WILEY-VCH

Wolfram Schnabel

Polymers and Electromagnetic Radiation

Fundamentals and Practical Applications



Lam Research Ex. 1047 - Page 1
Lam Research Corp. v. Inpria Corp.
IPR2024-00033 - U.S. Patent No. 9,823,564

Wolfram Schnabel

Polymers and Electromagnetic Radiation

Lam Research Ex. 1047 - Page 2
Lam Research Corp. v. Inpria Corp.
IPR2024-00033 - U.S. Patent No. 9,823,564

Related Titles

Theato, P., Klok, H. (eds.)

Functional Polymers by Post-Polymerization Modification
Concepts, Guidelines, and Applications
2013
ISBN: 978-3-527-33115-4, also available in digital formats

Thomas, S., Durand, D., Chassenieux, C., Jyotishkumar, P. (eds.)

Handbook of Biopolymer-Based Materials
From Blends and Composites to Gels and Complex Networks
2013
ISBN: 978-3-527-32884-0, also available in digital formats

Barner-Kowollik, C., Gruendling, T., Falkenhagen, J., Weidner, S. (eds.)

Mass Spectrometry in Polymer Chemistry
2012
ISBN: 978-3-527-32924-3, also available in digital formats

Mascia, L.

Polymers in Industry from A to Z
A Concise Encyclopedia
2012
ISBN: 978-3-527-32964-9, also available in digital formats

Yang, X. (ed.)

Semiconducting Polymer Composites
Principles, Morphologies, Properties and Applications
2012
ISBN: 978-3-527-33030-0, also available in digital formats

Schlüter, D.A., Hawker, C., Sakamoto, J. (eds.)

Synthesis of Polymers
New Structures and Methods
2012
ISBN: 978-3-527-32757-7, also available in digital formats

Makuuchi, K., Cheng, S.

Radiation Processing of Polymer Materials and itsIndustrial Applications
2012
ISBN: 978-0-470-58769-0, also available in digital formats

Knoll, W., Advincula, R.C. (eds.)

Functional Polymer Films
2 Volume Set
2011
ISBN: 978-3-527-32190-2, also available in digital formats

Leclerc, M., Morin, J. (eds.)

Design and Synthesis of Conjugated Polymers
2010
ISBN: 978-3-527-32474-3, also available in digital formats

Allen, N.S. (ed.)

Photochemistry and Photophysics of Polymer Materials
2010
ISBN: 978-0-470-13796-3, also available in digital formats

Matyjaszewski, K., Müller, A.H. (eds.)

Controlled and Living Polymerizations
From Mechanisms to Applications
2009
ISBN: 978-3-527-32492-7, also available in digital formats

Lam Research Ex. 1047 - Page 3
Lam Research Corp. v. Inpria Corp.
IPR2024-00033 - U.S. Patent No. 9,823,564

Wolfram Schnabel

Polymers and Electromagnetic Radiation

Fundamentals and Practical Applications

WILEY-VCH
Verlag GmbH & Co. KGaA

Lam Research Ex. 1047 - Page 4
Lam Research Corp. v. Inpria Corp.
IPR2024-00033 - U.S. Patent No. 9,823,564

Author

Prof. Dr. Wolfram Schnabel
Krottnaurer Str. 11
14129 Berlin
Germany

All books published by **Wiley-VCH** are carefully produced. Nevertheless, authors, editors, and publisher do not warrant the information contained in these books, including this book, to be free of errors. Readers are advised to keep in mind that statements, data, illustrations, procedural details or other items may inadvertently be inaccurate.

Library of Congress Card No.: applied for

British Library Cataloguing-in-Publication Data
A catalogue record for this book is available from the British Library.

Bibliographic information published by the Deutsche Nationalbibliothek
The Deutsche Nationalbibliothek lists this publication in the Deutsche Nationalbibliografie; detailed bibliographic data are available on the Internet at <http://dnb.d-nb.de>.

© 2014 Wiley-VCH Verlag GmbH & Co. KGaA, Boschstr. 12, 69469 Weinheim, Germany

All rights reserved (including those of translation into other languages). No part of this book may be reproduced in any form – by photoprinting, microfilm, or any other means – nor transmitted or translated into a machine language without written permission from the publishers. Registered names, trademarks, etc. used in this book, even when not specifically marked as such, are not to be considered unprotected by law.

Print ISBN: 978-3-527-33607-4
ePDF ISBN: 978-3-527-67774-0
ePub ISBN: 978-3-527-67773-3
Mobi ISBN: 978-3-527-67772-6
oBook ISBN: 978-3-527-67771-9

Cover Design Adam Design, Weinheim

Typesetting Thomson Digital, Noida, India

Printing and Binding Markono Print Media Pte Ltd, Singapore

Printed in Singapore
Printed on acid-free paper

Contents

Preface *IX*

Introduction *1*

Part I Non-Ionizing Radiation *5*

1 Sub-Terahertz Radiation Including Radiofrequency (RF) and Microwave Radiation *7*
1.1 Absorption *7*
1.1.1 General Aspects *7*
1.1.2 Dissipation of Energy *9*
1.1.2.1 Frequency Dependence *9*
1.1.2.2 Temperature Dependence *13*
1.2 Applications in Polymer Chemistry *15*
1.2.1 General Aspects *15*
1.2.2 Thermal Effects *16*
1.2.2.1 Polymer Synthesis *17*
1.2.2.2 Polymer Processing *21*
1.2.2.3 Modification of Polymers *22*
1.2.2.4 Polymer Degradation *22*
1.2.2.5 Polymer Supports for Solid-Phase Organic Synthesis (SPOS) *23*
1.2.3 Non-Thermal Effects *25*
1.2.3.1 Unresolved Questions *25*
1.2.3.2 Plasma-Assisted Chemistry *26*
1.3 Applications in Polymer Physics *38*
1.3.1 Dielectric Spectroscopy of Polymers *38*
1.3.2 Microwave Probing of Electrical Conductivity in Polymers *40*
1.3.3 Nondestructive Microwave Testing of Polymer Materials *43*
1.4 Industrial Applications *46*
References *49*

Lam Research Ex. 1047 - Page 6
Lam Research Corp. v. Inpria Corp.
IPR2024-00033 - U.S. Patent No. 9,823,564

2 Infrared Radiation *55*
2.1 Absorption *55*
2.1.1 General Aspects *55*
2.1.2 Crystalline Polymers *61*
2.1.3 Polarized IR Radiation *61*
2.1.4 Far-IR Radiation *62*
2.2 Applications *65*
2.2.1 General Aspects *65*
2.2.2 Mid-IR Analysis *67*
2.2.2.1 Identification of Synthetic Polymers *67*
2.2.2.2 Proteins *67*
2.2.2.3 Nucleic Acids *69*
2.2.3 NIR Analysis of Synthetic Organic Polymers *70*
2.2.4 Far-IR Analysis of Polymers: Terahertz Spectroscopy *73*
2.2.4.1 General Aspects *73*
2.2.4.2 Nondestructive Testing of Plastic Articles: THz Imaging *76*
2.2.4.3 THz Absorption by Biopolymers *77*
2.2.4.4 THz Studies of Biopolymers in Liquid Water *77*
2.2.4.5 Generation of THz Radiation in Poled Polymers *78*
2.2.5 Special Applications *79*
2.2.5.1 Thin Polymer Films *79*
2.2.5.2 Orientation Measurements *85*
2.2.5.3 IR Microspectroscopy and IR Imaging *90*
2.3 Polymer Characterization by Two-Dimensional IR Spectroscopy *91*
2.4 Time-Resolved Measurements in the mid-IR Range *93*
2.4.1 *In-Situ* Monitoring of Chemical Reactions *93*
2.4.2 Transient Two-Dimensional IR Spectroscopy *96*
2.4.2.1 T-Jump Studies *96*
2.4.2.2 Flash Photolysis *97*
2.5 Time-Resolved THz Spectroscopy *98*
2.5.1 Photoconductivity of Conjugated Polymers *98*
2.5.2 Folding of Proteins *100*
2.6 THz Optics Made From Polymers *101*
References *102*

3 Visible and Ultraviolet Light *109*
3.1 Absorption *109*
3.1.1 General Aspects *109*
3.1.2 The Molecular Orbital Model *111*
3.1.3 The Jablonski Diagram *113*
3.1.4 Absorption in Synthetic Nonconjugated Polymers *114*
3.1.5 Absorption in Synthetic Conjugated Polymers *115*
3.1.6 Absorption in Biopolymers *118*
3.1.7 Time-Resolved Spectroscopy *121*
3.2 Applications *122*

Lam Research Ex. 1047 - Page 7
Lam Research Corp. v. Inpria Corp.
IPR2024-00033 - U.S. Patent No. 9,823,564

3.2.1 General Aspects *122*
3.2.2 Applications in Polymer Chemistry *123*
3.2.2.1 Polymer Synthesis *123*
3.2.2.2 Modification of Synthetic Polymers *139*
3.2.2.3 Modification of Biopolymers *158*
3.2.3 Applications in Polymer Physics *164*
3.2.3.1 Spectroscopy *164*
3.2.3.2 Light Scattering *166*
3.2.3.3 Raman Scattering *174*
3.3 Technical Developments *176*
3.3.1 Introductory Remarks *176*
3.3.2 Photocuring *178*
3.3.3 Photolithography *183*
3.3.3.1 General Aspects *183*
3.3.3.2 248 nm Lithography *187*
3.3.3.3 193 nm Lithography *189*
3.3.3.4 157 nm Lithography *190*
3.3.4 Photovoltaics *192*
3.3.5 Polymeric Light Sources *196*
3.3.6 Holography *201*
3.3.7 Xerography *204*
3.3.8 Optical Waveguides *207*
References *210*

Part II Ionizing Radiation *225*

4 Elementary Processes of the Interaction of High-Energy Photons with Matter *227*
4.1 General Aspects *227*
4.2 Attenuation Coefficients *228*
4.3 Photoelectric Effect *230*
4.4 Compton Scattering *234*
4.5 Electron–Positron Pair Production *235*
4.6 Photonuclear Absorption *235*
4.7 Absorption of Swift Electrons *235*
References *237*

5 Chemical Reactions Induced by High-Energy Radiation *239*
5.1 General Aspects *239*
5.1.1 Radiation Sources and Electron Accelerators *242*
5.2 Polymer Synthesis *243*
5.2.1 Free-Radical Polymerization *243*
5.2.2 Ionic Polymerization *247*
5.2.3 Graft Copolymerization *251*

Lam Research Ex. 1047 - Page 8
Lam Research Corp. v. Inpria Corp.
IPR2024-00033 - U.S. Patent No. 9,823,564

5.2.4 Polymerization in the Solid State *253*
5.3 Radiolysis of Bulk Synthetic Polymers *257*
5.3.1 General Aspects *257*
5.3.2 Product Formation in the Absence of Molecular Oxygen *258*
5.3.3 Product Formation in the Presence of Molecular Oxygen *265*
5.3.4 Radiation Stability and Protection *265*
5.4 Radiolysis of Bulk Biopolymers *268*
5.4.1 General Aspects *268*
5.4.2 Nucleic Acids *268*
5.4.3 Polysaccharides *270*
5.4.4 Proteins *274*
5.5 Radiolysis of Polymers in Solution *275*
5.6 Technical Developments *285*
5.6.1 General Aspects *285*
5.6.2 Lithography *287*
5.6.2.1 Introduction *287*
5.6.2.2 Technical Performance *288*
5.6.2.3 Resists *292*
5.6.3 Crosslinking *303*
5.6.4 Curing *304*
5.6.5 Grafting *304*
5.6.6 Hydrogels *306*
References *307*

6 Applications of High-Energy Radiation in Polymer Physics *315*
6.1 General Aspects *315*
6.2 X-Ray Spectroscopy *316*
6.2.1 General Aspects *316*
6.2.2 Near-Edge X-Ray Absorption Fine Structure (NEXAFS) Spectroscopy *317*
6.2.3 Extended X-Ray Absorption Fine Structure (EXAFS) Spectroscopy *318*
6.2.4 X-Ray Photoelectron Spectroscopy (XPS) *318*
6.3 X-Ray Imaging and Microscopy *321*
6.4 X-Ray Scattering *322*
6.4.1 General Aspects *322*
6.4.2 Crystalline Polymers *322*
6.4.3 Polymer Solutions *330*
References *335*

Index *339*

Lam Research Ex. 1047 - Page 9
Lam Research Corp. v. Inpria Corp.
IPR2024-00033 - U.S. Patent No. 9,823,564

Preface

In 2006, the author completed a first monograph on the interaction of radiation with the vast family of polymers; this was titled *Polymers and Light. Fundamentals and Technical Applications*. The completion of that work coincided with the idea of a new project, this time covering the whole range of electromagnetic radiation, from sub-radiofrequency waves of only a few Hertz to gamma rays of some 10^{22} Hertz. Again, the objective was to cover in a concise manner the leading-edge results of the research community from a single author's perspective. This book, *Polymers and Electromagnetic Radiation*, is the result of that project.

It is the intention of the author to provide the reader with a guided tour through the panorama of polymers and their interactions with electromagnetic waves of different frequencies and wavelengths. Wherever needed, the reader is introduced to the basic physical and chemical concepts involved. Throughout all chapters, the book demonstrates how scientific results find their way into both industrial applications and further research.

To obtain an overview of a subject as immense as the present one requires a lot of reading. After all, the more than 800 citations compiled separately at the end of each chapter are only a fraction of the literature that had to be searched in order to obtain a representative impression of what the state-of-the art research is seeking. But, reading takes time, and after six years of work the project became a race against time for several reasons. First, as leading-edge technology ever advances, the work of a reviewer resembles the task of the well-known Sisyphos who, in Hades, was required to push the same huge bolder up a hill, again and again. Second, unlike the eternal setting in mythology, time is limited on Earth and this is felt even more strongly by a retired researcher. In fact, shortly after the studies and the text edition for this book were completed, my father's reading ability was impaired by a mini-stroke, and this is why he asked me to write this preface and handle the further printing of the book.

It is therefore in his name that I refer to the people supporting his work. Special thanks go to M. Wiencken, senior librarian of the Helmholtz-Zentrum Berlin für Materialien und Energie (HZB). The smooth and professional support by the personnel of the publisher, Wiley-VCH, is also gratefully acknowledged.

Munich, September 2013 *R. Florian Schnabel*

Lam Research Ex. 1047 - Page 10
Lam Research Corp. v. Inpria Corp.
IPR2024-00033 - U.S. Patent No. 9,823,564

Introduction

This book concentrates on the interaction of electromagnetic waves with polymers and deals only exceptionally with particle radiation. Electromagnetic waves comprise a very broad range of frequencies that extends over more than 20 orders of magnitude from the radiofrequency region up to the region of hard γ-rays emitted from radionuclides or being part of the cosmic rays (see Table I.1).

Table I.1 Electromagnetic waves.

Frequency (Hz)	Wavelength (m)	Photon energy (ev)	Designation of range
3×10^{1}	10^{7}	1.24×10^{-13}	Sub-radiofrequency waves
3×10^{2}	10^{6}	1.24×10^{-12}	
3×10^{3}	10^{5}	1.24×10^{-11}	Radiofrequency (RF) waves
3×10^{4}	10^{4}	1.24×10^{-10}	
3×10^{5}	10^{3}	1.24×10^{-9}	
3×10^{6}	10^{2}	1.24×10^{-8}	
3×10^{7}	10^{1}	1.24×10^{-7}	
3×10^{8}	10^{0}	1.24×10^{-6}	
3×10^{9}	10^{-1}	1.24×10^{-5}	Microwaves
3×10^{10}	10^{-2}	1.24×10^{-4}	
3×10^{11}	10^{-3}	1.24×10^{-3}	
3×10^{12}	10^{-4}	1.24×10^{-2}	Infrared (IR) radiation
3×10^{13}	10^{-5}	1.24×10^{-1}	
3×10^{14}	10^{-6}	1.24×10^{0}	Visible (VIS) - ultraviolet (UV) light
3×10^{15}	10^{-7}	1.24×10^{1}	Extreme ultraviolet (EUV) radiation
3×10^{16}	10^{-8}	1.24×10^{2}	
3×10^{17}	10^{-9}	1.24×10^{3}	X-rays
3×10^{18}	10^{-10}	1.24×10^{4}	
3×10^{19}	10^{-11}	1.24×10^{5}	
3×10^{20}	10^{-12}	1.24×10^{6}	γ-rays
3×10^{21}	10^{-13}	1.24×10^{7}	
3×10^{22}	10^{-14}	1.24×10^{8}	

Polymers and Electromagnetic Radiation: Fundamentals and Practical Applications, First Edition. Wolfram Schnabel
© 2014 Wiley-VCH Verlag GmbH & Co. KGaA. Published 2014 by Wiley-VCH Verlag GmbH & Co. KGaA.

Lam Research Ex. 1047 - Page 11
Lam Research Corp. v. Inpria Corp.
IPR2024-00033 - U.S. Patent No. 9,823,564

The various effects observed when electromagnetic radiation interacts with matter are interpreted on the basis of the so-called *wave-particle duality*, that is, electromagnetic radiation is considered to have both a wave-like and a particle-like character. Certain phenomena such as diffraction or interference can be interpreted only with the aid of the wave model, whereas energetic processes involving atoms or molecules such as absorption and emission can be understood only on the basis of the photon or quantum model. The particles of electromagnetic radiation are called *photons*, and the photon energy E is related to the frequency ν according to Eq. (I.1):

$$E = h\nu \tag{I.1}$$

where $h = 6.626 \times 10^{-34}\,J\,s$ $(6.626 \times 10^{-31}\,g\,m^2\,s^{-1})$ denotes Planck's constant. According to Einstein, a photon of energy E has the quality of mass m according to Eq. (I.2)

$$E = mc^2 \tag{I.2}$$

where $c = 3 \times 10^8\,m\,s^{-1}$ and denotes the velocity of electromagnetic radiation in free space.

Polymers are substances composed of macromolecules – that is, large molecules in excess of about 1000 atoms – and in many cases consist of long chains made up of small repeating units. Certain synthetic polymers are prepared via the polymerization of monomers and play important and ubiquitous roles in everyday life as plastic materials. Moreover, many biopolymers produced by living organisms are fundamental to biological functions.

Electromagnetic radiation can interact with matter – including polymers – in a variety of ways, the most prominent interaction modes being *absorption* and *scattering*. Radiation of frequencies below 10^{12} Hz (1 THz) is absorbed by polymers containing polar groups, and causes orientation polarization such that heat is generated. The absorption of infrared (IR) radiation causes the vibrations of atoms, but no bond breakages, while visible and ultraviolet (UV) light interacts with the shell electrons of the atoms, giving rise to the generation of electronically excited states that can undergo chemical reactions with surrounding molecules and thus causing chemical alterations. Also at frequencies higher than about 10^{15} Hz, photons interact with the shell electrons of the atoms. As the photon energies now exceed the shell electrons' ionization energy the latter can be expelled and, as a consequence, chemical bonds are broken, chemical alterations occur, and the physical properties of polymers are altered. When the expelled electrons possess relatively high kinetic energies they can dig their own tracks and ionize and electronically excite other molecules in the process. In the context of absorption, it is notable that electromagnetic radiation is an important tool for synthesizing polymers via the polymerization of small molecules.

Electromagnetic radiation passing through matter can also be attenuated by *scattering*. The electric field of the radiation is thought to cause vigorous vibrations of the shell electrons of atoms, thus forming oscillating dipoles which are themselves the source of electromagnetic waves that are emitted over the whole

Lam Research Ex. 1047 - Page 12
Lam Research Corp. v. Inpria Corp.
IPR2024-00033 - U.S. Patent No. 9,823,564

space. The wavelengths of the emitted waves are equal to those of the incident waves. Scattering can also be seen as elastic collision of photons with shell electrons. Recently, the scattering of both X-rays and of visible light has attracted analytical importance for synthetic and biopolymers.

This book describes in detail how the different types of electromagnetic radiation are attenuated by polymers, and highlights many of the applications related to the interaction of electromagnetic radiation with polymers. Typical applications refer to microwave heating used for the vulcanization of rubber and for recycling polymer waste. Radiofrequency or microwave-based plasma techniques are employed for the industrial processing of polymeric materials. Non-destructive microwave testing is an important tool for inspecting dielectric polymer coatings in a non-contact fashion. The IR region is related to important analytical applications, and IR analysis is nowadays an important tool for identifying and characterizing commercial polymers and for elucidating the spatial structure of proteins. Terahertz (10^{12} Hz) transmission spectroscopy has the potential for determining the content of additives in a polymer system in a contactless and non-destructive manner. Moreover, terahertz spectroscopy can also be used to identify nucleotide sequences in genes in a label-free manner and to measure the rate of folding and unfolding of proteins. Processes based on the interaction of visible and UV light with polymers have become important for a variety of applications. For example, polymers are used as photoresists in the production of computer chips, as core materials for optical wave guides, and as photoswitches and optical memories. Polymers are also employed in photocopying machines and in solar cells for the generation of energy. Moreover, VIS-UV light serves as a tool for the synthesis of polymers; that is, to initiate the polymerization of small molecules, a process that is applied not only in technical processes that involve the curing of coatings and adhesives but also in dentistry to cure tooth inlays.

Technical processes that employ ionizing radiation are widely applied in the polymer field, and include the production of crosslinked wire insulation and of heat-shrink food wrappings and tubings for electrical connections, the vulcanization of rubber tires and rubber lattices, and the curing of coatings and inks. Moreover, various X-ray methods can also be applied for the characterization and analysis of polymers, especially of the polymer surfaces. Both, X-ray imaging and X-ray microscopy allow the derivation of quantitative composition maps of polymer surfaces. Notable in this context are also near-edge X-ray absorption fine structure spectroscopy (NEXAFS), extended X-ray absorption fine structure spectroscopy (EXAFS) and X-ray photoelectron spectroscopy (XPS).

The phenomenon of X-ray scattering forms the basis of techniques that serve to characterize semicrystalline synthetic polymers, to elucidate the chemical structure of biopolymers (e.g., certain proteins), and to determine size, shape and state of aggregation of macromolecules in solution. X-ray scattering is also an important tool for characterizing biopolymers such as proteins and nucleic acids in the native state.

Within this book, the chemical and physical processes involving the interaction of electromagnetic radiation with polymers are addressed in two parts, with Part I

Lam Research Ex. 1047 - Page 13
Lam Research Corp. v. Inpria Corp.
IPR2024-00033 - U.S. Patent No. 9,823,564

being devoted to non-ionizing radiation and Part II to ionizing radiation. In Part I, the interaction of sub-terahertz radiation, infrared radiation and VIS-UV light with polymers, and their practical applications are detailed in separate chapters. In contrast, the three chapters of Part II relate to the absorption of high-energy photons (Chapter 4), to high-energy radiation-induced chemical reactions and related applications (Chapter 5), and to the application of high-energy radiation in polymer physics (Chapter 6).

It is customary to deal with the interaction of electromagnetic radiation with polymers separately with respect to the various frequency ranges, and a typical example of this can be found in the present author's book *Polymers and Light*, published in 2007 by Wiley-VCH. However, it was the author's notion to provide an overview in a single book covering the very broad frequency range referred to above and, of necessity, a concise working mode had to be applied and concentration on essentials was afforded.

Lam Research Ex. 1047 - Page 14
Lam Research Corp. v. Inpria Corp.
IPR2024-00033 - U.S. Patent No. 9,823,564

Part I
Non-Ionizing Radiation

Polymers and Electromagnetic Radiation: Fundamentals and Practical Applications, First Edition. Wolfram Schnabel
© 2014 Wiley-VCH Verlag GmbH & Co. KGaA. Published 2014 by Wiley-VCH Verlag GmbH & Co. KGaA.

Lam Research Ex. 1047 - Page 15
Lam Research Corp. v. Inpria Corp.
IPR2024-00033 - U.S. Patent No. 9,823,564

1
Sub-Terahertz Radiation Including Radiofrequency (RF) and Microwave Radiation

1.1
Absorption

1.1.1
General Aspects

The regime of the electromagnetic spectrum corresponding to frequencies lower than 1 THz $= 10^{12}$ Hz – that is, to photon energies lower than that of infrared (*IR*) light – is commonly divided into three sections: (i) the sub-radiofrequency (*RF*) region, ranging from 10^{-6} Hz to 3×10^{3} Hz; (ii) the RF region, ranging from 3×10^{3} Hz to 3×10^{8} Hz (1.24×10^{-11} to 1.24×10^{-6} eV, corresponding to wavelengths *in vacuo* of 10^{5} to 1 m); and (iii) the microwave region, ranging from 3×10^{8} Hz to 3×10^{11} Hz (1.24×10^{-6} to 1.24×10^{-3} eV, corresponding to wavelengths *in vacuo* of 1 m to 10^{-3} m). Both, RF and microwave radiation are widely used for all types of telecommunication techniques, including radio, television, wireless telephoning, and radar (radio detection and ranging), and therefore the use of these electromagnetic waves is regulated by government agencies. In many countries, the frequencies 0.869, 0.915 and 2.45 GHz, corresponding to $\lambda = 0.345$ m, 0.328 m and 0.122 m, respectively, are provided for industrial and private usage. Commonly, domestic microwave ovens are operated at 2.45 GHz.

Basically, the absorption of the various types of sub-THz radiation follows the same principle, and therefore its treatise will be coupled together here. The photon energy of sub-THz radiation is lower than about 10^{-3} eV, and thus at least about three orders of magnitude lower than the binding energies of atoms in molecules. This implies that chemical reactions cannot be induced directly by single photons of these radiations. However, if sub-THz radiation is absorbed, heat will be generated – that is, photon energy will be converted into translational energy. The phenomenon related to the fact that the absorption of sub-THz radiation results in heating is commonly referred to as *dielectric loss heating*. The resultant increase in temperature can be the cause of the initiation or acceleration of chemical reactions. Now, the question arises: How is photon energy converted into translational energy in this case? Actually, only polar materials consisting of molecules with a

Polymers and Electromagnetic Radiation: Fundamentals and Practical Applications, First Edition. Wolfram Schnabel
© 2014 Wiley-VCH Verlag GmbH & Co. KGaA. Published 2014 by Wiley-VCH Verlag GmbH & Co. KGaA.

Lam Research Ex. 1047 - Page 16
Lam Research Corp. v. Inpria Corp.
IPR2024-00033 - U.S. Patent No. 9,823,564

permanent dipole moment and materials containing mobile ions are capable of absorbing sub-THz radiation, whereas nonpolar materials are almost transparent. This explains why polar polymers such as poly(methyl methacrylate) and poly(vinyl acetate) are absorbing, but nonpolar polymers such as polyethylene, polypropylene and polytetrafluoroethylene are nonabsorbing materials. According to a model originating from P. Debye [1,2] (who received the Nobel Prize in Chemistry in 1936), sub-THz radiation interacts with nonionic systems containing polar entities via *orientation polarization* of the permanent dipoles; that is, the dipole moments tend to align parallel to the direction of the external electric field, provided that the mobility of the polar entities is sufficiently high. At relatively low frequencies, the dipoles have ample time to follow the variations of an external alternating electric field. However, as the frequency increases, the dipoles are unable to fully restore their original positions during field reversals; that is, the dipolar reorientation lags behind the applied field and eventually stops. Energy is absorbed by the system, as long as electric field-enforced motions of the polar entities take place.

The phenomenon of orientation polarization under the influence of an outer alternating electric field is referred to as *dielectric relaxation*. Relaxation, in its original meaning, relates to the re-establishment of an equilibrium state of a system that has been distorted by an outer force. In a frequently used broader sense, the term relaxation relates to the ability of a system to undergo distortions under the influence of an outer force. In the present case, the motions of polar groups contained in a system in the condensed state are enforced by an outer electric field; that is, dipole vectors orient themselves with respect to the direction of the outer electric field. In this sense, dielectric relaxation resembles mechanical relaxation involving strain release after strain build-up. The relaxation of a system is characterized by the relaxation time τ, which, generally speaking, corresponds to the time that the system needs to return to the equilibrium state after distortion by an outer force. With respect to polar groups being exposed to an outer electric field, τ characterizes their mobility and, in an extrapolated sense, the mobility of the whole system. The extent of energy absorption is essentially determined by the magnitude of the relaxation time τ (see Section 1.1.2.1). In the case of polymers, the determination of relaxation times is an important feature of dielectric spectroscopy (see Section 1.3.1).

The radiation-induced orientation polarization of dipolar molecules or groups consumes energy on a molecular scale (internally dissipated as heat) to overcome internal constraints induced by the external electric field. Electrically nonconducting materials capable of undergoing dielectric relaxation are commonly denoted as *dielectrics*.

In systems containing mobile charge carriers, another mechanism of energy absorption becomes operative. Here, electromagnetic waves induce an electric current which generates heat. In this context it is notable that microwave absorption can serve as a tool to detect charge carriers; for example, a characteristic microwave absorption signal can be detected (see Section 1.3.2) when charge carriers are generated in a nonconducting medium upon irradiation with a pulse of ultraviolet (*UV*) laser light.

Lam Research Ex. 1047 - Page 17
Lam Research Corp. v. Inpria Corp.
IPR2024-00033 - U.S. Patent No. 9,823,564

In heterogeneous dielectric systems comprising small fractions of electrically conducting phases, another mode of polarization arises from the charge build-up in *interfaces* between chemically different components, termed *interfacial* (space charge) or *Maxwell–Wagner polarization*. Both, orientation and interfacial polarization are the basis for energy absorption in many industrial materials subjected to alternating electric fields during processing.

1.1.2 Dissipation of Energy

The parameter characterizing the interaction of sub-THz radiation with matter is the complex relative dielectric constant ε (dimensionless), also called complex permittivity (Equation 1.1).

$$\varepsilon = \varepsilon' - \mathrm{j}\,\varepsilon'' \tag{1.1}$$

Here, $\mathrm{j} = \sqrt{-1}$. The term *relative* means relative to free space (*in vacuo*). Absolute values are obtained according to Equation 1.2 by multiplying ε with the permittivity of free space $\varepsilon_0 = 8.85 \times 10^{-12}\,\mathrm{F\,m^{-1}}$.

$$\varepsilon_{\mathrm{abs}} = \varepsilon\,\varepsilon_0 = (\varepsilon' - \mathrm{j}\,\varepsilon'')\varepsilon_0 \quad (\mathrm{F\,m^{-1}}) \tag{1.2}$$

The real part ε' of the complex dielectric constant relates to the energy reversibly stored and released per cycle of the alternating field; that is, ε' characterizes the ability of the irradiated material to be polarized and to propagate the wave. The imaginary part $-\mathrm{j}\varepsilon''$ relates to the energy absorbed per cycle; that is, ε'', which is also called the *loss factor*, characterizes the ability of the irradiated material to absorb (dissipate) energy – that is, to convert sub-THz energy quantums into heat. Frequently, the *dielectric performance* of materials is characterized by the ratio of ε'' to ε', denoted as $\tan\,\delta = \varepsilon''/\varepsilon'$. Polar materials contain a large number of permanent dipoles which all contribute to the loss factor. The latter is obtained experimentally and commonly denoted as the *effective loss factor* (for the sake of simplicity, the attribute *effective* is omitted in the following text). The dielectric properties of typical nonpolar and polar polymers are listed in Tables 1.1 and 1.2, respectively. Both ε' and ε'' vary with frequency and temperature.

1.1.2.1 Frequency Dependence

$\varepsilon(\omega)$, the complex dielectric function of a material, can be obtained by measuring the capacitance C_0 and C of a capacitor in the absence and presence of the material, respectively, with the aid of Equation 1.3:

$$\varepsilon(\omega) = \frac{C}{C_0} \tag{1.3}$$

By using a sinusoidal electric field $E(\omega) = E_0 \exp(\mathrm{j}\omega t)$ with an angular frequency $\omega = 2\pi\nu$, the complex permittivity can be obtained by measuring the complex

Lam Research Ex. 1047 - Page 18
Lam Research Corp. v. Inpria Corp.
IPR2024-00033 - U.S. Patent No. 9,823,564

Table 1.1 Dielectric properties of nonpolar polymers at 20 to 30 °C [3,7].

Polymer	Frequency (Hz)	ε' [a]	ε'' [b]
Polypropylene	10^3	2.4	$<1.2 \times 10^{-3}$
	10^5	2.4	$<1.2 \times 10^{-3}$
	10^7	2.4	$<(1.2–4.5) \times 10^{-3}$
	10^9	2.4	
Butadiene-styrene rubber	10^4	2.5	2.5×10^{-3}
	10^5	2.5	4.5×10^{-3}
	10^7	2.5	16.9×10^{-3}
	10^9	2.5	10.8×10^{-3}
Hevea rubber	10^4	2.4	3.4×10^{-3}
	10^5	2.4	3.4×10^{-3}
	10^7	2.4	7.7×10^{-3}
	10^8	2.2	12.0×10^{-3}
	10^9		6.4×10^{-3}
Polystyrene	10^3	2.5	4×10^{-3}
	10^9	2.5	4×10^{-3}
Poly(tetrafluoroethylene-*co*-hexa-fluoropropene) (90:10, w/w)	10^5	2.1	0.5×10^{-3}
	10^7	2.1	1.0×10^{-3}
	10^9	2.1	2.3×10^{-3}
	10^{10}	2.1	1.5×10^{-3}

a) Real part of the complex relative dielectric constant.
b) Loss factor.

Table 1.2 Dielectric properties of polar polymers at 20 to 30 °C [3].

Polymer	Frequency (Hz)	ε' [a]	ε'' [b]
Polychloroprene (1,4-poly(2-chloro-1,3-butadiene))	10^4	6.2	0.205
	10^5	6.1	0.183
	10^7	4.7	0.940
	10^9	2.84	0.136
Poly(methyl methacrylate)	10^4	3.0	0.100
	10^5	2.9	0.082
	10^7	2.8	0.048
	10^8	2.7	0.032
Poly(ethylene terephthalate)	10^3	3.3	0.016
	10^6	2.4	0.048
	10^9	2.4	0.008
Polyamide-6	10^3	3.5	0.035
	10^5	3.4	0.065
	10^7	3.2	0.096
	10^9	3.1	0.062
Cellulose	10^3	7.2	0.145
	10^4	7.0	0.21
	10^7	5.8	0.46
	10^8	5.6	0.39

a) Real part of the complex relative dielectric constant.
b) Loss factor.

Lam Research Ex. 1047 - Page 19
Lam Research Corp. v. Inpria Corp.
IPR2024-00033 - U.S. Patent No. 9,823,564

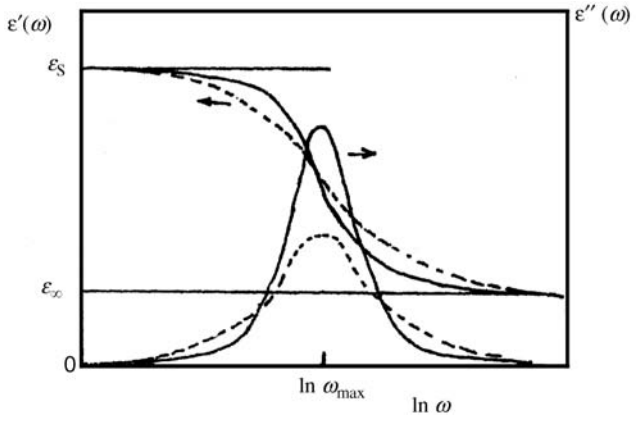


Figure 1.1 General frequency dependence of ε' and ε''. —, Debye dielectric; ---, real dielectric. Adapted with permission from Ref. [3]; © 1996, Pergamon/Elsevier.

impedance $Z(\omega)$. The latter is related to $\varepsilon(\omega)$ according to Equation 1.4.

$$\varepsilon(\omega) = \frac{1}{\mathrm{j}\omega Z(\omega) C_0} \tag{1.4}$$

From the dielectric function, the relaxation time can be extracted as a fitting parameter based on empirical functions. In the simplest case, the Debye function Equation 1.5 is applicable.

$$\varepsilon(\omega) = \frac{\varepsilon_\mathrm{s} - \varepsilon_\infty}{1 + \mathrm{j}\omega\tau} + \varepsilon_\infty \tag{1.5}$$

(see Figure 1.1 for the definition of ε_s and ε_∞)

Corresponding relations for ε' and ε'' are given by Equations 1.6 and 1.7, which show that the magnitude of the dielectric loss is governed by the relaxation time τ, more exactly speaking by the term $(\omega\tau)^2$ [3].

$$\varepsilon'(\omega) = \frac{\varepsilon_\mathrm{s} - \varepsilon_\infty}{1 + \omega^2\tau^2} + \varepsilon_\infty \tag{1.6}$$

$$\varepsilon''(\omega) = (\varepsilon_\mathrm{s} - \varepsilon_\infty)\frac{\omega\tau}{1 + \omega^2\tau^2} \tag{1.7}$$

Alternating orientation polarization is feasible at frequencies ranging from $\nu = 0$ (steady field) to about $\nu = 10^{12}$ Hz (lowest IR frequency). At higher frequencies, the dipoles can no longer follow the variations of an external alternating electric field, and here only electron distortion polarization is possible. In the frequency range from 0 to 10^{12} Hz, ε' decreases monotonically from the highest value $\varepsilon' = \varepsilon_\mathrm{s}$ at $\nu = 0$ (static dielectric constant) to the lowest value $\varepsilon' = \varepsilon_\infty$ (dielectric dispersion) at the upper limit of ν. On the other hand, ε'' equals zero at $\nu = 0$ and at far IR frequencies. However, at intermediate frequencies, Equation 1.7 predicts a

Lam Research Ex. 1047 - Page 20
Lam Research Corp. v. Inpria Corp.
IPR2024-00033 - U.S. Patent No. 9,823,564

symmetrical peak at $\omega\tau = 1$, corresponding to $\varepsilon'' = (\varepsilon_s - \varepsilon_\infty)/2$. The general frequency dependence of ε' and ε'' is demonstrated in Figure 1.1.

In many cases – including amorphous polymers – the peaks in dielectric spectra ($\varepsilon'' = f(\omega)$) are not symmetrical and are broader than predicted by the Debye model (Equation 1.7). To account for asymmetry and broadness of the spectra, modified equations characterized by the addition of exponential parameters to Equation 1.5 have been proposed. For example, the *Havriliak–Negami equation* (Equation 1.8) contains two exponents, α and β [4]:

$$\text{Havriliak-Negami equation} \qquad \varepsilon = \frac{\varepsilon_s - \varepsilon_\infty}{(1 + (j\omega\tau)^\alpha)^\beta} + \varepsilon_\infty \tag{1.8}$$

In a special case, the symmetry parameter β equals unity. This leads to the so-called *Cole–Cole equation* (Equation 1.9) [5]:

$$\text{Cole-Cole equation} \qquad \varepsilon = \frac{\varepsilon_s - \varepsilon_\infty}{1 + (j\omega\tau)^\alpha} + \varepsilon_\infty \tag{1.9}$$

As can be seen from Figure 1.2, the typical dielectric response of a polar amorphous polymer at constant temperature is characterized by a succession of descending steps in ε' and a corresponding series of ε'' peaks.

The multiplicity of dielectric relaxations becoming obvious from this graph reflects various different modes of orientation polarization occurring at distant frequencies. The α-relaxation at the lowest frequencies corresponding to the longest relaxation times is associated with the glass transition – that is, movements of the main chains of the polymer via cooperative motions of main chain segments. The subsidiary β- and γ-relaxations at higher frequencies corresponding to shorter relaxation times are related to motions of single structural elements including rotations and/or conformational changes of side groups.

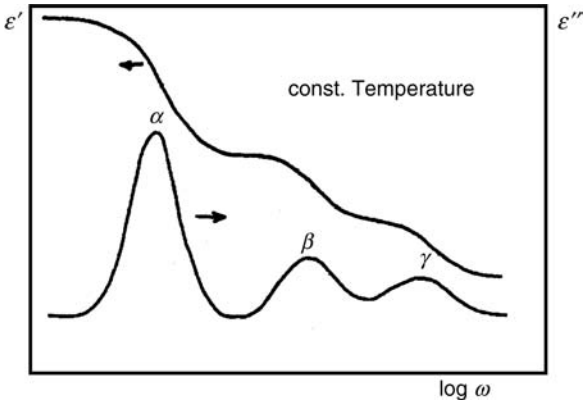


Figure 1.2 Typical dielectric response of a polar amorphous polymer. Frequency dependence of ε' and ε'' at constant temperature. Adapted with permission from Ref. [3]; © 1996, Pergamon/Elsevier.

Lam Research Ex. 1047 - Page 21
Lam Research Corp. v. Inpria Corp.
IPR2024-00033 - U.S. Patent No. 9,823,564

As sub-THz radiation penetrates a *lossy* dielectric ($\varepsilon'' > 0$), energy is dissipated and, therefore, the power of the radiation is attenuated. Equations relating the absorbed dose rate and the penetration depth with ε' and ε'' can be derived from Maxwell's equations; details (not given here) for this are available from the relevant literature [3,6].

The absorbed dose rate – that is, the radiation energy absorbed per volume and time unit – is given by Equation 1.10 [6]:

$$D_r^{abs} = 2\pi\nu\varepsilon_0\varepsilon'' E^2 \qquad (\mathrm{Js^{-1}\,m^{-3}}) \tag{1.10}$$

where ν is the frequency (in Hz) and E is the electric field strength (in $\mathrm{V\,m^{-1}}$).

The penetration depth, d_P – that is, the depth at which the incident radiation power is being reduced to $1/e$ (about 37%) – is given by Equation 1.11 [6]:

$$d_P = \frac{\lambda_0}{2\pi(2\varepsilon')^{0.5}}\left[\left(1+(\varepsilon''/\varepsilon')^2\right)^{0.5} - 1\right]^{-0.5} \quad (\mathrm{m}) \tag{1.11}$$

For low-loss dielectrics – that is, for $(\varepsilon''/\varepsilon') \ll 1$, d_P approximates to:

$$d_P = \frac{\lambda_0(\varepsilon')^{0.5}}{2\pi\varepsilon''} \quad (\mathrm{m}) \tag{1.12}$$

where λ_0 (m) denotes the wavelength *in vacuo*. Obviously, the penetration depth increases with larger wavelengths, that is, with decreasing frequency. This can be seen also from Table 1.3, where d_P values calculated with the aid of Equation 1.12 are listed for various frequencies and ε'' values. Typically, at $\nu = 10^9$ Hz, corresponding to $\lambda_0 = 0.3$ m, the penetration depth into poly(ethylene terephthalate), amounts to $d_P = 9.26$ m, with $\varepsilon' = 2.4$ and $\varepsilon'' = 8 \times 10^{-3}$.

1.1.2.2 Temperature Dependence

The variation of ε' and ε'' with temperature can be explained on the basis of the Debye model, according to which the absorption of sub-THz radiation in nonionic materials is caused by the orientation polarization of polar molecules or polar groups in polymers and, therefore, depends on the mobility of the polar entities. Since the extent to which absorption occurs via this mechanism is essentially

Table 1.3 Penetration depth d_P (m) of sub-THz radiation into a nonmagnetic material of relative dielectric constant $\varepsilon' = 3.0$, and different electric loss factors ε'' at various frequencies. Calculated with the aid of Equation 1.12.

ε''	Frequency (Hz)			
	10^4	10^6	10^8	10^{10}
0.01	8.27×10^5	8.27×10^3	8.27×10^1	8.27×10^{-1}
0.1	8.27×10^4	8.27×10^2	8.27	8.27×10^{-2}
1.0	8.27×10^3	8.27×10^1	8.27×10^{-1}	8.27×10^{-3}

Lam Research Ex. 1047 - Page 22
Lam Research Corp. v. Inpria Corp.
IPR2024-00033 - U.S. Patent No. 9,823,564

determined by the relaxation time τ (see Equations 1.6 and 1.7), the temperature dependence of ε' and ε'' is related to that of τ, as given by Equation 1.13.

$$\tau = \frac{\mathrm{h}}{\mathrm{k}T}\exp\left(\frac{\Delta \mathrm{G}^*}{RT}\right) = \frac{\mathrm{h}}{\mathrm{k}T}\exp\left(-\frac{\Delta S^*}{R}\right)\exp\left(\frac{\Delta H^*}{RT}\right) \tag{1.13}$$

where h is Planck's constant, k is Boltzmann's constant, and ΔG^*, ΔS^* and ΔH^* denote molar free energy, molar entropy and molar enthalpy of activation, respectively. For a limited temperature range, the pre-exponential and the entropy term can be combined in a practically temperature-independent term τ_0, as expressed by Equation 1.14:

$$\tau = \tau_0 \exp\left(\frac{\Delta H^*}{RT}\right) \tag{1.14}$$

According to Equation 1.14, $\ln(\tau)$ decreases with increasing temperature, which implies that in plots of ε'' versus $\omega = 2\pi\nu$, the peak of the absorption band is shifted to higher frequencies with rising temperature. This results from the fact that, at the peak's maximum, $\omega_{\max}\tau = 1$. Consequently, an increase in temperature resulting in a decrease in τ enforces an increase in $\omega_{\max}$ and vice versa, an increase in τ, caused by decreasing temperature, yields a lower $\omega_{\max}$. According to Equations 1.6 and 1.7, the magnitude of ε' is determined both by ε_∞ and the difference $\varepsilon_S - \varepsilon_\infty$, and that of ε'' by $\varepsilon_S - \varepsilon_\infty$. These terms depend in different modes on temperature for polymers with polar side groups and polymers containing in-chain or rigidly attached polar groups.

For many compounds, including certain polymers, both ε' and ε'' increase with increasing temperature. While this increase is marginal with respect to ε', it is quite significant in the case of ε''. Typically, in the case of polyamide 6,6, ε'' increases by a factor of about 10 as the temperature rises from 40 to 150 °C (see Figure 1.3).

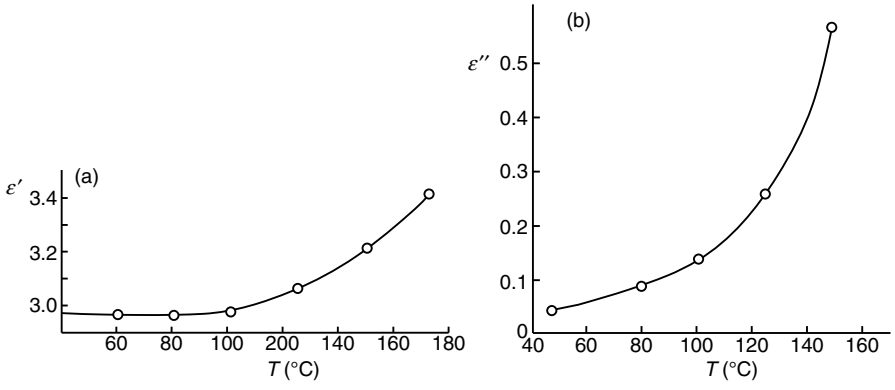


Figure 1.3 Dielectric properties of polyamide 6,6 at 3 GHz. ε' and ε'' as a function of temperature. Adapted with permission from Ref. [8]; © 1976, International Microwave Power Institute.

Lam Research Ex. 1047 - Page 23
Lam Research Corp. v. Inpria Corp.
IPR2024-00033 - U.S. Patent No. 9,823,564

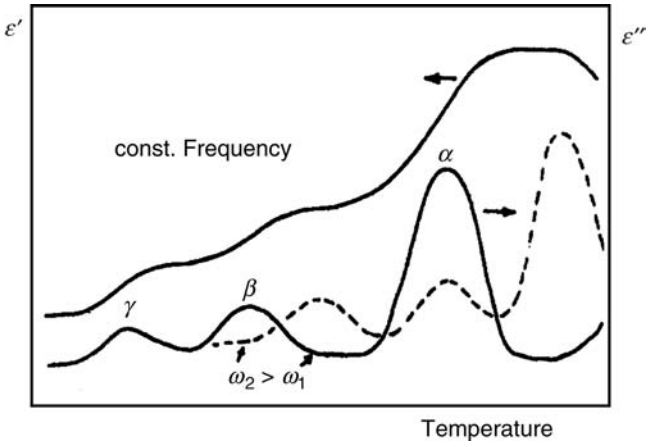


Figure 1.4 Typical dielectric response of a polar amorphous polymer. Temperature dependence of ε' and ε'' at constant frequency. Adapted with permission from Ref. [3]; © 1996, Pergamon/Elsevier.

It is interesting to note that, in the case of amorphous polar polymers, the temperature dependence of ε' and ε'' reflects alterations in the physical state of the system. This is due to the fact mentioned above that the absorption of sub-THz radiation is based on the orientation polarization of polar groups, which is determined by their mobility. As a polymeric system is heated up from low to high temperatures, various physical stages related to the mobility of structural elements are surpassed. As demonstrated in Figure 1.4, the temperature dependence of the dielectric response at constant frequency, typical for a polar amorphous polymer, is characterized by a succession of ascending steps in ε' and a corresponding series of ε'' peaks.

The peak at the highest temperature is associated with the α-relaxation – that is, to the motions of main-chain-segments becoming activated during the glass transition. The subsidiary weaker peaks refer to the β- and γ-relaxations associated with various motions, such as rotation or conformational changes of polar side groups.

It should be noted that a positive $d\varepsilon''/dT$ implies an increase in the absorbed dose rate during irradiation, as the latter heats the system up. Therefore, care must be taken during RF- and microwave-aided processing to avoid unwanted overheating, the so-called *runaway effects*.

1.2
Applications in Polymer Chemistry

1.2.1
General Aspects

Materials absorbing sub-THz radiation ($\nu < 10^{12}$ Hz) are rapidly heated up, which is an attractive feature for chemists since, in comparison with conventional heating

Lam Research Ex. 1047 - Page 24
Lam Research Corp. v. Inpria Corp.
IPR2024-00033 - U.S. Patent No. 9,823,564

techniques, many thermally induced chemical processes can be performed with a substantially shortened reaction time. In fact, reductions from many hours or days to several minutes, or even seconds, are common place.

As was noted in Section 1.1, the absorption of sub-THz radiation by organic materials is restricted to those containing ionic and/or polar components and, in the case of linear polymers, with polar groups incorporated in the main chain or in side chains. Provided that the penetration depth of the radiation is substantially larger than the sample's thickness, heating proceeds *volumetrically* – that is, simultaneously in the total irradiated volume – and does not rely on convection or the conduction of energy from the system's outside to its interior, as in the case of classical heating (such as a hot plate or oil-bath heating). Thus, microwave irradiation represents an attractive and safe alternative to classical heating, as it permits a required reaction temperature to be attained at a much faster rate.

In fact, the mode of action of sub-THz radiation-induced chemical reactions is still under debate [9]. Because of the low photon energy (0.0016 eV at 2.45 GHz), sub-THz radiation cannot break chemical bonds (which have binding energies of several eV), and so such radiation cannot directly induce chemical reactions. Therefore, frequently observed microwave effects – such as an acceleration of the reaction rate, increases in product yield and variations in product distribution – are commonly interpreted on the basis of purely thermal effects. The latter include very rapid heating, superheating to temperatures that substantially exceed the boiling point of the solvent, or a pressure increase if a closed system is irradiated. The selective excitation of dipoles, causing a large temperature increase in their vicinity and enhanced diffusion rates of small molecules, is thought to be responsible for an increase in reaction rate and a decrease in the apparent activation energy (for details, see Ref. [10]). Moreover, microwave phenomena are explained in terms of changes in thermodynamic properties under the influence of microwave fields [11]. This model comes close to speculations on *nonthermal radiation effects* that are still lacking convincing evidence [9]. On the other hand, nonthermal reactions can be induced by *plasmas* generated by sub-THz radiation, and plasma-assisted chemistry is widely applied in industrial processes, for example in processes related to the field of polymers.

Apart from the role that sub-THz radiations play in polymer chemistry, they are also very usefully applied in polymer physics. As an example, this might involve dielectric spectroscopy, which is used widely to characterize the molecular dynamics of polymers. Moreover, microwaves are employed for the nondestructive testing of polymer materials, an example being the detection of heterogeneities in plastic articles.

1.2.2 Thermal Effects

The advent of commercial laboratory microwave reactors and the corresponding industrial-scale equipment [10] has given rise to worldwide activity concerning the

Lam Research Ex. 1047 - Page 25
Lam Research Corp. v. Inpria Corp.
IPR2024-00033 - U.S. Patent No. 9,823,564

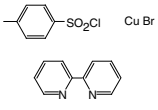
sub-THz radiation-assisted synthesis of organic compounds. Indeed, a plethora of reports has been made on the influence of microwave heating on chemical reactions with organic compounds [10,12–15]. Although most of these reports have involved the organic chemistry of low-molar-mass compounds, a respectful fraction is related to the field of polymers, including their synthesis via the polymerization of small molecules, the modification and degradation of polymers, and the use of polymer supports for solid-phase organic syntheses [9,16–20]. These topics are discussed in the following subsections.

1.2.2.1 Polymer Synthesis

Chain-Growth Polymerizations

Free-Radical Polymerization The free-radical polymerization of unsaturated compounds is readily performed with the aid of microwaves, provided that the monomer molecules have a permanent dipole moment and can, therefore, absorb microwaves. The classical polymerization mechanism – as described in textbooks [21–24] and involving steps of initiation, propagation, and termination – applies to the microwave-assisted polymerization. Prescriptions for milliliter-scale polymerizations have been described by Bogdal [18], and some typical cases are listed in Table 1.4. Whereas styrene (an unpolar monomer) polymerizes only very slowly if irradiated in bulk, the aqueous emulsion polymerization of styrene using potassium persulfate as an initiator proceeds very rapidly. This process is shown in Figure 1.5, where the conventional and microwave-initiated polymerizations are compared by plotting monomer conversion versus reaction time [25].

Table 1.4 Microwave-assisted free-radical polymerizations of unsaturated monomers at 300 W [18].

Monomer	Polymer	Initiator	Solvent[a)]	Reaction time and temperature	Polymer yield (%)
Methyl methacrylate	Poly(methyl methacrylate)	AIBN[b)]	Toluene	10 min 90 °C	>50
Isooctyl acrylate	Poly(isooctyl acrylate)	AIBN[b)]	Hexane	10 min 65 °C	>60
9-Vinylcarbazole	Poly(9-vinylcarbazole)	AIBN[b)]	Toluene	10 min 65 °C	>75
Styrene	Polystyrene			120 min 110 °C	>50

a) Monomer concentration: (ca. 50%, v/v).
b) 2,2′-Azobis(2-methylpropionitrile).

Lam Research Ex. 1047 - Page 26
Lam Research Corp. v. Inpria Corp.
IPR2024-00033 - U.S. Patent No. 9,823,564

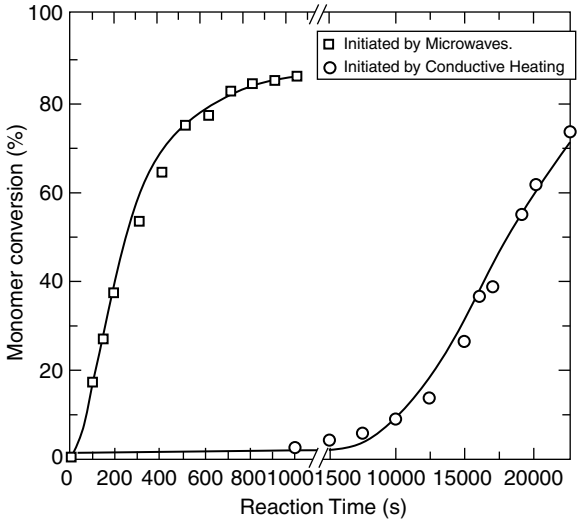
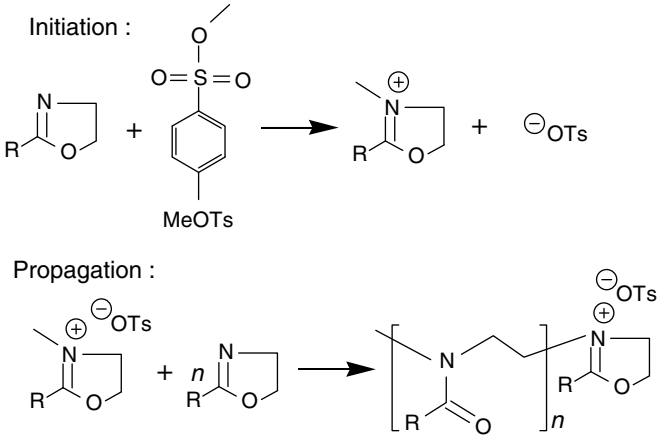


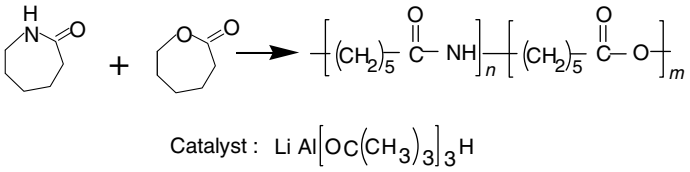
Figure 1.5 Conventional and microwave initiated emulsion polymerization of styrene. Adapted with permission from Ref. [25]; © 1996, VNU Science Press.

Ionic Polymerization A variety of polymerizations that proceed by ionic mechanisms are promoted if microwave heating is applied. Typical cases pertain to the living cationic ring-opening polymerization of 2-oxazolines [10,26] (see Scheme 1.1) and the anionic homo- and copolymerization of ε-caprolactone and ε-caprolactam [27] (see Scheme 1.2). The rate of polymerization of 2-ethyl-2-oxazoline at 200 °C in acetonitrile solution is accelerated by a factor of 400 as compared to conventional heating [26]. Notably, poly(2-ethyl-2-oxazoline), being both biocompatible and biodegradable, is applicable to drug-delivery systems.



Scheme 1.1 Ring-opening polymerization of 2-oxazolines. R: methyl, ethyl, nonyl, or phenyl [26].

Lam Research Ex. 1047 - Page 27
Lam Research Corp. v. Inpria Corp.
IPR2024-00033 - U.S. Patent No. 9,823,564



Scheme 1.2 Copolymerization of ε-caprolactam and ε-caprolactone [27].

ε-Caprolactone and ε-caprolactam, both of which are polar compounds capable of absorbing microwaves, were shown to homopolymerize more rapidly in catalyzed, solvent-free processes under microwave heating (at 4.2 to 5.2 GHz) than with conventional heating, producing yields of 92% and 87%, respectively [27]. The molar mass, melt temperatures and glass transition temperature (T_g) of the homopolymers obtained by the two heating methods were of comparable magnitude. The microwave-assisted anionic copolymerization of the two compounds, catalyzed by lithium tris-*tert*-butoxyalumino hydride, resulted in polymers with a molar mass of approximately $2 \times 10^4\,g\,mol^{-1}$ (yield: ca. 70%). The yields, amide-to-ester ratios and T_g-values were higher, and the molar masses of products equivalent, as compared to those obtained by conventional heating.

Subsequent studies on polymerization of the bisaliphatic epoxy compound 3,4-epoxycyclohexylmethyl, 3,4-epoxy-cyclohexylcarboxylate (see Chart 1.1) revealed that the compound does not polymerize thermally in the absence of an initiator. However, in the presence of diaryliodonium or triphenylsulfonium salts, an ionic polymerization was initiated and the onset of the polymerization shifted to higher temperatures upon microwave heating (see Table 1.5). This microwave effect could be explained in terms of the thermodynamic properties being different under the influence of a microwave field [11].

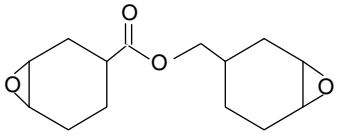
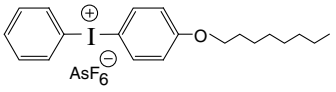
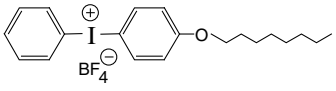
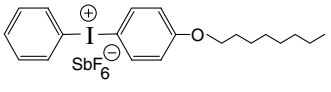


Chart 1.1 Chemical structure of 3,4-epoxycyclohexylmethyl,3,4-epoxy-cyclohexylcarboxylate.

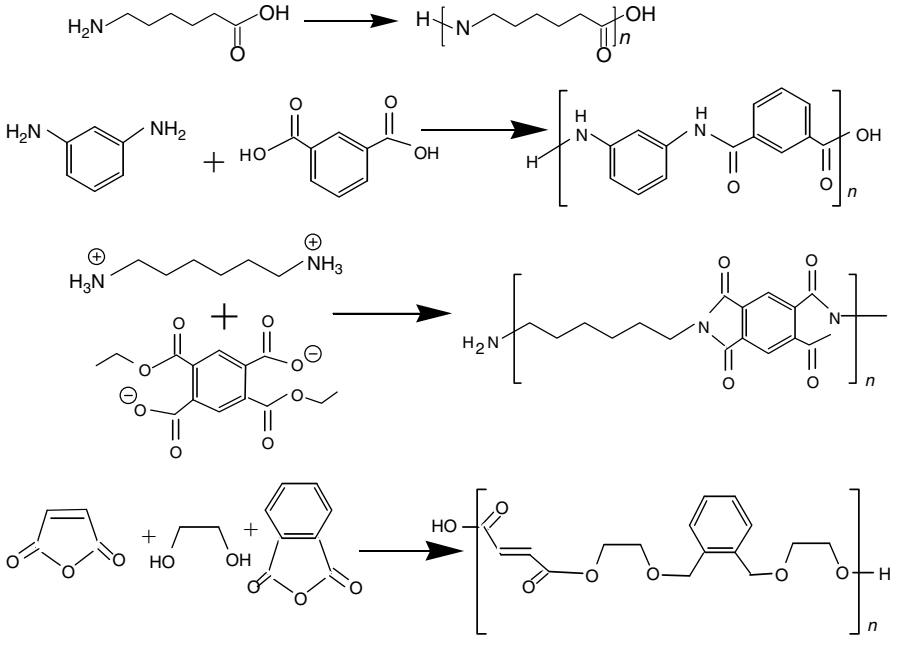
Step-Growth Polymerization Microwave-assisted step-growth polymerizations – that is, polycondensation and polyaddition reactions – have been studied extensively. According to a review by Wiesbrock *et al.* [10], a plethora of reports has been devoted to the microwave-assisted synthesis of polyamides, polyimides, polyethers, and polyesters. For the majority of polymerizations, the reaction rates were significantly increased under microwave irradiation as compared to conventional heating, whilst in many cases the reaction times were shortened from hours, and sometimes days, to about 10 minutes. Moreover, the product purity was improved and the polymers exhibited superior properties, most likely due to a reduction in

Lam Research Ex. 1047 - Page 28
Lam Research Corp. v. Inpria Corp.
IPR2024-00033 - U.S. Patent No. 9,823,564

Table 1.5 Polymerization of the epoxide compound shown in Chart 1.1 with the aid of different onium salts. Comparison of the onset temperatures for conventional and microwave heating [28].

Initiator	Conventional heating	Microwave heating
	212 °C	257 °C
	169 °C	216 °C
	191 °C	217 °C

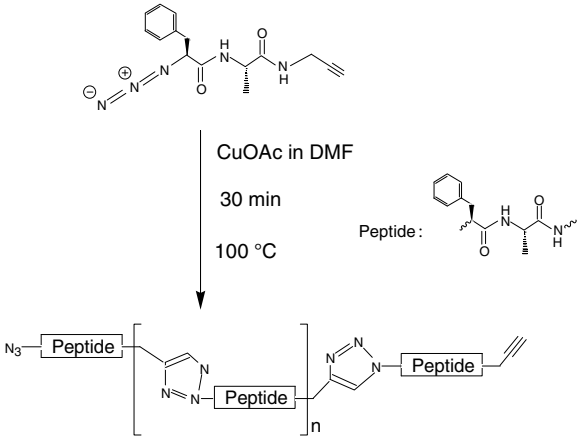
side reactions. A small selection of microwave-assisted step-growth polymerizations, as described in various reports, are presented in Scheme 1.3. It should be noted that these polymerizations were quite often performed in polar solvents with high boiling points, because of the low microwave absorbance of monomers; such solvents included *o*-cresol, dimethylacetamide, and *N*-methylpyrrolidone.



Scheme 1.3 Microwave-assisted step-growth polymerization. Typical systems [10,18].

Lam Research Ex. 1047 - Page 29
Lam Research Corp. v. Inpria Corp.
IPR2024-00033 - U.S. Patent No. 9,823,564

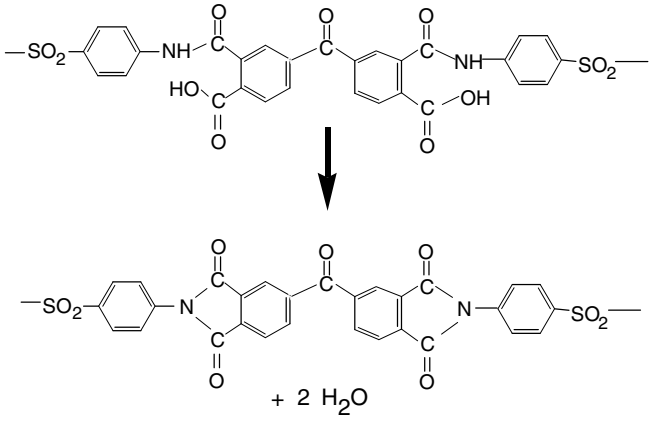
Another interesting example was the synthesis of peptide-based polymers via the Cu(I)-catalyzed N–C polymerization of azido-phenylalanyl-alanyl-propargyl amide [29] (see Scheme 1.4).



Scheme 1.4 Synthesis of peptide-based polymers via Cu(I)-catalyzed N---C polymerization of azido-phenylalanyl-alanyl-propargyl amide in dimethylformamide solution ($c > 250\,g\,l^{-1}$). $n = 80$ to 150 [29].

1.2.2.2 **Polymer Processing**

Thermoset systems including epoxide systems, polyesters, polyimides, and polyurethanes are cured more quickly by microwave heating than by conventional thermal heating. This benefit of microwave heating was concluded from many studies reviewed by Zong *et al.* [19], with one typical example pertaining to the unimolecular imidization of a polyamic acid in *N*-methylpyrrolidone solution (see Scheme 1.5).



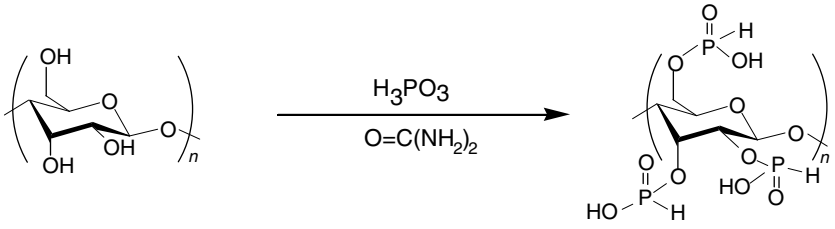
Scheme 1.5 Imidization of a polyamic acid [30].

Lam Research Ex. 1047 - Page 30
Lam Research Corp. v. Inpria Corp.
IPR2024-00033 - U.S. Patent No. 9,823,564

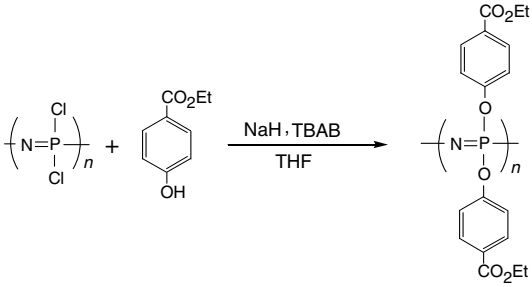
According to Lewis *et al.* [30], the rate constant of the imidization is increased and the activation energy reduced when the reaction is performed with microwaves rather than with conventional heating. In contrast to most other studies, however, Mijovic *et al.* found no difference in curing rates upon investigating epoxide systems and polyimides [31].

1.2.2.3 **Modification of Polymers**

There is a significant potential of microwave-assisted modification of linear polymers via side group substitution, and the details of two examples pertaining to cellulose and polyphosphazene are presented here. The phosphorylation of cellulose at OH groups, as achieved by the microwave irradiation of a mixture of cellulose, urea and phosphorous acid at 105 °C for 2 h, is shown in Scheme 1.6 [18], while Scheme 1.7 indicates how chlorine atoms of poly(dichlorophosphazene) can be substituted by microwave heating of the polymer in the presence of ethyl-4-hydroxybenzoate, tetrabutyl ammonium bromide (*TBAB*), tetrahydrofuran (*THF*), and NaH for 2 h at 65 °C [18].



Scheme 1.6 Modification of cellulose [18].



Scheme 1.7 Modification of poly(dichlorophosphazene) [18].

1.2.2.4 **Polymer Degradation**

Microwave heating is an appropriate tool for recycling polymer waste. For example, it can be applied to separate metal from polymer/metal laminates by pyrolysis, to depolymerize polyamide and poly(ethylene terephthalate) by solvolysis, or to devulcanize rubber (see Table 1.6). Detailed information on this topic is available in Ref. [19].

Lam Research Ex. 1047 - Page 31
Lam Research Corp. v. Inpria Corp.
IPR2024-00033 - U.S. Patent No. 9,823,564

Table 1.6 Typical processes based on microwave-assisted polymer degradation.

Process	System	Remarks	Reference
Pyrolysis	HDPE[a]/aluminum laminates	Clean Al is obtained	[32]
	Polysiloxane		
	Polysylazene	Conversion to ceramics	[33]
Depolymerization	Polyamide-6	Solvolysis within 4 to	[34]
	Poly(ethylene terephthalate)	10 min	[35]
Devulcanization	Vulcanized rubber	Cleavage of S–S bond, polymer chain remains intact	[36]

a) HDPE: high-density polyethylene.

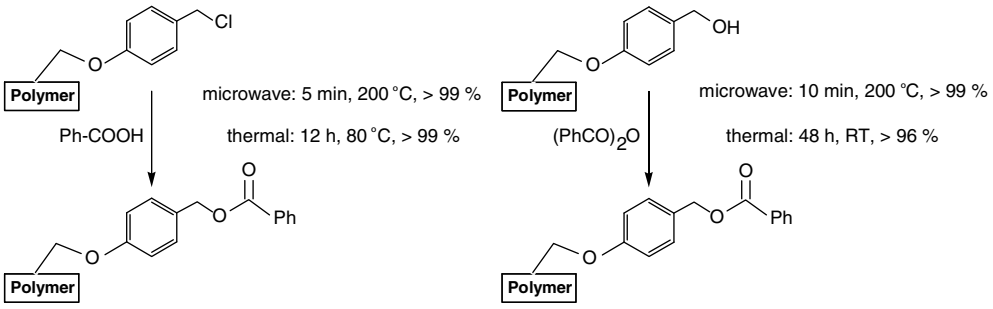
One very useful application of the microwave heating technique is in the hydrolysis of proteins and peptides for amino acid analysis [37]. Conventionally, protein analysis is performed by hydrolyzing samples in aqueous 6 N HCl solution at 110 °C for periods of at least 24 h, in conjunction with high-performance liquid chromatography (*HPLC*). By employing microwave heating, however, the reaction time can be reduced to less than 1 h, and in special cases to a few minutes. As microwave hydrolysis accelerates the reaction without altering the chemistry of amino acid analysis, the same acids, protective agents and derivatization procedures can be used as are employed in conventional processes. Interestingly, microwave heating is also appropriate for the generation of HCl vapor in the vapor-phase hydrolysis of proteins [37].

1.2.2.5 Polymer Supports for Solid-Phase Organic Synthesis (SPOS)

Based on the Merrifield synthesis for the preparation of peptides, SPOS using insoluble polymer supports has been developed for the rapid preparation of large libraries of small organic molecules with drug-like properties. Notably, SPOS contributes essentially to the field of *combinatorial chemistry*, which is the art and science of synthesizing and testing compounds for their bioactivity, aiming at the discovery of new drugs.

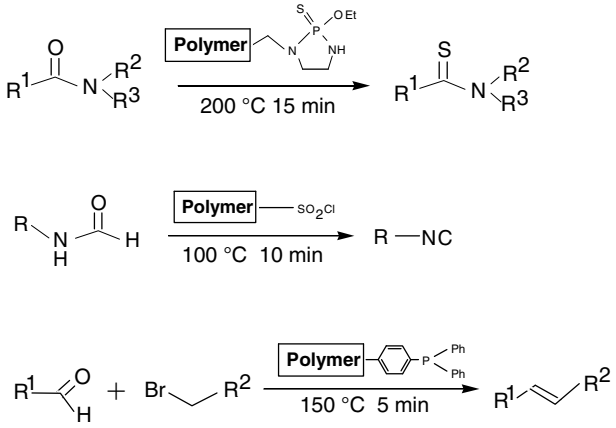
The polymer supports employed commonly include crosslinked polystyrene and membranes of polypropylene and cellulose. The general SPOS procedure involves several steps: following attachment of the educt to the polymer support, the latter is contacted with a solution of a reagent and subsequently heated to the desired temperature. This procedure can be repeated using a second or third reagent, after which the product is finally detached from the support and isolated. The main shortcomings of this method – notably the long reaction times required – can be overcome by using microwave heating (mostly with 2.45 GHz radiation), and significant increases in the reaction rates, yields, and purity of products have been observed [14,38,39]. A typical extent of rate enhancement is shown in Scheme 1.8, where the reaction times using conventional thermal and microwave heating are compared [40].

Lam Research Ex. 1047 - Page 32
Lam Research Corp. v. Inpria Corp.
IPR2024-00033 - U.S. Patent No. 9,823,564



Scheme 1.8 Typical examples demonstrating rate enhancement in the case of microwave-assisted solid-phase organic synthesis [40].

As an alternative approach, instead of performing the process with educts coupled to the support, polymer-supported reagents (*PSR*s) can be brought into contact with the educt dissolved in an appropriate solvent. In this case, the polymer support can be easily isolated from the product solution by filtration. Moreover, it is possible to apply a surplus of the PSR, and this frequently leads to higher product yields. Microwave heating has also been used to improve the PSR method, and some typical microwave-assisted reactions are shown in Scheme 1.9. More detailed information on this topic, and some appropriate references, are provided in Ref. [14].



Scheme 1.9 Typical examples of microwave-assisted reactions with polymer-supported reagents [14].

Another occasionally useful alternative to the above-described methods is to employ a liquid-phase synthesis on soluble polymeric supports. In this case, the reactive molecules such as poly(ethyleneoxide) are coupled to a polymer backbone and brought into contact with reagents within a homogeneous medium (solvent). On completion of the reaction, the polymeric matrix is separated from the system

Lam Research Ex. 1047 - Page 33
Lam Research Corp. v. Inpria Corp.
IPR2024-00033 - U.S. Patent No. 9,823,564

by precipitation, membrane filtration, or size-exclusion chromatography. The large number of thiohydantoins of the structure shown in Chart 1.2, and which have been synthesized in this way, represent an example of this approach [41]. Notably, the use of microwave heating led to a significant acceleration in the different steps of the process.

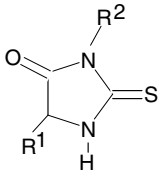


Chart 1.2 General structure of thiohydantoins prepared by microwave-assisted liquid-phase synthesis on poly(ethylene oxide) of molar mass 6000 g mol^{-1}.

It should be noted that solvents employed in microwave-assisted synthesis on polymer supports must fulfill various requirements. In particular, they should swell the polymer, have a high boiling point, exhibit a high chemical stability and last, but not least, they should absorb microwaves (i.e., they should possess a high ε''-value). 1-methyl-2-pyrrolidone (*NMP*; see Chart 1.3) fulfills these requirements, at least if used in conjunction with polystyrene supports, which swell strongly in this solvent.

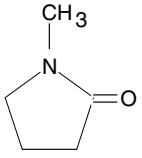


Chart 1.3 Chemical structure of 1-methyl-2-pyrrolidone (NMP).

1.2.3 Non-Thermal Effects

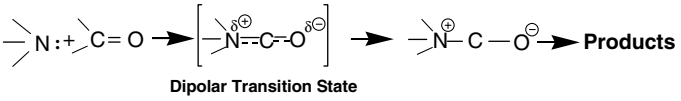
1.2.3.1 Unresolved Questions

Sub-THz radiation – especially microwave radiation – is a powerful tool for initiating classical thermal chemical reactions (as noted in Section 1.2.2). The most obvious sub-THz radiation phenomenon relates to the significantly reduced reaction times, which can be interpreted in terms of the efficient and rapid heating of the reaction mixtures. However, many research groups are currently debating the existence of specific, so-called "non-thermal" modes of action regarding the initiation or modulation of chemical reactions. In particular, it has been asked whether the steric course and the chemoselectivity or stereoselectivity of reactions are altered by the influence of sub-THz radiation, as this would result in new products that would not be formed after classical heating. Various aspects

Lam Research Ex. 1047 - Page 34
Lam Research Corp. v. Inpria Corp.
IPR2024-00033 - U.S. Patent No. 9,823,564

regarding specific microwave effects have been discussed by many authors [10,11,30,42,43], and in particular by Perreux and Loupy [44]. Accordingly, specific effects can be based on selective energy absorption by dipoles, with ensuing specific reactions of the latter. A temperature increase of 50 K in the vicinity of the absorbing dipoles has been predicted [30], a consequence of which would be an enhancement of the diffusion rates of small molecules. This situation would apply, for example, to the increase in reaction rate and decrease in apparent activation energy in ring-closing imidization reactions [42].

Specific effects are also feasible for reactions proceeding via polar transition states, which can give rise to an enhanced absorption of sub-THz radiation and thus influence the course of the reaction [44]. A typical case refers to the reaction of amines with ketones (see Scheme 1.10).



Scheme 1.10 Amine addition to a carbonyl group involving a polar transition state.

Provided that *thermodynamic properties* such as internal energy and Gibbs free energy of materials with permanent dipole moments undergo significant changes under the influence of microwave fields, shifts in the reaction equilibrium and in kinetics, as compared to thermal fields at the same temperature, can be foreseen [11]. At present, it seems that final conclusions about non-thermal effects can be arrived at only after much more carefully performed experiments have been carried out. However, it is clear that sub-THz radiations – and especially microwaves – can serve as a tool for rapid and efficient heating, with no further influence on most reactions [10].

While the present discussion on non-thermal chemical reactions induced by the direct specific action of sub-THz radiation is ongoing, it is well known that non-thermal reactions can also be initiated indirectly via plasmas generated by the same radiation. In fact, plasma-assisted chemistry is strongly related to the field of polymers, and its importance and major potential for industrial applications are described in the following subsections.

1.2.3.2 Plasma-Assisted Chemistry

General Aspects Radiofrequency or microwave electric fields of sufficient strength can break down a gas under appropriate conditions and produce an electrically conducting medium, denoted as "plasma." By definition, a plasma is a partially ionized gas, confined to a certain volume with equal numbers of positive and negative charges. The charged particles are free and exhibit a collective behavior. Similar to soap bubbles, plasmas possess at their boundaries a skin called the *plasma sheath* or *Debye sheath*. The main body of a plasma always has a positive

Lam Research Ex. 1047 - Page 35
Lam Research Corp. v. Inpria Corp.
IPR2024-00033 - U.S. Patent No. 9,823,564

potential relative to the walls, with most of the potential drop appearing across the sheath with voltages ranging from a few volts up to thousands of volts, depending on various parameters. Positive ions generated in the plasma zone are propelled through the sheath and strike the walls or a substrate placed close to the plasma zone at near-normal incidence.

Plasma techniques are employed for the deposition of thin polymer films on solid substrates, for the chemical modification of polymer surfaces, and for the etching of polymer coatings. These processes are usually performed with the aid of low-pressure, low-temperature continuous plasmas, so-called continuous wave (*CW*) plasmas. Some typical laboratory-scale set-ups for these plasma processes are shown in Figure 1.6 [45].

Plasma etching and plasma film deposition, with the latter frequently being denoted as plasma-enhanced chemical vapor deposition (*PE-CVD*) or somewhat incorrectly as *plasma polymerization*, were initially developed during the 1960s as CW processes. Some years later, processes utilizing afterglow (*AG*) discharge became very popular, and in many cases these were operated at pressures ranging from 13 to 4000 Pa (0.1 to 30 Torr) and at a field frequency of 13.56 MHz, though

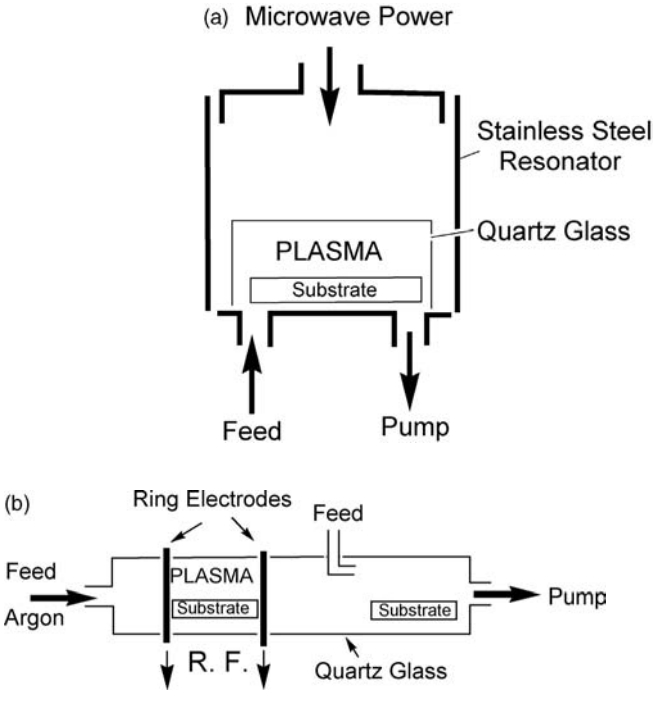


Figure 1.6 Deposition of polymer films with the aid of low-pressure, low-temperature continuous plasmas. (a, b) Typical set-ups with substrates positioned in the plasma zone. The set-up in (b) possesses also a substrate position downstream from the plasma zone for afterglow deposition. Adapted with permission from Ref. [45]; © 2004, The Electrochemical Society.

Lam Research Ex. 1047 - Page 36
Lam Research Corp. v. Inpria Corp.
IPR2024-00033 - U.S. Patent No. 9,823,564

frequencies in the kHz and GHz regimes were also utilized. In CW processes, the discharge runs continuously and the substrate is directly exposed to the plasma (in this context, frequently denoted as *glow*). As a result, the substrate is subjected to a direct interaction with reactive neutral and ionized species generated in the plasma by ionization and fragmentation of the feed molecules. In this way, thin films of highly crosslinked, quite irregular macromolecular structures (see Chart 1.4) are formed at the substrate's surface, when the molecular fragments eventually combine.

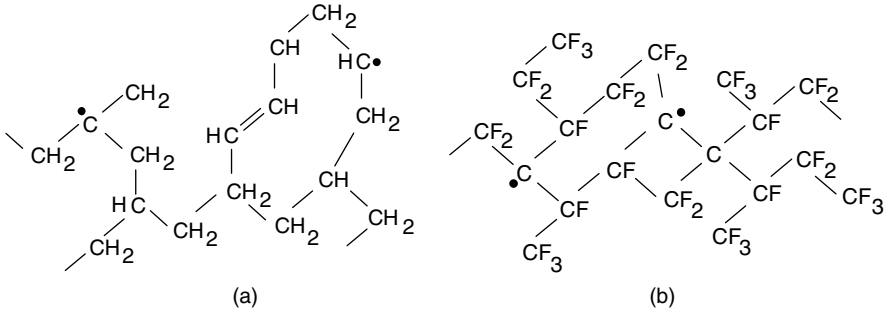


Chart 1.4 Chemical structures of macromolecular coatings formed by deposition at solid substrates positioned in the plasma zone using (a) an aliphatic hydrocarbon feed and (b) a fluorocarbon feed (b).

Commonly, these structures are referred to as *plasma polymers*, although they do not resemble conventional polymers with regular structural repeating units. Practically all organic substances of sufficiently high volatility can be employed for PE-CVD; for example, thin polymer films can form at the surface of appropriate substrates using plasmas generated from aliphatic or aromatic hydrocarbons such as methane, ethane and hexane or benzene and xylene, respectively. Halogenated compounds such as CF_4 and C_2F_3Cl, and organosilicon compounds such as tetramethylsilane, hexamethyldisiloxane and hexamethyldisilazane, can also be plasma-polymerized. Conventional monomers suitable for the plasma deposition of polymeric coatings include acrylic acid, allyl alcohol, ethylene, and styrene. A range of compounds that have been used in plasma polymerization studies are listed in Table 1.7. Interestingly, thin polymer films can also be deposited from plasma generated from a gas mixture consisting of CO_2, H_2, and NH_3.

In AG processes, the substrates are positioned downstream with respect to the plasma zone (see Figure 1.6b). Here, the substrate is not bombarded by ions but reacts only with longlived reactive species (especially free radicals) which are following the stream originating from the plasma. More regular macromolecular chemical structures with a high retention of the monomer structure are formed in this way, as indicated in Chart 1.5, which shows the chemical structure of a film deposited from C_2F_6 plasma onto a polymer substrate. Notably, in the case of AG PE-CVD the deposition rate is several orders of magnitude lower than for PE-CVD.

Lam Research Ex. 1047 - Page 37
Lam Research Corp. v. Inpria Corp.
IPR2024-00033 - U.S. Patent No. 9,823,564

Table 1.7 Selected compounds employed in plasma polymerization studies [46].

Class	Monomer
Hydrocarbons	Methane, ethane, hexane benzene, toluene, xylene, naphthalene, hexamethylbenzene
Halogenated hydrocarbons	Tetrafluoromethane, trifluorochloroethylene
Unsaturated compounds	Ethylene, tetracyanoethylene, propylene, isobutene, acrylic acid, allyl alcohol, allyl amine, vinyl trimethyl silane, acetylene
Organosilicon compounds	Tetraethyloxysilane, hexamethyldisiloxane, tetramethylsilane, hexamethyldisilazane
Sulfur-containing compounds	Thianthrene, thiophene, thioacetamide, thiourea
Nitrogen-containing compounds	Aniline, *p*-toluidine, picoline
Other compounds	Diphenyl mercury, diphenyl selenide

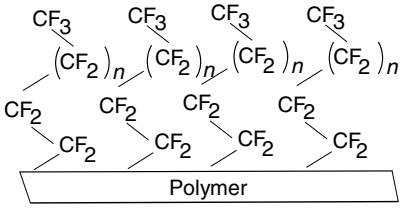


Chart 1.5 Chemical structure of a film deposited on a polymer substrate from C_2F_6 plasma by afterglow plasma-enhanced chemical vapor deposition (AG PE-CVD) [47].

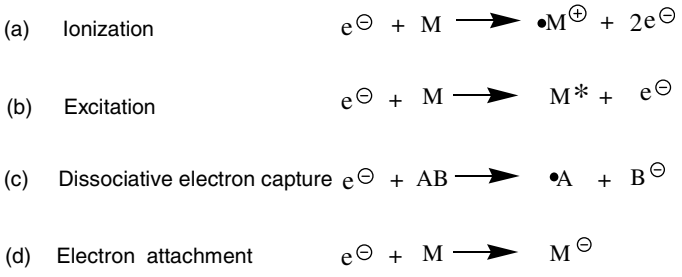
A high degree of monomer structure retention can be achieved also by employing a modulated plasma technique. In this case, the power input is delivered to the plasma for a period t_{on} and switched off for a period t_{off}, with $t_{off} \gg t_{on}$. As the substrate is positioned in the plasma zone, it is subjected to attack by reactive particles during the on-period, while reactive species that have been generated on its surface react with intact feed molecules during the off-period. Provided that the feed contains a conventionally polymerizable compound, the short plasma pulse will initiate its polymerization, exactly speaking the graft-copolymerization of the monomer at the polymer surface.

The great interest in the field of plasma-assisted chemistry is reflected by a large number of reviews and books [45,46,48–62], and by two journals devoted to the subject [63,64].

Mechanistic Aspects Usually, the breakdown of gases under the influence of an alternating electric field is initiated by a relatively small number of electrons produced from an external agency. These electrons acquire kinetic energy mainly from the electric field, and partially from elastic collisions with gas molecules. Upon multiplication of these processes, the kinetic energy of the electrons

Lam Research Ex. 1047 - Page 38
Lam Research Corp. v. Inpria Corp.
IPR2024-00033 - U.S. Patent No. 9,823,564

eventually becomes sufficiently high to accomplish electronic excitations and ionizations of feed molecules by electron impact (see reactions (a) and (b) in Scheme 1.11). The ionization produces additional electrons. It should be noted that the kinetic energy of the primary electrons is reduced by these processes. Subsequent fragmentation processes yield a variety of intermediates that include radical cations and free radicals. Negative ions can be formed by attachment processes of *sub-excitation electrons with gas molecules* (see reactions (c) and (d) in Scheme 1.11) [65]. Sub-excitation electrons have kinetic energies below the first electronic excitation potential of the feed molecules.



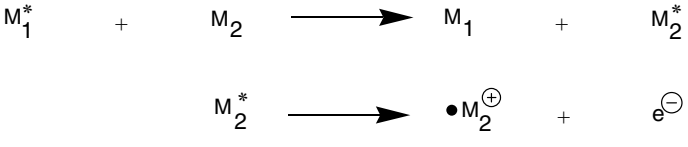
Scheme 1.11 Reactions of electrons with plasma feed molecules. The asterisk denotes an electronically excited state.

After having lost their kinetic energy, the electrons combine with positive ions, typically according to reaction (a) in Scheme 1.12. Often, radical cations disintegrate spontaneously into smaller cations and free radicals according to reaction (b) in Scheme 1.12.



Scheme 1.12 Reactions of radical cations. The asterisk denotes an electronically excited state.

Energy transfer from excited molecules M_1^* to molecules M_2 of a lower ionization potential might also result in ionization; this process is referred to as *Penning ionization* (see Scheme 1.13).

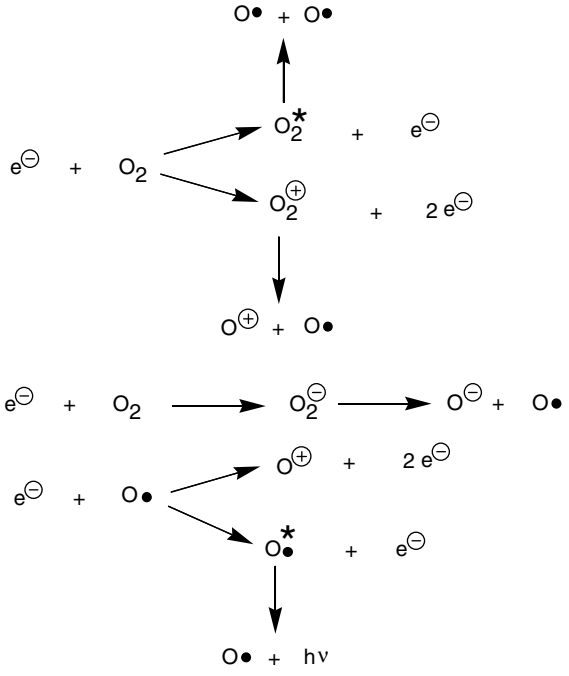


Scheme 1.13 Energy transfer from molecules of high ionization potential to molecules of lower ionization potential, resulting in ionization (Penning ionization). The asterisk denotes an electronically excited state.

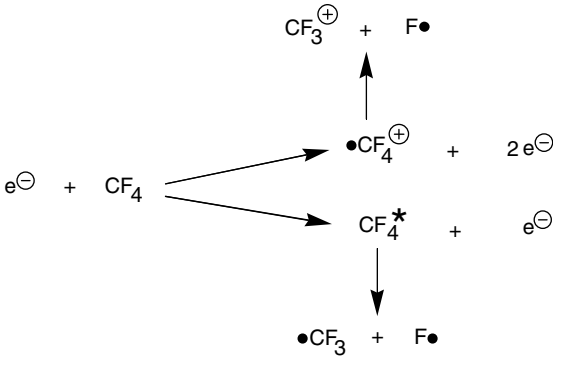
Lam Research Ex. 1047 - Page 39
Lam Research Corp. v. Inpria Corp.
IPR2024-00033 - U.S. Patent No. 9,823,564

Typical reaction schemes related to plasmas applied to the fabrication of microelectronic devices are presented in Schemes 1.14 and 1.15 (the former scheme refers to an oxygen plasma and the latter to a CF_4 plasma).

Actually, various fragments including $CF_3^{\oplus}$ and $CF_2^{\oplus}$ ions; CF_3, CF_2, CF radicals and F atoms have been detected in CF_4 plasmas, indicating the occurrence of additional processes such as those described in Scheme 1.16.

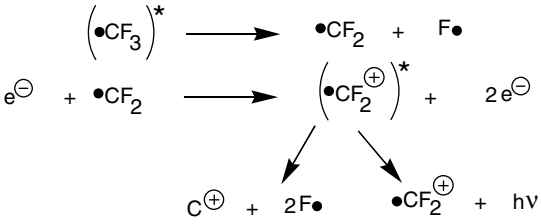


Scheme 1.14 Reactions of electrons in oxygen (O_2) plasmas. The asterisk denotes an electronically excited state.



Scheme 1.15 Reactions of electrons with tetrafluoromethane. The asterisk denotes an electronically excited state.

Lam Research Ex. 1047 - Page 40
Lam Research Corp. v. Inpria Corp.
IPR2024-00033 - U.S. Patent No. 9,823,564



Scheme 1.16 Processes occurring in a CF_4 plasma [66]. The asterisk denotes an electronically excited state.

A plasma formed by ionization of the feed molecules is maintained if the rates of charge production and charge loss are equal. Charge loss occurs by neutralization – that is, via the combination of electrons or negative ions with positive ions, and reaction (a) in Scheme 1.12 is a typical example of this. Details concerning breakdown mechanisms and the maintenance of fully developed plasmas have been described in detail (e.g., Ref. [6]).

If a substrate is to be plasma-modified, then photochemical processes must also be taken into account. This follows on from the fact that some of the electronically excited molecules emit photons (see Equation 1.15), which makes the plasma visible (via glow discharge).

$$M^* \rightarrow M + h\nu \tag{1.15}$$

To some extent, photons possessing energies corresponding to the UV range are likely to be absorbed by the substrate, thus initiating photochemical reactions. Plasma-induced intermolecular crosslinking and main-chain cleavage, as occurs in the case of substrates consisting of linear polymers, are thought to result from such photochemical processes.

In low-pressure (1 Torr = 133 Pa), high-frequency (1 MHz) plasmas (so-called *nonequilibrium plasmas*), which are of practical importance, the heavy particles (ions and intact molecules) are essentially at ambient temperature, while the electrons are *hot* – that is, they possess kinetic energies that are sufficiently high to cause ionizations and electronic excitations, and under these conditions plasma chemistry takes place at near-ambient temperature. However, the plasma temperature increases as the pressure is increased, and atmospheric plasmas can be applied as heat sources for the activation of endothermic chemical reactions. Relevant investigations with RF plasmas have included the pyrolysis of hydrocarbons such as methane and propane, and the decomposition of carbon tetrachloride [48]. With regards to polymers, surface treatment and thin-film deposition at atmospheric pressure can be performed, when He or Ar are used as carrier gases for the feed, and dielectric insulators are inserted between the electrodes in the discharge gap [67]. Detailed information on atmospheric plasmas, in the context of both thin-film deposition and polymer etching, is available elsewhere [67–69].

Lam Research Ex. 1047 - Page 41
Lam Research Corp. v. Inpria Corp.
IPR2024-00033 - U.S. Patent No. 9,823,564

Technical Applications Important applications in the field of polymers refer to the plasma etching of thin polymer coatings [70–74] and plasma-induced surface modifications of polymer materials, including polymer coatings [45,49–56,59,70,75–77]. *Plasma etching* – which involves the controlled partial removal of the surface of a body by subjecting the latter to an appropriate plasma – is widely applied in industrial processes. The removal of surface matter can be accomplished by *physical sputtering*, which relates to the removal of surface fragments by a physical process in which energetic positive ions transfer large amounts of energy and momentum to the substrate's surface, thus inducing a mechanical ejection of matter. *Chemical etching* is of greater practical importance than physical sputtering, and is based on the total conversion of surface matter into volatile products by reactions with neutral free radicals. In this case, the mass loss is totally evaporative; for example, a polyimide of the structure shown in Chart 1.6 is totally converted to CO, CO_2, N_2 and H_2O, with the aid of an O_2 plasma.

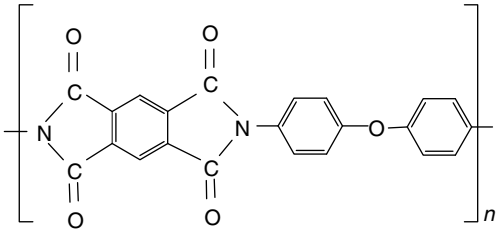


Chart 1.6 Chemical structure of a typical polyimide.

Plasma etching plays a prominent role in the industrial lithographic production of microelectronic devices such as dynamic random access memory (*DRAM*) chips and micro-electromechanical systems (*MEMS*), such as accelerometers for airbags in motor vehicles. For these purposes, silicon wafers are generally patterned using sophisticated methods, which results in small structures of dimensions down to the nanometer range. The plasma etching gases presently used in industrial processes are listed in Table 1.8, and the

Table 1.8 Plasma etching gases employed in the production of microelectronic devices [75].

Substrate material	Components of plasma feed
Al	Cl_2, BCl_3, $SiCl_4$, HBr, HJ
W	HBr, Cl_2, O_2
Si_3N_4	CHF_3, CF_4, CH_3F, SF_6
SiO_2	CHF_3, CF_4, C_2F_6, C_4F_8
Si	HBr, HCl, Cl_2, NF_3, CF_4, SF_6, BCl_3
Amorphous carbon hardmask	O_2, N_2/O_2
Photoresists	O_2, N_2/O_2

Lam Research Ex. 1047 - Page 42
Lam Research Corp. v. Inpria Corp.
IPR2024-00033 - U.S. Patent No. 9,823,564

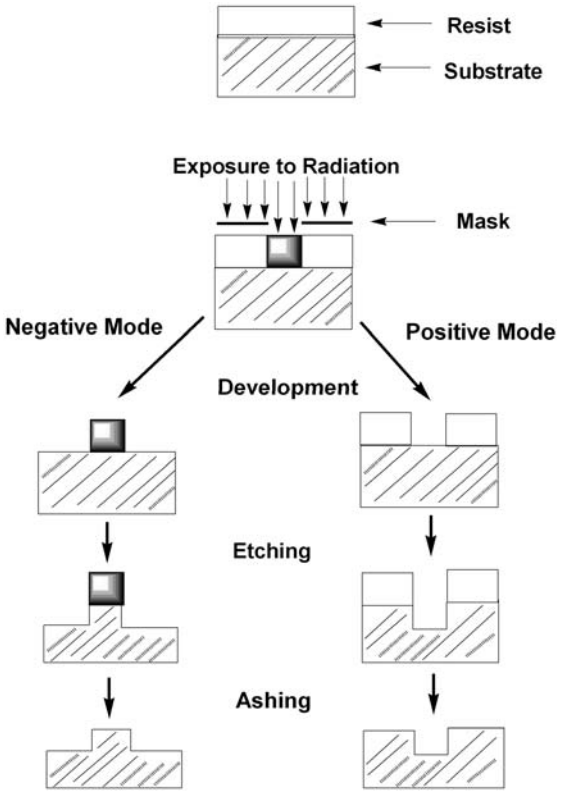


Figure 1.7 Schematic illustration of pattern generation in a silicon waver employing liquid development: irradiation makes the resist insoluble (negative mode) or soluble (positive mode).

process of pattern delineation is depicted in Figure 1.7. The process starts with a microlithographic step structuring a thin film on top of the wafer; this film, which most often consists of a plasma-resistant polymer (the *polymer resist*) is then subjected to a beam of light, X-rays or swift particles (electrons or ions). The subsequent development of latent structures, generated in this way, with appropriate liquids yields a pattern of covered and uncovered areas on the wafer. After liquid development, trenches and holes at places not covered by the resist are then formed when the wafer is subjected to a specific plasma.

Eventually, the polymer resist – which is not (or only weakly) attacked by the Si- and SiO_2-selective plasmas – is removed totally by a special treatment (referred to as "ashing" or "stripping") with the aid of an oxygen (O_2) plasma. One outstanding requirement for proper pattern delineation, namely the generation of trenches with vertical walls and flat floors, can be fulfilled by anisotropic (i.e., directional) etching (see Figure 1.8).

Lam Research Ex. 1047 - Page 43
Lam Research Corp. v. Inpria Corp.
IPR2024-00033 - U.S. Patent No. 9,823,564

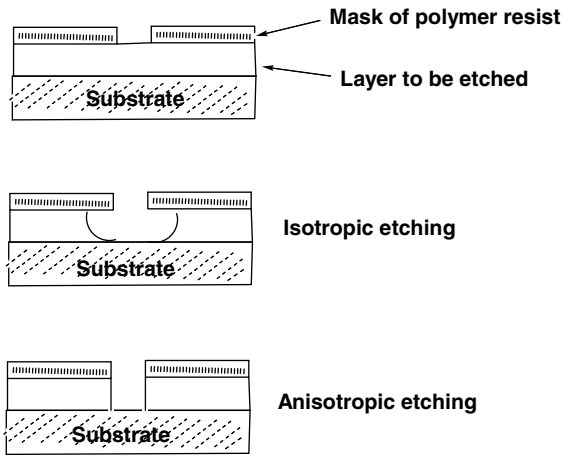


Figure 1.8 Schematic illustration of isotropic and anisotropic etching.

Anisotropic etching is accomplished by ion-enhanced etching, commonly referred to as reactive ion etching (*RIE*). This process is based on the reactions of free radicals with the substrate occurring under the simultaneous bombardment of directed ions. A directional negative-heading electric field that is always formed across the sheath at the plasma boundaries accelerates the positive ions which have been produced in the plasma up to kinetic energies of several hundred eV, and guides them vertically to the wafer's surface. In this way, not only trenches with depths of 10–20 μm (as in the case of DRAM circuits) but also features with depths of 600 μm or more (as afforded in the manufacture of MEMS devices) can be created. The generation of these extraordinarily deep features, which is referred to as *deep reactive ion etching*, may be based on chilling the wafer during etching to 163 K ($-110\,^{\circ}$C), which slows down the chemical reactions of the uncharged, isotropically acting reactive plasma species. Another process alternates repeatedly (up to several hundred times) between two modes. Mode 1 involves an almost anisotropic plasma etch, where ions attack the wafer from a near-vertical direction, while mode 2 involves the plasma deposition of a chemically inert passivation layer. The mode 2 approach protects the entire substrate from chemical attack of uncharged species, while ion etching using mode 1 is restricted to the bottom of the trench.

Surface modifications of polymeric substrates can be performed either with the aid of inorganic gas plasmas (e.g., with oxygen plasmas) or with CVD processes. In both cases the polymer surface is functionalized; that is, any functional groups that profoundly alter the surface properties become chemically attached to the polymer surface. Products obtained with both modification modes are depicted schematically in Figure 1.9.

Generally, the attachment of functional groups to the surface can result in either hydrophilicity or hydrophobicity of the substrate. For instance, it can improve the adhesive strength of polymer surfaces towards differently composed materials.

Lam Research Ex. 1047 - Page 44
Lam Research Corp. v. Inpria Corp.
IPR2024-00033 - U.S. Patent No. 9,823,564

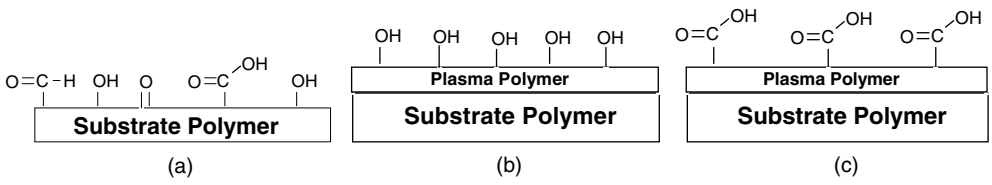


Figure 1.9 Schematic depiction of plasma-induced modifications of polymer surfaces. (a) Unspecific functionalization of the surface of a substrate polymer (e.g., polypropylene) by oxygen plasma treatment; (b, c) Specific functionalization via plasma polymerization of allyl alcohol or acrylic acid, respectively, in the presence of a substrate polymer.

Exactly how the treatment of polymer surfaces with an oxidizing plasma can cause a decrease in the water contact angle (i.e., an increase in wettability) is shown in Table 1.9. Normally, this is related to the surface energy and a reduction in surface energy will indicate a better bondability – that is, the ability of a polymer to bond to other materials.

The plasma treatment of a yarn of polymer fibers used for composite reinforcement provides a typical example of the improvement in adherence [78]. The result is an increase in the strength of the final composite, due to the plasma-induced formation of a very thin interphase layer between the fiber and the composite matrix, causing in turn an improved bonding between the two components (see Figure 1.10).

Substrate hydrophilicity is required for the adhesion of certain biomaterials, such as living tissues. This property has an important role for human body implants, such as orthopedic prostheses. A typical case in which substrate hydrophobicity is required relates to an ophthalmologic scenario, when the surfaces of an intraocular polymer lens should preferably not adhere to proteins in order to avoid the formation of inflammatory cells.

Table 1.9 Alterations in the surface wettability of selected polymers by low-pressure plasma treatment. Adapted from Ref. [78].

Polymer	Initial water contact angle (degrees)	Final water contact angle (degrees)
Polyethylene	87	22
Polypropylene	87	22
Polystyrene	72	15
Polyamide	63	17
Poly(tetrafluoroethylene-*co*-ethylene)	92	53
Poly(ethyleneterephthalate)	76	17
Polycarbonate	75	33
Poly(phenylene oxide)	75	38
Poly(ether sulfone)	92	9
Silicone	96	53

Lam Research Ex. 1047 - Page 45
Lam Research Corp. v. Inpria Corp.
IPR2024-00033 - U.S. Patent No. 9,823,564

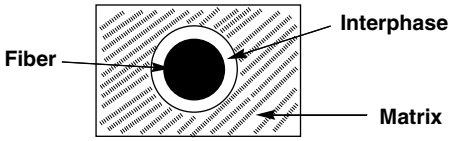


Figure 1.10 Cross-section of a plasma-treated fiber in a composite matrix.

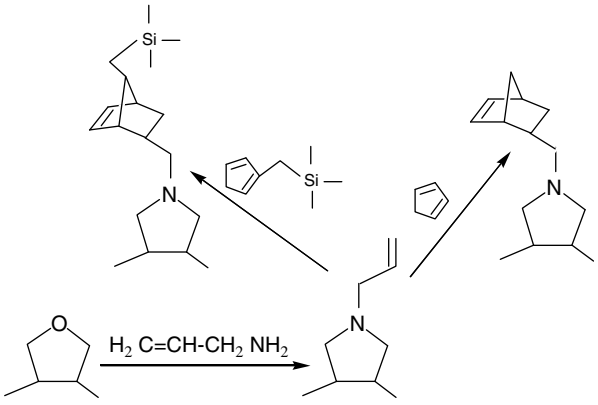
Plasma polymerization leading to functionalized surfaces, as depicted in Figure 1.9b and c, is an outstanding feature of plasma chemistry. Its importance derives from the fact that macromolecular structures can be formed not only from unsaturated substances but also from compounds that are incapable of forming polymers via conventional polymerization techniques. An interesting application here is the plasma-initiated homopolymerization and copolymerization of monomers bearing functional groups on polymer substrates. Relevant investigations have concerned the generation of a very thin adhesion-promoting polymer layer at the surface of polypropylene sheets. By deploying monomers with functional groups (such as allyl alcohol or acrylic acid), plasma polymer layers with up to 30 OH or 25 COOH groups per 100 C atoms can be attached to the surface of the polypropylene substrate, using a pulsed plasma technique with duty cycles of short on-periods and long off-periods, for example, 25 μs to 1200 μs. In this way, good adhesion properties (high peel strength) towards aluminum layers deposited onto the sheet by vacuum evaporation can be attained [53].

Another example relates to the plasma polymerization of maleic anhydride on silicon substrates [55]. After functionalization of the anhydride groups of the polymer with dienophile groups such as allyl amine groups, bicyclo[2.2.1]hept-2-ene groups are attached to the surface via the Diels–Alder cycloaddition of a diene. The cycloaddition of cyclopentadiene or [(trimethylsilyl)methyl]cyclopentadiene to the cyclic imide-functionalized plasma polymer is shown in Scheme 1.17. In this case, the extent to which maleic anhydride groups are converted is controllable, such that the number density of functionalized groups can be tailored to comply with the adhesion between different types of solid surface.

The plasma-assisted surface modification of polymers may also serve to create permselective membranes for gas purification. For example, thin membranes of natural rubber treated with a 4-vinyl pyridine plasma are capable of separating O_2 from N_2 [79]. For additional information on this topic, see Ref. [80].

In conclusion, plasma polymerization provided the possibility to deposit carefully designed, highly adherent and pinhole-free thin polymer films onto various substrates, and thus to control adhesion between various types of solid surface. Moreover, plasma-deposited polymer films can be used to protect metals and other substrates from environmental attacks, for instance by corrosive agents. Further information on these topics is available in Ref. [80].

Lam Research Ex. 1047 - Page 46
Lam Research Corp. v. Inpria Corp.
IPR2024-00033 - U.S. Patent No. 9,823,564



Scheme 1.17 Attachment of bicyclo[2.2.1]hept-2-ene groups to a cyclic imide functionalized thin layer of plasma-polymerized maleic anhydride [55].

1.3 Applications in Polymer Physics

1.3.1 Dielectric Spectroscopy of Polymers

Dielectric spectroscopy (*DS*), which is related to measurements of the complex dielectric permittivity $\varepsilon^* = \varepsilon' - j\varepsilon''$, has been used widely to study the dynamics of polymers, including heterogeneous polymer-containing systems [81–87]. DS complements other methods based on nuclear magnetic resonance (*NMR*), light scattering, and dynamic mechanical analysis. With the aid of commercially available instruments covering a broad frequency range of many orders of magnitude (10^{-6} Hz to 10^{12} Hz), it is possible to investigate molecular motions on quite different time scales, including fluctuations within base units, side group rotations, and cooperative glass transitions. One prerequisite for the application of this technique, however, is the presence of dipoles – that is, in the case of linear polymers of polar groups in the main chain and/or in pendant groups.

With regards to the performance of DS measurements, two modes have been identified: (i) measurements in the frequency domain; and (ii) measurements in the time domain [88–90]. These two terms refer to measurements of ε'' as a function of radiation frequency and of time, respectively. Details of, and references pertaining to, the measuring techniques are outlined by Kremer and Schönhals [88].

A typical example referring to frequency domain measurements is shown in Figure 1.11, where ε'', recorded with poly(methylacrylate) at various temperatures, is plotted as a function of frequency. The two peaks, related to α relaxation (low-frequency) and β relaxation (high-frequency) are shifted to higher frequencies with increasing temperature (details of this phenomenon were outlined in Section 1.1.2.2). It should be noted that the α-relaxation is

Lam Research Ex. 1047 - Page 47
Lam Research Corp. v. Inpria Corp.
IPR2024-00033 - U.S. Patent No. 9,823,564

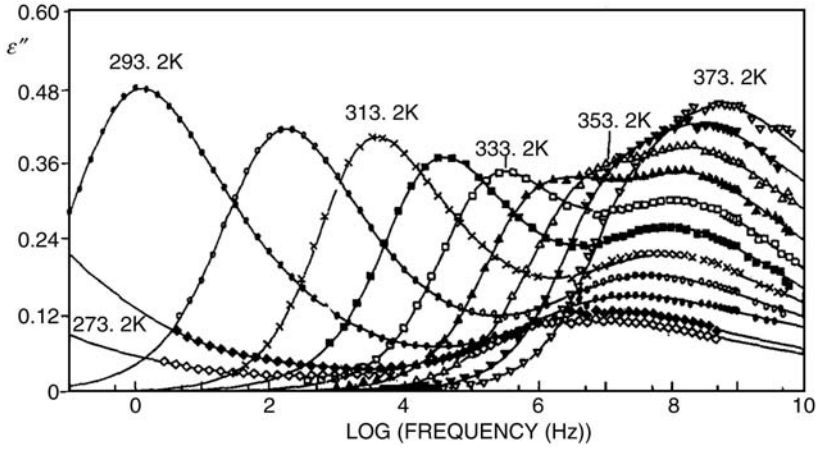


Figure 1.11 Dielectric loss spectra of poly(methyl acrylate) depicting ε'' versus frequency at different temperatures. Adapted with permission from Ref. [91]; © 1992, American Chemical Society.

attributed to a structural process, the dynamic glass transition related to segmental motions, while the β-relaxation originates from localized fluctuations of the dipole vector of the side groups, such as the rotation of methyl groups.

With the aid of modern dielectric spectrometers, real-time observations can be carried out. For example, DS can be used to monitor the curing of thermosetting resins, the absorption of water by polymers, or film formation and coalescence in polymer lattices [92].

In the case of nonpolar polymers such as polyolefins, attempts have been made to perform DS by doping the polymer with additives having a large dipole moment (so-called *dielectric probes*) [93]. Here, as a typical example, studies on atactic polypropylene (*aPP*), doped with 4,4′-(*N*,*N*-dibutylamino)-(*E*)-nitrostilbene (*DBANS*; see Chart 1.7) of dipole moment $\mu = 8$ Debye, is addressed [94]. Plots of ε'' versus temperature for both doped and undoped aPP are shown in Figure 1.12.

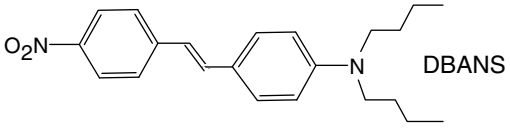


Chart 1.7 Chemical structure of 4,4′-(*N*,*N*-dibutylamino)-(*E*)-nitrostilbene.

The spectra contained two peaks above and below the T_g (250 K), according to differential scanning calorimetry (*DSC*) at about 150 K and 280 K, which were assigned to the β- and α-processes, respectively. The dopant significantly augmented the α-peak, and in the vicinity of T_g the probe relaxation time τ_α

Lam Research Ex. 1047 - Page 48
Lam Research Corp. v. Inpria Corp.
IPR2024-00033 - U.S. Patent No. 9,823,564

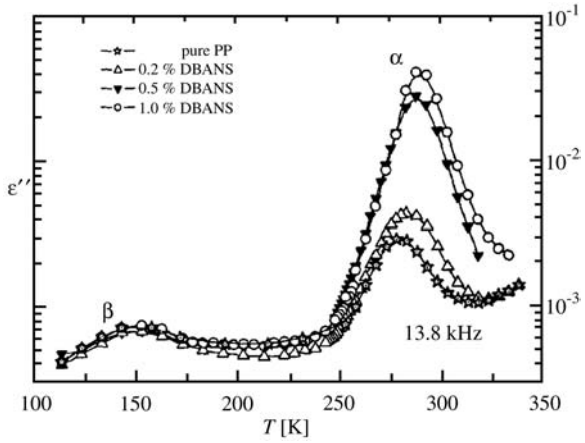


Figure 1.12 Plots of the dielectric loss ε'' versus temperature, recorded at $\nu = 1.38 \times 10^4$ Hz with atactic polypropylene, undoped and doped with different amounts of DBANS. Adapted with permission from Ref. [94]; © 2007, American Chemical Society.

reflected the intrinsic cooperative dynamics of the polymer. The dopant exerted only a very weak plasticizing effect; this was inferred from the fact that, in the presence of the dopant, the T_g values were only slightly lower than T_g (DSC). T_g is obtained, from the temperature dependence of τ_α with the aid of the Vogel–Fulcher–Tamman equation (Equation 1.16).

$$\tau_\alpha = \tau_\infty \exp\left[\frac{E_v}{R(T - T_v)}\right] \tag{1.16}$$

where τ_α and τ_∞ denote the structural relaxation time at temperature T and in the high-temperature limit, respectively, while E_v and T_v are the activation energy and the Vogel temperature, respectively.

More than two decades ago, W. N. Mie *et al.* proposed a model which involved electromagnetic energy coupling through acoustic vibrations along the axis of helical polymers. These authors predicted high absorption cross-sections at microwave frequencies [95], but the prediction could not be verified experimentally [96,97], despite earlier studies seeming to have provided evidence of a resonant microwave absorption of plasmid DNA molecules in aqueous solution in the frequency range 1 to 10 GHz [98]. Such a discrepancy in results is a consequence of pH changes; that is, changes in the ionic conductivity that had not been considered in earlier studies.

1.3.2
Microwave Probing of Electrical Conductivity in Polymers

As noted in Section 1.1, dipole rotation and ionic conduction are the fundamental mechanisms involved when dissipating microwave energy in matter. With regards to

Lam Research Ex. 1047 - Page 49
Lam Research Corp. v. Inpria Corp.
IPR2024-00033 - U.S. Patent No. 9,823,564

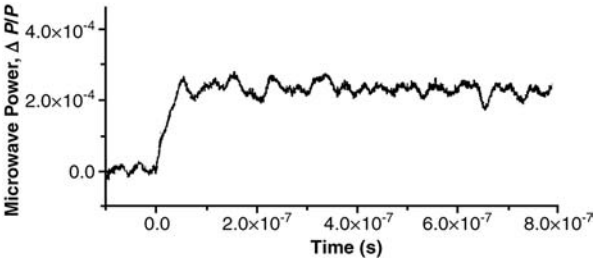


Figure 1.13 Increase in the microwave absorption of poly(methylphenylsilane) at $\nu = 30.4$ GHz, indicating the formation of electrical charge carriers after irradiation with a 12 ns pulse of 266-nm light. Reproduced from Ref. [101].

the ionic conduction mechanism, it is notable that microwave absorption measurements can serve as a very valuable tool for electrode-less electrical conductivity determinations. This may concern, for example, time-resolved measurements, and in this context the method of time-resolved microwave conductivity (*TRMC*), which is frequently applied to flash photolysis and pulse radiolysis investigations, should be mentioned [99,100]. For example, the TRMC method served to probe charge carriers in polysilanes generated by UV light. The data provided in Figure 1.13 indicate how microwave absorption, expressed here in terms of the relative decrease in incident microwave power, $\Delta P/P_{inc}$, was increased following the irradiation of poly(methylphenylsilane) with a 12 ns pulse of 266 nm light.

Time-resolved microwave absorption measurements also served to determine the intrachain mobility of charge carriers moving along the chains of ladder-type poly (*p*-phenylenes) and phenylene-vinylene polymers (see Chart 1.8) [102,103]. Upon irradiating O_2-saturated benzene solutions containing isolated polymer chains (low concentration, 10^{-4} to 10^{-3} base mol l^{-1}) with 10 ns pulses of 3 MeV electrons, benzene cations and excess electrons were generated. Although the electrons were scavenged by oxygen, the cations reacted with the polymer chains via a diffusion-controlled reaction, thus yielding positively charged polymer chains. Eventually, the oxygen anions and polymer cations combined in a neutralization reaction (see Scheme 1.18).

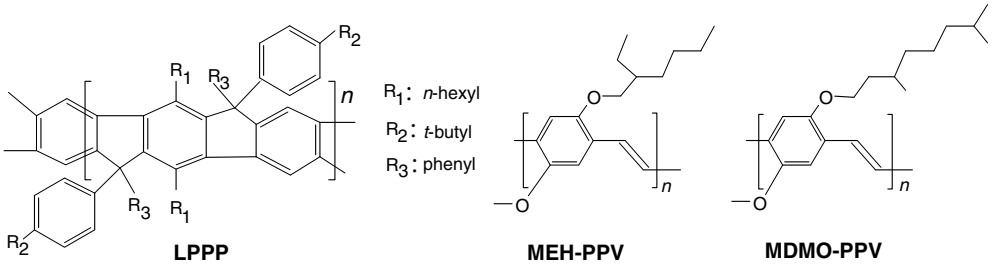
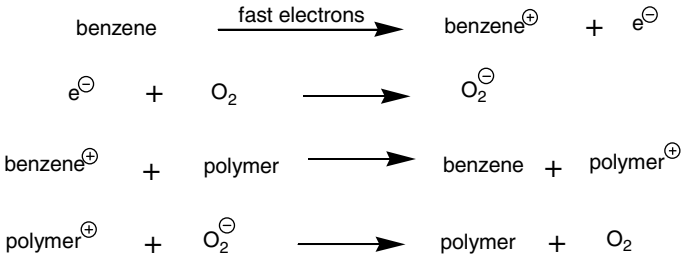


Chart 1.8 Chemical structures of *p*-phenylene and phenylene-vinylene polymers employed for the determination of the intrachain hole mobility [102,103].

Lam Research Ex. 1047 - Page 50
Lam Research Corp. v. Inpria Corp.
IPR2024-00033 - U.S. Patent No. 9,823,564



Scheme 1.18 Generation and decay of positively charged polymer chains in O_2-saturated benzene solutions upon irradiation with fast electrons.

The reaction of benzene cations with polymer chains was indicated by an increase in the electrical conductivity of the solution relative to that of neat O_2-saturated benzene (see Figure 1.14). The increase in conductivity was more pronounced the longer the polymer chain length – an effect that was attributed to the fact that the charges diffuse over the entire length of the chains and encounter chain ends within one period of the oscillating electric field. Consequently, the measured intrachain conductivity was seen to be frequency-dependent with a tendency to increase with increasing microwave frequency [104].

The measured electrical conductivity increase of the system $\Delta\sigma(t)$ is related to the mobility of the charge carriers $\mu_{ac,i}$ according to Equation 1.17:

$$\Delta\sigma(t) = e\Sigma\mu_{ac,i}n_i(t) \tag{1.17}$$

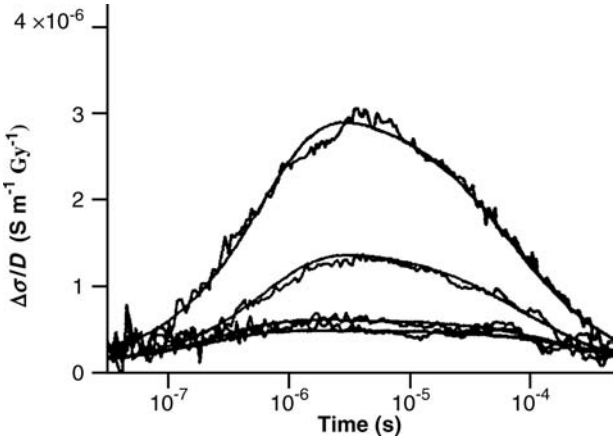


Figure 1.14 Electrical conductivity of benzene solutions containing the ladder-type polymer LPPP (3.15×10^{-4} base mol l^{-1}, average chain length: 13, 16, 35, 54, from bottom to top). $\nu = 34$ GHz, $E = 20$ V cm^{-1}. Absorbed dose: $D = 21$ Gy. Adapted with permission from Ref. [102]; © 2006, American Physical Society.

Lam Research Ex. 1047 - Page 51
Lam Research Corp. v. Inpria Corp.
IPR2024-00033 - U.S. Patent No. 9,823,564

where e is the elementary charge and n_i is the concentration of charged species i. Since the mobility of oxygen anions is negligibly small, the sum in Equation 1.17 reduces to the terms related to hole conduction. Moreover, the effective hole mobility μ_{ac} is dominated by the intrachain mobility $\mu_{intra,hole}$, provided that the magnitude of the latter is less than about $0.1\,cm^2\,V^{-1}\,s^{-1}$. At higher values of $\mu_{intra,hole}$, scattering of the charge carriers at the chain ends dominated the charge transport and μ_{ac} was much lower than $\mu_{intra,hole}$. On the basis of the chain length dependence of μ_{ac}, and using a theoretical model for one-dimensional diffusive motion of charge carriers between chain ends [104], a very high value of $\mu_{intra,hole}$ (close to $600\,cm^2\,V^{-1}\,s^{-1}$) was obtained for ladder-type poly(*p*-phenylene)s (*LPPP*s) [102]. Therefore, ladder-type polymers such as LPPPs might potentially be used as interconnecting wires in the molecular electronic devices of the future.

Notably, measurements of the electrical conductivity in stretch-oriented polymers such as I_2-doped polyacetylene, by employing the technique of *coherent microwave transient spectroscopy* [105] revealed a large orientation-dependence. In the case of polyacetylene, the conductivity values parallel and perpendicular to the stretch direction were $\sigma_{||} = 34.4$ and $\sigma_{\perp} = 3.3\,S\,cm^{-1}$ [106]. The higher $\sigma_{||}$-value was believed to be due to the higher electron mobility along the oriented polymer chains. σ-values have been obtained from transmission data with the aid of Equation (1.18):

$$T(\lambda) = \frac{1}{1 + 0.5\sigma L(\mu_0/\varepsilon_0)^{0.5}} \tag{1.18}$$

where $T(\lambda)$ is the transmission at wavelength λ, L denotes the sample length, and μ_0 and ε_0 are the vacuum permeability and permittivity, respectively [106].

1.3.3 Nondestructive Microwave Testing of Polymer Materials

Microwaves can be applied for the nonintrusive inspection of dielectric materials, including polymers, wood, and ceramics [107–117]. The inspection of dielectric polymeric materials is easily performed, because of their relatively high transparency towards microwaves. Of technical importance are methods based on reflection measurements on sheet materials, such as composites made from several layers adhesively bonded together. In this case, microwave techniques can be used to control composite processing and manufacturing.

Commonly, contact-free measurements with single-sided access to the sample via open-ended rectangular wave guides are performed, as can be seen from Figure 1.15. The signal recorded by the detector results from reflections and interference effects. This serves for the determination of dielectric properties (ε' and ε''), and of the absolute thickness of thick polymer slabs and dielectric composites made from plastics.

Lam Research Ex. 1047 - Page 52
Lam Research Corp. v. Inpria Corp.
IPR2024-00033 - U.S. Patent No. 9,823,564

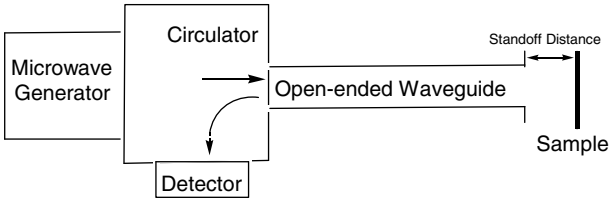


Figure 1.15 Schematic depiction of an open-ended waveguide arrangement for nondestructive inspection of polymer samples.

The importance of microwave nondestructive testing for coatings becomes more obvious when consulting the data in Table 1.10, which elucidate the potential of this method.

With an array of sensors – or, better, with the aid of two-dimensional raster scans – the images of any hidden flaws can be displayed (termed *microwave near-field imaging*). When the sample is located close to the open end of the waveguide, which is commonly referred to as *near-field geometry*, the resolution is about one-tenth of the wavelength. For example, at a frequency of 30 GHz corresponding to $\lambda_0 = 10$ mm, defects at distances of 1 mm can be detected individually. With regards to the determination of thickness variations, a resolution of a few micrometers has been claimed [107].

Thickness measurements on thin polymer layers (25–500 μm) being backed by a metal layer can be accomplished by a method depicted schematically in Figure 1.16. Here, a transmitter/receiver couple is positioned very close to the film surface, where a guided wave is excited. Both the thickness and dielectric properties can be calculated from the signal recorded by the receiver [118,119].

Interestingly, local anisotropies in dielectric materials can be probed and imaged by using a rotating rectangular waveguide which emits linear and polarized microwave radiation. The rotation modifies the relative orientation of the electric field vector, such that dielectric anisotropy will result in a modulation of the measured effective reflection. Both, the modulation depth and the angle of

Table 1.10 Microwave nondestructive testing of dielectric polymeric coatings in noncontact fashion. Access to only one side of the material is needed [107].

Property or Effect	Benefit of the method
Thickness	Determination of absolute values Evaluation of minute variations
Disbonds	Detection of very slight effects
Delaminations	Detection of slight effects
Porosity	Detection of voids and pores, including size estimation
Cracks	Detection of cracks in metals covered with dielectric coatings without the need for removal

Lam Research Ex. 1047 - Page 53
Lam Research Corp. v. Inpria Corp.
IPR2024-00033 - U.S. Patent No. 9,823,564

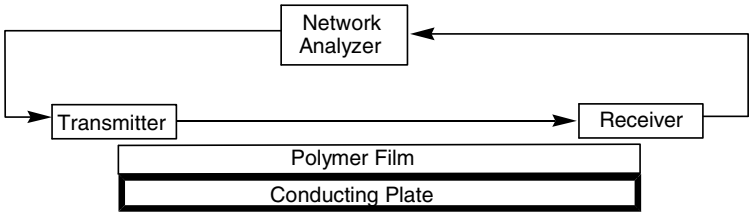


Figure 1.16 Schematic depiction of a set-up allowing nondestructive thickness measurements on thin layers of dielectric polymers. Waves in transverse magnetic mode launched from the transmitter are reflected from the sample and excite guided modes in the dielectric layer. Adapted from Refs [118,119].

maximum reflection, are related to the extent and the direction of local anisotropies, respectively. In this way, glass fiber-reinforced, injection-molded polymers can be characterized with respect to the orientation of the fibers [113]. As a typical example, the influence of injection speed on fiber orientation is depicted in Figure 1.17 [110].

It is also possible to monitor, during the injection molding of plastic articles, how molds are filled and the melt is cooled down [110]. The curing of resins, determination of the moisture content of polymeric materials, and corrosion phenomena represent further applications of this technique.

Compared to traditional nondestructive testing methods, microwave-based inspection yields a better contrast than X-ray absorption techniques, and a better signal-to-noise ratio than ultrasound inspection. The primary advantages of microwave testing are that measurements can be performed contact-free, and with single-sided access to the sample.

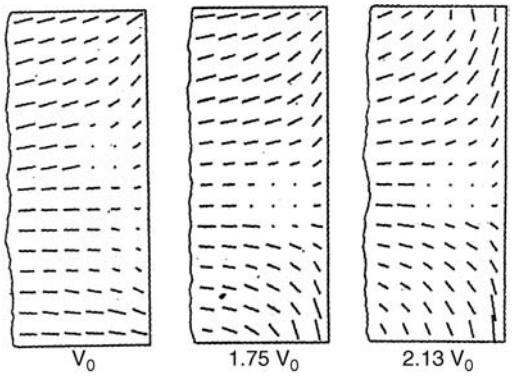


Figure 1.17 Microwave anisotropy images demonstrating the influence of the injection speed (varying between V_0 and $2.13V_0$) on the fiber orientation in the injection molding process. Adapted with permission from Ref. [110]; © 1996, Scientific.Net.

Lam Research Ex. 1047 - Page 54
Lam Research Corp. v. Inpria Corp.
IPR2024-00033 - U.S. Patent No. 9,823,564

1.4 Industrial Applications

While RF and microwave-based techniques each play important roles in industrial material processing involving plasmas, the use of these radiations as a heating source for thermally initiated chemical reactions is (at present) mainly restricted to the laboratory scale. However, there is one exemption, namely the application of microwave heating to the vulcanization of rubber. Microwave extrusion lines are operated worldwide in the automotive and construction industries for the vulcanization of carbon black-filled rubber [120]. Carbon black is a good microwave absorber, but in the case of white and colored rubbers special sensitizers that permit the absorption of microwaves must first be applied [121].

With regards to plasma applications, both RF- and microwave-based techniques (e.g., low-pressure plasma processes) have been employed since the 1960s for industrial materials processing. At present, plasma techniques are important in those technologies that involve plastics, notably in several areas of the automotive, aerospace, packaging, and textile industries. Although both RF and microwave plasma systems have been developed for specific tasks, plasma processing is generally aimed at increasing the surface energy of films, webs, and fibers so as to achieve better characteristics of printing, bonding wettability and wickability (the ability to transport perspiration away from the human body). Some typical arrangements, as applied to the surface modification of textiles, are shown in Figure 1.18.

It is remarkable, that not only flexible substrates such as films or fabrics but also large stiff objects (e.g., fenders for automobiles) that are made from polypropylene (*PP*) or ethylene-propylene-diene-terpolymer (*EPDM*) are plasma-treated on an industrial scale. It should be noted that a large proportion of these applications involve surface modifications for improved adhesion, and that such processes are commonly accomplished with the aid of air or oxygen plasmas [59,123,124].

Finally, the use of plasma techniques for the production of microelectronic devices must be emphasized (see also "Technical Applications" in Section 1.2.3.2), as this involves the technical polymer resist-based generation of microfeatures that now range down to a structure size of 40 nm, allowing a data storage capacity for DRAM chips of up to 2 GByte. Three etching configurations of a parallel-plate plasma reactor applicable to the etching of wafers at low pressure are shown in Figure 1.19. These configurations are distinguished by the manner in which the RF power supply is connected to the electrodes. Plasma etching, in conjunction with the photolithographic structuring of polymer resists, represents a powerful tool that permits a high grade of technical miniaturization that has subsequently led to the creation of products such as personal computers that are today of major importance in daily life.

Lam Research Ex. 1047 - Page 55
Lam Research Corp. v. Inpria Corp.
IPR2024-00033 - U.S. Patent No. 9,823,564

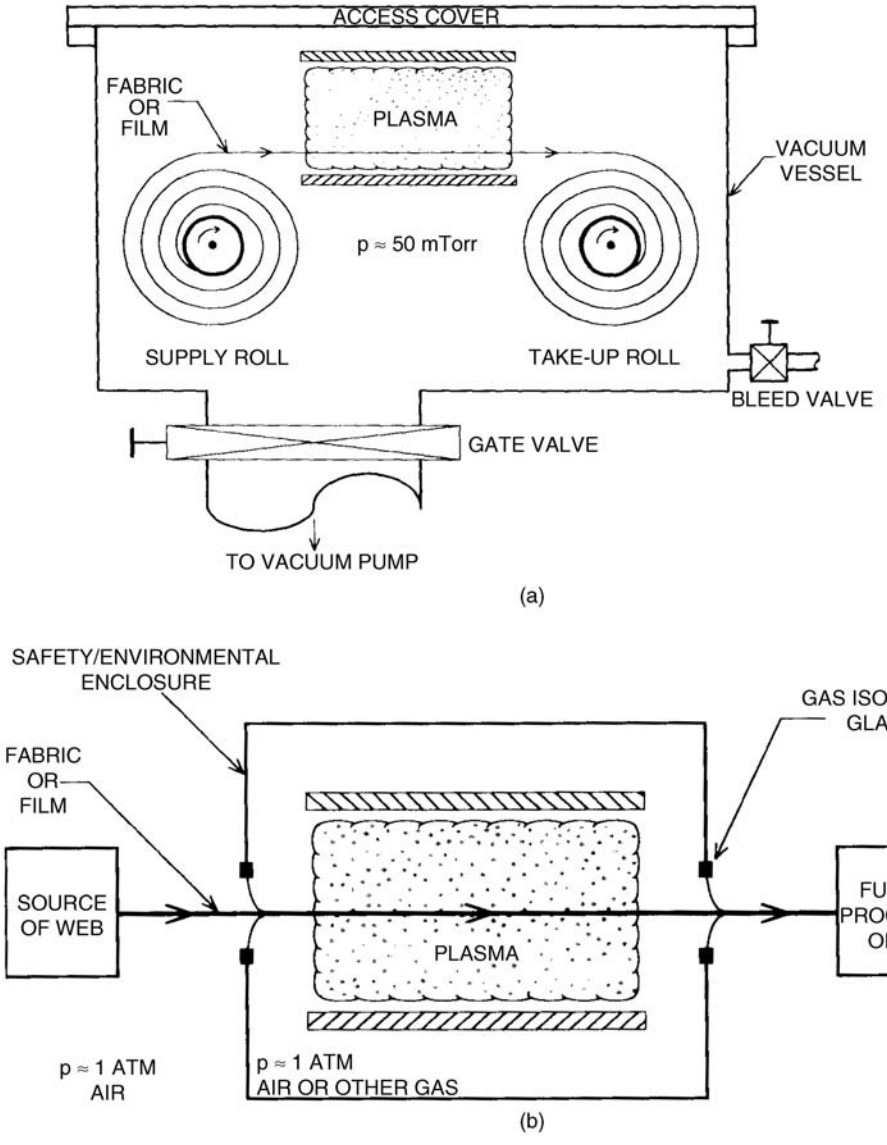


Figure 1.18 Industrial plasma modification of textile surfaces. Plasma reactor configurations for (a) low-pressure batch processing and (b) continuous processing at atmospheric pressure. Adapted with permission from Ref. [122]; © 1995, Institute of Physics Publishing.

Lam Research Ex. 1047 - Page 56
Lam Research Corp. v. Inpria Corp.
IPR2024-00033 - U.S. Patent No. 9,823,564

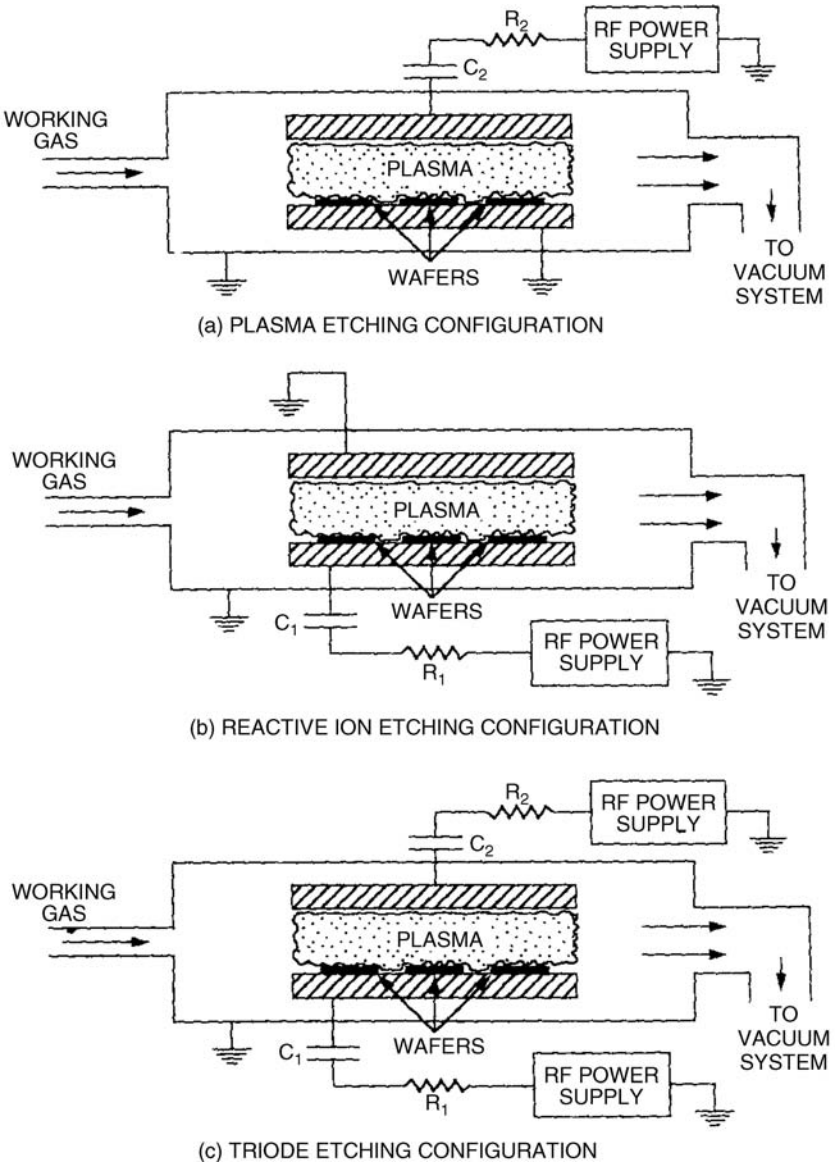


Figure 1.19 Industrial plasma etching of wafers. Plasma reactor configurations for low-pressure processing. Adapted with permission from Ref. [122]; © 1995, Institute of Physics Publishing.

Lam Research Ex. 1047 - Page 57
Lam Research Corp. v. Inpria Corp.
IPR2024-00033 - U.S. Patent No. 9,823,564

References

1 Debye, P. (1929) *Polar Molecules*, Chemical Catalog Co., New York.
2 Debye, P. (1935) Molecular rotation in liquids. *Phys. Z.*, **36**, 100.
3 Parodi, F. (1996) Physics and chemistry of microwave processing, Chapter 19, in *Comprehensive Polymer Science, Second Supplement* (eds S.L. Aggarwal and S. Russo), Pergamon, Oxford, p. 669.
4 (a) Havriliak, S. and Negami, S. (1966) A complex plane analysis of α-dispersions in some polymer systems. *J. Polym. Sci. C*, **14**, 99; (b) Havriliak, S. and Negami, S. (1967) A complex plane representation of dielectric and mechanical relaxation processes in some polymers. *Polymer*, **8**, 161.
5 Cole, K.S. and Cole, R.H. (1941) Dispersion and absorption in dielectrics. *J. Chem. Phys.*, **9**, 341.
6 Metaxas, A.C. and Meredith, R.J. (1983) *Industrial Microwave Heating*, Peregrinus, London.
7 Brandrup, J. and Immergut, E.H. (eds) (1989) *Polymer Handbook*, 3rd edn, John Wiley, New York.
8 Huang, H.T. (1976) Temperature control in a microwave resonant cavity system for rapid heating of nylon monofilament. *J. Microwave Power Electromagn. Energy*, **11**, 305.
9 Bogdal, D., Penczek, P., Pielichowski, J., and Prociak, A. (2003) Microwave-assisted synthesis, crosslinking, and processing of polymeric materials. *Adv. Polym. Sci.*, **163**, 193.
10 Wiesbrock, F., Hoogenboom, R., and Schubert, U. (2004) Microwave-assisted polymer synthesis: state-of-the-art and future perspectives. *Macromol. Rapid Commun.*, **25**, 1739.
11 Zhang, D., Crivello, J.V., and Stoffer, J.O. (2004) Polymerizations of epoxides with microwave energy. *J. Polym. Sci., Part B: Polym. Phys.*, **42**, 4230.
12 Loupy, A. (ed.) (2006) *Microwaves in Organic Synthesis*, 2nd edn, Wiley-VCH, Weinheim.
13 Kappe, C.O. and Stadler, A. (2005) *Microwaves in Organic and Medicinal Chemistry*, Wiley-VCH, Weinheim.
14 Kappe, C.O. (2004) Controlled heating with microwaves in modern organic synthesis. *Angew. Chem. Int. Ed.*, **43**, 6250.
15 Man, A.K. and Shahidan, R. (2007) Microwave-assisted chemical reactions. *J. Macromol. Sci., Pure Appl. Chem.*, **44**, 651.
16 Bogdal, D. and Prociak, A. (2007) *Microwave-Enhanced Polymer Chemistry and Technology*, Blackwell Publishing, Ames, IA, USA.
17 Bogdal, D. and Matras, K. (2006) Polymer Chemistry under the Action of Microwave Irradiation, in *Microwaves in Organic Synthesis* (ed. A. Loupy), 2nd edn, Wiley-VCH, Weinheim, Ch. 14.
18 Bogdal, D. (2005) *Microwave-Assisted Organic Synthesis: One Hundred Reaction Procedures*, Elsevier, Amsterdam.
19 Zong, L., Zhou, S., Sgriccia, N., Hawley, M.C., and Kempei, L.C. (2003) A Review of microwave-assisted polymer chemistry (MAPC). *J. Microwave Power Electromagn. Energy*, **38**, 49.
20 Mingos, D.M.P. and Baghurst, D.R. (1991) Applications of microwave dielectric heating effects to synthetic problems in chemistry. *Chem. Soc. Rev.*, **20**, 1.
21 Elias, H.-G. (2005) Macromolecules, in *Chemical Structures and Syntheses*, vol. 1, Wiley-VCH, Weinheim.
22 Mishra, M.K. and Yagci, Y. (eds) (1998) *Handbook of Radical Vinyl Polymerization*, Dekker, New York.
23 Cowie, J.M.G. and Arrighi, V. (2007) *Polymers, Chemistry and Physics of Modern Materials*, 3rd edn, CRC Press, Boca Raton.
24 Moad, G. and Solomon, D.H. (2005) *The Chemistry of Free Radical Polymerization*, 2nd edn, Elsevier Science, Oxford.
25 Palacios, J.J. and Valverde, C. (1996) Microwave initiated emulsion polymerization of styrene: reaction conditions. *New Polym. Mater.*, **5**, 93.
26 Hoogenboom, R., Wiesbrock, F., Huang, H., Leenen, M.A.M., Thijs, H.M.L., van Nispen, S.F.G.M., van der Loop, M., Fustin, C.-A., Jonas, A.M., Gohy, J.-F., and Schubert, U.S. (2006) Microwave-assisted ring-opening cationic polymerization of

Lam Research Ex. 1047 - Page 58
Lam Research Corp. v. Inpria Corp.
IPR2024-00033 - U.S. Patent No. 9,823,564

2-oxazolines: a powerful method for the synthesis of amphiphilic triblock terpolymers. *Macromolecules*, **39**, 4719.
27 Fang, X., Hutcheon, R., and Scola, D.A. (2000) Microwave syntheses of Poly (ε-caprolactam-*co*-ε-caprolactone). *J. Polym. Sci., Part A: Polym. Chem.*, **38**, 1379.
28 Stoffer, J.O., Zhang, D., and Crivello, J.V. (1999) Cationic polymerizations of epoxides using microwave energy. *Polym. Mater. Sci. Eng.*, **81**, 118.
29 van Dijk, M., Mustafa, K., Dechesne, A.C., van Nostrum, C.F., Hennink, W.E., Rijkers, D.T.S., and Liskamp, R.M.L. (2007) Synthesis of peptide-based polymers by microwave-assisted cycloaddition by backbone polymerization. *Biomacromolecules*, **8**, 327.
30 Lewis, D.A., Summers, J.D., Ward, T.C., and McGrath, E.J. (1992) Accelerated imidization reactions using microwave radiation. *J. Polym. Sci., Part A: Polym. Chem.*, **30**, 1647.
31 Mijovic, J., Corso, W.V., Nicolais, L., and d'Ambrosio, G. (1998) *In situ* real-time study of crosslinking kinetics in thermal and microwave fields. *Polym. Adv. Technol.*, **9**, 231.
32 Ludlow-Palafox, C. and Chase, H.A. (2001) Microwave-induced pyrolysis of plastic wastes. *Ind. Eng. Chem. Res.*, **40**, 4749.
33 Danko, G.A., Silberglitt, R., Colombo, P., Pippel, E., and Woltersdorf, J. (2000) Comparison of microwave hybrid and conventional heating of preceramic polymers to form silicon carbide and silicon oxycarbide ceramics. *J. Am. Ceram. Soc.*, **83**, 1617.
34 Klun, U. and Krzan, A. (2000) Rapid microwave induced depolymerization of polyamide-6. *Polymer*, **41** (11), 4361.
35 Krzan, A. (1998) Microwave irradiation as an energy source in poly(ethylene terephthalate) solvolysis. *J. Appl. Polym. Sci.*, **69**, 1115.
36 Kleps, T., Piaskiewicz, M., and Parasiewicz, W. (2000) The use of thermogravimetry in the study of rubber devulcanization. *J. Therm. Anal. Calorim.*, **60**, 271.
37 Engelhart, W.G. (1997) Microwave hydrolysis of proteins and peptides for amino acid analysis, in *Microwave-Enhanced Chemistry* (eds H.M. Kingston and S.J. Haswell), American Chemical Society, Washington DC, USA, Ch. 13.
38 Galema, S.A. (1997) Microwave chemistry. *Chem. Soc. Rev.*, **26**, 233.
39 Larhed, M. and Halberg, A. (2001) Microwave-assisted high-speed chemistry: a new technique in drug discovery. *Drug Disc. Today*, **6**, 406.
40 (a) Stadler, A. and Kappe, C.O. (2001) High-speed couplings and cleavages in microwave-heated, solid-phase reactions at high temperatures. *Eur. J. Org. Chem.*, 919; (b) Stadler, A. and Kappe, C.O. (2001) The effect of microwave irradiation on carbodiimide-mediated esterifications on solid support. *Tetrahedron*, **57**, 3915.
41 Lin, M.J. and Sun, C.M. (2003) Microwave-assisted traceless synthesis of thiohydantoin. *Tetrahedron Lett.*, **44**, 8739.
42 Mallon, F.K. and Ray, W.H. (1998) Enhancement of solid-state polymerization with microwave energy. *J. Appl. Polym. Sci.*, **69**, 1203.
43 de la Hoz, A., Diaz-Ortiz, A., and Moreno, A. (2005) Microwave in organic synthesis. thermal and non-thermal microwave effects. *Chem. Soc. Rev.*, **34**, 164.
44 Perreux, L. and Loupy, A. (2006) Non-thermal Effects of Microwaves in Organic Synthesis, in *Microwaves in Organic Synthesis* (ed. A. Loupy), 2nd edn, Wiley-VCH, Weinheim, Ch. 3.
45 Biederman, H. (ed.) (2004) *Plasma Polymer Films*, Imperial College Press, London.
46 Bradley, A.P. and Hammes, J.P. (1963) Electrical properties of thin organic films. *J. Electrochem. Soc.*, **10**, 15.
47 Favia, P. (2004) Plasma Deposition of Fluoropolymer Films in Different Glow Discharge Regimes, in *Plasma Polymer Films* (ed. H. Biederman), Imperial College Press, London, Ch. 2.
48 Hamblyn, S.M.L. and Reuben, B.G. (1975) Use of radio-frequency plasma in chemical synthesis. *Adv. Inorg. Radio Chem.*, **17**, 89.
49 Yasuda, H. (1985) *Plasma Polymerization*, Academic Press, Orlando.
50 Inagaki, N. (1995) *Plasma Surface Modification and Plasma Polymerization*, Technomic Publ. AG, Basel.
51 d'Agostino, R., Favia, P., Oehr, C., and Wertheimer, M.R. (eds) (2005) *Plasma*

Lam Research Ex. 1047 - Page 59
Lam Research Corp. v. Inpria Corp.
IPR2024-00033 - U.S. Patent No. 9,823,564

Processes and Polymers, Wiley-VCH, Weinheim.

52 Friedrich, J.F., Mix, R., and Kühn, G. (2005) Polymer Surface Modification with Monotype Functional Groups of Different Type and Density, in *Plasma Processes and Polymers* (eds R. d'Agostino, P. Favia, C. Oehr, M.R. Wertheimer), Wiley-VCH, Weinheim, p. 3.

53 Friedrich, J.F., Mix, R., Schulze, R.D., and Kühn, G. (2005) Contribution of chemical interaction to the adhesion between metals and functional groups of different (Mono-) type and density at polymer surfaces, in *Adhesion* (ed. W. Possart), Wiley-VCH, Weinheim, Ch. 18, p. 265.

54 Legeay, G. and Poncin-Epaillard, F. (2005) Surface engineering by coating of hydrophilic layers: bioadhesion and biocontamination, in *Adhesion* (ed. W. Possart), Wiley-VCH, Weinheim, Ch. 12, p. 175.

55 Siffer, F., Schultz, J., and Roucoules, V. (2005) Alkene pulsed plasma functionalized surfaces: an interfacial Diels–Alder study, in *Adhesion* (ed. W. Possart), Wiley-VCH, Weinheim, Ch. 19, p. 289.

56 Biederman, H. and Osada, Y. (1992) *Plasma Polymerization Processes*, Elsevier, Amsterdam.

57 Rossmann, K. (1956) Improvement of bonding properties of polyethylene. *J. Polym. Sci.*, **19**, 141.

58 Strobel, M., Lyons, C.S., and Mittal, K.L. (eds) (1994) *Plasma Surface Modification of Polymers*, VSP Press, Zeist, Netherlands.

59 Wertheimer, M.R., Martinu, L., Klemberg-Sapieha, J.E., and Czeremuszkin, G. (1999) Plasma treatment of polymers to improve adhesion, in *Adhesion Promotion Techniques, Technological Applications* (eds K.L. Mittal and A. Pizzi), Dekker, New York., Ch. 5.

60 Hegemann, D., Hossain, M.M., Körner, E., and Balazs, D.J. (2007) A Macroscopic Description of Plasma Polymerization, in *Proceedings, 10th International Conference on Plasma Surface Engineering, Garmisch-Partenkirchen, 2006* (eds A. Cavaleiro, R. Grün, U. Helmersson, W. Möller, J. Musil, and C. Oehr), Wiley-VCH, Weinheim, p. 229.

61 Hippler, R., Pfau, S., Schmidt, M., and Schoenbach, K.H. (eds) (2001) *Low Temperature Plasmas, Fundamental Aspects and Applications*, Wiley-VCH, Weinheim.

62 Hippler, R., Kersten, H., Schmidt, M., and Schoenbach, K.H. (eds) (2008) *Low Temperature Plasmas, Fundamentals, Technologies and Techniques*, Wiley-VCH, Weinheim.

63 *Plasma Processes and Polymers* (2013) vol. **10**, Wiley-VCH. Print-ISSN: 1612-8850; Online ISSN: 1612-8869.

64 *Plasmas and Polymers*. Springer. Print-ISSN: 1084-0184 (discontinued).

65 Christophorou, L.G. (1971) *Atomic and Molecular Radiation Physics*, Wiley-Interscience, London.

66 d'Agostino, R., Camarossa, F., Fracasse, F., and Illuzzi, F. (1990) Plasma Polymerization of Fluorocarbons, in *Plasma Deposition, Treatment and Etching of Polymers* (ed. R. d'Agostino), Academic Press, Boston, Ch. 2.

67 Kogoma, M. (2004) Application of Atmospheric Pressure Discharge for Plasma Polymer Processes, in *Plasma Polymer Films* (ed. H. Biederman), Imperial College Press, London, Ch. 8.

68 Becker, K.H., Kogelschatz, U., Schoenbach, K.H., and Barker, R.J. (eds) (2004) *Non-Equilibrium Plasmas at Atmospheric Pressure*, Institute of Physics Publ., Bristol.

69 Hopfe, V. and Scheel, D.W. (2007) Atmospheric Pressure Plasmas for Wide-Area Thin-Film Deposition and Etching, in *Proceedings 10th International Conference on Plasma Surface Engineering, Garmisch-Partenkirchen, 2006* (eds A. Cavaleiro, R. Grün, U. Helmersson, W. Möller, J. Musil, and C. Oehr), Wiley-VCH, Weinheim, p. 253.

70 d'Agostino, R. (ed.) (1990) *Plasma Deposition, Treatment and Etching of Polymers*, Academic Press, Boston.

71 Manos, D.M. and Flamm, D.L. (eds) (1989) *Plasma Etching – An Introduction*, Academic Press, Boston.

72 Mucha, J.A. and Hess, D.W. (1983) Plasma etching, in *Introduction to Microlithography* (eds L.F. Thompson, C.G., Willson, and M.J. Bowden), American Chemical Society, Washington, Ch. 5.

Lam Research Ex. 1047 - Page 60
Lam Research Corp. v. Inpria Corp.
IPR2024-00033 - U.S. Patent No. 9,823,564

73 Kay, E. (1982) Reactive ion etching and related polymerization processes, in *Methods and Materials in Microelectronic Technology* (ed. J. Bargon), Plenum Press, New York.

74 Richter, H.H. and Wolff, A. (2001) Plasma Etching in Microelectronics, in *Low Temperature Plasmas, Fundamental Aspects and Applications* (eds R. Hippler, S. Pfau, M. Schmidt, and K.H. Schoenbach), Wiley-VCH, Weinheim, Ch. 18.

75 Richter, H.H., Marschmeyer, S., and Wolff, A. (2008) Plasma Etching in Microelectronics, in *Low Temperature Plasmas, Fundamentals, Technologies and Techniques* (eds R. Hippler, H. Kersten, M. Schmidt, and K.H. Schoenbach), Wiley-VCH, Weinheim, Ch. 25.

76 Cavaleiro, A., Grün, R., Helmersson, U., Möller, W., Musil, J., and Oehr, C. (eds) (2007) Plasma surface engineering, in *Proceedings 10th International Conference on Plasma Surface Engineering, Garmisch-Partenkirchen, 2006*, Wiley-VCH, Weinheim.

77 Meichsner, J. (2001) Low Temperature Plasmas for Polymer Surface Modification, in *Low Temperature Plasmas, Fundamental Aspects and Applications* (eds R. Hippler, S. Pfau, M. Schmidt, and K.H. Schoenbach), Wiley-VCH, Weinheim, Ch. 19.

78 Liston, E.M. (1993) Plasmas and surfaces – a practical approach to good composites, in *The Interfacial Interaction in Polymeric Composites, NATO-ASI Series E: Applied Sciences* (ed. G. Akovali), Kluwer, Dordrecht, vol. 230, Ch. 10.

79 Kawakami, M., Yamashita, Y., Iwamoto, M., and Kagawa, S. (1984) Modification of gas permeabilities of polymer membranes by plasma coating. *J. Membrane Sci.*, **19**, 249.

80 Morosoff, N. (1990) An Introduction to Plasma Polymerization, in *Plasma Deposition, Treatment and Etching of Polymers* (ed. R. d'Agostino), Academic Press, Boston, Ch. 1.

81 Havriliak, S. and Havriliak, S.J. (1997) *Dielectric and Mechanical Relaxation in Materials: Analysis, Interpretation, and Application to Polymers*, Hanser, München.

82 Riande, E. and Diaz-Caleja, R. (2004) *Broadband Dielectric Spectroscopy*, Dekker, New York.

83 Kremer, F. and Schönhals, A. (eds) (2003) *Broadband Dielectric Spectroscopy*, Springer, Berlin.

84 Runt, J.P. and Fitzgerald, J.J. (eds) (1997) *Dielectric Spectroscopy of Polymeric Materials, Fundamentals and Applications*, American Chemical Society, Washington, DC, USA.

85 McCrum, N.G., Read, B.E., and Williams, G. (1991) *Anelastic and Dielectric Effects in Polymer Solids*, Dover, New York.

86 Schönhals, A. (2004) Dielectric Properties of Amorphous Polymers, in *Broadband Dielectric Spectroscopy* (eds E. Riande and R. Diaz-Caleja), Dekker, New York, Ch. 3.

87 Asami, K. (2002) Characterization of heterogeneous systems by dielectric spectroscopy. *Prog. Polym. Sci.*, **27**, 1617.

88 Kremer, F. and Schönhals, A. (2003) Broadband Dielectric Measurement Techniques (10^{-6} Hz to 10^{12} Hz), in *Broadband Dielectric Spectroscopy* (eds F. Kremer and A. Schönhals), Springer, Berlin, Ch. 2.

89 Feldman, Y.D., Zuev, Y.F., Polygalov, E.A., and Fedotov, V.D. (1992) Time domain dielectric spectroscopy. A new effective tool for physical chemistry investigations. *Colloid Polym. Sci.*, **270**, 768.

90 Cole, R.H., Berberian, J.G., Mashimo, S., Chryssikos, G., Burns, A., and Tombari, E. (1989) Time domain reflection methods for dielectric measurements to 10 GHz. *J. Appl. Phys.*, **66**, 793.

91 Kremer, F., Hofmann, A., and Fischer, E. W. (1992) Broadband dielectric measurements on the α-and β-relaxation of polymers – a test of mode coupling. *Am. Chem. Soc., Polym. Prepr.*, **33**, 96.

92 Pethrick, R.A. and Hayward, D. (2002) Real time dielectric relaxation studies of dynamic polymeric systems. *Prog. Polym. Sci.*, **27**, 1983.

93 van den Berg, O., Sengers, W.G.F., Jager, W.F., Picken, S.J., and Wübbenhorst, M. (2004) Dielectric and fluorescent probes to investigate glass transition, melt, and crystallization in polyolefins. *Macromolecules*, **37**, 2460.

Lam Research Ex. 1047 - Page 61
Lam Research Corp. v. Inpria Corp.
IPR2024-00033 - U.S. Patent No. 9,823,564

94 Kessairi, K., Napolitano, S., Cappacioli, S., Rolla, P., and Wübbenhorst, M. (2007) Molecular dynamics of atactic poly (propylene) investigated by broadband dielectric spectroscopy. *Macromolecules*, **40**, 1786.

95 Mie, W.N., Kohli, M., Prohofsky, E.W., and Van Zandt, L.L. (1981) Acoustic modes and nonbonded interactions of the double helix. *Biopolymers*, **20**, 833.

96 Gabriel, C., Grant, E.H., Tata, R., Brown, P. R., Gestblom, B., and Noreland, E. (1987) Microwave absorption in aqueous solutions of DNA. *Nature*, **328**, 145.

97 Bigio, I.J., Gosnet, T.R., Mukherjee, P., and Saffer, J.D. (1993) Microwave absorption spectroscopy of DNA. *Biopolymers*, **33**, 147.

98 Edwards, G.S., Davis, C.C., Saffer, J.D., and Swicord, M.L. (1984) Resonant microwave absorption of selected DNA molecules. *Phys. Rev. Lett.*, **53**, 1284.

99 Infelta, P.P., de Haas, M.P., and Warman, J.M. (1977) The study of the transient conductivity of pulse irradiated dielectric liquids on a nanosecond timescale using microwaves. *Radiat. Phys. Chem.*, **10**, 353.

100 Warman, J.M., de Haas, M.P., Pichat, P., Koster, T.M.P., van der Zouwen-Assink, E. A., Mackor, A., and Cooper, R. (1991) Electronic processes in semiconductor materials studied by nanosecond time-resolved microwave conductivity. *Radiat. Phys. Chem.*, **37**, 433.

101 Nespurek, S., Herden, V., Kunst, M., and Schnabel, W. (2000) Microwave photoconductivity and polaron formation in poly(methylphenyl silylene). *Synth. Met.*, **109**, 309.

102 Prins, P., Grozema, F.C., Schins, J.M., Patil, S., Scherf, U., and Siebbeles, L.D.A. (2006) High intrachain hole mobility on molecular wires of ladder type poly(*p*-phenylenes). *Phys. Rev. Lett.*, **96**, 146601.

103 Prins, P., Grozema, F.C., and Siebbeles, L.D.A. (2006) Efficient charge transport along phenylene–vinylene molecular wires. *J. Phys. Chem. B*, **110**, 14659.

104 Prins, P., Grozema, F.C., Schins, J.M., and Siebbeles, L.D.A. (2006) Frequency dependent mobility of charge carriers along polymer chains with finite length. *Phys. Status Solidi B*, **243**, 382.

105 Pastol, Y., Arjavalingam, G., Halbout, J.-M., and Kopcsay, G.V. (1989) Coherent broadband microwave spectroscopy using picosecond optoelectronic antennas. *Appl. Phys. Lett.*, **54**, 307.

106 Arjavalingam, G., Theophilou, N., Pastol, Y., Kopcsay, G.V., and Angelopoulos, M. (1990) Anisotropic conductivity in stretch oriented polymers measured with coherent microwave transient spectroscopy. *J. Chem. Phys.*, **93**, 6.

107 Zoughi, R. (2000) *Microwave Non-Destructive Testing and Evaluation*, Kluwer Academic Publ., Dordrecht.

108 Zoughi, R. (1995) Microwave and millimeter wave nondestructive testing: a succinct introduction. *Res. Nondestr. Eval.*, **7**, 71.

109 Diener, L. (1995) Microwave near-field imaging with open-ended waveguide – comparison with other techniques of non-destructive testing. *Res. Nondestr. Eval.*, **7**, 137.

110 Diener, L. and Busse, G. (1996) Non-destructive quality and process control in injection moulding polymer manufacture with microwaves. *Mater. Sci. Forum*, **210-213**, 665.

111 Green, R.E., Djordevic, B.B., and Hentschel, M.P. (eds) (2003) Nondestructive characterization of materials X, in *Proceedings of the 11th International Symposium, Berlin 2002*, Springer, Berlin.

112 Hinken, J.H. and Beilken, D. (2005) Microwave defectoscopy with extended eddy current system. *Online J. Nondestruct. Test.*, **NDT.net 10**, October. Available at: http://www.ndt.net/v10n09.htm.

113 Steegmüller, R., Diener, L., and Busse, G. (1999) Microwave characterization of glass fiber reinforced polymers with a multi-detector waveguide. *Progr. Quantit. Nondestr. Eval.*, **18**, 555.

114 Liu, J.M. (2003) Characterization of Layered Dielectric Composites by Radar Techniques, in *Proceedings of the 11th International Symposium, Berlin 2002* (eds R.E. Green, B.B. Djordevic, and M.P. Hentschel), Springer, Berlin, p. 291.

115 Predak, S., Solodov, I.Y., Busse, G., Bister, V.H., Vöhringer, M.C., Haberstroh, E., and Ehbing, H. (2006)

Lam Research Ex. 1047 - Page 62
Lam Research Corp. v. Inpria Corp.
IPR2024-00033 - U.S. Patent No. 9,823,564

Fiber orientation measurement on short fiber reinforced PUR-RIM components: combination of nondestructive testing methods for optimization of simulation and production processes. *Tech. Mess.*, **73**, 617.

116 Predak, S., Ringer, T., Aicher, S., and Busse, G. (2003) Inspection of Dielectric Materials with Microwaves, in *Proceedings of the 11th International Symposium, Berlin 2002* (eds R.E. Green, B.B. Djordevic, and M.P. Hentschel), Springer, Berlin, p. 281.

117 Otto, J., Pannert, W., and Hald, M. (2003) Detection of Hidden Corrosion under Paint, in *Proceedings of the 11th International Symposium, Berlin 2002* (eds R.E. Green, B.B. Djordevic, and M.P. Hentschel), Springer, Berlin, p. 297.

118 Han, H.C. and Mansueto, E.S. (1995) Thin film inspection with millimeter-wave reflectometer. *Res. Nondestr. Eval.*, **7**, 89.

119 Han, H.C. and Mansueto, E.S. (1997) Thick measurement for thin films and coatings using millimeter waves. *Res. Nondestr. Eval.*, **9**, 97.

120 Krieger, B. (1992) Vulcanization of rubber, a resounding success for microwave processing. *Polym. Mater. Sci. Eng.*, **66**, 339.

121 Parodi, F. (2013) Novel Specialty Microwave Heating Susceptors for the Fast UHF Vulcanization of White and Colored Rubber Compounds, Technical Brochure. Available at: http://www.fpchem.com/fap_6a2-en.html.

122 Reece Roth, J. (1995) Industrial Plasma Engineering, vol. **1**, *Applications to Nonthermal Plasma Processing*, vol. 2, *Principles*. IOP Publishing, Bristol (reprinted 2001).

123 Wertheimer, M.R., Fozza, A.C., and Hollander, A. (1999) Industrial processing of polymers by low-pressure plasmas: the role of VUV radiation. *Nucl. Instr. Meth., Phys. Res. B*, **151**, 65.

124 Wertheimer, M.R., Martinu, L., and Liston, E.M. (1996) Plasma sources for polymer surface treatment, in *Handbook of Thin Film Process Technology* (eds D.A. Glocker and S.I. Shah), IOP Publishing, Bristol.

Lam Research Ex. 1047 - Page 63
Lam Research Corp. v. Inpria Corp.
IPR2024-00033 - U.S. Patent No. 9,823,564

2
Infrared Radiation

2.1
Absorption

2.1.1
General Aspects

The infrared portion of the electromagnetic spectrum is commonly divided into the near-, mid-, and far-infrared (*IR*) regions, named for their relation to the visible part of the spectrum (see Table 2.1).

As regards organic molecules, IR photon energies correspond in the case of small molecules to rotational motions, and in the case of large molecules to collective intramolecular and intermolecular vibrational modes (far-IR), fundamental vibrations (mid-IR), and to overtone and combination vibrations (near-IR). The molecules rotate and the atoms of the molecules vibrate at frequencies corresponding to discrete energy levels that are determined by the shape of molecular potential energy surfaces, the mass of the atoms, and by associated vibronic coupling. Necessary conditions for the absorption or emission of IR of frequency ν are: (i) the photon energy $h\nu$ must correspond to the difference ΔE_v of discrete energy levels; and (ii) the transition between the two energy states must cause a change in the charge distribution in the molecule, that is, a change in the electric dipole moment of the molecule. In terms of quantum mechanics, the absorption of a photon occurs when the transition moment M has a nonzero value. Since M is a vector composed of three components ($M = M_x, M_y, M_z$), at least one component must have a nonzero value. There need be no permanent dipole moment. Vibrations fulfilling the requirements are termed IR-active, and whether or not a vibration is IR-active depends on the symmetry properties of the molecule. In totally asymmetric molecules all vibrations are associated with a change in the dipole moment, and therefore these are IR-active. In molecules possessing symmetry elements, certain vibrations are not associated with a change in the dipole moment, and these therefore are IR-inactive.

Polymers and Electromagnetic Radiation: Fundamentals and Practical Applications, First Edition. Wolfram Schnabel
© 2014 Wiley-VCH Verlag GmbH & Co. KGaA. Published 2014 by Wiley-VCH Verlag GmbH & Co. KGaA.

Lam Research Ex. 1047 - Page 64
Lam Research Corp. v. Inpria Corp.
IPR2024-00033 - U.S. Patent No. 9,823,564

Table 2.1 Regions of infrared radiation.

Region	λ (μm)[a]	λ^{-1} (cm^{-1})[b]	ν (Hz)[c]	E (eV)[d]
	0.8	12 500	3.75×10^{14}	1.551
Near-IR	↕	↕	↕	↕
	2.5	4000	1.2×10^{14}	0.496
Mid-IR	↕	↕	↕	↕
	50	200	6×10^{12}	0.025
Far-IR	↕	↕	↕	↕
	1000	10	3×10^{11}	$1{,}24 \times 10^{-3}$

a) Wavelength.
b) Wavenumber.
c) Frequency.
d) Photon energy.

To obtain an insight into the interaction of IR radiation with molecules it is helpful to consider a simple case, namely a diatomic oscillator undergoing harmonic oscillations. The respective potential energy function is depicted in Figure 2.1.

For a diatomic molecule, modeled as a harmonic oscillator, quantum mechanics reveals that the vibronic molecular energy levels are restricted to discrete values given by Equation 2.1

$$E_v = h\nu\left(n_v + \frac{1}{2}\right) \tag{2.1}$$

where ν is the vibration frequency and n_v is the vibration quantum number taking only the integer values 0, 1, 2, 3, and so on. Hence, the zero point energy ($n_v = 0$)

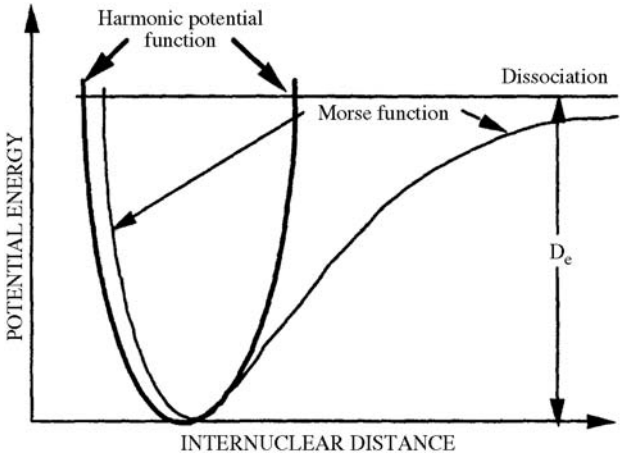


Figure 2.1 Potential energy versus interatomic distance for a diatomic molecule undergoing harmonic or anharmonic oscillations.

Lam Research Ex. 1047 - Page 65
Lam Research Corp. v. Inpria Corp.
IPR2024-00033 - U.S. Patent No. 9,823,564

corresponds to $E_v = 0.5\,h\nu$. When the molecules interact with IR radiation, transitions to higher energy levels are induced. Raising n_v from 0 to 1, a highly probable (allowed) process, corresponds to the *fundamental (normal) transition*, while raising n_v to higher levels, a (forbidden) process of low probability, results in *overtone transitions*. It should be noted that, in an IR absorption spectrum, the frequencies of overtone bands are multiples of those of fundamental mid-IR absorption bands. Therefore, frequencies of the first and second overtones can be estimated by multiplying the frequency of the fundamental by a factor two or three, respectively. The amplitudes of overtone bands are approximately one to two orders of magnitude smaller than the amplitudes of the corresponding fundamental absorption bands.

A more realistic approach towards atomic vibrations is the anharmonic oscillator (see Figure 2.1). Here, the vibronic molecular energy levels are given by Equation 2.2.

$$E_v = h\nu\left(n_v + \frac{1}{2}\right) - h\nu\, x_e\left(n_v + \frac{1}{2}\right)^2 \tag{2.2}$$

where x_e is the anharmonicity constant. In this case, the difference between vibronic levels decreases with increasing potential energy up to D_e, the dissociation energy corresponding to bond breakage. For a single vibronic stretch, the dependence of the potential energy on the interatomic distance r is fairly well described by the empirical Morse function (see Equation 2.3):

$$E_p = D_e\left(1 - e^{-\beta(r-r_e)}\right)^2 \tag{2.3}$$

where r_e is the equilibrium distance and β is a parameter governing the width of the function.

In contrast to diatomic molecules vibrating in a single mode only, polyatomic molecules can vibrate in many modes. A molecule containing N atoms has $3N-6$ vibrational degrees of freedom (linear molecules $3N-5$), which correspond to the number of possible fundamental vibrations (normal modes). As an example, Figure 2.2 shows the various vibration modes feasible for a 3-atomic side group. Here, $N>3$ due to the polymer rest (not shown).

It has been mentioned briefly before that, apart from fundamental vibrations, atoms in molecules also can undergo overtone vibrations. Moreover, combination vibrations (coupled vibrations) are possible. When two fundamental vibrations, corresponding to frequencies ν_1 and ν_2, are excited, transitions occur to combined levels corresponding to the sum of the frequencies $\nu_1 + \nu_2$, or to the difference

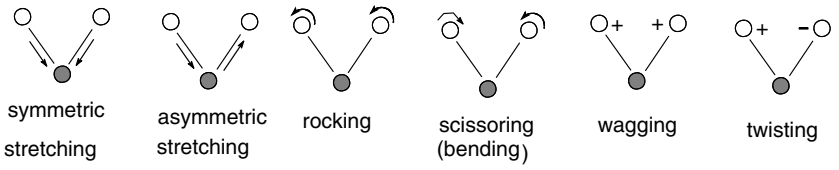


Figure 2.2 Vibration modes for an AX_2 side group (e.g., CH_2, NH_2).

Lam Research Ex. 1047 - Page 66
Lam Research Corp. v. Inpria Corp.
IPR2024-00033 - U.S. Patent No. 9,823,564

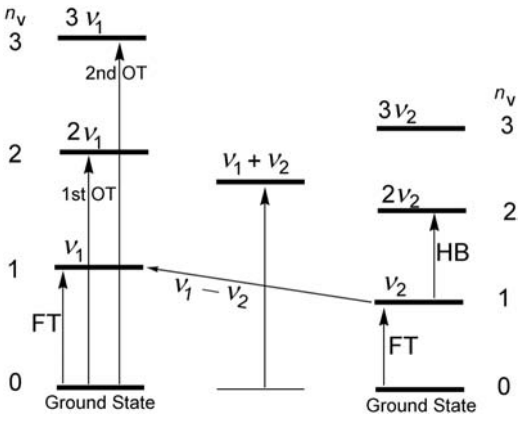


Figure 2.3 Vibrational energy levels and typical transitions regarding two vibrating modes with frequencies ν_1 and ν_2. n_v: vibrational quantum number, FT: fundamental transition, HB: hot band transition, 1st OT: first overtone transition, 2nd OT: second overtone transition.

$\nu_1 - \nu_2$ [1]. This can be seen from the energy level diagram in Figure 2.3, which also shows IR radiation-induced transitions commencing at the ground state. Obviously, transitions related to overtone and combination vibrations corresponding to the addition of frequencies are more energetic than fundamental transitions. Hence, the absorption bands are located in the near-infrared (*NIR*) region. Recently, NIR spectroscopy has gained importance with respect to the polymer field (see Section 2.2.3) [2,3]. The so-called "hot band" transition between higher energetic levels shown in Figure 2.3 is named for its increased occurrence probability at higher temperatures.

Difficulties in the assignment of IR bands of organic polymers in the region between 1500 and 650 cm^{-1} often arise because vibrations can become coupled. Coupling may involve part of the carbon backbone atoms, plus atoms of any adjacent groups, such that the energy levels mix and bands can no longer be assigned to one bond. This very common phenomenon occurs when adjacent bonds vibrate with closely similar frequencies [4].

The model developed for diatomic molecules serves as the basis to understand absorption and emission processes in polyatomic molecules. As pointed out before, linear *N*-atomic molecules can undergo $3N-5$ vibrations [5,6], and hence a polyethylene chain containing, for example, 10^4 CH_2 groups can vibrate in 9×10^4 modes. In fact, the IR absorption spectra of polyethylene and other polymers do not exhibit such a large number of lines. This is due not only to the similarity of force fields of the equivalent chemical groups in the macromolecules, with the consequence that many atoms vibrate with the same frequency, but also to the fact that the interaction of remote repeating units is almost negligible. The mutual interaction of atoms is restricted to those atoms being in close proximity, and IR absorption by polymers is characteristic of certain chemical groups. Hence, the interpretation and assignment of the IR spectra of polymers relies on the concept of group frequencies, which is based on theoretical concepts and computations on

Lam Research Ex. 1047 - Page 67
Lam Research Corp. v. Inpria Corp.
IPR2024-00033 - U.S. Patent No. 9,823,564

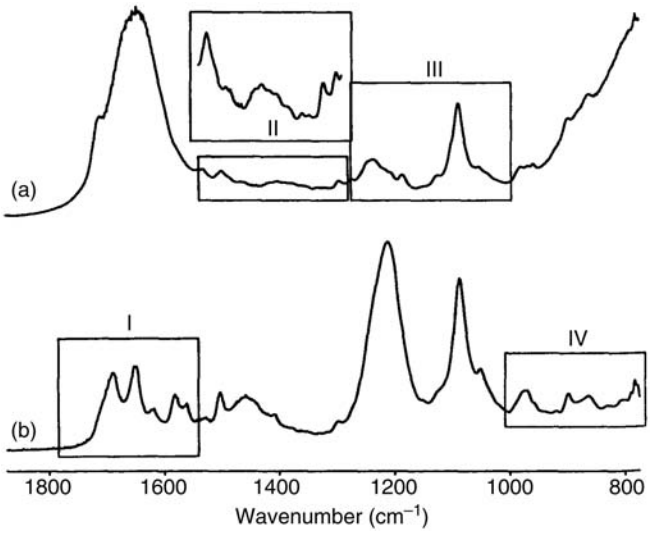


Figure 2.4 Mid-IR spectra of nucleic acids recorded in (a) H_2O and (b) in D_2O solution. Framed spectral domains: (I) in-plane base double-bond vibrations; (II) base-sugar bending motions; (III) phosphate group vibrations; (IV) phosphate-sugar backbone vibrations. Adapted with permission from Ref. [7]; © 1996, John Wiley & Sons.

small molecules. As a typical example, Figure 2.4 presents the mid-IR absorption spectra of double-stranded nucleic acids with framed spectral domains associated with characteristic groups.

Generally, resonant vibration frequencies are associated with particular bond types and particular chemical groups. The correlations between various specific chemical bonds and groups contained in organic polymers and mid-IR absorption bands are listed in Table 2.2, while overtone and combination bands associated with stretching and bending vibrations of hydrogenic functional groups contained in organic polymers are listed in Table 2.3.

The data in Table 2.2 and the spectra in Figure 2.4 denote absorption bands in terms of wavenumbers $n_w = \lambda^{-1}$ (cm^{-1}) instead of wavelength values. In this case, n_w is proportional to the frequency ν, and thus to the quantum energy $h\nu$ (see Equation 2.4):

$$n_w = \frac{1}{\lambda} = \frac{\nu}{c} \tag{2.4}$$

where c is the velocity of light *in vacuo* ($c \approx 3 \times 10^{10}$ cm s^{-1}). Both, wavenumber and wavelength values are presented in Table 2.3, because many authors present near-IR data in terms of wavelength values.

It should be noted that the photon energy of IR radiation does not surpass values of about 1.5 eV. In fact, it is lower than the binding energies of atoms in molecules, which implies that chemical reactions cannot be induced directly by single photons of IR radiation via bond breakage.

Lam Research Ex. 1047 - Page 68
Lam Research Corp. v. Inpria Corp.
IPR2024-00033 - U.S. Patent No. 9,823,564

Table 2.2 Mid-IR absorption bands of typical chemical groups contained in organic polymers.

Bond	Type of bond	Specific type of bond	Absorption range and intensity[a)]
C—H	Alkyl	Methyl	1380 (weak), 1260 (strong), 2870 and 2960 (both strong to weak)
	Vinyl	$C{=}CH_2$	900 (strong), 2975, 3080 (medium)
	Aromatic	Benzene	3070 (weak)
C—C	Acyclic C—C	Monosubstituted alkenes	1645 (medium)
C=O	Aldehyde, Ketone		1720
O—H	Alcohols, Phenols		3610 to 3670
	Carboxylic acids		3500 to 3560
N—H	Primary amines		Doublet between 3400 to 3500 and 1560 to 1640
C—O	Alcohols	Primary	1050 (strong)
		Secondary	1100 (strong)
		Tertiary	1150 to1200 (medium)
C—N	Aliphatic amines		1020 to 1220
	C=N		1650 to 1700
	CN	Nitriles	2210 to 2260
	R—C—N	Isonitriles	2165 to 2110
C—F	Fluoroalkanes		1000 to 1100
C—Cl	Chloroalkanes		540 to 760 (medium to weak)
C—Br	Bromoalkanes		500 to 600 (strong to medium)
N—O	Nitrocompounds	Aliphatic	1540 (strong), 1380 (weak)
		Aromatic	1520, 1350

a) Numbers denote wavenumbers n_w in units of (cm^{-1}).

Table 2.3 Near-IR absorption bands of hydrogenic functional groups contained in organic polymers.

Functional group	Wavelength range of absorption (nm)[a)]	Nature of bands
C—H, aliphatic	2000 to 2400 (5.0×10^3 to 4.17×10^3)	Combination
	1600 to 1800 (6.25×10^3 to 5.56×10^3)	1st Overtone
	1000 to 1200 (1×10^4 to 8.33×10^3)	2nd Overtone
C—H, aromatic	1685 (5.93×10^3)	1st Overtone
	1143 (8.75×10^3)	2nd Overtone
OH, alcohols, phenols	About 2000 (5.0×10^3)	Combination
	About 1400 (7.14×10^3)	1st Overtone
	About 1000 (1×10^4)	2nd Overtone
O—H, water	1940 (5.15×10^3)	Combination
	1440 (6.94×10^3)	1st Overtone
N—H, aliphatic amines	2000 (5.0×10^3)	Combination
	1500 (6.67×10^3)	1st Overtone
N—H, aromatic amines	1972 (5.07×10^3)	Combination
	1446 (6.92×10^3)	1st Overtone
	1020 (9.8×10^3)	2nd Overtone

a) Wavenumbers (in cm^{-1} units) in brackets.

Lam Research Ex. 1047 - Page 69
Lam Research Corp. v. Inpria Corp.
IPR2024-00033 - U.S. Patent No. 9,823,564

Among the plethora of books dealing generally with the absorption of IR radiation, only a few titles are cited here [1–4,8]. Other books notably relate especially to polymers [5,6,9–12].

2.1.2 Crystalline Polymers

If the molecules in the unit cell of crystalline polymers are placed close enough together, the interaction of polymer chains can result in a detectable effect. This occurs in the case of crystalline polyethylene, where *crystal field splitting* is observed, and each group mode of the isolated polyethylene molecule is split into two components. This holds also, for example, for the methylene rocking mode at $720\,cm^{-1}$ and for the methylene bending mode at $1460\,cm^{-1}$. In the case of polypropylene, crystal band splitting is not observed, because the molecules are not positioned close enough together [9].

2.1.3 Polarized IR Radiation

Photons are absorbed when the electric field vector **E** of the incident radiation interacts with the transition moment vector $\mathbf{M_i}$ associated with vibration *i*. The absorbance A_i for the respective band is proportional to the square of the scalar product of $\mathbf{M}_i$ and **E**, as shown by Equation 2.5:

$$A_i \propto \sum_k (\mathbf{M}_{ik} \bullet \mathbf{E})^2 \quad \propto \quad \sum_k (M_{ik} E)^2 \cos^2 \varphi_\kappa \tag{2.5}$$

where φ_κ is the angle between $\mathbf{M}_{ik}$ and **E**. For isotropic samples, A_i is independent of the polarization of the incident radiation, since the summation extends over all randomly oriented absorbing species, indicated by the index *k* in Equation 2.5. In anisotropic samples, the transition moments are oriented and, therefore, the absorbance of certain bands depends on the polarization of the incident radiation. A_i is maximum when $\mathbf{M}_i$ and **E** are parallel, and is zero when $\mathbf{M}_i$ and **E** are perpendicular. Anisotropic behavior is exhibited, for example, by stretched polymer films and fibers, liquid crystals, self-assembled monolayers, and multilayers. In these cases, the absorption of IR radiation is sensitive to the state of polarization of the incident light beam with respect to a reference direction. The latter can be given by the stretching direction of a polymer sample, the director of a liquid crystal or of a monolayer film. A typical case is shown in Figure 2.5 depicting the IR absorption bands of polyacrylonitrile recorded before and after stretching the film to the draw ratio 2 (extension by 100%).

The *IR linear dichroism* (i.e., the anisotropic absorption) is characterized by the integrated absorbances $A_{||}$ and $A_\perp$ measured at the band under inspection with light polarized parallel and perpendicular to the fixed reference direction, respectively. Commonly, the optical anisotropy of uniaxially oriented samples is characterized by the *dichroic ratio* $R_{dichro} = A_{||}/A_\perp$, the *dichroic difference* $\Delta A = A_{||} - A_\perp$, or by the

Lam Research Ex. 1047 - Page 70
Lam Research Corp. v. Inpria Corp.
IPR2024-00033 - U.S. Patent No. 9,823,564

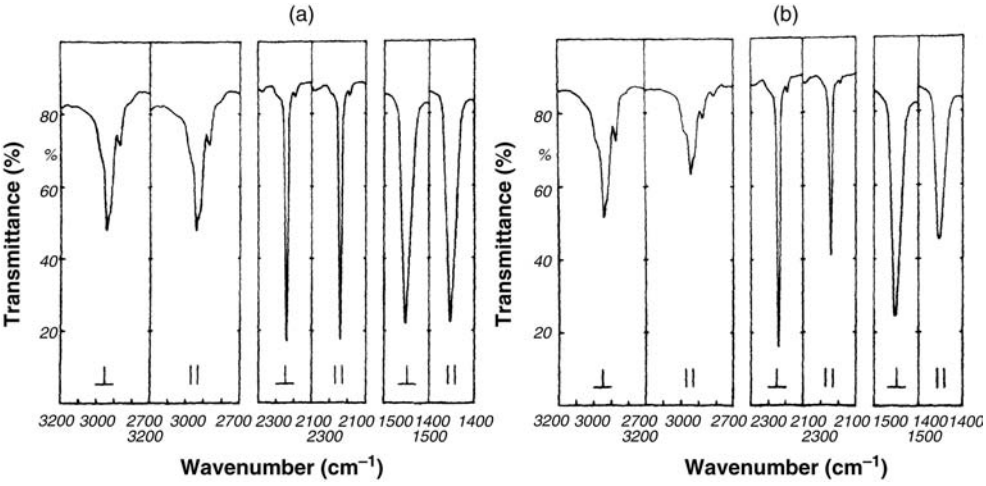


Figure 2.5 Absorption bands of polyacrylonitrile recorded before (a) and after (b) stretching the film to the draw ratio 2. Band assignment: 2940 cm^{-1} (antisymmetric CH_2-stretching); 2940 cm^{-1} (C≡N-stretching); 1452 cm^{-1} (CH_2-bending). Polarization of incident light: || parallel and ⊥ perpendicular to drawing direction. Adapted with permission from Ref. [6]; © 1980, Marcel Dekker.

in-plane order parameter $S = (A_{||} - A_{\perp})/(A_{||} + A_{\perp})$. In the case of biaxial orientation, polarized spectra must be recorded parallel to three independent reference axes. The determination of molecular orientation in polymers by polarized IR spectroscopy is of great importance from both practical and theoretical points of view. The technique serves to characterize industrially produced polymers, and is a very helpful tool for studying orientation in biomolecules such as fibrous proteins [13,14]. Notably, the orientation of specific groups can be determined selectively by performing measurements at wavelengths corresponding to these groups. It should be emphasized that IR polarization spectroscopy allows orientation studies to be performed on numerous polymers that do not absorb visible light.

2.1.4 Far-IR Radiation

Techniques applicable to far-IR radiation in the terahertz (THz) frequency region have become accessible only recently. The respective developments are particularly important in the field of polymers, as collective vibrational modes of macromolecules on a picosecond timescale are excited by far-IR radiation of THz frequencies. This involves dry polymers as well as biopolymers contained in aqueous systems. Collective vibrations involve portions of the macromolecules, and can be best described as large molecular pieces beating against each other. Extensive molecular dynamics simulations, including various proteins and DNA, have identified twisting and vibrational modes in the range from 0.6 to 6.0 THz. Effectively, all

Lam Research Ex. 1047 - Page 71
Lam Research Corp. v. Inpria Corp.
IPR2024-00033 - U.S. Patent No. 9,823,564

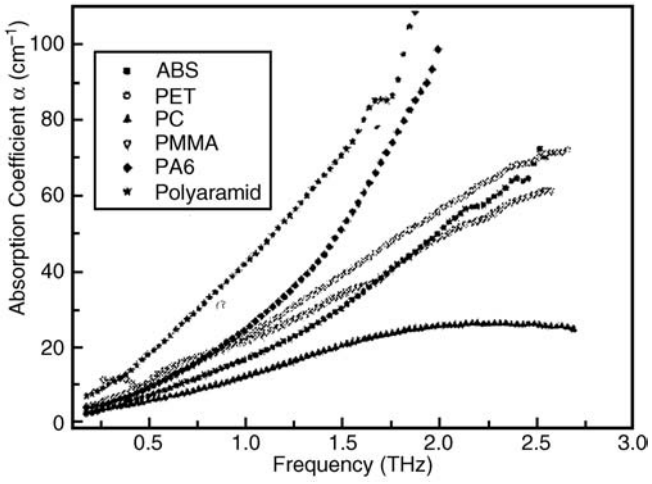


Figure 2.6 THz absorption spectra of synthetic polar polymers recorded with powdered samples dispersed in a polyethylene matrix. ABS: acrylonitrile-butadiene-styrene-*ter*-polymer; PET: poly (ethyleneterephthalate); PC: polycarbonate; PMMA: poly(methylmethacrylate); PA 6: polyamide 6. For chemical structures, see Chart 2.1. Adapted with permission from Ref. [17]; © 2006, Springer.

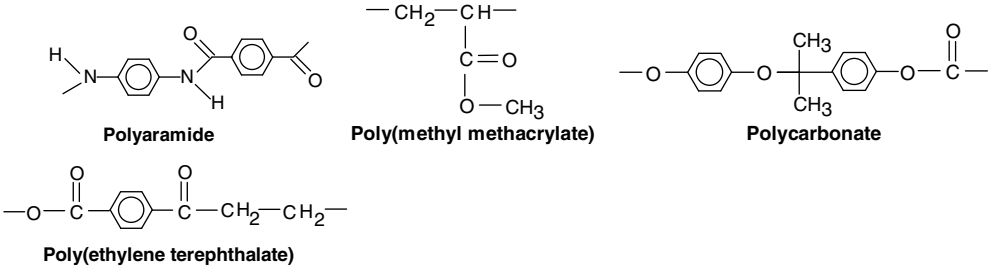


Chart 2.1 Chemical structures of the repeating units of polymers shown in Figure 2.6.

biomolecules containing more than about 500 atoms are expected to absorb rather strongly in the THz region due to the excitation of collective vibrational modes [15,16]. It should be noted that collective, relative motions between tertiary subunits in the biopolymer, or coherent movements within the subunit, represent functionally relevant motions.

In most cases, the THz absorption spectra of polymers do not exhibit specific features, but are characterized by absorption coefficients that increase monotonically with frequency. Some typical absorption spectra of synthetic polar polymers are presented in Figure 2.6. Unpolar polymers including polyethylene, polypropylene and poly(tetrafluoroethylene) absorb only weakly (at 1 THz, α is five- to 20-fold less than for the polar polymers in Figure 2.6). Some typical spectra of unpolar polymers are presented in Figure 2.7.

Lam Research Ex. 1047 - Page 72
Lam Research Corp. v. Inpria Corp.
IPR2024-00033 - U.S. Patent No. 9,823,564

Table 2.4 Molar extinction coefficients of typical biopolymers measured at $\lambda = 0.6$ THz obtained with powdered samples dispersed in a polyethylene matrix [21].

Polymer	Extinction coefficient α ($\mathrm{l\,mol^{-1}\,cm^{-1}}$)[a)]
Calf thymus DNA	1.9×10^5
Bovine serum albumin (BSA)	0.9×10^3
Collagen	4.1×10^3

a) Defined by $A = \alpha cl$, with A is absorbance, c is molar concentration, and l is the optical path length.

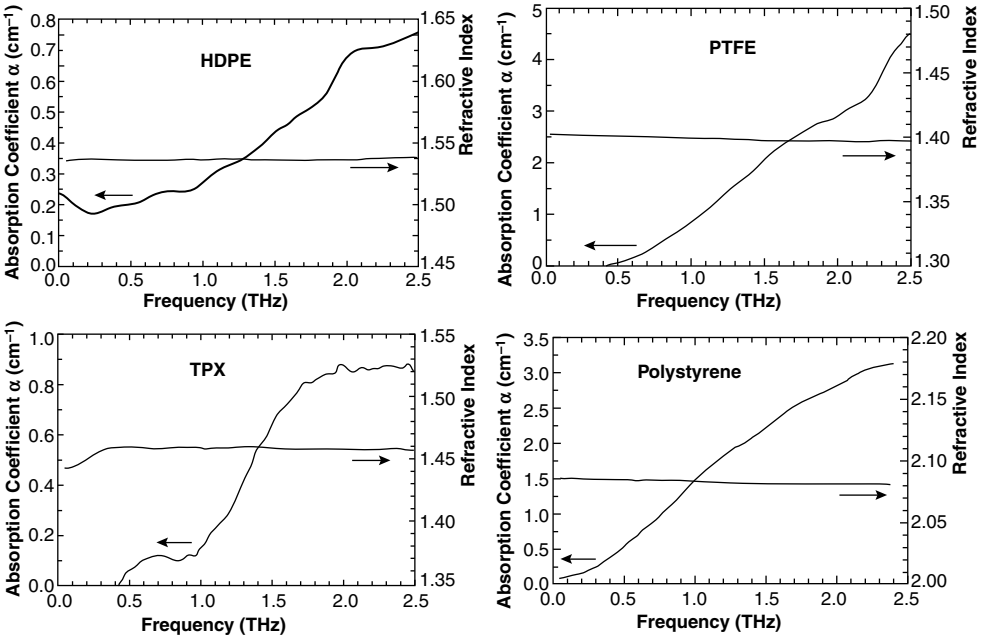


Figure 2.7 THz absorption spectra of synthetic unpolar polymers. Adapted with permission from Ref. [18]; © 2007, IEEE.

Broadband absorption without distinct absorption features reflects an overlapping of the collective vibrational modes resulting from a large density of the latter. Synthetic polymers (including those of Figures 2.6 and Figure 2.7) and biopolymers (including DNA, bovine serum albumin and collagen) behave similarly, but cellulose, which forms hydrogen-bonded triple helices with strands composed of polyglucose units, appears to be an exception. Rather, the THz absorption spectrum of cellulose exhibits distinct absorption features that can be attributed to inter-strand twisting or stretching motions [19], or to phonon-like modes along the polymer backbone [20].

Whenever checked for its validity, the Lambert–Beer law (absorbance $A = \alpha cl$) was observed [21]. The molar extinction coefficients, α, of some biopolymers are listed in Table 2.4.

Lam Research Ex. 1047 - Page 73
Lam Research Corp. v. Inpria Corp.
IPR2024-00033 - U.S. Patent No. 9,823,564

2.2
Applications

2.2.1
General Aspects

The absorption of mid-IR radiation by organic matter is characterized by the interaction of photons with specific chemical groups. In fact, this forms the basis for the technique of *IR spectroscopy*, which serves as a routine tool for studying the various chemical and physical properties of polymers. Today, IR spectroscopy is used not only to identify polymers and polymer additives but also to explore the composition of polymer blends. It is also used in manufacturing schemes, to monitor the quality of incoming monomers, to control the processes employed, and to confirm the quality of the intermediates and final products. The theoretical background of IR spectroscopy, as well as the technical aspects of relevant methods and an analysis of the results obtained, have been described exhaustively in numerous reviews and monographs [1–5,8–12,22–31]. The widespread use of IR spectroscopy for polymer characterization will be demonstrated below with various examples, including specialized applications devoted to orientation measurements and IR microscopy. In addition, topics which have become important quite recently, such as two-dimensional IR spectroscopy and time-resolved measurements on polymers, will be discussed. In this context it is important to note that the *in-situ* IR monitoring of the kinetics of chemical processes – including polymerization reactions – today represent an elegant and widely applied tool.

Although the aim of this book is not to describe in detail the instrumental and apparatus aspects of IR spectroscopy, a few more recent developments that are essentially responsible for the technique's current importance can be outlined here. Typically, the IR absorption spectra of polymers are recorded in normal-incident transmission mode, using sheets of polymers or solid matrices (e.g., KBr) that contain admixed polymer powder. The main problems associated with the technique, such as interference patterns in the spectra of micrometer-thick films, can be eliminated by using sophisticated reflection methods such as attenuated total reflection (*ATR*). In this case, a reflection element with a high refractive index, n_1, composed generally of ZnSe, As_2Se_3, or Ge, is brought into close contact with a sample having a lower refractive index, n_2. Subsequently, IR light introduced to the reflection element at an incident angle θ larger than the critical angle θ_{crit} will be totally reflected at the reflection element/sample interface (see Figure 2.8).

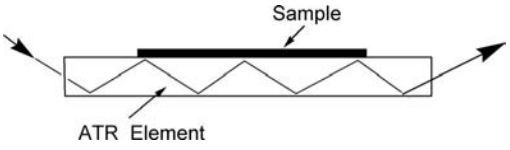


Figure 2.8 Attenuated total reflection accessory containing a multireflection single-pass element.

Lam Research Ex. 1047 - Page 74
Lam Research Corp. v. Inpria Corp.
IPR2024-00033 - U.S. Patent No. 9,823,564

The critical angle θ_{crit} is defined by Equation 2.6:

$$\sin \theta_{crit} = \frac{n_2}{n_1} \tag{2.6}$$

In this case, an evanescent field penetrating the sample is formed at the reflection element/sample interface. At the same time, IR light passing through the set-up (as shown in Figure 2.8) will be totally reflected at the interface unless it is absorbed by the sample, that is, at wavelengths where the sample is transparent. Absorption causes an attenuation of the intensity of the IR light passing through the reflection element, and consequently an absorption spectrum resembling a transmission spectrum will be obtained. The layer of light absorption is characterized by the penetration depth d_p, which is in turn determined by the angle θ, the ratio n_2/n_1, and the wavelength of the light within the reflection element, λ, according to Equation 2.7.

$$d_p = \frac{\lambda}{2\pi\sqrt{\sin^2\theta - \left(\frac{n_2}{n_1}\right)^2}} \tag{2.7}$$

Since d_p is at most a few micrometers in the IR region, an ATR spectrum provides information regarding the sample's surface. Thus, the ATR method is especially applicable to the case of thin macromolecular materials such as fibers and fabrics, and also to thin polymer layers (especially coatings and laminates) which often fail to yield useful transmission spectra. Other sophisticated methods that are useful for examining thin polymer layers include infrared ellipsometry (*IRE*) and infrared reflection absorption spectroscopy (*IRRAS*); the principles of these techniques are briefly described in Section 2.2.5.1.

It must be emphasized that IR spectroscopy has undergone major improvements in terms of light sources, detectors, and data systems, and particularly in developments of the Fourier transform technique which utilizes interferometers instead of salt prisms and grating monochromators. Modern commercial spectrometers operating with the aid of a Michelson interferometer produce interferograms which, upon mathematical decoding by means of Fourier transformation, deliver simultaneously whole absorption spectra that are commonly referred to as Fourier transform infrared (*FTIR*) spectra.

With regards to the above-mentioned improvements, developments concerning the far-IR region (i.e., THz spectroscopy) should also be emphasized. THz spectroscopy has become scientifically accessible only during the past two decades, with the aid of new broadband sources of moderate intensity. Frequently used THz sources operate with femtosecond near-IR laser pulses being emitted, for example, from biased semiconductors irradiated by a Ti:sapphire laser [32–35], in which case the THz pulses are generated by photoconductive antennas. A typical THz transmitter consists of an undoped GaAs wafer covered by metal strips at a distance of 30 to 60 μm. A direct current (*dc*) bias is applied across the gap such that, when the semiconductor area between the metal strips is hit by a near-IR pulse, electrons

Lam Research Ex. 1047 - Page 75
Lam Research Corp. v. Inpria Corp.
IPR2024-00033 - U.S. Patent No. 9,823,564

are generated. As these latter electrons are accelerated in the dc field, a femtosecond THz pulse is emitted. THz radiation can also be generated with the aid of beryllium-doped germanium (Ge:Be) lasers which, when operated at 4.2 K (liquid helium temperature) can be tuned from 1 to 4 THz [36]. Other modes of generating THz radiation have been described [32], and in this context the generation of THz radiation in poled polymers is to be noted (see Section 2.2.4.5). Recently, a high-power source of THz radiation has become available: coherent *synchrotron radiation* covers the frequency range from 0.1 to 1.0 THz (3 to 33 cm^{-1}, 0.4 to 4 meV) and is emitted from subpicosecond relativistic electron bunches [37–39].

2.2.2 Mid-IR Analysis

2.2.2.1 Identification of Synthetic Polymers

As IR spectroscopy can be used for the identification of functional groups, it is also a useful tool for identifying commercial polymeric materials that might be used, for example, in the wrapping and packaging of items, and of additives contained in such materials. In most cases it would be at least possible to place a sample into a certain class of polymer, such as polyolefins, polyesters, polyamides, and polyurethanes, and for this purpose it would be helpful to create a reference to a library of spectra. Noticeable in this context are the books of Hummel [28], as well as other libraries [40,41] containing large numbers of IR spectra of various polymer samples.

2.2.2.2 Proteins

Today, IR spectroscopy is widely used for analyzing the spatial structures of proteins [42,43]. The IR-spectra of proteins are characterized by the absorption bands of the amide (peptide) group (Chart 2.2) resulting from several in-plane vibrations; that is, the stretching vibrations of C=O, C—N, and N—H, the bending vibration of O=C, and the C—N torsion as an out-of-plane vibration. Details of these bands are listed in Table 2.5.

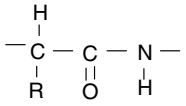


Chart 2.2 General chemical structure of the base unit of a protein chain. R: H, CH_3, $HOCH_2$, Ph-CH_2, etc.

The amide I band, located between 1700 and 1600 cm^{-1}, is especially sensitive to the secondary structure of proteins. It represents 80% of the C=O stretching vibration coupled to the in-plane N—H bending and C—N stretching modes. The

Lam Research Ex. 1047 - Page 76
Lam Research Corp. v. Inpria Corp.
IPR2024-00033 - U.S. Patent No. 9,823,564

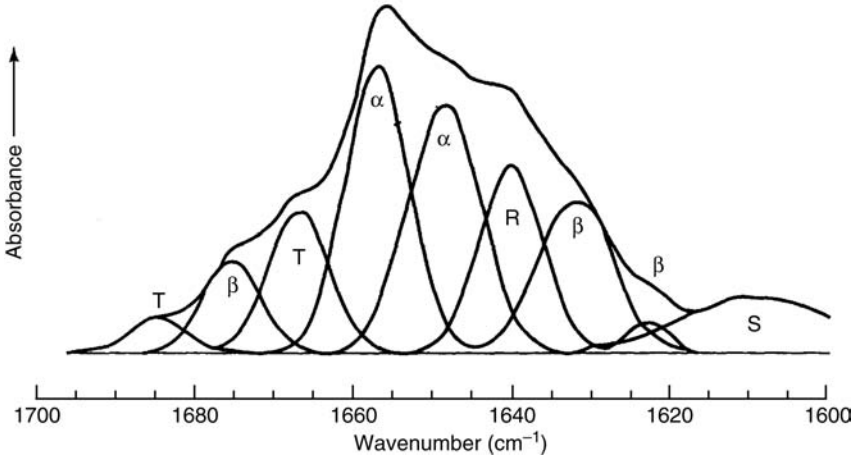


Figure 2.9 Curve-fitted amide I band of lysozyme recorded in D_2O solution. Denotations: T (turns), β (β-structure), α (α-helix), R (random coil), S (amino acid side-chain vibration). Adapted with permission from Ref. [43]; © 1997, John Wiley & Sons.

Table 2.5 Characteristic IR absorption bands of proteins [43].

Denotation	Wavenumber (cm^{-1})	Assignment
A	3300	N-H stretching (overtone)
B	3110	N-H stretching (overtone)
I	1653	80% C=O stretching, 10% C—N stretching, 10% N—H bending
II	1567	60% N—H bending, 40% C—N stretching
III	1299	30% C—N stretching, 30% N—H bending, 10% C=O stretching, 20 others
IV	627	40% O=C—N bending, 60% others
V	725	N—H bending
VI	600	C=O bending
VII	200	C—N torsion

exact position of the band in the spectrum depends on the nature of hydrogen bonding involving C=O and N—H groups, which is determined by the particular secondary structure of the protein. Generally, proteins contain a variety of segments with different conformations – that is, helices, β-structures, turns, and random structures. Hence, the amide I band consists of several overlapping component bands arising from these different secondary structure domains. In the case of globular proteins, band assignments can be made on the basis of empirical rules and X-ray crystallography studies (see Table 2.6).

Lam Research Ex. 1047 - Page 77
Lam Research Corp. v. Inpria Corp.
IPR2024-00033 - U.S. Patent No. 9,823,564

Table 2.6 Assignment of amide-I bands to secondary structures [42,43].

Wavenumber (cm^{-1})	Assignment
1695 to 1670	Intermolecular β-structure
1690 to 1680	Intramolecular β-structure
1666 to 1659	"3-turn" helix
1657 to 1648	α-helix
1645 to1640	Random coil
1640 to 1630	Intramolecular β-structure
1625 to 1610	Intermolecular β-structure

Quantitative protein analyses can be performed by applying a technique of resolution enhancement such as Fourier self-deconvolution and by referring to empirical rules on the correspondence between the wavenumbers of amide I bands and secondary structures [42,43]. Figure 2.9 shows, as a typical example, the deconvolved amide I band of lysozyme recorded in D_2O solution [43].

Noticeably, the denaturation of proteins as a consequence of changes in temperature, pH and pressure can be studied by measuring changes in the amide I band.

2.2.2.3 Nucleic Acids

In the 2000 to 500 cm^{-1} region, the IR spectrum of nucleic acids contains around 40 well-defined absorption bands with different relative intensities and dichroic ratios [7,44]. These bands are related to characteristic vibration modes of the

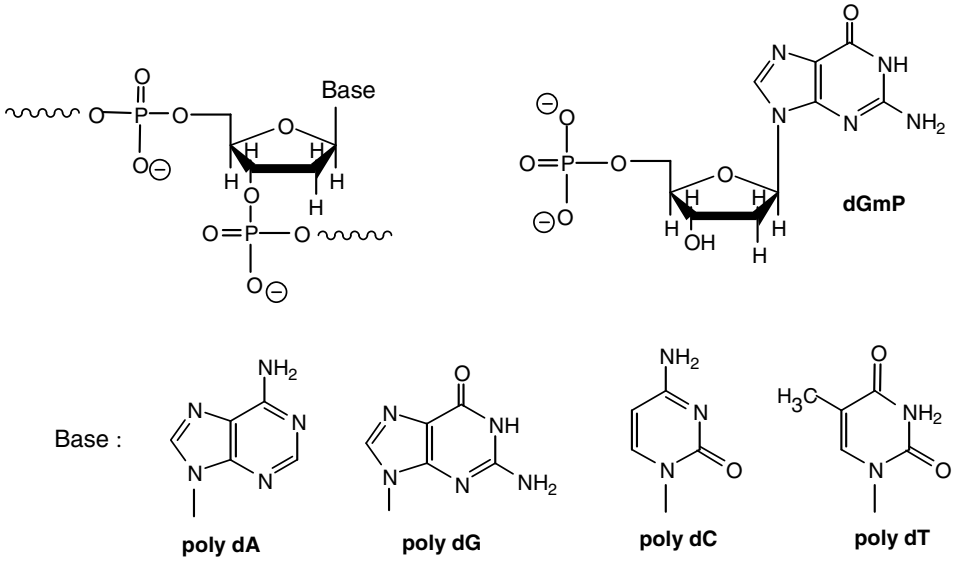


Chart 2.3 Chemical structures of nucleic acids.

Lam Research Ex. 1047 - Page 78
Lam Research Corp. v. Inpria Corp.
IPR2024-00033 - U.S. Patent No. 9,823,564

Table 2.7 Modes of vibrations of nucleic acids.

Wavenumber (cm^{-1})	Assignment
1800 to 1500	Purinic and pyridinic vibrations
1500 to 1250	Vibrational coupling between base and sugar
1250 to 1000	Sugar-phosphate chain vibration
1000 to 800	Sugar and sugar-phosphate vibrations

Table 2.8 Major absorption bands of DNA [45].

Wavenumber (cm^{-1})	Assignment
2960 to 2850	CH_2 stretching
1660 to 1655	C=O stretching, N—H bending
1610	C=C imidazole ring stretching
1578	C=N imidazole ring stretching
1230	PO_2^- asymmetric stretching
1089	PO_2^- symmetric stretching
1015	Ribose stretching
970 and 915	Ribose-phosphate skeletal motions

constituent base, sugar, and phosphate groups (see Table 2.7). The major IR absorption bands of DNA are listed in Table 2.8.

The nucleic acid bases thymine, adenine, cytosine, guanine and uracil give rise to purinic and pyridinic vibrations which are sensitive to base-pairing and base-stacking effects. Figure 2.10 shows as an example the base-pairing effect on spectra of poly dG.poly dC and $dA_{12}.dT_{12}$ recorded in D_2O solution [32]. Base-pairing causes important modifications: in the first case (left side of Figure 2.10), the guanine C=O stretching vibration is shifted from 1668 cm^{-1} to 1689 cm^{-1}, and the relative intensity of the 1581 cm^{-1} guanine band is strongly reduced; moreover, the cytosine ring vibration at 1524 cm^{-1} vanishes on base-pairing. In the second case (right side of Figure 2.10), the thymine band is shifted from 1632 cm^{-1} to 1641 cm^{-1}, and the adenine band from 1626 cm^{-1} to 1622 cm^{-1}.

2.2.3 NIR Analysis of Synthetic Organic Polymers

The absorption spectra recorded with synthetic organic polymers exhibit bands in the NIR region (0.8 to 2.5 μ), this being due mainly to hydrogenic functional groups, in particular C—H, N—H, and O—H groups [2]. The absorptions arise from overtones of fundamental stretch vibrations and from combinations of stretching and bending vibrations (see Table 2.3). Notably, the amplitudes of these bands are approximately one to two orders of magnitude less than the amplitudes

Lam Research Ex. 1047 - Page 79
Lam Research Corp. v. Inpria Corp.
IPR2024-00033 - U.S. Patent No. 9,823,564

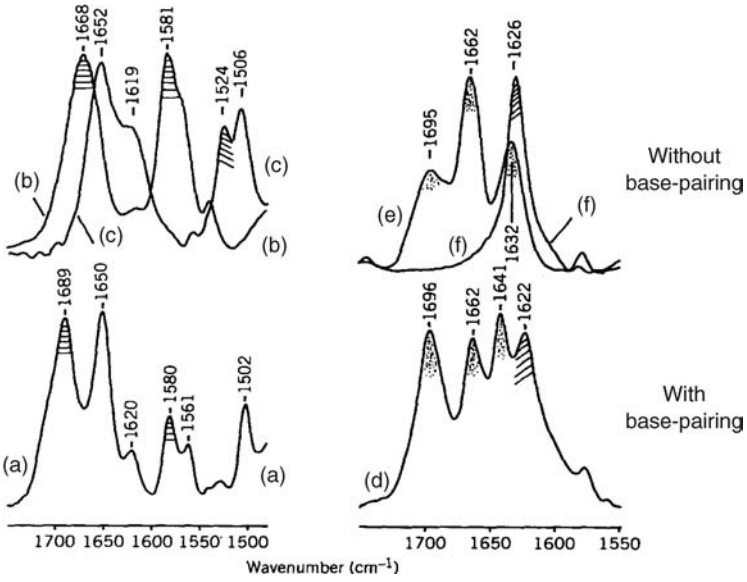


Figure 2.10 Effects of base-pairing on the IR spectra of nucleic acids (for chemical structures, see Chart 2.3) recorded in D_2O solution. (a) Poly dG.poly dC; (b) dGmP; (c) poly dC; (d) $dA_{12}.dT_{12}$; (e) dT_{12}; (f) dA_{12}. Acronyms: d, deoxyribo; A, adenylic acid; C, cytidylic acid; T, thymidylic acid; GmP, guanosine-5′-monophosphate. Adapted with permission from Ref. [7]; © 1996, John Wiley & Sons.

of the corresponding fundamental absorption bands. The diminished amplitude of NIR bands is very useful for the analysis of samples absorbing strongly in the mid-IR region. For example, rather thick polymer sheets (up to several millimeters) can be tested directly by using NIR techniques, while aqueous systems such as polymer lattices with up to 99% water content can be analyzed directly for copolymer ratio. Although the overtone bands of water are very strong, they are confined to the region of 1400–1500 nm and 1900–2000 nm, leaving the C—H and N—H overtone region (1500–2000 nm) relatively unaffected by the large concentration of water (see Figure 2.11).

Currently, there exists a wide spectrum of applications of NIR-based analysis in the field of polymers. As can be seen from the data in Table 2.9, NIR analysis serves to determine quantitatively terminal double bonds, OH groups, and the content of not only moisture but also of additives such as plasticizers or stabilizers.

The information in Table 2.10 shows that NIR techniques also allow the characterization of textile products made from natural fibers (cotton, wool, blends) or from synthetic fibers (polyamide, polyester, blends). In this case, *NIR reflectance spectroscopy* is mostly applied, and provides the advantage of testing a sample rapidly (within minutes), without destroying its integrity. Moreover, with the aid of sophisticated commercial instruments, not only quantitative analyses but also

Lam Research Ex. 1047 - Page 80
Lam Research Corp. v. Inpria Corp.
IPR2024-00033 - U.S. Patent No. 9,823,564

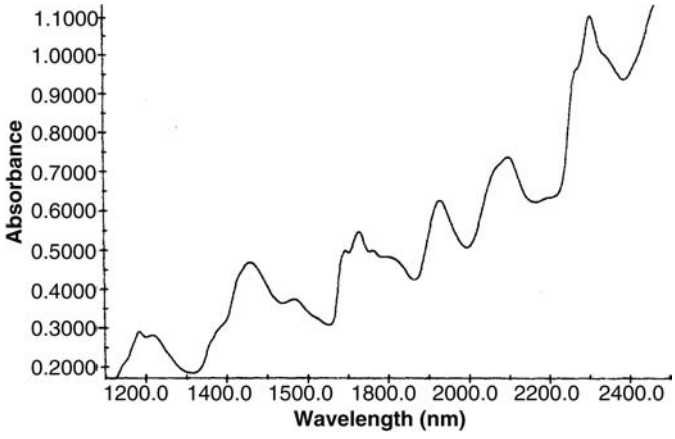


Figure 2.11 NIR spectrum of typical latex exhibiting C—H and N—H bands between 1500 and 1900 nm and above 2000 nm. The O—H bands of water are located from 1400–1500 nm and from 1900–2000 nm. Adapted with permission from Ref. [46]; © 2007, CRC Press.

Table 2.9 NIR analysis of synthetic organic polymers. Typical examples. Further details can be found in Ref. [46].

Polymer	Object of analysis
Polyethylene	Terminal double bonds
Poly(vinyl chloride)	Plasticizer content
Poly(vinyl alcohol)	OH number, moisture, and additive content
Polystyrene	Stabilizer content

morphological investigations of fibers and yarns can be rapidly performed, thus allowing the qualitative identification of sample sets. NIR analysis is also used to monitor the moisture content and finish-on-fiber of fibers and yarns, the content of sugars and the maturity of cotton fibers, the degree of mercerization of cotton fabrics, the polyester content in polyester/cotton blends, and the heat-set temperature of polyamide carpet yarns. By permitting the characterization of textile materials both accurately and quickly, with simple and easy-to-use procedures, NIR

Table 2.10 NIR analysis of textiles. Typical examples. Further details can be found in Ref. [47].

Polymer	Object of analysis
Cotton	Sugar and moisture content, fiber maturity, degree of mercerization, finish on the fiber surface
Polyester/cotton blends	Polyester content
Polyamide-6, polyamide-6,6	Moisture content, finish on the fiber surface, heat-set temperature

Lam Research Ex. 1047 - Page 81
Lam Research Corp. v. Inpria Corp.
IPR2024-00033 - U.S. Patent No. 9,823,564

methods demonstrate a clear potential for the online real-time analysis of textiles in production lines [36].

2.2.4
Far-IR Analysis of Polymers: Terahertz Spectroscopy

2.2.4.1 General Aspects

Terahertz spectroscopy emerged when it was first appreciated that THz radiation (covering the frequency range from about 0.1 to 10 THz) could propagate through air, from a transmitter to a detector [48]. Since then, sophisticated technological developments have led to a method that can be now considered as another weapon in the physical chemist's arsenal. The THz radiation sources applied to the field of polymers are mostly based on short-pulsed visible lasers with pulse widths ranging from 10 to 100 femtoseconds (fs), and consequently time-resolved far-IR studies with subpicosecond time resolution can be performed (see Section 2.5). Whilst this type of time-resolved investigation is most often related to *terahertz-time-domain spectroscopy*, there is also a significant potential for the use of THz spectroscopy in non-time-resolved studies, as will be demonstrated in the following subsections.

A schematic diagram of a time-domain spectrometer is shown in Figure 2.12, where a laser beam generated by a Ti:sapphire system (central wavelength 800 nm) is split into pump and probe beams. On striking the emitter, the pump beam generates THz pulses that are collimated and focused onto the sample by using parabolic reflectors. After transmitting the sample, the THz pulses are collimated and focused onto the detector. The probe beam is then used to gate the detector, so that the instantaneous THz electric field can be measured. A delay stage is used to

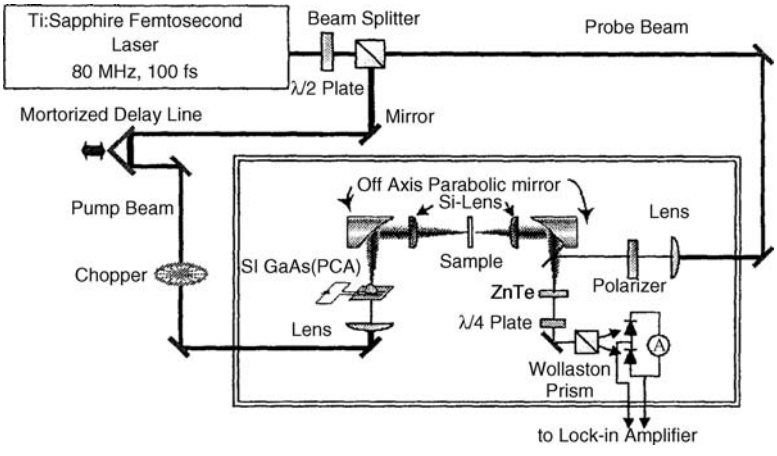


Figure 2.12 Schematic diagram of a time-domain spectrometer. Adapted with permission from Ref. [17]; © 2006, Korean Physical Society.

Lam Research Ex. 1047 - Page 82
Lam Research Corp. v. Inpria Corp.
IPR2024-00033 - U.S. Patent No. 9,823,564

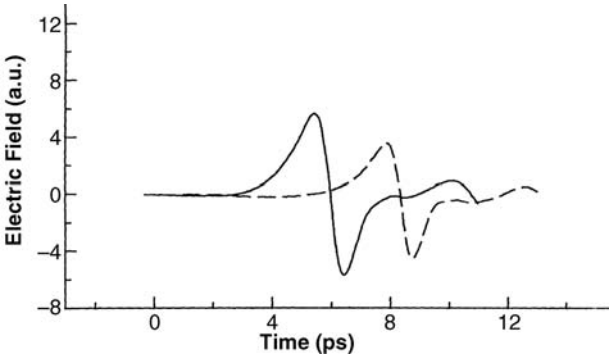


Figure 2.13 Waveforms of THz pulses propagating freely (solid line) and transmitting a silicon wafer (dashed line). Adapted with permission from Ref. [49]; © 2002, M.A. Kazan.

offset the pump and probe beams, which allows measurement of the temporal profile of the pulse's electric field.

When the THz wave transmits the sample, both the strength of the incident electric field and the phase speed are reduced. Figure 2.13 shows how, in the case of a silicon wafer, the waveform of a freely propagating THz pulse is changed, when the beam is passing the wafer. The waveform of a pulse propagating through a polyethylene sample, and the respective amplitude spectrum, are shown in Figure 2.14.

Taking into account both the reduced electric field strength and the reduced phase speed, the complex refractive index n^* can be obtained. For this purpose, the complex absorption spectrum of the pulse transmitting the sample is divided by the

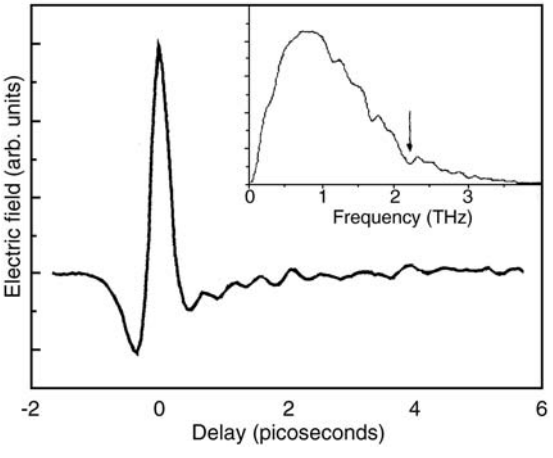


Figure 2.14 Waveform of a THz pulse propagating through a 1 cm-thick polyethylene sample. The inset shows the respective amplitude spectrum. Adapted with permission from Ref. [50]; © 2003, Springer.

Lam Research Ex. 1047 - Page 83
Lam Research Corp. v. Inpria Corp.
IPR2024-00033 - U.S. Patent No. 9,823,564

reference spectrum obtained by removing the sample from the beam. This yields $T^*(\omega)$, the frequency-dependent complex transmission function (complex transmittance) of the sample expressed by Equation 2.8:

$$\mathrm{T}^*(\omega) = \frac{\mathrm{E}(\omega)}{\mathrm{E}_{\mathrm{ref}}(\omega)} \tag{2.8}$$

where ω is the angular frequency ($\omega = 2\pi\nu$), and $E(\omega)$ and $E_{\mathrm{ref}}(\omega)$ denote the Fourier transforms of the pulse profiles recorded with the beam passing the sample or the reference, respectively. For flat samples placed in air, the complex refractive index $n^*(\omega) = n(\omega) - \mathrm{j}\kappa(\omega)$, can be calculated by numerically solving the Fresnel transmission equation (Equation 2.9) with the aid of an appropriate algorithm such as the Newton–Raphson algorithm [49].

$$T^*(\omega) = \frac{4n^* \exp\left[-\mathrm{i}\frac{\omega}{\mathrm{c}}(n^* - 1)d\right]}{(n^* + 1)^2\left(1 - \left(\frac{n^* - 1}{n^* + 1}\right)^2 \exp\left[-2\mathrm{i}\frac{\omega}{\mathrm{c}}(n^*)d\right]\right)} \tag{2.9}$$

where d is the sample thickness, c is the speed of light *in vacuo*, and $\kappa(\omega)$ is the extinction coefficient indicating the absorption of the radiation, and is related to the absorption coefficient $\alpha(\omega)$ via Equation 2.10:

$$\kappa(\omega) = \frac{\alpha(\omega)\mathrm{c}}{2\omega} \tag{2.10}$$

Data extraction algorithms developed for the evaluation of the real and the imaginary part of the complex refractive index – that is, of n and κ – are based on various assumptions such as homogeneity and flat and parallel surfaces of the sample, dry atmosphere at the measurement, and orthogonal incidence of the THz rays. Details of this have been described elsewhere [51–54]. According to Pupeza *et al.* [51], the decrease in the maximum signal amplitude $\mathrm{A}^{\max}$ is given by Equation 2.11:

$$\mathrm{A}^{\max}_{\mathrm{sample}} = \mathrm{A}^{\max}_{\mathrm{reference}} \exp\left(-\frac{\omega\kappa L}{\mathrm{c}}\right) \tag{2.11}$$

where $\mathrm{A}^{\max}_{\mathrm{sample}}$ and $\mathrm{A}^{\max}_{\mathrm{reference}}$ are the maximum signal amplitudes of sample and reference, respectively, and L is the sample thickness. κ, derived from Equation 2.11, is given by Equation 2.12:

$$\kappa = -\frac{\mathrm{c}}{\mathrm{L}\omega}\ln\frac{\mathrm{A}^{\max}_{\mathrm{sample}}}{\mathrm{A}^{\max}_{\mathrm{reference}}} \tag{2.12}$$

An initial value for the real refractive index n is derived from Δt, the time delay between $\mathrm{A}^{\max}_{\mathrm{sample}}$ and $\mathrm{A}^{\max}_{\mathrm{reference}}$. Δt is related to $\Delta n = n - n_0$, the difference in the refractive indices of the sample and reference (see Equation 2.13):

$$\Delta t = \frac{L\Delta n}{\mathrm{c}} \tag{2.13}$$

Lam Research Ex. 1047 - Page 84
Lam Research Corp. v. Inpria Corp.
IPR2024-00033 - U.S. Patent No. 9,823,564

From Equation 2.13 the refractive index n is obtained (see Equation 2.14):

$$n = \frac{c\Delta t}{L} + n_0 \tag{2.14}$$

2.2.4.2 Nondestructive Testing of Plastic Articles: THz Imaging

THz transmission time-domain spectroscopy (*TDS*) has the potential for determining the content of additives in polymeric systems in a contactless and nondestructive manner. The prerequisites are transparency or low absorptivity of the polymer matrix, and large differences in the refractive indices of polymer and additive at THz frequencies. THz TDS allows the determination of refractive index n and absorption coefficient α. Figure 2.15 shows typical results referring to polyethylene, polypropylene and polyamide containing the mineral additives $Mg(OH)_2$, $CaCO_3$, and SiO_2, respectively. From Figure 2.15a it can be seen that n is constant over frequency, while Figure 2.15b shows that n increases linearly with increasing additive content [55]. Therefore, the volumetric additive content in compounded polymeric systems can be obtained by making offline measurements of n. Moreover, THz measurements can also serve for the inline control of compounding processes, as demonstrated by taking real-time measurements of the refractive index of molten polymers passing an extruder, namely polypropylene containing $CaCO_3$ and polyamide-12 containing glass fibers [56].

The THz imaging of welded plastic sheets represents another interesting application where, in order to obtain images, the sheets are placed perpendicular to the THz beam and scanned in a raster pattern in two dimensions at a step width of 0.5 mm [57]. At each position, the waveforms of several pulses are acquired and averaged. On plotting the intensity of the transmitted beam, integrated over a

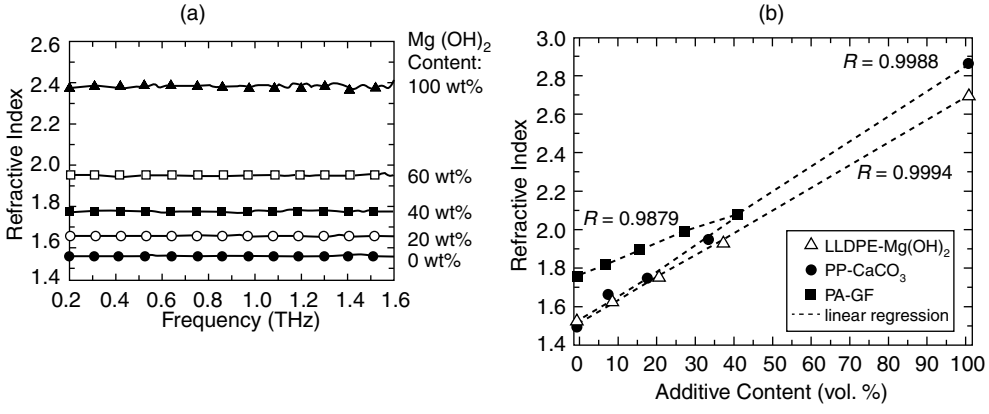


Figure 2.15 THz spectroscopy of additive/polymer systems. (a) Frequency dependence of the refractive index of the system polyethylene/$Mg(OH)_2$; (b) Refractive index as a function of additive content in polyethylene (LLDPE), polypropylene (PP) and polyamide (PA). GF: glass-fiber. Adapted with permission from Ref. [55]; © 1999, Elsevier.

Lam Research Ex. 1047 - Page 85
Lam Research Corp. v. Inpria Corp.
IPR2024-00033 - U.S. Patent No. 9,823,564

Table 2.11 Biopolymers examined with THz spectroscopy [58][a].

Polymer family	Polymer
Nucleic acids	DNA
	RNA
Polypeptides and Proteins	Bovine serum albumin
	Collagen
	Rhodopsin, bacteriorhodopsin, isorhodopsin
	Hen egg white lysozyme
	Horse heart myoglobin
	Cytochrome c
Polysaccharides	Cellulose
	Chitin

a) Spectra were taken by irradiating the polymer in the form of films or polyethylene pellets.

certain frequency range, two-dimensional images of the sheet are obtained that reveal the presence of any contaminating particles and delaminations. In addition, the thickness of the air layer between the sheets can be determined at any unwelded area.

2.2.4.3 THz Absorption by Biopolymers

THz absorption studies on nucleic acids, polysaccharides, polypeptides and proteins have been reviewed by Plusquellic and colleagues [58] (see also Table 2.11).

All biopolymers absorb THz radiation in the frequency range between 0.3 and 3 THz (10 and 100 cm^{-1}). Broadband absorption without any identifiable peaks was observed to increase with increasing frequency, and to level off in the range of 1.2 to 1.6 THz (40–60 cm^{-1}). The absorption coefficients depend on the state of conformation and the degree of hydration, the latter factor being determined by the relative humidity of the environment. In the case of cellulose, the THz absorption spectrum reportedly exhibits distinct absorption features which are attributed to interstrand twisting or stretching motions [58]. The otherwise-observed lack of distinct spectral features represents a severe limitation for biological applications, although with the aid of carefully determined absorption coefficients, information concerning the biomacromolecule and its environment can be obtained. Owing to associated differences in refractive indices between single- and double-stranded molecules, DNA samples of free strands and hybridized pairs can be readily distinguished using THz spectroscopy. Further modes of application pertain to label-free methods used in DNA analyzers and gene chips to identify polynucleotide base sequences. With regards to all types of biological macromolecules, it should be noted that THz spectroscopy can be used to acquire information relating to their conformational state and the dynamics of their hydrate shells (see Section 2.5.2).

2.2.4.4 THz Studies of Biopolymers in Liquid Water

In bulk liquid water, the molecules will form a hydrogen-bonded network that undergoes collective vibrations. In fact, the hydrogen bonds between single water

Lam Research Ex. 1047 - Page 86
Lam Research Corp. v. Inpria Corp.
IPR2024-00033 - U.S. Patent No. 9,823,564

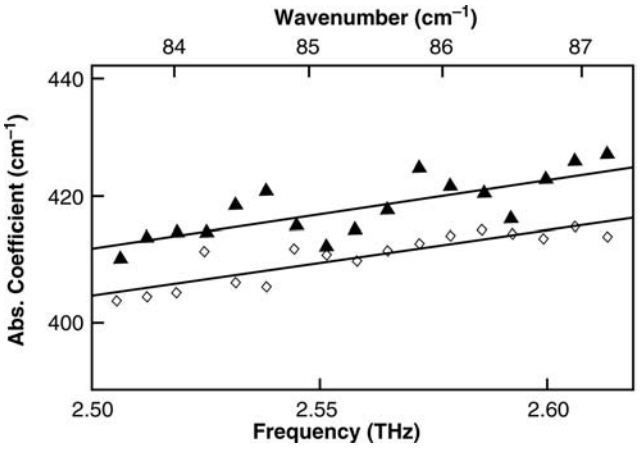


Figure 2.16 Absorption of THz radiation by an aqueous solution of ubiquitin. Absorption coefficient versus frequency. Upper curve: ubiquitin (0.59×10^{-3} mol l^{-1}) in magnesium acetate buffer solution (50×10^{-3} mol l^{-1}). Lower curve: buffer solution without ubiquitin. Sample thickness: 52.6 μm. Adapted with permission from Ref. [59]; © 2009, Royal Society of Chemistry.

molecules are continuously broken and reformed within picoseconds. As revealed by THz spectroscopy, the water network is disturbed by solutes, and even at low concentrations the protein molecules will bring the water molecules more in line with each other; that is, the motions of the water molecules are altered by the protein. This influence extends over several solvation shells, and can involve up to 1000 water molecules per macromolecule. The addition of a protein to water can result in either an increase or a decrease in the THz absorption, depending on the way in which the protein couples with the collective vibrations of the water network. The determining factors in this respect are the protein's configuration and flexibility [59]. In the case of ubiquitin, absorption is increased upon addition of the protein to a buffer solution as can be seen from Figure 2.16. Such an increase in absorption can be explained by assuming an increase in the absorption coefficient of the dynamic hydration shell formed around the protein molecule relative to that of bulk water. The presence of protein molecules affects the reorientation rate of the dipole moments of proximate water molecules in the hydrogen-bonded network. As the effect of the protein on the molecules of the hydration shell depends sensitively on the protein structure, the rate of structural changes such as protein folding and unfolding can be followed by using THz spectroscopy. In fact, folded proteins exhibit a different influence on the network of water molecules in the surrounding hydration shell than do unfolded proteins.

2.2.4.5 Generation of THz Radiation in Poled Polymers

Terahertz radiation can be generated with the aid of certain polymer systems that are irradiated with 800 nm pulses (duration of less than 200 fs) emitted from a Ti: sapphire laser system. A prerequisite for the generation of THz radiation is the

Lam Research Ex. 1047 - Page 87
Lam Research Corp. v. Inpria Corp.
IPR2024-00033 - U.S. Patent No. 9,823,564

presence of electro-optic properties; that is, the polymers should possess a sufficiently large macroscopic second-order nonlinear optical susceptibility, $\chi^{(2)}$. This property can be induced in certain polymers by poling – that is, by annealing the polymer under the influence of a strong electric field. When the electric field is switched off, the polymers retain a dipole moment such that they have become *ferroelectric*. This behavior has been observed, for example, with guest/host mixtures of dye molecules (25%) embedded in poly(methylmethacrylate) (*PMMA*) [60] or with a copolymer of 4-*N*-ethyl-*N*-(2-methacryloxyethyl)amine-4′-nitroazobenzene (*MA1*) (16.5 mol%), and methylmethacrylate (*MMA*) (Chart 2.4). In the latter case, Corona poling was performed with 16 μm-thick standing films at a poling field of 1.75 MV cm^{-1} [61]. Radially polarized THz radiation can be produced from a metal wire which has been partially overcoated with a copolymer of MMA and MA1 [62].

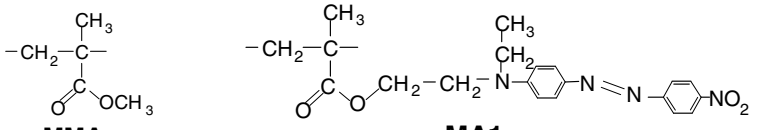


Chart 2.4 Chemical structures of repeating units of copolymers suitable for poling by an electric field.

The generation mechanism is related to *optical rectification*, a nonlinear optical process that involves the mixing of waves – for example, two waves having frequencies ν_1 and ν_2. The mixing process may result in the generation of radiation of the difference frequency ($\nu_1 - \nu_2$). As the NIR pulses emitted from a Ti:sapphire laser have a rather large bandwidth, the high-frequency component can mix with the low-frequency component within a given pulse to produce a pulse of the difference frequency. This difference falls into the THz range in the case of pulse durations of approximately 100 fs [32].

2.2.5 Special Applications

2.2.5.1 Thin Polymer Films

One interesting aspect of the application of IR spectroscopy relates to thin (micrometer) and ultrathin (≤50 nm) polymer films, polymer surfaces, and polymer–substrate interfaces [23]. So-called *external reflection* methods can be used to determine the important properties of thin films (comprising monolayers and multilayers) such as thickness, anisotropy, molecular orientation, and composition. The most frequently applied methods include IR ellipsometry (IRE) [63–67] and IR reflection absorption spectroscopy (IRRAS), which may also be referred to as reflection absorption infrared spectroscopy (*RAIRS*) [1,23].

IRE Techniques IRE involves taking measurements of the state of polarization of reflected light. As illustrated in Figure 2.17, linearly polarized light is specularly

Lam Research Ex. 1047 - Page 88
Lam Research Corp. v. Inpria Corp.
IPR2024-00033 - U.S. Patent No. 9,823,564

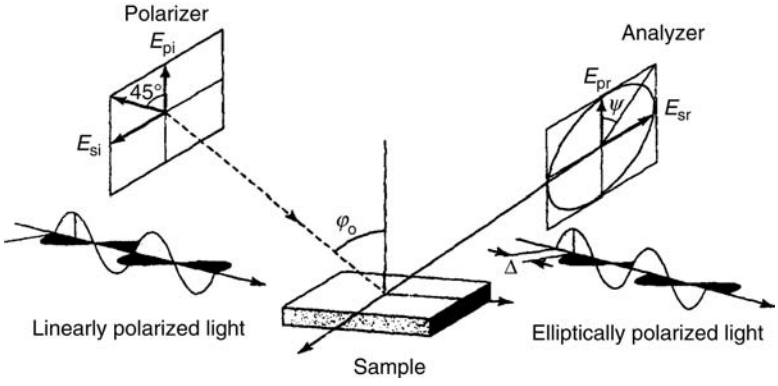


Figure 2.17 Typical optical system used for infrared ellipsometry (IRE) measurements. Adapted with permission from Ref. [68]; © 2005, Society for Applied Spectroscopy.

reflected from the sample's surface and becomes elliptically polarized (which gives the method its name).

The orthogonal vibrational amplitudes r_p and r_s (complex reflection coefficients) for p- and s-polarized incident light are defined according to the expressions given by Equation 2.15:

$$r_p = \frac{E_{pr}}{E_{pi}} \qquad r_s = \frac{E_{sr}}{E_{si}} \tag{2.15}$$

Here, p- and s-polarization refers to the polarization of the electric field vector within (p) and orthogonal to (s) the plane of incidence, as depicted in Figure 2.17.

The phase difference Δ and the ratio ρ of the orthogonal vibrational amplitudes are related according to Equation 2.16:

$$\rho = \frac{r_p}{r_s} = \tan\psi e^{i\Delta} \tag{2.16}$$

Equation 2.16 is valid for homogeneous systems with smooth and parallel interfaces. Δ and $\tan\psi$ are functions of the angle of incidence, the wavelength, the optical constants of substrate, layer and ambient medium, and of the layer thickness.

Typically, $\tan\psi$ and Δ are determined from intensity (I) measurements at four azimuthal angles (0°, 45°, 90°, 135°) of the polarizer at a fixed position of the analyzer (45°) with the aid of Equations 2.17 and 2.18 [68]:

$$\cos 2\psi = \frac{I(90^\circ) - I(0^\circ)}{I(90^\circ) + I(0^\circ)} \tag{2.17}$$

$$\sin 2\psi \cos\Delta = \frac{I(45^\circ) - I(135^\circ)}{I(45^\circ) + I(135^\circ)} \tag{2.18}$$

By fitting the parameters of an optical model to the experimental values of Δ and $\tan\psi$, the layer thickness and the optical constants of the sample can be obtained [64,65,67,68].

Lam Research Ex. 1047 - Page 89
Lam Research Corp. v. Inpria Corp.
IPR2024-00033 - U.S. Patent No. 9,823,564

A more straightforward method of evaluating ellipsometric data involves the determination of the so-called pseudo-optical constant $\langle \check{n} \rangle$ with the aid of Equation 2.19. $\langle \check{n} \rangle$ is the square-root of the pseudo-dielectric function $\langle \varepsilon \rangle$ ($\langle \check{n} \rangle = \langle \varepsilon \rangle^{0.5}$).

$$\langle \check{n} \rangle = \sin^2 \varphi_0 \left[1 + \left(\frac{1-\rho}{1+\rho} \right)^2 \tan^2 \varphi_0 \right] \tag{2.19}$$

where φ_0 is the angle of incidence. $\langle \check{n} \rangle$ represents the optical properties of the total sample, that is, layer plus substrate and, therefore, Equation 2.19 can be utilized only if the substrate is transparent.

By using IRE, optical constants (refractive indices, absorption constants) of thin polymer layers having thicknesses ranging from micrometers down to single molecular layers can be determined [68,69]. Some typical results are presented in Figure 2.18, where the wavelength dependence of optical constants of two isotropic polymers is shown. This type of data serves to characterize multilayer systems with respect to important properties such as composition, miscibility, interdiffusion, and interaction at interfaces [68].

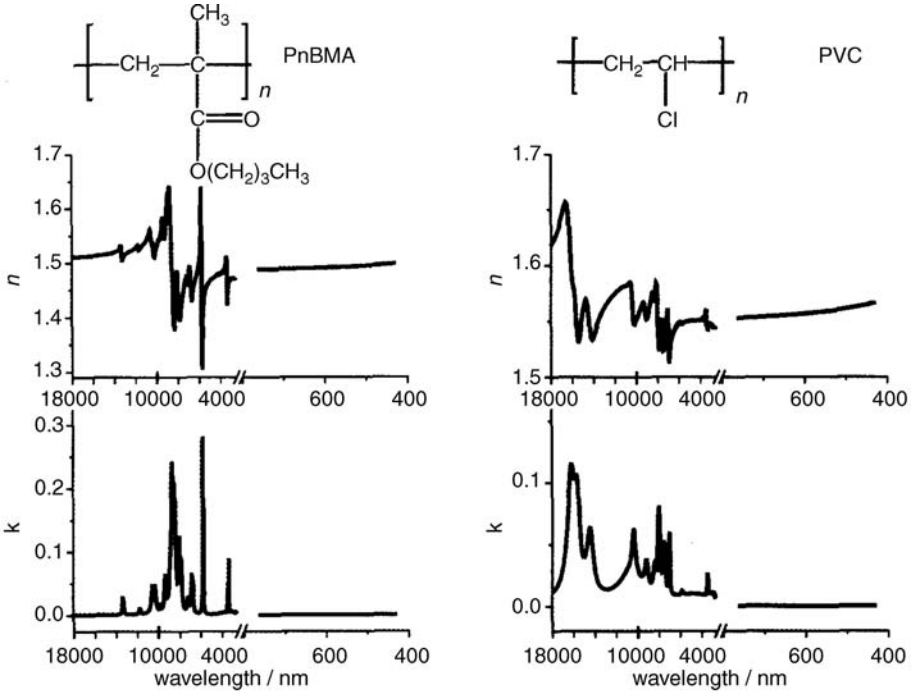


Figure 2.18 Infrared ellipsometry (IRE). Wavelength dependence of refractive index (n) and absorption constant (k) of single isotropic polymer films on gold-coated glass substrates. PnBMA: poly(n-butyl methacrylate), $d = 98.5$ nm. PVC: poly(vinyl chloride), $d = 104$ nm. Adapted with permission from Ref. [69]; © 2007, John Wiley & Sons.

Lam Research Ex. 1047 - Page 90
Lam Research Corp. v. Inpria Corp.
IPR2024-00033 - U.S. Patent No. 9,823,564

With regards to stratified systems, it is noticeable that the layer thickness can, in principle, be determined by using the ellipsometric method. However, this does not hold for ultrathin films (monolayers and multilayers) because the influence of anisotropy, molecular density, and thickness cannot be discriminated in this case [68].

IRRAS Techniques IRRAS is based on measuring the wavelength dependence of the reflectance R, as defined by Equation 2.20:

$$R = \frac{I_{\text{reflected}}}{I_{\text{incident}}} \tag{2.20}$$

where $I_{\text{reflected}}$ and I_{incident} denote the intensity of the reflected light beam and the corresponding light beam incident on the sample at a grazing angle, respectively. IRRAS is commonly employed to examine thin layers on metal substrates characterized by a high reflectivity, the latter effect being due to the absorption of light by conduction band electrons, followed by a rapid emission. The use of metal substrates has the advantage that the incident and reflected waves can combine to form a standing wave. When radiation is reflected from a metal surface, a phase change occurs, with the phase of s-polarized radiation always changing by 180°. As a result, a standing wave is not formed since the electromagnetic field intensity is zero. For p-polarized radiation, however, a standing wave forms and the phase change depends heavily on the incident angle φ_0. At $\varphi_0 = 87°$, the phase change is 90° and the incident and reflected beams strengthen each other at the metal's surface. The strong electric field of the combined rays is polarized in the plane defined by the beam direction and the surface normal, and this determines the appearance of reflection-absorption spectra. In fact, only vibrational modes with dipole moment components perpendicular to the reflecting surface will give rise to absorption bands, which allows the evaluation of molecular orientation in ultra-thin films. When light of a certain wavelength is absorbed by a thin film on a metal surface, the change in reflectance is given by Equation 2.20:

$$\frac{\Delta R}{R_0} = \frac{R_0 - R}{R_0} = \frac{4n_1^3 \sin^2 \varphi_0}{n_2^3 \cos \varphi_0} \alpha d \tag{2.20}$$

where R_0 and R are the reflectance without and with film, respectively, n_1 and n_2 are the refractive indices of the ambient medium and film, respectively, φ_0 is the incident angle, α is the absorption coefficient, and d is the film thickness. In practice, reflection spectra are often represented in terms of the reflectance absorbance (RA) defined by Equation 2.21:

$$\text{RA} = -\log \frac{R}{R_0} \tag{2.21}$$

Typical IRRAS spectra of polymer films deposited by the plasma polymerization of hexamethyldisilane, $(CH_3)_3$-Si-Si-$(CH_3)_3$, on metal substrates (gold-coated glass, pure iron) in a microwave reactor are shown in Figure 2.19.

Lam Research Ex. 1047 - Page 91
Lam Research Corp. v. Inpria Corp.
IPR2024-00033 - U.S. Patent No. 9,823,564

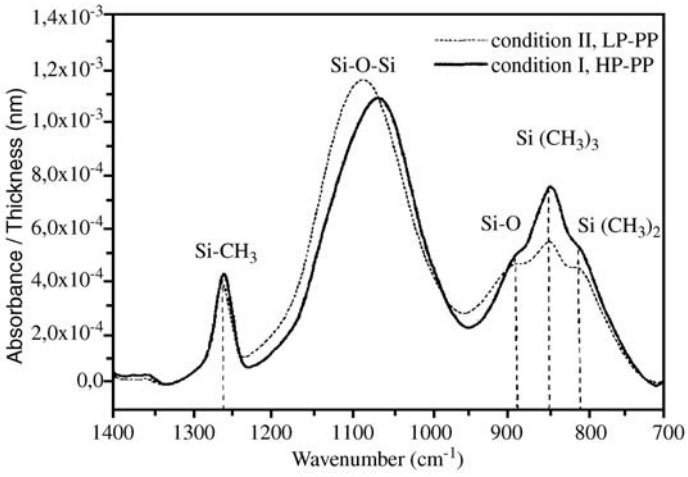
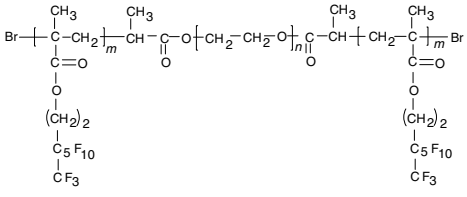
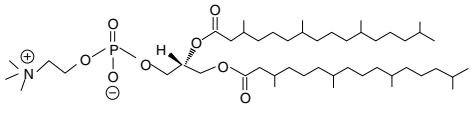


Figure 2.19 Reflection absorption infrared spectroscopy (IRRAS). Absorption spectra of polymer films formed by plasma deposition of hexamethyldisilane on a metal substrate at 0.18 mbar (condition I) and 0.05 mbar (condition II). Adapted with permission from Ref. [70]; © 2003, Elsevier.

The IRRAS method is also employed for liquid samples that can be poured into a Teflon® trough [71]. In this context, IRRAS investigations on protein monolayer films at the air/water interface pertaining to the orientation of secondary structures are worthy of mention [71,72]. Figure 2.20 shows the IRRA spectra of monolayer films of an amphiphilic triblock copolymer and of the lipid DPhPC (Chart 2.5) spread at water.



PFMA-*b*-PEO-*b*-PFMA



DPhPC

Chart 2.5 Chemical structure of triblock copolymer of ethylene oxide and perfluorohexylethyl methacrylate, PFMA-*b*-PEO-*b*-PFMA and 1,2-diphytanoyl-*sn*-glycero-3-phosphocholine, DPhPC.

Both spectra exhibit a strong band at about 3600 cm^{-1} due to the O—H stretching vibration of water, while the broad band at 1090 cm^{-1} of the block copolymer spectrum is due to the C—O vibration. In the case of mixed monolayers containing both triblock copolymer and DPhPC, the C—O band decreases with increasing surface pressure π and is no longer detectable at $\pi > 33\,mN\,m^{-1}$, indicating that the polymer chains are being squeezed out of the lipid monolayer [73].

Lam Research Ex. 1047 - Page 92
Lam Research Corp. v. Inpria Corp.
IPR2024-00033 - U.S. Patent No. 9,823,564

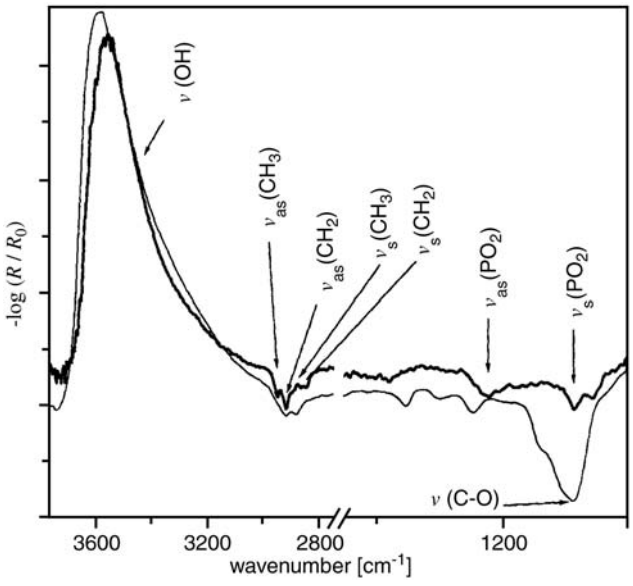


Figure 2.20 IRRA spectra of DPhPC (bold line) and of PFMA-*b*-PEO-*b*-PFMA (full line) films at the air/water interface, recorded at a surface pressure of 36.7 and 40.0 mN m^{-1}, respectively. Adapted with permission from Ref. [73]; © 2004, American Chemical Society.

When applying the IRRAS method, problems often arise due to the very weak reflection signal and to disturbing atmospheric absorption caused by water vapor and CO_2. However, these problems can be overcome with the aid of a polarization modulation technique, a schematic diagram of which is shown in Figure 2.21. Here, the incident light beam is directed to a photoelastic modulator (*PM*) which produces a periodic change between the p- and s-polarization of the beam at a fixed frequency (typically 62 kHz). After being reflected by the sample the beam strikes the detector, where the modulated reflectivity is recorded. Further details of this method are available elsewhere [71,74].

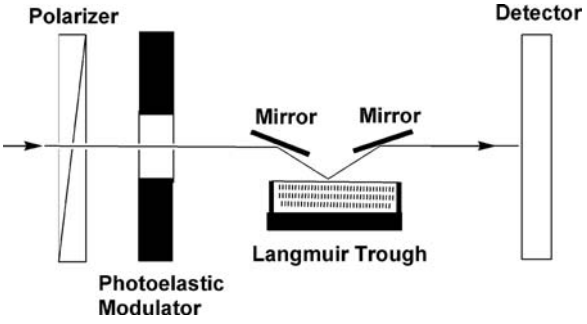


Figure 2.21 Schematic diagram of a PM-IRRAS set-up. In part adapted with permission from Ref. [74]; © 1994, Elsevier Sequoia.

Lam Research Ex. 1047 - Page 93
Lam Research Corp. v. Inpria Corp.
IPR2024-00033 - U.S. Patent No. 9,823,564

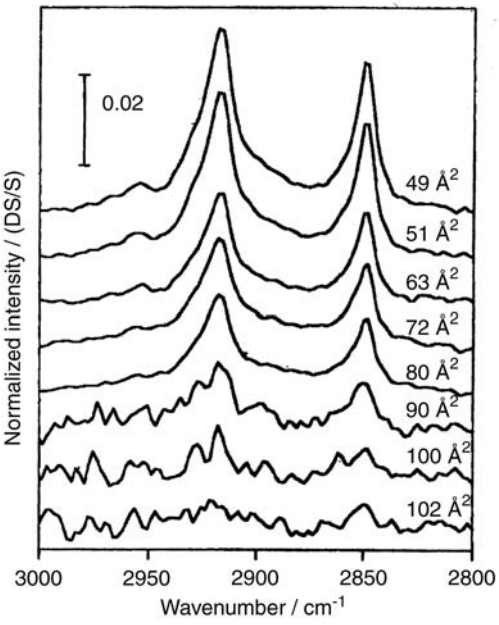


Figure 2.22 Normalized PM-IRRA spectra of HPC-C16 spread as a monolayer at the air/water interface, recorded at various surface pressures as indicated in the graph in units of area per anhydroglucose repeat unit. Adapted with permission from Ref. [75]; © 1998, Elsevier Science.

The high-frequency modulation between s- and p-polarization allows a simultaneous measurement of the difference spectrum between s- and p-polarized incident light. The PM-IRRA method yields the polarization modulated reflectivity S, as defined by Equation 2.23 [71,74].

$$S = \mathrm{C}\frac{J_2(\Phi_0)(R_\mathrm{p} - R_\mathrm{s})}{(R_\mathrm{p} + R_\mathrm{s})J_0(\Phi_0)(R_\mathrm{p} - R_\mathrm{s})} \tag{2.23}$$

where R_p and R_s are the reflectivities for p- and s-polarization, J_0 and J_2 are the zero- and second-order Bessel functions of the maximum dephasing Φ_0 introduced by the photoelastic modulator, and C is an apparatus constant. Commonly, spectral data are plotted as $(S - S_0)/S_0$ as a function of the wavenumber. Here, S and S_0 denote the polarization-modulated reflectivities of the film-covered and film-free water surface, respectively. Figure 2.22 shows typical PM-IRRA spectra recorded with monolayers of a cellulose alkyl ether, HPC-C16 (Chart 2.6). The increase in intensity of the bands with decreasing molecular area is due to an increase in the surface density of the absorbing groups, and also to changes in the alkyl side-chain orientation.

2.2.5.2 **Orientation Measurements**

The IR dichroism technique is frequently applied for the characterization of anisotropy in polymers (see Section 2.1.3). Optical anisotropy is exhibited by highly

Lam Research Ex. 1047 - Page 94
Lam Research Corp. v. Inpria Corp.
IPR2024-00033 - U.S. Patent No. 9,823,564

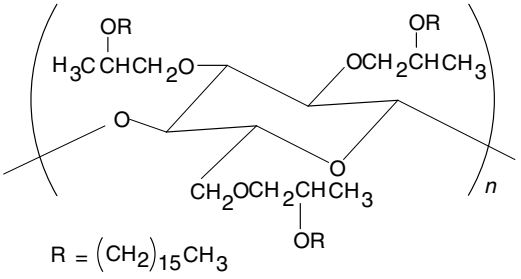


Chart 2.6 Chemical structure of 2-hydroxypropyl cellulose (HPC-C16) substituted by reaction with 1-bromohexadecane.

viscous or rigid polymeric materials containing macromolecules aligned in a specific direction. Orientation can be achieved in various ways, including mechanical alignment, Langmuir–Blodgett film deposition, liquid crystalline self-organization, and by alignment on specific substrates. Often, polymer systems are subjected to stress during fabrication, with such stress being applied either in one direction (uniaxial stretching) or along two perpendicular directions (biaxial stretching). Anisotropy in polymer materials can be detected by measuring the absorption of linearly polarized light, both parallel and perpendicular to the draw direction (see Section 2.1.3). The extent of anisotropy is characterized either by the dichroic ratio $R_{\text{dichro}} = A_{||}/A_{\perp}$, the ratio of the absorbance parallel and perpendicular to the draw direction, respectively, by the dichroic difference $\Delta A = A_{||} - A_{\perp}$, or by the in-plane order parameter $S = (A_{||} - A_{\perp})/(A_{||} + A_{\perp})$. Figure 2.23 a and b show the IR spectra of an isotactic polypropylene specimen recorded during uniaxial stretching. Here, the radiation was polarized either parallel or perpendicular to the draw direction, and the increase in the dichroic ratio of the bands at 975 and 999 cm^{-1} with strain is characterized by several ranges with plateau regions (see Figure 2.23c). The 975 cm^{-1} band is due to strongly coupled CH_3 and C—C backbone vibrations, while the 999 cm^{-1} band is due to strongly coupled CH_3, C—CH_3, CH, and CH_2 vibrations. The changes in the range from 50% to 150% strain are due to the alignment of methyl side groups and parallel alignment of the polymer helix axes in relation to the draw direction. Changes above 250% strain reflect slippage processes of conformationally regular polymer chains in the crystalline phase.

Interestingly, IR dichroism studies on liquid crystalline polymers can reveal some insight into the mechanism of mechanical stress-induced orientation processes. For example, in studies with polyurethanes carrying mesogenic side chains (Chart 2.7), it was found that an initially stress-induced orientation system would be broken up and reoriented when the strain surpassed a critical value [77].

The copolymer of the structure depicted in Chart 2.7 consists of hard and soft segments. Both of these are largely incorporated into domains, with the hard segments in H-bonded domains and the soft segments in liquid crystalline smectic layers.

Lam Research Ex. 1047 - Page 95
Lam Research Corp. v. Inpria Corp.
IPR2024-00033 - U.S. Patent No. 9,823,564

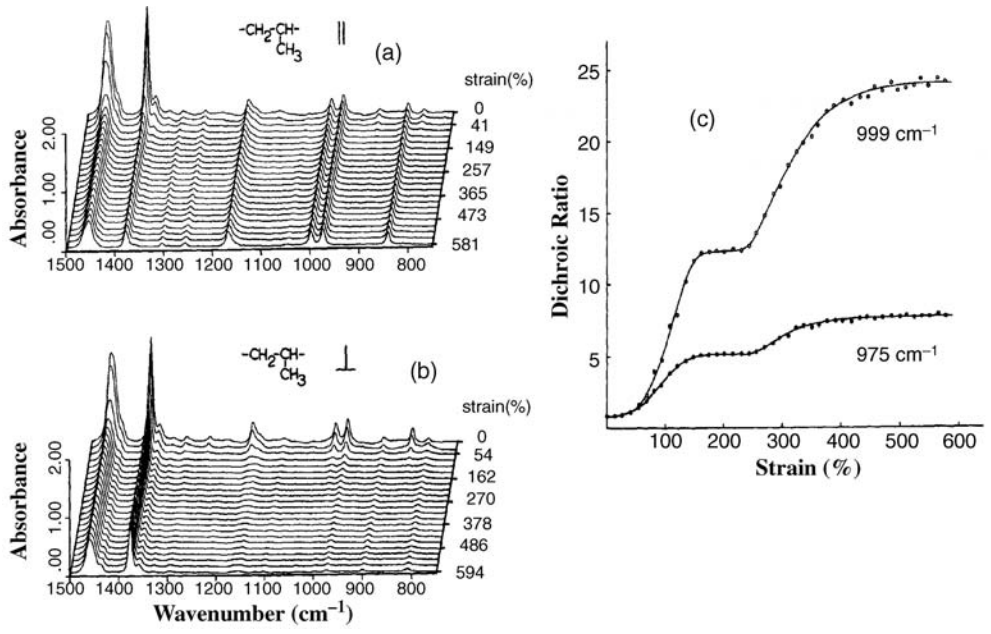


Figure 2.23 Infrared spectra recorded during uniaxial deformation of isotactic polypropylene with radiation polarized either parallel (a) or perpendicular (b) to the draw direction. (c) Dichroic ratio at 975 and 999 cm^{-1} as a function of strain. Adapted with permission from Ref. [76]; © 1980, Marcel Dekker.

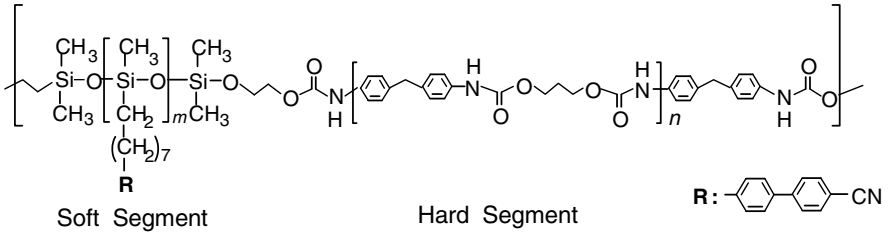


Chart 2.7 Chemical structure of a copolymer consisting of polyurethane segments and polysiloxane segments with a cyanodiphenyl mesogen groups. The latter are capable of forming smectic phases.

Under a strain below 40%, both domains tend to align perpendicular to the stress direction, and the individual mesogens are aligned parallel to the stress direction. At a strain above 40%, however, both the liquid crystalline smectic domains and the hard segment domains reorient parallel to the stress direction; this is shown schematically in Figure 2.24.

Note that the transverse anchoring of the liquid crystalline smectic layers with respect to the hard domains is maintained during the reorientation process. These conclusions are based on the strain dependence of the dichroic ratio of the bands at

Lam Research Ex. 1047 - Page 96
Lam Research Corp. v. Inpria Corp.
IPR2024-00033 - U.S. Patent No. 9,823,564

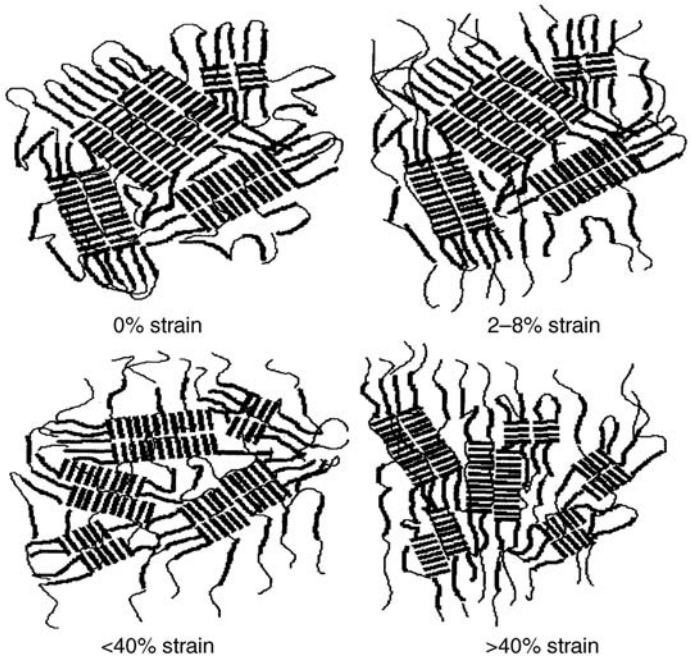


Figure 2.24 Schematic depiction of stress-induced changes in orientation of domains consisting of soft and hard segments of a polysiloxane/polyurethane copolymer of the structure presented in Chart 2.7. Adapted with permission from Ref. [78]; © 2000, Elsevier.

2225 cm^{-1} and 1717 cm^{-1}, which pertain to the cyano groups of the soft segments and the carbonyl groups of the hard segments, respectively. In both cases, the dichroic ratio increases with strain and passes through a maximum at about 40% strain, as can be seen in Figure 2.25.

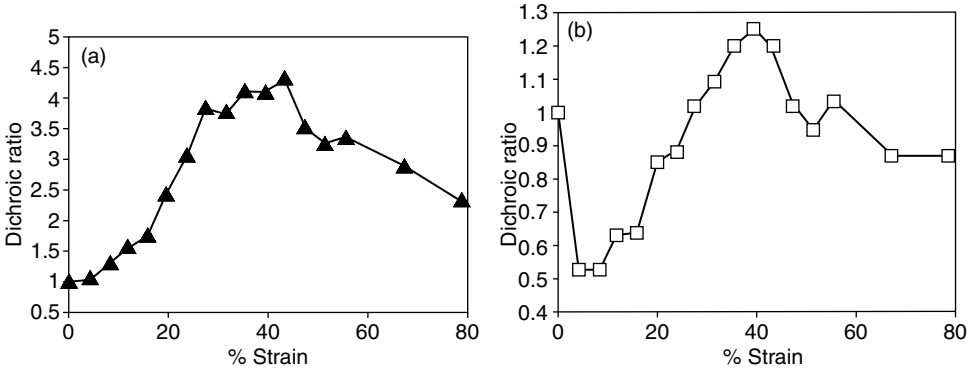


Figure 2.25 Dichroic ratio of the cyano group band at 2225 cm^{-1} (a) and the carbonyl group band at 1717 cm^{-1} (b) as a function of strain. Adapted with permission from Ref. [78]; © 2000, Elsevier.

Lam Research Ex. 1047 - Page 97
Lam Research Corp. v. Inpria Corp.
IPR2024-00033 - U.S. Patent No. 9,823,564

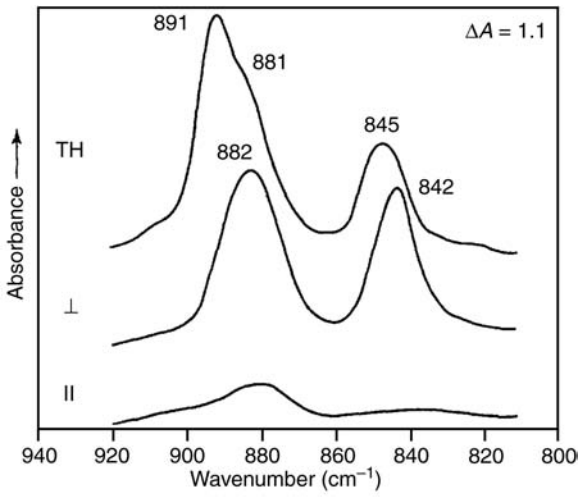


Figure 2.26 Infrared spectra of stretched poly(vinylidene fluoride) recorded through the thickness (TH) and in the directions parallel (||) and perpendicular (⊥) to the draw direction. Adapted with permission from Ref. [79]; © 1986, Wiley-VCH.

As noted above, IR dichroic measurements can be used to measure the orientation in thin films. However, in reality polymeric materials often have orientation with a three-dimensional character, which can be characterized by using trichroic IR measurements with the aid of a tilting apparatus [9b]. The latter is constructed such that the sample can be rotated about a horizontal and a vertical axis, both of which are orthogonal to the light propagation direction. Three-dimensional information is obtained by rotating the sample on the axis perpendicular to the incident electric vector. Typical results referring to poly (vinylidene fluoride), when oriented and annealed under stress, are presented in Figure 2.26. Apart from differences in the peak amplitude of $A_{||}$, $A_{\perp}$, and A_{TH}, there are also frequency shifts which are attributed to defect structures in the crystal lattice [79].

Finally, reference is made to the *dynamic dichroic absorption difference*, which is related to an absorption change induced by an external time-dependent perturbation. *Dynamic absorption spectroscopy* is performed with linearly polarized IR light and serves for example to detect intermolecular hydrogen bonds in polyamides of the structure

$$> N—H \cdots O = C <$$

Here, the H-bonds enforce an increase in the length of adjacent bonds, which leads to lower stretching frequencies. When H-bonds are weakened or destroyed, however, the position of IR absorption bands related to the stretching vibrations of N—H and C=O are blue-shifted. This technique has been employed to detect hydrogen bonds in polyester urethanes and polyamide-6 that had been exposed to sinusoidally varying strain at a stretching frequency of

Lam Research Ex. 1047 - Page 98
Lam Research Corp. v. Inpria Corp.
IPR2024-00033 - U.S. Patent No. 9,823,564

10 Hz [80]. In such experiments, dynamic spectra were obtained by subtracting the recorded spectra from a reference spectrum. Further details on this topic are available in Ref. [1].

Dynamic absorption spectroscopy has also been used to study the molecular origins of macroscopic rheological properties of organic polymers, and several relevant reports on this topic have been reviewed by Gregoriou *et al.* [77].

2.2.5.3 IR Microspectroscopy and IR Imaging

The so-called *microspectroscopy mapping technique* has been developed by attaching a microscope equipped with special reflecting-type optics and focal plane array detectors to FTIR spectrophotometers.

This technique allows microscopic areas to be examined and, in the case of polymers, it has been used to study multicomponent systems, and in particular to characterize heterogeneities in solid-state polymer blends. The most popular types of analysis involve transmittance and reflectance techniques, whereby FTIR microscopes employ reflecting mirrors rather than the lenses which are used in microscopes operating with visible light (see Figure 2.27).

The mid-IR region of the spectrum is particularly suited to polymers, and in this context it is notable that IR synchrotron radiation can serve as a high-brightness source for microspectroscopy in the mid-IR region [81,82]. The brightness advantage of IR synchrotron radiation over thermal IR light sources amounts to almost three orders of magnitude. The most important applications of the IR mapping technique involve biological objects, notably because very small specimens (down to the size of single biological cells) can be

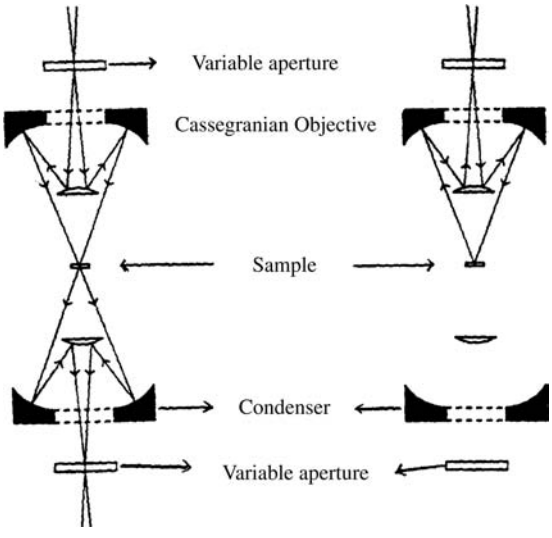


Figure 2.27 General layout of FTIR microspectroscopy mapping set-ups operating in transmission (left) and reflection (right) modes. Adapted with permission from Ref. [1]; © 2001, Elsevier.

Lam Research Ex. 1047 - Page 99
Lam Research Corp. v. Inpria Corp.
IPR2024-00033 - U.S. Patent No. 9,823,564

examined. One such example is the ability to analyze single lymphocytes, with normal cells being differentiated from their leukemic counterparts on the basis of their DNA/protein and RNA/protein ratios [45,83]. Another example has involved the identification of the secondary structure of amyloid plaques in the brains of humans with Alzheimer's disease, as these tissues can be readily imaged using synchrotron FTIR microspectroscopy [82]. Additional, detailed information relating to the IR microspectroscopy of polymeric systems is available in various reviews [31,84,85].

The subject of IR and Raman-spectroscopic imaging has been covered comprehensively in a recent book [86]. In contrast to mapping, modern imaging techniques are based on the use of focal plane array detectors which allow the rapid characterization of multicomponent polymer samples such as blends of PMMA or poly(ethylacrylate) with polystyrene, or of poly(3-hydroxybutyrate) with poly(lactic acid).

2.3 Polymer Characterization by Two-Dimensional IR Spectroscopy

The development of laser systems generating high-power femtosecond pulses (typical length 100 fs) has led to the creation of nonlinear two-dimensional infrared spectroscopy (*2D-IRS*) which could be termed the IR version of correlation spectroscopy [87]. This technique allows couplings and correlations between molecular vibrations to be detected whilst, in the case of polymers, investigations can also be made into the secondary structure and dynamics of proteins by performing experiments in the 1600–1700 cm^{-1} region, pertaining to amide I vibration modes.

Two main techniques are available to perform 2D-IRS, namely a *pulsed-frequency-domain technique* [88] and a *time-domain-pulsed-Fourier transform technique* [89]. A hybrid method using acousto-optic modulation has also been proposed recently [90]. In the pulsed-frequency-domain experiments, an intense broadband femtosecond pulse is split into a pump pulse, which passes a filter to reduce the band width to sections of typically 10 cm^{-1}, and an unfiltered probe pulse. Both pulses are focused into the sample within an adjustable time delay. The probe pulse (full bandwidth) measures the spectral changes of the sample after the arrival of the pump pulse. For this purpose, the intensity of the probe light beam is recorded using a spectrometer equipped with a broadband array detector.

In time-domain-pulsed Fourier transform experiments, the pumping is done by two phased-locked spectrally broad femtosecond pulses that interfere on the sample. Identical probe processes are employed for both techniques, and the recorded signals are displayed two-dimensionally; thus, the probe axis represents the frequency of the spectrometer and the pump axis the frequency of the narrow band pump pulse. 2D-IR spectra referring to a two-vibrator system in the uncoupled and coupled states are shown schematically in Figure 2.28a and b, respectively, together with the corresponding energy level schemes.

Lam Research Ex. 1047 - Page 100
Lam Research Corp. v. Inpria Corp.
IPR2024-00033 - U.S. Patent No. 9,823,564

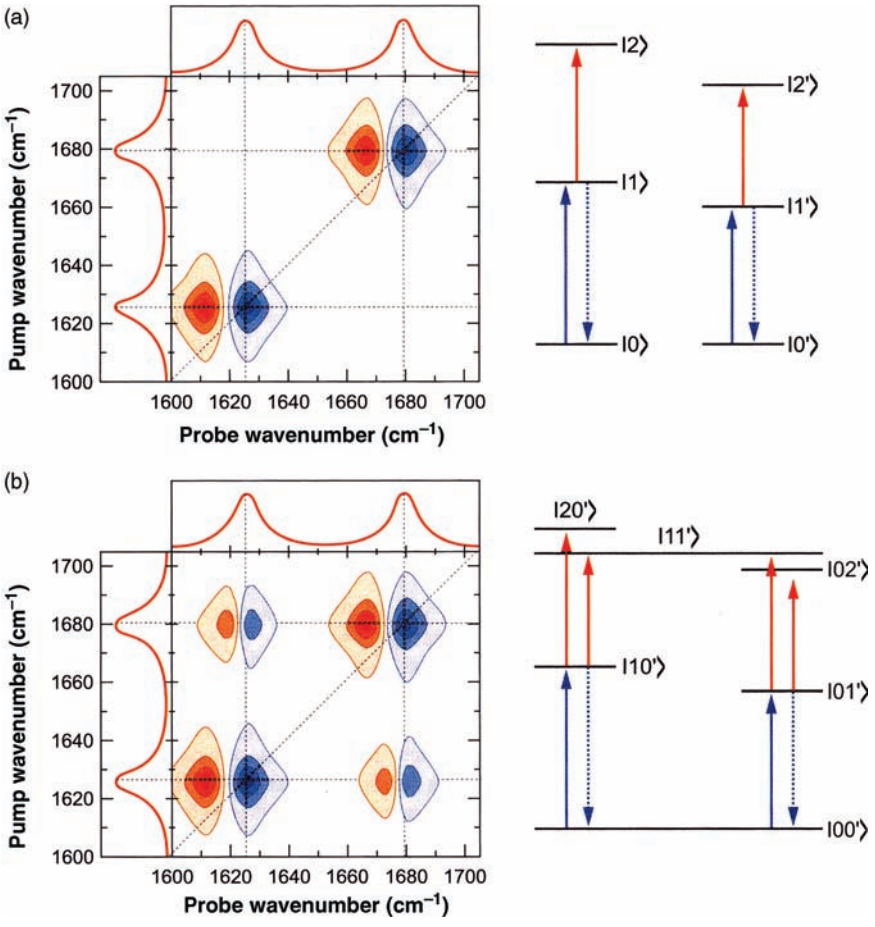


Figure 2.28 General representation of two-dimensional IR spectra and corresponding energy level schemes of a two-vibrator system in the uncoupled (a) and coupled (b) state. Blue peaks on the right side: negative peaks (related to bleaching and stimulated emission). Red peaks on the left side: positive peaks (related to excited state absorption). Adapted with permission from Ref. [91]; © 2008, Annual Reviews.

If the vibrators are not coupled, the spectrum will exhibit two peaks for each vibrator on the diagonal. These peaks are related to the $0 \rightarrow 1$ transition, reflecting bleaching and stimulated emission, and to the $1 \rightarrow 2$ transition, reflecting excited state absorption. The separation of the peaks is due to the anharmonicity – that is, to the fact that $\Delta E_{1\rightarrow 2} < \Delta E_{0\rightarrow 1}$ (see Section 2.1.1). If the vibrators are coupled, additional peaks (so-called *cross peaks*) appear in the off-diagonal areas of the spectrum. The appearance of the cross-peaks can be explained in terms of an additional energy level denoted by "$|11'>$" in the energy level scheme of Figure 2.28b. In fact, 2D-IR spectra contain both positive and negative peaks, the

Lam Research Ex. 1047 - Page 101
Lam Research Corp. v. Inpria Corp.
IPR2024-00033 - U.S. Patent No. 9,823,564

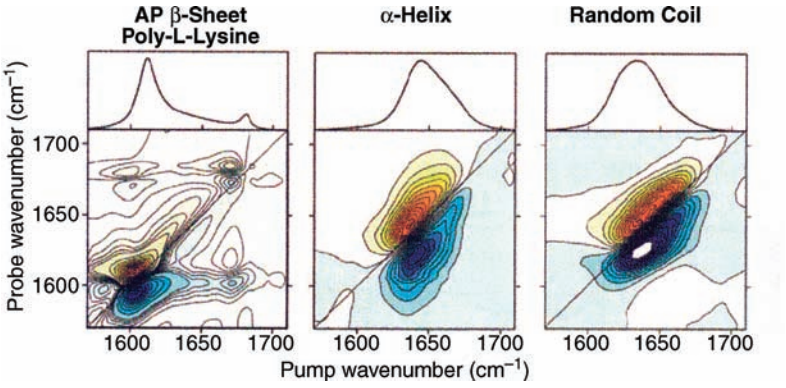


Figure 2.29 FTIR spectra (upper) and 2D-IR spectra (lower) of three secondary structure motifs of poly-L-lysine. Adapted with permission from Ref. [93]; © 2008, American Chemical Society.

former being related to excited-state absorptions and the latter to bleaching and stimulated emission.

Recently, 2D-IR spectroscopy has been applied successfully to peptides and proteins, with the most important features pertaining to cross-peaks arising from anharmonic coupling between the $1620\,cm^{-1}$ and the $1680\,cm^{-1}$ amide I vibrations, and revealing details of the delocalization of vibrational excitation energy. In this context, it is notable that cross-peaks in experimental 2D-IR spectra have been theoretically reproduced on the basis of an excitonic coupling model (see Section 3.1.5). On this basis, accessible peptide excitons are estimated to be delocalized over a length of about 8 Å [92]. The shape of the cross-peaks is related to the spatial conformation and the ordered state of the proteins. This is shown in Figure 2.29, where the FTIR and 2D-IR spectra of the three most common secondary structure motifs are shown for the case of poly-L-lysine. Ordered antiparallel (AP) β-sheets give rise to a Z-shaped contour profile, while α-helices show a flattened figure-8 line shape, and random coils yield unstructured, diagonally elongated bands [93]. Several reports have been made relating to the 2D-IRS characterization of DNA and various proteins including RNase, ubiquitin, concanavalin, lysozyme, and the human islet amyloid polypeptide [90,93,94].

2.4
Time-Resolved Measurements in the mid-IR Range

2.4.1
In-Situ Monitoring of Chemical Reactions

With modern commercial spectrometers equipped with a mercury-cadmium-tellurium detector, interferograms can be collected and stored at a high rate, typically 50 to 80 spectra per second, corresponding to a time resolution of 12 to

Lam Research Ex. 1047 - Page 102
Lam Research Corp. v. Inpria Corp.
IPR2024-00033 - U.S. Patent No. 9,823,564

20 ms [9a]. Therefore, by studying the time dependence of the intensity change of absorption bands of functional groups of reactants, the rate of chemical reactions can be measured. Early studies employing rapid-scanning FTIR spectroscopy date back to the 1980s, when the curing of isocyanate coatings [95] and the polymerization of acrylic monomers were first investigated [96].

Today, the IR real-time monitoring of polymerization rates during the curing of resins is a frequently applied analytical tool. Indeed, many important technical processes utilized by the coatings industry are commonly based on solvent-free formulations that can be dried very rapidly by radiation-curing. The formulations contain, apart from a photoinitiator, polymerizable monomers and functionalized oligomers as reactive components and, importantly, unreactive additives such as inorganic fillers. Upon irradiation with UV light, the formulations are cured within a few seconds, or sometimes even within less than one second. Two main classes of industrially applied UV-curable systems have been developed, in which polymerization proceeds by either a radical-type or a cationic-type mechanism. Formulations containing unsaturated compounds on acrylate or styrene basis are polymerized by a radical mechanism, whereas formulations on expoxide or vinyl ether basis are polymerized by a cationic mechanism.

IR spectroscopy is highly appropriate for the direct recording of curing rates – that is, the degree of conversion as a function of time [97,98]. Typical polymerization profiles obtained upon UV exposure of an urethane-acrylate resin and an acrylate/epoxide blend (diacryl derivative of bis-phenol A/bicycloaliphatic diepoxide) are shown in Figure 2.30. While the radical polymerization of the acrylate monomer occurred faster than the cationic polymerization of the epoxide

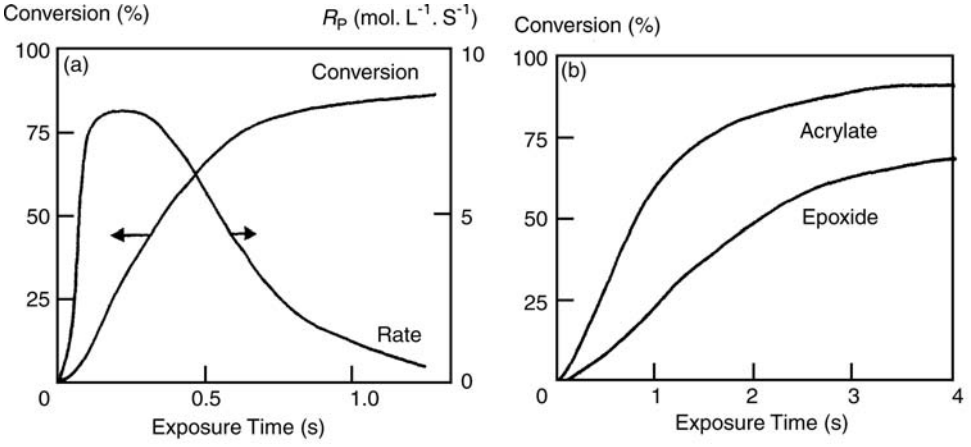


Figure 2.30 UV-light-initiated polymerization of an urethane-acrylate system (a) and an acrylate/epoxide blend (1:1, w/w); (b) Conversion as a function of exposure time, monitored in real time by following the decay of the acrylate band at 1410 cm^{-1}, and the build-up of the ether band at 1082 cm^{-1}. Adapted with permission from Ref. [97]; © 2005, Taylor & Francis.

Lam Research Ex. 1047 - Page 103
Lam Research Corp. v. Inpria Corp.
IPR2024-00033 - U.S. Patent No. 9,823,564

Table 2.12 Wavenumbers appropriate for real-time IR monitoring of the polymerization of functional groups.

Functional group	Absorption decrease at wavenumber (cm^{-1})	Absorption increase at wavenumber (cm^{-1})	Appropriate layer thickness
Acrylate	812		<50 μm
	1410		
	6160		Up to several mm
Vinyl ether	1623		
Epoxides	865		
	795		
Ether bond		1080	
		1210	

monomer, polymerization of the latter continued in the dark and led to almost complete curing after only one day [97].

Appropriate wavenumbers at which the conversion of functional groups, or the formation of newly formed bonds can be monitored, are listed in Table 2.12.

Interesting applications of the IR real-time monitoring method involve the formation of interpenetrating polymer networks (*IPN*s) by the polymerization (or condensation) of multifunctional monomers reacting via different mechanisms. The data shown in Figure 2.30b relate to an IPN system containing polymer networks formed separately from acrylate and epoxide moieties, respectively. Another example refers to the case of a hybrid organic–inorganic sol–gel material formed from methacryloxypropyltrimethoxysilane (*MAPTMS*) or acryloxypropyltrimethoxysilane (*APTMS*) (Chart 2.8) that were condensed to a certain extent prior to photopolymerization. The rate of photopolymerization was measured by recording the decrease in IR absorption of the carbon–carbon double bonds [99]. Currently, such sol–gel materials are used in the production of optical devices such as gratings, microlenses, and waveguides.

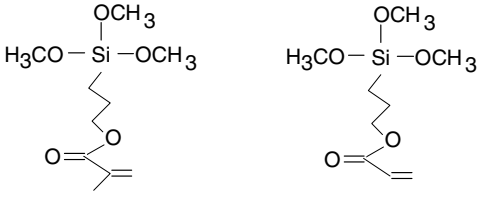


Chart 2.8 Chemical structures of methacryloxypropyltrimethoxysilane (MAPTMS) and acryloxypropyltrimethoxysilane (APTMS).

Lam Research Ex. 1047 - Page 104
Lam Research Corp. v. Inpria Corp.
IPR2024-00033 - U.S. Patent No. 9,823,564

The IR real-time monitoring method is versatile with respect to sample thickness. At a thickness exceeding 0.5 mm, measurements can be performed at overtone bands of weak absorption, whereas in the case of thin layers (<2 μm) the attenuated total reflectance (*ATR*) method (see Section 2.2.1) is applicable. Generally, this method is well suited to monitoring the UV-curing of varnishes, printing inks, and paints that have been coated onto metallic substrates.

Another field of time-resolved FTIR spectroscopy relates to polymeric liquid crystals, with the rate of electric field reorientation of nematic liquid crystals [100] and the orientation of strands in liquid crystals [101] each having been monitored using this technique.

2.4.2 Transient Two-Dimensional IR Spectroscopy

Transient 2D-IRS has been used to study the dynamics of reversible and irreversible processes that are initiated by an external force; typical investigations have included temperature jump (*T-jump*) [102] and flash photolysis experiments [103].

2.4.2.1 T-Jump Studies

In T-jump studies with aqueous systems, an intense nanosecond NIR laser pulse (<10 ns) excites the overtone transition of the O—H (1.5 μm) or O—D (2.0 μm) stretching vibration of water molecules. The absorbed energy is dissipated by picosecond relaxation, thus raising the kinetic energy of water and solute molecules in the time scale of the pulse duration. Structurally or chemically evolving transient species are detected in real time by using 2D-IRS as a time-delayed probe of the system. Varying the time delay between the initiation pulse and the 2D-IRS experiment allows a *molecular movie* of the system to be obtained. The T-jump technique has been utilized to monitor conformational transitions of macromolecules; an example is the thermal unfolding of proteins, including RNase [104] and ubiquitin [105]. As a typical example, Figure 2.31 shows the transient 2D-IR difference spectra of ubiquitin recorded in the amide I region between 1600 and 1750 cm^{-1} at various time delays after a T-jump from 63 to 72 °C.

Ubiquitin is a small, 76-residue-containing protein that can be covalently attached to target proteins for intracellular degradation. It has a five-stranded β-sheet and an α-helix (Chart 2.9). The changes in the contour profiles in the 2D-IR spectra presented in Figure 2.31 are related to the loss of β-sheet modes as a consequence of hydrogen bonds being weakened and cleaved by the temperature increase. The simultaneously observed blue shift of the band center is caused by an increase in the random coil region. The kinetic analysis of the data reveals that thermal unfolding of ubiquitin involves sequential stages: the less-stable strands III to V unfold (3 μs) before the protein's hydrophobic core unfolds (80 μs) [106].

Lam Research Ex. 1047 - Page 105
Lam Research Corp. v. Inpria Corp.
IPR2024-00033 - U.S. Patent No. 9,823,564

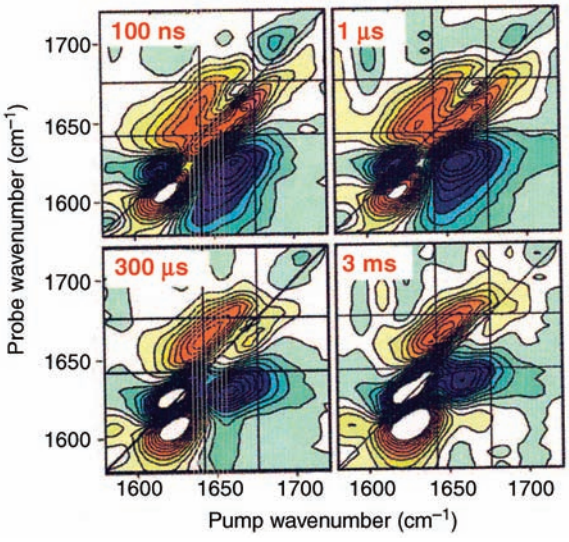


Figure 2.31 Transient 2D-IR difference spectra of ubiquitin in aqueous pH 1 DCl/D_2O solution (30 g l^{-1}) recorded at various time delays after T-jump from 63 to 72 °C. Adapted with permission from Ref. [93]; © 2008, American Chemical Society.



Chart 2.9 Structures of folded and unfolded ubiquitin.

2.4.2.2 Flash Photolysis

In the case of flash photolysis experiments, the initiation light pulse of UV/visible wavelength is absorbed by the substrate (solute), causing a chemical alteration. The resultant conformational changes in macromolecules can be examined via a sequence of 2D-IR experiments. In typical studies with peptides and proteins containing disulfide bridges, the latter are cleaved by a 260 nm light pulse within 20 ps, after which the subsequent unfolding of the molecule is examined using 2D-IRS [103]. In the case of the cyclic disulfide-bridged peptide cyclo(Boc-Cys-Pro-Aib-OMe) dissolved in CD_3CN solution (Chart 2.10), the Cys(1) C=O band undergoes a blue shift indicating breaking or weakening of the hydrogen bond, and an

Lam Research Ex. 1047 - Page 106
Lam Research Corp. v. Inpria Corp.
IPR2024-00033 - U.S. Patent No. 9,823,564

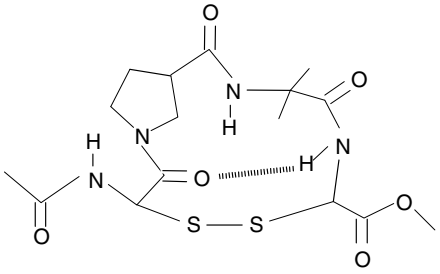
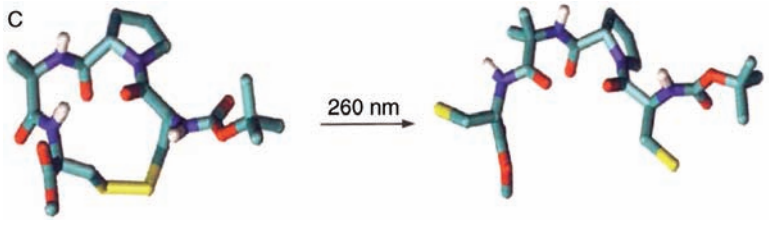


Chart 2.10 Chemical structure of peptide cyclo(Boc-Cys-Pro-Aib-OMe).

additional transient cross-peak forms. These processes, which proceed with a life time of 160 ps, are attributed to β-turn opening [107]. The unfolding of the peptide is depicted in Scheme 2.1.



Scheme 2.1 UV-light-induced unfolding of peptide cyclo(Boc-Cys-Pro-Aib-OMe).

2.5 Time-Resolved THz Spectroscopy

THz spectroscopy is an important tool for studying the dynamics of stimulus-induced processes, and this can be demonstrated by two typical examples: (i) the UV light-induced generation of charge carriers in semiconducting polymers; and (ii) the folding of proteins in the mixing chamber of a stopped-flow apparatus.

2.5.1 Photoconductivity of Conjugated Polymers

Due to the generation of charge carriers, conjugated polymers become electrically conductive when irradiated with UV/visible light. The quantum yield for charge carrier generation is increased by additives, such as fullerene compounds. With the aid of time-resolved THz spectroscopy, the time- and frequency-dependent complex conductivity with its real and imaginary parts can be measured. THz radiation is absorbed by the polymer due to the dielectric

Lam Research Ex. 1047 - Page 107
Lam Research Corp. v. Inpria Corp.
IPR2024-00033 - U.S. Patent No. 9,823,564

polarization of bound charge pairs (excitons) generated by an antecedent UV light pulse. The strength of the electric field $E(\omega)$ of a THz pulse transmitting a polymer sample is reduced when it is preceded by an UV pulse. This frequency-dependent decrease $\Delta E(\omega)$ is proportional to the electric conductivity $\sigma(\omega)$ according to Equation 2.23:

$$\sigma(\omega) = -\frac{2\varepsilon_0 nc}{d_{\text{exc}}}\frac{\Delta E(\omega)}{E(\omega)} \tag{2.23}$$

where d_{exc} is the excitation thickness, n is the refractive index of the medium, c is the speed of light, and ε_0 is permittivity *in vacuo*.

Investigations with poly(2-methoxy-5-(2′ethylhexyloxy)-*p*-phenylene-vinylene (MEH-PPV; Chart 2.11) have revealed that photoexcitation generates excitons with near-unity quantum yield. However, only a small fraction of them ($<10^{-2}$) is converted to free charge carriers by the rapid (100 fs) dissociation of hot excitons. The free charges relax on a subpicosecond time scale, while other excitons persist over longer times [108]. The change in field transmission, ΔE, as a function of the delay time τ between the optical pump and the THz probe pulse is shown in Figure 2.32. Here, the MEH-PPV sample was irradiated with 150 fs pulses of 400 nm light at 30 K, and the conductivity was probed by THz pulses (1 ps, 0.3 to 1.2 THz). As can be seen in Figure 2.32a, ΔE increases very rapidly (rise time $\approx$ 0.3 ps) after the absorption of a 400 nm light pulse. The decay dynamics exhibit two distinct modes with lifetimes of 0.9 ps and 200 ps, which are attributed to hot excitons yielding free charges and primary excitons, respectively. Both, the real and imaginary conductivity increase with increasing frequency (see Figure 2.32b). After 10 ps the conductivity is essentially determined by the imaginary fraction [108].

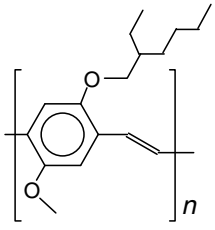


Chart 2.11 Chemical structure of MEH-PPV.

In conclusion, THz time domain spectroscopy allows the simultaneous quantitative detection of real and imaginary electrical conductivity. The real component of the complex conductivity is related to the free charge carrier yield, while the imaginary component is related to the yield of bound charge pairs (excitons). Moreover, time-resolved THz measurements may provide data on charge transport along isolated polymer chains [108].

Lam Research Ex. 1047 - Page 108
Lam Research Corp. v. Inpria Corp.
IPR2024-00033 - U.S. Patent No. 9,823,564

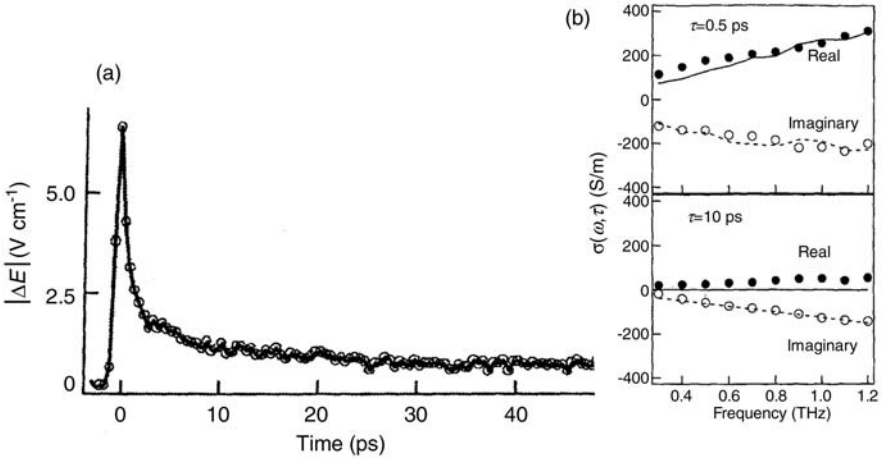


Figure 2.32 Photogeneration of charge carriers in MEH-PPV (see Chart 2.11) as probed by time-resolved THz spectroscopy. (a) Change in the electric field strength of the THz probe pulses after the UV pump pulse ($\lambda = 400$ nm); (b) Real and imaginary electric conductivity as a function of THz frequency recorded at 0.5 and 10 ps after the pump pulse. Adapted with permission from Ref. [108]; © 2004, American Physical Society.

2.5.2 Folding of Proteins

Proteins in aqueous solution unfold upon the addition of specific agents, and refold when the concentration of the latter is significantly lowered. For example, ubiquitin (see Chart 2.9) unfolds in 6 M guanidinium solution (Chart 2.12) and refolds when the guanidinium concentration is reduced to 0.86 mol l^{-1} [109].

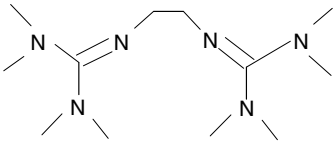


Chart 2.12 Chemical structure of guanidine.

In this case, the refolding has been triggered by diluting the protein solution in the mixing chamber of a stopped-flow apparatus. The rate of subsequent refolding was measured by transmitting a series of THz pulses through the mixing chamber and recording the change in the electric field strength of the THz pulses as a function of time after mixing. Figure 2.33 shows the exponential decrease of $(E_{\text{buffer}} - E_{\text{protein}})/E_{\text{buffer}}$, where E_{buffer} and E_{protein} represent the electric field strength before and after mixing, respectively. The lifetime amounts to about 10 ms [109].

Lam Research Ex. 1047 - Page 109
Lam Research Corp. v. Inpria Corp.
IPR2024-00033 - U.S. Patent No. 9,823,564

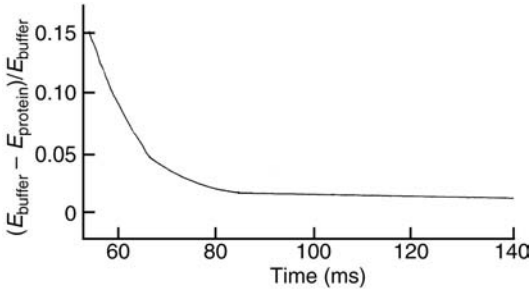


Figure 2.33 Folding of ubiquitin at −20 °C probed by time-resolved THz spectroscopy. Change in the electric field strength of the THz probe pulses (0.1 to 1 THz) after dilution of the solution in the mixing chamber of a stopped-flow apparatus. Solvent: ethylene glycol/water (45:55) containing sodium phosphate (4×10^{-2} mol l^{-1}), pH 5.9. Adapted with permission from Ref. [109]; © 2008, Wiley-VCH.

The decrease in $(E_{buffer} - E_{protein})/E_{buffer}$ after mixing reflects the reorientation of water molecules located in the neighborhood of the protein molecules. As noted in Section 2.2.4.4, the absorption coefficient of the dynamic hydration shell depends on the structure of the protein molecule. Folding and unfolding involves hydrogen-bonds between backbone sites of the protein and solvating water molecules. Upon folding, these hydrogen-bonds are broken and new hydrogen-bonds between different backbone sites are formed. In fact, such processes are detectable by performing THz absorption measurements reflecting collective vibrations of the hydrogen-bonded network around protein molecules. Interestingly, the THz-detectable folding process is about two to three orders of magnitude faster than folding processes detectable by other techniques (e.g., fluorescence, circular dichroism and small angle X-ray scattering), indicating that the process observable by the THz detection method corresponds to an early phase of the total folding mechanism.

2.6 THz Optics Made From Polymers

Polymeric materials are widely used in THz systems as transmissive optics, including lenses, windows and prisms, owing to their rather high transparency in this frequency range. Currently, high-density polyethylene (*HDPE*), polypropylene (*PP*), polytetrafluoroethylene (*PTFE*) and picarin (a cycloolefin-based polymer, also named tsurupica) are used for the fabrication of THz optics. HDPE is a good choice as an optical material, with its very low absorption at frequencies between 0.2 and 2.5 THz, minimal dispersion and small Fresnel reflection loss, but unfortunately it is opaque towards visible light. The alignment of complex THz optical systems is greatly simplified if visible light

Lam Research Ex. 1047 - Page 110
Lam Research Corp. v. Inpria Corp.
IPR2024-00033 - U.S. Patent No. 9,823,564

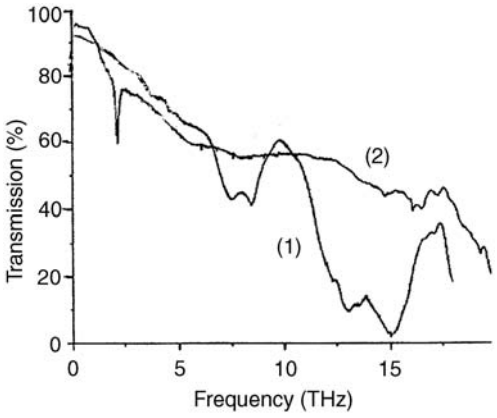


Figure 2.34 Transmission spectra of polyethylene (1) and picarin (2) [110].

can be used as a guide, and this requirement is fulfilled by picarin, which is quite transparent at both UV/visible and THz frequencies, with almost identical refractive indices of about 1.51. The transmission spectra of picarin and polyethylene are shown in Figure 2.34.

Other polymers with properties similar to those of picarin include a copolymer of norbornene and ethylene (NEC), which has a transmission of about 90% (for a 2 mm-thick sample) in the frequency range between 0.2 and 1.2 THz [111], and poly(4-methyl pentene-1) (TPX^{TM}; Mitsui Chemicals). The latter is transparent at UV, visible and far-IR frequencies [112]. The chemical structures of the base units of these polymers are provided in Chart 2.13.

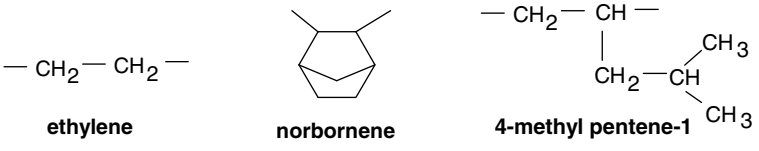


Chart 2.13 Chemical structures of base units of polymers used to fabricate THz optics.

References

1 Christy, A.A., Ozaki, Y., and Gregoriou, V.G. (2001) *Modern Fourier Transform Infrared Spectroscopy*, Elsevier, Amsterdam.
2 Burns, D.A. and Ciurczak, E.W. (2007) *Handbook of Near Infrared Analysis*, 3rd edn, CRC Press, Boca Raton, FL, USA.
3 Siesler, H.W., Ozaki, Y., Kawata, S., and Heise, H.M. (eds) (2002) *Near-Infrared Spectroscopy, Principals, Instruments, Applications*, Wiley-VCH, Weinheim.
4 Stuart, B. (2004) *Infrared Spectroscopy, Fundamentals and Applications*, Wiley, Chichester, UK (reprinted 2008).
5 Elliott, A. (1969) *Infrared Spectra and Structure of Organic Long-Chain Polymers*, Arnold, London.

Lam Research Ex. 1047 - Page 111
Lam Research Corp. v. Inpria Corp.
IPR2024-00033 - U.S. Patent No. 9,823,564

6 Siesler, H.W. and Holland-Moritz, K. (1980) *Infrared and Raman Spectroscopy of Polymers*, Dekker, New York.

7 Liquier, J. and Taillandier, E. (1996) Infrared Spectroscopy of Nucleic Acids, in *Infrared Spectroscopy of Biomolecules* (eds H.M. Mantsch and D. Chapman), Wiley, New York, Ch. 6.

8 Chalmers, J.M. and Griffiths, P.R. (eds) (2002) *Handbook of Vibrational Spectroscopy*, Wiley, Chichester.

9 (a) Koenig, J.L. (1999) *Spectroscopy of Polymers*, 2nd edn, Elsevier, Amsterdam; (b) Koenig, J.L. (1998) Trichroic Infrared Measurements of Orientation, in *Handbook of FT Raman and IR Spectra of Polymers* (eds A.H. Kuptsov and G.N. Zhizhin), Elsevier, Oxford, p. 305.

10 Everall, N., Griffiths, P.R., and Chalmers, J.M. (eds) (2007) *Vibrational Spectroscopy of Polymers, Principles and Practice*, Wiley-VCH, Weinheim.

11 Kuptsov, A.H. and Zhizhin, G.N. (1998) *Handbook of FT Raman and IR Spectra of Polymers*, Elsevier, Oxford.

12 Mantsch, H.M. and Chapman, D. (eds) (1996) *Infrared Spectroscopy of Biomolecules*, Wiley, New York.

13 Ward, M. (ed.) (1997) *Structure and Properties of Oriented Polymers*, Chapman & Hall, London.

14 Buffeteau, T. and Pézolet, M. (2007) Infrared Linear Dichroism of Polymers, in *Vibrational Spectroscopy of Polymers, Principles and Practice* (eds N. Everall, P.R. Griffiths, and J.M. Chalmers), Wiley-VCH, Weinheim, p. 255.

15 Xu, J., Ramian, G.J., Galan, J.F., Savvidis, P.G., Scopatz, A.M., Birge, R.R., Allen, S.J., and Plaxco, K.W. (2003) Terahertz circular dichroism spectroscopy: a potential approach to the *in situ* detection of life's metabolic and genetic machinery. *Astrobiology*, **3**, 489.

16 Xu, J., Ramian, G.J., Galan, J.F., Savvidis, P.G., Scopatz, A.M., Birge, R.R., Allen, S. J., and Plaxco, K.W. (2004) Terahertz circular dichroism of biopolymers. *Proc. SPIE Int. Soc. Opt. Eng.*, **19-26**, 5268.

17 Jin, Y.-S., Kim, G.-J., and Jeon, S.-G. (2006) Terahertz dielectric properties of polymers. *J. Korean Phys. Soc.*, **49**, 513.

18 Naftaly, M. and Miles, R.E. (2007) Terahertz time domain spectroscopy for material characterization. *Proc. IEEE*, **95**, 1658.

19 Plusquellic, D.F., Siegrist, K., Heilweil, E.J., and Esenturk, O. (2007) Applications of terahertz spectroscopy in biosystems. *ChemPhysChem*, **8**, 2412.

20 Fischer, B., Hoffmann, M., Helm, H., Modjesch, G., and Jepson, P.U. (2005) Chemical recognition in terahertz time-domain spectroscopy and imaging. *Semicond. Sci. Technol.*, **20**, S246.

21 Markelz, A.G., Roitberg, A., and Heilweil, E.J. (2000) Pulsed terahertz spectroscopy of DNA bovine serum albumin and collagen between 0.1 and 2.0 THz. *Chem. Phys. Lett.*, **320**, 42.

22 Hannah, R.W. and Mayo, D.W. (2004) Infrared Spectra of Polymers, in *Course Notes on the Interpretation of Infrared and Raman Spectra* (eds D.W. Mayo, F.A. Miller, and R.W. Hannah), Wiley, New York, Ch. 10.

23 Tolstoy, V.P., Chernyshova, I.V., and Skryshevsky, V.A. (2003) *Handbook of Infrared Spectroscopy of Ultrathin Films*, Wiley-Interscience, Hoboken, N.J. USA.

24 Garton, A. (1992) *IR Spectroscopy of Polymer Blends, Composites and Surfaces*, Hanser Gardner Publications, Oxford, New York.

25 Urban, M. and Craver, C.D. (1993) *Surface Property Relations in Polymers, Spectroscopy and Performance*, American Chemical Society, Washington, DC.

26 Gregoriou, V.G. and Braiman, M.S. (eds) (2006) *Vibrational Spectroscopy of Biological and Polymeric Materials*, CRC Press, Taylor & Francis, Boca Raton, FL, USA.

27 DeSilvestri, S., Cerullo, G., and Lanzani, G. (eds) (2008) *Coherent Vibrational Dynamics*, CRC Press, Taylor & Francis, Boca Raton, FL, USA.

28 (a) Hummel, O.D. (2001) *IR Hummel Defined Polymers Basic Collection*, Wiley-VCH, Weinheim, and (2005); (b) Hummel, O.D. (2006) *IR Hummel Industrial Polymers, Volume 1, Natural and Synthetic Polymers, Elastomers and Fibers*, Wiley-VCH, Weinheim; (c) Hummel, O.D. (2006) *IR Hummel Industrial Polymers, Volume 2, Monomers and Technical Solvents*, Wiley-VCH,

Lam Research Ex. 1047 - Page 112
Lam Research Corp. v. Inpria Corp.
IPR2024-00033 - U.S. Patent No. 9,823,564

Weinheim; (d) Hummel, O.D. (2006) *IR Hummel Industrial Polymers, Volume 3, Additives and Auxiliaries*, Wiley-VCH, Weinheim; (e) Hummel, O.D. (2005) *Atlas of Polymer and Plastics Analysis*, 3rd edn, Wiley-VCH, Weinheim.

29 Claybourn, M. (1998) *Infrared Reflectance Spectroscopy of Polymers. Analysis of Films, Surfaces and Interfaces*, Adhesion Society, Blacksburg, VA.

30 (a) Workman, J. (2000) *Handbook of Organic Compounds, NIR, IR, Raman and UV-Vis Spectra Featuring Polymers and Surfactants*, Academic Press, San Diego; (b) Workman, J. and Weyer, L. (2008) *Practical Guide to Interpretive Near-Infrared Spectroscopy*, CRC Press, Taylor & Francis, Boca Raton, FL, USA.

31 Messerschmidt, R.G. and Harthcock, M.A. (eds) (1988) *Infrared Microspectroscopy: Theory and Applications*, Marcel Dekker, New York.

32 Schmuttenmaer, C.A. (2004) Exploring dynamics in the far-infrared with terahertz spectroscopy. *Chem. Rev.*, **104**, 1759.

33 Auston, D.H., Cheung, K.P., Valmanis, J. V., and Kleinman, D.A. (1984) Čerenkov radiation from femtosecond optical pulses in electro-optic media. *Phys. Rev. Lett.*, **53**, 1555.

34 Ferguson, B. and Zhang, X.C. (2002) Materials for terahertz science and technology. *Nat. Mater.*, **1**, 26.

35 Dexheimer, S.L. (ed.) (2008) *Terahertz Spectroscopy, Principles and Applications*, CRC Press, Taylor & Francis, Boca Raton, FL, USA.

36 Bründermann, E., Chamberlin, D.R., and Haller, E.E. (1998) Novel design concepts if widely tunable germanium terahertz lasers. *Appl. Phys. Lett.*, **73**, 2757.

37 Carr, G.L., Martin, M.C., McKinney, W.R., Jordan, K., Neil, G.R., and Williams, G.P. (2002) High power THz radiation from relativistic electrons. *Nature*, **420**, 153.

38 (a) Abo-Bakr, M., Feikes, J., Holldack, K., Kuske, P., Peatman, W.B., Wüstefeld, G. and Hübers, H.-W. (2003) Brilliant, coherent far-infrared (THz) synchrotron radiation. *Phys. Rev. Lett.*, **90**, 094801; (b) Abo-Bakr, M., Feikes, J., Holldack, K., Wüstefeld, G., and Hübers, H.-W. (2002) Steady-state far-infrared coherent synchrotron radiation detected at BESSY II. *Phys. Rev. Lett.*, **88**, 254801.

39 Schade, U., Ortolani, M., and Lee, J. (2007) THz experiments with coherent synchrotron radiation from BESSY II. *Synchrotron Rad. News*, **20**, 17.

40 Nicodom (2006) IR Polymers and Fibers (2072 Spectra). Praha, Czek Republic. Available at: http://www.ir-spectra.com.

41 Interspectrum. Fireash Data Management (FDM) FTIR Spectra of Polymers and Polymer Additives (580 Spectra). Toravere, Tartumaa, Estonia. Available at: http://www.interspectrum.ee.

42 Torii, H. and Tasumi, M. (1996) Theoretical Analyses of the Amide I Infrared Bands of Globular Proteins, in *Infrared Spectroscopy of Biomolecules* (eds H.M. Mantsch and D. Chapman), Wiley, New York, Ch. 1.

43 Stuart, B. (1997) *Biological Applications of Infrared Spectroscopy*, Wiley, Chichester, UK.

44 Taillandier, E. and Liquier, J. (2002) Vibrational Spectroscopy of Nucleic Acids, in *Handbook of Vibrational Spectroscopy* (eds J.M. Chalmers and P.R. Griffiths), Wiley, Chichester, Vol. 5.

45 Benedetti, Ed., Bramanti, E., Papineschi, F., Rossi, I., and Benedetti, En. (1997) Determination of the relative amount of nucleic acids and proteins in leukemic and normal lymphocytes by means of Fourier transform infrared microspectroscopy. *Appl. Spectrosc.*, **51**, 792.

46 Kradjel, C. and Lee, K.A. (2007) NIR Analysis of Polymers, in *Handbook of Near Infrared Analysis* (eds D.A. Burns and E.W. Ciurczak) 3rd edn, CRC Press, Boca Raton, FL, USA, Ch. 26.

47 Ghosh, S. and Rodgers, J. (2007) NIR Analysis of Textiles, in *Handbook of Near Infrared Analysis* (eds D.A. Burns and E.W. Ciurczak) 3rd edn, CRC Press, Boca Raton, FL, USA, Ch. 22.

48 Smith, D.M. and Chugtai, A.R. (2007) Polymer Optical and Dielectric Properties through Vibrational Spectroscopy, in *Vibrational Spectroscopy of Polymers, Principles and Practice* (eds N. Everall, P.R. Griffiths, and J.M. Chalmers), Wiley-VCH, Weinheim, p. 237.

Lam Research Ex. 1047 - Page 113
Lam Research Corp. v. Inpria Corp.
IPR2024-00033 - U.S. Patent No. 9,823,564

49 Khazan, M.A. (2002) Time Domain Terahertz Spectroscopy and its Application to the Study of High Tc Superconductor Thin Films, Doctoral Thesis, University of Hamburg.

50 Mittleman, D. (2003) Terahertz Imaging, in *Sensing with Terahertz Radiation* (ed. D. Mittleman), Springer, Berlin.

51 Pupeza, J., Wilk, R., and Koch, M. (2007) Highly accurate optical material parameter determination with THz time-domain spectroscopy. *Opt. Express*, **15**, 4335.

52 Hangyo, M., Nakashima, T., and Nashima, S. (2002) Spectroscopy by pulsed terahertz radiation. *Meas. Sci. Technol.*, **13**, 1727.

53 Dorney, T.D., Baraniuk, B., and Mittleman, D.M. (2001) Material parameter estimation with terahertz time-domain spectroscopy. *J. Opt. Soc. Am. A*, **18**, 1562.

54 Duvillaret, L., Garet, F., and Coutaz, J.-L. (1999) Highly precise determination of optical constants and sample thickness in terahertz time-domain spectroscopy. *Appl. Opt.*, **38**, 409.

55 Wietzke, S., Jansen, C., Rutz, F., Mittleman, D.M., and Koch, M. (2007) Determination of additive content in polymeric compounds with terahertz time-domain spectroscopy. *Polymer Testing*, **26**, 614.

56 Hochrein, T., Krumbholz, N., Wietzke, S., Kretschmer, K., Bastian, M., and Koch, M. (2008) Terahertz-spektroskopie zur schmelzanalyse in der compoundierung. *Gummi, Fasern, Kuntstoffe*, **61**, 517.

57 Wietzke, S., Jördens, C., Krumbholz, N., Baudrit, B., Bastian, M., and Koch, M. (2007) Determination of additive content in polymeric compounds with terahertz imaging: a new non-destructive technique for quality control of plastic weld joints. *J. Eur. Opt. Soc. Rapid Publ.*, **2**, 0713614.

58 Plusquellic, D.F., Siegrist, K., Heil, E.J., and Esenturk, O. (2007) Applications of terahertz spectroscopy in biosystems. *ChemPhysChem*, **8**, 2412.

59 Born, B., Kim, S.J., Ebbinghaus, S., Gruebele, M., and Havenith, M. (2009) The terahertz dance of water with the proteins: the effect of protein flexibility on the dynamical hydration shell of ubiquitin. *Faraday Discuss.*, **141**, 161.

60 Sinyukov, A.M. and Hayden, L.M. (2002) Generation and detection of terahertz radiation with multilayered electro-optic polymer films. *Opt. Lett.*, **27**, 55.

61 Nahata, A., Auston, D.H., Wu, C.J., and Yardley, J.T. (1995) Generation of terahertz radiation from a poled polymer. *Appl. Phys. Lett.*, **67**, 1358.

62 Zhu, W., Agarwal, A., Cao, H., and Nahata, A. (2008) Generation of broadband radially polarized terahertz radiation directly from a cylindrical metal wire. *Opt. Express*, **16**, 8433.

63 Tompkins, H.G. and Irene, E.A. (2005) *Handbook of Ellipsometry*, William Andrew Publishing-Springer, Norwich, NY.

64 Azzam, R.M.A. and Bashara, N.M. (1977) *Ellipsometry and Polarized Light*, North Holland Publishing, New York.

65 Röseler, A. (1990) *Infrared Spectroscopic Ellipsometry*, Akademie Verlag, Berlin.

66 Smith, P.R., Auston, D.H., and Nuss, M. (1988) Subpicosecond photoconducting dipole antennas. *IEEE J. Quantum Electron.*, **24**, 255.

67 Fujiwara, H. (2007) *Spectroscopic Ellipsometry, Principles and Applications*, Wiley, Chichester.

68 Hinrichs, K., Gensch, M., and Esser, N. (2005) Analysis of organic films and interfacial layers by infrared spectroscopic ellipsometry. *Appl. Spectrosc.*, **59**, 272 A.

69 Hinrichs, K. and Eichhorn, K.J. (2007) Combined infrared and visible spectroscopic ellipsometry study of thin polymer layers. *Appl. Spectrosc. Europe*, **19**, 11.

70 Grundmeier, G., Thiemann, P., Carpentier, J., and Barranco, V. (2003) Tailored thin plasma polymers for the corrosion protection of metals. *Surface Coat. Technol.*, **174**, 996.

71 Mendelsohn, R., Brauner, J.W., and Gericke, A. (1995) External infrared reflection- absorption spectroscopy of monolayer films at the air/water interface. *Annu. Rev. Phys. Chem.*, **46**, 305.

72 Mendelsohn, R. and Flach, C.R. (2002) Infrared Reflection-Absorption Spectroscopy of Lipids, Peptides and Proteins in Aqueous Monolayers, Peptide-Lipid Interactions, in *Current Topics in Membranes*, vol. **52** (eds D.M. Fambrough

Lam Research Ex. 1047 - Page 114
Lam Research Corp. v. Inpria Corp.
IPR2024-00033 - U.S. Patent No. 9,823,564

and D.J. Benos), Elsevier Science, San Diego, p. 57.

73 Hussain, H., Kerth, A., Blume, A., and Kressler, J. (2004) Amphiphilic block copolymers of Poly(ethylene oxide) and Poly(perfluorohexylethyl methacrylate) at the water surface and their penetration into the lipid monolayer. *J. Phys. Chem. B.*, **108**, 9962.

74 Blaudez, D., Buffeteau, T., Cornut, J.C., Desbat, B., Escafre, N., Pézolet, M., and Turlet, J.M. (1994) Polarization modulation FTIR spectroscopy at the air-water interface. *Thin Solid Films*, **242**, 146.

75 Xiao, Y., Bourque, H., Pézolet, M., and Ritcey, A.M. (1998) Polarization modulation IRRAS investigation of a cellulose ether at the air/water interface. *Thin Solid Films*, **327-329**, 299.

76 Siesler, H.W. and Holland-Moritz, K. (1980) in *Infrared and Raman Spectroscopy of Polymers* (eds H.W. Siesler and K. Holland-Moritz), Dekker, New York, Ch. 4.3.

77 Gregoriou, V.G., Rodman, S.E., Nair, B.R., and Hammond, P.T. (2006) Studying the Viscoelastic Behavior of Liquid Crystalline Polyurethanes Using Static and Dynamic FTIR Spectroscopy, in *Vibrational Spectroscopy of Biological and Polymeric Materials* (eds V.G. Gregoriou and M.S. Braiman), CRC Press, Taylor & Francis, Boca Raton, FL, USA, Ch. 1.

78 Nair, B.R., Gregoriou, V.G., and Hammond, P.T. (2000) FT-IR studies of side chain liquid crystalline thermoplastic elastomers. *Polymer*, **41**, 2961.

79 Fina, L.J. and Koenig, J.L. (1986) Analysis of tichroic infrared absorption in solids. II. One-way drawn poly(ethylene terephthalate). *J. Polym. Sci. Part B: Polym. Phys.*, **24**, 2525.

80 Kischel, M., Kisters, D., Strohe, G., and Veeman, W.S. (1998) Dynamic infrared spectroscopy, a tool to detect hydrogen bonds in polymers? *Eur. Polym. J.*, **34**, 1571.

81 Schexnaydre, R.J. and Mitchell, B.S. (2007) Synchrotron infrared microspectroscopy characterization of heterogeneities in solid state blended polymers. *Mater. Lett.*, **6**, 2151.

82 Zhong, Z., Bennet, D., Chapman, D., Chen, J., Connor, D., Dilmanian, A., Faulconer, L., Kao, T., Lekovjan, A.C., Liu, J.L.T., Miller, L.M., Muehleman, C., Parham, C. *et al.* (2008) Probing Alzheimer's decease pathology and early detection at the NSLS with infrared, XRF and DEI. *Synchrotron Rad. News*, **21**, 11.

83 Benedetti, E., Vergamini, P., and Spremolla, G. (1988) FT-IR analysis of single human normal and leukemic lymphocytes. *Microchim. Acta*, **94**, 139.

84 Koenig, J.L. (1992) *Microspectroscopy of Polymers*, American Chemical Society, Washington, DC.

85 Bhargara, R., Wang, S.-Q., and Koenig, J.L. (2003) Infrared microspectroscopy of polymeric systems. *Adv. Polym. Sci.*, **163**, 137.

86 Salzer, R. and Siesler, H.W. (2009) *Infrared and Raman Spectroscopic Imaging*, Wiley-VCH, Weinheim.

87 Hunt, N.T. (2008) Ultrafast 2D-IR spectroscopy – method and applications. *Spectrosc. Europe*, **20**, 7.

88 Cervetto, V., Helbing, J., Bredenbeck, J., and Hamm, P. (2004) Double-resonance versus pulsed Fourier transform two-dimensional infrared spectroscopy: an experimental and theoretical comparison. *J. Chem. Phys.*, **121**, 5935.

89 Khalil, M., Demirdöven, N., and Tokmakoff, A. (2003) Coherent 2D IR spectroscopy: molecular structure and dynamics in solution. *J. Phys. Chem. A*, **107**, 5258.

90 Shim, S.-H., Strasfeld, D.B., Ling, Y.L., and Zanni, M.T. (2007) Automated 2D IR spectroscopy using a mid-IR pulse shaper and application of this technology to the human islet amyloid polypeptide. *Proc. Natl Acad. Sci. USA*, **104**, 14197.

91 Hamm, P., Helbing, J., and Bredenbeck, J. (2008) Two-dimensional infrared spectroscopy of photoswitchable peptides. *Annu. Rev. Phys. Chem.*, **59**, 291.

92 Hamm, P., Lim, M., and Hochstrasser, R.M. (1998) Structure of amide i band of peptides measured by femtosecond nonlinear-infrared spectroscopy. *J. Phys. Chem. B*, **102**, 6123.

93 Ganim, Z., Chung, H.S., Smith, A.W., DeFlores, L.P., Jones, K.C., and

Lam Research Ex. 1047 - Page 115
Lam Research Corp. v. Inpria Corp.
IPR2024-00033 - U.S. Patent No. 9,823,564

Tokmakoff, A. (2008) Amide I two-dimensional infrared spectroscopy of proteins. *Acc. Chem. Res.*, **41**, 432.

94 Demirdöven, N., Cheatum, C.M., Chung, H.S., Khalil, M., Knoester, J., and Tokmakoff, A. (2004) Two-dimensional infrared spectroscopy of antiparallel β-sheet secondary structure. *J. Am. Chem. Soc.*, **126**, 7981.

95 Provder, T., Neag, C.M., Carlson, G.M., Kuo, C., and Holsworth, R.M. (1984) Cure reaction kinetics characterization of some model organic coating systems by FTIR and thermal mechanical analysis, in *Analytical Calorimetry* (eds J.F. Johnson and P.S. Gill), Plenum Press, New York.

96 Decker, C. and Moussa, K. (1988) A new method for monitoring ultra-fast photopolymerizations by real-time infrared (RTIR) spectroscopy. *Makromol. Chem.*, **189**, 2381.

97 Decker, C. (2005) *In situ* monitoring of ultrafast photopolymerizations by real-time infrared spectroscopy. *Polym. News*, **30**, 34.

98 Decker, C. (2005) Linked by light. advances in the UV-curing of organic coatings. *Eur. Coat. J.*, **7-8**, 28.

99 Croutxé-Barghorn, C., Soppera, O., and Carré, C. (2007) Real time study of hybrid sol-gel photopolymerization by UV light. *J. Sol-Gel Sci. Technol.*, **41**, 93.

100 Gregoriou, V.G., Chao, J.L., Toriumi, H., and Palmer, R.A. (1991) Time-resolved vibrational spectroscopy of an electric field-induced transition in a nematic liquid crystal by use of step-scan 2D FT-IR. *Chem. Phys. Lett.*, **179**, 491.

101 Kaito, A., Kyotani, M., and Nanayama, K. (1991) Orientation profiles in the strands of thermotropic liquid-crystalline polymer studies by polarized Fourier transform infrared microspectroscopy. *Macromolecules*, **24**, 3244.

102 Chung, H.S., Khalil, M., Smith, A.W., and Tokmakoff, A. (2007) Transient two-dimensional IR spectrometer for probing nanosecond temperature-jump kinetics. *Rev. Sci. Instrum.*, **78**, 063101.

103 Bredenbeck, J., Helbing, J., Kolano, C., and Hamm, P. (2007) Ultrafast 2D-IR spectroscopy of transient species. *ChemPhysChem*, **8**, 1747.

104 Chung, H.S., Khalil, M., and Tokmakoff, A. (2004) Nonlinear infrared spectroscopy of protein conformational change during thermal unfolding. *J. Phys. Chem. B*, **108**, 15332.

105 Chung, H.S., Khalil, M., Smith, A.W., Ganim, Z., and Tokmakoff, A. (2005) Conformational changes during the nanosecond-to-millisecond unfolding of ubiquitin. *Proc. Natl Acad. Sci. USA*, **102**, 612.

106 Chung, H.S., Ganim, Z., Jones, K.C., and Tokmakoff, A. (2007) Transient 2D IR spectroscopy of ubiquitin unfolding dynamics. *Proc. Natl Acad. Sci. USA*, **104**, 14237.

107 Kolano, C., Helbing, J., Kozinski, M., Sander, W., and Hamm, P. (2006) Watching hydrogen-bond dynamics in a β-turn by transient two-dimensional infrared spectroscopy. *Nature*, **444**, 469.

108 Hendry, E., Schins, J.M., Candeias, L.P., Siebbeles, L.D.A., and Bonn, M. (2004) Efficiency of exciton and charge carrier photogeneration in a semiconducting polymer. *Phys. Rev. Lett.*, **92**, 196601.

109 Kim, S.J., Born, B., Havenith, M., and Gruebele, M. (2008) Real-time detection of protein-water dynamics upon protein folding by terahertz absorption spectroscopy. *Angew. Chem. Int. Ed.*, **47**, 6486.

110 MichroTech Instruments, Product Information. Available at: http://www.mtinstruments.com.

111 Sengupta, A., Bandyopadhyay, A., Bowden, B.F., Harrington, J.A., and Federici, J.F. (2006) Characterization of olefin copolymers using terahertz spectroscopy. *Electron. Lett.*, **42**, 1477.

112 Tydex, Product Information. Available at: http://www.tydex.ru/products/products6/thz_materials.html.

Lam Research Ex. 1047 - Page 116
Lam Research Corp. v. Inpria Corp.
IPR2024-00033 - U.S. Patent No. 9,823,564

3
Visible and Ultraviolet Light

3.1
Absorption

3.1.1
General Aspects

The absorption of photons of energies ranging from about 1.6 eV ($\lambda = 800$ nm) to about 6.2 eV ($\lambda = 200$ nm) is related to their interacting with outer shell electrons, also called the valence electrons of the atoms. The absorption occurs on a time scale of about 10^{-15} s and causes an alteration of the electronic structure. The position of the atomic nuclei, vibrating on a time scale of 10^{-12} s, is practically not changed during the absorption act. There are two prerequisites for the absorption of a photon of energy $h\nu$ by a polymer molecule. First, the molecule must contain a chromophoric group with excitable energy states corresponding to the photon energy according to Equation 3.1.

$$h\nu = E_n - E_o \tag{3.1}$$

where E_n and E_o denote the energies of the excited and the ground state, respectively. Typical chromophoric groups are listed in Table 3.1.

Second, the transition between the two energy states must cause a change in the charge distribution in the molecule – that is, a change in the dipole moment. In terms of quantum mechanics, the absorption of a photon is possible (allowed) if the transition moment $\boldsymbol{M}$ has a nonzero value. Since M is a vector, it can be composed of three components parallel to the three coordinates (see Equation 3.2), and at least one component must have a nonzero value.

$$\boldsymbol{M} = \boldsymbol{M_x} + \boldsymbol{M_y} + \boldsymbol{M_z} \tag{3.2}$$

The higher the value of M, the more efficient is the absorption. According to Equation 3.3, M is composed of three integrals:

$$\boldsymbol{M} = \int \psi_v{}^* \psi_v d\tau_v \int \psi_e{}^* \boldsymbol{\mu_{dp}} \psi_e d\tau_e \int \psi_s{}^* \psi_s d\tau_s \tag{3.3}$$

Polymers and Electromagnetic Radiation: Fundamentals and Practical Applications, First Edition. Wolfram Schnabel
© 2014 Wiley-VCH Verlag GmbH & Co. KGaA. Published 2014 by Wiley-VCH Verlag GmbH & Co. KGaA.

Lam Research Ex. 1047 - Page 117
Lam Research Corp. v. Inpria Corp.
IPR2024-00033 - U.S. Patent No. 9,823,564

Table 3.1 Typical chromophoric groups for visible and ultraviolet light [1].

Chromophore	Typical compound	λ_{max} (nm)[a]	ε_{max} ($l\,mol^{-1}\,cm^{-1}$)[b]	Mode of electron transition[c]
	Ethene	193	10^4	$\pi \rightarrow \pi^*$
—C ≡ C—	Ethyne	173	6×10^3	$\pi \rightarrow \pi^*$
	Acetone	187	10^3	$\pi \rightarrow \pi^*$
		271	15	$n \rightarrow \pi^*$
—N ≡ N—	Azomethane	347	5	$n \rightarrow \pi^*$
—N=O	*t*-Nitrosobutane	300	100	$\pi \rightarrow \pi^*$
		665	20	$n \rightarrow \pi^*$
—O—N=O	Amyl nitrite	219	1120	$\pi \rightarrow \pi^*$
		357	56	$n \rightarrow \pi^*$

a) Wavelength of maximum optical absorption.
b) Decadic molar extinction coefficient ($\log I_0/I = \varepsilon cd$).
c) See Section 3.1.2 for explanations.

where ψ_v, ψ_e, and ψ_s are the vibronic, electronic, and electron-spin wave functions of the absorbing molecule, respectively. The asterisk denotes an "excited state". $\boldsymbol{\mu}_{dp}$ is the electronic dipole moment operator, and $d\tau_v$, $d\tau_e$, and $d\tau_s$ refer to the three respective coordinates; $d\tau = dx \cdot dy \cdot dz$.

The three integrals in Equation 3.3 are the basis of the so-called *selection rules*, which determine whether a transition is allowed or forbidden. $\left(\int \psi_v^* \psi_v d\tau_v\right)^2$ is the Franck–Condon factor, and $\int \psi_s^* \psi_s d\tau_s$ applies to the spin properties of the excited and the ground states. If any of the three integrals in Equation 3.3 is zero, the corresponding transition is forbidden – that is, a final probability could only result from a second-order approximation. This applies, for example, to the forbidden transitions between levels of the singlet and the triplet system. The magnitude of the Franck–Condon factor determines the probability of transitions with respect to molecular geometry. The rule states that the transition probability is highest if the geometries of the ground and excited states are equal. For more detail, the reader is referred to relevant monographs [1–3].

The probability of the occurrence of an electronic transition is given by the (dimensionless) oscillator strength *f*, which is proportional to the square of the transition moment (Equation 3.4):

$$f = 8.75 \times 10^{-2}\, \Delta E |M|^2 \tag{3.4}$$

where ΔE is equal to $E_n - E_0$ (given in eV). A large value of f corresponds to a strong absorption band and a short lifetime of the excited state. The maximum value is $f = 1$. f is related to the measured integrated extinction coefficient $\int \varepsilon d\nu'$ by Equation 3.6, where ε and ν' are given in units of $l\,mol^{-1}\,cm^{-1}$ and

Lam Research Ex. 1047 - Page 118
Lam Research Corp. v. Inpria Corp.
IPR2024-00033 - U.S. Patent No. 9,823,564

cm^{-1}, respectively:

$$f = (2.3 \times 10^3\ c^2 m/Ne^2\pi)F \int \varepsilon d\nu' = 4.32 \times 10^{-9}\ F \int \varepsilon d\nu' \tag{3.6}$$

where c is the velocity of light, m and e are the mass and charge of an electron, respectively, and N is Avogadro's number. The factor F, which reflects solvent effects and depends on the refractive index of the absorbing medium, is close to unity. ε_{max}, the extinction coefficient at the maximum of an absorption band, is a measure of the intensity (magnitude) of the band and an indicator of the *allowedness* of the corresponding electronic transition.

Experimentally, the absorption of light is recorded as a function of the wavelength λ or the wavenumber $\nu' = \lambda^{-1}$ by measuring the change in the intensity of a light beam passing through a sample of unit path length (1 cm). For a homogeneous, isotropic medium containing an absorbing compound at concentration c (in $mol\,l^{-1}$), the light absorption is described by Equation 3.5, the Lambert–Beer law:

$$A = \lg_{10}(I_0/I) = \varepsilon c d \tag{3.5}$$

where A is the absorbance (extinction, optical density), and I_0 and I denote the light intensity before and after absorption, respectively. Equivalent denotations for I_0 and I are *incident* and *transmitted radiant flux*, respectively. ε ($l\,mol^{-1}\,cm^{-1}$) is the decadic molar extinction coefficient at a given wavelength. The Lambert–Beer law does not hold at high light intensities, as experienced, for example, with lasers.

3.1.2 The Molecular Orbital Model

Changes in the electronic structure of a molecule can be visualized with the aid of the molecular orbital (*MO*) model [1,3]. Molecular orbitals are thought to be formed by the linear combination of the valence shell orbitals of the atoms linked together in the molecule. The combination of two single orbitals of two adjacent atoms results in two molecular orbitals, one of lower and the other of higher energy than before the combination. The low-energy orbital, denoted as the "bonding" orbital, is occupied by a pair of electrons of antiparallel spin. The high-energy molecular orbital (also called an "antibonding" orbital) is unoccupied in the ground state but may be occupied by an electron upon electronic excitation of the molecule.

Different types of molecular orbital exist, including bonding σ and π orbitals, nonbonding n orbitals, and antibonding σ^* and π^* orbitals. σ and σ^* orbitals are symmetrical about the internuclear axis, whereas π and π^* orbitals are antisymmetric about a plane including the internuclear axis. n orbitals, which are located on heteroatoms such as oxygen, nitrogen, or phosphorus, are nonbonding and are of almost the same energy as in the case of the isolated atom. A pair of electrons occupying an n orbital is regarded as a lone pair on the atom in question.

Lam Research Ex. 1047 - Page 119
Lam Research Corp. v. Inpria Corp.
IPR2024-00033 - U.S. Patent No. 9,823,564

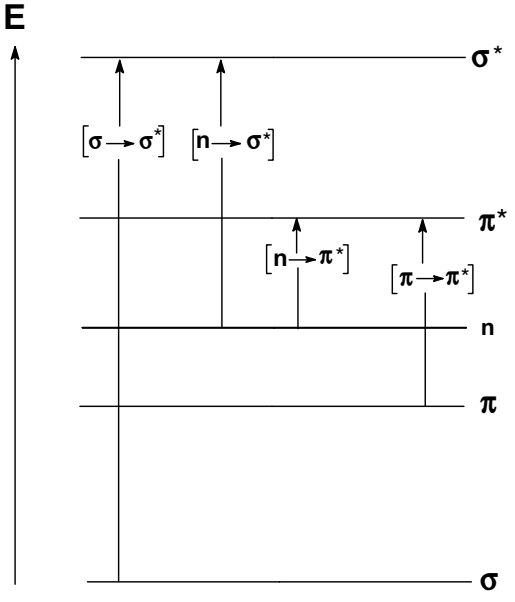


Figure 3.1 Energy of molecular orbitals (not to scale) and electronic transitions induced by the absorption of a photon.

The simple MO model is based on several assumptions. For instance, σ and π orbitals are assumed not to interact. Moreover, molecules are described by localized orbitals each covering two nuclei only. Delocalized orbitals involving more than two nuclei are thought to exist only in the case of π-bonding in conjugated systems.

When a molecule in its ground state absorbs a photon, an electron occupying a σ, π, or n orbital is promoted to a higher-energy σ^* or π^* orbital. In principle, the following transitions are possible: $\sigma \rightarrow \sigma^*$, $\pi \rightarrow \pi^*$, $n \rightarrow \pi^*$, and $n \rightarrow \sigma^*$. As can be seen in Figure 3.1, the orbital energy increases in the series $\sigma < \pi < n < \pi^* < \sigma^*$.

According to the differences in the orbital energies, the electron transitions indicated in Figure 3.1 correspond to light absorption in different wavelength regions. This is illustrated in Table 3.2.

At $\lambda > 200$ nm, photon absorption initiates transitions of n or π electrons rather than those of σ electrons.

Commonly, molecular orbitals are classified as *occupied* (doubly), *singly occupied*, and *unoccupied*. The acronyms HOMO and LUMO denote the frontier orbitals – that is, the Highest Occupied and the Lowest Unoccupied Molecular Orbital, respectively. SOMO represents a Singly Occupied Molecular Orbital (Figure 3.2).

Lam Research Ex. 1047 - Page 120
Lam Research Corp. v. Inpria Corp.
IPR2024-00033 - U.S. Patent No. 9,823,564

Table 3.2 Correspondence of electron transition and optical absorption.

Electron transition	Absorption region (nm)	Extinction coefficient (l mol^{-1} cm^{-1})
$\sigma \rightarrow \sigma^*$	100–200	10^3
$n \rightarrow \sigma^*$	150–250	10^2–10^3
$\pi \rightarrow \pi^*$	180–250	102–104
(Isolated π-bonds)	220–IR	
(Conjugated π-bonds)		
$n \rightarrow \pi^*$	220–320	1–400
(Isolated groups)	250–IR	
(Conjugated segments)		

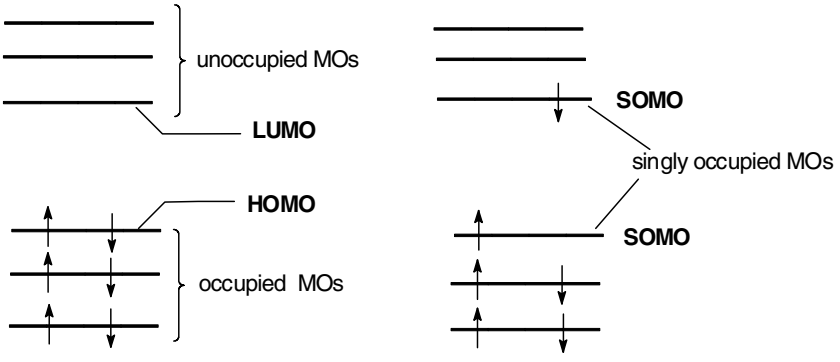


Figure 3.2 Classification of molecular orbitals with respect to electron occupancy.

3.1.3 The Jablonski Diagram

Photon-induced excitations of molecules also include vibrations of nuclei. This fact can be visualized with the aid of the Jablonski diagram (Figure 3.3). The diagram shows the various energy states of a molecule, and further indicates the transitions related to the formation and deactivation of excited states. Here, photon absorption leads to electron transitions from the ground state S_0 to the excited states S_1, S_2, and so on. Electron release occurs when the photon energy exceeds the ionization energy E_I. This is not the case within the wavelength range of UV and visible light, that is, $\lambda = 200$ to 800 nm ($h\nu = 6.2$ to 1.6 eV).

Lam Research Ex. 1047 - Page 121
Lam Research Corp. v. Inpria Corp.
IPR2024-00033 - U.S. Patent No. 9,823,564

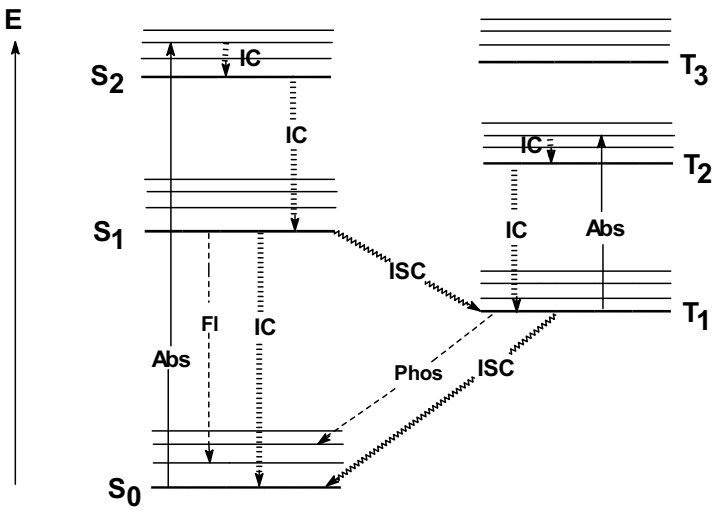


Figure 3.3 Jablonski-type diagram. Abbreviations and acronyms: Abs: absorption, Fl: fluorescence, Phos: phosphorescence, IC: internal conversion, ISC: intersystem crossing.

3.1.4
Absorption in Synthetic Nonconjugated Polymers

The absorption spectra of the typical unconjugated linear polymers presented in Chart 3.1 are shown in Figure 3.4.

Due to the fact that electronic excitations also involve vibronic and rotational sublevels (the latter are not shown in Figure 3.3), the absorption spectra of molecules consist of bands rather than single lines. It is notable that the maxima of the absorption spectra shown in Figure 3.4 are located in the UV region. These reflect spin-state-conserving electronic transitions – that is, transitions in the singlet manifold: upon photon absorption, molecules in the singlet ground state S_0 are converted into molecules in an excited singlet

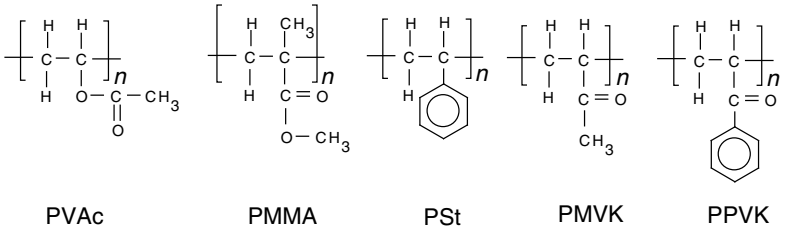


Chart 3.1 Chemical structures of: poly(vinyl acetate), PVAc; poly(methylmethacrylate), PMMA; polystyrene, PSt; poly(methylvinyl ketone), PMVK; and poly(phenylvinyl ketone), PPVK.

Lam Research Ex. 1047 - Page 122
Lam Research Corp. v. Inpria Corp.
IPR2024-00033 - U.S. Patent No. 9,823,564

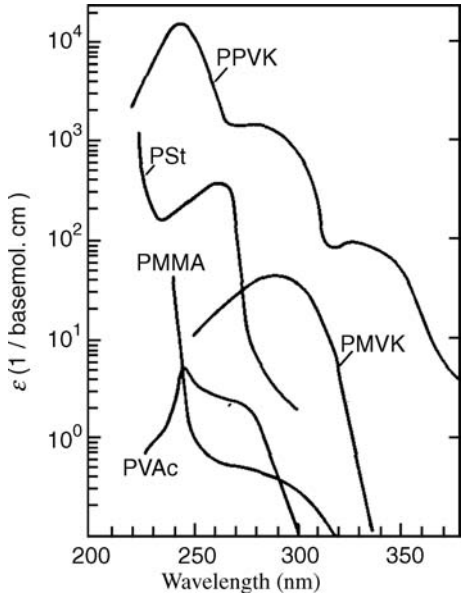


Figure 3.4 Absorption spectra of synthetic nonconjugated polymers. PPVK: poly(phenyl vinyl ketone); PMVK: poly(methylvinylketone); PSt: polystyrene; PMMA: poly(methyl methacrylate); PVAc: poly(vinyl acetate). Adapted with permission from Ref. [4]; © 2007, Wiley-VCH.

state, S_n. At long wavelengths (low photon energies), photon absorption generates S_1 states, but at shorter wavelengths, S_2 and higher states are excited. In the case of polymers containing carbonyl groups, the absorption bands located at long wavelengths correspond to $n \rightarrow \pi^*$ transitions with low extinction coefficients – that is, low values of the transition moment. At shorter wavelengths, $\pi \rightarrow \pi^*$ transitions with larger transition moments are excited. In this context, the reader's attention is directed to Table 3.2, which indicates the relative orders of magnitude of the extinction coefficients of the different electron transitions.

3.1.5
Absorption in Synthetic Conjugated Polymers

During recent years, carbon-catenated π-conjugated and silicon-catenated σ-conjugated polymers have attracted great interest with regards to their application in the fields of electroluminescence (organic light-emitting diodes) and photovoltaics (energy conversion of sunlight). Some typical polymers that exhibit electric conductivity upon light absorption are listed in Table 3.3, while typical optical absorption spectra are presented in Figure 3.5. As can be seen from Figure 3.5, the maxima of the absorption spectra of conjugated polymers are located in the visible wavelength region.

Lam Research Ex. 1047 - Page 123
Lam Research Corp. v. Inpria Corp.
IPR2024-00033 - U.S. Patent No. 9,823,564

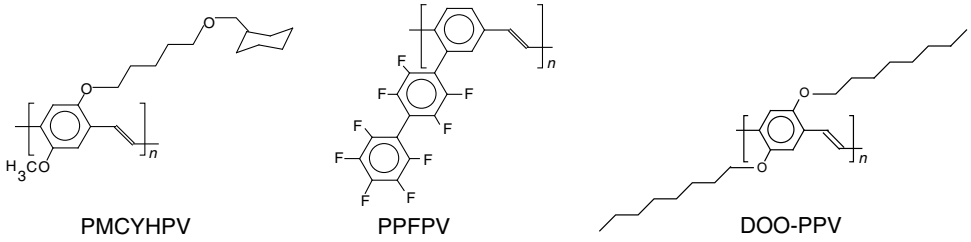
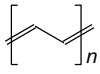
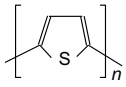
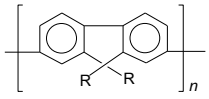
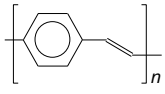
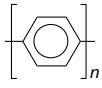
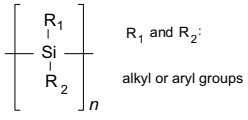
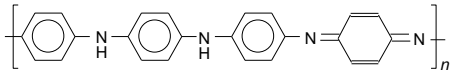


Chart 3.2 Chemical structures of PPV derivatives.

Certain phenomena observed with conjugated polymers cannot be explained in terms of the model described in Section 3.1. This concerns, above all, the generation of charge carriers with the aid of UV and visible light, and the conduction of photogenerated charge carriers. An explanation for these

Table 3.3 Typical synthetic conjugated polymers.

Chemical structure	Acronym	Denotation
	PAC	*trans*-Polyacetylene
	PT	Polythiophene
	PFO	Poly(dialkyl fluorene)
	PPV	Poly(*p*-phenylene vinylene)
	PPP	Poly(*p*-phenylene)
		Polysilylene
	PANI	Polyaniline

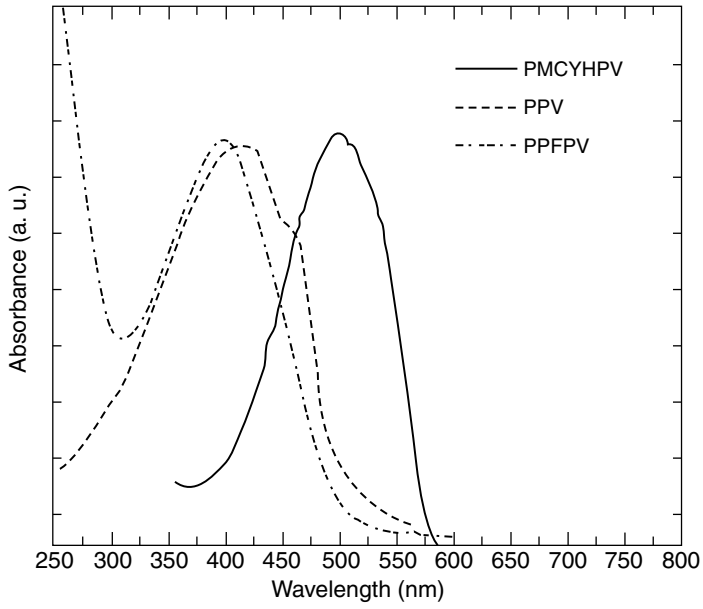


Figure 3.5 Absorption spectra of synthetic conjugated polymers. For chemical structures, see Chart 3.2. Adapted with permission from Ref. [5]; © 2002, Springer Verlag.

phenomena is provided by the *exciton model*, which was originally developed for inorganic semiconductors and dielectrics [6–8]. According to this model, the light-induced transition of an electron to an excited state located above the valence state causes a pronounced polarization of the chromophoric group. This excited state – called an exciton – is considered to be an entity of special nature of quasi-particle character. It resembles a hydrogen-like system with a certain binding energy which, besides other nonradiative deactivation routes, can give rise to the formation of a geminate electron/hole pair which can dissociate into free independent charge carriers, as presented in Equation 3.7.

$$\text{exciton} \quad \rightarrow \quad [h^+/e^-] \quad \rightarrow \quad h^+ \quad + \quad e^- \tag{3.7}$$

The dissociation is induced or strongly assisted by an external electric field. It is conjectured that excitons diffuse over certain distances and dissociate into free charge carriers, preferentially at specially structured sites on the surface of the sample, or on structural defects in the macromolecular system such as conformational kinks or chain twists. The electric conductivity in the polymers shown in Table 3.3 is thought to be due to hole conduction.

Lam Research Ex. 1047 - Page 125
Lam Research Corp. v. Inpria Corp.
IPR2024-00033 - U.S. Patent No. 9,823,564

3.1.6
Absorption in Biopolymers

Biopolymers such as nucleic acids, proteins and polysaccharides and lignins (Chart 3.3) absorb UV light to quite different extents. The absorption spectra of DNA and bovine serum albumin, which exhibit maxima at about 260 and 280 nm, respectively, are shown in Figure 3.6. Whereas common proteins absorb light measurably in the UV region with the aromatic amino acids phenylalanine,

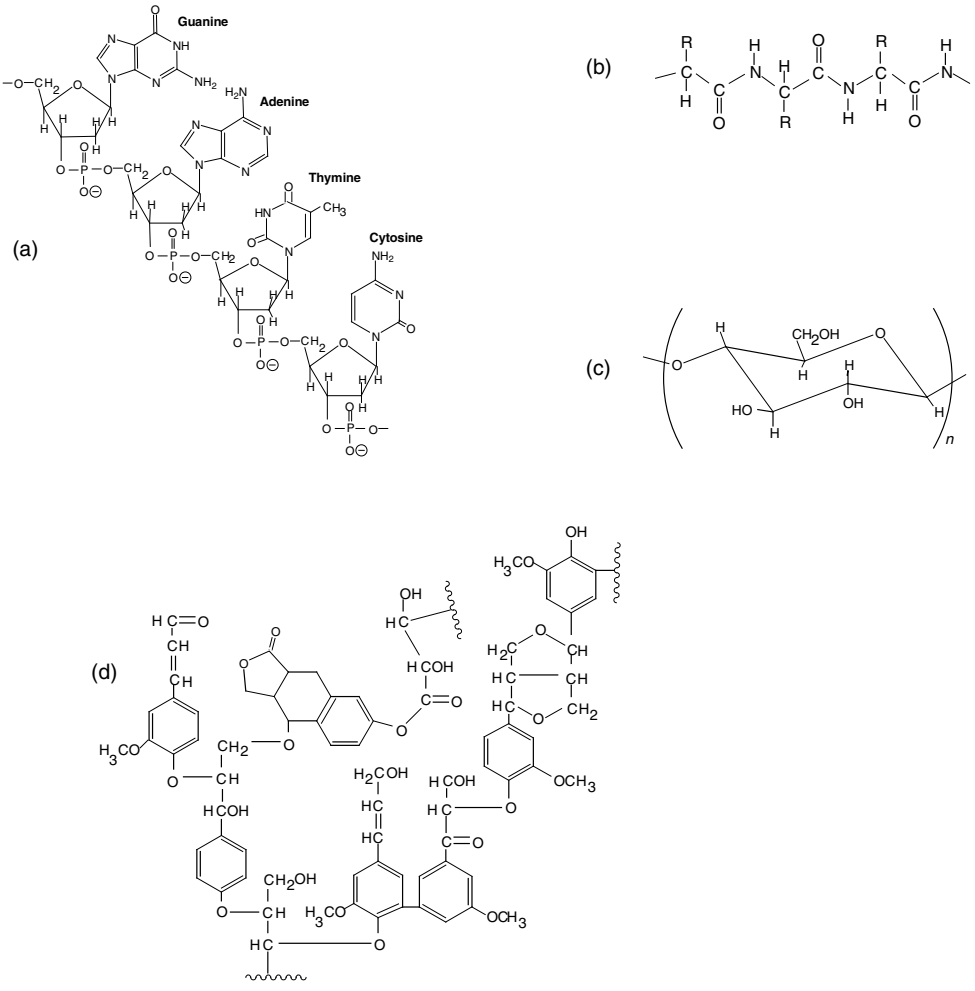


Chart 3.3 Biopolymer structures depicting: (a) different nucleotides contained in human deoxyribonucleic acid, DNA; (b) part of a protein chain consisting of various amino acid residues with R being H (glycine), CH_3 (alanine), $(CH_2)_4NH_2$ (lysine), CH_2SH (cysteine), and so on; (c) the base unit of the cellulose chain, representing the class of polysaccharides; and (d) part of a lignin with typical structural elements.

Lam Research Ex. 1047 - Page 126
Lam Research Corp. v. Inpria Corp.
IPR2024-00033 - U.S. Patent No. 9,823,564

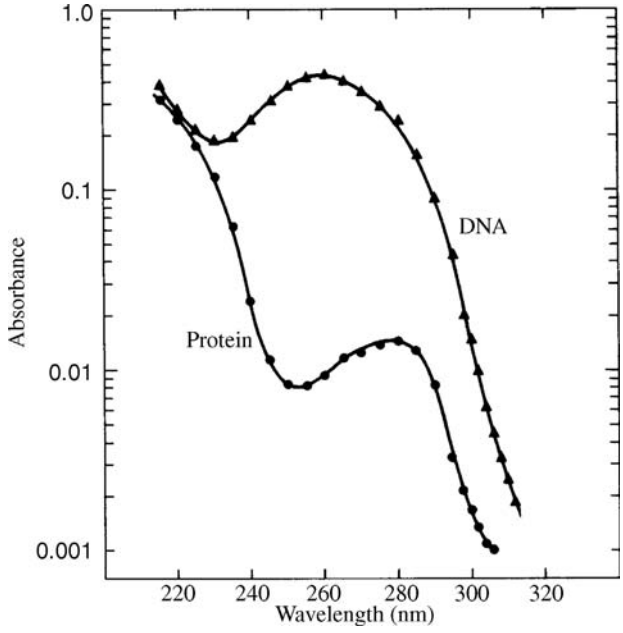


Figure 3.6 Optical absorption spectra of DNA and bovine serum albumin in aqueous solution ($c = 1.97 \times 10^{-2}\,g\,l^{-1}$). Adapted with permission from Ref. [9]; © 1980, Cambridge University Press.

tyrosine, and tryptophan (Chart 3.4) acting as chromophores, photoreceptor proteins containing covalently bound chromophoric groups absorb visible light.

Typical photoreceptor proteins are chlorophyllic protein complexes, and proteins belonging to the carotenoid (rhodopsin), phytochrome, and cryptochrome families [10]. These function as light-harvesting antenna pigments and auxiliary cofactors in the photosynthetic process, or they may play a regulatory role in biological processes. The chemical structures of typical chromophoric groups contained in these proteins are presented in Table 3.4.

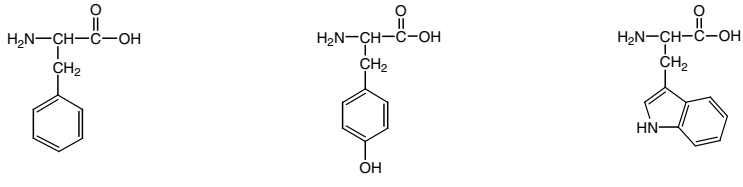
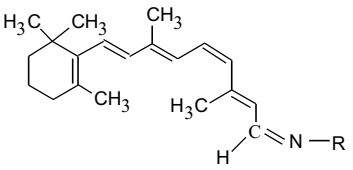
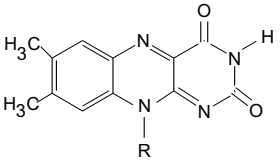
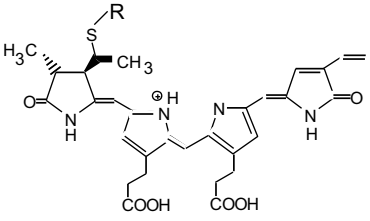
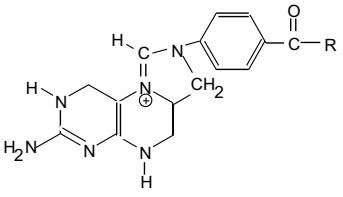
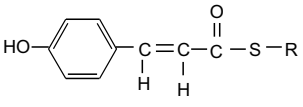


Chart 3.4 Chemical structures of aromatic amino acids.

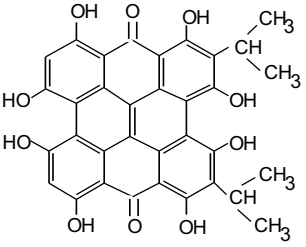
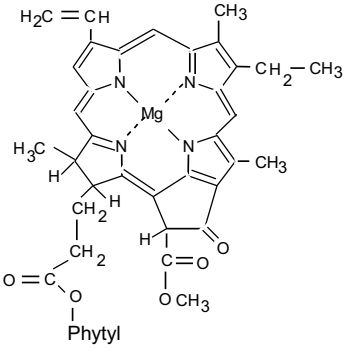
Lam Research Ex. 1047 - Page 127
Lam Research Corp. v. Inpria Corp.
IPR2024-00033 - U.S. Patent No. 9,823,564

Table 3.4 Photoactive chromophores (pigments) of photoreceptor proteins [11–17].

Typical chromophore	Photoreceptor class	Typical functions
 11-*cis* Retinal	Carotenoids	(a) Photoantennas in the photosynthetic system of plants. (b) Catalytic pigments in animal and bacterial rhodopsins.
 Flavin	Flavins	(a) Photoantennas in enzymes. (b) Cofactors for photolyase/blue-light photoreceptors.
 Phytochromobilin	Phytochromes	(a) Photoreceptors exerting morphogenic control in plants. (b) Accessory antennas in the light-harvesting complexes of photosynthetic systems.
 5,10-Methenyltetrahydrofolate (MTHF)	Pterins	Photoantennas in the majority of photolyase/cryptochrome blue-light photoreceptors.
 4-Hydroxycinnamate	Xanthopsins, Yellow Proteins	Sensory blue light receptors, water-soluble, controlling the life of bacteria in saline lakes.

Lam Research Ex. 1047 - Page 128
Lam Research Corp. v. Inpria Corp.
IPR2024-00033 - U.S. Patent No. 9,823,564

Table 3.4 (*Continued*)

Typical chromophore	Photoreceptor class	Typical functions
 Stentorin	Naphthodianthrones, Blepharismins	Photosensors in ciliated protozoans exhibiting step-up photophobic and negative phototactic responses.
 Chlorophyll *a*	Chlorophylls	Photoantennas in the light-harvesting complexes and electron donors in the reaction center of the photosynthetic system.

The optical absorption spectra of lignins extend into the visible wavelength region and exhibit peaks at about 205 and 280 nm, and shoulders at 230 and 340 nm [17a]. Polysaccharides such as cellulose and amylose essentially do not absorb light at $\lambda > 200$ nm.

3.1.7 Time-Resolved Spectroscopy

Powerful lasers that are capable of generating short light pulses, in conjunction with effective detection techniques, allow the detection of short-lived intermediates such as electronically excited molecules, free radicals and ions, and the determination of their lifetimes. At present, lasers generating light pulses ranging from the microsecond ($1\,\mu s = 10^{-6}$ s) to the femtosecond ($1\,fs = 10^{-15}$ s) time region are applied for *flash photolysis* studies. The flash photolysis method is used for time-resolved measurements of physical property changes caused by chemical processes induced by the absorption of a light flash (pulse). In this way, short-lived intermediates can be identified and the rate constants of reactions that they

Lam Research Ex. 1047 - Page 129
Lam Research Corp. v. Inpria Corp.
IPR2024-00033 - U.S. Patent No. 9,823,564

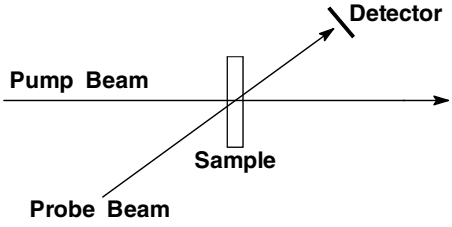


Figure 3.7 Schematic depiction of a set-up for time-resolved optical absorption measurements.

undergo can be determined. Consequently, this method is appropriate for elucidating reaction mechanisms. In many cases, time-resolved transient absorption experiments are performed with the aid of the pump-and-probe technique, as depicted in Figure 3.7. In this case, a pump beam is directed onto the sample, causing excited species to be generated. The formation and decay of these species can be monitored with the aid of an analyzing (probe) light beam that passes through the sample, perpendicular to the direction of the pump beam. In principle, a set-up of this type is also suitable for recording luminescence, if it is operated without the probe beam.

In picosecond and femtosecond flash photolysis studies, commercially available laser systems based on Ti:sapphire oscillators that are tunable between 720 and 930 nm (optimum laser power about 800 nm), and/or systems based on mode-locked dye lasers can be employed. For nanosecond investigations, Nd^{3+}:YAG (neodymium-doped yttrium-aluminum-garnet; optimum power at 1064 nm) and ruby (optimum power at 694.3 nm) laser systems are commonly used. Light pulses of lower wavelengths are produced with the aid of appropriate nonlinear crystals through second, third, or fourth harmonic generation. For example, short pulses of $\lambda = 532$, 355, and 266 nm are generated by means of Nd^{3+}:YAG systems. Apart from optical absorption measurements, detection methods based on electrical conductivity or light-scattering measurements are employed.

For further information on this subject, the reader is directed to Chapter 1 of Ref. [4].

3.2 Applications

3.2.1 General Aspects

During the past few decades, processes based on the interaction of visible and ultraviolet (Vis/UV) light with polymers have become important for various technical applications. The latter include the use of polymeric photoresists in the production of computer chips, and the use of nonlinear optical polymeric materials as core materials for optical wave guides. Polymers are employed in

Lam Research Ex. 1047 - Page 130
Lam Research Corp. v. Inpria Corp.
IPR2024-00033 - U.S. Patent No. 9,823,564

photocopying machines, in solar cells and in light-emitting diodes (*LED*s). UV/Vis light-based methods are employed for the analysis of polymers and also for the synthesis of polymers – that is, for the initiation of the polymerization of small molecules, a method which is applied in technical processes that involve the curing of coatings and adhesives and which may also be used by the dentist to cure tooth inlays. As all of these topics cannot be treated in detail within the framework of the present book, the reader should consult the author's book *Polymers and Light* [4] for further information. The following subsections are devoted to applications in polymer chemistry, including polymer synthesis and modifications of polymers, and also to applications in polymer physics including spectroscopy, light scattering, and holography. Technical developments concerning the curing of coatings, photolithography, LEDs and photovoltaics are covered later in this chapter.

3.2.2 Applications in Polymer Chemistry

3.2.2.1 Polymer Synthesis

Free-Radical Polymerization The free-radical chain polymerization of appropriate monomers can be initiated with the aid of Vis/UV light. Here, light serves only as an initiating tool, and does not interfere with the propagation and termination stages of the chain process. The initiation affords the presence of an appropriate light-absorbing initiator, as shown in Scheme 3.1.

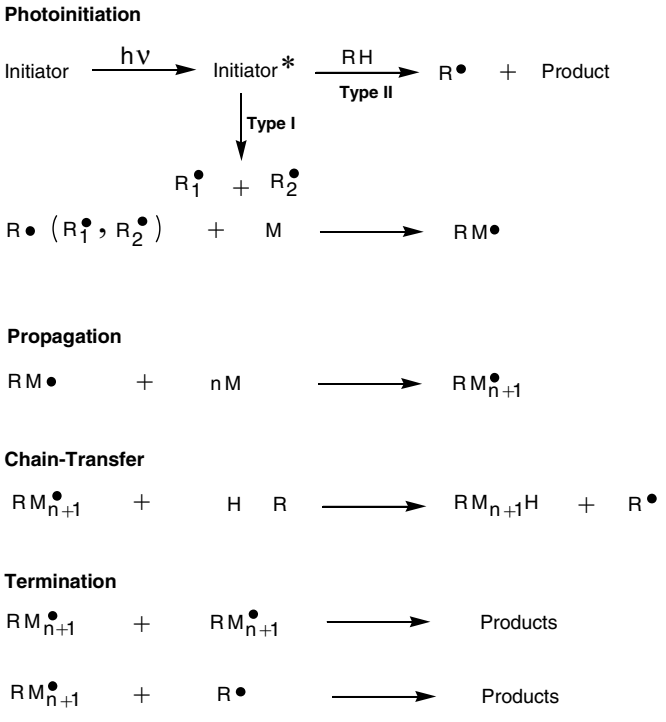
Two types of photoinitiator that differ in their mode of action of generating free radicals can be used. *Type I initiators* undergo a very rapid bond cleavage after the absorption of a photon, whereas *type II initiators* form relatively long-lived excited states capable of undergoing hydrogen abstraction or electron transfer reactions with a coinitiator that is deliberately added to the reaction system. Typical type I initiators are listed in Table 3.5. Most of these contain aromatic carbonyl groups which act as chromophores.

The dissociation energy of the C—C bond adjacent to a carbonyl group is lower than the energy of the excited state formed by absorption of a photon. Therefore, bond cleavage resulting in the formation of a pair of radicals, one of which is a benzoyl-type radical, occurs very rapidly (Scheme 3.2).

There are large differences in the reactivity of the free radicals generated from type I photoinitiators towards unsaturated monomers. For example, the rate constants for the addition of diphenylphosphinoyl radicals to vinyl monomers are of the order of 10^6 to $10^8\,\mathrm{mol\,l^{-1}\,s^{-1}}$ – that is, several orders of magnitude larger than those for benzoyl or other carbon-centered radicals [18b].

Typical type II initiators are listed in Table 3.6. Certain amines and alcohols (e.g., those presented in Table 3.7) serve as coinitiators by reacting with electronically excited initiators. As shown in Scheme 3.3, this reaction may involve an exciplex (excited complex) between the diaryl radical anion and the amine radical cation formed after electron transfer.

Lam Research Ex. 1047 - Page 131
Lam Research Corp. v. Inpria Corp.
IPR2024-00033 - U.S. Patent No. 9,823,564



Scheme 3.1 Reaction scheme illustrating the photoinitiated free-radical polymerization of monomer M, commonly a compound with a C=C bond.

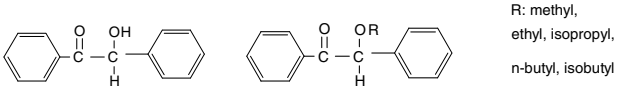
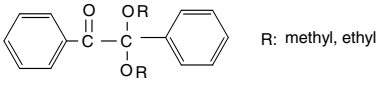
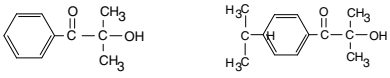
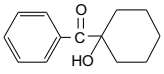
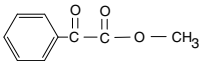
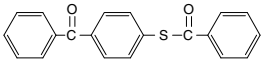
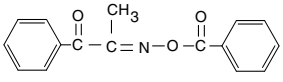
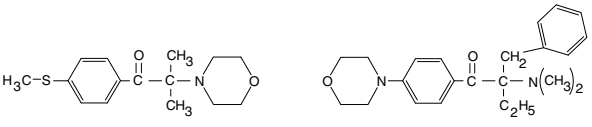
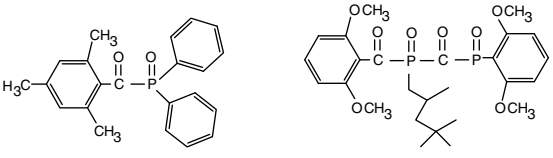
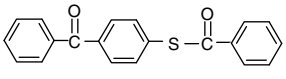
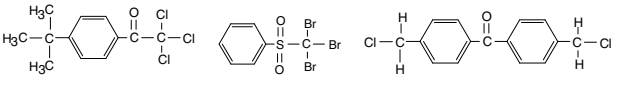
Commonly, industrially employed photopolymerization processes are performed in the 300–400 nm wavelength range, which is covered by most of the photoinitiators described so far.

For special applications including maskless photoimaging, production of holograms, color printing and the curing of dental fillings, initiating systems that absorb visible light are required. Photoinitiators operating with visible light include organometallic initiators, dyes, quinones, and α-diketones; some typical examples are listed in Table 3.8.

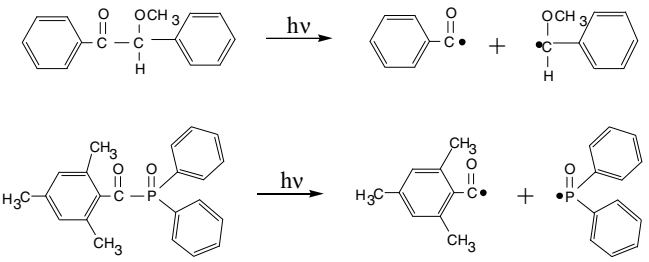
In general, the initiators listed in Table 3.8 are type II, and so are employed in conjunction with a coinitiator. An example of these would be an electronically excited dye molecule reacting with a tertiary amine to form amino radical cations that would then lose a proton to produce α-amino radicals capable of initiating free-radical polymerizations. Notably, the titanocene presented in Table 3.8 functions without a coinitiator, as it is thermally stable (it decomposes at 230 °C) and it absorbs light up to $\lambda = 560$ nm. Upon the absorption of a photon, the complex is isomerized and, in the presence of a monomer, the resulting coordinatively unsaturated isomer can undergo a ligand exchange

Lam Research Ex. 1047 - Page 132
Lam Research Corp. v. Inpria Corp.
IPR2024-00033 - U.S. Patent No. 9,823,564

Table 3.5 Chemical structures of typical type I free-radical photoinitiators.

Class	Chemical structure
Benzoin and benzoin ethers	
Benzil ketals	
Acetophenones	
Hydroxyalkylphenones	
Phenylglyoxylates	
S-Phenyl thiobenzoates	
O-Acyl-α-oximo ketones	
4-Morpholino-α-dialkylamino acetophenones	
Acylphosphine oxides	
Thiobenzoates	
Halogenated compounds	

Lam Research Ex. 1047 - Page 133
Lam Research Corp. v. Inpria Corp.
IPR2024-00033 - U.S. Patent No. 9,823,564

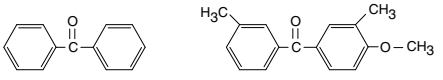
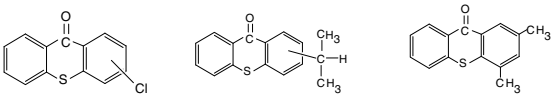
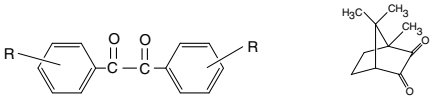
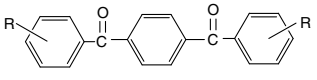
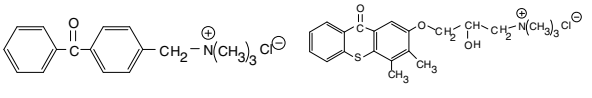


Scheme 3.2 Photofragmentation by α-cleavage of benzoin methyl ether and 2,4,6-trimethylbenzoyl diphenylphosphine oxide.

reaction to yield a biradical capable of initiating the polymerization (Scheme 3.4).

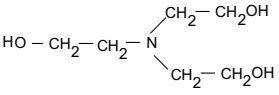
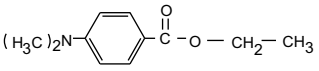
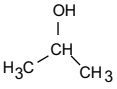
Interestingly, ketones containing germanium act as visible light initiators [20]. In this case, a coinitiator is not needed because these ketones are type I photoinitiators – that is, they undergo α-cleavage upon irradiation (Scheme 3.5).

Table 3.6 Chemical structures of typical type II photoinitiators.

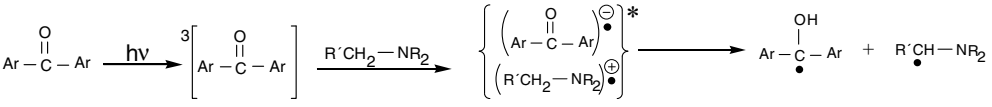
Class	Chemical structure
Benzophenone derivatives	
Thioxanthone derivatives	
1,2-Diketones (benzils and camphorquinone)	
Terephthalophenones	
Water-soluble aromatic ketones	

Lam Research Ex. 1047 - Page 134
Lam Research Corp. v. Inpria Corp.
IPR2024-00033 - U.S. Patent No. 9,823,564

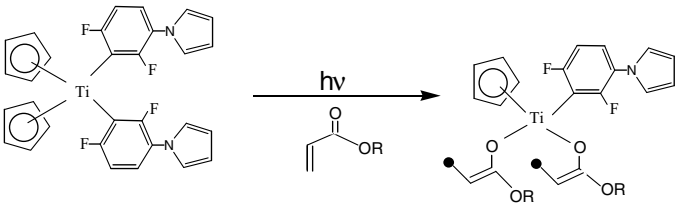
Table 3.7 Chemical structures of amines and alcohols functioning as co-initiators for type II free-radical photoinitiators.

Denotation	Chemical structure
Methyl diethanolamine	$H_3C—N(CH_2—CH_2OH)_2$
Triethanolamine	
Ethyl 4-(dimethylamino)benzoate	
2-Propanol	

Ionic Polymerization Ionic chain polymerizations can also be initiated with the aid of Vis/UV light although, as in the case of free-radical photopolymerization, the light serves only as an initiating tool. Most studies on ionic photopolymerization have focused on cationic polymerization, which proceeds rapidly and is not inhibited by oxygen [18,21–24]. Moreover, cationic photopolymerization is apt to polymerize monomers such as vinyl ethers, oxiranes (epoxides), and other heterocyclic compounds that do not polymerize via a free-radical mechanism (Table 3.9).



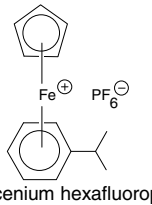
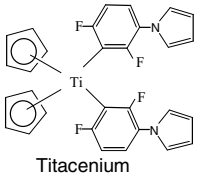
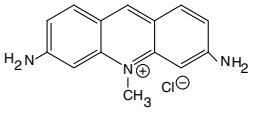
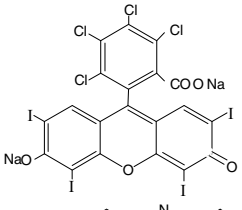
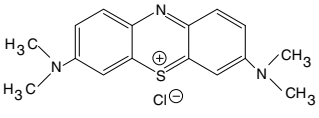
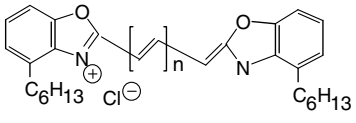
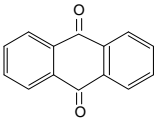
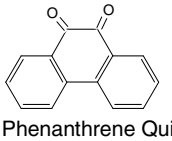
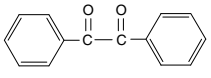
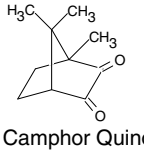
Scheme 3.3 Reaction of a diaryl ketone with a tertiary amine. Typical example of radical formation with the aid of type II initiators.



Scheme 3.4 Photoinitiation of the free-radical polymerization of an alkyl acrylate with the aid of a titanocene [19].

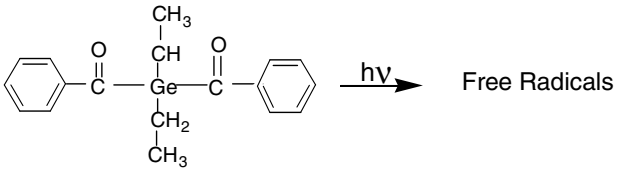
Lam Research Ex. 1047 - Page 135
Lam Research Corp. v. Inpria Corp.
IPR2024-00033 - U.S. Patent No. 9,823,564

Table 3.8 Photoinitiators for visible light.

Class	Example
Transition metal complexes	$Mn_2(CO)_{10}$, $Fe(CO)_5$, $Cr(CO)_6$, $W(CO)_6$, $Mo(CO)_6$, $CpMn(CO)_3$[a)]
	 Ferrocenium hexafluorophosphate
	 Titacenium
Dyes	
	Acriflavin 
	Rose Bengal 
	Methylene blue 
	Cyanine dye 
Quinones and α-Diketones	 Anthraquinone
	 Phenanthrene Quinone
	 Benzil
	 Camphor Quinone

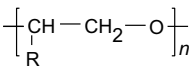
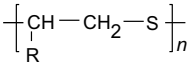
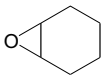
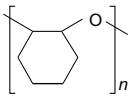
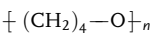
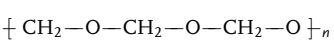
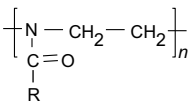
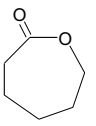
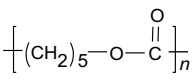
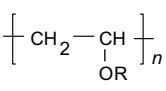
a) Cp: cyclopentadienyl.

Lam Research Ex. 1047 - Page 136
Lam Research Corp. v. Inpria Corp.
IPR2024-00033 - U.S. Patent No. 9,823,564



Scheme 3.5 Photolytic cleavage of a diacylgermane [20].

Table 3.9 Chemical structures of monomers that can be photopolymerized by a cationic mechanism [21].

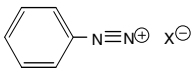
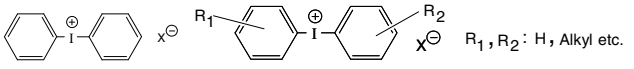
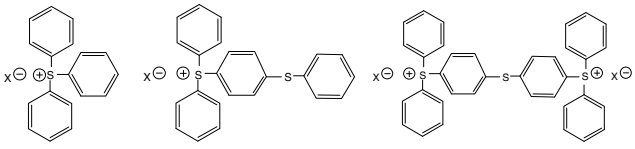
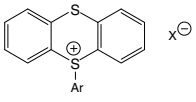
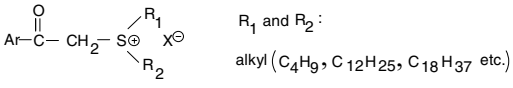
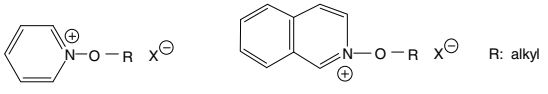
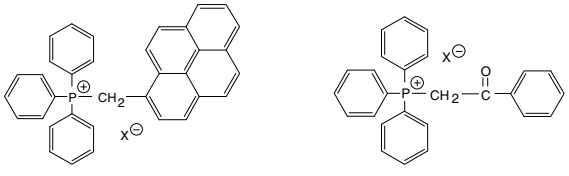
Monomer	Polymer
	
	
	
	
	
	
	
$H_2C{=}CH{-}O{-}R$	

Lam Research Ex. 1047 - Page 137
Lam Research Corp. v. Inpria Corp.
IPR2024-00033 - U.S. Patent No. 9,823,564

Cationic polymerizations proceed as chain reactions involving initiation and propagation. In most cases, there is no termination by neutralization, and the growing chains are terminated by nucleophilic impurities. Cationic chain reactions are photoinitiated by special initiators (Table 3.10) which date back to the pioneering studies of Crivello on sulfonium and iodonium salts containing non-nucleophilic anions such as $PF_6^{(-)}$ and $AsF_6^{(-)}$.

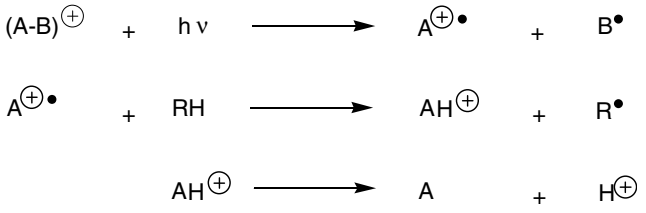
The direct photolysis of onium salt-type initiators of the general structure $\{(A-B)^{(+)}X^{(-)}\}$ results in the formation of Brønsted acids (superacids) of the structure $H^{(+)}X^{(-)}$), as shown in Scheme 3.6. In this mechanism, radical cations

Table 3.10 Chemical structures of cationic photoinitiators [25–28].

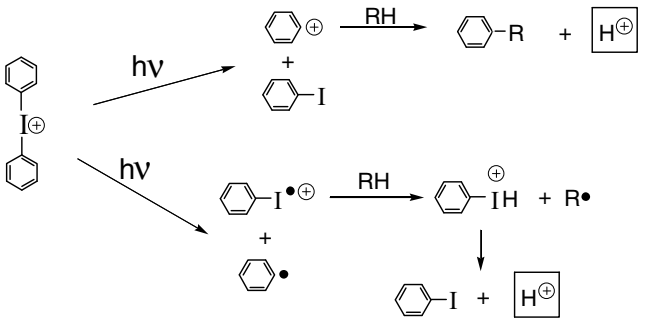
Class	Typical example[a)]
Diazonium salts	
Diaryl iodonium salts	
Triaryl sulfonium salts	
5-Arylthianthrenium salts	
Dialkylphenacyl sulfonium salts	
N-Alkoxy pyridinium and isoquinolinium salts	
Phosphonium salts	

a) $X^{(-)}$ denotes a non-nucleophilic anion such as $BF_4^{(-)}$, $PF_6^{(-)}$, $AsF_6^{(-)}$, $SbF_6^{(-)}$, $CF_3SO_3^{(-)}$, $CF_3(CF_2)_3SO_3^{(-)}$, $(C_6F_5)_4B^{(-)}$, $(C_6F_5)_4Ga^{(-)}$.

Lam Research Ex. 1047 - Page 138
Lam Research Corp. v. Inpria Corp.
IPR2024-00033 - U.S. Patent No. 9,823,564



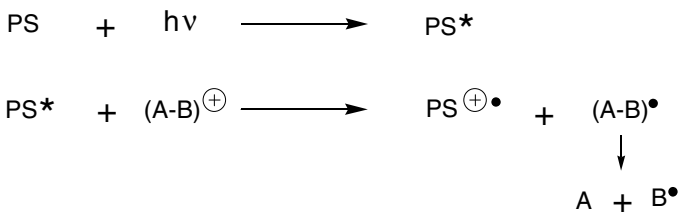
Scheme 3.6 Photolysis of an onium ion $(A-B)^{(+)}$.



Scheme 3.7 Mechanism of the photolysis of diphenyl iodonium ions.

$(A^{(+)\bullet})$ are supposed to abstract hydrogens from surrounding molecules, and the resulting cations $(AH^{(+)})$ release then protons.

As a typical example, Scheme 3.7 presents the detailed mechanism of the photolysis of diphenyl iodonium ions. The initiation of the polymerization can be accomplished by both Brønsted acids and radical cations $A^{(+)\bullet}$. Many onium salts do not, or only weakly, absorb light at $\lambda > 300$ nm, and in this case a photosensitizer (PS) that absorbs strongly at longer wavelengths may be employed in conjunction with an onium salt. Provided that the free energy, ΔG, has a sufficiently high negative value, excited PS molecules (PS^*) are oxidized by the onium ions, such that radical cations $PS^{+\bullet}$ are formed (Scheme 3.8).

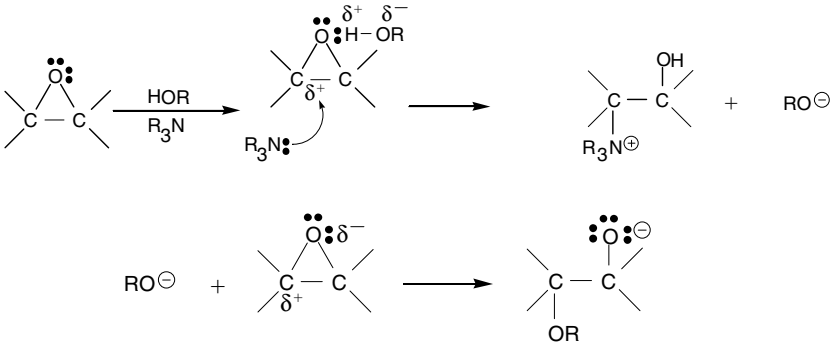


Scheme 3.8 Oxidation of an electronically excited sensitizer PS^* by an onium ion $(A-B)^{(+)}$.

Lam Research Ex. 1047 - Page 139
Lam Research Corp. v. Inpria Corp.
IPR2024-00033 - U.S. Patent No. 9,823,564

The $PS^{+\bullet}$ ions are apt to initiate the polymerization of an appropriate monomer M by direct reaction ($PS^{+\bullet} + M \rightarrow {}^{\bullet}PS\text{-}M^{+}$), or by abstracting hydrogens from the surrounding molecules (RH), thus forming proton-releasing $PSH^{+\bullet}$ ions ($PS^{+\bullet} + RH \rightarrow PSH^{+} + R^{\bullet} \rightarrow PS + R^{\bullet} + H^{+}$). Alternatively, commercially available free-radical photoinitiators absorbing at longer wavelengths can be employed in conjunction with onium salts. Free radicals generated by photolysis of the initiators can be oxidized by onium ions, and the so-formed carbocations can add directly to appropriate monomers; alternatively, they may form Brønsted acids by abstracting hydrogens from the surrounding molecules. This method is commonly referred to as *free-radical-promoted cationic polymerization*. Further details of this process are provided in Ref. [18a].

Anionic photopolymerization was pioneered by Kutal *et al.* [29–31]. The initial studies were performed with 2-cyanoacrylates (CAs) that are known to polymerize readily by an anionic mechanism. Upon exposure to light, potassium reineckate ($[Cr(NH_3)_2\ (NCS)_4]^{(-)}\ K^{(+)}$) was found to release $(NCS)^{(-)}$ ions, that add to CA molecules and thus initiate the anionic polymerization. More recent studies have focused on the photogeneration of organic bases capable of curing epoxidized resins through intermolecular crosslinking [26,32]. Photo-released strong organic bases such as tertiary amines can function as curing agents in the presence of polyols (oligomers bearing OH groups), as shown in Scheme 3.9.

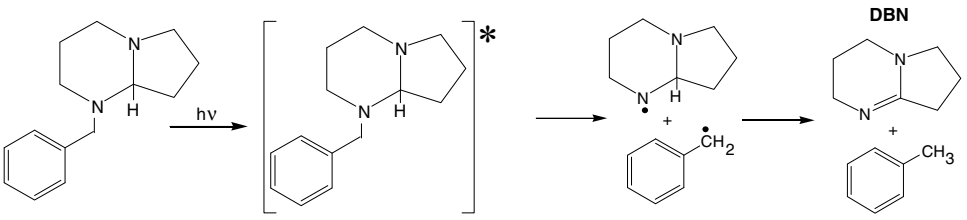


Scheme 3.9 Initiation of the anionic polymerization of epoxides by a tertiary amine in conjunction with a polyol [32b].

Reportedly, 5-benzyl-1,5-diazabicyclo[4.3.0]nonane is a very effective photolatent initiator [26,32]. It releases 1,5-diazabicyclo[4.3.0]non-5-ene (DBN), a bicyclic amidine possessing a high basicity ($pK_a = 12 - 13$) due to the strong conjugative interaction between the two nitrogens. The suggested release mechanism is depicted in Scheme 3.10.

As compared with the classical curing of ready-to-use formulations with curing times of several hours, phototriggered curing has the advantage of being performed on demand, with a working window extending to a full day [32].

Lam Research Ex. 1047 - Page 140
Lam Research Corp. v. Inpria Corp.
IPR2024-00033 - U.S. Patent No. 9,823,564



Scheme 3.10 Photoinduced release of DBN from 5-benzyl-1,5-diazabicyclo[4.3.0]nonane [32a].

Block and Graft Copolymerization Block and graft polymers of the general structures indicated in Chart 3.5 possess a specific combination of physical properties, and are therefore of interest for the development of new high-tech devices.



Block Copolymer **Graft Copolymer**

Chart 3.5 General chemical structures of block copolymers and graft copolymers consisting of monomer units A and B.

Most photochemical procedures for the synthesis of block and graft copolymers are based on the modification of already existing polymers with photolabile groups incorporated at defined positions – that is, at the chain end, at side chains, or in the main chain (Chart 3.6) [33].

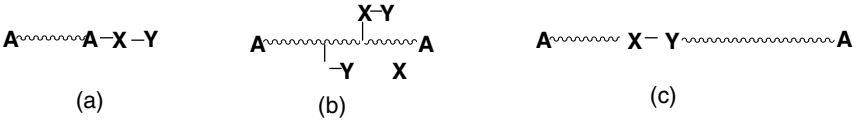
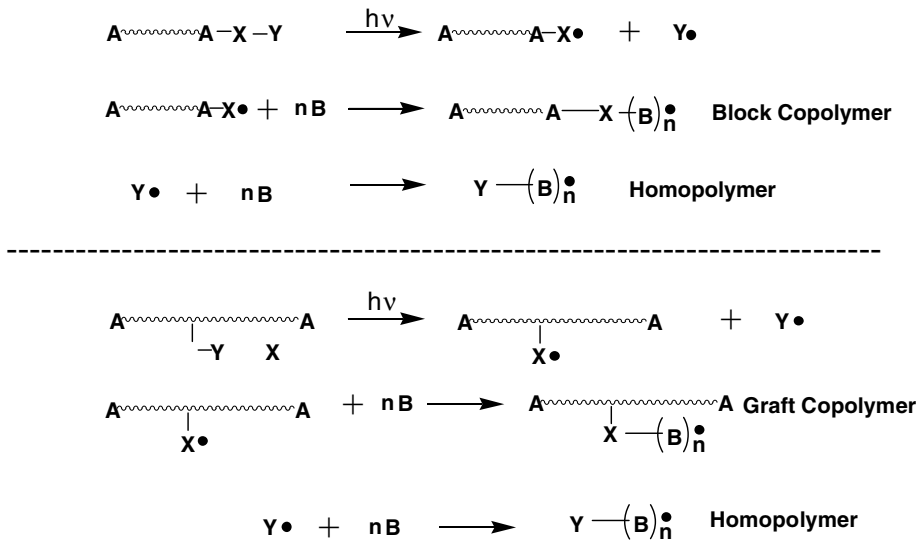


Chart 3.6 General structures of polymers bearing photolabile groups X-Y at the chain end (a), at side chains (b), or incorporated into the main chain (c).

Both types of copolymer can be synthesized by means of photochemical methods based on free radical or cationic mechanisms [33–46], although for practical applications cationic polymerizations are less attractive than free-radical polymerizations. In the latter case, light absorption induces the dissociation of the photolabile groups into pairs of free radicals capable of initiating the polymerization of a monomer present in the system (Scheme 3.11).

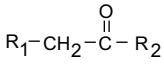
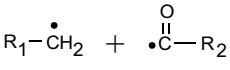
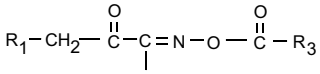
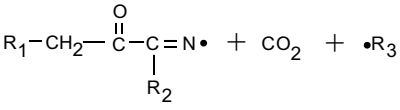
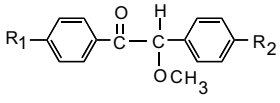
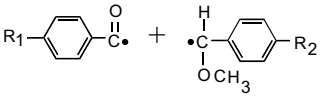
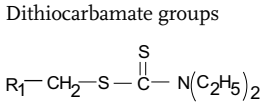
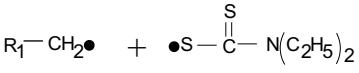
Typical chromophoric groups that have been chemically incorporated into or attached to linear macromolecules for the purpose of photosynthesizing block or graft copolymers are compiled in Table 3.11. With regards to the last entry in

Lam Research Ex. 1047 - Page 141
Lam Research Corp. v. Inpria Corp.
IPR2024-00033 - U.S. Patent No. 9,823,564



Scheme 3.11 Formation of block and graft copolymers following the photodissociation of chromophoric groups X-Y. For the sake of simplicity, chain-termination reactions are not included.

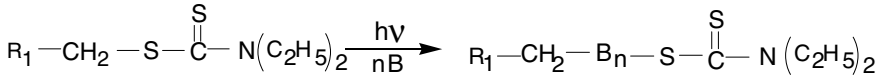
Table 3.11 Photolabile groups, chemically incorporated into linear polymers at in-chain, lateral or terminal positions, giving rise to the formation of reactive free radicals [33].

Photolabile groups[a)]	Free radicals
Carbonyl groups	
	
Keto oxime ester groups	
	
Benzoin methyl ether groups	
	
Dithiocarbamate groups	
	

a) R_1 denotes a macromolecular substituent.

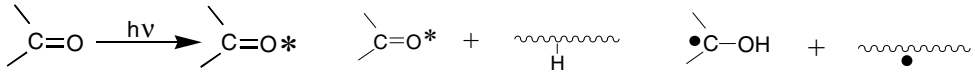
Lam Research Ex. 1047 - Page 142
Lam Research Corp. v. Inpria Corp.
IPR2024-00033 - U.S. Patent No. 9,823,564

Table 3.11, the low reactivity of the sulfur-centered radical should be noted as it does not react with vinyl monomers to initiate kinetic chains but rather acts as a terminator of the growing chains. An initiator behaving in this way is termed an *iniferter* (initiator-transfer-agent-terminator) (Scheme 3.12) [47,48].



Scheme 3.12 Formation of a diblock copolymer with the aid of an iniferter. R_1 denotes a macromolecular substituent.

Block and graft copolymerization can also be initiated indirectly by generating photochemically reactive species that attack the polymer so as to generate free radical sites on the latter that are capable of reacting with monomer molecules. A typical system is presented in Scheme 3.13.



Scheme 3.13 Indirect generation of lateral radical sites at a linear polymer. The carbonyl group is supposed to be part of an aromatic molecule (benzophenone or anthraquinone).

Photografting of the surface of polymeric articles is a technically applied method that can lead to changes in the surface properties of polymeric articles. For example, photografting can impart hydrophilicity to the hydrophobic surfaces of polyalkenes and thus impart antifogging, antistatic and antistaining properties, as well as providing improvements in surface dyeability, adhesiveness, printability, and biocompatibility. Surface grafting can also be accomplished using high-energy radiation of a low penetration depth, including electron beam radiation and soft X-rays (see Section 5.2.3). Photografting may be advantageous over high-energy radiation grafting in that it is virtually restricted to a very thin surface layer, which means that it can be applied with minimal effort with respect to the radiation sources.

Polyalkenes and other polymers that are produced industrially in large quantities lack chromophoric groups capable of absorbing UV light emitted from commonly available light sources. To circumvent this problem, procedures based on the adsorption of monomers and initiators by presoaking have been elaborated. For example, acrylic acid, acrylamide, vinylpyridine or glycidyl acrylate can be grafted onto low-density polyethylene or linear polyesters in layers ranging from 2 to 8 nm in thickness, by using a continuous process that employs benzophenone as a hydrogen abstraction-type initiator. In this case, the polymer foil is drawn from a roll through a solution of the initiator and monomer to a reaction chamber where it

Lam Research Ex. 1047 - Page 143
Lam Research Corp. v. Inpria Corp.
IPR2024-00033 - U.S. Patent No. 9,823,564

Table 3.12 Surface grafting of monomers; recent investigations.

Substrate	Monomers	Remarks	Reference(s)
Low-density polyethylene	Acrylic acid, acrylamide, vinyl pyridine, glycidyl acrylate	Enhanced hydrophilicity and dye adsorption, adhesion to different substrates	[40,41]
Low-density polyethylene Polypropylene	Acrylic acid, hydroxypropyl acrylate	Enhanced hydrophilicity, wettability	[49]
Low-density polyethylene Polypropylene	Maleic anhydride, vinyl acetate/maleic anhydride	Enhanced hydrophilicity	[50,51]
Polyurethane	Methacrylic acid	Enhanced hydrophilicity, enhanced biological cell compatibility	[52]
Ultrafine inorganic particles (silica, titania)	Acrylic acid, acrylamide, acrylonitrile, styrene	Grafted materials give stable dispersions in appropriate liquids	[53,54]

is irradiated at $\lambda \approx 250$ nm and subsequently rolled up [40]. Batch processes such as immersion grafting and vapor-phase grafting can also be employed for this purpose; in the latter process the initiator-coated polymer is irradiated in an atmosphere of the monomer.

Various studies demonstrating the enhancement of hydrophilicity and wettability of hydrophobic polymers, as well as the improvement of adhesion of polymers to various substrates, are listed in Table 3.12. The grafting of ultrafine inorganic particles, such as nanosized silica and titania, with vinyl monomers is also an attractive prospect [49–54].

Topochemical Polymerization The light-induced solid-state polymerization of certain monomers at ambient temperature is a very intriguing phenomenon that has been dealt with in numerous articles and books [55–64]. Diacetylenes and dialkenes (see Charts 3.7 and 3.8) polymerize under crystal-lattice control

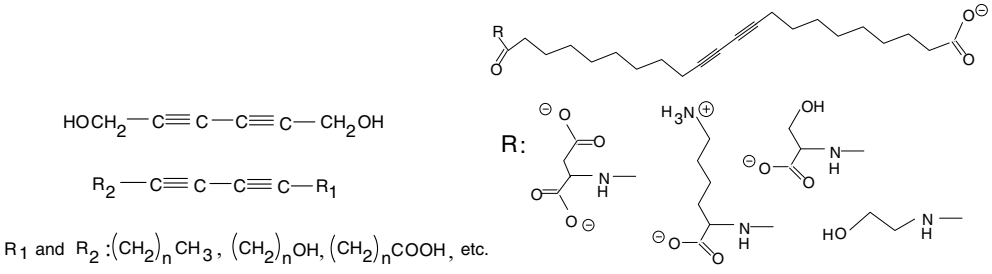


Chart 3.7 Diacetylene derivatives capable of undergoing topochemical photopolymerization [56,65].

Lam Research Ex. 1047 - Page 144
Lam Research Corp. v. Inpria Corp.
IPR2024-00033 - U.S. Patent No. 9,823,564

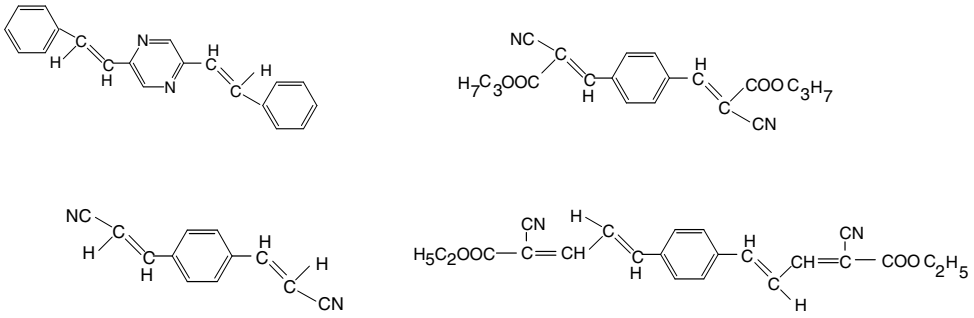


Chart 3.8 Dialkenes capable of undergoing topochemical photopolymerization [59].

upon absorption of light [55,57]. The reactivity of the monomers and the structure of the resulting products are governed by the molecular geometry in the reactant crystal, and the reaction proceeds with a minimum of atomic and molecular movement. An essential prerequisite for the topochemical polymerization of diacetylenes is a packing of the monomer molecules at a distance of $d = 4.7 - 5.2$ Å and a tilt angle of about 45° between the molecular axis and the packing axis [64].

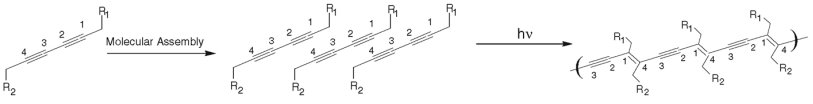
The topochemical diacetylene photopolymerization is applicable to various organized structures, including Langmuir–Blodgett films, liposomes, vesicles, and self-assembled monolayers (*SAM*s) on metal oxide or graphite surfaces. Scheme 3.14 depicts an assembly of diacetylene molecules and the subsequent photopolymerization at 254 nm. At ambient temperatures, the polymerization proceeds as a chain reaction by 1,4-addition, and results in alternating ene–yne polymer chains with exclusive *trans* selectivity. The quantum yield for initiation is low (about 0.01) [60].

In polymer monolayers obtained in this way, a color change from blue to red is induced by changes in temperature or pH, or by mechanical stress, and in conjugated polydiacetylenes this accompanies conformational changes. This phenomenon has been exploited in the construction of direct sensing devices [67–72], for example, in the detection of a virus [67] and of cholera toxin [68]. Such devices consist of polydiacetylene bilayers functionalized with covalently attached receptors. The binding of biological entities (large molecules or cells) provides a mechanical stimulus that results in a chromatic shift [65].

The photopolymerization of diolefinic crystals was discovered in the case of the [2 + 2] photocyclopolymerization of 2,5-distyrylpyrazine (DSP) crystals, and was termed *four-center-type polymerization* (Scheme 3.15) [58,59].

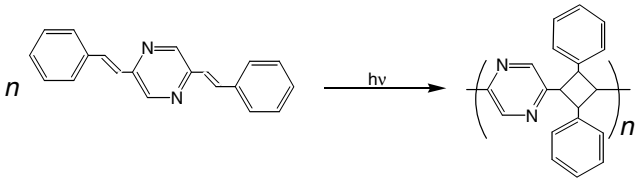
It should be noted that the polymerization of dialkenes proceeds as a stepwise process, and not as a chain reaction. In other words, the addition of each repeating unit to the chain requires the absorption of a further photon (Scheme 3.16).

Lam Research Ex. 1047 - Page 145
Lam Research Corp. v. Inpria Corp.
IPR2024-00033 - U.S. Patent No. 9,823,564



Scheme 3.14 Schematic representation of the polymerization of assembled functional diacetylenes by 1,4-addition upon exposure to UV light. R_1 and R_2 denote functionalized alkyl chains [66].

Lam Research Ex. 1047 - Page 146
Lam Research Corp. v. Inpria Corp.
IPR2024-00033 - U.S. Patent No. 9,823,564



Scheme 3.15 Four-center-type photopolymerization of crystalline 2,5-distyrylpyrazine [59].

3.2.2.2 Modification of Synthetic Polymers

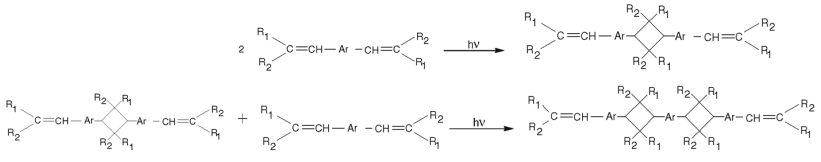
Alterations in the Absence of Oxygen As noted above (see Section 3.1), light is absorbed by chromophoric groups incorporated into polymers. The chemical activity of a chromophoric group may originate from two features:

- The bonding strength between adjacent atoms is strongly reduced when an electron is promoted to a higher level, and therefore a chemical bond can be cleaved if the atoms separate upon vibration. This type of monomolecular bond cleavage is a very rapid process (ca. 10^{-12} s) that cannot be prevented by any means after the absorption of a photon.
- The electronic excitation leads to a relatively stable state. The lifetime of the excited state is so long (occasionally approaching the millisecond range) that, in the condensed phase, chromophoric groups have many encounters with the surrounding molecules, thus enabling bimolecular chemical interactions. Thereby, the original chemical bond is relinquished and a new bond is formed. This type of bond cleavage can be prevented by *energy quenching*, that is, through energy transfer from the excited chromophore to an additive functioning as an energy acceptor.

The bond-scission processes mentioned above are energetically feasible as the photon energies associated with radiation of wavelengths ranging from 250 nm (4.96 eV) to 400 nm (3.1 eV) correspond to the bond-dissociation energies of common covalent bonds – that is, about 3.5 eV for C—H, C—C, and C—O bonds (in aliphatic compounds). The deactivation of identical electronically excited chromophores can result in the cleavage of different chemical bonds. This common phenomenon is demonstrated for polystyrene in Scheme 3.17. Note that the bond cleavage probabilities are not equal; indeed, the quantum yields for the individual processes may differ by orders of magnitudes.

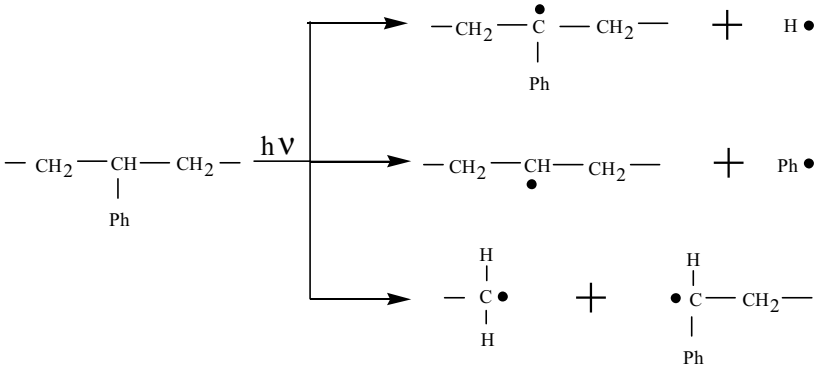
As indicated in Scheme 3.17, several different free radicals are generated upon exposure to light. These radicals undergo various reactions, including hydrogen-abstraction reactions, thereby generating new free radicals, and also coupling reactions. In this way, a variety of products is eventually formed, as is shown in Scheme 3.18 for the case of polystyrene.

Lam Research Ex. 1047 - Page 147
Lam Research Corp. v. Inpria Corp.
IPR2024-00033 - U.S. Patent No. 9,823,564

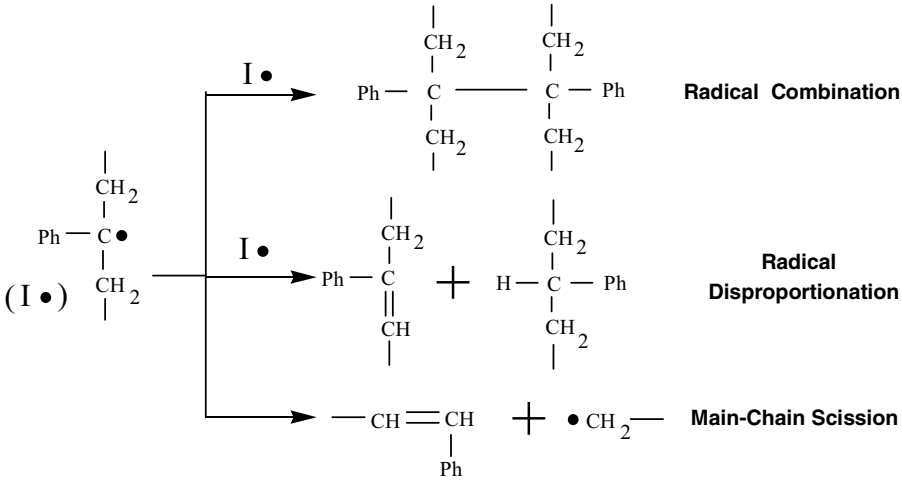


Scheme 3.16 Stepwise [2 + 2] photocyclopolymerization of a dialkene [58,59].

Lam Research Ex. 1047 - Page 148
Lam Research Corp. v. Inpria Corp.
IPR2024-00033 - U.S. Patent No. 9,823,564



Scheme 3.17 Primary reactions in the photolysis of polystyrene [73].



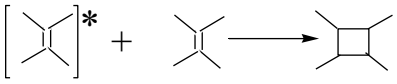
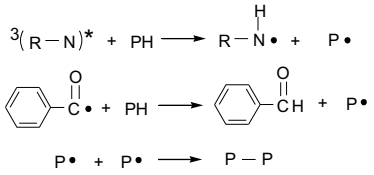
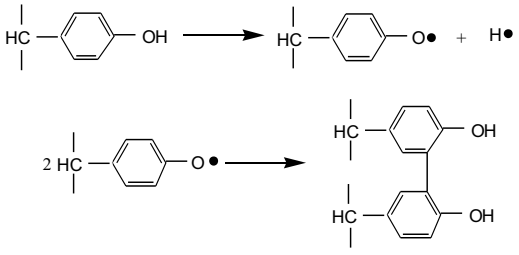
Scheme 3.18 Reactions of a benzyl-type macroradical (I•) formed in the photolysis of polystyrene.

Photochemical methods based on the direct absorption of light by the polymer can hardly be envisaged for chemical modifications of commercial polymers. For some time, practical applications which have been devoted to photolithography have played an important role and involved light-induced changes in the solubility of polymers as a consequence of intermolecular crosslinking or main-chain scission. Of note in this context are the methods listed in Table 3.13, which can be used to crosslink linear polymers (for further details, see Ref. [4]).

With regards to the hydrogen-abstraction method referred to in Table 3.13, it should be noted that triplet nitrene and benzoyl radicals can be formed by the photodecomposition of azides (Scheme 3.19), and of type I free radical photo-initiators (see Table 3.5), respectively.

Lam Research Ex. 1047 - Page 149
Lam Research Corp. v. Inpria Corp.
IPR2024-00033 - U.S. Patent No. 9,823,564

Table 3.13 Photo-crosslinking of linear polymers.

Method	Characterization
Cycloaddition of C=C bonds incorporated laterally or in the chain	
Coupling of macroradicals generated by hydrogen abstraction through reactive radicals for example, triplet nitrene or benzoyl radicals	
Cleavage of pendant phenolic OH groups with ensuing coupling of phenoxyl radicals	

$$RN_3 + h\nu \rightarrow {}^1(RN)^* + N_2$$
$${}^1(RN)^* \rightarrow {}^3(RN)$$

Scheme 3.19 Formation of singlet and triplet excited nitrene by photodecomposition of azides.

As noted above, different macromolecules in a polymer sample commonly undergo simultaneously different types of bond rupture upon exposure to light; that is, bond cleavage processes occur both in the side chains and in the main chain of linear polymers. Bond rupture in side chains results in the formation of lateral macroradicals, which can give rise to the release of low-molar-mass compounds and can also form intermolecular and intramolecular crosslinks. In contrast, bond rupture in the main chain can result in a reduction in chain length. The quantum yields of photoproducts of selected linear polymers are listed in Table 3.14. The quantum yields for main-chain cleavage and crosslinking, $\Phi(S)$ and $\Phi(X)$, are low (<0.1), and those of volatile products resulting from side-chain degradation are also quite low for most polymers.

Lam Research Ex. 1047 - Page 150
Lam Research Corp. v. Inpria Corp.
IPR2024-00033 - U.S. Patent No. 9,823,564

Table 3.14 Photoproduct quantum yields of polymers in the rid state, determined at room temperature *in vacuo* [74].

Polymer	$\Phi(S)/\Phi(X)$	$\Phi(S) \times 10^2$	$\Phi(X) \times 10^2$	λ(nm)	Volatile products ($10^2\ \Phi$)
Poly-α-methyl-styrene		0.1–0.6		253.7	α-methylstyrene H_2 (1.7×10^{-2})
Poly(methyl methacrylate)		1.2–3.9		253.7	CH_3OH (48); $HCOOCH_3$ (14); CO; H_2; CO_2
Poly(phenyl vinyl ketone)		6.0		313	
Poly(vinyl acetate)	1.4	6.6	4.7	253.7	CH_3COOH (1.0); CO_2 (0.65); CO (0.69); CH_4 (0.38)
Poly(ethylene terephthalate)	2.7	0.16	0.06	313	
Poly(methyl acrylate)	1.0	0.19	0.19	253.7	HCHO (2); CH_3OH (0.2); $HCOOCH_3$ (0.8)
Poly(*p*-methyl-styrene)	0.52			253.7	H_2 (6); CH_4 (0.04)

In fact, it is often the case that the processes of main-chain scission and crosslinking occur simultaneously and cause changes in the molar mass distribution, and also in the average molar mass of the polymer. Theoretical studies on this topic have revealed that the dependence of the weight-average molar mass M_w ($g\,mol^{-1}$) of linear polymers undergoing simultaneous main-chain cleavage and crosslinking on the absorbed dose D_{abs} (photons g^{-1}) is given by Equation 3.8 [74a]:

$$\frac{1}{M_{w,D}} = \frac{1}{M_{w,0}} + \left(\frac{\Phi(S)}{2} - 2\Phi(X)\right)\frac{D_{abs}}{N_A} \tag{3.8}$$

where $\Phi(S)$ and $\Phi(X)$ denote the quantum yields for main-chain cleavage and crosslinking, respectively, and N_A is Avogadro's number. Equation 3.8 holds for the case that the initial molar mass distribution is of the most probable type, and that main-chain ruptures and crosslinks are randomly distributed along the polymer chains. Crosslinking predominates if $\Phi(S) < 4\ \Phi(X)$, and in this case the reciprocal average molar mass decreases – that is, M_w increases – with increasing absorbed dose. In contrast, main-chain cleavage predominates if $\Phi(S) > 4\ \Phi(X)$, in which case the reciprocal average molar mass increases – that is, M_w decreases – with increasing absorbed dose. In this context, it should be noted that predominant main-chain cleavage causes a deterioration in the important mechanical properties that are related to the molar mass of the polymer. Several linear polymers have

Lam Research Ex. 1047 - Page 151
Lam Research Corp. v. Inpria Corp.
IPR2024-00033 - U.S. Patent No. 9,823,564

Table 3.15 Predominant effects upon UV irradiation of rigid polymers in the absence of oxygen [74].

Polymer	Predominant effect
Poly(methyl methacrylate)	Degradation
Poly(α-methyl styrene)	Degradation
Poly(phenyl vinyl ketone)	Degradation
Polyacrylonitrile	Crosslinking
Poly(methyl acrylate)	Crosslinking
Polystyrene	Crosslinking

been characterized with respect to the predominance of crosslinking or main-chain cleavage in Table 3.15.

When linear polymers undergo predominantly crosslinking, a three-dimensional insoluble network is formed. The absorbed dose at which the insoluble network begins to form is termed the *gel dose*, D_{gel}, and this corresponds to an average of one crosslink per weight-average molecule [74a]. As a consequence, a simple equation may be derived from Equation 3.8 for the relationship between D_{gel} and $\Phi(X)$ (see Equation 3.9):

$$D_{gel} = \frac{N_A}{2\Phi(X)M_{w,0}} \tag{3.9}$$

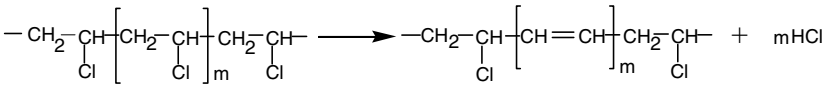
Equation 3.9 holds in the absence of main-chain scission, that is, at $\Phi(S) = 0$. In this case, the molar mass approaches infinity at the gel dose, that is, $1/M_{w,D_{gel}} = 0$.

Regarding the outdoor application of commercial polymers such as polyolefins, photo-oxidation reactions are of prominent importance. Photooxidation processes will be discussed in the next subsection.

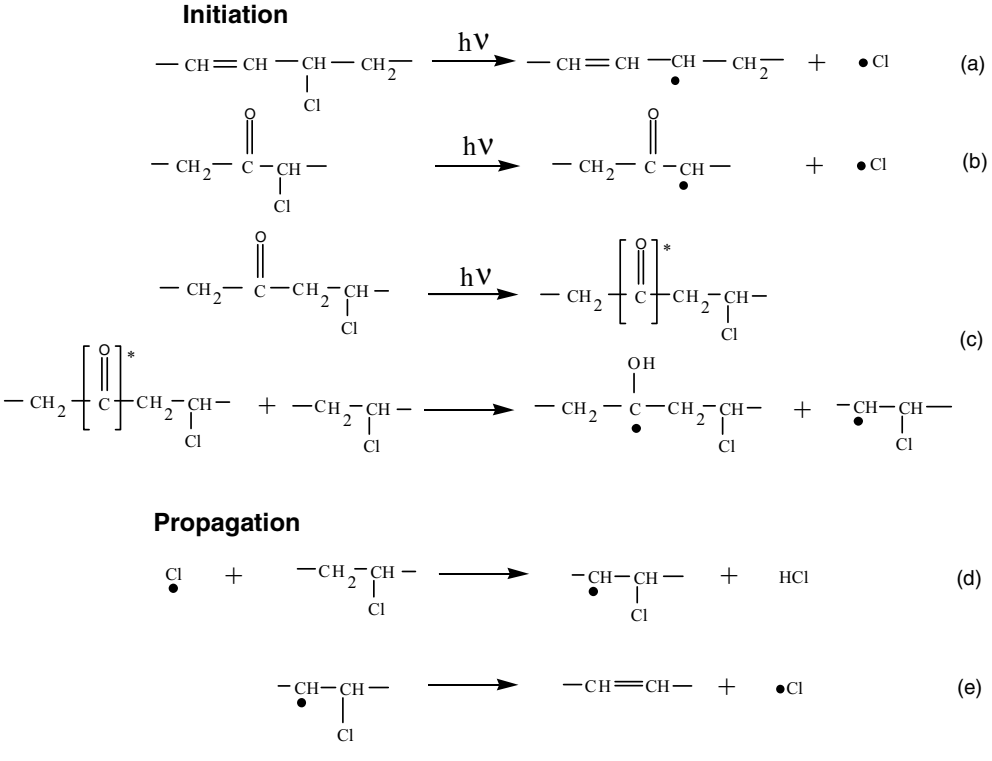
Light-induced chemical alterations of polymers have been extensively investigated during the past decades, as becomes evident from a plethora of research reports, patents, and various books and reviews on the subject [75–100]. While it is not the intention here to review those photoreactions in detail, the properties of poly(vinyl chloride) (*PVC*) will be briefly discussed as it is one of the most widely used polymers and it behaves differently compared to many polymers when exposed to light. Upon exposure to UV/Vis light, PVC products suffer from a deterioration of their mechanical and electrical properties and eventually become discolored [84,92,94]. Such discoloration is due to a dehydrochlorination process that results in the formation of long conjugated polyene sequences in the polymer chain (Scheme 3.20). Polyenes can give rise to photo-crosslinking reactions.

It is generally accepted that the elimination of HCl occurs by way of a free-radical chain reaction initiated by chromophore impurities. Whilst chlorine atoms may function as the propagating species, as shown in Scheme 3.21, unsaturated

Lam Research Ex. 1047 - Page 152
Lam Research Corp. v. Inpria Corp.
IPR2024-00033 - U.S. Patent No. 9,823,564



Scheme 3.20 Elimination of HCl with polyene formation at the exposure of poly(vinyl chloride) to UV/visible light.



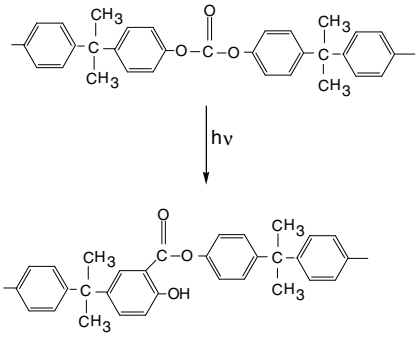
Scheme 3.21 Mechanism of the light-induced dehydrochlorination of poly(vinyl chloride).

moieties are believed to be the most important initiator species, with carbonyl groups the next most important. The latter can undergo Norrish-type reactions while excited carbonyl groups can transfer energy to unsaturated moieties, or even abstract hydrogens. In addition, hydroperoxide and peroxide groups formed during autoxidation of the polymer can contribute to the initiation process [84] (see next subsection).

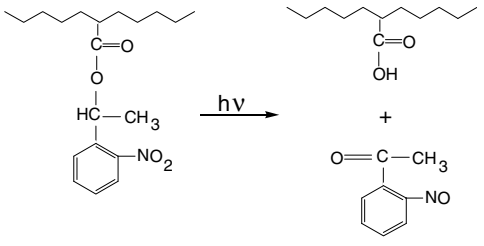
Commercial PVC products commonly contain plasticizers (up to 40%) such as phthalates or mellitates. In the past, phthalates were found to exert a weak protective effect with respect to C—Cl bond cleavage and polyene formation by quenching the electronically excited states of impurity chromophores [101].

Lam Research Ex. 1047 - Page 153
Lam Research Corp. v. Inpria Corp.
IPR2024-00033 - U.S. Patent No. 9,823,564

One special type of light-induced alterations concerns the rearrangement of constituent groups in either the main chain or the pendant groups of linear polymers. Typical processes that have gained importance are the photo-Fries rearrangement of aromatic esters, amides, and urethanes, and the *o*-nitrobenzyl ester rearrangement. Some typical examples are illustrated in Schemes 3.22 and 3.23.



Scheme 3.22 Photo-Fries rearrangement in the main chain of a polycarbonate.



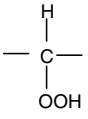
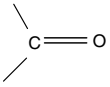
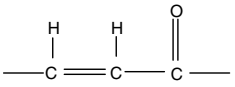
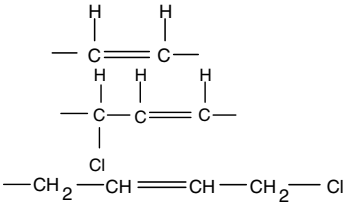
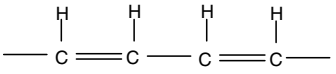
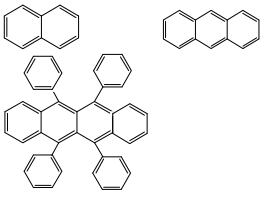
Scheme 3.23 Light-induced *o*-nitrobenzyl ester rearrangement in pendant groups of a linear polymer.

Photorearrangements in polymers can lead to pronounced property changes. For example, polymers containing *o*-nitrobenzyl pendant groups become soluble in aqueous solution, since the benzyl ester groups are converted into carboxyl groups.

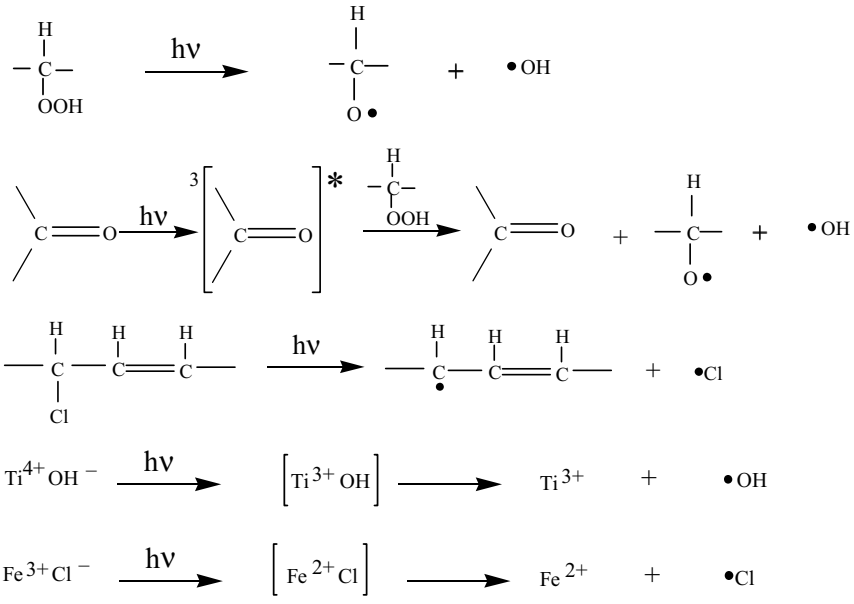
Photo-Oxidation Oxidation processes are initiated, when polymers absorb visible or UV light in the presence of air [102–106]. According to the structures of their repeating units, several important commercial linear polymers, including polyethylene, polypropylene and PVC, are transparent to light of $\lambda > 250\,\text{nm}$. However, in these cases impurities originating from the polymerization or from the processing may act as light-absorbing entities (Table 3.16).

Lam Research Ex. 1047 - Page 154
Lam Research Corp. v. Inpria Corp.
IPR2024-00033 - U.S. Patent No. 9,823,564

Table 3.16 Impurity chromophores commonly contained in commercial polyalkenes or poly(vinyl chloride)s.

Structure of chromophore	Denotation
	Hydroperoxide group
	Carbonyl group
	α,β-Unsaturated carbonyl group
	Double bonds
	Conjugated double bonds
	Polynuclear aromatics (e.g., naphthalene, anthracene, rubrene)
Ti^{4+} Al^{3+} Fe^{3+}	Metal ions
$[RH \ldots . O_2]_{CT}$	Charge-transfer complexes

Lam Research Ex. 1047 - Page 155
Lam Research Corp. v. Inpria Corp.
IPR2024-00033 - U.S. Patent No. 9,823,564



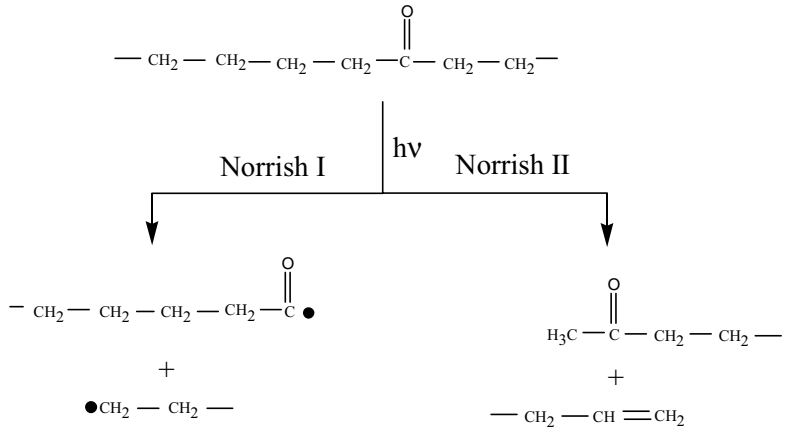
Scheme 3.24 Generation of free radicals by photoreactions of impurity chromophores.

Moreover, these impurities are capable of absorbing the near-UV portion (290–400 nm) of the solar radiation that reaches the Earth, and may therefore jeopardize or curtail the stability of polymers in outdoor applications, hastening their degradation.

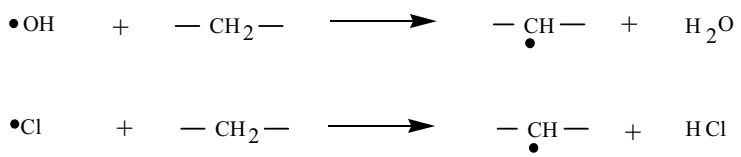
Some of the chromophores shown in Table 3.16, such as carbonyl groups or carbon–carbon double bonds, are chemically incorporated into the polymers, whereas others such as polynuclear aromatic compounds and metal salts, are adventitiously dispersed. The latter are almost invariably present in many polymers. The impurity chromophores function as free-radical generators, as shown in Scheme 3.24. Hydroperoxide groups – the most common and important of the chromophores – yield highly reactive hydroxyl radicals. Carbonyl groups can mediate the decomposition of hydroperoxide groups via triplet energy transfer, and may also give rise to the formation of free radicals via the so-called Norrish type I reaction; this is illustrated in Scheme 3.25 for the case of a copolymer of ethylene and carbon monoxide. Metal salts produce free radicals by electron-transfer processes whereby, in the case of PVC, allyl-type chlorine atoms are split off. In most cases, photo-oxidation processes proceed as chain reactions, with free macroradicals generated in the initiation step via hydrogen abstractions (Scheme 3.26).

In the propagation step, macroradicals P$^{\bullet}$ react with dioxygen to produce hydroperoxide groups and additional macroradicals (Scheme 3.27); this process is frequently referred to as *autoxidation*. The hydroperoxide groups can then

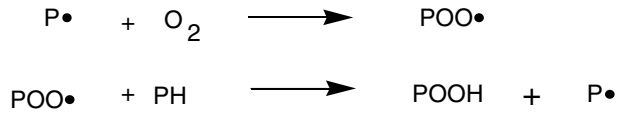
Lam Research Ex. 1047 - Page 156
Lam Research Corp. v. Inpria Corp.
IPR2024-00033 - U.S. Patent No. 9,823,564



Scheme 3.25 Photoreactions of carbonyl groups.



Scheme 3.26 Generation of macroradicals via hydrogen abstraction.



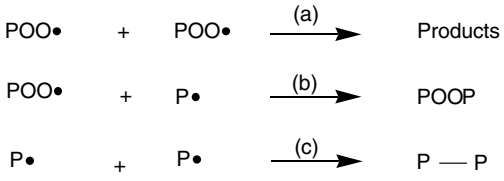
Scheme 3.27 Propagation of the chain reaction in the autoxidation process.

be decomposed photolytically, provided that the wavelength of the incident light is less than about 300 nm (see Scheme 3.24). Radicals generated in this way can initiate additional chain reactions (chain branching) by abstracting hydrogens from neighboring macromolecules, for instance by the reaction according to Equation 3.10:

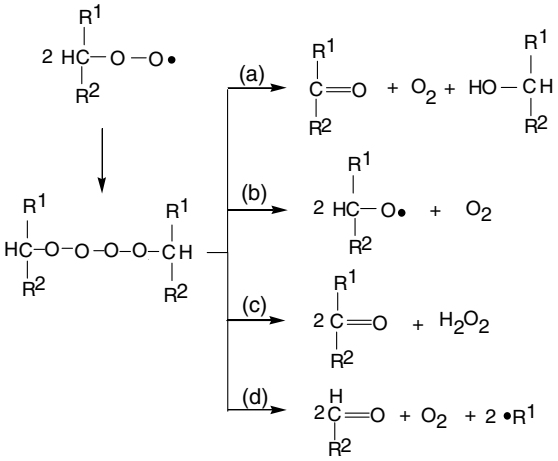
$$^{\bullet}OH + PH \rightarrow H_2O + P^{\bullet} \tag{3.10}$$

The kinetic chains are terminated by radical coupling reactions (Scheme 3.28). The combination of peroxyl radicals (reaction (a) in Scheme 3.28) is assumed to proceed via a tetroxide P–O_4–P, a short-lived intermediate (Scheme 3.29).

Lam Research Ex. 1047 - Page 157
Lam Research Corp. v. Inpria Corp.
IPR2024-00033 - U.S. Patent No. 9,823,564



Scheme 3.28 Termination reactions in the autoxidation process.



Scheme 3.29 Decay processes of secondary peroxyl radicals (Russel mechanism) [107].

As a consequence of autoxidation, the most important mechanical properties of polymeric materials may undergo a sudden breakdown during continuous exposure to light. This is shown in Figure 3.8, where the impact strength of an ABS polymer is seen to fall drastically after a certain exposure time [108].

Oxyl radicals, such as those formed by reaction (b) in Scheme 3.29, can abstract hydrogen via intermolecular and/or intramolecular reactions, but alternatively they can decompose and form carbonyl groups (Scheme 3.30).

In conclusion, the light-induced oxidation of polymers results in the formation of hydroperoxide, peroxide, and carbonyl groups. In the case of commercial polymers consisting of linear macromolecules, oxidation leads to main-chain cleavage and causes the deterioration of certain important mechanical properties. Appropriate stabilization measures to avoid these problems are discussed in the following subsection.

Stabilization In order for commercial polymers to withstand prolonged exposure to solar radiation, they are commonly stabilized with small amounts (between 0.25 and 3.0%) of additives denoted as *light stabilizers* [109–120]. It might be recalled that

Lam Research Ex. 1047 - Page 158
Lam Research Corp. v. Inpria Corp.
IPR2024-00033 - U.S. Patent No. 9,823,564

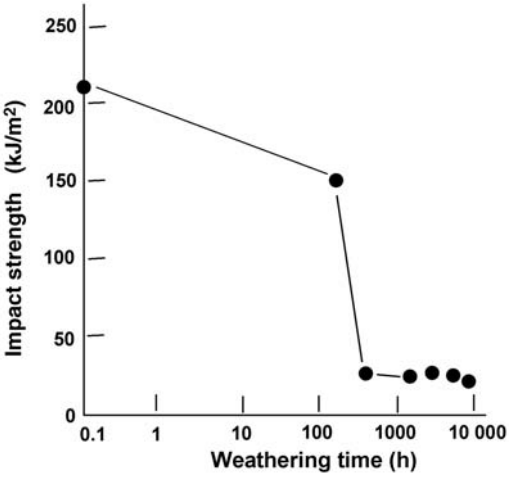
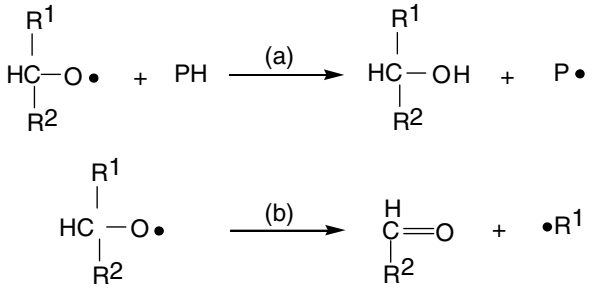


Figure 3.8 Photodegradation of an acrylonitrile/butadiene/styrene (*ABS*) copolymer at 30 °C. Plot of impact strength versus simulated natural exposure time (Xenon-arc radiation, 0.55 W m^{-2} at 340 nm). Adapted with permission from Ref. [108]; © 2004, Elsevier.

the absorption of a photon by a chromophoric group generates an electronically excited state, and that the latter can undergo various deactivation modes; the subsequent deactivation frequently results in the formation of free radicals that attack intact molecules. Autoxidation processes can also be initiated in the presence of dioxygen (see previous subsection). Strategies currently employed to stabilize commercial polymers are targeted at interfering with the absorption of light, at deactivating excited states, and at the reactions of free radicals. Thus, the stabilizers used may be allocated to three classes – UV absorbers, energy quenchers, and radical scavengers – though some stabilizers may employ more than one of these mechanisms to afford protection to a polymer. Radical scavengers are commonly denoted as *chain terminators*, *chain breakers*, or *antioxidants*. Light stabilizers for polymers are required to be physically compatible with the polymers, and should not be readily transformed into reactive species. Moreover, they should not alter the mechanical or other physical properties of the polymer before, during, or after



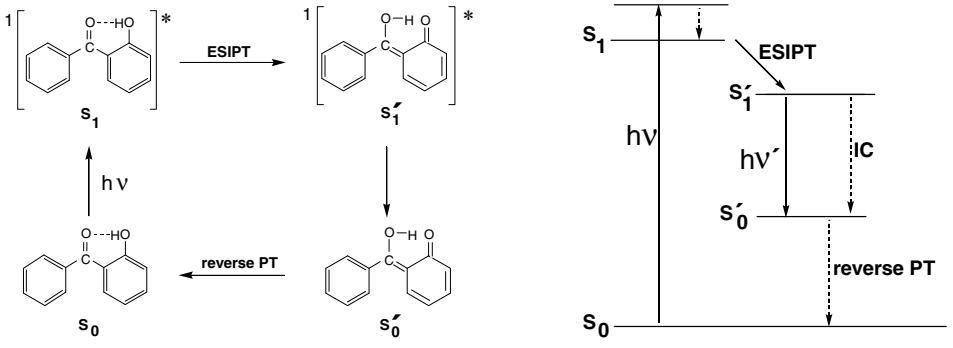
Scheme 3.30 Reactions of oxyl radicals.

Lam Research Ex. 1047 - Page 159
Lam Research Corp. v. Inpria Corp.
IPR2024-00033 - U.S. Patent No. 9,823,564

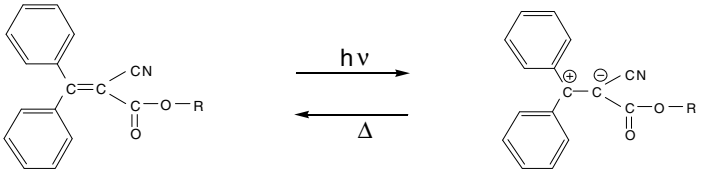
exposure to light. It should be noted, however, that stabilizers generally undergo a sacrificial consumption which determines the ultimate outdoor lifetime of polymer articles.

Screening is the most obvious method of protection. Although surface painting is not applicable to most plastics due to incompatibility problems, intrinsic screening is widely applied. This is based on the addition of effective light absorbers, known as *pigments*; these are hyperfinely dispersed compounds with extinction coefficients that significantly exceed those of the polymers. The most prominent pigment is carbon black, but other industrially important pigments and fillers include ZnO, MgO, $CaCO_3$, $BaSO_4$, and Fe_2O_3.

UV absorbers are colorless, highly photostable compounds that have absorption maxima lying between 300 and 380 nm, as well as high absorption coefficients; some examples are listed in Table 3.17. UV absorbers transform the absorbed radiation energy into harmless thermal energy by way of photophysical processes that involve the ground state and the excited state of the molecule. The mechanisms proposed for phenolic UV absorbers, benzotriazoles and nonphenolic oxanilides are based on proton tunneling; this process is referred to as excited state intramolecular proton transfer (*ESIPT*). The mechanism involved, as discussed for 2-hydroxybenzophenone, is shown in Scheme 3.31. Intramolecular charge separation after photoexcitation serves to explain the UV-absorbing properties of cyanoacrylates (Scheme 3.32).



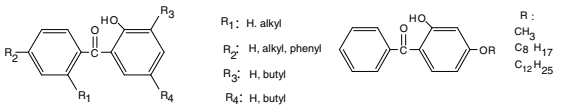
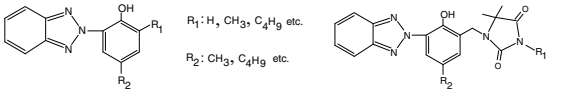
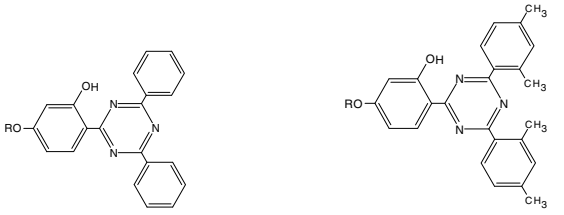
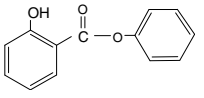
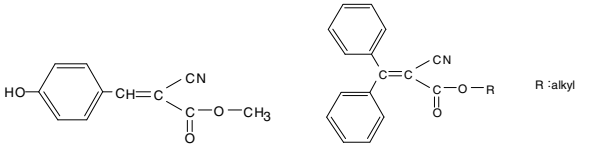
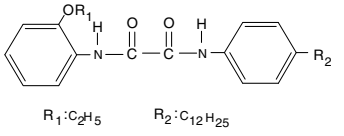
Scheme 3.31 Mechanism of excited state intramolecular proton transfer (*ESIPT*) in the case of 2-hydroxybenzophenone.



Scheme 3.32 Mechanism of intramolecular charge separation in the excited state of cyanoacrylates.

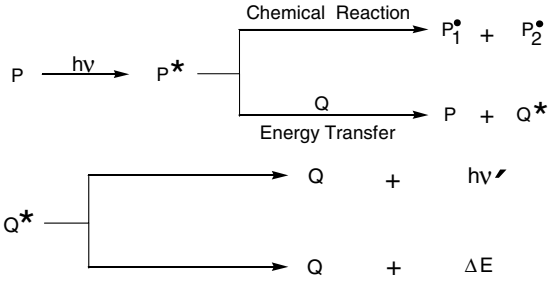
Lam Research Ex. 1047 - Page 160
Lam Research Corp. v. Inpria Corp.
IPR2024-00033 - U.S. Patent No. 9,823,564

Table 3.17 Typical UV absorbers [109,121].

Denotation	Chemical structure
o-Hydroxybenzophenones	
2-(2-Hydroxyphenyl)benzo-triazoles	
2-(2-Hydroxyphenyl)-1,3,5-triazines	
Phenyl salicylates	
Cyanoacrylates	
Oxanilides	

Energy quenchers accept energy from excited chromophores tethered to polymers, and thus prevent harmful chemical transformations (Scheme 3.33). Commercially available energy quenchers include complexes and chelates of transition metals, such as those shown in Chart 3.9. The importance of these quenchers derives mainly from their ability to interact with excited carbonyl groups, which are present in many thermoplastics, especially in polyalkenes.

Lam Research Ex. 1047 - Page 161
Lam Research Corp. v. Inpria Corp.
IPR2024-00033 - U.S. Patent No. 9,823,564



Scheme 3.33 Schematic illustration of the action of energy quenchers. P and Q denote polymer and quencher, respectively, and the asterisk denotes an electronically excited state.

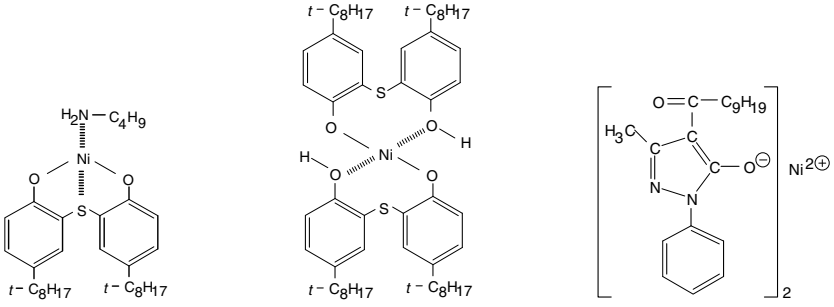
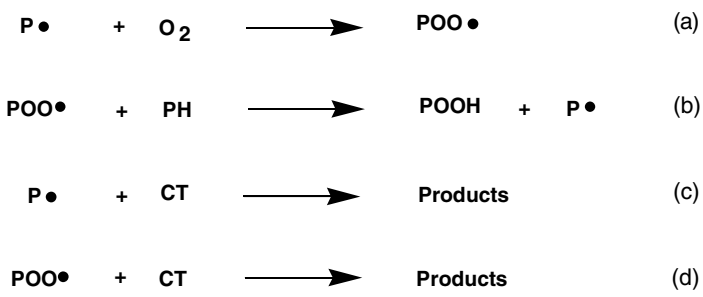


Chart 3.9 Chemical structures of typical nickel chelates used as quenchers in polyalkenes [113].

Chain terminators interrupt the propagation of the oxidative chain reaction (reactions (a) and (b) in Scheme 3.34). The chain propagation would be totally prevented if all macroradicals $P^•$ generated during the initiation stage were scavenged according to reaction (c). However, reaction (a) proceeds at a relatively large rate, even at ambient temperature and low O_2 pressure. Therefore, in practically relevant situations, the concentration of $P^•$ will be much lower than that of $POO^•$ [117]. Consequently, an effective chain terminator is required to react rapidly with $POO^•$ (reaction (d)). Hindered amines based on the 2,2′,6,6′-tetramethylpiperidine (TMP) structure (Chart 3.10) satisfactorily fulfill these requirements, especially in the case of polyalkenes. They are generally referred to as *hindered amine stabilizers* (*HAS*s), and frequently also as *hindered amine light stabilizers* (*HALS*s). HALS are transparent to visible and terrestrial UV light (300–400 nm), and in polymeric matrices are oxidized in a sacrificial reaction (by way of a not yet fully understood mechanism) to stable nitroxyl(aminoxyl) radicals >N—O•. A mechanism based on the reaction of HASs with alkyl hydroperoxides and alkyl peroxyl radicals is presented in Scheme 3.35 [109].

Besides hindered amines, compounds also exist that are capable of functioning as long-term hydroperoxide decomposers. These include alkyl and aryl phosphites,

Lam Research Ex. 1047 - Page 162
Lam Research Corp. v. Inpria Corp.
IPR2024-00033 - U.S. Patent No. 9,823,564



Scheme 3.34 Schematic illustration of elementary reactions occurring in a polymeric matrix containing O_2 and a radical scavenger (chain terminator, *CT*).

and organosulfur compounds such as dialkyl dithiocarbamates, dithiophosphates, and dithioalkyl propionates (Chart 3.11). These compounds are commonly used to stabilize thermoplastic polymers during processing in the melt at temperatures up to 300 °C. Their contribution to the long-term stabilization of polymers at ambient temperatures is small, but not negligible.

Laser Ablation Material can be ejected when a laser beam or, more generally speaking, a high-intensity light beam is directed onto a polymer sheet. On the basis of this phenomenon, which is commonly known as *laser ablation*, microstructures can be generated and mechanical machining such as cutting and drilling of polymeric materials is possible. For these purposes, excimer lasers operating at wavelengths of 157, 193, 248, 308, and 351 nm, and diode-pumped solid-state Nd:YAG lasers, generating 10 ns light pulses at the harmonic wavelengths of 266, 355, and 532 nm (pulse energy: several mJ) have been applied. Laser ablation can also be exploited for other practical applications, such as laser desorption mass spectrometry or laser plasma thrusters for the propulsion of small satellites [122–124]. Both, photochemical and photothermal reactions contribute to the release of volatile fragments, a process that leads to the breakage of a certain number of chemical bonds in the polymer within a short period. According to a presently accepted model [125], the absorption of laser light leads to the electronic excitation of chromophoric groups in the polymer. The subsequent deactivation processes involve both direct bond breakage in the excited state and relaxation; that is, an internal conversion to a highly excited vibrational state of the electronic ground state. In the latter case, thermal activation of surrounding molecules can lead to further bond breakage. If the number of broken bonds exceeds a threshold value, a thin layer of the polymer is ablated, and the ablated material forms a *plume* that consists of gaseous products and particulate fragments. This plume expands three-dimensionally and continues to absorb laser radiation. The chemical structures of polymers that have proved appropriate for laser ablation are shown in Chart 3.12.

Lam Research Ex. 1047 - Page 163
Lam Research Corp. v. Inpria Corp.
IPR2024-00033 - U.S. Patent No. 9,823,564

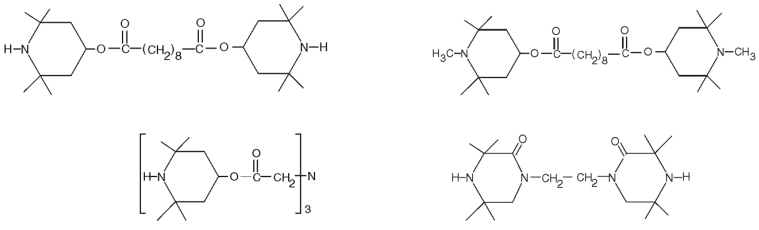
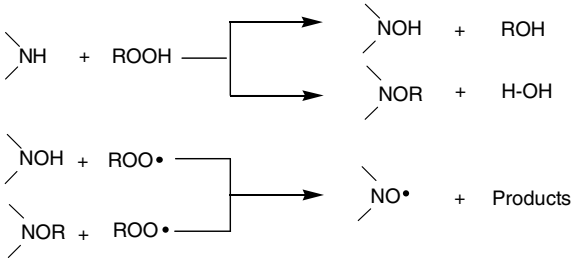


Chart 3.10 Chemical structures of typical commercial hindered amine stabilizers [120].

Lam Research Ex. 1047 - Page 164
Lam Research Corp. v. Inpria Corp.
IPR2024-00033 - U.S. Patent No. 9,823,564



Scheme 3.35 Schematic illustration of the oxidation of hindered amine stabilizers by alkyl hydroperoxides and alkyl peroxyl radicals [109].

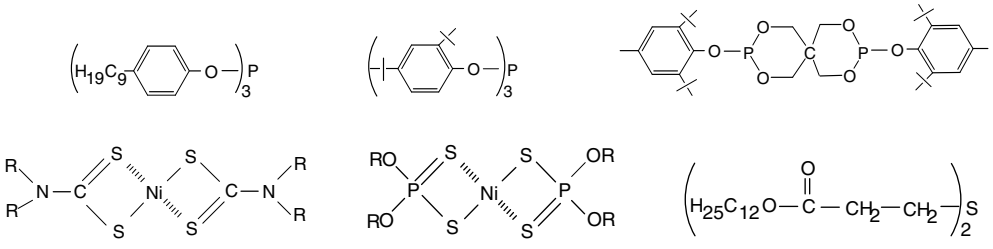


Chart 3.11 Chemical structures of hydroperoxide decomposers [113–116].

Applications employing laser ablation of polymers include film deposition and the synthesis of certain organic compounds. Laser beam ablation in conjunction with mass spectrometry is an important tool for polymer analysis, which is referred to as laser desorption mass spectrometry (*LDMS*). One particular type of LDMS, termed matrix-assisted laser desorption/ionization (*MALDI*), has contributed essentially to the analysis of proteins (Nobel prize for chemistry to K. Tanaka in 2002) [126,127]. Further information on this subject is available in Ref. [4].

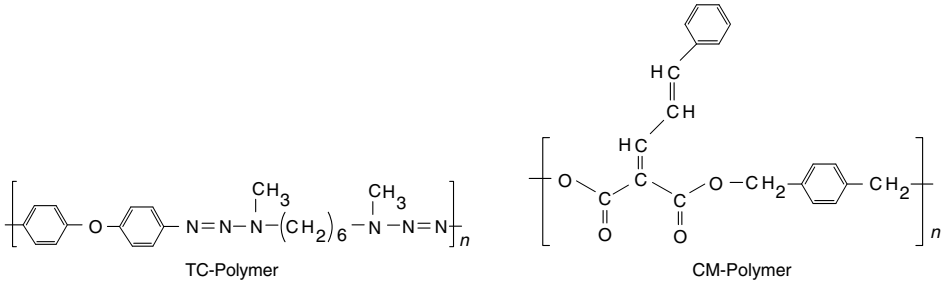


Chart 3.12 Chemical structures of polymers appropriate for laser ablation at $\lambda = 308$ nm.

Lam Research Ex. 1047 - Page 165
Lam Research Corp. v. Inpria Corp.
IPR2024-00033 - U.S. Patent No. 9,823,564

Table 3.18 Effects of UV/Vis light on biopolymers.

Quality of effect	Mode of action	Typical cases
Beneficial	Regulatory action, for example, light-triggered biological processes	Photomorphological processes in plants, Photomovements in bacteria
	Energy transduction processes	Conversion of solar energy into chemical energy (photosynthesis), Conversion of chemical energy into light (bioluminescence)
Deleterious	Light-induced chemical damage in biopolymers due to cleavage of chemical bonds	Photolesions in DNA resulting in skin cancer due to mutations in the cell nucleus. Deactivation of biological activity of proteins, in particular denaturation of enzymes

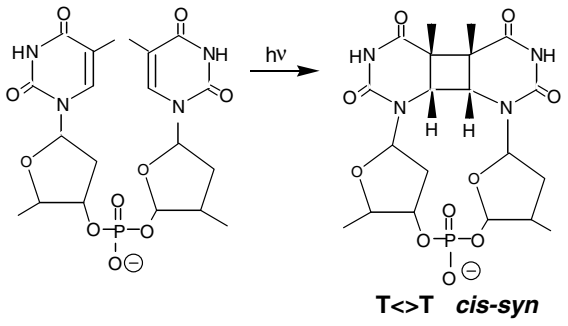
3.2.2.3 **Modification of Biopolymers**

The irradiation of biopolymers with UV/Vis light may cause both beneficial and deleterious effects (Table 3.18) [10,11,128–142]. While the deleterious action is commonly restricted to the wavelength region between 200 and 320 nm – that is, to the absorption of photons having energies high enough to cleave chemical bonds – the beneficial action relates to UV light of longer wavelengths (320–400 nm) and to visible light (400–800 nm). The deleterious effects on nucleic acids, proteins and polysaccharides will be discussed based on some typical examples in the following subsections.

UV-light-induced harmful modifications in *nucleic acids*, commonly termed UV-induced DNA lesions, are essentially due to reactions of the bases. Upon the absorption of light, the bases are converted into their excited singlet or triplet state, from which chemical reactions can ensue. The resulting modifications are accompanied by changes in the base-pairing properties which, in turn, causes mutations [143–146]. Photolesions can be caused through the cleavage of chemical bonds with the concurrent generation of free radicals, and through molecular mechanisms, for instance the dimerization of pyrimidine bases. The pyrimidine bases thymine (T) and cytosine (C) form dimers at sites with adjacent pyrimidine moieties, so-called dipyrimidine sites, in the DNA chain. The dimerization presented in Scheme 3.36 is a $[2\pi + 2\pi]$ cycloaddition (see Section 3.36) involving the two C(5)=C(6) double bonds, leading to cyclobutane structures denoted by the symbol T<>T, or generally Pyr<>Pyr.

The dimerization can, in principle, lead to three isomers: *cis-syn*, *trans-syn* I, and *trans-syn* II; however, due to the constraints imposed by the DNA double strand, the *cis-syn* dimer shown in Scheme 3.36 is the major photoproduct [144]. Pyrimidine–pyrimidone (Pyr[6-4]Pyr) dimers represent another type of dimeric lesion that is formed by a Paterno–Büchi-type reaction at dipyrimidine sites between the

Lam Research Ex. 1047 - Page 166
Lam Research Corp. v. Inpria Corp.
IPR2024-00033 - U.S. Patent No. 9,823,564



Scheme 3.36 Dimerization of adjacent thymine moieties in DNA by [2π + 2π] cycloaddition.

C(5)=C(6) double bond of the first pyrimidine and the C(4)=O carbonyl group of the second base (Scheme 3.37)

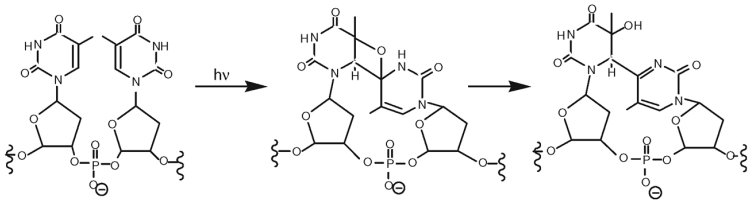
The UV-induced generation of cyclobutane dimers is heavily dependent on double-helix conformational factors. In certain cases, proteins bind specifically to DNA, so as to enforce a particular conformation that is unfavorable for the formation of cyclobutane-type lesions. Notably, photodimers of the cyclobutane type are cleaved by irradiation with far-UV light (240 nm) with a quantum yield of almost unity by way of the so-called [2 + 2] cycloreversion reaction. In living cells, dimer lesions can be repaired by the nucleotide excision repair pathway, which is based on the excision of a small piece of DNA around the lesion. Any lesions not removed from the genome will lead to either cell death or mutagenesis.

Photoproducts generated via free-radical mechanisms include single-strand breaks, and also crosslinks between the strands of the same double helix, and between different DNA strands and adjacent protein molecules.

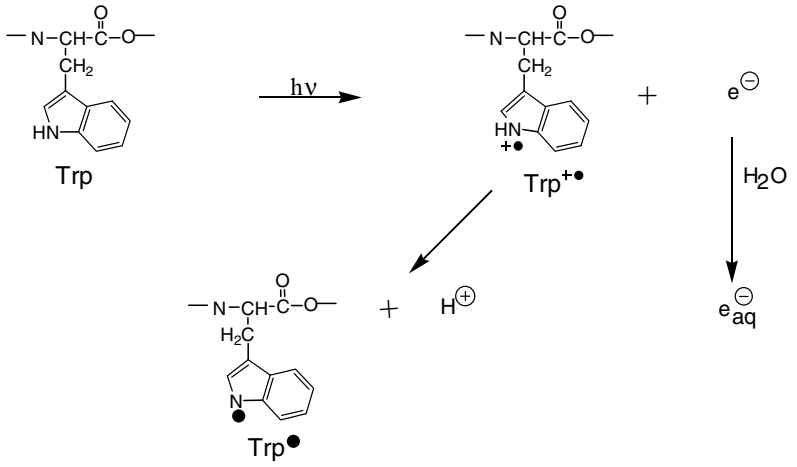
Chemical alterations in *proteins* due to UV irradiation can induce disturbances of the natural conformation, aggregation, and chain cleavage, all of which lead to denaturation. The structural proteins keratin (wool), collagen, elastin, and fibroin (silk) undergo losses in mechanical strength and elasticity (wool is said to *tender*) and sometimes also color changes (*yellowing*).

In many proteins, the tryptophan (Trp), tyrosine (Tyr), cystine (Cys) and phenylalanine (Phe) moieties play a determinant role with regards to UV-light-induced chemical alterations. Following the absorption of light, these moieties undergo photoionization and participate in energy-transfer and electron-transfer processes. This situation holds true not only for structural proteins such as keratin and fibroin [136], but also for enzymes in aqueous media such as lysozyme, trypsin, papain, ribonuclease A, and insulin [133]. The photoionization of Trp and/or Tyr residues is the major initial photochemical event, and in the case of enzymes this will result in their inactivation. A typical mechanism pertaining to Trp residues (Scheme 3.38) commences with the absorption of a photon and the subsequent release of an electron. In aqueous media, the latter is rapidly solvated. By the release of a proton, the tryptophan cation radical $Trp^{\bullet+}$ is converted to the tryptophan radical $Trp^{\bullet}$.

Lam Research Ex. 1047 - Page 167
Lam Research Corp. v. Inpria Corp.
IPR2024-00033 - U.S. Patent No. 9,823,564

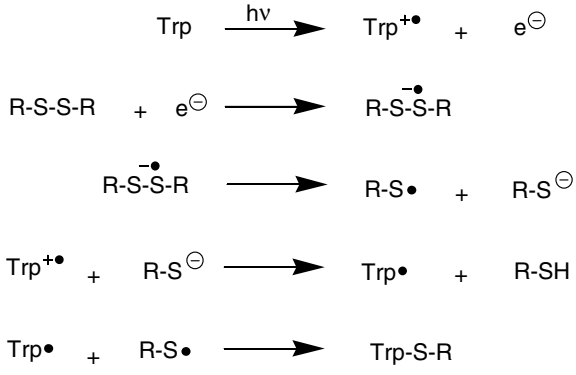


Scheme 3.37 Dimerization of adjacent thymine moieties in DNA by a Paterno–Büchi-type reaction.



Scheme 3.38 Photolysis of proteins. Reactions involving tryptophan [133].

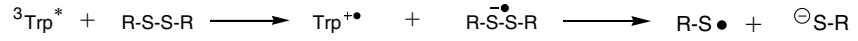
In other proteins, such as α-lactalbumin, which consists of 123 amino acid moieties, the electron released from a Trp moiety is attached, by way of an intramolecular process, to a disulfide group of a cystine bridge in a position adjacent to the indole ring of the Trp moiety [147]. As shown in Scheme 3.39, the resulting disulfide anion radical dissociates into a thiolate ion $R-S^-$ and a thiyl radical $R-S^\bullet$. Proton transfer from the tryptophan cation radical to the thiolate ion leads to the tryptophan radical $Trp^\bullet$ and the thiol RSH. The final stage of the process is governed by radical coupling, which may result in sulfenylation of the Trp moiety yielding $Trp-S-R$, or in intermolecular crosslinking – that is, in the formation of enzyme dimers or trimers.



Scheme 3.39 Rupture of cystine bridges by the attachment of electrons stemming from the photoionization of tryptophan [147,148].

Lam Research Ex. 1047 - Page 169
Lam Research Corp. v. Inpria Corp.
IPR2024-00033 - U.S. Patent No. 9,823,564

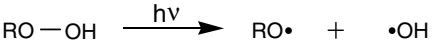
Disulfide bridges can also be ruptured by reaction with the triplet excited moieties $^3Trp^*$ or $^3Tyr^*$, the formation of which accompanies the electron release. In this process, the triplet species undergo an electron transfer with cystine moieties, thus forming the disulfide radical anion (Scheme 3.40).



Scheme 3.40 Reaction of tryptophan triplets with cystine moieties.

In many proteins, crosslinks are formed; in the case of keratin and collagen they are of the tryptophan–histidine and dityrosine types [136]. Crosslinks formed by the combination of R−S$^\bullet$ or R−S−S$^\bullet$ radicals, both intermolecularly and intramolecularly, with incorrect sites are considered to be an important source of photoaggregation effects [134]. Electron spin resonance (*ESR*) measurements have also yielded evidence of C—H and C—N bond ruptures [134].

Polysaccharides do not absorb light at $\lambda > 200$ nm, and therefore any photochemical alterations caused by light of longer wavelengths are due to the action of impurity chromophores. This holds also for cellulose, a major component of plants (in jute, flax, hemp, and cotton up to 90%). *Neat* cellulose forms gaseous products (CO, CO_2, and H_2) upon exposure to UV light ($\lambda = 253.7$ nm), whereby the degree of crystallinity of the cellulose fibrils is reduced [142]. However, if O_2 is present during the irradiation, then carbonyl, carboxyl and peroxide groups will be formed, even at $\lambda > 340$ nm. Typically, main-chain scission will occur and the brightness will be reduced [149], because irradiation at $\lambda < 360$ nm leads to homolysis of the previously formed hydroperoxide groups (Scheme 3.41).

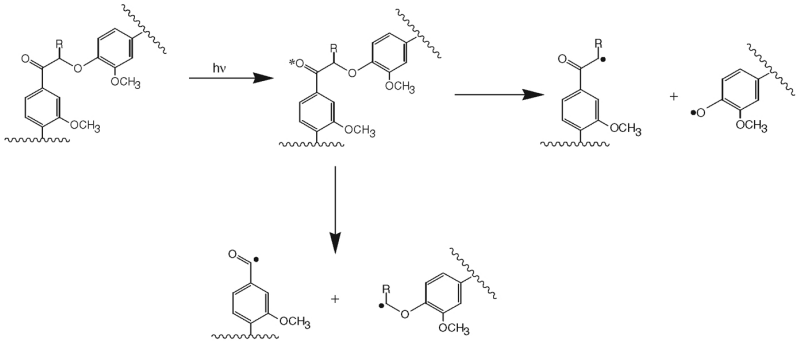


Scheme 3.41 Generation of hydroxyl radicals during the photolysis of hydroperoxide groups.

The OH radicals resulting from this process are highly reactive; that is, they abstract hydrogens from neighboring molecules and thus initiate further decomposition processes. Detailed information on the photochemistry of cellulose is available elsewhere [142,150,151]. Wood is known to contain 15–30% of lignin, an aromatic UV- and visible-light-absorbing polymer with a very complex structure (see Chart 3.3(d)). Although photochemical changes in wood are essentially determined by reactions initiated by bond breakages in the lignin component, little is known of the complex mechanism of the photoreactions in lignins; some of those which have been proposed [141,152] are shown in Scheme 3.42. Phenoxyl radicals generated in this way can be transformed into the quinoid structures (Scheme 3.43) that are thought to be responsible for the surface yellowing of wood products.

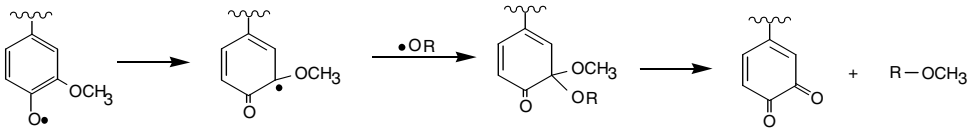
Because lignins have the ability to absorb both near-UV and visible light, they undergo slow photo-oxidation processes such that, even indoors, a yellowing and

Lam Research Ex. 1047 - Page 170
Lam Research Corp. v. Inpria Corp.
IPR2024-00033 - U.S. Patent No. 9,823,564



Scheme 3.42 Photoreactions of lignins.

Lam Research Ex. 1047 - Page 171
Lam Research Corp. v. Inpria Corp.
IPR2024-00033 - U.S. Patent No. 9,823,564



Scheme 3.43 Formation of quinoid structures in lignins.

darkening of wooden surfaces is unavoidable. Detailed information on the photochemistry of lignins and wood are provided in Refs [141,152].

3.2.3 Applications in Polymer Physics

3.2.3.1 Spectroscopy

A variety of applications for optical absorption spectroscopy related to polymers has been proposed:

- The analysis and identification of polymers with chromophores absorbing UV/Vis photons (e.g., carbonyl and aromatic groups).
- The investigation of polymer degradation processes.
- The investigation of alterations in the tertiary structure of proteins and nucleic acids.

With regards to the final entry here, it should be noted that structural alterations can often be conveniently monitored simply by recording changes in optical absorption at a certain wavelength. This applies, for example, to the thermal denaturation of biomacromolecules, such as proteins and nucleic acids in aqueous solution. In these cases, the optical absorption is increased as a consequence of the unfolding caused by the destruction of intramolecular hydrogen bonds. Generally, changes in optical absorption related to molecular alterations not involving chemical bond breakages are denoted by the terms *hypochromicity* (also known as hypochromy) and *hyperchromicity* (also known as hyperchromy), depending on whether the optical absorption decreases or increases, respectively. With regards to nucleic acids in solution, hypochromicity applies to a decrease in optical absorbance when single-stranded nucleic acids combine to form double-stranded helices. The hypochromicity phenomenon and relevant theories are discussed in detail elsewhere [153].

Circular dichroism (*CD*) spectroscopy is a form of absorption spectroscopy that is based on measuring the difference in the absorbance by a substance of right- or left-circularly polarized light. CD is exhibited by *chiral molecules*, and represents a powerful tool for revealing the structures of biological macromolecules such as polypeptides, proteins and nucleic acids in solution. In the case of proteins, CD spectroscopy not only allows the discrimination between the different structural types, such as α-helix, parallel and antiparallel β-pleated sheets and β-turns, but also permits an estimation of the relative contents of these structures. This is

Lam Research Ex. 1047 - Page 172
Lam Research Corp. v. Inpria Corp.
IPR2024-00033 - U.S. Patent No. 9,823,564

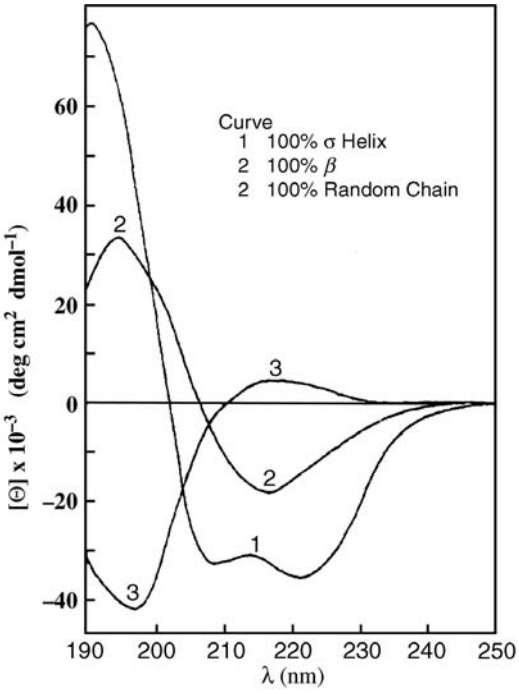


Figure 3.9 Circular dichroism spectra of poly(L-lysine) in its α-helical, β-sheet, and random coil conformations. Adapted with permission from Ref. [154]; © 1969, American Chemical Society.

shown in Figure 3.9 for the case of poly(L-lysine), a polymer that can adopt three different conformations depending on the pH and temperature: a random coil at pH 7.0; an α-helix at pH 10.8; and a β-sheet at pH 11.1 (after heating to 52 °C and cooling to room temperature once more).

For detailed information on the CD of chiral polymers, the reader is referred to relevant publications [149,155–157]. One important feature of CD spectroscopy is the possibility to monitor conformational changes in optically active macromolecules (for a review, see Ref. [158]).

Attention should also be paid here to *ultraviolet photoelectron spectroscopy* (*UPS*), which employs light of a wavelength greater than the ionization energy of the valence electrons. UPS is related to the absorption of photons by the outer shell electrons of the atom and the subsequent release of an electron. The kinetic energy E_{kin} of the emitted electron is given by Equation 3.11, Einstein's photoelectric law:

$$E_{kin} = h\nu - I \tag{3.11}$$

where I is the ionization energy corresponding to the energy of an occupied molecular orbital. Spectra can be recorded with synchrotron radiation or with conventional UV light sources, such as helium discharge lamps emitting photons

Lam Research Ex. 1047 - Page 173
Lam Research Corp. v. Inpria Corp.
IPR2024-00033 - U.S. Patent No. 9,823,564

of 21.2 and 40.8 eV. From the energy distribution of the emitted electrons, conclusions can be drawn concerning the molecular energy levels in the valence region [159,160]. UPS has served, for example, to directly observe occupied and unoccupied electronic states of bulk π-conjugated polymers and to study the electronic band structure of these polymers at interfaces with substrates [161,162]. In this way it has helped, in particular, to provide an understanding of charge injection – that is, the transport of electrons and holes across electrode–polymer interfaces, and transport through thin polymer films in light-emitting devices. The UPS method has been further developed by using X-ray radiation instead of UV light (see Section 6.2.3).

3.2.3.2 Light Scattering

General Aspects Light is scattered elastically (no energy transfer) by matter when its electric field interacts with electrons located in atomic orbitals. Under the influence of the electric field, the electrons oscillate and thereby emit – in all directions – electromagnetic waves of a frequency equal to that of the incident light. Based on the measurement of the intensity of light scattered by small particles in solution or suspension, two powerful techniques with important applications in the polymer field have been developed, namely *static* and *dynamic* light-scattering methods, denoted respectively by the acronyms SLS and DLS.

In the case of SLS, a light beam is continuously incident upon a sample, and the intensity of the scattered light is measured using a photomultiplier. In the case of DLS, time-dependent fluctuations in the intensity of the scattered light arising from thermal motions of the scattering particles are measured using photomultipliers that are capable of operating in photon-counting mode. Usually, the measurements are performed at various scattering angles. The SLS method serves to determine molar mass, radius of gyration and second virial coefficient of macromolecules in dilute solution, as described elsewhere [163–171]. The most important applications of the DLS method pertain to the direct determination of translational diffusion coefficients of macromolecules in solution (it has been the preferred method since about 1970), as well as monitoring the size distribution of small particles in dilute solution. Relaxation processes in a concentrated polymer solution can also be studied (Table 3.19).

Table 3.19 Processes investigated by dynamic light scattering. Adapted from Refs [172–175,177].

System	Processes
Dilute solutions	Translational diffusion of polymer coils, internal diffusion modes of homopolymer or diblock copolymer chains
Semidilute solutions	Cooperative diffusion of transient polymer networks, heterogeneity mode related to polymer self-diffusion in diblock copolymers, entanglement mode, chain reptation, viscoelastic relaxation, diffusion of clusters
Concentrated solutions	Viscoelastic relaxation, α- and β-relaxation

Lam Research Ex. 1047 - Page 174
Lam Research Corp. v. Inpria Corp.
IPR2024-00033 - U.S. Patent No. 9,823,564

The theory and applications of the DLS method (which may also be referred to as quasi-elastic light scattering and photon-correlated spectroscopy) are covered in a variety of books and articles [172–183].

Details related to both SLS and DLS methods are provided in the following subsections.

SLS from Dilute Polymer Solutions The intensity $i_{u,\Theta(one)}$ of light scattered by one isolated small isotropic particle being much smaller than the wavelength λ of incident *unpolarized* light of intensity I_0 is given by Equation 3.12:

$$i_{u,\Theta(one)} = I_0 \frac{8\pi^4 \alpha_{pol}^2}{\lambda^4 R^2} (1 + \cos^2\Theta) \tag{3.12}$$

where R is the distance from specimen to detector, Θ is the scattering angle, and α_{pol} is the polarizability of the molecule. The factor $(1 + \cos^2 \Theta)$ results from the superposition of the horizontally and vertically polarized components of the scattered light.

If N_v molecules of molar mass M are contained in a volume V, the scattering intensity per unit volume is $i_{u,\Theta} = i_{u,\Theta(one)} N_v/V = i_{u,\Theta(one)} c\ N_A/M$, where c denotes the concentration (in g cm^{-3}) and N_A is Avogadro's number. Substitution into Equation 3.12 yields Equation 3.13:

$$i_{u,\Theta} = I_0 (1 + \cos^2 \Theta) \frac{2\pi^2}{\lambda^4\ R^2\ N_A} \left(\frac{dn}{dc}\right)^2 Mc \tag{3.13}$$

Here, it is also taken into account that α_{pol} is proportional to the refractive index increment (dn/dc) according to Equation 3.14

$$\alpha_{pol} = \frac{M}{2\pi N_A} \left(\frac{dn}{dc}\right) \tag{3.14}$$

The proportionality of $i_{u,\Theta}$ to M indicates that the light-scattering intensity of systems containing macromolecules significantly exceeds that of small molecules.

In compact systems, such as crystals and fluid solutions, the scattered light is extinguished by interference. The scattered light that is nevertheless detectable is due to impurities (crystal-lattice defects or voids) in the case of crystals, and due to concentration fluctuations in the case of fluid solutions. The fluctuation theory developed for macromolecules in solution takes into account that the light-scattering intensity (*LSI*) of a solution is larger than that of the solvent. The increase in LSI is ascribed to δc, the fluctuation in solute concentration within volume elements having dimensions much smaller than the wavelength of incident light. The intensity of light scattered from a dilute polymer solution is proportional to $\langle \delta c^2 \rangle$, the average square concentration fluctuation. Based on the fluctuation theory, the basic light scattering Equation 3.15 which pertains to light scattered from dilute solutions during irradiation with unpolarized light, has been derived. The derivation of Equation 3.15 and the description of the theory which

Lam Research Ex. 1047 - Page 175
Lam Research Corp. v. Inpria Corp.
IPR2024-00033 - U.S. Patent No. 9,823,564

has been developed by Einstein [184] and Debye [168] can be found in the textbook of Tanford [164].

$$i_{u,\Theta} = I_0\left(1+\cos^2\Theta\right)\frac{2\pi^2 n_0^2}{\lambda^4 R^2 N_A}\left(\frac{\mathrm{d}n}{\mathrm{d}c}\right)^2 c\,\frac{1}{M^{-1}+2A_2c+3A_3c^2+\ldots} \tag{3.15}$$

where n_0 is the refractive index of the solvent, $\mathrm{d}n/\mathrm{d}c$ is the refractive index increment, and A_2 and A_3 are the second and third virial coefficients, respectively. The so-called Rayleigh ratio R_Θ (see Equation 3.16), which commonly serves to present light-scattering results, is obtained by transforming Equation 3.15.

$$R_\Theta = \frac{i_{u,\Theta}R^2}{I_0(1+\cos^2\Theta)} = \frac{Kc}{M^{-1}+2A_2c+3A_3c^2+\ldots} \tag{3.16}$$

where $K = \dfrac{2\pi^2 n_0^2}{\lambda^4 N_A}\left(\dfrac{\mathrm{d}n}{\mathrm{d}c}\right)^2$. Note the difference in dimensions of $i_{u,\Theta}$,(energy $\cdot$ time$^{-1}\cdot$ area^{-1} $\cdot$ volume^{-1}) and I_0 (energy $\cdot$ time$^{-1}\cdot$ area^{-1}).

For small macromolecules (dimensions smaller than $\lambda/20$) in dilute solution, the Rayleigh ratio, as defined by Equation 3.16, does not depend on the angle of observation, and the following basic Equation 3.17 is obtained:

$$\frac{Kc}{R_\Theta} = \frac{1}{M} + 2A_2c + 3A_3c^2 + \ldots \tag{3.17}$$

At infinite dilution ($c \to 0$) Equation 3.18 holds:

$$\lim_{c\to 0}\frac{Kc}{R_\Theta} = \frac{1}{M} \tag{3.18}$$

It must be pointed out here, that the scattering of light by small particles is determined by a spherical symmetric scattering function, P_Θ. Upon using *vertically* polarized incident light, i_Θ is equal to i_0, the intensity of light scattered at zero observation angle, that is, $P_\Theta = i_\Theta/i_0 = 1$.

In the case of large particles, light scattered from different mass points of the same macromolecule can interfere (*intramolecular interference*), resulting in a nonsymmetric scattering function, P_Θ; that is, in a monotonous decrease in the LSI with increasing Θ. The intramolecular interference depends on the distance between the different scattering units and their distribution within the macromolecule and is, therefore, related to their sizes and shapes. This is taken into account by the particle scattering function P_Θ in Equation 3.19. It holds for dilute solutions where terms with higher concentration power can be neglected.

$$\frac{Kc}{R_\Theta} = \frac{1}{MP_\Theta} + 2A_2c \tag{3.19}$$

P_Θ reflects the intramolecular interference and is determined by both size and shape of the particle. As Θ approaches zero, P_Θ becomes independent of the particle shape and, under these limiting conditions, is a measure of the radius of gyration. This is expressed by Equation 3.20, where $\langle R_G^2\rangle_z$ denotes the square of the z-average radius

Lam Research Ex. 1047 - Page 176
Lam Research Corp. v. Inpria Corp.
IPR2024-00033 - U.S. Patent No. 9,823,564

of gyration of macromolecules; that is, the square of the average distance of all atoms of the particle from the center of gravity of the particle [163].

$$\lim_{\Theta\to 0}\frac{1}{P_\Theta} = 1 + \frac{16\pi^2}{3\lambda^2}\left\langle R_G^2\right\rangle_z \sin^2(\Theta/2) \tag{3.20}$$

It follows, that the molar mass and the radius of gyration of macromolecules of any shape can be determined from the angular dependence of the intensity of scattered light. Note that the equations presented above pertain to monodisperse systems with respect to molar mass and particle size. However, in most practical cases, polymers are polydisperse in molar mass and particle size, and light-scattering measurements bring about certain average values. As can be seen from relevant textbooks [163,164,166], light-scattering measurements deliver the mass-average molar mass M_w and the z-average radius of gyration $\langle R_G\rangle_z$. In practice, however, light-scattering measurements are carried out with polymer solutions of different concentrations at various angles. One widely used method for handling light-scattering data obtained with dilute polymer solutions has been introduced by Zimm [165], and is based on Equation 3.21:

$$\left(\frac{Kc}{R_\Theta}\right)_{c=0} = \frac{1}{M_w} + \frac{16\pi^2}{3\lambda^2 M_w}\langle R_G^2\rangle_z \sin^2(\Theta/2). \tag{3.21}$$

Here, Kc/R_Θ is plotted versus $\sin^2(\Theta/2) + kc$, where k is used as a fitting parameter. From Figure 3.10 it can be seen how M_w and $\langle R_G\rangle_z$ are found from a Zimm plot. As a typical example, Figure 3.11 presents a Zimm plot obtained with polystyrene in toluene solution yielding $M_w = 5.83\times10^5\,\mathrm{g\,mol^{-1}}$, $A_2 = 4.8\times10^{-4}\,\mathrm{mol\,cm^3\,g^{-2}}$, and $\langle R_G\rangle_z = 33\,\mathrm{nm}$. Additional typical results are presented in

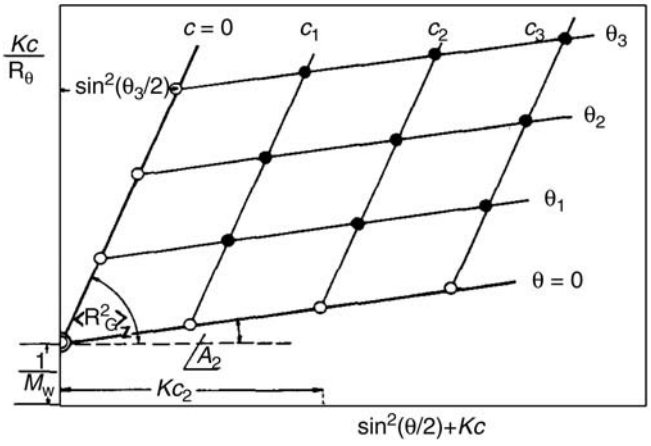


Figure 3.10 Schematic representation of a Zimm plot. •, Experimental points; ○, extrapolated points. Adapted with permission from Ref. [163]; © 1987, Elsevier.

Lam Research Ex. 1047 - Page 177
Lam Research Corp. v. Inpria Corp.
IPR2024-00033 - U.S. Patent No. 9,823,564

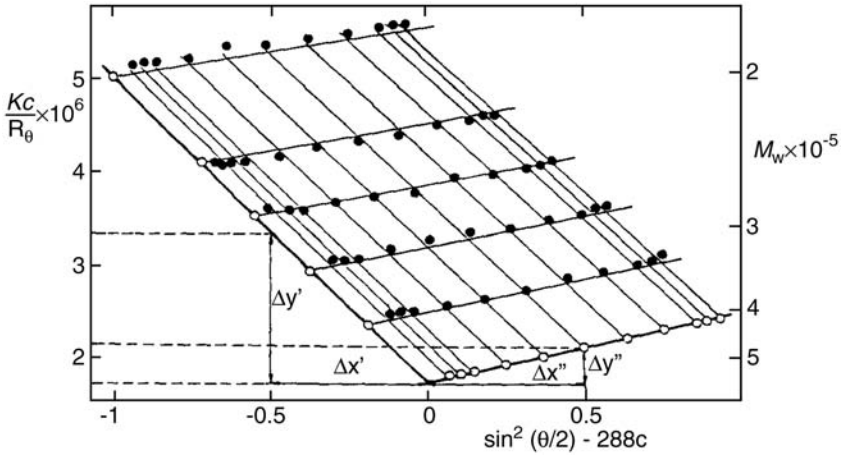


Figure 3.11 Zimm plot for polystyrene in toluene solution. $\lambda_0 = 546$ nm. $T = 25\,^{\circ}$C. ●, Experimental points; ○, extrapolated points. A negative *k*-value has been chosen to render the plot more synoptic. $A_2 = 1/2\ (\Delta y'/\Delta x')$. $\langle R_G^2 \rangle_z^{1/2} = \left(\sqrt{3}/4\pi\right)\left(\lambda_0/n\right)\sqrt{M_w\left(\Delta\gamma''/\Delta x''\right)}$. Adapted with permission from Ref. [163]; © 1987, Elsevier.

Table 3.20. In this context, it is notable, that X-ray scattering (see Section 5.2.1.5) rather than light-scattering has to be used if $\langle R_G \rangle_z$ is small. This pertains to many biopolymers such as serum albumin ($\langle R_G \rangle_z = 3$ nm or catalase ($\langle R_G \rangle_z \approx 4$ nm).

Interestingly, light-scattering measurements can serve to characterize the chain-stiffness of rod-like (worm-like) linear polymers (Kratky–Porod model). The extent of stiffness can be expressed by a special parameter, the *persistence length*, *p*. This can be evaluated from light-scattering measurements of the molar mass and the mean-square radius of gyration if the samples are not polydisperse, or if the polydispersity can be determined. According to Benoit and colleagues [185,186], the radius of gyration of rod-like polymers can be expressed as a function of the contour length *L* and the persistence length, *p* (cf. Equation 3.22). *L* is the maximum possible displacement length (maximum possible end-to-end distance) of the chain, which is obtained from the molar mass M_w and the mass

Table 3.20 Characterization of typical synthetic linear polymers by LS measurements in solution at $\lambda = 546$ nm. Adapted from Ref. [163].

Polymer	Solvent	M_w (g mol^{-1})	A_2 (mol cm^3 g^{-1})	$<R_G>_z$ (nm)
Polystyrene	Toluene	5.83×10^5	4.8×10^{-4}	33
Polybutadiene	Dioxane	2.35×10^5	-0.2×10^{-4}	36
Poly(ethyl methacrylate)	2-Methoxy ethanol	4.78×10^5	1.14×10^{-4}	41

Lam Research Ex. 1047 - Page 178
Lam Research Corp. v. Inpria Corp.
IPR2024-00033 - U.S. Patent No. 9,823,564

per unit length.

$$\langle R_G^2 \rangle_z = \frac{Lp}{3} - p^2 + \frac{2p^3}{L} - \frac{2p^4}{L^2}\left(1 - e^{\frac{-L}{p}}\right) \tag{3.22}$$

In the case of double-stranded DNA, the light-scattering method yields $p = 54.0 \pm 5.6$ nm [187].

Dynamic Light Scattering (DLS) Time-dependent fluctuations in the intensity of the scattered light can be observed, when a monochromatic laser light beam impinges a very small volume of a polymer solution or particle dispersion. The fluctuations in the intensity of the scattered light arise from thermal motions of the scattering particles, whose distance is constantly varying, so as to cause varying interference (constructive and destructive) of the scattered light. The intensity fluctuations are measured with the aid of photomultipliers capable of operating in photon-counting mode. The "signal" is, in this case, the number of photons counted in one sampling interval. Signals are fed into a digital correlator, which generates the intensity (or second-order) autocorrelation function $g_{(2)}(t)$, which is defined by Equation 3.23.

$$g_{(2)}(t) = \frac{\langle I(t_S) I(t_S + t) \rangle}{\langle I(t_S) \rangle^2} \tag{3.23}$$

Here, $I(t_S)$ and $I(t_S + t)$ denote the light intensity recorded at the sampling time t_S and at a time augmented by the delay time t, respectively. The brackets $\langle\ \rangle$ denote the *average* over sampling time.

The autocorrelation function $g_{(2)}(t)$ is related to $g_{(1)}(t)$, the electric field correlation function (or first-order autocorrelation function) via the so-called *Siegert relation* (Equation 3.24):

$$g_{(2)}(t) = B\left(1 + \beta\left(g_{(1)}(t)\right)^2\right) \tag{3.24}$$

where B and β are instrumental parameters. For monodisperse and spherical particles, $g_{(1)}(t)$ is a single-exponential function with decay rate constant Γ (the reciprocal of the decay time τ, also referred to as relaxation time) as described by Equation 3.25.

$$g_{(1)}(t) = e^{-\Gamma t} \tag{3.25}$$

Figure 3.12 presents an autocorrelation function recorded with a solution of a polymer blend consisting of equal parts of almost monodisperse polystyrene and PMMA that exhibits a single exponential decay.

Γ is related to D_c, the cooperative diffusion coefficient of translation motion, according to Equation 3.26:

$$\Gamma = q^2 D_c \tag{3.26}$$

Lam Research Ex. 1047 - Page 179
Lam Research Corp. v. Inpria Corp.
IPR2024-00033 - U.S. Patent No. 9,823,564

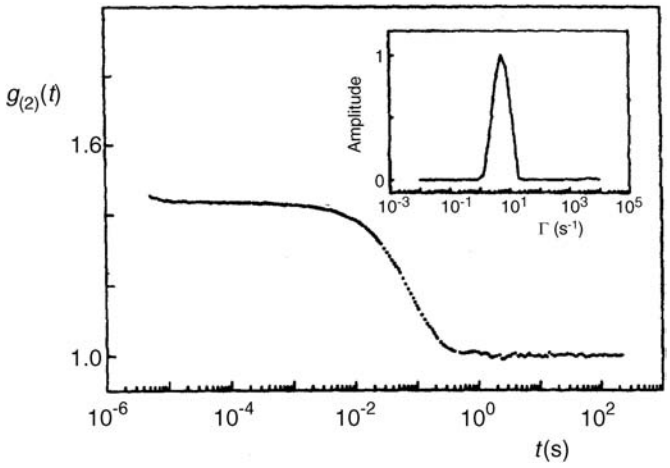


Figure 3.12 Autocorrelation function $g_{(2)}(t)$ recorded with a solution of a polymer blend consisting of equal parts of polystyrene (*PS*) and poly(methylmethacrylate) (PMMA) in deuterated benzene (Bnz-d_6). PS: $M_w = 1.26 \times 10^6$ g mol^{-1}, $M_w/M_n = 1.05$. PMMA: $M_w = 1.09 \times 10^6$ g mol^{-1}, $M_w/M_n = 1.08$. Adapted with permission from Ref. [188]; © 2000, Gordon & Breach Science Publishers.

where q denotes the wave vector: $q = (4\pi n/\lambda)$ sin $(\Theta/2)$, with n and Θ being the refractive index of the solution and the scattering angle, respectively. Thus, the diffusion coefficient D_c is obtained by plotting experimentally determined rate constants Γ as a function of q^2. From Table 3.21, which presents typical results, it becomes obvious that D_c decreases with increasing molar mass.

DLS measurements allow the determination of the size of scattering particles, because the diffusion coefficient D_c is related to the hydrodynamic radius r_{hyd} via the Stokes–Einstein equation (Equation 3.27).

Table 3.21 Translational diffusion coefficients D_c of linear macromolecules determined in dilute solution at a concentration of 0.5 g l^{-1}.

Polymer	Solvent	D_c (m^2 s^{-1})	M_w (g mol^{-1})[a]	Reference
Polystyrene	Toluene	1.3×10^{-11}	1×10^6	[181]
Polystyrene	Toluene	0.6×10^{-11}	13×10^6	
Poly(styrene-*co*-methyl methacrylate)	Butyl acrylate	1.6×10^{-11}	0.6×10^6	[181]
Poly(vinyl trimethylsilane)	Cyclohexane	1.6×10^{-11}	0.5×10^6	[181]
Starch LD16[b]	0.5 M aq. NaOH	0.62×10^{-11}	1.7×10^6	[189]
Starch LD19		0.26×10^{-11}	14.5×10^6	
Starch LD17		0.1×10^{-11}	64.0×10^6	

a) Weight average molar mass.
b) Randomly branched degraded starch.

Lam Research Ex. 1047 - Page 180
Lam Research Corp. v. Inpria Corp.
IPR2024-00033 - U.S. Patent No. 9,823,564

$$D_c = \frac{kT}{6\pi\eta\, r_{hyd}} \tag{3.27}$$

where k is the Boltzmann constant, T is the temperature, and η is the viscosity of the solvent.

Note that the validity of Equation 3.26 is limited; it does not hold, for example, for polymer gels, worm-like micelles, and polymer aggregates. Higher-power dependencies of Γ on q have been reported (where Γ is proportional to q^3 or q^4) [190]. In the case of a polydisperse system, which frequently refers to synthetic polymers, the measured correlation function is related to a distribution of relaxation times. Sophisticated algorithms, such as the cumulant method or CONTIN, have been developed to analyze these correlation functions [191]. This topic is beyond the scope of this book, and so is not dealt with further here; however, within this context attention might be paid to studies involving the determination of molecular weight distributions of polymers by DLS [179], and also to studies related to systems consisting of various components that differ in size. In this case, the correlation function $g_{(1)}(t)$ is related to $A(\tau)$, the distribution of relaxation times as shown by Equation 3.28 [177]:

$$g_{(1)}(t) = \int A(\tau) e^{-\frac{t}{\tau}} d\tau \tag{3.28}$$

$A(\tau)$ can be extracted from the measured intensity correlation function $g_{(2)}(t)$ by a computer program that performs the inverse Laplace transformation of $g_{(2)}(t)$ according to Equation 3.29:

$$g_{(2)}(t) = 1 + \beta\left(\int A(\tau) e^{-\frac{t}{\tau}} d\tau\right)^2 \tag{3.29}$$

This procedure allows the simultaneous analysis and detection of separated relaxation modes resulting from different components of the system under investigation. This is demonstrated in Figure 3.13, where the distribution of relaxation times obtained at several scattering angles in a tetrahydrofuran solution of a diblock copolymer polystyrene-*b*-poly(ethylene-propylene) is presented.

The peaks in Figure 3.13a (counted from the left) are ascribed to the following modes: peak 3 (dominant) to cooperative or translational diffusion, peak 4 to self-diffusion of the copolymer chain, and peak 5 to the diffusion of clusters of a hydrodynamic radius equal to about 120 nm, as estimated via the Stokes–Einstein relation (Equation 3.27). Peaks 1 and 2 correspond to thermal diffusion and to self-diffusion of solvent molecules, respectively.

In the pioneering days, linear correlators with a low number of channels (16–64) were used to determine translational diffusion coefficients in particle dispersions or dilute polymer solutions. Today, much more complicated systems can be studied with the aid of logarithmic multi-tau correlators covering a dynamic range of many decades of relaxation times. In fact, the fastest correlators allow the determination

Lam Research Ex. 1047 - Page 181
Lam Research Corp. v. Inpria Corp.
IPR2024-00033 - U.S. Patent No. 9,823,564

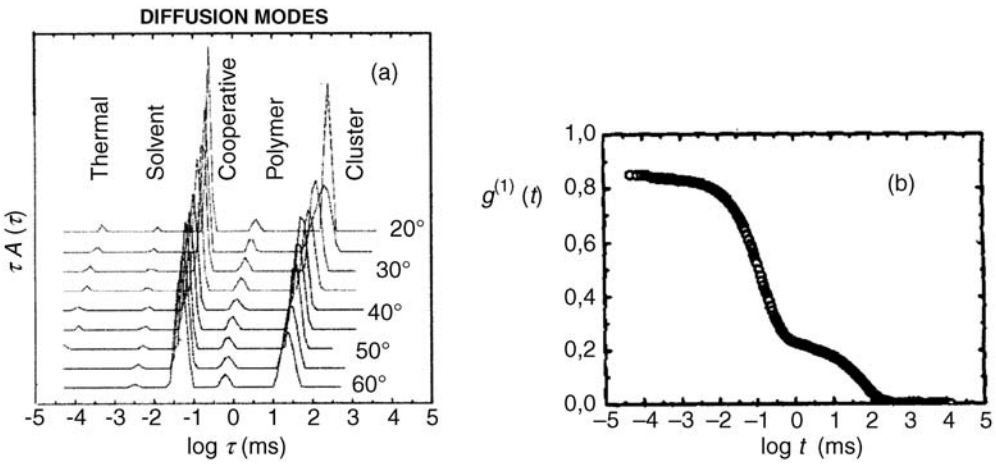


Figure 3.13 (a) Distribution of relaxation times for a 5 wt% solution of polystyrene-*b*-poly(ethylene-propylene) in tetrahydrofuran at 25 °C and at several scattering angles (indicated). $M_w = 9.6 \times 10^4\,g\,mol^{-1}$, $M_w/M_n < 1.2$, styrene weight fraction: 0.43; (b) Typical correlation curve obtained at scattering angle 30°. Adapted with permission from Ref. [192]; © 2007, American Chemical Society.

of relaxation times of a few nanoseconds. Details on the performance of DLS measurements are available elsewhere [169,193].

3.2.3.3 **Raman Scattering**

If light (Vis/UV or near-infrared range) of frequency ν_0 is scattered upon passing through matter, then one out of 10^6 photons will be scattered inelastically. This fraction of scattered light, which is referred to as *Raman scattering*, can be understood as a collision process between photons and molecules. After collision, the photon energy may be either decreased ($h\nu < h\nu_0$) or increased ($h\nu > h\nu_0$), resulting in Stokes lines or anti-Stokes lines, respectively. The energy difference of the incident and scattered photons corresponds to vibrational levels of the scattering molecules. Raman spectroscopy, in contrast to infrared (IR) absorption spectroscopy, yields different types of information, because Raman scattering is related to symmetric vibrations and IR absorption to asymmetric vibrations, respectively. The Raman spectra of polyethylene with different amorphous/crystalline phase fractions are shown as typical examples in Figure 3.14.

Raman spectroscopy is a technique appropriate for the analysis and characterization of polymers, as it provides information on the chemical and morphological structures of polymers. One advantage of Raman spectroscopy over IR spectroscopy is the greater sensitivity to homonuclear bonds such as >C—C<, —C=C—, and —C≡C—. Raman spectroscopy can serve to measure the degree of crystallinity of partly crystalline polymers, and notable in this context are the longitudinal acoustic vibrations in linear chain polymers (also

Lam Research Ex. 1047 - Page 182
Lam Research Corp. v. Inpria Corp.
IPR2024-00033 - U.S. Patent No. 9,823,564

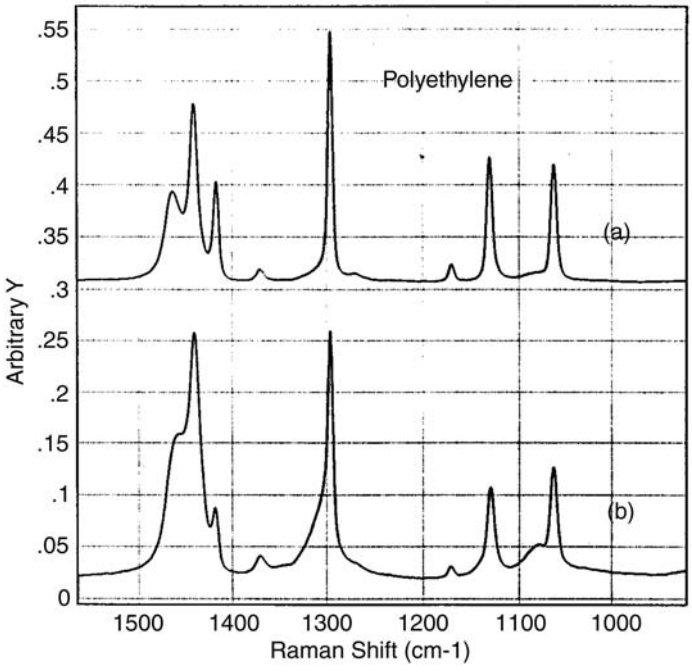


Figure 3.14 Raman spectra of polyethylene. Phase fractions: (a) 30% amorphous, 68% crystalline; (b) 70% amorphous, 15% crystalline. Remainder: interfacial phase. Adapted with permission from Ref. [194]; © 1995, American Chemical Society.

termed *accordion vibrations*; see Figure 3.15) that serve to study parameters such as crystallization, melting, growth, and thickness of the lamellae.

Commonly, Raman scattering is observed using charge-coupled device (*CCD*) detectors upon exposure of the sample to monochromatic visible laser light. The spatial resolution of measurements can be optimized (down to 1 μm) by coupling an optical microscope to a Raman spectrometer. A schematic layout of a Raman microscope system is shown in Figure 3.16, where the laser beam passes through the microscope and is focused onto the sample.

Raman microspectroscopy allows the *mapping* (surveying) of polymer surfaces with the aid of CCD array detectors. In this case, mapping is accomplished by recording

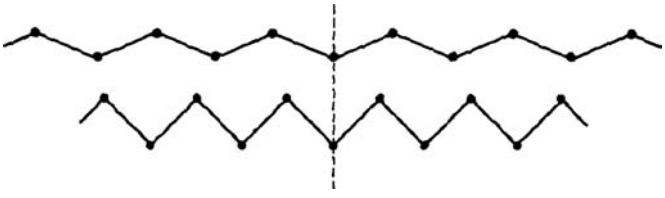


Figure 3.15 Fundamental acoustic vibration of a linear chain polymer. Adapted with permission from Ref. [195]; © 1984, Springer.

Lam Research Ex. 1047 - Page 183
Lam Research Corp. v. Inpria Corp.
IPR2024-00033 - U.S. Patent No. 9,823,564

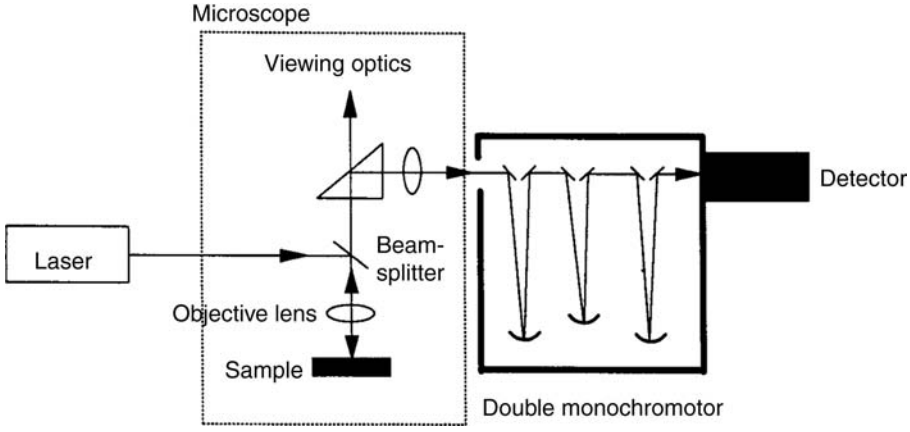


Figure 3.16 Schematic layout of a Raman microscope system. Adapted with permission from Ref. [194]; © 1995, American Chemical Society.

spectra at various points of the sample in a point-by-point manner and dispersing the spectra across the detector. After each measurement the sample is moved by a small amount. In this way the spatial distribution of components in heterogeneous systems can be determined; for example, the phase structure in polymer blends can be elucidated.

The outer form of an object can be visualized by using *wide-field Raman imaging*, where the entire sample is illuminated by defocusing the laser beam and the image of the sample is then obtained by focusing the scattered radiation of a single wavelength to an array detector. The wavelength is changed after each measurement. Rayleigh radiation is removed by passing the scattered radiation through an appropriate filter. A typical example of the Raman images of polystyrene beads is shown in Figure 3.17.

Detailed information on the Raman spectroscopy of polymers is available elsewhere [197–210].

3.3 Technical Developments

3.3.1 Introductory Remarks

During recent years, a wide variety of technical developments involving the use of Vis/UV light for monitoring polymers and polymerization have been made (Table 3.22) that refer not only to photochemical applications such as photocuring and photolithography but also to photophysical applications such as photovoltaics and optical waveguides. Some of these applications are discussed in the following subsections.

Lam Research Ex. 1047 - Page 184
Lam Research Corp. v. Inpria Corp.
IPR2024-00033 - U.S. Patent No. 9,823,564

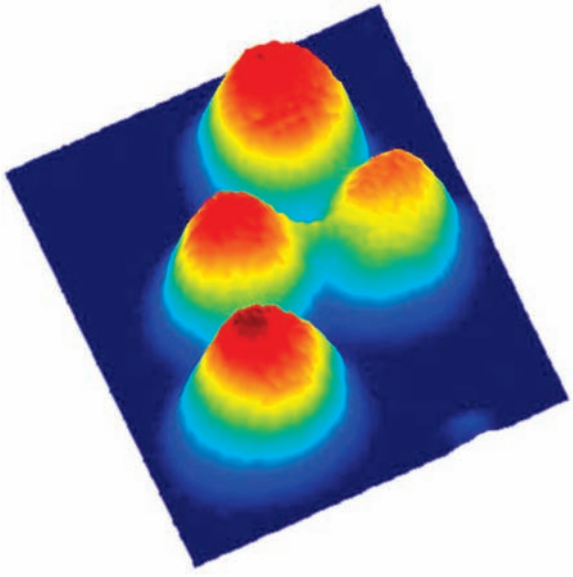


Figure 3.17 Raman images of polystyrene beads located on a Si plate mapped with 100 nm steps. Bead diameter: 2.8 μm. Adapted from Ref. [196].

Table 3.22 Technical developments regarding the use of UV/Vis light in the polymer field.

Subject	Typical applications
Photocuring	Furniture coatings, printing plates, dental restorative systems, insulation of electrical conductor wires, volume phase holography
Photolithography	Generation of structured patterns in the manufacture of micro-devices (computer chips)
Photovoltaics	Conversion of sunlight to electric power with the aid of organic solar cells
Polymeric light sources	Conversion of electric power to light with organic light-emitting diodes. Conjugated polymers in laser materials
Holography	Production of three-dimensional images of objects; optical data storage
Xerography	Copying of documents; desktop printing
Optical waveguides	Polymeric optical fibers for short-distance data communication systems
Electro-optics and non-linear optics	Devices for telecommunications (Bragg wavelength filters, signal modulators, electrical-to-optical signal transducers), optical data storage
Photorefractivity	Real-time recording of optically encoded information, Holography

Lam Research Ex. 1047 - Page 185
Lam Research Corp. v. Inpria Corp.
IPR2024-00033 - U.S. Patent No. 9,823,564

3.3.2 Photocuring

Photocuring refers to the methods employed for various practical applications that are based on the light-induced polymerization of low-molar-mass liquid compounds (monomers and oligomers), and result in the formation of rigid intermolecularly crosslinked materials that are insoluble in most solvents. The most important applications here include surface coatings, the preparation of printing plates, the curing of dental preventive and restorative systems, and microfabrication with the aid of stereolithography. Further detailed information on this topic is available in books and reviews [46,211–229]

In contrast to thermal curing, photocuring can be performed at ambient temperatures with solvent-free formulations. In many cases, photocuring processes that proceed within a fraction of a second have replaced the conventional thermal curing of solvent-containing formulations. The main industrially applied photocuring processes are based on four chemical systems that are converted into three-dimensional networks upon irradiation [225]: (i) unsaturated maleic/fumaric acid-containing polyesters (*UPE*s) dissolved in styrene; (ii) acrylate/methacrylate systems; (iii) thiol/ene systems; and (iv) epoxide- or vinyl ether-containing systems. In the first three systems, free-radical polymerizations are operative, whilst in the fourth system cationic species are involved (see Section 3.2.2.1). Industrially applied polymerizable formulations are composed of mixtures of monofunctional and multifunctional monomers and oligomers (Table 3.23) containing a photoinitiator and, if required, also additives such as polymers (pre-polymers, resins) and pigments. The composition of a formulation applied for microfabrication, as a typical example, is presented in Table 3.24. With regards to the thiol/ene systems, the mechanism of free radical thiol/alkene polymerization outlined in Scheme 3.44 is assumed to be operative [229]. Moreover, by employing polyfunctional thiol compounds it is possible to form very tough, abrasion-resistant coatings [217].

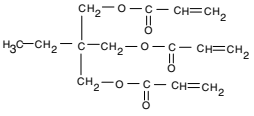
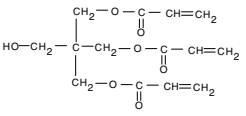
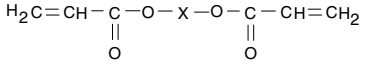
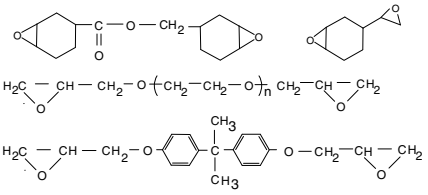
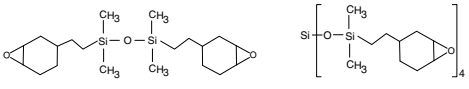
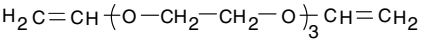
The UV-curing of coatings is widely used, and all types of substrate – including paper, plastic, and metal – are coated using this technique (Table 3.25). The main benefits of the method are that it delivers short production times, provides high-quality products, has low energy needs and equipment costs, and is also environment-friendly because of the greatly reduced emissions of volatile organic compounds (*VOC*s).

Silicones have the advantage of softness, biological inertness, good substrate wettability, and superb permeability of gases. Consequently, UV-cured silicones are suitable for various interesting product applications [229], including ophthalmic devices (hard and soft contact lenses, intraocular lens implants), gaskets, sealings, and optical fiber coatings. Photocurable formulations appropriate for the fabrication of such products contain siloxane derivatives bearing unsaturated carbon–carbon double bonds (Chart 3.13).

Apart from acrylate-based systems, which are cured by a free-radical mechanism, epoxide-based systems that are cured cationically are also used. Epoxide-based formulations yield excellent overprint varnishes on tin-free steel and aluminum for rigid packaging, especially when producing steel food cans and aluminum beer and

Lam Research Ex. 1047 - Page 186
Lam Research Corp. v. Inpria Corp.
IPR2024-00033 - U.S. Patent No. 9,823,564

Table 3.23 Typical di- and trifunctional compounds used for photocuring.

Class	Chemical structure	Mode of polymerization
Trifunctional acrylates	 Trimethylolpropane  Pentaerythritol triacrylate	Free radical
Oligomeric diacrylates	 X : Polyester, Polyether, Polyurethane, Polysiloxane	Free radical
Thiol/Enes Difunctional epoxides	$C(X{-}SH)_4 / H_2C{=}CH{-}X'{-}CH{=}CH_2$ 	Free radical Cationic
Epoxidized siloxanes		Cationic
Difunctional vinyl ethers	  X : Polyester, Polyether, Polyurethane, Polysiloxane	Cationic

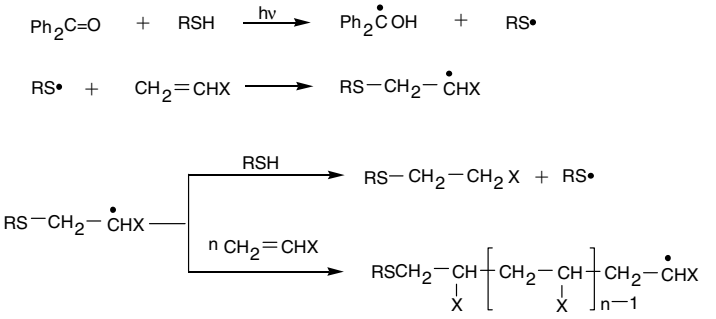
beverage cans. The cured films exhibit good adhesion, flexibility and abrasion resistance, while the high production rates (up to 1600 cans per minute) are astounding [221]. As coatings containing cycloaliphatic epoxides tend to be brittle, other compounds (e.g., oligomeric polyols) are frequently added as flexibilizing agents. When polyfunctional alcohols react with polyfunctional epoxides, a three-dimensional polymer network is formed as the alcohols react with oxonium ions formed by the addition of protons to epoxide groups (Scheme 3.45), and are thereby copolymerized with the epoxides. It should be noted that the protons formed in this reaction can, in turn, react with epoxide groups, so as to accomplish a chain-transfer process. The structure of part of a three-dimensional network that is formed upon reaction of a difunctional epoxide with a trifunctional polyol is depicted in Chart 3.14.

One major difference between cationic and free radical curing is the degree of shrinkage caused by the polymerization. Typically, cationic ring-opening polymerization (*ROP*) leads to a shrinkage of 1–2%, compared to 5–20% shrinkage for the

Lam Research Ex. 1047 - Page 187
Lam Research Corp. v. Inpria Corp.
IPR2024-00033 - U.S. Patent No. 9,823,564

Table 3.24 Composition of a formulation applied for microfabrication [227].

Monomer/Oligomer	wt.%
Alkoxylated trifunctional acrylate	10
Tris(2-hydroxyethyl) isocyanurate triacrylate	10
Trifunctional methacrylate	11
Ethoxylated trimethylolpropane triacrylate	10
Triethyleneglycol diacrylate	11
Isobornyl acrylate	2.5
Trimethylolpropane trimethacrylate	2.75
Brominated urethane acrylate (oligomer)	7.5
Aliphatic polyester-based urethane dimethacrylate (oligomer)	8.25
Aromatic urethane acrylate (oligomer)	27



Scheme 3.44 Free radical thiol/alkene polymerization [217].

Table 3.25 Typical commercial applications of radiation-cured coatings in major industries [4].

Industrial sector	Mode of application
Furniture and construction	Hardwood flooring, PVC flooring, wood and metal furniture, particle board sealer, galvanized tubing, fencing, and so on.
Electronics and telecommunications	Electrical conductor wires, printed circuit board coatings, optical fibers, magnetic media, coatings, computer disc clearcoats, coatings for metallized substrates
Printing and packaging	Inks, release coatings, overcoats for graphic art, magazine covers, coatings on beverage cans, coatings on non-food packaging, barrier coatings, DVD laminates
Automotive	Headlamps, printed dashboard components, refinishing coatings
Consumer goods	Release coatings for adhesives, pressure-sensitive adhesives, leather coatings, coatings on plastic housings (cell phones, computers, etc.), eyeglass lenses, mirror coatings

Lam Research Ex. 1047 - Page 188
Lam Research Corp. v. Inpria Corp.
IPR2024-00033 - U.S. Patent No. 9,823,564

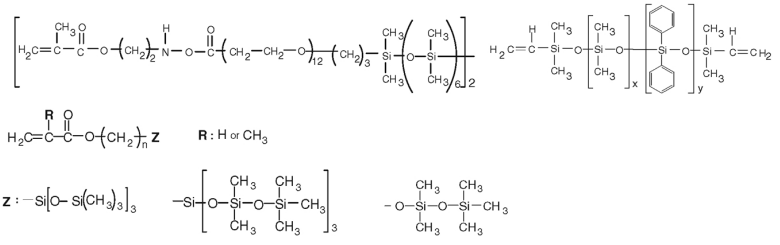
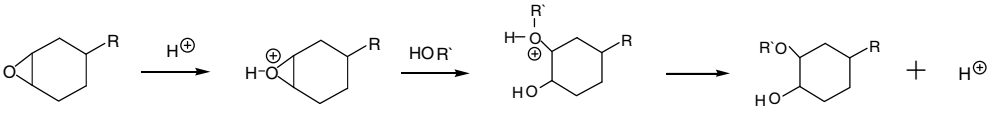


Chart 3.13 Chemical structures of typical siloxane-derived monomers [229].

Lam Research Ex. 1047 - Page 189
Lam Research Corp. v. Inpria Corp.
IPR2024-00033 - U.S. Patent No. 9,823,564



Scheme 3.45 Formation of oxonium ions by the addition of protons to epoxides, and their subsequent reaction with alcohols.

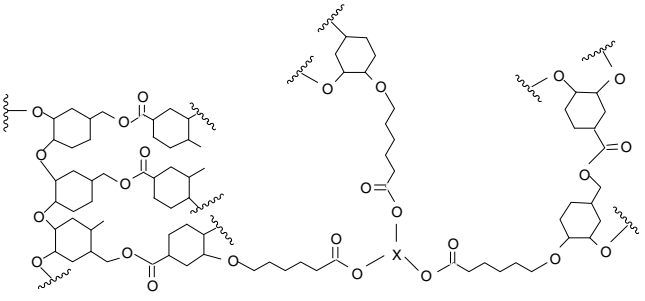


Chart 3.14 Structure of part of a network formed by the reaction of a difunctional epoxide with a trifunctional polyol.

radical polymerization of double bonds. Notably, a lower degree of shrinkage implies a stronger adhesion of the coating to the substrate.

The photocuring of coatings is paralleled by high-energy radiation curing (see Section 5.6.4), which does not require initiators; rather, the latter process is performed industrially with the aid of fast electrons.

The photocuring of *printing plates* is a widely used and important application for transferring images to paper or other substrates, the image being applied to the printing plate by means of photomechanical, photochemical or laser-engraving processes. The so-called *letterpress technique*, which is based on light-sensitive relief-structured polymer printing plates, is used to print newspapers, paperback books, business stationery, postage stamps, adhesive labels, and many other items. During the printing process, ink that is dispensed onto the raised areas is transferred to the substrate. As shown in Table 3.26, polymer letterpress plates consist of various layers, including a protective cover layer, a photosensitive layer, an adhesion layer, and a support layer.

Table 3.26 Layer sequence of a typical polymer letterpress plate. Adapted with permission from Ref. [230]; © 1989, Wiley-VCH.

Nature of layer	Layer thickness (μm)
Protective	Approx. 100 μm
Photosensitive	30 to 6500
Adhesion	Approx. 20
Support	100 to 200

Lam Research Ex. 1047 - Page 190
Lam Research Corp. v. Inpria Corp.
IPR2024-00033 - U.S. Patent No. 9,823,564

The photosensitive layers are generally composed of a mixture of reactive monomers and multifunctional oligomers (pre-polymers), polymeric binders, and photoinitiators. Both, free-radical polymerization and cationic polymerization are applicable in this process [230].

The printing plate, covered with the polymerizable material (which often is incorrectly referred to as the *photopolymer*) is irradiated through a film negative (mask) to initiate photocuring. In this way, the areas of the photosensitive layer corresponding to the transparent regions of the mask become polymerized and thus insoluble in the developer. Following irradiation, the plate is developed with an appropriate liquid (mostly water or alcohol/water mixtures), washed, dried and, if necessary, re-exposed. One modern technique employs a solvent-free thermal development [231], whereby the irradiated plate is fixed onto an internally heated drum in a processor heated to about 50 °C. At this temperature, the unexposed monomer forms a fluid that can be lifted from the plate with a fleece that is pressed against the plate.

Recently, printing plate fabrication techniques employing computer-to-plate digital laser exposure have been introduced, thus rendering the negative film process obsolete [232]. These techniques rely on the use of IR lasers, particularly fiber lasers emitting at $\lambda = 1110\,\text{nm}$ [233]. In this case, the photosensitive material, which is adhered to the substrate layer, is coated with a layer of carbon black only a few micrometers thick. The black layer is then ablated by the IR laser beam, resulting in a digital image on the surface of the plate. The printing plate is subsequently processed by exposure to UV light, washout, drying, and finishing. Computer-to-plate printing is also accomplished with printing plates bearing a heat-sensitive mask layer containing IR absorbers. Prior to UV exposure, these plates are irradiated with a computer-guided IR laser in order to generate a mask through imagewise exposure [234]. Besides letterpress printing, photosensitive systems are also employed in other printing modes, such as gravure and screen printing [230,235,236].

The *photocuring of inks* dispensed on the raised areas of the printing plate is another interesting application. Besides pigments, appropriate inks typically contain unsaturated polymers based on polyacrylates and polyesters, photoinitiators, and additives [236a]. The ink is cured after printing by exposing the printed items to UV light. As the ink hardens within a fraction of a second, printing speeds of up to $300\,\text{m}\,\text{min}^{-1}$ can be attained. UV-cured printing inks are superior to water-based, thermally cured inks due to their higher gloss and better fastness (i.e., abrasion resistance).

Photocuring involving photopolymerization can also be used to write *volume phase holograms* that form the basis of a variety of commercial products; this process is described in greater detail in Section 3.3.6.

3.3.3 Photolithography

3.3.3.1 General Aspects

The lithographic method used for the industrial production of microelectronic devices, such as computer chips, has already been introduced in Chapter 1; Section 1.2.3.2 (a schematic illustration of the lithographic process is shown in

Lam Research Ex. 1047 - Page 191
Lam Research Corp. v. Inpria Corp.
IPR2024-00033 - U.S. Patent No. 9,823,564

Figure 1.7). The topic has been covered in several books [237–241]. Principally, structured patterns can be generated by different types of radiation, although at present photolithography using UV or visible light is the key technology for the manufacture of microdevices [242–249]. The generation of fine structures with the aid of extreme ultraviolet (*EUV*) radiation and X-rays is described in Section 5.6.2. Charged particle beam lithography using electron or ion beams (e.g., H^+, He^{2+}, Ar^+) serves to fabricate photomasks, but is inappropriate for the large-scale production of chips. Key criteria for the selection of a special type of electromagnetic radiation are the wavelength dependence of LW_{min}, the minimum achievable feature size, and of the depth-of-focus (*DOF*), which is given by Equations 3.31a and 3.31b:

$$LW_{min} = \frac{k_1 \lambda}{NA} \tag{3.31a}$$

$$DOF = \frac{k_2 \lambda}{(NA)^2} \tag{3.31b}$$

where LW_{min} is equal to $p/2$, also called the *node*, where p denotes the *pitch* – that is, the distance comprising a pair of a line and a space in a periodic fine structure assembly. λ is the exposure light wavelength, k_1 and k_2 are system factors, depending on various parameters such as resist response, pattern geometry in the mask, and so on, and NA is the numerical aperture.

Industrial lithographic set-ups use an optical projection system, which provides a demagnification ratio of up to $\times 4$ in projecting the pattern of the mask onto the resist layer (Figure 3.18) [246]. In this case, NA is given by Equation 3.32:

$$NA = n \sin \theta \tag{3.32}$$

where n is the refractive index of the immersion medium and θ is the acceptance angle of the projection lens.

According to Equation 3.31a, a decrease in LW_{min} can be accomplished by decreasing k_1 and λ and by increasing NA. In the past, all three approaches have been implemented following the industry's roadmap for the miniaturization of electronic devices. A significant enhancement in resolution was brought about by using excimer lasers operating at short wavelengths: 248 nm (KrF), 193 nm (ArF) and 157 nm (F_2). Sub-100 nm features can be generated with the aid of ArF and F_2 lasers.

The numerical aperture may be increased with the aid of lenses with an increased acceptance angle. Moreover, a quite radical approach to enhanced resolution concerns *liquid immersion lithography* [247,249], a new technology that is based on an increase in the refractive index n by replacing the ambient gas (air, nitrogen) with a transparent liquid. A schematic illustration is presented in Figure 3.19. By using water with $n = 1.4366$ at $\lambda = 193$ nm and $T = 21.5\,^{\circ}C$, the numerical aperture NA is increased by 44% at a given $\sin \theta$.

The revolutionary development in miniaturization becomes evident by realizing that the storage capacity of dynamic random access memory (*DRAM*) devices has been increased from 4 Megabit ($1\,Mb = 10^6$ bit) to several Gigabit ($1\,Gb = 10^9$ bit).

Lam Research Ex. 1047 - Page 192
Lam Research Corp. v. Inpria Corp.
IPR2024-00033 - U.S. Patent No. 9,823,564

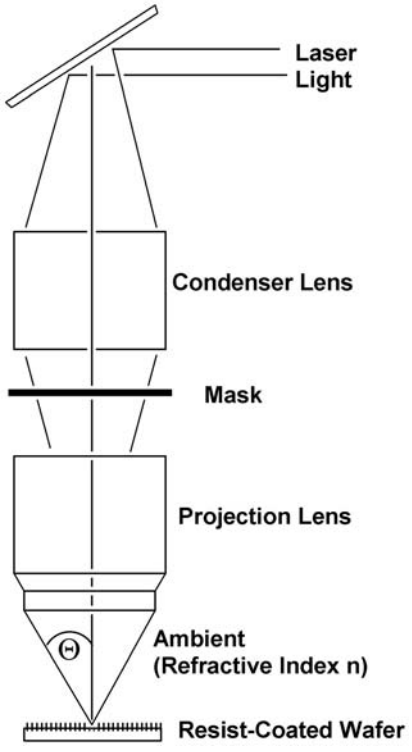


Figure 3.18 Schematic illustration of an optical projection system employed in photolithography.

This increase in storage capacity has been accomplished by lowering LW_{min} from 0.8 μm to 0.04 μm. Additional approaches to enhance resolution, such as *zone-plate array lithography* [250], or the use of phase-shifting masks and maskless lithography [251] cannot be treated here.

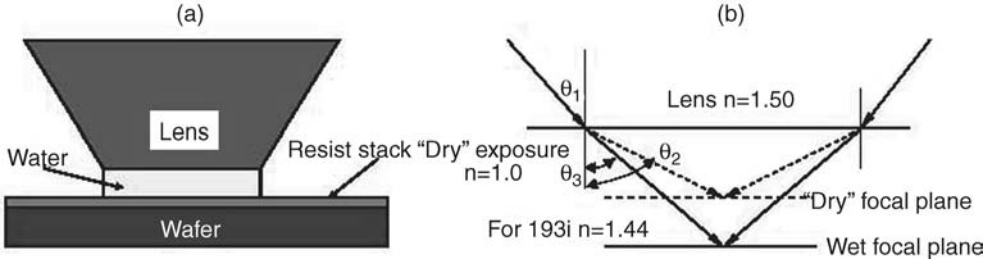


Figure 3.19 (a) Schematic illustration of a 193 nm immersion (193i) exposure head with water filling the gap between final lens and wafer; (b) Optical paths of two-beam interference for both ambient gas-filled and water-filled gap. Adapted with permission from Ref. [247]; © 2007, International Society for Optics and Photonics.

Lam Research Ex. 1047 - Page 193
Lam Research Corp. v. Inpria Corp.
IPR2024-00033 - U.S. Patent No. 9,823,564

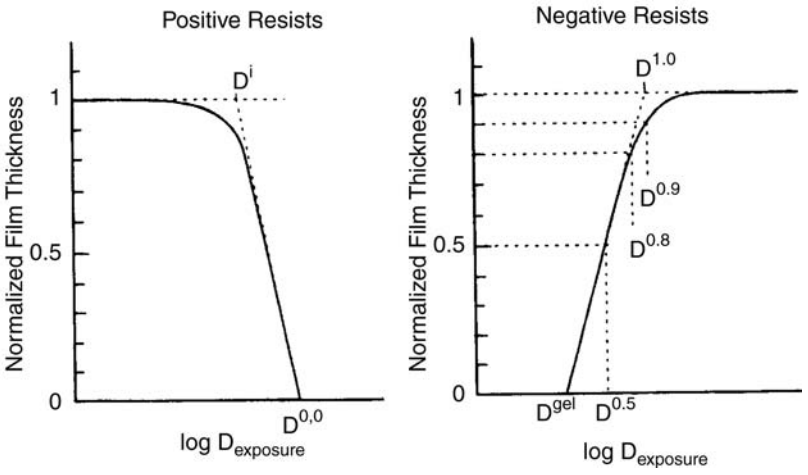


Figure 3.20 Exposure characteristic curves for resists. The film thickness normalized with respect to its initial value (d/d_0) as a function of the exposure dose ($D_{exposure}$).

Most of the resists that have been employed to date are polymer-based – that is, they consist wholly or partly of an amorphous polymer. A resist material must fulfill various requirements: (i) it must be suited for spin casting from solution into a thin and uniform film that adheres to various substrates; and (ii) it must possess a high *radiation sensitivity* and a high *resolution capability*. Commonly, the radiation sensitivity S is defined by *exposure characteristic curves* (Figure 3.20).

In the case of positive tone resists, S is equal to $D^{0.0}$, where $D^{0.0}$ is the exposure dose that corresponds to the total removal of the resist during development (thickness $d = 0$). In the case of negative tone resists, S is equal to $D^{0.5}$, with $D^{0.5}$ being the exposure dose that corresponds to $d = 0.5\, d_0$. Occasionally, S is given by $D^{0.8}$ or $D^{0.9}$.

The *line edge roughness* (LER) is of key importance for the resolution, for example, when features in sub-100 nm node region must be generated. The LER is defined as the local line edge variation determined along a distance equal to four times the node [238]. For certain applications, the *aspect ratio* of radiation-generated fine-line features (the height-to-width ratio of lines) should be high. Moreover, the resist material must withstand extremely harsh environments, for example, high temperatures, strong acids, and plasmas.

As noted above, major advances in resolution have been achieved by reducing the wavelength of incident light. It appears that optical lithography, with all foreseeable extensions, can reach a half-pitch of 19 nm [239]. For this aim, new resist materials with low absorptivities (optical density <0.4) at the shorter wavelengths are needed, because near-uniform exposure throughout the resist layer needs to be maintained.

Liquid development, which is commonly applied in lithographic processes, depends on a radiation-induced alteration of the solubility of resist areas (see Figure 1.7). Provided that the resist consists of a linear polymer, the solubility is either lowered by intermolecular crosslinking (negative tone) or is augmented by

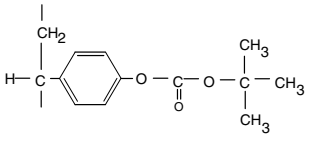
Lam Research Ex. 1047 - Page 194
Lam Research Corp. v. Inpria Corp.
IPR2024-00033 - U.S. Patent No. 9,823,564

main-chain degradation of the polymer (positive tone). Moreover, radiation-induced chemical alterations of functional groups attached to polymer backbones can lead to a solubility change. Very importantly, the radiation-induced conversion of additives controlling the solubility behavior of the polymer can also bring about the desired effect. For example, an additive that normally functions as a *dissolution inhibitor* may accelerate the dissolution after exposure to light.

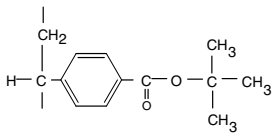
Major advances in radiation sensitivity have been achieved by applying the concept of *chemical amplification* to photolithography [252–254]. Chemical amplification is related to a cascade of chemical reactions that are initiated by a single photon. In fact, strategies based on chemical amplification have played a key role in the development of novel resist systems, as will be outlined in the following subsection. It is to be noted, that the chemical amplification concept has served the semiconductor industry as a workhorse for the past few decades.

3.3.3.2 **248 nm Lithography**

In order to reduce the minimum achievable feature size and to increase the manufacture throughput rate, novel resist systems exhibiting a high radiation sensitivity and containing polymers of low absorptivity were needed. Moreover, novel high-intensity light sources were afforded. In this respect, the invention of chemical amplification, the synthesis of appropriate new polymers and the advent of KrF excimer lasers, generating light of $\lambda = 248\,\text{nm}$, proved to be of key importance. Chemical amplification applies, commonly, to the photogeneration of a Brønsted (protonic) acid capable of catalyzing the deprotection of functional groups attached to the backbone of linear polymers such as PBOCSt or PTBVB (Chart 3.15). Deprotection makes these polymers base-soluble.



PBOCSt



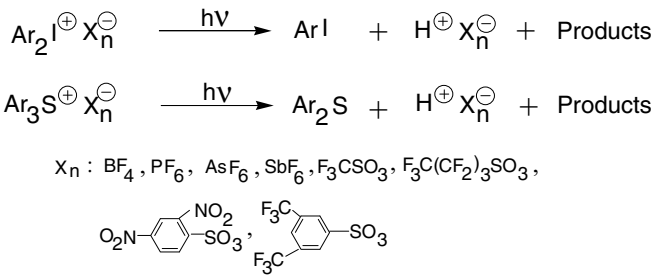
PTBVB

Chart 3.15 Chemical structures of poly(*t*-butoxycarbonyl oxystyrene), PBOCSt, and poly(*t*-butyl-*p*-vinyl benzoate), PTBVB.

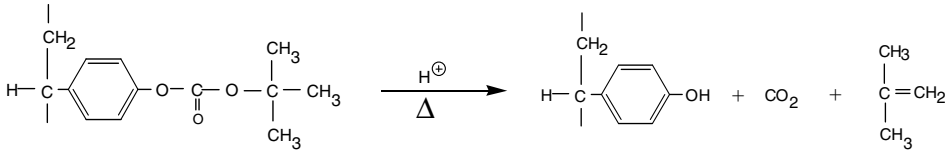
The protonic acid is formed upon irradiation, when the resists contain a small amount of an appropriate acid generator such as an iodonium or sulfonium salt (Scheme 3.46). A detailed mechanism of the photolysis of a diphenyl iodonium salt is presented in Scheme 3.7.

When the exposed resist system is baked at elevated temperatures (>100 °C), the photogenerated acid catalyzes the cleavage of C—O bonds (Scheme 3.47). The deprotected polymer host is soluble in aqueous base developers. Typical turnover rates for one acid molecule are in the range of 800–1200 cleavages. Resists thus amplified may attain a photosensitivity of $S = 1\text{–}5\,\text{mJ}\,\text{cm}^{-2}$ [255],

Lam Research Ex. 1047 - Page 195
Lam Research Corp. v. Inpria Corp.
IPR2024-00033 - U.S. Patent No. 9,823,564



Scheme 3.46 Generalized mechanism of proton generation by photolysis of diphenyliodonium and triphenyl sulfonium salts. Ar: aromatic group.



Scheme 3.47 Acidolysis of PBOCSt, a protected poly(*p*-hydroxystyrene).

significantly surpassing the sensitivity of nonamplified commercial resists such as RD 2000N (poly(vinyl phenol) containing diazidodiphenyl sulfone) with $S = 20\,\mathrm{mJ\,cm^{-2}}$, and Kodak KTFR (cyclized polyisoprene rubber containing azide) with $S = 20\,\mathrm{mJ\,cm^{-2}}$ [245]. Resist systems based on PBOCSt emerged as being highly sensitive towards airborne impurities, but these difficulties were overcome by employing a random copolymer consisting of *p*-hydroxystyrene and *t*-butyl acrylate (Chart 3.16) instead of PBOCSt. This system, denoted as *Environmentally Stable Chemical Amplification Positive Photoresist* (*ESCAP*), has become the standard 248 nm resist in device manufacture by leading chip makers, and is capable of printing features with a density of 125 nm [254]. Besides the onium salts considered above, a variety of organic compounds has been identified that are capable of acting as acid generators; some typical examples are listed in Table 3.27.

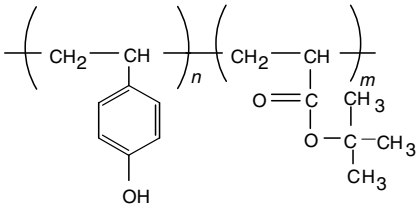
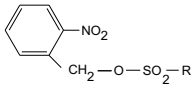
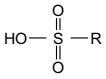
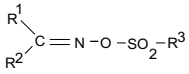
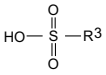
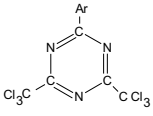
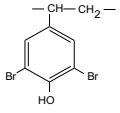


Chart 3.16 Structure of a random copolymer forming the host polymer of ESCAP [254].

Lam Research Ex. 1047 - Page 196
Lam Research Corp. v. Inpria Corp.
IPR2024-00033 - U.S. Patent No. 9,823,564

Table 3.27 Organic photoacid generators.

Acid generator	Acid
o-Nitrobenzyl sulfonates 	
Imino sulfonates 	
2-Aryl-4,6-bis(trichloromethyl)triazines 	HCl
o,*o*′-Dibromophenols 	HBr

With regards to the generation of protons in chemically activated resists (*CAR*s), diffusion emerged as a major problem. It is possible that protons generated in exposed regions diffuse into unexposed regions, thus causing blurring of the latent image.

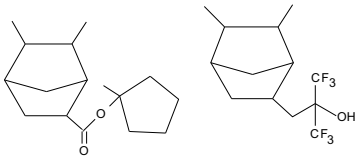
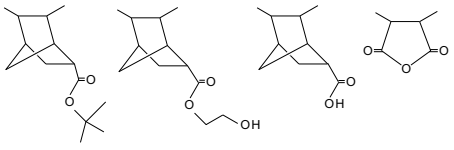
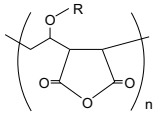
3.3.3.3 193 nm Lithography

The protected *p*-hydroxystyrene-based polymers that function well at 248 nm are too opaque at 193 nm, the wavelength of light emitted by ArF lasers. However, there are acrylate- and cycloalkene-based polymers of much lower absorptivity at this wavelength, which withstand dry etching agents and become base-soluble by chemical amplification based on the release of protective groups. Details of families of random copolymers with cycloaliphatic structures in the main chain or in side groups that are appropriate for 193 nm lithography are listed in Table 3.28.

A typical example of this class of polymers is presented in Chart 3.17, where cycloaliphatic moieties (i.e., adamantyl groups) offer etch durability, while carboxylic acid groups – which become available through amplified deprotection processes – impart base solubility.

Lam Research Ex. 1047 - Page 197
Lam Research Corp. v. Inpria Corp.
IPR2024-00033 - U.S. Patent No. 9,823,564

Table 3.28 Chemical amplification resists applicable in 193 nm lithography.

Resist system	Chemical structure of typical base units	Reference(s)
Random copolymers of norbornene methylcyclopentyl ester and norbornene hexafluoroisopropanol		[254,256a]
Random co- and terpolymers containing norbornene derivatives and maleic anhydride		[256b]
Alternating copolymers of vinyl ether and maleic anhydride	 R: alicyclic group	[256c]

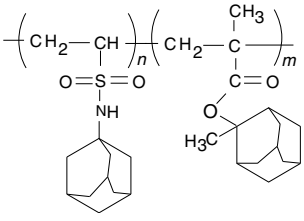


Chart 3.17 Structure of poly[*N*-(1-adamantyl)vinylsulfonamide-*co*-(2-methyl)adamantyl methacrylate], a random copolymer that absorbs light only weakly at $\lambda = 193$ nm [257].

A high sensitivity value $S = 2\ \mathrm{mJ\ cm^{-2}}$ was found for the copolymer presented in Chart 3.17, with $n = 0.4$ and $m = 0.6$. (Resist thickness $d = 220$ nm, acid generator: triphenylsulfonium perfluoro-1-butane sulfonate, developer: aqueous tetramethylammonium hydroxide solution). At present, dry 193 nm lithography operating with the aid of commercially available 193 nm liquid immersion scanners allows the production of devices with 45 nm half-pitch features. Moreover, the production of devices with even smaller features seems feasible [248].

3.3.3.4 157 nm Lithography

Photoresists employed at 248 nm and 193 nm are too opaque at 157 nm, the wavelength of light emitted by F_2 lasers. However, sufficiently transparent fluorocarbon-based polymers containing nonabsorbing C—F bonds function satisfactorily as acid-amplified resists at 157 nm [256a,258]. Chart 3.18 shows the

Lam Research Ex. 1047 - Page 198
Lam Research Corp. v. Inpria Corp.
IPR2024-00033 - U.S. Patent No. 9,823,564

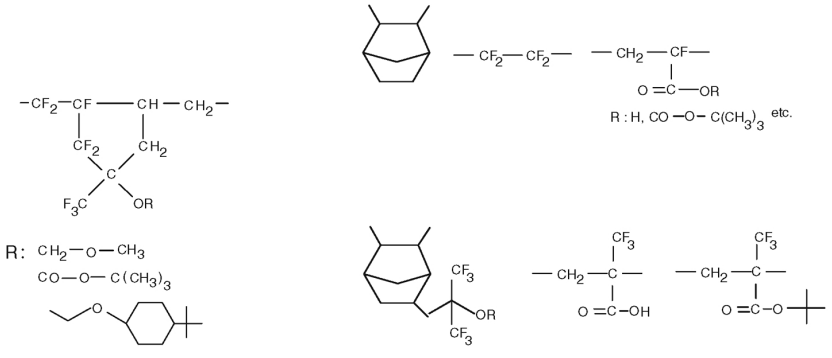
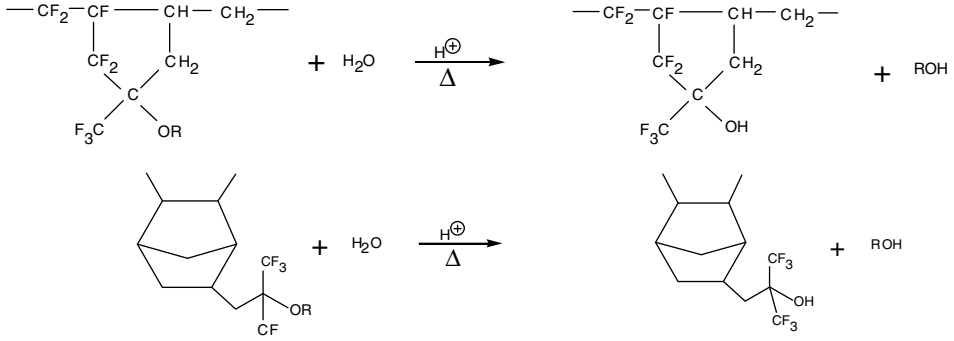


Chart 3.18 Chemical structures of monomer moieties of homopolymers and random copolymers capable of acting as 157 nm resists [259–261].

Lam Research Ex. 1047 - Page 199
Lam Research Corp. v. Inpria Corp.
IPR2024-00033 - U.S. Patent No. 9,823,564

chemical structures of monomer moieties of typical polymers, which have absorption coefficients ranging from 3.0 to 4.0 μm^{-1} [259–264]. At a resist thickness lower than 100 nm, these were found to be capable of imaging 50 nm half-pitch features [264].

The mechanism of the acidolysis of typical polymers is presented in Scheme 3.48.



Scheme 3.48 Acidolysis of polymers appropriate for 157 nm lithography [262,263].

The application of 157 nm lithography for production purposes was delayed by several technical problems concerning pattern development. Moreover, there are difficulties regarding lenses and masks. As yet, CaF_2 is the only feasible lens material, since fused quartz is not transparent at 157 nm, whilst CaF_2 is crystalline and is therefore intrinsically birefringent. Consequently, lenses must be made from elements with different crystal orientations.

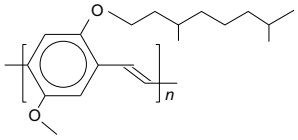
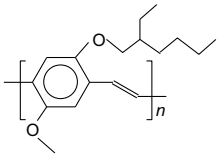
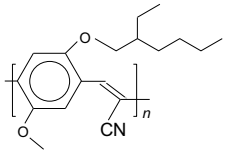
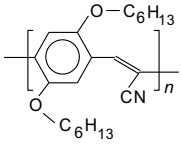
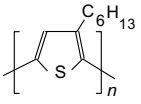
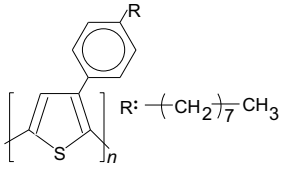
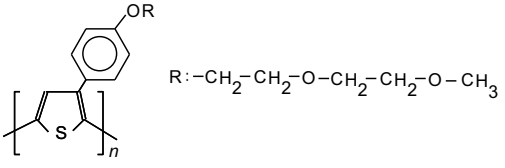
3.3.4 Photovoltaics

An interesting technical development is related to the use of polymers in photovoltaic devices. This applies to semiconducting polymers [265–272], and typical examples of relevant polymers are listed in Table 3.29.

Compared to inorganic photovoltaic cells, efficient organic photovoltaic cells resemble the heterojunction type. Inorganic heterojunction-type photovoltaic cells contain layers of two chemically different semiconductors with different band gaps that are doped with small amounts of additives that provide p-type (electron) and n-type (hole) conductivity, respectively [273–281]. The absorption of photons having energies greater than the band gap energy promotes electrons from the valence to the conduction band, thus generating hole–electron pairs. The latter rapidly dissociate into free carriers that move independently of each other. As these approach the junction, they come under the influence of the "built-in" internal electric field existing across the junction between the two layers. In this way,

Lam Research Ex. 1047 - Page 200
Lam Research Corp. v. Inpria Corp.
IPR2024-00033 - U.S. Patent No. 9,823,564

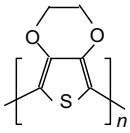
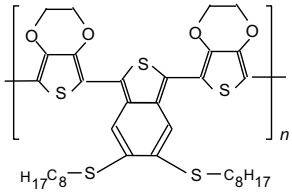
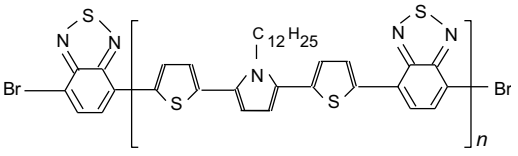
Table 3.29 Chemical structures of semiconducting polymers used in organic solar cell devices [266–272].

Chemical structure	Acronym	Denotation
	MDMO-PPV	Poly[2-methoxy-5-(3′,7′-dimethyl-octyloxy)-1,4-phenylene vinylene]
	MEH-PPV	Poly[2-methoxy-5-(2′-ethyl-hexyloxy)-1,4-phenylene vinylene]
	MEH-CN-PPV	Poly[2-methoxy-5-(2′-ethyl-hexyloxy)-1,4-phenylene (1-cyano) vinylene]
	CN-PPV	Poly[2,5-di-*n*-hexyloxy-1,4-phenylene (1-cyano)vinylene]
	P3HT	Poly(3-hexylthiophene)
	POPT	Poly[3-(4′-octylphenyl)thiophene]
	PEOPT	Poly{3-[4′-(1″,4″,7″-trioxaoctyl)phenyl] thiophene}

(*continued*)

Lam Research Ex. 1047 - Page 201
Lam Research Corp. v. Inpria Corp.
IPR2024-00033 - U.S. Patent No. 9,823,564

Table 3.29 (*Continued*)

Chemical structure	Acronym	Denotation
	PEDOT	Poly(3,4-ethylene-dioxy thiophene)
	PDTI	Thiophene-isothia-naphthene copoly-mer
	PTPTB	Benzothiadiazole-pyrrole copolymer

electrons are swept from the p to the n side and holes from the n to the p side, and recombination is prevented.

The development of effective polymeric photovoltaic cells led to the creation of architectures consisting of phase-separated polymer blends [282–286]. Such systems consist of interpenetrating bicontinuous networks of donor and acceptor phases with domain sizes of 5−50 nm, and provide donor/acceptor heterojunctions distributed throughout the layer thickness (Figure 3.21).

The following model serves to explain the generation of a photocurrent. The absorption of a photon is confined to a molecule or to a region of a polymer chain, where an excited state is created. This localized excited state is frequently termed an *exciton* (see Section 3.1.5), which stems from the terminology for an electron–hole pair in semiconductors. Charge separation occurring at the interphase requires that the difference in energies of the hole states and the electron states exceeds the binding energy of the electron–hole pairs. This amounts to about 100 meV, and is much larger than the input energy required for charge separation in inorganic semiconductors. The efficiency of charge separation is critically determined by the exciton diffusion range since, after its generation, the exciton must reach the junction in order to dissociate into two free charge carriers. Actually, the exciton diffusion range is at most a few nanometers and, therefore, a portion of the excitons generated

Lam Research Ex. 1047 - Page 202
Lam Research Corp. v. Inpria Corp.
IPR2024-00033 - U.S. Patent No. 9,823,564

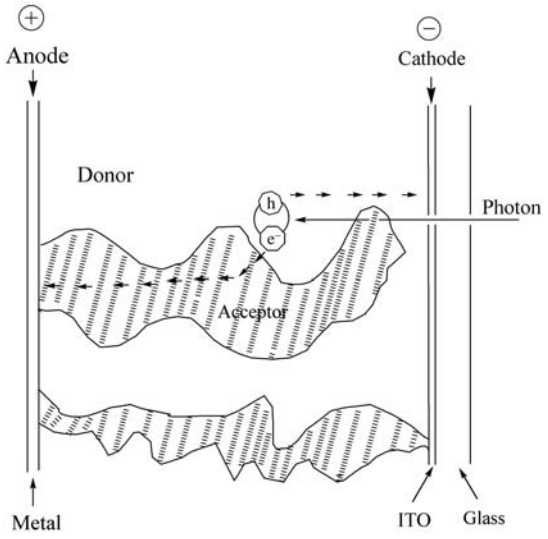


Figure 3.21 Schematic diagram depicting charge transfer from an exciton at a donor/acceptor heterojunction in a composite of two conducting polymers.

in the bulk of the layer do not dissociate. Such systems can be formed, for example, from blends of donor and acceptor polymers such as MEH-PPV and CN-PPV [282,283], or from composites of conducting polymers with buckminsterfullerenes such as MEH-PPV + C_{60} or poly(3-hexylthiophene) (P3HT) + C_{60} [284–289]. The preparation of appropriate composites is facilitated by using fullerene derivatives with improved solubility such as PCBM, the structure of which is shown in Chart 3.19 [271,290].

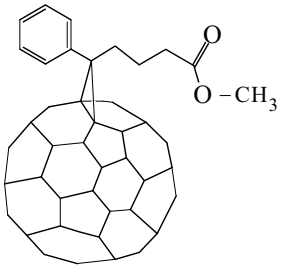


Chart 3.19 Chemical structure of 1-(3-methoxycarbonyl)-propyl-1-phenyl-[6,6]C_{61}, PCBM.

The performance characteristics of some organic photovoltaic cells and those of silicon cells are shown in Table 3.30. Efficiencies for the conversion of incident photons to electric current of up to 50% have been achieved, but the power conversion efficiency of about 5% remains far inferior to that of silicon cells.

Lam Research Ex. 1047 - Page 203
Lam Research Corp. v. Inpria Corp.
IPR2024-00033 - U.S. Patent No. 9,823,564

Table 3.30 Performance characteristics of solar cells.

Material system	η_{mp} (%)[a)]	Φ_{cc}[b)]	Reference
P3HT/PCMB (1:0.8)	5.1		[284]
P3HT/PCMB (1: 1)	4.4		[285]
MDMO-PPV/PCBM	2.5	0.50 (470 nm)	[286]
POPT/MEH-CN-PPV	1.9	0.29	[291]
Amorphous silicon	12.7	∼0.90	[267]
Monocrystalline silicon	24.7	>0.90	[267]

a) Maximum power conversion efficiency.
b) Quantum efficiency for charge carrier generation.

It seems that certain organic materials and especially polymers are attractive for use in photovoltaics. Provided that further progress is brought about by future research, there is the prospect of inexpensive production of large-area solar cells at ambient temperature, since high-throughput manufacture using simple procedures such as spin-casting or spray deposition and reel-to-reel handling is feasible. It is possible to produce very thin, flexible devices, which may be integrated into appliances or building materials.

3.3.5 Polymeric Light Sources

Polymers play a prominent role in organic light-emitting diodes (*OLED*s), which operate on the basis of electroluminescence (*EL*) – that is, luminescence generated by the application of high electric fields to thin polymer layers. Polymer-based EL was first demonstrated in the case of poly(*p*-phenylene vinylene); PPV), ($\pi-\pi^*$ energy gap: 2.5 eV) [291,292], and was later also observed with many PPV derivatives and other fully π-conjugated polymers. Typical representatives are shown in Tables 3.31 and 3.32.

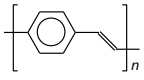
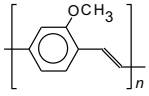
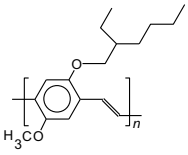
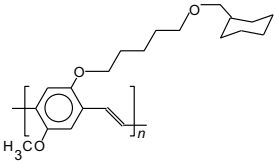
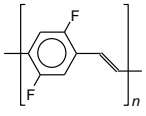
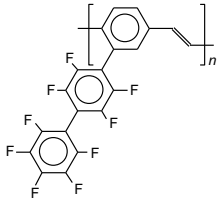
Devices based on the EL of organic materials – commonly denoted as OLEDs – are used for various purposes, including mini-displays in wrist watches and chip cards, for flexible screens, and for emitting wallpaper, as documented in several reviews [265,293,294,296–306]. In contrast to liquid-crystal displays (*LCD*s), OLED displays can be seen from all viewing angles.

As can be seen in Figure 3.22a, an OLED consists, in the simplest case, of a polymer film placed between two electrodes, one of them being light-transparent such as indium tin oxide (*ITO*) and the other being a metal of low work function, such as barium, calcium, or aluminum. More sophisticated OLEDs possess multilayer structures, as shown in Figure 3.22b.

The major steps in the EL mechanism are injection, transport, and the recombination of charge carriers. Electrons are injected from the metal electrode (cathode) and holes from the ITO electrode (anode). A model explaining the phenomenon of the EL of disordered organic materials assumes a "hopping" mechanism for the transport of electric charge carriers. Electrons are injected from

Lam Research Ex. 1047 - Page 204
Lam Research Corp. v. Inpria Corp.
IPR2024-00033 - U.S. Patent No. 9,823,564

Table 3.31 Poly(p-phenylene vinylene)s used in light-emitting diodes [293–295].

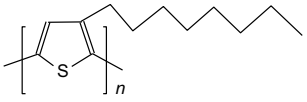
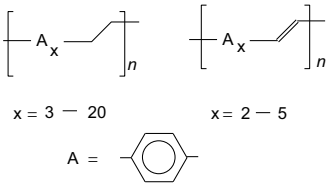
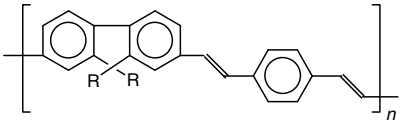
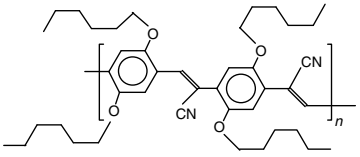
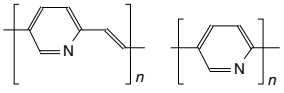
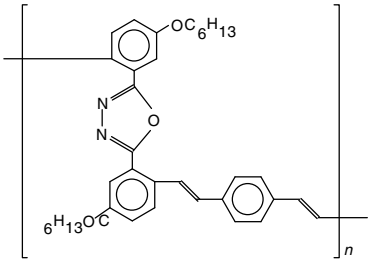
Polymer	Acronym	EL maximum (nm)[a]
	PPV	540
	PMPPV	560
	MEH-PPV	590
	PMCYH-PV	590
	PDFPV	600
	PPFPV	520

a) Wavelength of the maximum of the electroluminescence spectrum.

the Fermi level of the metal electrode into the manifold of hopping states of the organic system. The charge carriers are not very mobile because they are localized, and the transport involves localized discrete hopping steps within a distribution of energy states. Under the influence of the applied electric field, the injected oppositely charged carriers migrate through the system towards the electrodes, and a portion of them eventually combines to form excited electron-hole singlet states,

Lam Research Ex. 1047 - Page 205
Lam Research Corp. v. Inpria Corp.
IPR2024-00033 - U.S. Patent No. 9,823,564

Table 3.32 Polymers employed in light-emitting diodes [296].

Polymer class	Structure of typical polymer	Characteristics
Polythiophenes		p-Type (hole-transporting) polymers. Alkyl groups provide for solubility in organic solvents. Emission tunable from UV to IR by varying the substituent.
Poly-*p*-phenylenes		p-Type polymers of rather high thermal stability, mostly used in the form of polymers containing oligo-*p*-phenylene sequences. Emit light in the blue wavelength range.
Polyfluorenes		p-Type polymers of improved thermal and photostability (relative to PPV). Emit light primarily in the blue wavelength range.
Cyano polymers		Polymers, for example, PPV derivatives, containing electron-withdrawing cyano groups. The latter provide for electron transport, thus complementing the hole-transport property.
Pyridine-containing polymers		Highly luminescent polymers soluble in organic solvents. High electron affinity affords improved electron transport. Quaternization of nitrogen allows manipulation of the emission wavelength.
Oxadiazole-containing polymers		Oxadiazole groups provide for efficient electron transport. Insertion of these groups into p-type polymers facilitates bipolar carrier transport.

Lam Research Ex. 1047 - Page 206
Lam Research Corp. v. Inpria Corp.
IPR2024-00033 - U.S. Patent No. 9,823,564

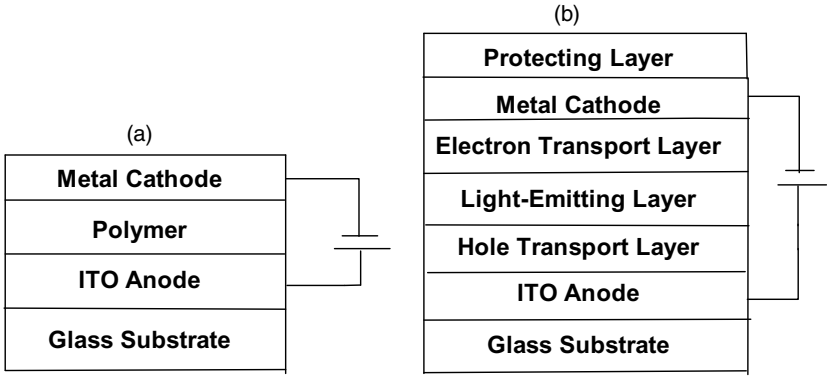


Figure 3.22 (a) Structure of a single-layer polymer LED; (b) Structure of a multilayer polymer LED.

so-called *singlet excitons*. The latter undergo radiative decay to only a small extent – that is to say, the EL quantum yields (in terms of emitted photons per injected electron) are relatively low and amount to only a few percent even in the best cases. Competing processes are operative, such as singlet-triplet crossing and singlet-exciton quenching. The energy level diagram of a single-layer polymer LED under forward bias is shown in Figure 3.23.

Good carrier transport and efficient recombination in the same material are antagonists, because the combination probability is low if the charge carriers swiftly migrate to the electrodes without interaction with their oppositely charged counterparts. A solution to this dilemma was found with devices consisting of several layers (Figure 3.22b). In many cases, a layer allowing swift hole transport and blocking of the passage of electrons has been combined with a layer that permits only electron transport and serves as an emitting layer. Typical hole and electron transport materials employed in polymer LEDS are listed in Table 3.33 [296].

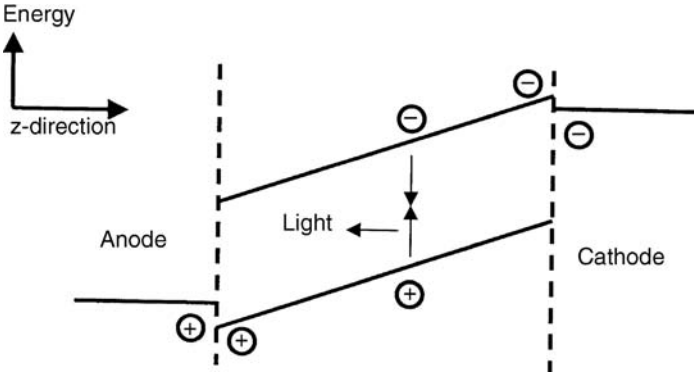
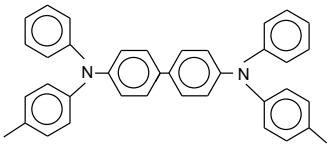
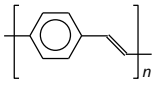
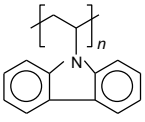
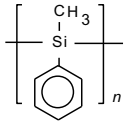
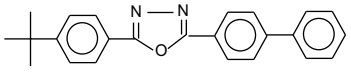
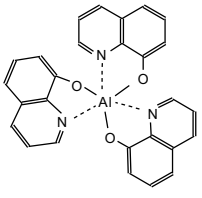
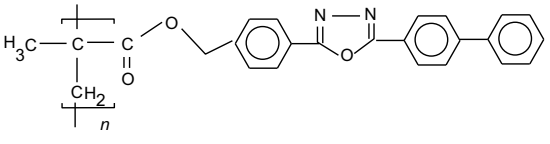


Figure 3.23 Energy level diagram of a single-layer polymer LED under forward bias. The *z*-direction is parallel to the current direction and hence perpendicular to the layer. Adapted with permission from Ref. [298]; © 2002, Center for Photochemical Sciences, Bowling Green.

Lam Research Ex. 1047 - Page 207
Lam Research Corp. v. Inpria Corp.
IPR2024-00033 - U.S. Patent No. 9,823,564

Table 3.33 Hole and electron transport materials employed in polymer LEDs [296].

Chemical structure	Acronym
Hole transport materials:	
	TPD
	PPV
	PVK
	PMPS
Electron transport materials:	
	PBD
	Alq_3
	PMA-PBD

Lam Research Ex. 1047 - Page 208
Lam Research Corp. v. Inpria Corp.
IPR2024-00033 - U.S. Patent No. 9,823,564

A review detailing the various classes of polymers tested for LED application is provided in Ref. [296], while a list of appropriate commercially available materials is provided in Ref. [307].

Interestingly, polymers are used as hole-transport media in white light-emitting OLED devices, which contain a polymer and low-molar mass organic or inorganic compounds as emitting materials. A typical white light-emitting device, which contains CdSe nanoparticles embedded in PPV (Chart 3.20), produces almost white light under a forward bias of 3.5–5.0 V [308].

ITO anode/PEI/(CdSe-PPV)/Al cathode

Chart 3.20 Device used to produce almost white light. ITO: indium tin oxide; PEI: poly(ethylene imine).

3.3.6 Holography

Holography is a technique developed to create three-dimensional images [309–312]. A hologram is a two-dimensional recording, but produces a three-dimensional image. Apart from recording the images of objects, holography has other uses, an example being data storage. Holography relates to recording the complete wave field scattered by an object; that is, both the phase and the amplitude of the light waves diffracted by the object are recorded. As recording media respond only to the light intensity, phase information must be converted into intensity variations, and this is accomplished by using coherent illumination in conjunction with an interference technique.

The way in which a hologram is written is depicted schematically in Figure 3.24a. Light generated by a laser falls simultaneously on the object and a mirror. The light waves diffracted from the object, and those reflected by the mirror, produce an interference pattern on the detection plate by generating a local refractive index modulation (phase hologram) or an absorption coefficient modulation (amplitude hologram). After processing, the image can be reconstructed by illuminating the hologram with the reference light beam only. As shown in Figure 3.24b, light diffracted by the hologram appears to come from the original object.

There are three polymeric systems appropriate for holography: photopolymerizable systems; photochromic systems; and photorefractive systems (Table 3.34). Detailed information on the topic of *polymers in holography* is available in various reviews [313–320].

With regards to commercialized data storage products, photopolymerizable systems (commonly referred to as photopolymers) have shown the most promise [321–323]. In this case, *volume holography* is applied with thick memory devices (typical thickness 1 cm), such that a large number of holograms can be superimposed in one volume element in conjunction with angular multiplexing methods. Notably, holographic storage materials appropriate for the commercial

Lam Research Ex. 1047 - Page 209
Lam Research Corp. v. Inpria Corp.
IPR2024-00033 - U.S. Patent No. 9,823,564

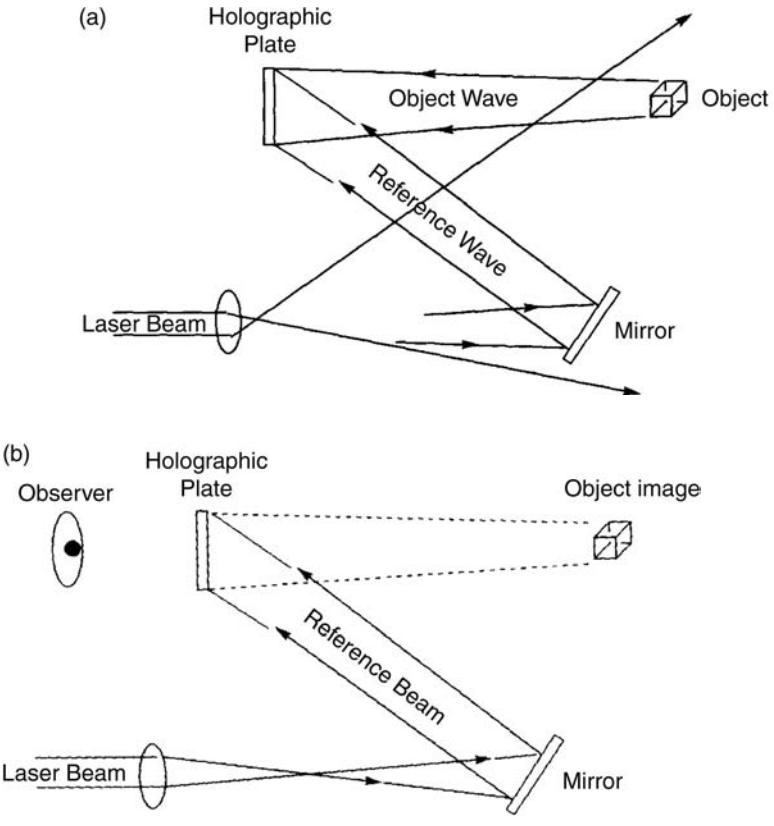


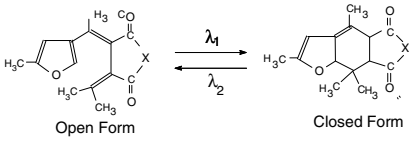
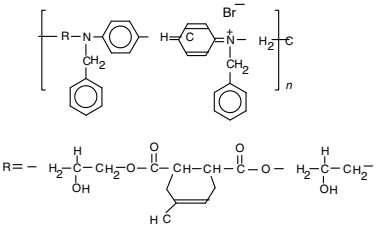
Figure 3.24 (a) Recording of a hologram of an object by generating an interference pattern on the detection plate; (b) Reconstruction of the image of an object recorded in a hologram by illuminating the detection plate with the reference light wave.

application must fulfill various requirements, the most important being a high storage density ($>1\,\mathrm{GB\,cm^{-2}}$), a fast writing time (ms), high sensitivity (mW), long memory (years), fast access time (μs), and reversibility ($>10^4$ cycles) for write/erase systems [322]. Reportedly, commercialized read-only-memory (*ROM*) products possess storage densities of $1.9\,\mathrm{GB\,cm^{-2}}$, with negligible shrinkage occurring during writing [321].

Photopolymerizable systems appropriate for writing holograms typically comprise one or more monomers, a photoinitiator system, an inactive component (binder), and occasionally substances that serve to regulate pre-exposure shelf-life or viscosity. The resulting formulation is typically a viscous fluid, or a solid with a low glass transition temperature. For exposure, the formulation is coated onto a solid or flexible substrate, or is dispensed between two optically flat glass slides. In this case the formation of a hologram is due to the generation of a refractive index grating comprised of bright and dark regions [324]. When the holographic

Lam Research Ex. 1047 - Page 210
Lam Research Corp. v. Inpria Corp.
IPR2024-00033 - U.S. Patent No. 9,823,564

Table 3.34 Polymeric systems suitable for holography.

Polymeric system	Mode of action of generating refractive index gratings	Typical system
Photopolymerizable systems	Photopolymerization of appropriate monomers	Mono- and multifunctional acrylate and methacrylate monomers, photoinitiator, binder
Photochromic systems	Photochromic transformation (color change) $A \rightleftarrows^{\lambda_1}_{\lambda_2,\Delta} B$	Dispersion of fulgides or fulgimides in polystyrene  (X = O) (X = NR)
Photorefractive systems	Photogeneration, migration and trapping of charge carriers	Fully functionalized polymer 

formulation is exposed to a light interference grating, the dispersed monomer polymerizes rapidly in the regions of high intensity (i.e., in the bright regions). As the monomer concentration is depleted in these regions, concentration gradients are generated that cause *component segregation*; that is, the gradients drive the diffusion of the monomer from the dark into the depleted bright regions, where it polymerizes. Ultimately, the bright regions are characterized as areas of high concentration of newly formed polymer molecules, and the dark regions as areas of high binder concentration. As the two materials differ in their refractive indices, a phase grating results. In order to increase the reaction rate, the hologram may be heated for a short period to temperatures of 100–160 °C [324]. Any unreacted monomer can be finally converted by briefly exposing the plate to incoherent UV light (360–400 nm). No wet-processing is required with modern holographic formulations.

Although the precise composition of relevant commercial formulations has not been disclosed by the manufacturers, it is generally agreed that in most cases acrylate- and methacrylate-based monomers are used as polymerizable components [314]. In typical holographic storage studies, the formulation comprises a difunctional acrylate oligomer, *N*-vinyl carbazole, and isobornyl acrylate [325]. In

Lam Research Ex. 1047 - Page 211
Lam Research Corp. v. Inpria Corp.
IPR2024-00033 - U.S. Patent No. 9,823,564

these cases, the polymerization proceeds by a free-radical mechanism, and initiator systems operating in the visible or near-IR wavelength region are employed. Multifunctional monomers are often added to the formulation so as to produce a molecular architecture that consists of a crosslinked polymer network, which improves dimensional stability and image fidelity. Moreover, cationically polymerizable epoxide monomers capable of undergoing ring-opening polymerization (Chart 3.21) are used in volume holographic recording [326,327].

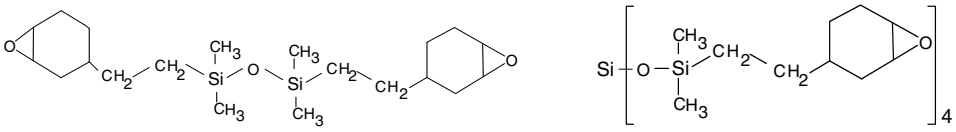


Chart 3.21 Structures of typical epoxide monomers employed in volume holography [326].

Multicolor holographic recording is also possible with the aid of *color mixing*. By utilizing three recording laser wavelengths (usually red, green, and blue) which are simultaneously incident on the holographic plate, the impression of a wide variety of colors is created. In fact, the image of an object obtained from a color hologram is the superposition of the images of three holograms written with three laser beams. If photopolymerizable formulations are employed, then color holograms can be created by writing the holograms in a single holographic plate containing polymerization-initiating systems that are sufficiently sensitive at the specific wavelengths of the laser beams.

Competitor materials in the race to the market are inorganic crystals such as $LiNiO_3$ or $BaTiO_3$ doped with Fe, Cr, Cu, Mg or Zn, and also inorganic chalcogenide glasses containing As_2S_3 or As_2Se_3. However, these are much less sensitive than polymerizable systems, and also provide poor photosensitivity and minimal stability against the light used to read the holograms. Consequently, they must be heat-fixed after writing.

3.3.7
Xerography

Xerography, a form of electrophotography, involves the formation of images by the combined interaction of light and electricity that requires the development of electrostatic charge patterns on the surface of photoconducting substrates. The term *xerography* originates from the Greek words "xeros" (dry) and "graphein" (to write) which, together, means *dry writing*. The importance of the xerographic process, as invented by Carlson in 1938 [328], derives from its application in copying documents with the aid of copying machines. The principle of the xerographic process is depicted schematically in Figure 3.25.

The key role in the process is played by the photoreceptor, which nowadays mostly consists of an organic material. In order to make a copy of a document, the photoreceptor surface is first positively or negatively corona charged. The charge

Lam Research Ex. 1047 - Page 212
Lam Research Corp. v. Inpria Corp.
IPR2024-00033 - U.S. Patent No. 9,823,564

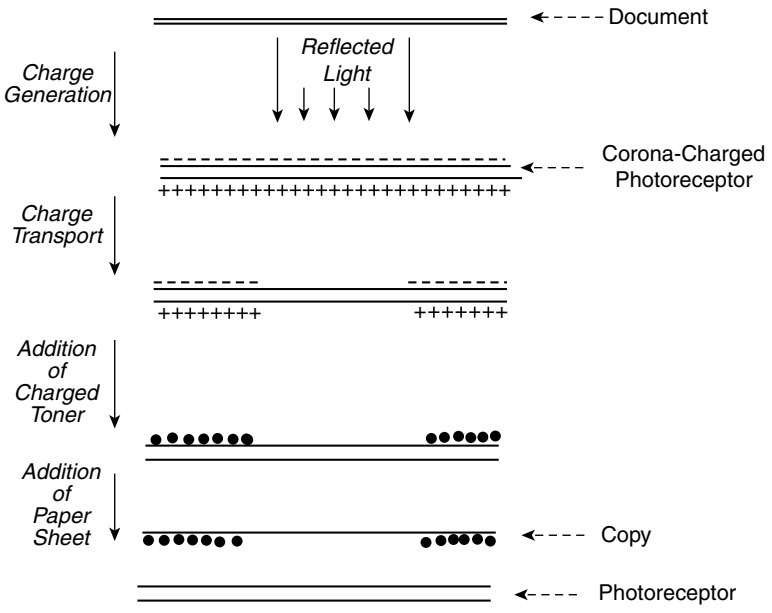


Figure 3.25 Schematic depiction of the xerographic process in the case of a positively corona-charged single photoreceptor layer. Adapted with permission from Ref. [4]; © 2007, Wiley-VCH.

carriers generated in the receptor layer during the subsequent exposure to light reflected from the document neutralize the corona charges. The result is a pattern of exposed and unexposed areas at the photoreceptor layer that corresponds to areas where the corona charges were neutralized or remained unaltered, respectively. Electrostatically charged toner particles brought into contact with the exposed photoreceptor stick exclusively to those areas that still carry charges. For completion of the copying process, the toner particles are transferred to a sheet of paper which is pressed to the photoreceptor and then fixed (fused) by a thermal (infrared) treatment. Improved Xerox copying machines employ dual-layer photoreceptors (Figure 3.26), where charge generation and charge transport are separated. The charge generation layer (CGL) is 0.5–5.0 μm thick, and is optimized for the spectral response and the quantum yield of charge carrier formation. The charge transport layer (CTL) is 15–30 μm thick and is optimized for the drift mobility of the charge carriers and for wear resistance.

Numerous compounds have been tested and applied commercially as charge generation and charge transport materials [329,330]. The first all-organic photoreceptor was a single-layer device, consisting of a 1 : 1 molar mixture of an electron-donor polymer, poly(*N*-vinyl carbazol), and an electron acceptor, trinitrofluorenone (*TNF*). Effective dual-layer systems developed at a later stage were operated with polymeric systems, most commonly with molecularly doped polymers – that is, solid solutions of active compounds with a low molar mass in inert polymeric matrices, typically consisting of polycarbonate or poly(vinyl butyral). Highly

Lam Research Ex. 1047 - Page 213
Lam Research Corp. v. Inpria Corp.
IPR2024-00033 - U.S. Patent No. 9,823,564

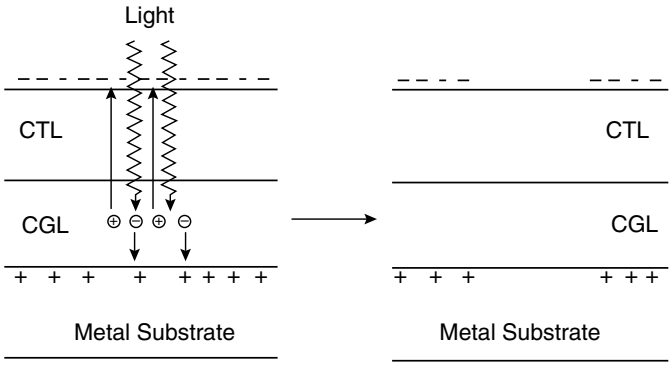
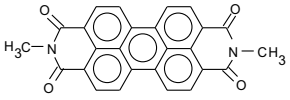
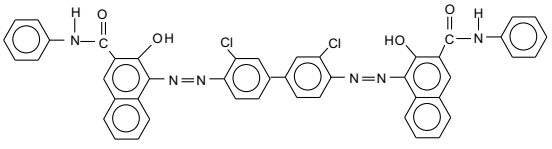
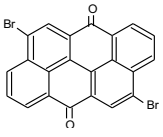
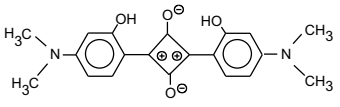


Figure 3.26 The light-induced discharge process schematically depicted for a negatively corona-charged dual-layer photoreceptor. CGL and CTL denote the charge generation layer and charge transport layer, respectively. Adapted with permission from Ref. [4]; © 2007, Wiley-VCH.

sensitive charge-generation systems, appropriate for visible and also for near-IR light, were obtained by doping polymers with pigment particles of dyes. In this case, the CGLs consisted of a light-sensitive crystalline phase dispersed in the polymeric matrix. Typical dopants are shown in Table 3.35.

Table 3.35 Typical dyes applicable as dopants in polymeric charge generation systems.

Formula	Denotation
	Perylene dye
	Azo dye
	Quinone dye
	Squaraine dye

Lam Research Ex. 1047 - Page 214
Lam Research Corp. v. Inpria Corp.
IPR2024-00033 - U.S. Patent No. 9,823,564

Improved sensitivities can be achieved with dual-layer systems containing pigment mixtures [331,332]. An example of this is a system with a CGL consisting of a dispersion of the triphenyl amine triazo pigment AZO-3 (Chart 3.22) in poly (vinyl butyral) and a CTL of a mixture of bisphenol-A polycarbonate and the triaryl amine derivative MAPS (see Chart 3.22).

3.3.8 Optical Waveguides

Modern communication systems with high bandwidth demands are operated with branching optical networks consisting of fibers that permit optical data transfer via laser light pulses. Optical fibers consist of a highly transparent core and a surrounding cladding of refractive indices n_{core} and $n_{cladding}$, respectively. Provided that $n_{core} > n_{cladding}$, light entering the fiber at an angle $\theta < \theta_{max}$ will be totally reflected at the cladding boundary and thus transmitted through the fiber. Polymer optical fibers have become attractive competitors to inorganic glass fibers [333–346]. When compared to erbium- or germania-doped silica fibers, polymer fibers have a larger caliber, are cheaper to prepare and easier to process, but suffer from a larger light attenuation and lower bandwidth. Therefore, polymer fibers can be employed over distances of only several hundred meters, for instance in information networks requiring a large number of connections. The typical properties of polymer and inorganic glass optical fibers are compared in Table 3.36.

Generally, polymer optical fiber systems are applicable in local area networks (*LAN*s), fiber-to-the-home systems, fiber optic sensors, and media-oriented system transport (*MOST*) devices in automobiles. With presently existing and commercially available polymer optical fibers, a bandwidth of up to 400 Mbit s^{-1} can be obtained. Another interesting field of application involves lighting and illumination, in which context a discrimination should be noted between end or point-source lighting and side or line-lighting devices. Typically, the former are used for motorway signaling, and the latter for night illumination of buildings [345].

Polymeric optical fibers have been prepared from various amorphous polymers such as polycarbonate, poly(methyl methacrylate), polystyrene and diglycol diallylcarbonate resin [339,340]. In these cases, the light attenuation of the respective optical fibers is due to absorption by the higher harmonics of C—H vibrations. The substitution of hydrogen by deuterium, fluorine or chlorine results in a shift to higher wavelengths of the absorption due to overtone vibrations, and reduces the attenuation at key communication wavelengths (as shown in Table 3.37).

In fact, commercial polymeric optical fibers prepared from the perfluorinated polymer poly(perfluorobutenyl vinyl ether), of the structure shown in Chart 3.23, exhibit an attenuation of 15 dB km^{-1} at $\lambda = 1310$ nm.

Single-channel systems can be operated at a transmission rate of 2.5 Gbit s^{-1} over a distance of 550 m at $\lambda = 840$ or 1310 nm [339,346]. Besides the intrinsic factors for optical propagation loss – namely, absorption and Rayleigh light scattering – there are extrinsic factors such as dust, interface asymmetry

Lam Research Ex. 1047 - Page 215
Lam Research Corp. v. Inpria Corp.
IPR2024-00033 - U.S. Patent No. 9,823,564

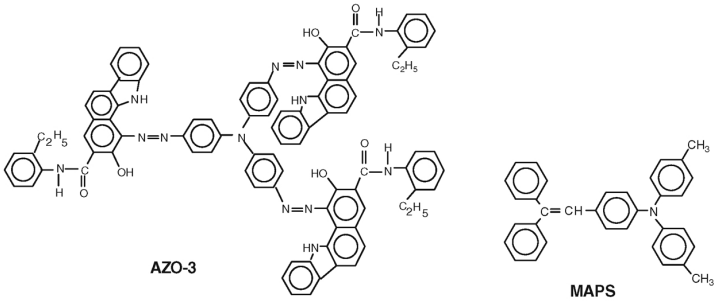


Chart 3.22 Chemical structures of the triphenyl amine triazo pigment AZO-3 and the triaryl amine derivative MAPS.

Lam Research Ex. 1047 - Page 216
Lam Research Corp. v. Inpria Corp.
IPR2024-00033 - U.S. Patent No. 9,823,564

Table 3.36 Typical properties of *step-index optical fibers*, which are characterized by a single refractive index extending over the entire core up to the core/cladding interface [345].

Property	PMMA[a)]	Polycarbonate	Silica glass
Attenuation coefficient α ($dB\,km^{-1}$)[b)]	125 @ 650 nm	1000 @ 650 nm	0.2 @ 1300 nm
Transmission capacity C_{trans}[c)] (MHz km)	<10	<10	10^2 to 10^3
Numerical aperture	0.3 to 0.5	0.4 to 0.6	0.10 to 0.25
Fiber diameter (mm)	0.25 to 10	0.25 to 10	9×10^{-3} to 1.25×10^{-1}
Maximum operating temperature (°C)	85	85	Approx. 150

a) Poly(methyl methacrylate).
b) $\alpha = (10/L) \log (P_0/P_L)$, P_0 and P_L: input and output power, L: fiber length.
c) C_{trans}: product of bandwidth W_{band} and fiber length L, $C_{trans} = W_{band}\ L$, $W_{band} \approx 0.44\,L\ \Delta t^{-1}$, $\Delta t = \left(t_{out}^2 - t_{in}^2\right)^{1/2}$, t_{out} and t_{in}: width (FWHM) of output and input pulse.

Table 3.37 Light attenuation (approximate values) caused by absorption due to overtone vibrations at key communication wavelengths, in units of $dB\,km^{-1}$ [339].

λ (nm)	Bond			
	C—Cl	C—F	C—D	C—H
840	$<10^{-8}$	10^{-4}	10^{1}	10^{4}
1310	10^{-5}	10^{0}	10^{3}	10^{5}
1550	10^{-3}	10^{1}	10^{5}	10^{6}

between core and clad, and changes in core diameter, that may also affect the light transmission.

Waveguide components are also applied in photonic devices. Based on polymers, these can be easily manufactured at low cost, with typical applications ranging from computer backplanes that combine electrical and optical cables, thermo-optical switches, optical splitters of multichannel high-density planar lightwave circuits to polyimide-based electro-optical (*EO*) modulators.

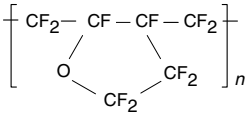


Chart 3.23 Chemical structure of poly(perfluorobutenyl vinyl ether).

Lam Research Ex. 1047 - Page 217
Lam Research Corp. v. Inpria Corp.
IPR2024-00033 - U.S. Patent No. 9,823,564

References

1 Becker, H.G.O. (ed.) (1983) *Einführung in die Photochemie*, Thieme Verlag, Stuttgart.

2 Jaffe, H.H. and Orchin, M. (1962) *Theory and Applications of Ultraviolet Spectroscopy*, John Wiley, New York.

3 Barrow, G.M. (1962) *Introduction to Molecular Spectroscopy*, McGraw-Hill Kogakusha, Tokyo.

4 Schnabel, W. (2007) *Polymers and Light, Fundamentals and Practical Applications*, Wiley-VCH, Weinheim.

5 Shim, H.-K. and Jin, J.-I. (2002) Light-emitting characteristics of conjugated polymers, in *Polymers for Photonics Applications I, Advances in Polymer Science*, 158 (ed. K.-S. Lee), Springer, Berlin, p. 193.

6 Sariciftci, N.S. (ed.) (1997) *Primary Photoexcitations in Conjugated Polymers: Molecular Exciton versus Semiconductor Band Model*, World Scientific, Singapore.

7 Cornil, J., dosSantos, D.A., Beljonne, D., Shuai, Z., and Bredas, J.-L. (2000) Gas phase to solid state evolution of the electronic and optical properties of conjugated chains: a theoretical investigation, in *Semiconducting Polymers* (eds G. Hadziioannou and P.F.vanHutten), Wiley-VCH, Weinheim, p. 235.

8 Pichler, K., Halliday, D., Bradley, D.C., Burn, P.L., Friend, R.H., and Holmes, A.B. (1993) Optical spectroscopy of highly ordered poly(*p*-phenylene vinylene). *J. Phys. Cond. Matter*, 5, 7155.

9 Harm, W. (1980) *Biological Effects of Ultraviolet Radiation*, Cambridge University Press, Cambridge.

10 Horspool, W.M. and Lenci, F. (eds) (2004) *CRC Handbook of Organic Photochemistry and Photobiology*, 2nd edn, CRC Press, Boca Raton, Florida.

11 Sancar, A. (2000) Cryptochrome: the second photoactive pigment in the eye and its role in circadian photoreception. *Annu. Rev. Biochem.*, 69, 31.

12 Schaffner, K. and Gärtner, W. (1999) Open-chain tetrapyrroles in light sensor proteins: phytochromes. *The Spectrum*, 12, 1.

13 Borgstahl, G.E.O., Williams, D.E., and Getzoff, E.D. (1995) Structure of photoactive yellow protein, a cytosolic photoreceptor: unusual fold, active site, and chromophore. *Biochemistry*, 34, 6278.

14 Hendriks, J. and Hellingwerf, K.J. (2004) Photoactive Yellow Protein, the Prototype Xanthopsin, in *CRC Handbook of Organic Photochemistry and Photobiology*, 2nd edn (eds W.M. Horspool and F. Lenci), CRC Press, Boca Raton, Florida, Ch. 123.

15 Muto, Y., Matsuoka, T., Kida, A., Okano, Y., and Kirino, Y. (2001) Blepharismins, produced by the protozoan, *Blepharisma japonicum*, form ion-permeable channels in planar lipid bilayer membranes. *FEBS Lett.*, 508, 423.

16 Dai, R., Yamazaki, T., Yamazaki, I., and Song, P.S. (1995) Initial spectroscopic characterization of the ciliate photoreceptor stentori. *Biochim. Biophys. Acta*, 1231, 58.

17 (a) Shichida, Y., and Yoshizawa, T., Photochemical Aspects of Rhodopsin, in *CRC Handbook of Organic Photochemistry and Photobiology*, 2nd edn (eds W.M. Horspool and F. Lenci), CRC Press, Boca Raton, Florida, Ch. 125; (b) Sakakibara, A. and Sano, Y. (2001) Chemistry of lignin, in *Wood and Cellulosic Chemistry*, 2nd edn (eds D.N.S. Hon and N. Shiraishi), Dekker, New York, Ch. 4.

18 (a) Schnabel, W. (1995) Photoinitiation of ionic polymerizations, in *Current Trends in Polymer Photochemistry* (eds N.S. Allen, M. Edge, I.R. Bellobono, and E. Selli), Ellis Horwood, New York, Ch. 7; (b) Sumiyoshi, T. and Schnabel, W. (1985) On the reactivity of phosphonyl radicals towards olefinic compounds. *Makromol. Chem.*, 186, 1811.

19 Finter, J., Riediker, M., Rohde, O., and Rotzinger, B. (1989) Photosensitive systems for microlithography based on organometallic photoinitiators. *Makromol. Chem. Macromol. Symp.*, 24, 177.

20 Ganster, B., Fischer, U.K., Moszner, N., and Liska, R. (2008) New photocleavable structures: diacylgermane-based

Lam Research Ex. 1047 - Page 218
Lam Research Corp. v. Inpria Corp.
IPR2024-00033 - U.S. Patent No. 9,823,564

photoinitiators for visible light curing. *Macromolecules*, 41, 2394.
21 Crivello, J.V. (1999) The discovery and development of onium salt cationic photoinitiators. *J. Polym. Sci. Part A, Polym. Chem.*, 37, 4241.
22 Crivello, J.V. (1993) Latest developments in the chemistry of onium salts, in *Radiation Curing in Polymer Science and Technology*, vol. III (eds J.P. Fouassier and J.F. Rabek), Elsevier Applied Science, London, Ch. 8.
23 Yağci, Y. and Reetz, I. (1998) Externally stimulated initiator systems for cationic polymerization. *Prog. Polym. Sci.*, 23, 1485.
24 Lazauskaite, R. and Grazulevicius, J.V. (2003) Cationic photopolymerization, in *Handbook of Photochemistry and Photobiology*, vol. 2 (ed. H.S. Nalwa), American Scientific Publishers, Stevenson Ranch, CA, USA, Ch. 7.
25 Dietliker, K. (1991) Photoinitiators for free radical and cationic polymerization, in *Chemistry and Technology of UV and EB Formulations for Coatings, Inks and Paints*, vol. III (ed. P.K.T. Oldring), SITA Technology, London.
26 Dietliker, K., Jung, T., Benkhoff, J., Kura, H., Matsumoto, A., Oka, H., Hristova, D., Gescheidt, G., and Rist, G. (2004) New developments in photoinitiators. *Macromol. Symp.*, 217, 77.
27 Crivello, J.V., Ma, J., and Jiang, F. (2002) Synthesis and photoactivity of novel 5-arylthianthrenium salt cationic photoinitiators. *J. Polym. Sci. Part A, Polym. Chem.*, 40, 3465.
28 Li., H., Ren, K., and Neckers, D.C. (2001) Substituted cyclopropenium salts as photoinitiators for cationic polymerization of glycidyl phenyl ether. *Macromolecules*, 34, 8637.
29 Kutal, C., Grutsch, P.A., and Yang, D.B. (1991) A novel strategy for photoinitiated anionic polymerization. *Macromolecules*, 24, 6872.
30 Kutal, C. (2001) Generation of bases and anions from inorganic and organometallic photoinitiators. *Coord. Chem. Rev.*, 211, 353.
31 Yamaguchi, Y., Palmer, B.J., Kutal, C., Wakamatsu, T., and Yang, D.B. (1998) Ferrocenes as anionic photoinitiators. *Macromolecules*, 31, 5155.
32 (a) Dietliker, K., Jung, T., and Benkhoff, J. (2004) Photolatent Amines: New Opportunities in Radiation Curing, in *Technical Conference Proceedings, UV & EB Technology Expo & Conference, Charlotte, NC, USA*, p. 217; (b) Mejiritski, A., Sarker, A.M., Wheaton, B., and Neckers, D.C. (1997) Novel method of thermal epoxy curing based on photogeneration of polymeric amines and negative-tone image formation. *Chem. Mater.*, 9, 1488.
33 Yağci, Y. and Schnabel, W. (1990) Light-induced synthesis of block and graft copolymers. *Prog. Polym. Sci.*, 15, 551.
34 Muftuoglu, A.E., Tasdelen, M.A., Yağci, Y., and Mishra, M.K. (2009) Block and graft copolymers, Chapter 11, in *Handbook of Radical Vinyl Polymerization, Radical Polymerization, Process and Technology*, 2nd edn (eds M.K. Mishra and Y. Yağci), CRC Press, Boca Raton, FL.
35 Muftuoglu, A.E., Tasdelen, M.A., and Yağci, Y. (2006) Photoinduced synthesis of block copolymers, in *Photochemistry and UV Curing: New Trends* (ed. J.P. Fouassier), Research Signpost, Trivandrum, India, Ch. 29.
36 Arthur, J.C. (1980) Photoinitiated Grafting of Monomers onto Cellulose Substrates, in *Developments in Polymer Photochemistry*, 1 (ed. N.S. Allen), Appl. Science Publ., London, p. 69.
37 Arthur, J.C. (1981) Photografting of monomers onto synthetic polymer substrates, in *Developments in Polymer Photochemistry*, 2 (ed. N.S. Allen), Appl. Science Publ., London, p. 39.
38 Dyer, D.J. (2006) Photoinitiated synthesis of grafted polymers. *Adv. Polym. Sci.*, 197, 47.
39 Mittal, K.L. (ed.) (1996) *Polymer Surface Modification: Relevance to Adhesion*, VSP, Utrecht.
40 Rånby, B. (1996) Surface photografting onto polymers–a new method in adhesion control, in *Polymer Surface Modification: Relevance to Adhesion* (ed. K.L. Mittal), VSP, Utrecht, Part 3.
41 Rånby, B. (1999) Surface modification and lamination of polymers by photografting. *Int. J. Adhes. Adhes.*, 19, 337.

Lam Research Ex. 1047 - Page 219
Lam Research Corp. v. Inpria Corp.
IPR2024-00033 - U.S. Patent No. 9,823,564

42 Rånby, B. (1995) Photoinitiated modification of synthetic polymers: photocrosslinking and surface photografting, in *Current Trends in Polymer Photochemistry* (eds N.S. Allen, M. Edge, I. R. Bellobono, and E. Selli), Ellis Horwood, New York, Ch. 2.

43 Swanson, M.J. and Oppermann, G.W. (1996) Photochemical Surface Modification. Photografting of Polymers for Improved Adhesion, in *Polymer Surface Modification: Relevance to Adhesion* (ed. K.L. Mittal), VSP, Utrecht, Part 3.

44 Bilz, J.P. and Lottle, C.B. (eds) (1999) *Fundamental and Applied Aspects of Chemically Modified Surfaces*, The Royal Chemical Society, London.

45 Dworjanyn, P.A. and Garnett, J.L. (1993) Role of Grafting in UV- and EB-Curing Reactions, in *Radiation Curing in Polymer Science and Technology*, vol. 1 (eds J.P. Fouassier and J.F. Rabek), Elsevier Applied Science, London, Ch. 6.

46 Fouassier, J.P. and Rabek, J.F. (eds) (1993) *Radiation Curing in Polymer Science and Technology*, Elsevier Applied Science, London.

47 Otsu, T. and Yoshida, M. (1982) Role of initiator-transfer agent-terminator (Iniferter) in radical polymerizations: polymer design by organic disulfides as iniferters. *Makromol. Chem. Rapid Commun.*, 3, 127.

48 Sebenik, A. (1998) Living free radical block copolymerization using thio-iniferters. *Prog. Polym. Sci.*, 23, 875.

49 Zahouilly, K. (2002) Proceedings RadTech North America 2002, Indianapolis, IN, April 28–May 1, 2002, vol. 1, 1079.

50 Deng, J. and Yang, W. (2005) Surface photografting polymerization of vinyl acetate, maleic anhydride, and their charge-transfer complex. V. Charge-transfer complex (1). *J. Appl. Polym. Sci.*, 97, 2230.

51 Deng, J. and Yang, W. (2005) Surface photografting polymerization of vinyl acetate, maleic anhydride, and their charge-transfer complex. IX. Charge-transfer complex (5). *J. Appl. Polym. Sci.*, 95, 903.

52 Zhu, Y., Gao, C., Guan, J., and Shen, J. (2003) Engineering porous polyurethane scaffolds by photografting polymerization of methacrylic acid for improved endothelial cell compatibility. *J. Biomed. Mater. Res.*, 67, 1367.

53 Satoh, M., Shirai, K., Saitoh, H., Yamauchi, T., and Tsubokawa, N. (2005) Photografting of polymers onto nanosized silica surface initiated by eosin moieties immobilized onto the surface. *J. Polym. Sci. Part A: Polym. Chem.*, 43, 600.

54 Tsubokawa, N., Shirai, Y., Tsuchida, H., and Handa, S. (1994) Photografting of vinyl polymers onto ultrafine inorganic particles: photopolymerization of vinyl monomers initiated by azo groups introduced onto these surfaces. *J. Polym. Sci. Part A: Polym. Chem.*, 32, 2327.

55 Wegner, G. (1969) Polymerisation von derivaten des 2,4-Hexadiin-1,6-diols. Topochemical reactions of monomers with conjugated triple bonds. *Z. Naturforsch.*, 24, 824.

56 Wegner, G. (1977) Solid-state polymerization mechanisms. *Pure Appl. Chem.*, 49, 443.

57 Hasegawa, M. and Susuki, Y. (1967) Four-center type photopolymerization in the solid state: Poly-2,5-distyrylpyrazine. *J. Polym. Sci. B*, 5, 813.

58 Hasegawa, M. (1983) Photopolymerization of diolefin crystals. *Chem. Rev.*, 83, 507.

59 Hasegawa, M. (1995) Product control in topochemical photoreactions, in *Current Trends in Polymer Photochemistry* (eds N.S. Allen, M. Edge, I.R. Bellobono, and E. Selli), Ellis Horwood, New York., Ch. 10.

60 Sixl, H. (1984) Spectroscopy of the intermediate state of the solid-state polymerization reaction in diacetylene crystals. *Adv. Polym. Sci.*, 63, 49.

61 Bässler, H. (1984) Photopolymerization of polydiacetylenes. *Adv. Polym. Sci.*, 63, 1.

62 Bloor, D. and Chance, R.R. (eds) (1985) *Polydiacetylenes, Synthesis, Structures and Electronic Properties*, Nijhoff, Dordrecht.

63 Schwoerer, M. and Niederwald, H. (1985) Photopolymerization of diacetylene single crystals. *Makromol. Chem. Suppl.*, 12, 61.

64 Enkelmann, V. (1984) Structural aspects of the topochemical polymerization of diacetylenes. *Adv. Polym. Sci.*, 63, 91.

Lam Research Ex. 1047 - Page 220
Lam Research Corp. v. Inpria Corp.
IPR2024-00033 - U.S. Patent No. 9,823,564

65 Song, J., Cisar, J.S., and Bertozzi, C.R. (2004) Functional self-assembling bolaamphiphilic polydiacetylenes as colorimetric sensor scaffolds. *J. Am. Chem. Soc.*, 126, 8459.

66 Kim, J.-M., Ji, E.-K., Woo, S.M., Lee, H., and Ahn, D.J. (2003) Immobilized polydiacetylene vesicles on solid substrates for use as chemosensors. *Adv. Mater.*, 15, 1118.

67 Charych, D.H., Nagy, J.O., Spevak, W., and Benarski, M.D. (1993) Direct colorimetric detection of a receptor-ligand interaction by a polymerized bilayer assembly. *Science*, 261, 585.

68 Charych, D.H., Cheng, Q., Reichert, A., Kuziemko, G., Stroh, M., Nagy, J.O., Spevak, W., and Stevens, R.C. (1996) A litmus test for molecular recognition using artificial membranes. *Chem. Biol.*, 3, 113.

69 Cheng, Q. and Stevens, R.C. (1997) Coupling of an induced fit enzyme to polydiacetylene thin films: colorimetric detection of glucose. *Adv. Mater.*, 9, 481.

70 Morigaki, K., Baumgart, T., Offenhäuser, A., and Knoll, W. (2001) Patterning solid-supported lipid bilayer membranes by lithographic polymerization of a diactylene lipid. *Angew. Chem. Int. Ed.*, 40, 172.

71 Kim, T.S., Chan, K.C., and Crooks, R.M. (1997) Polymeric self-assembled monolayers. 4. Chemical, electrochemical, and thermal stability of ω-functionalized self-assembled diacetylenic and polydiacetylenic monolayers. *J. Am. Chem. Soc.*, 119, 189.

72 Huo, Q., Russel, K.C., and Leblanc, R. M. (1999) Chromatographic studies of a polymerizable diacetylene hydrogen-bonding self-assembly: a self-folding process to explain the chromatic changes of polydiacetylenes. *Langmuir*, 15, 3972.

73 Schnabel, W. and Reetz, I. (1996) Polystyrene and Derivatives, Photolysis, in *Polymeric Materials Encyclopedia*, vol. 9 (ed. J.C. Salamone), CRC Press, Boca Raton, FL, USA, p. 6786.

74 (a) Schnabel, W. and Kiwi, J. (1979) Photodegradation, in *Aspects of Degradation and Stabilization of Polymers* (ed. H.H.G. Jellinek), Elsevier, Amsterdam; (b) Charlesby, A. (1960) Chapter 10, in *Atomic Radiation and Polymers*, Pergamon Press, Oxford; (c) Saito, O. (1972) Statistical theory of crosslinking, in *The Radiation Chemistry of Macromolecules* (ed. M. Dole), Academic Press, New York., Ch. 11.

75 (a) Salamone, J.C. (ed.) (1996) *Polymeric Materials Encyclopedia*, CRC Press, Boca Raton, FL, USA; (b) Salamone, J.C. (ed.) (1999) *Concise Polymeric Materials Encyclopedia*, CRC Press, Boca Raton, FL, USA.

76 Scott, G. (1999) *Polymers and the Environment*, Royal Society of Chemistry, Cambridge.

77 Timpe, H.-J. (1997) Polymer Photochemistry and Photo-Crosslinking, in *Desk Reference of Functional Polymers: Synthesis and Applications* (ed. R. Arshady), American Chemical Society, Washington, D.C, p. 273.

78 Hong, S.I., Joo, S.Y., and Kang, D.W. (1997) Photosensitive polymers, in *Desk Reference of Functional Polymers: Synthesis and Applications* (ed. R. Arshady), American Chemical Society, Washington, D.C., p. 293.

79 Rånby, B., Qu, B., and Shi, W. (1996) Photocrosslinking (Overview), in *Polymeric Materials Encyclopedia*, vol. 7 (ed. J.C. Salamone), CRC Press, Boca Raton, FL, USA, p. 5155.

80 Paczkowski, J. (1996) Photocrosslinkable Photopolymers (Effect of Cinnamate Group Structure), in *Polymeric Materials Encyclopedia*, vol. 7 (ed. J.C. Salamone), CRC Press, Boca Raton, FL, USA, p. 5142.

81 Rabek, J.F. (1996) *Photodegradation of Polymers, Physical Characteristics and Applications*, Springer, Berlin.

82 Clough, R.L., Billingham, N.C., and Gillen, K.T. (eds) (1996) *Polymer Durability Stabilization, and Lifetime Prediction, Advances in Chemistry Series 249*, American Chemical Society, Washington, D.C.

83 Krongauz, V.V. and Trifunac, A.D. (1995) *Processes in Photoreactive Polymers*, Chapman & Hall, New York.

84 Andrady, A.L. (1995) Ultraviolet radiation and polymers, in *Physical Properties of Polymers Handbook* (ed. J.E. Mark), AIP Press, Woodbury, NY, Ch. 40.

Lam Research Ex. 1047 - Page 221
Lam Research Corp. v. Inpria Corp.
IPR2024-00033 - U.S. Patent No. 9,823,564

85 Scott, G. (ed.) (1993) *Atmospheric Oxidation and Antioxidants*, Elsevier, Amsterdam.

86 Allen, N.S. and Edge, M. (1992) *Fundamentals of Polymer Degradation and Stabilisation*, Elsevier Applied Science, London.

87 Osawa, Z. (1992) Photoinduced degradation of polymers, in *Handbook of Polymer Degradation* (eds S.H. Hamid, M.B. Amin, and A.G. Maadhah), Dekker, New York.

88 Böttcher, H., Bendig, J., Fox, M.A., Hopf, G., and Timpe, H.-J. (1991) *Technical Applications of Photochemistry*, Deutscher Verlag für Grundstoffindustrie, Leipzig.

89 Strehmel, V. (2003) Epoxies, structures, photoinduced cross-linking, network properties, and applications, in *Handbook of Photochemistry and Photobiology*, vol. 2 (ed. H.S. Nalwa), American Scientific Publishers, Stevenson Ranch, CA, USA, p. 2.

90 Reiser, A. (1989) *Photoreactive Polymers. The Science and Technology of Resists*, Wiley, New York.

91 Guillet, J. (1985) *Polymer Photophysics and Photochemistry*, Cambridge University Press, Cambridge.

92 Decker, C. (1984) Photodegradation of PVC, in *Degradation and Stabilization of PVC* (ed. E.D. Owen), Elsevier Applied Science, London, p. 81.

93 Tazuke, S. (1982) Photocrosslinking of polymers, in *Developments in Polymer Photochemistry*, vol. 3 (ed. N.S. Allen), Applied Science, London, Ch. 2, p. 53.

94 Owen, E.D. (1982) Photodegradation and stabilization of PVC, in *Developments in Polymer Photochemistry*, vol. 3 (ed. N.S. Allen), Applied Science, London, Ch. 5, p. 165.

95 Ozawa, Z. (1982) Photodegradation and stabilization of polyurethanes, in *Developments in Polymer Photochemistry*, vol. 3 (ed. N.S. Allen), Applied Science, London, Ch. 6, p. 209.

96 Schnabel, W. (1982) Laser flash photolysis of polymers, in *Developments in Polymer Photochemistry*, vol. 3 (ed. N.S. Allen), Applied Science, London, Ch. 7, p. 237.

97 Schnabel, W. (1981) *Polymer Degradation, Principles and Practical Applications*, Hanser, München.

98 Arnaud, R. and Lemaire, J. (1981) Photocatalytic oxidation of polypropylenes and polyundecanoamides, in *Developments in Polymer Photochemistry*, 2 (ed. N.S. Allen), Applied Science, London, Ch. 4, p. 135.

99 Garton, A., Carlsson, D.J., and Wiles, D. M. (1980) Photo-oxidation mechanisms in commercial polyolefins, in *Developments in Polymer Photochemistry*, 1 (ed. N.S. Allen), Applied Science, London, Ch. 4, p. 93.

100 McKellar, J.F. and Allen, N.S. (1979) *Photochemistry of Man-Made Polymers*, Applied Science, London.

101 Balabanovich, A.I., Denizligil, S., and Schnabel, W. (1997) Photolysis of dialkyl phthalates and poly(vinyl chloride) plasticized with dialkyl phthalates at wavelengths exceeding 290nm. *Vinyl Add. Technol.*, 3, 42.

102 Rabek, J.F. (1996) *Photodegradation of Polymers, Physical Characteristics and Applications*, Springer, Berlin.

103 Scott, G. (ed.) (1993) *Atmospheric Oxidation and Antioxidants*, Elsevier, Amsterdam.

104 Schnabel, W. (1981) Photodegradation, in *Polymer Degradation, Principles and Practical Applications*, Hanser, München, Ch. 4.

105 Arnaud, R. and Lemaire, J. (1981) Photocatalytic oxidation of polypropylenes and polyundecanoamides, in *Developments in Polymer Photochemistry*, vol. 2 (ed. N.S. Allen), Applied Science, London, Ch. 4, p. 135.

106 Garton, A., Carlsson, D.J., and Wiles, D.M. (1980) Photo-oxidation mechanisms in commercial polyolefins, in *Developments in Polymer Photochemistry*, vol. 1 (ed. N.S. Allen), Applied Science, London, Ch. 4, p. 93.

107 Sonntag, C.v. (1987) Chapter 4, in *The Chemical Basis of Radiation Biology*, Taylor & Francis, London.

108 Davis, P., Tiganis, B.E., and Burn, L.S. (2004) The effect of photo-oxidative degradation on fracture in ABS pipe resins. *Polym. Degrad. Stab.*, 84, 233.

109 Pospiŝil, J. and Nešpurek, S. (2000) Photostabilization of coatings. mechanisms and performance. *Prog. Polym. Sci.*, 25, 1261.

Lam Research Ex. 1047 - Page 222
Lam Research Corp. v. Inpria Corp.
IPR2024-00033 - U.S. Patent No. 9,823,564

110 Pospiŝil, J. (1995) Aromatic and heteroaromatic amines in polymer degradation. *Adv. Polym. Sci.*, 124, 87.

111 Pospiŝil, J. and Klemchuk, P.P. (1990) *Oxidation Inhibition in Organic Materials*, vols. I and II, CRC Press, Boca Raton, FL, USA.

112 Zweifel, H. (2001) *Plastics Additives Handbook*, 5th edn, Hanser, München.

113 Zweifel, H. (1998) *Stabilization of Polymeric Materials*, Springer, Berlin.

114 Scott, G. (1999) *Polymers and the Environment*, Royal Society of Chemistry, Cambridge.

115 Scott, G. (ed.) (1993) *Atmospheric Oxidation and Antioxidants*, Elsevier, London.

116 Scott, G. (1990) *Mechanisms of Polymer Degradation and Stabilisation*, Elsevier Applied Science, London.

117 Yu, A., Shlapnikov, S.G., and Kiryushkin, A.P. (1996) *Marin, Antioxidative Stabilization of Polymers*, Taylor & Francis, London.

118 Grassie, N. and Scott, G. (1985) *Polymer Degradation and Stabilisation*, Cambridge University Press, Cambridge.

119 Al-Malaika, S., Golovoy, A., and Wilkie, C. A. (eds) (2001) *Specialty Polymer Additives*, Blackwell, Oxford.

120 Sedlář, J. (1990) Hindered Amines as Photostabilizers, in *Oxidation Inhibition in Organic Materials* (eds J. Pospiŝil and P.P. Klemchuk), CRC Press, Boca Raton, FL, USA, vol. II, Ch. 1.

121 Lee, R.E., Neri, C., Malatesta, V., Riva, R.M., and Angaroni, M. (2001) A New Family of Benzotriazoles: How to Modulate Properties within the Same Technology, in *Specialty Polymer Additives* (eds S. Al-Malaika, A. Golovoy, and C.A. Wilkie), Blackwell, Oxford, Ch. 7.

122 Masuhara, H. and Allen, N.S. (eds) (2001) Photoablation of materials. *J. Photochem. Photobiol. A: Chem.*, Special Issue, 145, 3.

123 Georgiou, S. and Hillenkamp, F. (eds) (2003) Laser ablation of molecular substrates. *Chem. Rev.*, Special Issue, 103, 2.

124 Ostendorf, A., Körber, K., Nether, T., and Temme, T. (2000) Material processing applications for diode pumped solid state lasers. *Lambda Physics Highlights*, 57, 1.

125 Schmidt, H., Ihlemann, J., Wolff-Rottke, B., Luther, K., and Troe, J. (1998) Ultraviolet laser ablation of polymers: spot size, pulse duration, and plume attenuation effects explained. *J. Appl. Phys.*, 83, 5458.

126 Tanaka, K., Waki, H., Ido, Y., Akita, S., Yoshida, Y., and Yoshida, T. (1988) Protein and polymer analyses up to m/z 100 000 by laser ionization time-of-flight mass spectrometry. *Rapid Commun. Mass Spectrom.*, 2, 151.

127 Bahr, U., Deppe, A., Karas, M., Hillenkamp, F., and Giessman, U. (1992) Mass spectrometry of synthetic polymers by UV-matrix-assisted laser desorption/ionization. *Anal. Chem.*, 64, 2866.

128 Horspool, W.M. and Song, P-.S. (eds) (1995) *CRC Handbook of Organic Photochemistry and Photobiology*, 1st edn, Boca Raton, Florida.

129 Morrison, H. (ed.) (1990) *Bioorganic Photochemistry*, John Wiley, New York.

130 Young, A.R., Bjorn, L.O., Moan, J., and Nultsch, W. (eds) (1993) *Environmental UV Photobiology*, Plenum Press, New York.

131 Nalwa, H.S. (ed.) (2003) *Handbook of Photochemistry and Photobiology*, American Scientific Publ., Stevenson Ranch, California.

132 Sancar, A. (2003) Structure and function of DNA photolyase and cryptochrome blue-light photoreceptors. *Chem. Rev.*, 103, 2203.

133 Grossweiner, L.I. (1984) Photochemistry of proteins: a review. *Curr. Eye Res.*, 3, 137.

134 Schaich, K.M. (1980) Free radical initiation in proteins and amino acids by ionizing and ultraviolet radiation and lipid oxidation. Part II: ultraviolet radiation and photolysis. *CRC Crit. Rev. Food Sci. Nutr.*, 13, 131.

135 Veksin, N.L. (2002) *Photonics of Biopolymers*, Springer, Berlin, Heidelberg.

136 Smith, G.J. (1995) New trends in photobiology (Invited Review). Photodegradation of keratin and other structural proteins. *J. Photochem. Photobiol. B: Biol.*, 27, 187.

137 Harm, W. (1980) *Biological Effects of Ultraviolet Radiation*, Cambridge University Press, Cambridge.

Lam Research Ex. 1047 - Page 223
Lam Research Corp. v. Inpria Corp.
IPR2024-00033 - U.S. Patent No. 9,823,564

138 Nicholls, C.H. (1980) Photodegradation and photoyellowing of wool, in *Developments in Polymer Photochemistry*, vol. 1 (ed. N.S. Allen), Applied Science Publ., London, Ch. 5, p. 125.

139 Armitage, B. (1998) Photocleavage of nucleic acids. *Chem. Rev.*, 98, 1171.

140 Barber, J. (ed.) (1987) *The Light Reactions*, Elsevier, Amsterdam.

141 Hon, D.N.S. and Shiraishi, N. (eds) (2001) *Wood and Cellulosic Chemistry*, 2nd edn, Dekker, New York.

142 Baugh, P.J. (1981) Photodegradation and photooxidation of cellulose, in *Developments in Polymer Photochemistry*, vol. 2 (ed. N.S. Allen), Applied Science Publ., London, Ch. 5, p. 165.

143 Friedel, M.G. (2004) DNA Damage and Repair: Photochemistry, in *CRC Handbook of Organic Photochemistry and Photobiology* (eds W.M. Horspool and F. Lenci), 2nd edn, CRC Press, Boca Raton, Florida, Ch. 141.

144 Wang, S.Y. (ed.) (1976) *Photochemistry and Photobiology of Nucleic Acids*, Academic Press, New York.

145 Cadet, F. and Vigny, P. (1990) The Photochemistry of Nucleic Acids, in *Bioorganic Photochemistry*, vol. 1 (ed. H. Morrison), John Wiley, New York, Ch. 1.

146 Mitchell, D.L. and Karentz, D. (1993) The Induction and Repair of DNA Photodamage in the Environment, in *Environmental UV Photobiology* (eds A.R. Young, L.O. Bjorn, J. Moan, and W. Nultsch), Plenum Press, New York, p. 345.

147 Vanhooren, A., Devreese, B., Vanhee, K., VanBeeumen, J., and Hanssens, I. (2002) Photoexcitation of tryptophan groups induces reduction of two disulfide bonds in goat α-lactalbumin. *Biochemistry*, 41, 11035.

148 Bent, D.V. and Hayon, E. (1975) Excited state chemistry of aromatic amino acids and related peptides. III. Tryptophan. *J. Am. Chem. Soc.*, 97, 2612.

149 Fasman, G.D. (ed.) (1996) *Circular Dichroism and the Conformational Analysis of Biomolecules*, Plenum Press, New York.

150 Malešic, J., Kolar, J., Strlič, M., Kočar, D., Fromageot, D., Lemaire, J., and Hailland, O. (2005) Photodegradation of cellulose. *Polym. Degrad. Stab.*, 89, 64.

151 Hon, D.N.S. (2001) Weathering and Photochemistry of Wood, in *Wood and Cellulosic Chemistry* (eds D.N.S., Hon and N. Shiraishi), 2nd edn, Dekker, New York, Ch. 11.

152 George, B., Suttie, E., Merlin, A., and Deglise, X. (2005) Photodegradation and photostabilisation of wood – the state of the art. *Polym. Degrad. Stab.*, 88, 268.

153 Veksin, N.L. (2002) *Photonics of Biopolymers*, Springer, Berlin.

154 Greenfield, N.J. and Fasman, G.D. (1969) Computed circular dichroism spectra for the evaluation of protein conformation. *Biochemistry*, 8, 4108.

155 Rodger, A. and Norden, B. (1997) *Circular Dichroism and Linear Dichroism*, Oxford University Press, Oxford.

156 Nakanishi, K., Berova, N., and Woody, R. W. (eds) (1994) *Circular Dichroism: Principles and Applications*, VCH Publishers, Weinheim.

157 Woody, R.W. (1985) Circular dichroism of peptides, in *The Peptides: Analysis, Synthesis, Biology*, vol. 7 (eds E. Gross and J. Meienhofer), Academic Press, New York, p. 14.

158 Woody, R.W. (1995) Circular dichroism. *Methods Enzymol.*, 246, 34.

159 deJong, M.P., Friedlein, R., Osikowicz, E., Salaneck, W.R., and Fahlman, M. (2006) Ultraviolet photoelectron spectroscopy of polymers. *Molec. Crystals Liq. Crystals*, 455, 193.

160 Salaneck, W.R. (2009) Classical ultraviolet photoelectron spectroscopy of polymers. *J. Electr. Spectrosc. Related Phenomena*, 174, 3.

161 Löglund, M., Salanek, W.R., Meyers, W.R., Brédas, J.-L., Arbuckle, J.L., Friend, G., Holmes, A.B., and Froyer, G. (1993) Evolution of the electronic structure of a conjugated polymer series: Polyacetylene, Poly(*p*-phenylene) and Poly(*p*-phenylene vinylene. *Macromolecules*, 26, 3815.

162 Hwang, J., Kim, E.G., Liu, J., Brédas, J.-L., Duggal, A., and Kahn, A. (2007) Photoelectron spectroscopy study of the electronic band structure of polyfluorene and fluorene-acrylamine copolymers at interfaces. *J. Phys. Chem. C*, 111, 1378.

Lam Research Ex. 1047 - Page 224
Lam Research Corp. v. Inpria Corp.
IPR2024-00033 - U.S. Patent No. 9,823,564

163 Kratochvil, P. (1987) *Classical Light Scattering from Polymer Solutions*, Elsevier, Amsterdam.

164 Tanford, C. (1961) *Physical Chemistry of Macromolecules*, Wiley, New York.

165 Zimm, B.H. (1948) Apparatus and methods for measurement and interpretation of angular variation of light scattering; preliminary results on polystyrene solutions. *J. Chem. Phys.*, 16, 1099 (reprinted in Ref. [167], p. 157).

166 Kerker, M. (1969) *The Scattering of Light and other Electromagnetic Radiation*, Academic Press, New York.

167 McIntyre, D. and Gornick, F. (eds) (1964) *Light Scattering from Dilute Polymer Solutions*, Gordon & Breach, New York.

168 Debye, P.P. (1944) Light scattering in solutions. *J. Appl. Phys.*, 15, 338.

169 Chu, B. (1991) *Laser Light Scattering, Basic Principles and Practice*, 2nd edn, Academic Press, New York.

170 van deHulst, H.C. (1981) *Light Scattering by Small Particles*, Dover Publ., New York.

171 Brown, W. (1996) *Light Scattering: Principles and Development*, Oxford University Press, Oxford.

172 Schmitz, K.S. (1990) *An Introduction to Dynamic Light Scattering by Macromolecules*, Academic Press, Boston.

173 Brown, W. (ed.) (1993) *Dynamic Light Scattering: The Method and Some Applications*, Oxford Science Publications, Oxford.

174 Brown, W. and Mortensen, K. (eds) (2000) *Scattering in Polymeric and Colloidal Systems*, Gordon & Breach, Amsterdam.

175 Berne, B.J. and Pecora, R. (1976) *Dynamic Light Scattering in Solutions*, Dover Publications, New York.

176 Berne, B.J. and Pecora, R. (2000) *Dynamic Light Scattering in Solutions: With Applications to Chemistry, Biology and Physics*, Dover Publ., New York.

177 Štěpánek, P. (1993) Data Analysis in Dynamic Light Scattering, in *Dynamic Light Scattering: The Method and Some Applications*, (ed. W. Brown), Oxford Science Publications, Oxford, p. 177.

178 Schärtl, W. (2007) *Light Scattering from Polymer Solutions and Nanoparticle Dispersions*, Springer, Berlin.

179 Raczek, J. (1982) A general method for determination of molecular weight distributions by dynamic light scattering. *Eur. Polym. J.*, 18, 847.

180 Raczek, J. (1982) Examples of the determination of molecular weight distributions by dynamic light scattering. *Eur. Polym. J.*, 18, 863.

181 Skazka, V.S. (1984) Dynamic light scattering and thermal motion of macromolecules in solution. *Russ. Chem. Rev.*, 53, 506.

182 Helmstedt, M. (2000) *Data Evaluation in Light Scattering of Polymers*, Wiley-VCH, Weinheim.

183 Xu, R.L. (2000) *Particle Characterization: Light Scattering Methods*, Kluwer Academic Publ., Dordrecht.

184 Einstein, A. (1910) Theorie der Opaleszenz von homogenen Flüssigkeiten und Flüssigkeitsgemischen in der Nähe des kritischen Punktes. *Ann. Phys.*, 33, 1275.

185 Benoit, H.C. and Doty, P. (1953) Light scattering from non-Gaussian chains. *J. Phys. Chem.*, 57, 958.

186 Higgins, J.S. and Benoit, H.C. (1994) *Polymers and Neutron Scattering*, Clarendon Press, Oxford.

187 Godfrey, J.E. and Eisenberg, H. (1976) The flexibility of low molecular weight double-stranded DNA as a function of length. *Biophys. Chem.*, 5, 301.

188 Nose, T. and Miyashita, N. (2000) Critical Behaviour in Polymer Blend Solutions, in *Scattering in Polymeric and Colloidal Systems* (eds W. Brown and K. Mortensen), Gordon & Breach, Amsterdam, Ch. 7.

189 Galinsky, G. and Burchard, W. (1997) Starch fractions as examples for nonrandomly branched macromolecules. 4. Angular dependence in dynamic light scattering. *Macromolecules*, 30, 6966.

190 Mays, H., Mortensen, K., and Brown, W. (2000) Microemulsions Studies by Scattering Techniques, in *Scattering in Polymeric and Colloidal Systems* (eds W. Brown and K. Mortensen), Gordon & Breach, Amsterdam, Ch. 6.

191 Chu, B. (1991) Methods of Data Analysis, in *Laser Light Scattering, Basic Principles and Practice*, 2nd edn (ed. B. Chu), Academic Press, New York, Ch. 7.

Lam Research Ex. 1047 - Page 225
Lam Research Corp. v. Inpria Corp.
IPR2024-00033 - U.S. Patent No. 9,823,564

192 Štěpánek, P., Tuzar, Z., Kadlec, P., and Kříž, J. (2007) A dynamic light scattering study of fast relaxations in polymer solutions. *Macromolecules*, 40, 2165.

193 Berne, B.J. and Pecora, R., (1976) The Light Scattering Experiment, in *Dynamic Light Scattering in Solutions* (eds B.J. Berne and R. Pecora), Dover Publications, New York, Ch. 4.

194 Clayborn, M., Luget, A., and Williams, K.P. J. (1995) Raman Microscopy and Imaging of Polymers, in *Multidimensional Spectroscopy of Polymers, Vibrational, NMR and Fluorescence Techniques* (eds M.W. Urban and T. Provder), American Chemical Society, Washington, DC, Ch. 3.

195 Klöppfer, W. (1984) *Introduction to Polymer Spectroscopy*, Springer, Berlin.

196 Horiba Scientific Raman Image Gallery, www.horiba.com/de/scientific/products/raman-spectroscopy/raman-imaging/image-galery.

197 Zoubir, A. (ed.) (2012) *Raman Imaging, Techniques and Applications*, Springer, Berlin.

198 Salzer, R. and Sisler, H.W. (eds) (2009) *Infrared and Raman Spectroscopic Imaging*, Wiley-VCH, Weinheim.

199 DeSilvestri, S., Cerullo, G., and Lanzani, G. (eds) (2006) *Coherent Vibrational Dynamics*, CRC Press, Taylor & Francis, Boca Raton, FL, USA.

200 Raghavendra, R., Byrne, H., Martin, S., Howard, R., and Toal, V. (2008) Raman spectroscopy for the characterization of the polymerization rate in an acrylamide-based photopolymer. *Appl. Opt.*, 47, 206.

201 Lewis, I.R. (2002) *Handbook of Raman Spectroscopy: From the Research Laboratory to the Process Line*, CRC Press, Boca Raton, FL, USA.

202 Gregoriou, V.G. and Braiman, M.S. (eds) (2006) *Vibrational Spectroscopy of Biological and Polymeric Materials*, CRC Press, Taylor & Francis, Boca Raton, FL, USA.

203 Galiotis, C. and Parthenios, J. (2006) Stress/Strain Measurements in Fibers and Composites Using Raman Spectroscopy, in *Vibrational Spectroscopy of Biological and Polymeric Materials* (eds V.G. Gregoriou and M.S. Braiman), CRC Press, Taylor & Francis, Boca Raton, FL, USA, Ch. 2.

204 Siesler, H.W., Ozaki, Y., Kawata, S., and Heise, H.M. (eds) (2002) *Near-Infrared Spectroscopy*, Wiley-VCH, Weinheim.

205 Furukawa, Y. (2002) Near-Infrared FT Raman Spectroscopy, in *Near-Infrared Spectroscopy* (eds H.W. Siesler, Y. Ozaki, S. Kawata, and H.M. Heise), Wiley-VCH, Weinheim, Ch. 5.

206 Koenig, J.L. (1999) Raman Spectroscopy of Polymers, in *Spectroscopy of Polymers*, 2nd edn (ed. J.L. Koenig), Elsevier, Amsterdam, Ch. 5.

207 Everall, N. (1999) Raman Spectroscopy of Synthetic Polymers, in *Analytical Applications of Raman Spectroscopy* (ed. M.J. Pelletier), Blackwell, Oxford, p. 127.

208 Urban, M.W. and Provder, T. (eds) (1995) *Multidimensional Spectroscopy of Polymers, Vibrational, NMR and Fluorescence Techniques*, American Chemical Society, Washington, DC.

209 Hendra, P.J. and Agbenyega, J.K. (1993) *The Raman Spectra of Polymers*, Wiley, Chichester.

210 Siesler, H.W. and Holland-Moritz, K. (1980) *Infrared and Raman Spectroscopy of Polymers*, Dekker, New York.

211 Roffey, C.G. (1997) *Photogeneration of Reactive Species for UV Curing*, Wiley, New York.

212 (a) Pappas, S.P. (ed.) (1978) *UV Curing: Science and Technology*, vol. I, Technology Marketing Corp., Norwalk, CT, USA; (b) Pappas, S.P. (ed.) (1985) *UV Curing: Science and Technology*, vol. II, Technology Marketing Corp., Norwalk, CT, USA.

213 Pappas, S.P. (ed.) (1992) *Radiation Curing, Science and Technology*, Plenum Press, New York.

214 Hoyle, C.E. and Kinstle, J.F. (eds) (1990) *Radiation Curing of Polymeric Materials, ACS Symposium Series 417*, American Chemical Society, Washington, DC.

215 Oldring, P.K.T. (ed.) (1991) *Chemistry and Technology of UV and EB Formulations for Coatings, Inks and Paints*, vols. I–IV, SITA Technology, London.

216 Böttcher, H. (1991) *Technical Applications of Photochemistry*, Deutscher Verlag für Grundstoffindustrie, Leipzig.

217 Allen, N.S. and Edge, M. (1993) UV and Electron Beam Curable Pre-Polymers and Diluent Monomers. Classification,

Lam Research Ex. 1047 - Page 226
Lam Research Corp. v. Inpria Corp.
IPR2024-00033 - U.S. Patent No. 9,823,564

Preparation and Properties, in *Radiation Curing in Polymer Science and Technology* (eds J.P. Fouassier and J.F. Rabek), Elsevier Applied Science, London, vol. I, p. 225.

218 Mehnert, R., Pincus, A., Janorski, I., Stowe, R., and Berejka, A. (1998) *UV and EB Technology and Equipment*, SITA Technology, London.

219 (a) Webster, G. (1998) *Prepolymers & Reactive Diluents*, SITA Technology, London; (b) Webster, G., Bradley, G., and Lowe, C. (2001) *A Compilation of Oligomers and Monomers Commercially Available for UV Today*, SITA Technology, London.

220 Lowe, C., Webster, G., Kessel, S., and McDonald, I. (1999) *Formulation*, SITA Technology, London.

221 Crivello, J.V. (1999) The discovery and development of onium salt cationic photoinitiators. *J. Polym. Sci. Part A: Polym. Chem.*, 37, 4241.

222 Davidson, R.S. (2001) *Radiation Curing*, Rapra Technology, Shawbury, Shrewsbury.

223 Dietliker, K. (2002) *A Compilation of Photoinitiators Commercially Available for UV Today*, SITA Technology, London.

224 Neckers, D.C. and Jager, W. (1999) *Photoinitiation for Polymerisation*, SITA Technology, London.

225 Dufour, P. (1993) State-of-the-Art and Trends in the Radiation Curing Market, in *Radiation Curing in Polymer Science and Technology*, vol. I (eds J.P. Fouassier and J. F. Rabek), Elsevier Applied Science, London, p. 1.

226 Jacobine, A.F. (1993) Thiol-Ene Photopolymers, in *Radiation Curing in Polymer Science and Technology*, vol. III (eds J.P. Fouassier and J.F. Rabek), Elsevier Applied Science, London, Ch. 7.

227 Nguyen, L.H., Straub, M., and Gu, M. (2005) Acrylate-based photopolymer for two-photon microfabrication and photonic applications. *Adv. Funct. Mater.*, 15, 209.

228 Decker, C. (1994) Photoinitiated curing of multifunctional monomers. *Acta Polym.*, 45, 333.

229 Jacobine, A.F. and Nakos, S.T. (1993) Polymerizable Silicone Monomers, Oligomers, and Resins, in *Radiation Curing in Polymer Science and Technology* (eds J.P. Fouassier and J.F. Rabek), Elsevier Applied Science, London, Ch. 5.

230 Frass, W., Hoffmann, H., and Bronstert, B. (1989) Imaging technology, in *Ullmann's Encyclopedia of Industrial Chemistry*, vol. A13 (eds B. Elvers, S. Hawkins, M. Ravenscroft, and G. Schulz), VCH, Weinheim, p. 629.

231 *The Seybold Report on Publishing Systems* (2000), vol. 30, 5.

232 Chinnis, D. (2003) Improving Corrugated Post Printing, Newsletter for the Flexographic Pre-Press Platemakers Association. Available at: http://fppa.net/newsletter/summer03/members.htm.

233 Johansson, C., Johnson, J., and Järnström, L. (March 2001) Photopolymer printing plates: Changes in performance and properties, Flexo and Gravure International.

234 Ichii, Y., Ichikawa, S., and Tanaka, S. (2005) Japanese Patent (Toray Industries), Photopolymer Printing Plate Precurser, Its Manufacturing Method of Plastic Letterpress Printing Plate Using It. JP 2005326442.

235 Bendig, J. and Timpe, H.-J. (1991) Photostructuring, in *Technical Applications of Photochemistry* (ed. H. Böttcher), Deutscher Verlag für Grundstoffindustrie, Leipzig, p. 172.

236 Vollmann, H., Frass, W., and Mohr, D. (1986) Polymere in der Drucktechnik. *Angew. Makromol. Chem.*, 145/146, 411; (a) Bean, A.J. (1992) Radiation Curing of Printing Inks, in *Radiation Curing, Science and Technology* (ed. S.P. Pappas), Plenum Press, New York, Ch. 8.

237 Levinson, H.J. (2011) *Principles of Lithography*, 3rd edn, SPIE Press, Bellingham, Washington USA.

238 Okoroanyanwu, U. (2010) *Chemistry and Lithography*, SPIE Press, Bellingham, Washington USA.

239 Lin, B.J. (2010) *Optical Lithography, Here is Why*, SPIE Press, Bellingham, Washington USA.

240 Lin, Q., Pearson, R.A., and Hedrick, J.C. (eds) (2004) *Polymers for Microelectronics and Nanoelectronics, ACS Symp. Ser. 874*, American Chemical Society, Washington, DC.

241 Sheats, J.R. and Smith, B.W. (eds) (1998) *Microlithography, Science and Technology*, Marcel Dekker, New York.

Lam Research Ex. 1047 - Page 227
Lam Research Corp. v. Inpria Corp.
IPR2024-00033 - U.S. Patent No. 9,823,564

242 Ito, H. (2005) Chemical amplification resists for microlithography. *Adv. Polym. Sci.*, 172, 37–245.

243 Ito, H. (1997) Functional polymers for microlithography: amplified imaging systems, in *Desk Reference of Functional Polymers. Syntheses and Applications* (ed. R. Arshady), American Chemical Society, Washington, DC, Ch. 2.4.

244 Ito, H. (1997) Functional polymers for microlithography: nonamplified imaging systems, in *Desk Reference of Functional Polymers. Syntheses and Applications* (ed. R. Arshady), American Chemical Society, Washington, DC, Ch. 2.3.

245 Reiser, A. (1989) *Photoreactive Polymers. The Science and Technology of Resists*, Wiley, New York.

246 Rothschild, M. (2005) Projection optical lithography. *Mater. Today*, 8, 18.

247 Wei, Y. and Back, D. (2007) *193nm Immersion Lithography: Status and Challenges*, SPIE Newsroom.

248 Wei, Y. (2008) *Extendibility of 193nm Immersion Lithography*, SPIE Newsroom.

249 Wei, Y. and Brainard, R.L. (2009) *Advanced Processes for 193nm Immersion Lithography*, SPIE Press, Bellingham, Washington USA.

250 Menon, R., Patel, A., Gil, D., and Smith, H. I. (2005) Maskless lithography. *Mater. Today*, 8, 26.

251 Levenson, M.D. (1994) Extending optical lithography to the gigabit era. *Microlithogr. World*, 3/4, 5.

252 Ito, H., Willson, C.G., and Frechet, J.M.J. (1985) Positive and Negative Working Resist Compositions with Acid Generating Photoinitiator and Polymer with Acid Labile Groups Pendant from Polymer Backbone. US Patent 4,491, 628.

253 Ito, H. and Willson, C.G. (1983) Chemical amplification in the design of dry developing resist materials. *Polym. Eng. Sci.*, 23, 1012.

254 Ito, H. (2003) Chemical amplification resists: inception, implementation in device manufacture, and new developments. *J. Polym. Sci.: Part A, Polym. Chem.*, 41, 3863.

255 Madou, M. (1997) *Fundamentals of Microfabrication*, CRC Press, Boca Raton, FL, USA.

256 (a) Li, W., Varanasi, P.R., Lawson, M.C., Kwong, R.W., Chen, K.J., Ito, H., Truong, H., Allen, R.D., Yamamoto, M., Kobayashi, E., and Slezak, M. (2003) Rational design in cyclic olefin resists for sub-100 nm lithography. *Proc. SPIE*, 5039, 61; (b) Jung, J.-C., Jung, M.-H., Lee, G., and Baik, H.-H. (2001) Amine gradient process for DUV lithography. *Polymer*, 42, 161; (c) Kim, H. W., Choi, S.J., Woo, S.G., and Moon, J.T. (2000) A new platform for ArF lithography. *Photopolym. Sci. Technol.*, 13, 419.

257 Fukuhara, T., Shibasaki, Y., Ando, S., Kishimura, S., Endo, M., Sasago, M., and Ueda, M. (2005) Synthesis of Poly[*N*-(1-adamantyl)vinylsulfonamide-*co*-2-(2-methyl)adamantyl methacrylate] for 193nm lithography. *Macromolecules*, 38, 3041.

258 Bates, A.K., Rothschild, M., Bloomstein, T. M., Fedynyshyn, T.H., Kunz, R.R., Liberman, V., and Switkes, M. (2001) Review of technology for 157nm lithography. *IBM J. Res. & Dev.*, 45, 605.

259 Kodama, S., Kaneko, T., Takebe, Y., Okada, S., Kawaguchi, Y., Shida, N., Ishikawa, S., Toriumi, M., and Itani, T. (2002) Synthesis of novel fluoropolymers for 157nm photoresists by cyclo-polymerization. *Proc. SPIE*, 4690, 76.

260 Yamazaki, T., Furukawa, T., Itani, T., Ishikawa, T., Koh, M., Araki, T., Toriumi, M., Kodani, T., Aoyama, H., and Yamashita, T. (2003) Development and characterization of new 157nm photoresists based on advanced fluorinated polymers. *Proc. SPIE*, 5039, 103.

261 Ito, H., Wallraff, G.M., Brock, P., Fender, N., Truong, H., Brayta, G., Miller, D.C., Sherwood, M.H., and Allen, R.D. (2001) Polymer design for 157nm chemically amplified resists. *Proc. SPIE*, 4345, 273.

262 Hohle, C., Sebald, M., and Zell, T. (2003) Ein Hauch von Elektronik: Entwicklungen in der Photolithographie und bei Photolacken für Halbleiterchips. *Metalloberfläche*, 57, 45.

263 Houlihan, F., Sakamuri, R., Romano, A., Rentkiewicz, D., Dammel, R.R., Conley, W., Miller, D., Sebald, M., Stepanenko, N., Markert, K., Mierau, U., Vermeir, I., Hohle, C., Itani, T., Shigematsu, M., and Kawaguchi, E. (2004) Recent advances in

Lam Research Ex. 1047 - Page 228
Lam Research Corp. v. Inpria Corp.
IPR2024-00033 - U.S. Patent No. 9,823,564

fluorinated resists for application at 157 nm. *Proc. SPIE*, 5376, 134.

264 (a) Fedynshyn, T.H., Kunz, R.R., Sinta, R. F., Sworin, M., Mowers, W.A., Goodman, R.B., and Doran, S.P. (2001) High resolution fluorocarbon based resists for 157 nm lithography. *Proc. SPIE*, 4345, 296; (b) Fedynshyn, T.H., Mowers, W.A., Kunz, R.R., Sinta, R.F., Sworin, M., Cabral, A. and Curtin, J. (2004) Fluorocarbon-Polymer-Based Photoresists for 157 nm Lithography, in *Polymers for Microelectronics and Nanoelectronics* (eds Q. Lin, R.A. Pearson, and J.C. Hedrick), ACS Symposium Series 874, American Chemical Society, Washington, DC, Ch. 5.

265 Schwoerer, M. and Wolf, H.C. (2005) Elektrolumineszenz und Photovoltaik, in *Organische Molekulare Festkörper* (eds M. Schwoerer and H.C. Wolf), Wiley-VCH, Weinheim, Ch. 11.

266 (a) Assender, H. and Barkhouse, A. (2010) Photovoltaic polymer materials, in *Photochemistry and Photophysics of Polymeric Materials* (ed. N.S. Allen), John Wiley, Hoboken, NJ, USA, Ch. 8; (b) Sariciftci, N.S. (2004) Plastic photovoltaic devices. *Mater. Today*, 7, 36; (c) Brabec, C. J., Dyakonov, V., Parisi, J., and Sariciftci, N. S. (eds) (2003) *Organic Photovoltaics, Concept and Realization*, Springer, Berlin.

267 (a) Nelson, J. (2003) Organic and Plastic Solar Cells, in *Practical Handbook of Photovoltaics: Fundamentals and Applications* (eds T. Markvart and L. Catañer), Elsevier, Oxford, Ch. IIe-2; (b) Nelson, J. (2011) Polymer fullerene bulk heterojunction solar cells. *Mater. Today*, 14 (10), 462–470.

268 Halls, J.J.M. and Friend, R.H. (2001) Organic photovoltaic devices, in *Clean Electricity from Photovoltaics* (eds M.D. Archer and R. Hill), Imperial College Press, London, p. 377.

269 Nierengarten, J.-F., Hadziioannou, G., and Armaroli, N. (2001) Molecular photovoltaic devices. *Mater. Today*, 4, 16.

270 (a) Brabec, C.J. (2004) Organic photovoltaics: technology and markets. *Solar Energy Mater. Solar Cells*, 83, 273; (b) Brabec, C.J. and Sariciftci, N.S. (2000) Polymeric photovoltaic devices. *Mater. Today*, 3, 5.

271 Dhanabalan, A., vanDuren, J.K.J., vanHal, P.A., vanDongen, J.L.J., and Jannssen, R.A. J. (2001) A low bandgap semiconducting polymer for photovoltaic devices and infrared emitting diodes. *Adv. Funct. Mater.*, 11, 255.

272 Shaheen, S.E., Vangeneugden, D., Kiebooms, R., Vanderzande, D., Fromherz, T., Padinger, F., Brabec, C.J., and Sariciftci, N.S. (2001) Low band-gap polymeric photovoltaic devices. *Synth. Met.*, 121, 1583.

273 Archer, M.D. and Hill, R. (eds) (2001) *Clean Electricity from Photovoltaics*, Imperial College Press, London.

274 Messenger, R. and Ventre, G. (1999) *Photovoltaic Systems Engineering*, CRC Press, Boca Raton, FL, USA.

275 Perlin, J. (1999) *From Space to Earth: The Story of Solar Electricity*, Aatec Publications, Ann Arbor, MI, USA.

276 Bube, R.H. (1998) *Photovoltaic Materials*, Imperial College Press, London.

277 Lewerenz, H.-J. and Jungblut, H. (1995) *Photovoltaik*, Springer, Berlin.

278 Green, M.A. (1995) *Silicon Solar Cells: Advanced Principles and Practice, Centre for Photovoltaic Devices and Systems*, University of New South Wales, Sydney.

279 Wenham, S.R., Green, M.A., and Watt, M. E. (1995) *Applied Photovoltaics, Centre for Photovoltaic Devices and Systems*, University of New South Wales, Sydney.

280 Partain, L.D. (ed.) (1995) *Solar Cells and Their Applications*, Wiley-Interscience, New York.

281 Markvart, T. (ed.) (1994) *Solar Electricity*, Wiley, Chichester.

282 Halls, J.J.M., Walsh, C.A., Greenham, N. C., Marseglia, E.A., Friend, R.H., Moratti, S.C., and Holmes, A.B. (1995) Efficient photodiodes from interpenetrating networks. *Nature*, 376, 498.

283 Yu, G., Gao, J., Hummelen, J.C., Wudl, F., and Heeger, A.J. (1995) Polymeric photovoltaic cells: enhanced efficiencies via a network of internal donor-acceptor heterojunctions. *Science*, 270, 1789.

284 Hoppe, H. and Sariciftci, N.S. (2006) Morphology of polymer/fullerene bulk heterojunction solar cells. *J. Mater. Chem.*, 16, 45.

285 Li, G., Shrotriya, V., Huang, J., Yao, Y., Moriarty, T., Emery, K., and Yang, Y. (2005)

Lam Research Ex. 1047 - Page 229
Lam Research Corp. v. Inpria Corp.
IPR2024-00033 - U.S. Patent No. 9,823,564

High efficiency solution processable polymer photovoltaic cells by self-organization of polymer blends. *Nature Mater*, 4, 864.

286 Shaheen, S.E., Brabec, C.J., Sariciftci, N.S., Padinger, F., Fromherz, T., and Hummelen, J.C. (2001) 2.5% efficient organic plastic solar cells. *Appl. Phys. Lett.*, 78, 841.

287 Armaroli, N., Barigeletti, E., Ceroni, P., Eckert, J.-F., Nicoud, J.-F., and Nierengarten, J.-F. (2000) Photoinduced energy transfer in a fullerene–oligophenylenevinylene conjugate. *Chem. Commun.*, 599.

288 Eckert, J.-F., Nicoud, J.F., Nierengarten, J.-F., Liu, S.-G., Echegoyen, L., Barigelletti, F., Armaroli, N., Ouali, L., Krasnikov, V., and Hadziioannou, G. (2000) Fullerene–oligophenylenevinylene hybrids: synthesis, electronic properties, and incorporation in photovoltaic devices. *J. Am. Chem. Soc.*, 122, 7467.

289 Nierengarten, J.-F., Eckert, J.-F., Nicoud, J. F., Ouali, L., Krasnikov, V., and Hadziioannou, G. (1999) Synthesis of a C_{60}-Oligophenylenevinylene hybrid and its incorporation in a photovoltaic device. *Chem. Commun.*, 617.

290 (a) Brabec, C.J. and Dyakonov, V. (2003) Photoinduced charge transfer in bulk heterojunction composites, in *Organic Photovoltaics, Concept and Realization* (eds C.J. Brabec, V. Dyakonov, J. Parisi, and N. S. Sariciftci), Springer, Berlin; (b) Dennler, G., Scharber, M.C., and Brabec, C.J. (2009) Polymer-fullerene bulk-heterojunction solar cells. *Adv. Mater.*, 21, 1323.

291 Burroughes, J.H., Bradley, D.D.C., Brown, A.R., Marks, R.N., Mackay, K., Friend, R. H., Burns, P.L., and Holmes, A.B. (1990) Light-emitting diodes based on conjugated polymers. *Nature*, 347, 539.

292 Greenham, N.C. and Friend, R.H. (2004) Light-emitting diodes based on Poly(p-phenylene vinylene) and its derivatives, in *Organic Light-Emitting Devices, A Survey* (ed. J. Shinar), Springer, New York, Ch. 5.

293 Shim, H-.K. and Jin, J.-I. (2002) Light-emitting characteristics of conjugated polymers, in *Polymers for Photonics Applications I, Advances in Polymer Science 158* (ed. K.-S. Lee), Springer, Berlin, p. 193.

294 Bernius, T., Inbasekaran, M., O'Brien, J., and Wu, W.-S. (2000) Progress with light-emitting polymers. *Adv. Mater.*, 12, 1737.

295 Friend, R.H., Gymer, R.W., Holmes, A.B., Burroughes, J.H., Marks, R.N., Taliani, C., Bradley, D.D.C., dosSantos, D.A., Bredas, J.L., Lögdlund, M., and Salaneck, W.R. (1999) Electroluminescence in conjugated polymers. *Nature*, 397, 121.

296 (a) Forget, S., Chenais, S., and Siove, A. (2010) Organic light-emitting diodes, in *Photochemistry and Photophysics of Polymeric Materials* (ed. N.S. Allen), John Wiley, Hoboken, NJ, USA, Ch. 9; (b) Akcelrud, L. (2003) Electroluminescent polymers. *Prog. Polym. Sci.*, 28, 875.

297 Mullen, K. and Scherf, U. (eds) (2006) *Organic Light-Emitting Devices: Synthesis, Properties and Applications*, Wiley, New York.

298 Graupner, W. (2002) Science and technology of organic light-emitting diodes. *The Spectrum*, 15, 20.

299 Ruhstaller, B., Carter, S.A., Barth, S., Riel, H., Riess, W., and Scott, J.C. (2001) Transient and steady-state behavior of space charges in multilayer organic light-emitting diodes. *J. Appl. Phys.*, 89, 4575.

300 Kim, D.Y., Cho, H.N., and Kim, C.Y. (2000) Blue light emitting polymers. *Prog. Polym. Sci.*, 25, 1089.

301 Greiner, A. (1998) Design and synthesis of polymers for light-emitting diodes. *Polym. Adv. Technol.*, 9, 371.

302 Sheats, J.R., Chang, Y.L., Roitman, D.B., and Socking, A. (1999) Chemical aspects of polymeric electroluminescent devices. *Acc. Chem. Res.*, 32, 193.

303 Rothberg, L.J. and Lovinger, A.J. (1996) Status and prospects for organic electroluminescence. *J. Mater. Res.*, 11, 3174.

304 Kraft, A., Grimsdale, A., and Holmes, A.B. (1998) Electroluminescent conjugated polymers – seeing polymers in a new light. *Angew. Chem. Int. Ed.*, 37, 402.

305 Bolognesi, A., Botta, C., Facchinetti, D., Jandke, M., Kreger, K., Strohriegl, P., Relini, A., Rolandi, R., and Blumstengel, S. (2001) Polarized electroluminescence in double-layer light-emitting diodes with perpendicularly oriented polymers. *Adv. Mater.*, 13, 1072.

Lam Research Ex. 1047 - Page 230
Lam Research Corp. v. Inpria Corp.
IPR2024-00033 - U.S. Patent No. 9,823,564

306 Miyata, S. and Nalwa, H.S. (eds) (1997) *Organic Electroluminescent Materials and Devices*, Gordon & Breach, Amsterdam.

307 OLED Cross Reference by Material Function. H.W. Sands Corp. Available at: http://www.hwsands.com/Chemicals.aspx.

308 Gao, M., Richter, B., and Kirstein, S. (1997) White-light electroluminescence from self-assembled Q-CdSe/PPV multilayer structures. *Adv. Mater.*, 9, 802.

309 Hariharan, P. (1996) *Optical Holography, Principles, Techniques, and Applications*, Cambridge University Press, Cambridge.

310 Hariharan, P. (2002) *Basics of Holography*, Cambridge University Press, Cambridge.

311 Lipson, A., Lipson, S.G., and Lipson, H. (2011) *Optical Physics*, Cambridge University Press, Cambridge.

312 Toal, V. (2012) *Introduction to Holography*, CRC Press, Boca Raton, FL, USA.

313 Reich, S. (1977) Photodielectric polymers for holography. *Angew. Chem. Int. Ed.*, 16, 441.

314 Ingwall, R.T. and Waldmann, D. (2000) Photopolymer systems, in *Holografic Data Storage* (eds H.J. Coufal, D. Psaltis, and G. T. Singerbox), Springer, Berlin, p. 171.

315 Dhar, I., Schnoes, M.G., Katz, H.E., Hale, A., Schilling, M.T., and Harris, A.L. (2000) Photopolymers for digital holographic data storage, in *Holografic Data Storage* (eds H. J. Coufal, D. Psaltis, and G.T. Singerbox), Springer, Berlin, p. 199.

316 (a) Sponsler, M.B. (2000) Photochemical and photophysical processes in the design of holographic recording materials. *The Spectrum*, 13, 7; (b) Ramamurthy, V. and Schanze, K.S. (eds) (2001) Hologram Switching and Erasing Strategies with Liquid Crystals, in *Optical Sensors and Switches*, Marcel Dekker, New York, p. 363.

317 Lougnot, D.J. (1993) Photopolymers and Holography, in *Radiation Curing in Polymer Science and Technology* (eds J.P. Fouassier and J.F. Rabek), Elsevier Applied Science, London, vol. III, Ch. 3.

318 Lougnot, D.J. (1996) Self-processing photopolymer materials for holographic recording. *Crit. Rev. Opt. Sci. Technol. CR*, 63, 190.

319 Schilling, M.L., Colvin, V.L., Dhar, I., Harris, A.L., Schilling, F.C., Katz, H.E., Wysocki, T., Hale, A.L., Blyer, L.L., and Boyd, C. (1999) Acrylate oligomer-based photopolymers for optical storage applications. *Chem. Mater.*, 11, 247.

320 Natarajan, L.V., Sutherland, R.L., Tondiglia, V., Bunning, T.J., and Adams, W. W. (1999) Photopolymer materials, development of holographic gratings, in *Concise Polymeric Materials Encyclopedia* (ed. J.C. Salamone), CRC Press, Boca Raton, Florida, USA, p. 1052.

321 Lucchetti, L. and Simoni, F. (2000) Soft materials for optical data storage. *Rivista del Nuovo Cimento*, 23, 1.

322 Anscombe, N. (2003) Holographic data storage: When will it happen? *Photonics Spectra*, June, 54.

323 Imlau, M., Bieringer, T., Odoulov, S.G., and Woike, T. (2005) Holographic data storage, in *Nanoelectronics and Information Technology* (ed. R. Waser), Wiley-VCH, Weinheim, p. 657.

324 Stevenson, S.H., Armstrong, M.L., O'Connor, P.J., and Tipton, D.F. (1994) Advances in photopolymer films for display holography. *Proc. SPIE*, 2333, 60.

325 Colvin, V.L., Larson, R.G., Harris, A.L., and Schilling, M.L. (1997) Quantitative model of volume hologram formation in photopolymers. *J. Appl. Phys.*, 81, 5913.

326 (a) Waldman, D.A., Ingwall, R.T., Dal, P.K., Horner, M.G., Kolb, E.S., Li, H.-Y.S., Minns, R.A., and Schild, H.G. (1996) Cationic ring-opening photopolymerization methods for volume hologram recording. *Proc. SPIE*, 2689, 127; (b) (1998) Holographic Medium and Process for Use Thereof. US Patent 5,759,721.

327 Strehmel, V. (2003) Epoxies: structures, photoinduced crosslinking, network properties and applications, in *Handbook of Photochemistry and Photobiology*, vol. 2 (ed. H.S. Nalwa), American Scientific Publ., Stevenson Ranch, CA, USA, p. 102.

328 Carlson, C.F. (1942) Electrophotography. US Patent 2,297,691.

329 Borsenberger, P.M. and Weiss, D.S. (1998) *Organic Photoreceptors for Xerography*, Dekker, New York.

330 Borsenberger, P.M. and Weiss, D.S. (1993) *Organic Photoreceptors for Imaging Systems*, Dekker, New York.

Lam Research Ex. 1047 - Page 231
Lam Research Corp. v. Inpria Corp.
IPR2024-00033 - U.S. Patent No. 9,823,564

331 Williams, E.M. (1984) *The Physics and Technology of Xerographic Processes*, Wiley, New York.

332 Umeda, M. and Yokoyama, M. (1997) Carrier photogeneration processes in layered organic systems incorporating bisazo pigment: xerographic and electroabsorption study. *J. Appl. Phys.*, 81, 6179.

333 Peters, K. (2011) Polymer optical fiber sensors – a review. *Smart Mater. Struct.*, 20, 1.

334 Ziemann, O., Krauser, J., Zamzow, P.E., and Daum, W. (2008) *POF Handbook – Optical Short Range Transmission Systems*, 2nd edn, Springer.

335 Möllers, I., Jäger, D., Gaudino, R., Nocivelli, A., Kragl, H., Ziemann, O., Weber, N., Koonen, T., Lezzi, C., Bluschke, A., and Randel, S. (2009) Plastic optical fiber technology for reliable home networking – overview and results of the EU project POF-ALL. *IEEE Communications Magazine, Optical Commun. Series*, 47, 58.

336 Randel, S. and Bunge, C. (2011) Spectrally efficient polymer optical fiber transmission. *Proc. SPIE*, 7960.

337 Zanger, H. (1991) *Fiber Optics Communication and Other Applications*, McMillan, New York.

338 Nalwa, H.S. (ed.) (2004) *Polymer Optical Fibers*, American Scientific Publishers, Stevenson Ranch, CA, USA.

339 Daum, W., Krauser, J., Zamzow, P.E., and Ziemann, O. (2002) *POF – Polymer Optical Fibers for Data Communication*, Springer, Berlin.

340 Horie, K., Ushiki, H., and Winnik, F.M. (2000) *Molecular Photonics, Fundamentals and Practical Aspects*, Kodansha-Wiley-VCH, Weinheim.

341 Weinert, A. (1999) *Plastic Optical Fibers, Principles, Components, Installation*, MCD Verlag, Erlangen.

342 Hecht, J. (1999) *City of Light, The Story of Fiber Optics*, Oxford University Press, New York.

343 Kaino, T. (1992) *Polymers for Light Wave and Integrated Optics* (ed. L.A. Hornak), Dekker, New York.

344 Kitazawa, M. (1993) *POF Data Book*, MCR Techno Research, Tokyo.

345 deGraaf, M.A. (2002) *Transmissive and Emissive Polymer Waveguides for Communication and Illumination*, University Press Facilities, Eindhoven, The Netherlands.

346 Khoe, G.-D., van denBoom, H., and Monroy, I.T. (2004) High Capacity Transmission Systems, in *Polymer Optical Fibers* (ed. H.S. Nalwa), American Scientific Publishers, Stevenson Ranch, CA, USA, Ch. 6.

Lam Research Ex. 1047 - Page 232
Lam Research Corp. v. Inpria Corp.
IPR2024-00033 - U.S. Patent No. 9,823,564

Part II
Ionizing Radiation

Polymers and Electromagnetic Radiation: Fundamentals and Practical Applications, First Edition. Wolfram Schnabel
© 2014 Wiley-VCH Verlag GmbH & Co. KGaA. Published 2014 by Wiley-VCH Verlag GmbH & Co. KGaA.

Lam Research Ex. 1047 - Page 233
Lam Research Corp. v. Inpria Corp.
IPR2024-00033 - U.S. Patent No. 9,823,564

4
Elementary Processes of the Interaction of High-Energy Photons with Matter

4.1
General Aspects

The energy range of photons related to ionizing radiation extends over several orders of magnitude, and is commonly divided into energy regions, as shown in Table 4.1.

The interaction of high-energy photons with matter includes absorption and scattering processes. It occurs in this energy range nonspecifically – that is, there are no *chromophores* for X- and γ-rays, and is related to interactions of photons with both atomic nuclei and the electron clouds surrounding them. The elementary processes involved in the attenuation of high-energy photons include the photoelectric effect, Compton scattering, the production of electron–positron pairs (Figure 4.1) and, at very high photon energy, photonuclear absorption.

Details concerning the elementary processes are given below in Sections 4.3–4.6. Prior to that, it will be shown in Section 4.2 how the interaction of high energy photons with matter is described quantitatively in terms of attenuation coefficients.

Chemical reactions are induced by high-energy photons in polymers due to the fact that, during the absorption process, electronically excited states are formed and, moreover, radical cations and fast electrons are generated, when the photon energy exceeds the ionization energy of atoms and molecules. Radical cations are positively charged molecules possessing an unpaired electron ($M^{+\bullet}$). They are unstable and are converted to stable species by chemical reactions with surrounding molecules and other unstable products. Electrons formed during the primary ionization act lose their kinetic energy by collisions with neighboring molecules, thus generating electronically excited molecules, namely radical cations and secondary electrons. In conclusion, organic materials – including polymers – undergo chemical alterations upon the absorption of high-energy photons.

Polymers and Electromagnetic Radiation: Fundamentals and Practical Applications, First Edition. Wolfram Schnabel
© 2014 Wiley-VCH Verlag GmbH & Co. KGaA. Published 2014 by Wiley-VCH Verlag GmbH & Co. KGaA.

Lam Research Ex. 1047 - Page 234
Lam Research Corp. v. Inpria Corp.
IPR2024-00033 - U.S. Patent No. 9,823,564

Table 4.1 Denotations for high-energy photon radiations.

Photon energy range (eV)	Denotation
10 eV to 1 keV	Extreme UV radiation and ultrasoft X-rays
1 keV to 10 keV	Soft X-rays
10 keV to 100 keV	Hard X-rays
≈100 keV	Ultrahard X-rays
≫100 keV	γ-rays

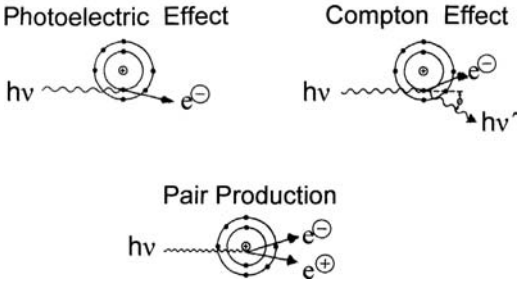


Figure 4.1 Schematic representation of elementary processes occurring during the interaction of high-energy photons with matter.

4.2 Attenuation Coefficients

The attenuation of a beam of high-energy photons traversing matter can be described by a Lambert–Beer-type law according to Equation 4.1:

$$I = I_0\, e^{-\mu L} = I_0\, e^{-\mu_m \xi} \tag{4.1}$$

where I_0 and I are the intensities of the original and attenuated beams, respectively, μ is the *attenuation coefficient*, $\mu_m = \mu/\rho$ is the *mass attenuation coefficient*, ρ is the density, L is the thickness of the absorbing layer, and $\xi = \rho L$. The interaction of high-energy photons with matter can also be described quantitatively by using the *atomic cross-section*, σ. The relationship between the mass attenuation coefficient and atomic cross-section is given by Equation 4.2:

$$\frac{\mu}{\rho}\left(\frac{m^2}{kg}\right) = \sigma\left(\frac{barns}{atom}\right)\frac{N_A}{A} \tag{4.2}$$

where N_A is the Avogadro constant ($6.022 \times 10^{23}\,mol^{-1}$), and A is the atomic weight, $1\ barn = 10^{-28}\,m^2$.

Not all photons involved in the attenuation process lose their energy in the irradiated system. In the case of coherent (Rayleigh) scattering, photons are scattered without a change in photon energy, whereas in the case of incoherent (Compton) scattering, part of the incident photon energy ($h\nu$) is released with the

Lam Research Ex. 1047 - Page 235
Lam Research Corp. v. Inpria Corp.
IPR2024-00033 - U.S. Patent No. 9,823,564

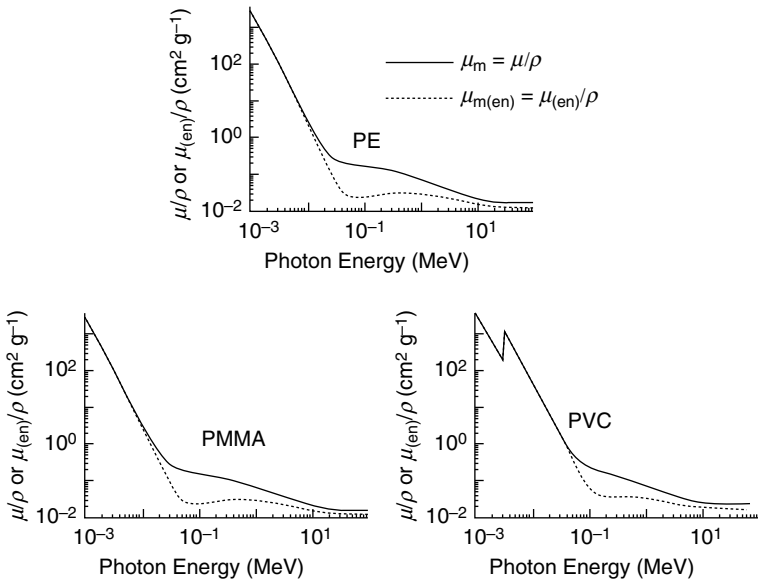


Figure 4.2 Mass attenuation coefficients, $\mu_m = \mu\,\rho^{-1}$, and mass energy attenuation coefficients $\mu_{m(en)} = \mu_{(en)}\,\rho^{-1}$ as a function of photon energy for polyethylene (PE), poly(methyl methacrylate) (PMMA), and poly(vinyl chloride) (PVC). Adapted with permission from Ref. [1]; © 1996, National Institute of Standards and Technology, MD, USA.

outgoing photon ($h\nu'$). In the case of pair formation, gamma radiation (photon energy $= 2\,m_0c^2$) generated during electron–positron annihilation is emitted. Since the yield of radiation-induced chemical alterations in an irradiated system is related to the energy absorbed by the system (absorbed dose), it is appropriate to operate with attenuation coefficients related to the absorbed energy, namely the energy attenuation coefficient $\mu_{(en)}$ and the mass energy attenuation coefficient $\mu_{m(en)} = \mu_{(en)}/\rho$. Figure 4.2 presents μ_m and $\mu_{m(en)}$ as a function of photon energy for three polymers. Attenuation coefficients of various polymers have been tabulated as a function of photon energy covering the range from 1 keV to 20 MeV by J. H. Hubbel and S. M. Seltzer [1]. Mass attenuation coefficients covering the energy range from 50 to 30 000 eV have been compiled by B. L. Henke [2].

The total atomic cross-section σ_{total} can be expressed as the sum of the cross-sections of the different elementary processes – that is, the photoelectric effect (τ), coherent (Rayleigh) scattering (σ_{coh}), incoherent (Compton scattering) (σ_{incoh}), photonuclear absorption $\sigma_{PH,N}$ and pair production, which is to be distinguished in nuclear-field pair production (κ_n) and electron-field pair production (κ_e) (see Equation 4.3).

$$\sigma_{total} = \tau + \sigma_{coh} + \sigma_{incoh} + \sigma_{PH,N} + \kappa_n + \kappa_e \tag{4.3}$$

Tables of total atomic cross-sections and mass attenuation coefficients of elements of atomic number (proton number) $Z = 1$ to 100, covering the photon energy range from 1 MeV to 100 GeV are presented in Ref. [3].

Lam Research Ex. 1047 - Page 236
Lam Research Corp. v. Inpria Corp.
IPR2024-00033 - U.S. Patent No. 9,823,564

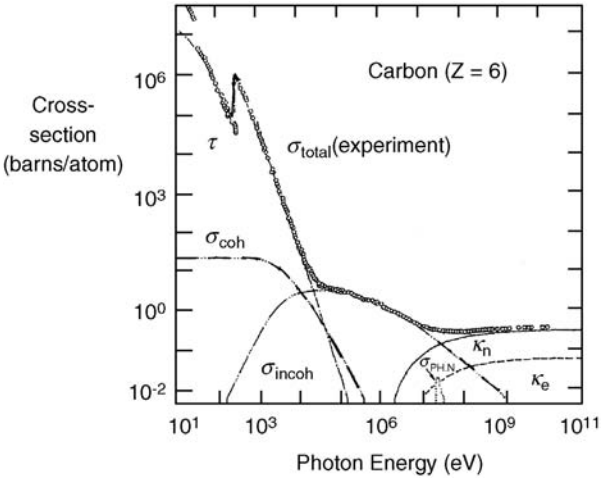


Figure 4.3 Partial calculated (lines) and total measured (circles) cross-sections of carbon (C) as a function of photon energy. Adapted with permission from Ref. [1]; © 1996, National Institute of Standards and Technology, MD, USA.

The attenuation of high-energy photons by matter depends on the one hand on the penetrating photon's energy, hν, and on the other hand on the properties of the penetrated material, namely the electron density $n_{e,c}$ (number of electrons per cm^3) and the atomic number Z. The energy dependence of σ_{total} for the element carbon (Z = 6) is illustrated in Figure 4.3. Other elements that constitute organic polymers exhibit a similar behavior. Note the large cross-section at low photon energies, which implies a very high absorption of extreme ultraviolet (*EUV*) radiation (hν of about 100 eV), which has recently been applied to the lithographic generation of microstructures.

At low photon energy, the attenuation is almost exclusively due to the photoelectric effect. At photon energies exceeding about 1 keV, the attenuation is dominated by Compton scattering, whilst at energies higher than 100 MeV pair production dominates the attenuation.

The dependence of the single cross-sections on photon energy E_{photon}, atomic number Z and electron density $n_{e,c}$ (number of electrons per unit volume) will not be discussed here in detail. Literature covering these aspects can be found in a review by Hubbell *et al.* [3]. Note, that τ is proportional to Z^5 and $E_{photon}^{-3.5}$, σ_{incoh} is proportional to $n_{e,c}$ and independent of Z, and κ_n, the cross-section for nuclear-field pair production, is approximately proportional to the square of the target nuclear charge ($\kappa_n \sim Z^2$). Finally, κ_e, the cross-section for triplet production, is proportional to Z ($\kappa_e \sim Z$) [4].

4.3 Photoelectric Effect

As noted above, the attenuation at low photon energy is largely dominated by the *photoelectric effect*, which is characterized by the fact that the incident photon is

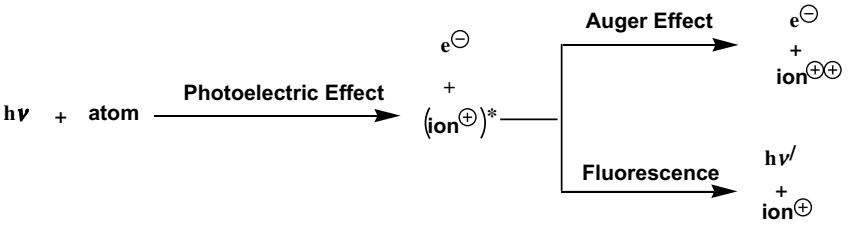
Lam Research Ex. 1047 - Page 237
Lam Research Corp. v. Inpria Corp.
IPR2024-00033 - U.S. Patent No. 9,823,564

completely consumed (absorbed) during the attenuation act. Part of the photon energy ($E_{binding}$) is used to eject an electron, and the rest is carried by its kinetic energy $E_{kinetic}$. The energy balance is given by Equation 4.4:

$$E_{binding} = E_{photon} - (E_{kinetic} + \phi) \tag{4.4}$$

where E_{photon} is the energy of the incident photon and φ is the work-function of the instrument used to measure electron emission.

Electrons may be ejected from the various shells of the atom. Low-energy photons interact with the outer electrons but, as the photon energy is increased, the interaction involves also the more tightly bound electrons, including those located close to the core (core electrons). When E_{photon} is greater than $E_{binding}$ of the innermost shell (K shell), all electrons of the atom can take part in the photoelectric effect. The process is most likely to occur with electrons of a given shell, when E_{photon} is just slightly greater than $E_{binding}$ of these electrons. As indicated in Scheme 4.1, there are two routes for the deactivation of the excited positive ion generated by electron emission, namely the *Auger effect* and *fluorescence*.



Scheme 4.1 Representation of the photoelectric effect and of two deactivation routes of excited ions.

In the case of the Auger effect, discovered by L. Meitner in 1922 [5], the hole left behind by an ejected core electron is filled rapidly by an outer shell electron. Thereby, the electron moving to the core level loses an amount of energy equal to the difference in orbital energies. This transition energy can be coupled to a second outer shell electron and thus induce the latter's emission from the atom, provided that the transition energy is greater than the orbital binding energy.

The fluorescence deactivation route is important in the case of elements having a relatively high atomic number Z. In the case of light elements ($Z < 15$), the probability of fluorescence is very low. Consequently, fluorescent deactivation plays a minor role in the case of organic polymers.

With regards to soft X-rays, absorption spectra presenting the dependence of the cross-section or the absorption coefficient on the photon energy are characterized by abrupt absorption edges (Figure 4.4) that are related to the binding energy of electrons in specific shells denoted by the uppercase letters K, L, M, N, and so on, with K assigned to the innermost shell. The binding energy of core electrons increases strongly with the atomic number Z (Table 4.2). This is why X-ray absorption spectra of compounds containing atoms of different atomic number are defined by absorption edges related to the binding energy of the respective core

Lam Research Ex. 1047 - Page 238
Lam Research Corp. v. Inpria Corp.
IPR2024-00033 - U.S. Patent No. 9,823,564

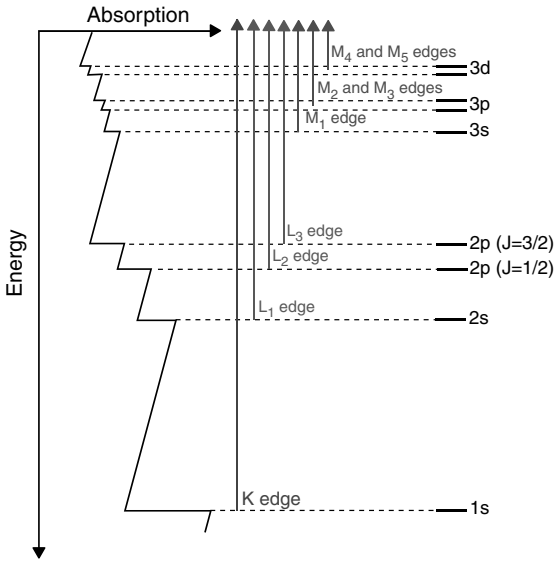


Figure 4.4 X-ray absorption spectra with corresponding electron transitions. Reproduced from Ref. [6].

Table 4.2 Binding energies of core electrons (1s).

Element	Atomic number Z	$E_{binding}$ (eV)
C	6	290
N	7	400
O	8	530
P	15	2150
S	16	2500

electrons. Therefore, the elemental composition of a sample can be readily accomplished from X-ray absorption spectra.

At present, X-ray spectroscopic methods, based on the photoelectric effect, are widely used in the polymer field (see Section 6.2). The importance of these methods relies on the fact that X-ray absorption spectra exhibit fine structures in an energy window of about 1000 eV above the absorption edge, as can be seen from Figure 4.5. Commonly, two spectral regions are distinguished: (1) the region up to about 30 eV past the absorption edge, denoted as the near-edge X-ray absorption fine structure (*NEXAFS*) region or the X-ray absorption near-edge structure (*XANES*) region; and (2) the region from 30 to about 1000 eV, denoted as the *EXAFS* (extended X-ray absorption fine structure) region.

In the case of molecules, the existence of these fine structures in the range up to 30 or 40 eV past the edge has been explained formerly in terms of multiple scattering resonances of low kinetic energy photoelectrons. More recently, however,

Lam Research Ex. 1047 - Page 239
Lam Research Corp. v. Inpria Corp.
IPR2024-00033 - U.S. Patent No. 9,823,564

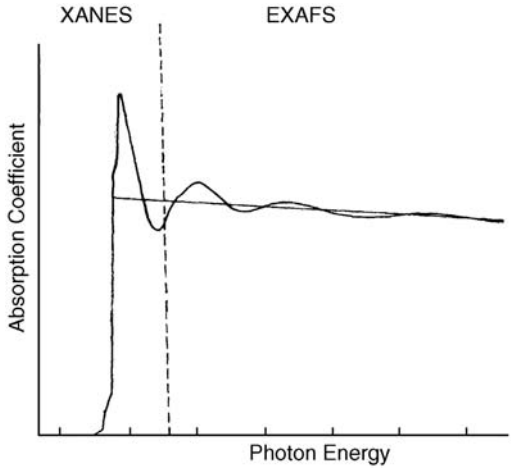


Figure 4.5 Schematic representation of fine structures observed with X-ray absorption spectra. XANES: X-ray absorption near-edge structure; EXAFS: extended X-ray absorption fine structure.

they have been considered to be related to excitations of electrons from core states to unoccupied valence and Rydberg states, and to vacuum states [7]. This is schematically demonstrated for a diatomic molecule in Figure 4.6.

Fine structures at higher energies – that is, in the EXAFS range – are of an oscillatory nature and are thought to be due to interference effects caused by the interaction of the outgoing photoelectron wave with the wave(s) backscattered from surrounding atoms (Figure 4.7). The interference depends on the distance between the absorbing atom and the backscattering atoms.

The advances in X-ray spectroscopy are related to the development of X-ray sources, and in this context, electron synchrotron sources play an important role. Notably, they provide a broad continuum of photon energies and generate radiation of high intensity and pronounced brightness also called *brilliance*. (The brightness

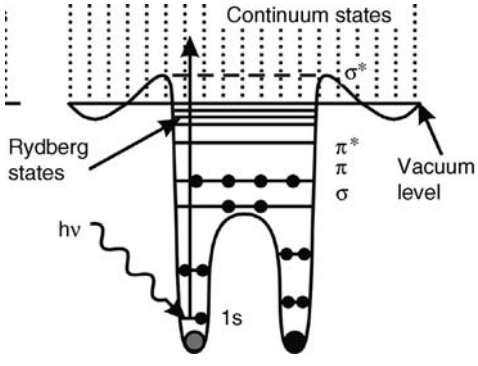


Figure 4.6 Schematic representation of core electron transitions in a diatomic molecule during the absorption of an X-ray photon. Adapted with permission from Ref. [8]; © 2013, Springer-Verlag.

Lam Research Ex. 1047 - Page 240
Lam Research Corp. v. Inpria Corp.
IPR2024-00033 - U.S. Patent No. 9,823,564

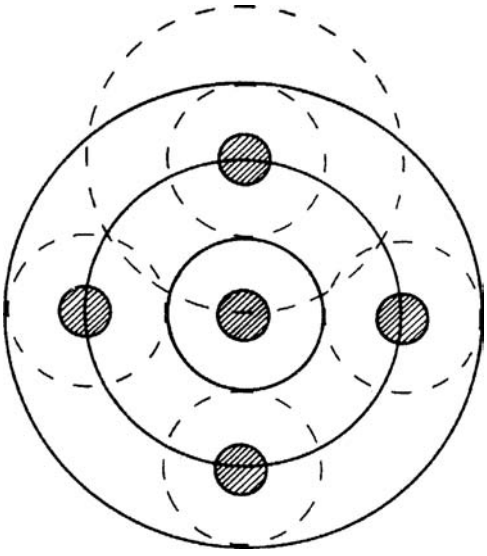


Figure 4.7 Schematic representation of the interaction of the original photoelectron wave (solid lines) with waves scattered by surrounding atoms (dashed lines). Adapted with permission from Ref. [7]; © 1988, Wiley.

of a radiation source is expressed in the dimensions: the number of photons per second per unit solid angle per unit source area per unit band width. A higher brightness can be achieved by increasing the number of photons and by reducing the solid angle of emission.)

4.4 Compton Scattering

Apart from the photoelectric effect, electrons can be emitted from atoms or molecules of the absorbing matter via another elementary process known as *Compton scattering*. The latter can be described as an elastic collision, in which some of the energy $h\nu$ and the momentum of the incident photon is transferred to an electron of the absorbing matter. Both, energy and momentum are conserved. After collision, the outgoing photon's energy is $h\nu'$ and the electron has acquired a kinetic energy E_{kin}. Thus, conservation of energy yields:

$$h\nu = h\nu' + E_{kin} \tag{4.5}$$

By considering conservation of momentum, it can be shown that the wavelength of the outgoing photon λ' is related to the wavelength of the incident photon λ by Equation 4.6:

$$\lambda' - \lambda = \left(\frac{h}{m_e c}\right)(1 - \cos\Theta) \tag{4.6}$$

Lam Research Ex. 1047 - Page 241
Lam Research Corp. v. Inpria Corp.
IPR2024-00033 - U.S. Patent No. 9,823,564

where h is Planck's constant, m_e is the resting mass of the electron, c is the speed of light, and Θ is the scattering angle.

The combination of factors $h/m_e c = 2.43 \times 10^{-12}$ m is known as the Compton wavelength. The collision causes the photon wavelength to increase by an amount between 0 (for a scattering angle of 0°) and twice the Compton wavelength (for a scattering angle of 180°).

4.5 Electron–Positron Pair Production

At photon energies exceeding twice the rest mass of an electron ($2m_e c^2 =$ 1.022 MeV), electron–positron pairs can be produced when photons interact in the vicinity of the nuclei with the Coulomb field of the nucleus. Pair production can also occur when a photon of energy in excess of $4m_e c^2$ (2.044 MeV) interacts with atomic electrons. In this case, the process is called *triplet production* due to the track of the recoiling atomic electron that appears in addition to the track of the created electron–positron pair.

4.6 Photonuclear Absorption

This effect refers to the absorption of a high-energy photon by a nucleus. The most likely result of such an interaction is the emission of a neutron, but the emission of charged particles or of several neutrons is also feasible [3]. The nuclear absorption of photons is characterized by *giant resonance*, that is, its occurrence is restricted to a relatively narrow range of photon energies in the MeV range. For carbon, the peak of the cross-section per target atom $\sigma_{PH.N}$ is centered at about 24 MeV (see Figure 4.3). This peak decreases in energy with increasing atomic number to about 12 MeV for the heaviest stable nuclei.

4.7 Absorption of Swift Electrons

There are two questions which arise on this topic: (1) What is the fate of the swift electrons that are generated during the absorption of high-energy photons? (2) How do high-energy electrons of an electron beam interact with matter?

Swift electrons generated during the absorption of high-energy photons lose energy by inelastic collisions with molecules, and the latter become ionized or electronically excited. Figure 4.8 shows that, within the absorbing matter, the energy is deposited in small packages that line-up to so-called *spurs* that are randomly distributed in the system.

Lam Research Ex. 1047 - Page 242
Lam Research Corp. v. Inpria Corp.
IPR2024-00033 - U.S. Patent No. 9,823,564

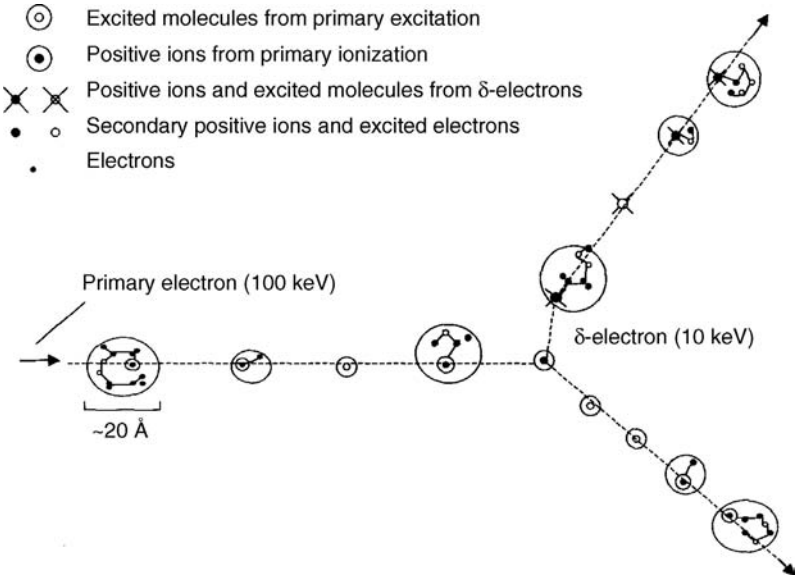


Figure 4.8 Schematic depiction of the energy deposition by a swift electron passing through absorbing matter. Adapted with permission from Ref. [9]; © 1969, Wiley-VCH.

The amount of energy deposited in the spurs varies. Energy-loss events have been classified more or less arbitrarily into three categories: small spurs (<100 eV, roughly corresponding to single-ionizations); large spurs or *blobs* (100–500 eV); and *short tracks* (500–5000 eV) [10]. In rare cases, the collision of the primary electron with a molecule generates *δ-electrons* which possess more than 10 keV and dig their own tracks – so-called *branched tracks*. The event abundance depends on the energy of the primary electron. From Table 4.3 it can be seen that, in the case of solid dry DNA, the fraction of small spurs increases up to about 50% with increasing primary electron energy, whereas the fraction of short tracks decreases [11].

The local deposition of high amounts of energy corresponds to high local concentrations of reactive intermediates, which might have consequences for chemical reactions if the modifications caused by different types of spurs are examined. Notable in this context is a hypothesis concerning linear polymers that

Table 4.3 Fraction of energy loss in solid dry DNA [11].

Energy of primary electron (eV)	Small spurs	Large spurs (blobs)	Short tracks
10^4	0.27	0.12	0.61
10^5	0.48	0.20	0.32
10^6	0.51	0.20	0.29

Lam Research Ex. 1047 - Page 243
Lam Research Corp. v. Inpria Corp.
IPR2024-00033 - U.S. Patent No. 9,823,564

postulates different chemical effects being associated with single-ionization or multi-ionization spurs. The latter are thought to be responsible for main-chain breaks, and the former for the induction of various other processes [12].

High-energy electrons of an electron beam impinging on matter can lose kinetic energy by interaction with the shell electrons, by Rutherford scattering in the Coulomb field of an atomic nucleus (Bremsstrahlung), and by collision with the nucleus. This can be described in terms of the linear energy transfer (energy loss per unit distance) according to Equation 4.7 with the following subscript denotations: I/E = ionization/excitation, R = electromagnetic radiation (bremsstrahlung), and C = collision.

$$-\frac{dE}{dx} = \left(-\frac{dE}{dx}\right)_C + \left(-\frac{dE}{dx}\right)_R + \left(-\frac{dE}{dx}\right)_{I/E} \tag{4.7}$$

As to high-energy electrons with energies of up to several MeV being absorbed by organic polymers that consist of low Z elements, the C and R terms can be neglected. This results from the following considerations.

C-term: Owing to the considerable difference in the masses involved, very little energy is transferred from the swift electron to the atomic nucleus. Only electrons of very high energy are capable of chemical change by direct displacement of the nucleus during collision acts.

I/E- and R-terms: Equations 4.8 and 4.9 show the dependence of the I/E- and R-term on electron energy E and atomic number Z.

$$\text{Ionization and excitation:} \quad \left(-\frac{dE}{dx}\right)_{I/E} \propto Z \ln\frac{E}{m_e} \tag{4.8}$$

$$\text{Bremstrahlung:} \quad \left(-\frac{dE}{dx}\right)_R \propto Z^2\frac{E}{m_e^2} \tag{4.9}$$

where m_e is the electron resting mass.

The ratio of energy loss by bremstrahlung to that by excitation and ionization is about $EZ/800$ (with E expressed in MeV) [13]. Thus, for polymer specimens in which Z rarely exceeds 8, the energy loss due to bremsstrahlung is about 2%, if $E = 2$ MeV. With respect to electron beam-induced alterations in polymeric specimens dealt with in this book, it follows that excitation and ionization acts are the dominating processes. Thus, a situation similar to that discussed above for the case of the absorption of high-energy electromagnetic radiation also applies here.

References

1 Hubbell, J.H. and Seltzer, S.M. (1996) Tables of X-Ray mass attenuation coefficients and mass energy-absorption coefficients. *NISTIR*, **5632**. Available at: http://www.nist.gov/pml/data/xraycoef/index.cfm.

2 Henke, B.L., Gullikson, E.M., and David, J.C. (1993) X-Ray interactions:

Lam Research Ex. 1047 - Page 244
Lam Research Corp. v. Inpria Corp.
IPR2024-00033 - U.S. Patent No. 9,823,564

photoabsorption, scattering, transmission and reflection at E=50-30000eV, Z=1–91. *Atomic Data Nucl. Data Tables*, **54**, 181.
3 Hubbell, J.H., Grimm, H.A., and Øverbø, I. (1980) Pair, triplet, and total atomic cross sections (and mass attenuation coefficients) for 1 MeV to 100 GeV photons in elements Z = 1 to 100. *J. Phys. Chem. Ref. Data*, **9**, 1023.
4 Hubbell, J.H. (2006) Electron positron pair production by photons: a historical overview. *Rad. Phys. Chem.*, **75**, 614.
5 Meitner, L. (1922) Über die Entstehung der beta-Strahl-Spektren radioaktiver Substanzen. *Z. Phys.*, **9**, 131.
6 Tenderholt, A. (2009) https://en.wikipedia.org/wiki/X-ray_absorption_spectroscopy. Last accessed 1 August 2013.
7 Bianconi, A. (1988) Xanes Spectroscopy, in *X-Ray Absorption, Principles, Applications, Techniques of EXAFS, SEXAFS and XANES* (eds D.C. Koningsberger and R. Prins), John Wiley, New York, Ch. 11.
8 Bracco, G. and Holst, B. (eds) (2013) *Surface Science Techniques,* Springer Series in Surface Science, vol. 51, Springer-Verlag, Berlin, pp. 277–306.
9 Henglein, A., Schnabel, W., and Wendenburg, J. (1969) *Einführung in die Strahlenchemie*, Verlag Chemie, Weinheim.
10 Mozumder, A. and Magee, J.L. (1966) Model of tracks of ionizing radiation for radical reaction mechanisms. *Radiat. Res.*, **28**, 203.
11 LaVerne, J.A. and Pimblott, S.M. (1995) Electron energy-loss distribution in solid dry DNA. *Radiat. Res.*, **141**, 208.
12 Zagorski, Z.P. (2002) Modification, degradation and stabilization of polymers in view of the classification of radiation spurs. *Rad. Phys. Chem.*, **63**, 9.
13 Charlesby, A. (1960) *Atomic Radiation and Polymers*, Pergamon Press, Oxford.

Lam Research Ex. 1047 - Page 245
Lam Research Corp. v. Inpria Corp.
IPR2024-00033 - U.S. Patent No. 9,823,564

5
Chemical Reactions Induced by High-Energy Radiation

5.1
General Aspects

X- and γ-rays, that is, electromagnetic radiation comprising photon energies in the keV and MeV range, generate unstable reactive species when absorbed by organic materials, including polymers. During the primary absorption processes radical cations ($M^{+\bullet}$) and free electrons are generated, and these species react rapidly with the surrounding molecules. The free electrons lose their relatively high initial kinetic energy by collisions with neighboring molecules, thus generating additional radical cations, free electrons, and electronically excited molecules. After thermalization, a large proportion of the ejected electrons is captured by parent radical ions. These neutralization reactions result in electronically (highly) excited molecules (M^{*}), which are likely to deactivate via bond breakage leading to free radicals ($M^{*} \rightarrow R_1^{\bullet} + R_2^{\bullet}$). Consequently, free radical reactions play a dominant role regarding radiation-induced transformations in organic materials, including polymers.

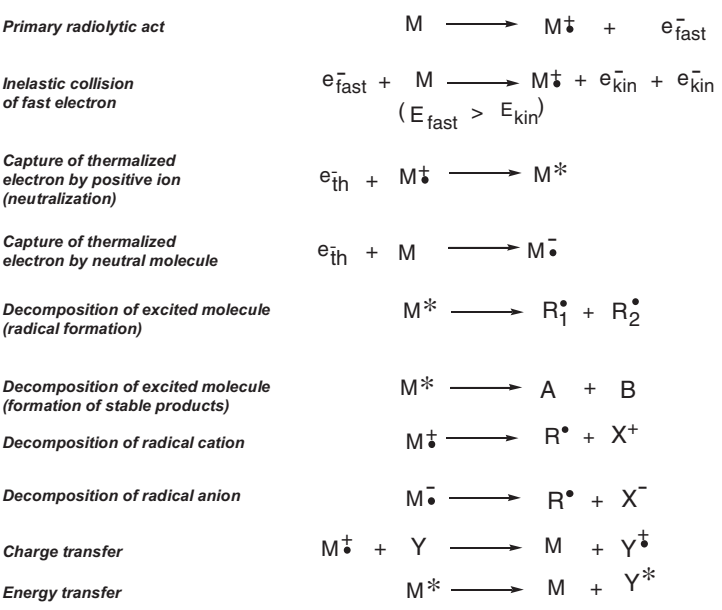
When thermalized free electrons collide with molecules of sufficiently high electron affinity, radical anions ($M^{-\bullet}$) can be formed, which decompose rapidly to form stable anions and free radicals ($R^{\bullet}$). This process is referred to as dissociative electron capture: $e^{-} + M \rightarrow M^{-\bullet} \rightarrow R^{\bullet} + X^{-}$.

Radical cations can decay via various routes. In the condensed phase they can interact, apart from being neutralized by thermal electrons, with neighboring intact molecules and undergo, for example, addition reactions or charge-transfer reactions. Moreover, they can decompose to form cations and free radicals ($R^{\bullet}$). The important primary processes that occur during the absorption of high-energy radiation by organic polymers are shown in Scheme 5.1.

In conclusion, X- and γ-rays are capable of inducing free-radical and ionic reactions, when absorbed by organic compounds; notably, a catalyst is not needed. Moreover, since the absorption of X- and γ-rays is independent of the ambient temperature, chemical reactions can be induced at any temperature. If penetrating radiation such as ^{60}Co-γ-radiation is employed, reactions can be initiated even in metal vessels.

Polymers and Electromagnetic Radiation: Fundamentals and Practical Applications, First Edition. Wolfram Schnabel
© 2014 Wiley-VCH Verlag GmbH & Co. KGaA. Published 2014 by Wiley-VCH Verlag GmbH & Co. KGaA.

Lam Research Ex. 1047 - Page 246
Lam Research Corp. v. Inpria Corp.
IPR2024-00033 - U.S. Patent No. 9,823,564



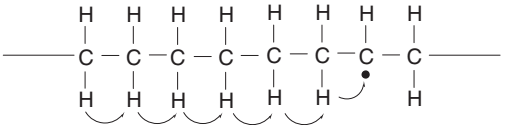
Scheme 5.1 Primary processes that take place during the absorption of high-energy photons by organic substances.

At this point, the analogy of chemical transformations induced by high-energy photons and fast electrons generated by accelerators should be addressed. Actually, apart from the primary radiolytic process, all processes presented in Scheme 5.1 also occur during the absorption of fast electrons impinged on organic matter by an electron beam (*EB*). Both, electron beams and X- and γ-rays induce the same chemical transformations in polymeric materials. Often, the use of EB radiation is advantageous because, in contrast to radioactive sources such as ^{60}Co and ^{137}Cs, accelerators can be switched on and off deliberately. In fact, among the processing techniques applied commercially for polymer modifications, electrically generated accelerated electrons are the preferred mode of radiation.

Notably, the absorption of high-energy radiation, comprising photon energies in the keV and MeV range, is nonspecific with respect to different atoms and groups of atoms except for their electron densities – that is, every chemical bond can potentially be cleaved. This contrasts with ultraviolet (UV) radiation, which is absorbed by specific chromophoric groups (chromophores). It follows, that all parts of molecules subjected to this form of high-energy radiation may be affected with regards to the primary absorption processes. However, in spite of the chemical and spatial randomness of energy absorption, chemical change may be quite non-random. In the case of linear polymers, a dominance of specific chemical reactions may be supported by transfer or migration processes along

Lam Research Ex. 1047 - Page 247
Lam Research Corp. v. Inpria Corp.
IPR2024-00033 - U.S. Patent No. 9,823,564

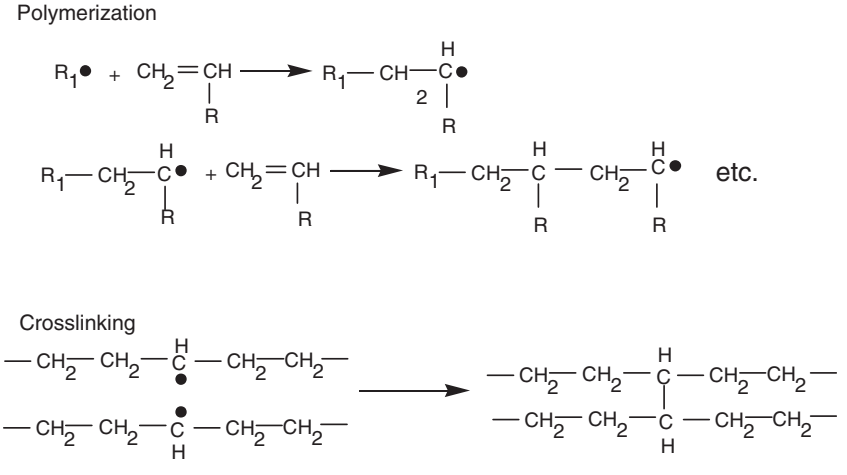
the polymer chain, in conjunction with trapping at specific sites according to various mechanisms should be considered. The transfer of excitation energy via a donor–acceptor mechanism ($D^* + A \rightarrow D + A^*$), as described in Chapter 3, is feasible provided that the polymer contains appropriate donating and accepting moieties. However, as this is only seldom the case, alternative mechanisms also apply. They include charge transfer via positive holes or electrons, and the transfer of free-radical sites via hydrogen atom transfer (Scheme 5.2).



Scheme 5.2 Radical migration via hydrogen atom transfer.

Evidence for free-radical migration derives from the fact that crosslinking in solid polyolefins (e.g., polyethylene) is inhibited by only small amounts of radical scavenger molecules that are, on average, located far away from the primary radical site.

The important role that free radicals are playing with regards to chemical reactions induced by high-energy radiation, and the potential of initiating free-radical reactions at any temperature, has already been noted above. Thus, high-energy-electromagnetic radiation, comprising photon energies in the keV and MeV range, is a convenient tool to initiate chemical reactions such as the polymerization of unsaturated monomers or the crosslinking of linear polymers (Scheme 5.3).



Scheme 5.3 Typical free-radical reactions that can be initiated by high-energy radiation.

Lam Research Ex. 1047 - Page 248
Lam Research Corp. v. Inpria Corp.
IPR2024-00033 - U.S. Patent No. 9,823,564

The initiation of free radical and ionic polymerization will be described in Section 5.2, while chemical transformations in neat linear synthetic polymers and biopolymers, and in polymers both in the solid state and in solution, will be treated in Sections 5.3, 5.4, and 5.5, respectively. The importance of high-energy radiation-induced processes for technical applications will be discussed in Section 5.6.

A radiation-chemical yield is commonly expressed as a *G-value*; this is the number of molecules or atoms or chemical bonds produced or decomposed per 100 eV of absorbed energy. For example, G(S) denotes the number of cleaved main-chain bonds in a linear polymer by the absorption of 100 eV. The unit of the absorbed dose is the *Gray* (Gy), which corresponds to the energy-absorption of 1 Joule (J) by 1 kg ($1\,Gy = 1\,J\,kg^{-1}$). Frequently, the absorbed dose is also given in units of $eV\,g^{-1}$.

5.1.1 Radiation Sources and Electron Accelerators

Radiation sources that are widely used in research studies and for industrial applications include the radioactive nuclei ^{60}Co and ^{137}Cs, which have half-lives of 5.26 and 30.2 years, respectively. During its decay, ^{60}Co emits two photons of 1.1 and 1.3 MeV, and ^{137}Cs emits 0.6 MeV photons.

X-rays are produced when a beam of fast electrons strikes an appropriate target; thereby, a continuous spectrum of bremsstrahlung is generated by interaction of the fast electrons with atomic nuclei. In contrast, characteristic electromagnetic radiation is produced if an electron of the innermost shells is expelled by electron impact, and the leaving electron is replaced by an electron from an outer orbital. In this case, the energy of the emitted photons corresponds to the energy differences between the two orbitals.

Recently, electron synchrotrons – that is, electron storage rings – have gained importance as bright sources of high-energy photons. Synchrotron radiation is incoherent electromagnetic radiation that is emitted when relativistic electrons circulating in a storage ring are accelerated normal to the direction of motion by a magnetic field. The emission spectrum extends over an energy range covering several orders of magnitude. Filters are used to select a portion of the spectrum for particular applications.

Swift electrons – that is, electrons having high kinetic energy – are generated with the aid of an *electron accelerator*. Today, industrial accelerators can provide electron energies greater than 10 MeV and average beam powers as high as 700 kW. Low-energy (75 to 300 keV) electron accelerators are used to crosslink polymers and to cure coatings, adhesives and inks on paper, plastic and metal substrates (see Sections 5.6.3 and 5.6.4, respectively). Schematic diagrams of two types of commercially available electron accelerators used for crosslinking and curing, namely the scanned beam and the electron curtain-type accelerator, are shown in Figure 5.1.

In most industrial electron accelerators, the energy of the electrons is increased by accelerating them with either a steady electric field or an electric field varying at

Lam Research Ex. 1047 - Page 249
Lam Research Corp. v. Inpria Corp.
IPR2024-00033 - U.S. Patent No. 9,823,564

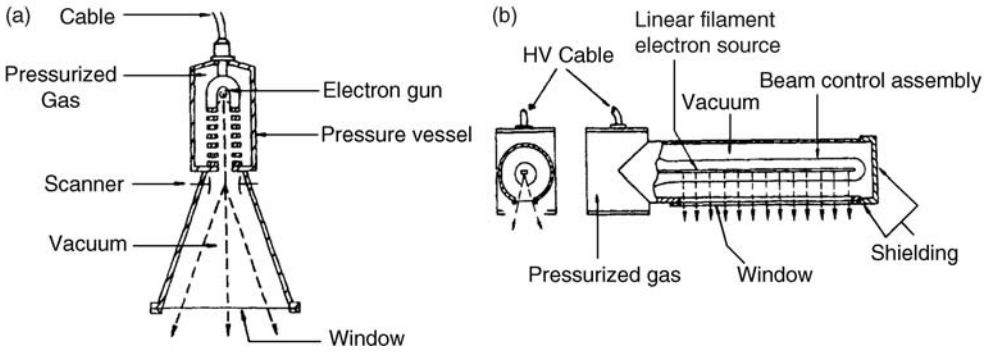


Figure 5.1 Schematic diagrams of (a) a scanned-beam electron accelerator and (b) an electron-curtain accelerator. Adapted with permission from Ref. [1]; © 1993, Elsevier.

a frequency in the microwave range. The former type of accelerator is known as a *DC* (direct current) accelerator, while the latter type is an *RF* (radiofrequency) linear accelerator. RF linear accelerators are also referred to as *RF linacs* or *microwave linacs*. A third type of accelerator, the linear induction accelerator, accelerates electrons by using a series of magnetic switches [2–4]. The reader is also referred to several books [5–11] dealing with the fundamentals and applications of radiation chemistry.

5.2
Polymer Synthesis

5.2.1
Free-Radical Polymerization

Practically, all monomers capable of undergoing free-radical polymerization can be polymerized upon irradiation with γ- or X-rays. An initiator is not needed because free radicals generated by radiolysis of the monomer can initiate the polymerization. The generation of initiator radicals is temperature-independent and, therefore, the activation energy E_{Pol} of the overall rate of polymerization v_{Pol}, is lower than in chemically initiated polymerizations.

Monomers dissolved in solvents can also be polymerized. In this case, free radicals generated from both the monomer and solvent initiate the polymerization. Energy transfer between monomer and solvent molecules may affect the radiation chemical yield of radical generation G(R), which can cause sensitization or retardation of the polymerization rate. The pioneering investigations in this field, which were performed during the 1950s, have been summarized by A. Chapiro [12].

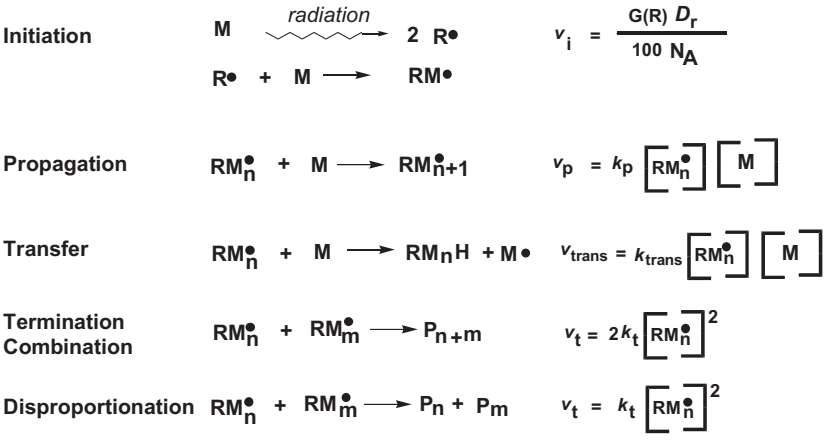
The kinetics of high-energy radiation-induced polymerization in homogeneous liquid phase can be treated conventionally in terms of initiation, propagation and

Lam Research Ex. 1047 - Page 250
Lam Research Corp. v. Inpria Corp.
IPR2024-00033 - U.S. Patent No. 9,823,564

termination, if it is considered that the initiation rate v_i in (mol L^{-1} s^{-1}) is given by Equation 5.1:

$$v_i = \frac{G(R) D_r}{100 N_A} \tag{5.1}$$

where G(R) is the number of free radicals generated by an absorbed dose of 100 eV, N_A is Avogadro's number, and D_r is the absorbed dose rate (in eV L^{-1} s^{-1}). The kinetic scheme of free-radical chain polymerization is presented in Scheme 5.4.



Scheme 5.4 Kinetic scheme of free-radical chain polymerization in homogeneous liquid phase. M: monomer; P: polymer.

Early discussions concerning high-energy radiation-induced polymerization were based on the applicability of the stationary state concept in homogeneous liquid systems which includes various assumptions: $v_i = v_t$, $v_t \gg v_{trans}$, and v_{Pol}, the overall rate of polymerization, is equal to the propagation rate: $v_{Pol} = v_p$. On the grounds of these assumptions, relationships describing the dependence of the rate of polymerization v_{Pol}, the 100 eV yield of monomer consumption G(-M) and the average molar mass M_n on both the absorbed dose rate D_r and the 100 eV yield of radical generation G(R) can be derived (see Equations 5.2–5.4):

$$v_{Pol} - \frac{d[M]}{dt} = \frac{k_p}{k_t^{1/2}} \left(\frac{G(R)}{100 N_A} \right)^{1/2} D_r^{1/2} [M] \tag{5.2}$$

$$G(-M) = -\frac{v_{Pol} 100 N_A}{D_r} = \frac{k_p}{k_t^{1/2}} \left(\frac{100 G(R) N_A}{D_r} \right)^{1/2} [M] \tag{5.3}$$

$$M_n = \frac{v_{Pol}}{v_i} = \frac{k_p}{k_t^{1/2}} \left(\frac{100 N_A}{G(R) D_r} \right)^{1/2} [M] \tag{5.4}$$

Lam Research Ex. 1047 - Page 251
Lam Research Corp. v. Inpria Corp.
IPR2024-00033 - U.S. Patent No. 9,823,564

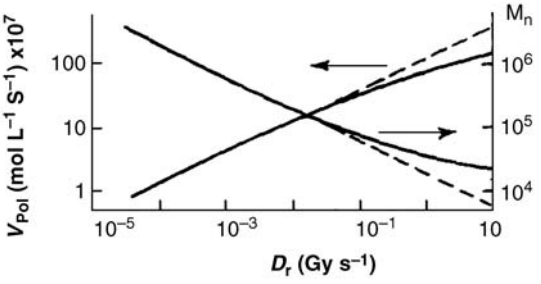


Figure 5.2 ^{60}Co-γ-ray-induced polymerization of styrene. Dependence of the overall rate of polymerization ν_{Pol} and the average molar mass M_n on the absorbed dose rate D_r. Data of various authors, compiled and generalized and reproduced with permission from Ref. [12]; © 1962, Interscience Publishers.

Figure 5.2 presents typical results obtained with styrene [12]. Cationic polymerization was suppressed, because the monomer was not rigorously dried in these studies. As expected from Equation 5.2, the polymerization proceeded by free-radical mechanisms, with ν_P being proportional to $D_r^{1/2}$ when D_r was low (indicated by a slope of 0.5). The deviation from this dependence at high absorbed dose rate is explained in terms of termination becoming partially controlled by the coupling of growing chain radicals with low-molar-mass free radicals according to Equation 5.5:

$$RM_n^{\bullet} + R^{\bullet} \rightarrow RM_nR \tag{5.5}$$

Various polymers including poly(acrylonitrile), poly(vinyl chloride) and poly (acrylic acid) are insoluble in their monomers. In these cases, growing chains precipitate at a critical chain length and termination does not occur via mutual coupling of macroradicals. Then, $\nu_i > \nu_t$ and ν_{Pol} is proportional to D_r^p with $0.5 < p < 1.0$.

The free-radical polymerization of monomer solutions and emulsions was investigated extensively during the 1950s, the respective findings were well documented [12]. In this context, investigations on the radiation-induced polymerization of vinyl monomers in dense CO_2 (supercritical fluid) are to be noted [13]. CO_2 is a good solvent for most vinyl monomers, but a poor solvent for most high-molar-mass polymers. With the aid of a dispersion technique, a high-molar-mass polymer ($M_w \approx 10^6\,g\,mol^{-1}$) with a narrow molar mass distribution can be obtained. This was achieved when methyl methacrylate dissolved in CO_2 and containing a polysiloxane stabilizer as surfactant was submitted to ^{60}Co-γ-radiation at 7 MPa and 30 °C. At early nucleation, the surfactant is attached to the surface of the particles, thus preventing coagulation and precipitation [14].

Free-radical polymerization in aqueous solution is of practical interest regarding the production of *hydrogels* [15]. Free radicals stemming from the radiolysis of water (Scheme 5.4) initiate first the polymerization of the monomer,

Lam Research Ex. 1047 - Page 252
Lam Research Corp. v. Inpria Corp.
IPR2024-00033 - U.S. Patent No. 9,823,564

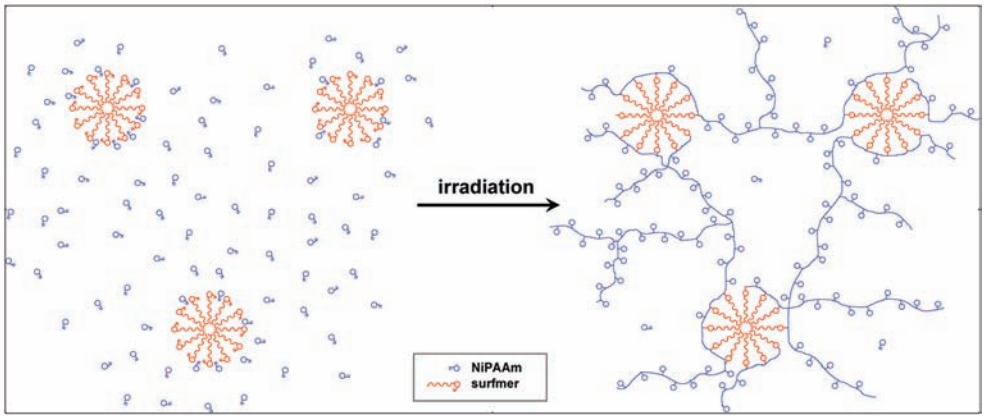


Figure 5.3 Formation of an intelligent hydrogel via γ-ray-induced polymerization of micellar aqueous comonomer solutions and microemulsions containing a cationic surfactant monomer (surfmer) such as *N*-isopropylacrylamide (NIPAM). Red: poly-surfmer blocks; Blue: poly-NiIPAAm blocks. Adapted with permission from Ref. [18]; © 2010, American Chemical Society.

and later the intermolecular crosslinking of the formed polymer. Hydrogel dressings obtained in this way may serve as temporary coverings for burn wounds [16] (see Section 5.6.6). Other interesting studies in this line refer to the preparation of *intelligent hydrogels* via γ-ray-induced polymerization of micellar monomer solutions [17,18]. Intelligent hydrogels are polymer networks with a high water content that are capable of undergoing reversible phase transitions under the influence of external stimuli such as changes in temperature, pH, magnetic field strength, or ionic strength. These gels can be prepared by the ^{60}Co-γ-irradiation-induced polymerization of micellar aqueous comonomer solutions and microemulsions containing a cationic surfactant monomer (surfmer), such as 11-acryloyloxyundecyltrimethylammonium bromide (AUTMAB) and *N*-isopropylacrylamide (NIPAAM). As shown in Figure 5.3 and Chart 5.1, a chemically and physically crosslinked network structure is formed consisting of blocks of P-NIPAAm and P-AUTMAB.

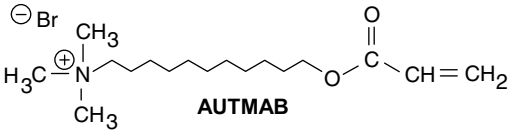


Chart 5.1 Chemical structure of 11-acryloyloxyundecyltrimethylammonium bromide (AUTMAB).

Reversibility of the transition renders the hydrogels attractive for sensor applications or controlled drug release. The hydrophobic core can be used to solubilize organic molecules such as fluorescent dyes or magnetic nanoparticles so

Lam Research Ex. 1047 - Page 253
Lam Research Corp. v. Inpria Corp.
IPR2024-00033 - U.S. Patent No. 9,823,564

as to introduce functional properties into the hydrogels. NIPAAM-based hydrogels are known to change volume and transparency upon heating to temperatures above 32 °C, which is the lower critical solution temperature (*LCST*) of the gel. Phase transition involves clouding of the hydrogel network and the expulsion of incorporated water [17,18].

Important technical applications of radiation-induced free-radical polymerization are presented in Section 5.6.4, which is devoted to *curing*.

5.2.2
Ionic Polymerization

Substances capable of undergoing cationic polymerization, such as isobutene, styrene and α-methylstyrene, polymerize by a cationic mechanism if subjected to irradiation with γ- or X-rays, provided that they have been rigorously purified from impurities, in particular from traces of water. Scheme 5.5 presents a kinetic scheme of cationic polymerization which takes into account that an impurity X interferes with the polymerization. The initiation comprises the generation of free ions A^+ and B^-, the latter being a free electron or a molecular ion.

Initiation :

$$M \xrightarrow{radiation} A^{\oplus} + B^{\ominus} \qquad v_i = \frac{G(I)\ D_r}{100\ N_A} \qquad (a)$$

Propagation :

$$A^{\oplus} + nM \longrightarrow AM_n^{\oplus}$$

$$AM_n^{\oplus} + M \longrightarrow AM_{n+1}^{\oplus} \qquad v_p = k_p [AM_n^{\oplus}][M] \qquad (b)$$

$$[AM_n^{\oplus}][M] \qquad (c)$$

Termination by Neutralization :

$$AM_n^{\oplus} + B^{\ominus} \longrightarrow \text{Polymer} \qquad v_t = k_t [AM_n^{\oplus}][B^{\ominus}] \qquad (d)$$

Termination by Impurity :

$$AM_n^{\oplus} + X \longrightarrow AM_n + X^{\oplus} \qquad v_X = k_X [AM_n^{\oplus}][X] \qquad (f)$$

Neutralization :

$$X^{\oplus} + B^{\ominus} \longrightarrow \text{Products} \qquad v_N = k_t [X^{\oplus}][B^{\ominus}] \qquad (g)$$

Transfer to Monomer

$$AM_n^{\oplus} + M \longrightarrow AM_n + M^{\oplus} \qquad v_{trans} = k_{trans} [AM_n^{\oplus}][M] \qquad (h)$$

Scheme 5.5 Kinetic scheme of cationic chain polymerization.

Lam Research Ex. 1047 - Page 254
Lam Research Corp. v. Inpria Corp.
IPR2024-00033 - U.S. Patent No. 9,823,564

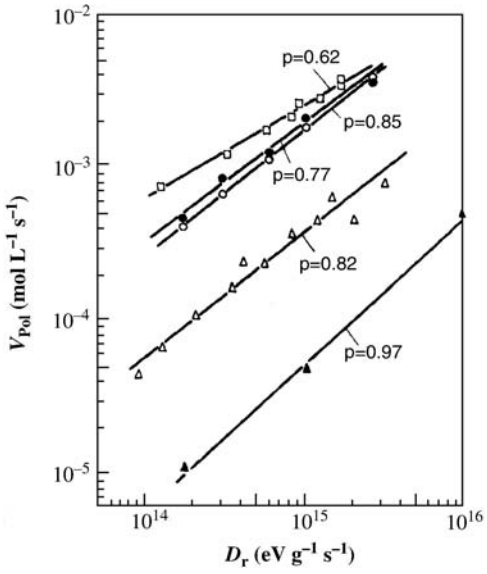


Figure 5.4 Polymerization of styrene at 15 °C. Plots of ν_{Pol} versus D_r with the monomer containing decreasing amounts of water (Δ, ○, ●, □) or 10^{-5} mol L^{-1} trimethyl amine (▲). Adapted with permission from Ref. [19]; © 1967, Royal Chemical Society.

Provided that the stationary state concept for the homogeneous liquid phase is applicable (i.e., $\nu_i = \nu_t$, $\nu_t \gg \nu_{trans}$, and $\nu_{Pol} = \nu_p$), and growing chain termination occurs exclusively by neutralization according to reaction (d) in Scheme 5.5, the overall rate of polymerization is proportional to the square-root of the absorbed dose rate D_r according Equation 5.6 [12]:

$$\nu_{Pol} = -\frac{d[M]}{dt} = \frac{k_p}{k_t^{1/2}} \left(\frac{G(I)}{100\, N_A} \right)^{1/2} D_r^{1/2} [M] \tag{5.6}$$

If the growing chains are terminated by impurity X according to reaction (f) in Scheme 5.5 and the resulting ion X^- cannot initiate the growth of new chains, ν_{Pol} is directly proportional to D_r according to Equation 5.7:

$$\nu_{Pol} = -\frac{d[M]}{dt} = \frac{k_p}{k_X} \frac{[M]}{[X]} \frac{G(I)}{100\, N_A} D_r \tag{5.7}$$

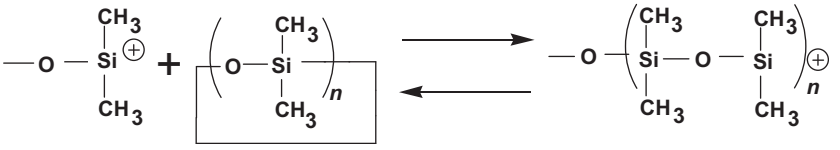
If growing chains are terminated both by reaction (d) and (f), ν_{Pol} is proportional to D_r^p with p-values between 0.5 and 1.0.

This behavior has been validated by the classical work of Ueno *et al.* [19]. Results are presented in Figure 5.4.

Another classical example pertains to the polymerization of rigorously dried cyclic dimethylsiloxanes at 90 °C [20]. A square-root dependence of ν_{Pol} on the absorbed dose rate, as expected for the ionic polymerization in the absence of

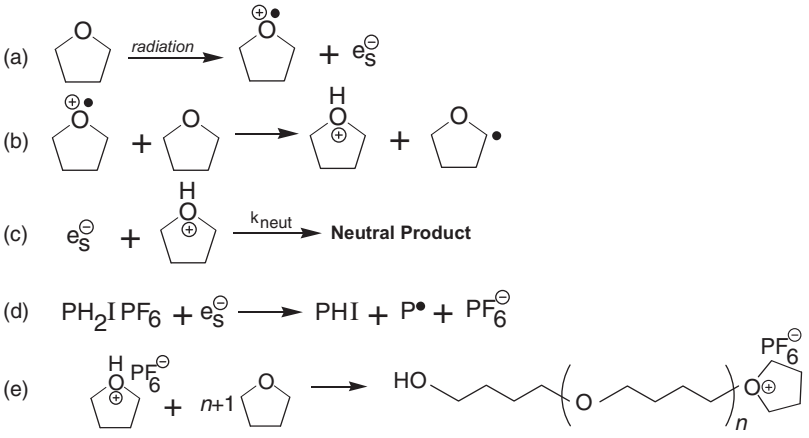
Lam Research Ex. 1047 - Page 255
Lam Research Corp. v. Inpria Corp.
IPR2024-00033 - U.S. Patent No. 9,823,564

terminating impurities (see Equation 5.6), was observed after repeated contact of the monomer with sodium mirrors (12 or more). The fact, that apart from the polymer, also oligomers are formed, led to the conclusion that propagation and ring formation proceed through the same type of cationic center (Scheme 5.6).



Scheme 5.6 Propagation in the high-energy radiation-induced polymerization of dimethylcyclosiloxanes D_3, D_4, and D_5 ($n = 3$, 4, or 5), via the mechanism proposed in Ref. [20].

In many cases, the initiation of cationic polymerizations is severely impeded or totally prevented by the diffusion-controlled neutralization of radical cations by secondary electrons. In the case of tetrahydrofuran (THF) the respective rate constant, as determined by pulse radiolysis measurements, is $k_{neut} = 2 \times 10^{12}\,l\,mol^{-1}\,s^{-1}$ (see Scheme 5.7, reaction (c) [21]. Therefore, high-energy radiation does not induce the polymerization of neat epoxides and vinyl ethers.



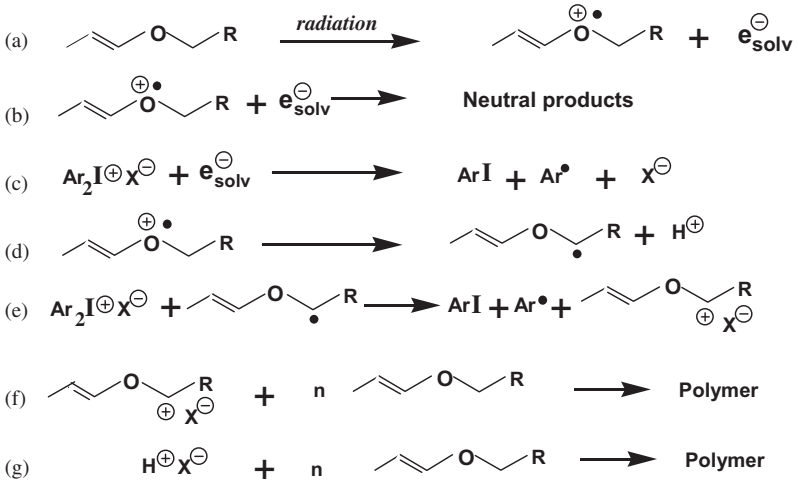
Scheme 5.7 High-energy-radiation-induced cationic polymerization of tetrahydrofuran [21].

However, if onium salts such as diphenyliodonium hexafluorophosphate are present in the system, solvated electrons can be scavenged according to reaction (d) in Scheme 5.7, and the cationic polymerization can be initiated (reaction (e)). The onium salts, which are mostly applied as electron scavengers, are widely applied photoinitiators (see Table 3.10). However, the mechanism of action becoming effective in conjunction with high-energy irradiation differs drastically from that occurring during photopolymerization, where the photoinitiator is the major light-absorbing species. If a system containing a small amount of onium salt as electron

Lam Research Ex. 1047 - Page 256
Lam Research Corp. v. Inpria Corp.
IPR2024-00033 - U.S. Patent No. 9,823,564

scavenger is submitted to high-energy radiation, the major fraction of the incident energy is absorbed by the solvent or monomer and only an almost negligible fraction by the onium salt.

The radiation-induced cationic polymerization in the presence of onium salts has attained practical importance for the EB curing of systems containing epoxides or vinyl ethers [22,23]. The chemical structures of typical compounds were presented in Table 3.23. THF does not play a role in this context, because of its very low propagation rate constant ($k_p \approx 4 \times 10^{-3}\,l\,mol^{-1}\,s^{-1}$). A reaction mechanism for the polymerization of vinyl ethers in the presence of an iodonium salt, as proposed by Crivello [22], is shown in Scheme 5.8.



Scheme 5.8 High-energy radiation-induced cationic polymerization of vinyl ethers in the presence of an iodonium salt. Ar: phenyl: X: PF_6 [22].

During the early investigations, nucleophobic anions contained in onium salts were considered to be chemically inert and to act partially as stabilizing entities in ion pair formation. However, the results of later studies suggested that they might be involved to some extent and in some cases in the initiation of cationic polymerizations. For example, in the case of Ph_2IPF_6 dissolved in a diepoxide (Chart 5.2), the hexafluorophosphate anion was found to decompose during irradiation simultaneously with conversion of the diepoxide [23].

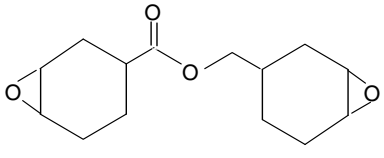


Chart 5.2 Chemical structure of a typical diepoxide.

Lam Research Ex. 1047 - Page 257
Lam Research Corp. v. Inpria Corp.
IPR2024-00033 - U.S. Patent No. 9,823,564

Therefore, PF_6^- has been supposed to react with oxonium ions of the diepoxide to form hexafluorophosphoric acid, which in turn decomposes into hydrofluoric acid and phosphorus pentafluoride. HPF_6, HF and PF_5 are considered to be potential initiators for cationic polymerizations [23].

Anionic polymerizations can be induced by high-energy radiation, provided that any electrons escaping the recombination of primary ion pairs are capable of attaching to monomer molecules, thus forming anion radicals as polymerization-initiating species. In fact, this is the case with compounds possessing a high electron affinity, such as nitroethylene and acrylonitrile. Bulk nitroethylene was shown to polymerize when irradiated with γ-rays at 10 °C [24]. β-Nitrostyrene, which does not polymerize in the solid state at room temperature, can be polymerized with γ-rays in solution of hexamethylphosphoric triamide and other aprotic solvents [25,26]. In this case, the polymerization is initiated by monomer radical anions generated by the reaction of solvated electrons with the β-nitrostyrene. To date, polymerizations initiated by anions generated by dissociative electron capture according to Equation 5.8 have not been identified.

$$AB + e^- \rightarrow A^- + B^\bullet \tag{5.8}$$

5.2.3 Graft Copolymerization

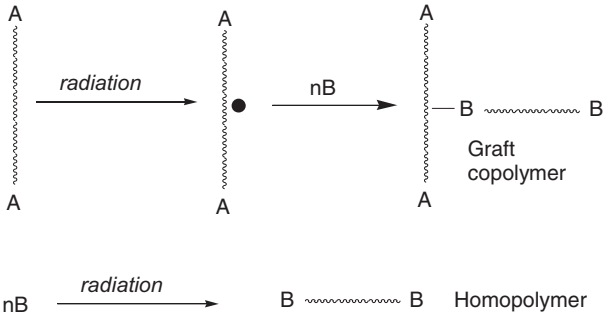
Graft copolymers are composed of chains of repeating units A, onto which side chains composed of repeating units B are grafted. High-energy radiation is an ideal tool to create graft copolymers. Radiation grafting is of particular importance for the surface modification of polymeric materials, and neither chromophoric groups (as in photografting; see Section 3.2.2.1) nor catalysts are needed. The thickness of the grafted layer can be varied with the aid of radiations that differ in their penetration depth. Commonly, high-energy radiation-induced graft copolymerization is accomplished by two different methods, both of which proceed via a free-radical mechanism: (1) the *direct or simultaneous method*; and (2) *the pre-irradiation method*.

In the direct or simultaneous method, polymer A_m is irradiated in the presence of monomer B (Scheme 5.9); free macroradicals generated by the radiolysis of A_m then initiate the polymerization of B, thus forming grafts. Simultaneously, monomer B is homopolymerized because, apart from polymer A_m, also monomer B is radiolyzed (though this might be an unwanted effect). Notably, this scheme operates in the absence of oxygen.

The pre-irradiation method (Scheme 5.10) can be performed in two modes:

- Polymer A_m is irradiated in the absence of O_2, and free macroradicals are formed. When, subsequently, monomer B is added to the irradiated polymer, a graft copolymer is formed.

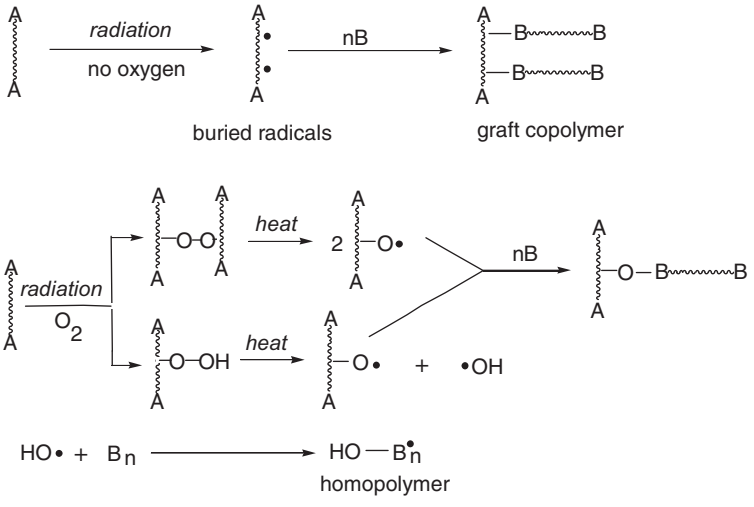
Lam Research Ex. 1047 - Page 258
Lam Research Corp. v. Inpria Corp.
IPR2024-00033 - U.S. Patent No. 9,823,564



Scheme 5.9 High-energy radiation-induced graft copolymerization according to the direct method.

- Polymer A_m is irradiated in the presence of O_2 and peroxide and hydroperoxide groups are generated. A graft copolymer is subsequently formed, when these groups are decomposed upon heating in the presence of monomer B.

As shown in Scheme 5.10, OH radicals capable of initiating the homopolymerization of B are formed upon the thermolysis of hydroperoxide groups. To avoid this, a low-temperature treatment in the absence of B may be employed to solely decompose hydroperoxide groups prior to initiating the grafting by decomposing peroxide groups at a higher temperature.



Scheme 5.10 High-energy-radiation-induced graft copolymerization according to the pre-irradiation method.

High-energy-radiation grafting is of technical importance due to the fact that the hydrophobic surface of bulk polymers can be turned hydrophilic by growing a

Lam Research Ex. 1047 - Page 259
Lam Research Corp. v. Inpria Corp.
IPR2024-00033 - U.S. Patent No. 9,823,564

hydrophilic polymer on the bulk. This is of particular interest when the dyeability of fabrics and fibers made from hydrophobic polymers such as polyamide, polypropylene or wool fibers, is to be increased. Further practical applications of interest are described in Section 5.6.5.

5.2.4 Polymerization in the Solid State

A unique feature of high-energy-radiation applications relates to solid-state polymerizations [27–31]. In this case, a catalyst is not required and the irradiations can be performed at deliberately chosen temperatures, because the absorption of radiation is temperature-independent. Of particular interest in this context are compounds such as trioxane, hexamethylcyclotrisiloxane, β-propiolactone and diketene, all of which polymerize readily in the solid state but slowly, or not at all, in the liquid state. Other compounds such as styrene, acrylonitrile and formaldehyde polymerize faster in the crystalline state than in the liquid state just above the melting point. Compounds that undergo solid-state polymerization upon γ-irradiation are listed in Table 5.1. In contrast, vinyl chloride, vinyl acetate and methyl methacrylate do not polymerize in the solid state.

Evidence for the occurrence of solid-state polymerization has been obtained by measurements employed *in situ* (Table 5.2).

Commonly, a significant conversion of solid monomers is observed at temperatures close to the melting point. For example, solid trioxane is not converted at 25 °C but polymerizes at 55 °C. Above this temperature, the conversion increases in proportion to the dose of radiation absorbed (Figure 5.5).

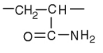
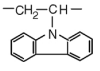
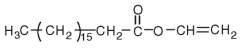
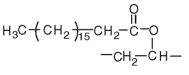
The solid-state polymerizations of trioxane [32,33] and of diacetylenes [34], proceed as topochemical reactions – that is, the polymerization is crystal-lattice controlled and proceeds with a minimum of atomic and molecular movement. Upon ring-opening, trioxane molecules form helical polyoxymethylene chains lying in the direction of the c-axis of the trioxane crystals. Such polymerization affords only a very small volume change.

By contrast, crystalline vinyl monomers cannot undergo topochemical polymerizations. In this case, the distance between the double bonds is 3.5 to 4.0 Å, which is much greater than the distance of C-atoms in a C—C bond of 1.5 Å. Therefore, the addition polymerization of vinyl-monomer molecules requires extended molecular motions, which explains why crystalline structural irregularities such as lattice dislocations and defects play an important role with respect to monomer conversion. Commonly, the vinyl-monomer conversion increases first and then levels off, thus approaching a constant (often quite low) limiting value with an increasing absorbed dose of radiation. In some cases, exponentially increasing monomer conversion–dose relationships have also been observed.

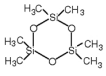
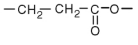
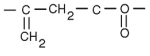
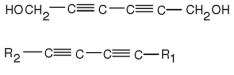
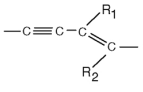
The mechanisms of high-energy-radiation-induced solid-state polymerization have not yet been firmly elucidated. Vinyl compounds supposedly polymerize by

Lam Research Ex. 1047 - Page 260
Lam Research Corp. v. Inpria Corp.
IPR2024-00033 - U.S. Patent No. 9,823,564

Table 5.1 Monomers that undergo high-energy radiation-induced polymerization in the solid state.

Monomer	Melting point (°C)	Irradiation temperature[a)] (°C)	Base unit of polymer
Acrylamide 	83	0–80	
Acrylonitrile 	−83	−196 to −140	
N-vinylcarbazol 	64	−20 to 40	
Vinylstearate 	35–37	−30 to 25	
Trioxane 	61	40 to 50	

Lam Research Ex. 1047 - Page 261
Lam Research Corp. v. Inpria Corp.
IPR2024-00033 - U.S. Patent No. 9,823,564

Hexamethylcyclotrisiloxane 	64	5 to 62	
β-Propiolactone 	−33	−196 to −70	
Diketene 	−6.5	−196 to −70	
Cyclohexene oxide 	−36		
Diacetylenes 	>60		

R_1 and R_2 : $(CH_2)_nCH_3$, $(CH_2)_nOH$, $(CH_2)_nCOOH$, etc.

a) Temperature range at which polymerizations were performed in relevant studies.

Lam Research Ex. 1047 - Page 262
Lam Research Corp. v. Inpria Corp.
IPR2024-00033 - U.S. Patent No. 9,823,564

Table 5.2 Experimental evidence for solid-state polymerization of certain monomers.

Method	Phenomenon	Monomer
X-ray diffraction	Destruction of crystal structure	Acrylamide
IR spectroscopy	Disappearance of double bonds	*p*-Benzamido styrene
Birefringence of light	Decrease	Acrylic acid, methacrylic acid
Calorimetry	Heat development	Acrylonitrile

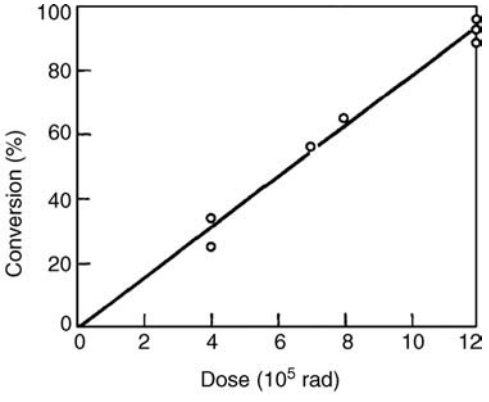


Figure 5.5 ^{60}Co-γ-irradiation of solid trioxane at 55 °C. Monomer conversion versus absorbed dose. Adapted with permission from Ref. [11]; © 1969, Wiley-VCH.

free-radical mechanisms, and cyclic compounds by ionic mechanisms. Generally, rigorous dehydration enforced by crystallization is likely to alleviate cationic polymerizations.

Finally, an interesting application referring to diacetylenes may be noted. Diacetylenes with melting points around 90 °C are used for low-dose dosimeters [35–37]; these compounds are colorless prior to irradiation but become blue or red when irradiated with high-energy radiation. The structure of a typical compound is depicted in Chart 5.3. Generally, the color intensity increases in proportion to the absorbed dose, and SIRAD, a *self-indicating-instant-radiation-alert dosimeter*, has been developed on this basis for the dose range up to 20 Gy [37].

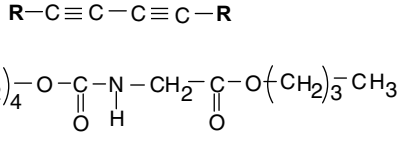


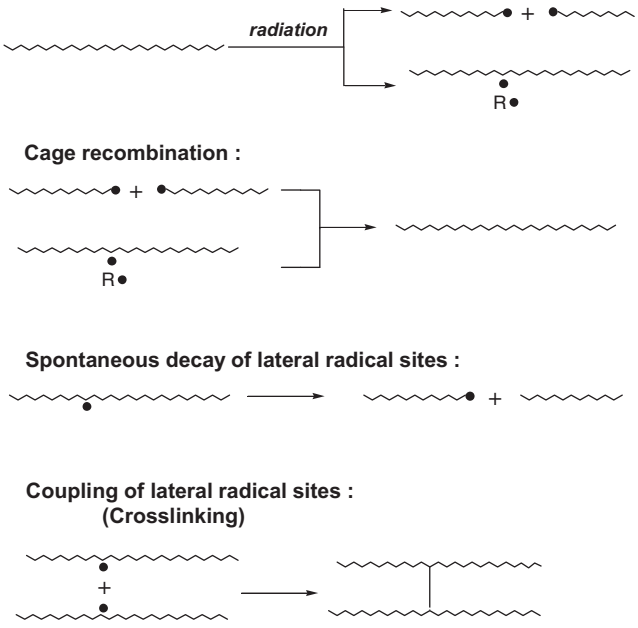
Chart 5.3 Chemical structure of a diacetylene applicable for dosimetry [35].

Lam Research Ex. 1047 - Page 263
Lam Research Corp. v. Inpria Corp.
IPR2024-00033 - U.S. Patent No. 9,823,564

5.3
Radiolysis of Bulk Synthetic Polymers

5.3.1
General Aspects

Irradiation effects in organic polymers result from the cleavage of chemical bonds and the subsequent reactions of intermediates generated thereby. These reactions lead to significant alterations in the physical properties of polymeric materials, and this topic has been covered in numerous books and articles [12,38–54]. As far as linear chain polymers are concerned, any changes in physical properties are due mainly to the formation of permanent main-chain scissions and intermolecular crosslinks. A general free-radical-based mechanism related to these processes is presented in Scheme 5.11.

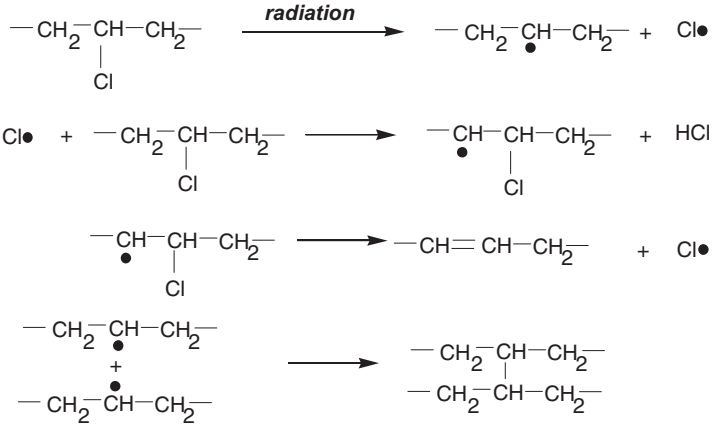


Scheme 5.11 Principal free-radical reactions occurring in linear chain molecules under the influence of high-energy radiation.

Apart from main-chain cleavage and crosslinking, radiation-induced modifications of linear polymers include the formation and disappearance of double bonds and the destruction of side groups. Commonly, the latter reaction results in the formation of gaseous products. In this context, the dehydrochlorination of poly (vinyl chloride), a polymer of great technical importance, is notable. Under the influence of high-energy radiation, carbon–halogen bonds are broken and

Lam Research Ex. 1047 - Page 264
Lam Research Corp. v. Inpria Corp.
IPR2024-00033 - U.S. Patent No. 9,823,564

hydrogen chloride gas is released. The resulting lateral macroradicals are prone to undergo intermolecular crosslinking (Scheme 5.12).



Scheme 5.12 High-energy-radiation-induced dehydrochlorination and crosslinking of poly(vinyl chloride).

Kinetically, the dehydrochlorination is a chain reaction, since chlorine radicals generated during double-bond formation can abstract hydrogens, thus forming new lateral macroradicals. Dehydrochlorination causes an intense discoloration which becomes more pronounced as the absorbed dose is increased, because of the increasing content of conjugated double bonds (polyene formation).

Molecular oxygen (O_2) has a significant effect on the radiolysis of polymers, because it adds readily to free radicals (see Section 5.3.3), a fact which is of great importance for practical applications. The radiolysis of polymers in the absence of O_2 is detailed in the following section.

When elucidating the mechanism of high-energy-radiation-induced reactions, credit must be given to the *pulse radiolysis method*, which allows the study of fast reactions that are initiated by exposing a sample for a short time (usually 10^{-12} to 10^{-6} s) to a beam of energetic electrons or synchrotron X-rays. During and after the pulse, any property changes of the sample are detected by a variety of methods that include light absorption and emission [55–57], electrical conductivity [58], and light scattering [59,60].

5.3.2
Product Formation in the Absence of Molecular Oxygen

In the case of linear chain polymers, intermolecular crosslinking and main-chain cleavage reactions cause an increase or decrease in the average molar mass, respectively, which in turn leads to dramatic changes in certain physical

Lam Research Ex. 1047 - Page 265
Lam Research Corp. v. Inpria Corp.
IPR2024-00033 - U.S. Patent No. 9,823,564

properties. Most vinyl polymers undergo simultaneously main-chain cleavage and intermolecular crosslinking. Theoretical studies exist for an initially random molar mass distribution and for main-chain ruptures and crosslinks being randomly distributed along the polymer chains. In this case, the dependence of weight-average molar mass M_w ($g\,mol^{-1}$) on the absorbed dose D_{abs} ($eV\,g^{-1}$) is given by Equation 5.9 [39]:

$$\frac{1}{M_{w,D}} = \frac{1}{M_{w,0}} + \left(\frac{G(S)}{2} - 2G(X)\right)\frac{D_{abs}}{N_A} \tag{5.9}$$

where G(S) and G(X) denote the 100 eV yields for main-chain cleavage and crosslinking, respectively, and N_A is Avogadro's number. Crosslinking predominates if the ratio of G-values for main-chain scission and crosslinking is lower than four – that is, $G(S)/G(X) < 4$. In this case, the average molar mass of the polymer increases at low absorbed doses. At absorbed doses exceeding a critical dose, the *gel dose* D_{gel}, the polymer becomes partially insoluble; this is shown in Figure 5.6 for the case of polybutene-1.

Depending on the ability to gel, two types of linear polymer can be discerned, namely those which gel and those which do not gel. Typical gelling and non-gelling polymers are listed in Table 5.3. Main-chain scission in linear polymers is highly favored if the polymer chains contains tertiary carbon atoms; for example, polystyrene and poly(methyl acrylate) crosslink predominantly, whereas poly (α-methyl styrene) and poly(methyl methacrylate) (PMMA) undergo predominantly main-chain scission.

Radiation effects are remarkably sensitive to molecular structure. G(S) and G(X) values vary from 0.1 to 10 (as can be seen in Table 5.4). The G(X) of polyethylene is about one order of magnitude larger than that of polystyrene, which demonstrates that aromatic rings exert a protective effect.

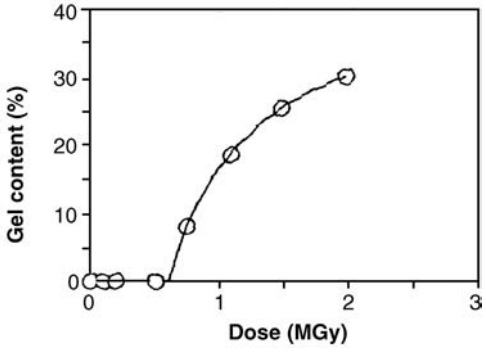


Figure 5.6 Irradiation of polybutene-1 with ^{60}Co-γ-rays *in vacuo* at $D_r = 2.8\,kGy\,h^{-1}$. Gel content as a function of the absorbed dose. Adapted with permission from Ref. [61]; © 1996, American Chemical Society.

Lam Research Ex. 1047 - Page 266
Lam Research Corp. v. Inpria Corp.
IPR2024-00033 - U.S. Patent No. 9,823,564

Table 5.3 Linear polymers that predominantly undergo crosslinking or main-chain scission if irradiated with high-energy radiation at room temperature in vacuo or in an oxygen-free atmosphere.

Predominant main-chain scission (average molar mass decreases)	Predominant crosslinking (average molar mass increases)
Polymethacrylates	Polyacrylates
Poly(methacryl amide)	Polyacrylamide
Poly(α-methacrylonitrile)	Polyacrylonitrile
Poly(α-methylstyrene)	Polystyrene
Polyisobutene	Polyethylene
Polytetrafluoroethylene	Polypropylene
Polytrifluorochloroethylene	Polyisoprene
Poly(vinyl fluoride)	Polybutadiene
Poly(vinylidene chloride)	Polyamides
Poly(hexene-1 sulfone)	Poly(vinyl acetate)
Poly(propylene sulfide)	Poly(vinyl alcohol)
Polyoxymethylene	Poly(vinyl pyrrolidone)
Polycarbonates	Polyurethanes
Poly(vinyl butyral)	Polychloroprene
Poly(phenyl vinyl ketone)	Natural rubber
Polysaccharines (cellulose, chitosan)	Polysiloxanes
Polysine, Polyalanine	Copolymers of butadiene with styrene or acrylonitrile
Nucleic acids (DNA)	Copolymers of acrylonitrile with styrene

Table 5.4 Radiation chemical yields G(S) and G(X) for main-chain cleavage and crosslinking, respectively. Irradiation of polymers with high-energy radiation at room temperature in vacuo or in an oxygen-free atmosphere [54].

Polymer	G(S)	G(X)	Predominant process
Polyethylene		0.5 to 2.0[a)]	Crosslinking
Polypropylene	0.24	0.27	Crosslinking
Poly(ethylene oxide)	2.0	1.8	Crosslinking
Poly(dimethyl siloxane)	0.07	2.3	Crosslinking
Polystyrene	0.02	0.03	Crosslinking
Poly(α-methyl styrene)	0.25		Main-chain scission
Poly(methyl methacrylate)	1.2–2.6		Main-chain scission
Polyisobutene	1.5 .5.0	<0.05	Main-chain scission
Polytetrafluoroethylene	0.1–0.2		Main-chain scission
Poly(phenyl vinyl ketone)	0.35		Main-chain scission
Poly(butene-1 sulfone)	12.2		Main-chain scission
Amylose	1.3–2.7		Main-chain scission
Cellulose	3.3–6.8		Main-chain scission
Polylysine	4.1		Main-chain scission

a) Depending on the degree of crystallinity.

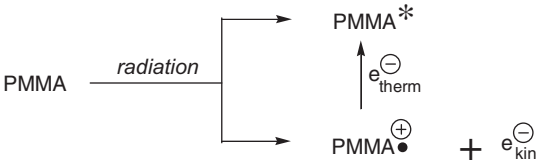
Lam Research Ex. 1047 - Page 267
Lam Research Corp. v. Inpria Corp.
IPR2024-00033 - U.S. Patent No. 9,823,564

Table 5.5 Major low-molar-mass products formed by ^{60}Co-γ-radiolysis of various linear polymers.

Polymer	Volatile products
Poly(methyl methacrylate)	CO, CO_2, $HCOOCH_3$, CH_4, H_2, CH_3OH, CH_3OCH_3, HCOOH
Poly(tetrafluoro ethylene)	CF_4, C_2F_6, C_3F_8
Poly(propylene oxide)	H_2, CO, CH_4
Poly(vinyl acetate)	H_2, CH_4, CO, CO_2
Polypropylene	H_2, CH_4

A general phenomenon is the evolution of small molecular products under the influence of high-energy radiation (as can be seen in Table 5.5). Volatile products result from the decomposition of radiation-sensitive lateral groups such as —COOH and —SO_2—, that give rise to the formation of CO and CO_2, and SO_2, respectively.

A comprehensive treatment of the mechanisms of radiation-induced processes in polymers is beyond the scope of this book. The primarily generated species – that is, electronically excited molecules, radical cations, and thermalized electrons – either decompose or react rapidly with the surrounding molecules. Extended electron spin resonance (ESR) studies with many linear polymers have revealed that, in all cases, free radicals are formed which either decompose or are transformed to different radicals by abstracting hydrogens from neighboring molecules. Frequently, the final products are formed via radical-coupling reactions. Key reactions pertaining to the initial stages of the radiolysis of PMMA, which may serve here as a typical example [62], are presented in Schemes 5.13–5.15.

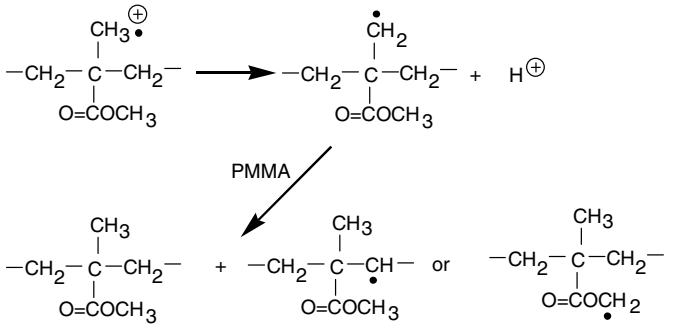


Scheme 5.13 Radiolysis of poly(methyl methacrylate). Generation of primary transients.

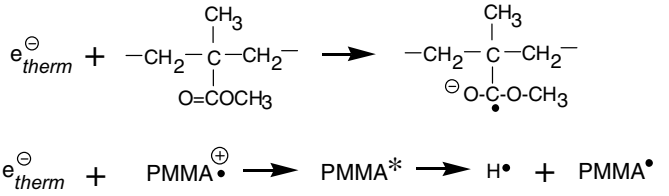
When PMMA radical cations deprotonate, side-group radicals are formed that abstract hydrogen atoms from intact macromolecules. In solid PMMA, the protons have a long lifetime (several hundred minutes) and can migrate through the polymer matrix [63]. Thermalized electrons are either captured by carbonyl groups, thus forming anion radicals, or they can couple with radical cations so as to generate additional, electronically excited molecules; the latter decay by splitting off either hydrogen atoms or side groups. Certain side-group radicals, formed by the release of hydrogen atoms, decompose via main-chain cleavage, as shown in

Lam Research Ex. 1047 - Page 268
Lam Research Corp. v. Inpria Corp.
IPR2024-00033 - U.S. Patent No. 9,823,564

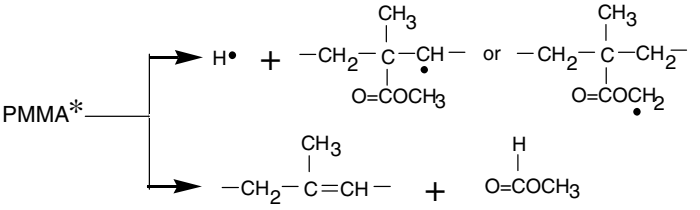
Fate of primary radical cations:



Fate of thermalized electrons:



Fate of electronically excited base units:

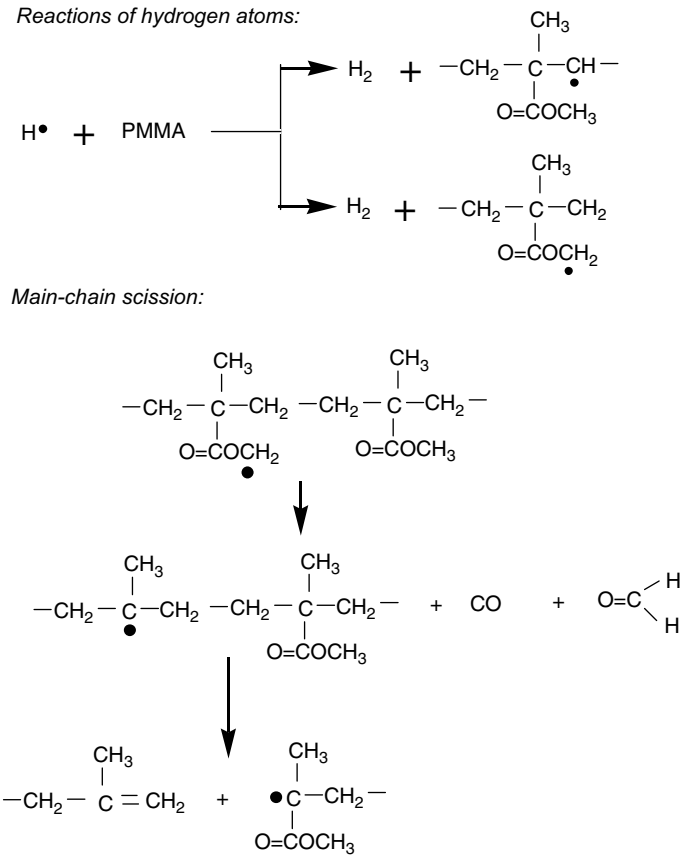


Scheme 5.14 Radiolysis of poly(methyl methacrylate) (PMMA). Fate of primary transients [62].

Scheme 5.15. Main-chain-scission-type radicals are also formed when free hydrogen atoms abstract hydrogen from polymer side groups (see upper part of Scheme 5.15).

It should be noted that a large proportion of primary bond breakages is nullified by recombination reactions, referred to in Scheme 5.11 as *cage recombination*. Evidence of temporary bond scissions has been obtained by investigating radiation-induced changes in the stereoregularity of certain ordered polymers, including isotactic polypropylene, isotactic polybutene-1 and isotactic PMMA. These changes are due to the fact that there is sufficient time for bond rotation and configurational inversion between bond scission and the recombination of radicals. For example, by measuring changes in the full-pentade distribution of isotactic polypropylene, a G-value for configurational

Lam Research Ex. 1047 - Page 269
Lam Research Corp. v. Inpria Corp.
IPR2024-00033 - U.S. Patent No. 9,823,564



Scheme 5.15 Radiolysis of poly(methyl methacrylate) (PMMA). Reactions of hydrogen atoms and decomposition of side-chain radicals that subsequently undergo main-chain cleavage via β-scission [62].

inversion greater than 20 was found. This G-value is considerably higher than the G-values for any other chemical event. Further details on this topic are available in Ref. [61].

In this context, the influence of temperature on radiation-chemical yields is also remarkable. To a great extent, these temperature effects are due to an increased segment mobility, which affects the course of radical reactions. In the case of amorphous linear polymers, an increase in segment mobility will diminish the probability for cage recombination. Therefore, quite often the radiation chemical yields G(S) and G(X) increase at temperatures above the glass transition temperature, T_g. Moreover, secondary transitions pertaining to the rotation of lateral groups can affect radiation chemical yields. As a typical example, Figure 5.7 shows the temperature dependence of G(S) measured in

Lam Research Ex. 1047 - Page 270
Lam Research Corp. v. Inpria Corp.
IPR2024-00033 - U.S. Patent No. 9,823,564

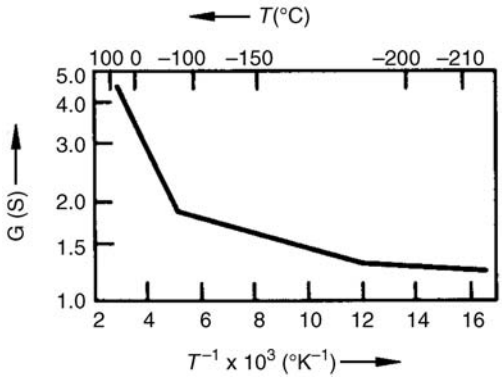


Figure 5.7 Irradiation of polyisobutene *in vacuo* with ^{60}Co-γ-rays. The radiation chemical yield of main-chain scission as a function of the temperature. Adapted with permission from Ref. [64]; © 1974, Elsevier.

the case of polyisobutene. Here, the inflection points at about −70 °C and −190 °C reflect T_g and the relaxation of lateral methyl groups, respectively.

The behavior of crystalline or partially crystalline polymers deserves special mention. In contrast to amorphous districts, chemical reactions are hindered in crystalline districts by their rigidity, which makes chemical reactions such as crosslinking less likely, or even impossible. Moreover, radicals can be trapped in crystalline districts. Therefore, G-values increase at temperatures above the crystalline melting point, when macromolecules become mobile; some typical results are shown in Figure 5.8.

Most striking in this context is the fact that polytetrafluoroethylene (PTFE), a semicrystalline polymer that undergoes predominantly main-chain scission at room temperature, can be crosslinked when irradiated in the absence of O_2 with

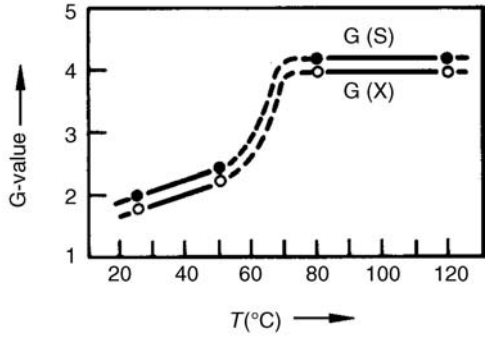


Figure 5.8 Irradiation of poly(ethylene oxide) *in vacuo* with ^{60}Co-γ-rays. Radiation chemical yields of crosslinking and main-chain scission as a function of temperature. Adapted with permission from Ref. [65]; © 1970, Wiley-VCH.

Lam Research Ex. 1047 - Page 271
Lam Research Corp. v. Inpria Corp.
IPR2024-00033 - U.S. Patent No. 9,823,564

γ-rays or swift electrons at 330 to 340 °C, that is, just above the crystalline melting point at 327 °C [66–69]. Opaque PTFE sheets can be made transparent by this procedure.

High-energy radiation can induce the depolymerization of polymers when irradiated at temperatures close to or above the ceiling temperature for the liquid-phase polymerization. This has been demonstrated in the cases of poly (butane sulfone) and poly(hexane sulfone) that possess ceiling temperatures at about 60 °C [70].

It should be noted that, with increasing absorbed dose, the physical properties of linear polymers are deteriorated severely by radiolysis, a fact which prohibits most plastic materials to be used in permanent radiation fields that exist, for example, in nuclear reactors. Radiation-induced damage plays an important role, when the structure of protein crystals shall be determined with the aid of X-ray diffraction measurements. Actually, radiation damage can bring about a loss in resolution or can prevent the solution of a structure during a diffraction experiment, because diffraction spots can fade away before the data set is complete [71–73].

5.3.3
Product Formation in the Presence of Molecular Oxygen

Molecular oxygen, O_2, readily reacts with free radicals, and since free radicals play a dominant role in the radiolysis of polymers, O_2 can significantly affect radiation-induced chemical alterations. For instance, it enhances the radiation-induced degradation of most polymers. Linear polymers, including polyethylene, polypropylene, polystyrene and poly(vinyl chloride), that crosslink in the absence of oxygen undergo predominantly main-chain scission in its presence. As a typical example, a free-radical-based reaction mechanism proposed for the oxidative degradation of polyethylene is shown in Scheme 5.16.

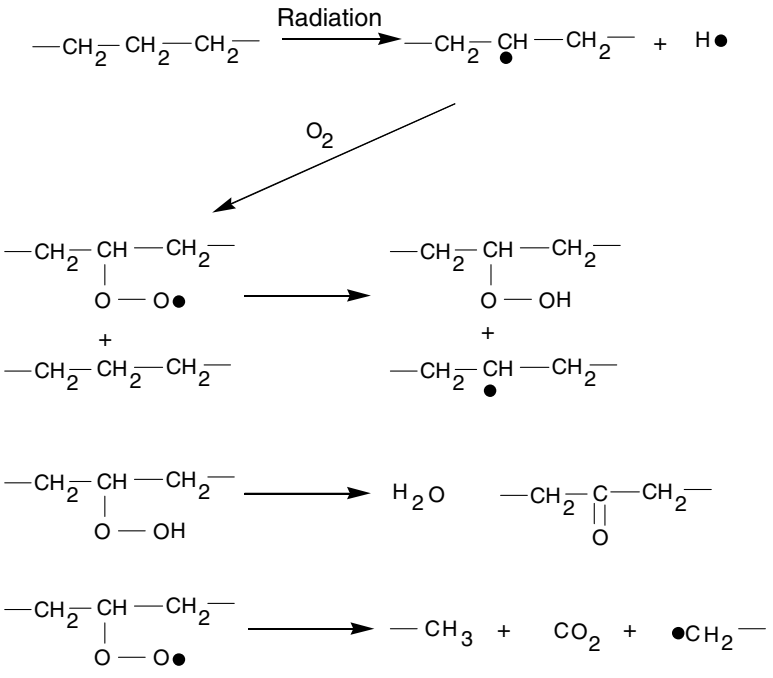
In some cases, such as PMMA and amylase, the presence of oxygen causes a diminution of the main-chain scission yield G(S) – that is, oxygen exerts a protective effect.

The oxidation of bulk polymers often emerges as being dose rate-dependent, as shown in Figure 5.9. This dependence arises from the fact that the oxygen concentration in the bulk is depleted at high dose rates because oxygen is consumed more rapidly than it can diffuse into the sample. However, a reverse situation is encountered at low absorbed dose rates. Clearly, sample thickness plays an important role during the oxidative degradation of polymers.

5.3.4
Radiation Stability and Protection

The mechanical properties of polymers of the crosslinking type are improved upon irradiation with low absorbed doses (up to 0.1 MGy): for example, the

Lam Research Ex. 1047 - Page 272
Lam Research Corp. v. Inpria Corp.
IPR2024-00033 - U.S. Patent No. 9,823,564



Scheme 5.16 Mechanism of the oxidative high-energy-radiation-induced degradation of polyethylene.

elastic modulus, tensile strength and hardness are each increased, whereas the solubility is decreased with increasing absorbed dose. On this basis, cable insulations and shrinkable foils made from polyethylene are crosslinked industrially. However, at high absorbed doses, polymers of the crosslinking type become hard and brittle. On the other hand, polymers of the degradation type undergo a deterioration of their mechanical properties, even at low absorbed doses.

Measures to really protect polymers do not exist. Protective agents (*antirads*) added to the polymer in small amounts are only effective to a limited extent, and function via different mechanisms. Typically, they can act as antioxidants by preventing radiation-induced oxidative chain reactions or, more generally, as scavengers of free radicals. Moreover, additives may act as energy sinks in accepting electronic excitation energy transferred from the polymer. Aromatic compounds, including polymers with aromatic constituents or fillers consisting of inorganic material or carbon black, operate protectively in this manner. Electronic excitation energy transported to or directly absorbed by aromatic groups is delocalized due to the π-electron-based resonant structure of the aromatic ring, and converted to heat by collision with neighboring groups or molecules. Hence, bond rupture is much less likely than in the case of nonaromatic compounds. As a consequence, technically important aromatic

Lam Research Ex. 1047 - Page 273
Lam Research Corp. v. Inpria Corp.
IPR2024-00033 - U.S. Patent No. 9,823,564

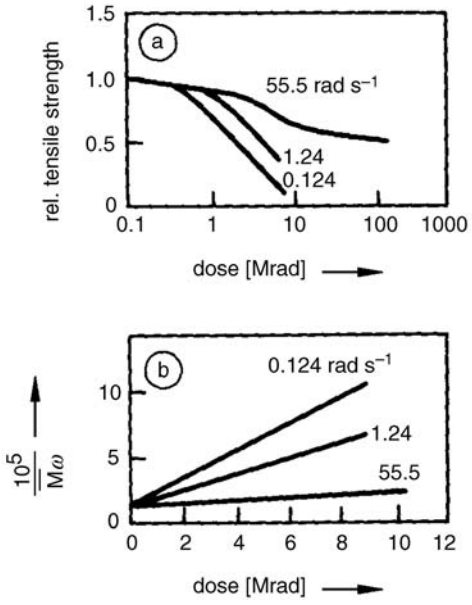


Figure 5.9 Oxidative degradation of polyethylene irradiated in the presence of air at different dose rates (as indicated in the graphs). (a) Relative ultimate tensile strength and (b) reciprocal average molar mass as a function of absorbed dose. Adapted with permission from Ref. [74]; © 1973, Springer Verlag.

polymers such as polyimides and poly(aryl sulfones) (Chart 5.4) are rather resistant to high-energy radiation when compared to nonaromatic polymers.

The mechanical and electrical properties of a polypyromellitimide (see Chart 5.4) are reported to remain satisfactory in the presence of air up to absorbed doses of 10^2 MGy [75], although most aromatic polymers proved to be radiation-resistant only in the absence of O_2. For example, the mechanical properties of polystyrene were not appreciably deteriorated when the polymer was exposed in the absence of O_2 to absorbed doses up to 10 MGy, but they were decreased to 50% of their initial value at an absorbed dose of only about 0.80 MGy [76].

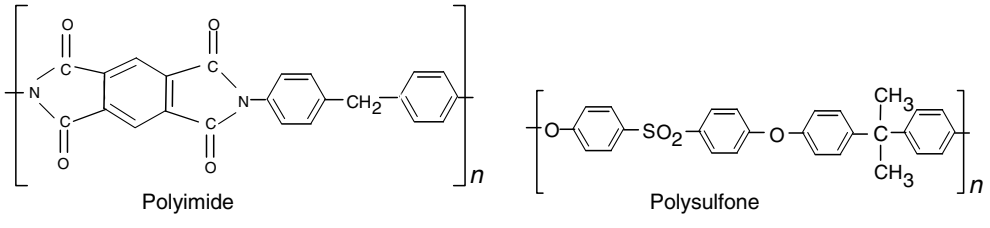


Chart 5.4 Chemical structures of radiation-resistant polymers.

Lam Research Ex. 1047 - Page 274
Lam Research Corp. v. Inpria Corp.
IPR2024-00033 - U.S. Patent No. 9,823,564

5.4
Radiolysis of Bulk Biopolymers

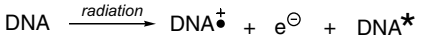
5.4.1
General Aspects

Irradiation effects in biopolymers result from the cleavage of chemical bonds. Because of the very complex composition of most biopolymers, many different chemical reactions are initiated and in each case a host of products are formed under the influence of high-energy radiation. Within the framework of this book only a few aspects of this broad field can be covered, and detailed information is available from the relevant literature [77–101]. Radiation chemistry and radiation biology are intimately connected, and this connection has been made the subject of various books [81,102]. A variety of biopolymers composed of linear strands, including certain polysaccharides, proteins and nucleic acids, undergo predominantly main-chain scission, and this is of outstanding importance in the case of deoxyribonucleic acids (*DNA*), because the killing of biological cells correlates well with double-strand breaks.

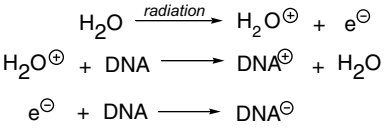
5.4.2
Nucleic Acids

DNA is the most important target with regards to the killing of biological cells by ionizing radiation, and consequently DNA and its related low-molar-mass compounds have been the subject of a plethora of publications [77–79,87–94]. High-energy radiation directly absorbed by DNA generates electronically excited moieties, radical cations and electrons (Scheme 5.17). *In vivo*, however, DNA occurs always in an aqueous environment where the indirect radiation effect prevails – that is, the lesions are predominantly due to the attack of DNA molecules by reactive species stemming from the radiolysis of water. High-energy radiation, when directly absorbed by DNA, generates electronically excited moieties, radical cations, and electrons (Scheme 5.17).

Direct effect:



Indirect effect:



Scheme 5.17 Direct and indirect radiation effects in DNA.

Lam Research Ex. 1047 - Page 275
Lam Research Corp. v. Inpria Corp.
IPR2024-00033 - U.S. Patent No. 9,823,564

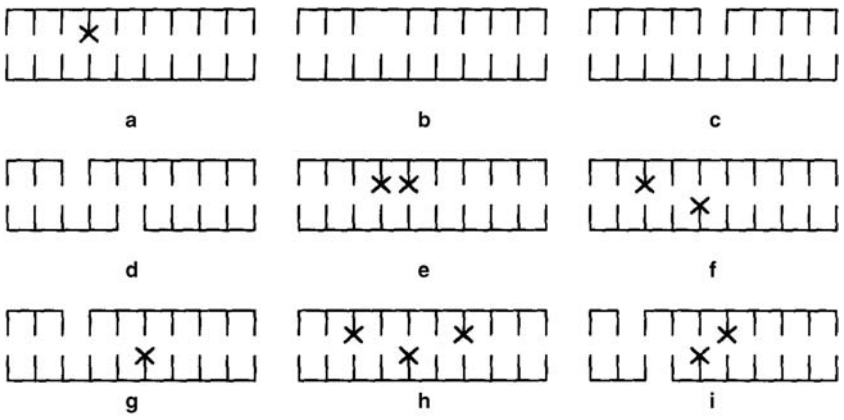


Figure 5.10 Schematic depiction of high-energy-induced lesions generated in double-stranded DNA. Adapted with permission from Ref. [78]; © 2006, Springer Verlag.

It should be noted that DNA can hardly be totally freed from water. Commonly, a certain number of water molecules (about 8–12 per nucleotide) are tightly associated with the different parts of the macromolecule, forming a primary solvation shell. However, when the water molecules are ionized, hole transfer to the DNA molecules can occur and electrons ejected from the water molecules can be scavenged by DNA molecules (Scheme 5.17). In fact, the existence of a primary solvation shell can cause an increase in the radiation-induced damage to DNA by about 50% [90].

Important radiolysis products and events due to the direct effect are single- and double-strand breaks, crosslinking, base release, and lesions in bases and sugar moieties. Moreover, hydrogen bonds between the two strands of the double helix are ruptured. The typical damage sites in double-stranded DNA are marked in Figure 5.10. A large number of radiolysis products occur with low molar masses; typical products resulting from base damage are compiled in Chart 5.5 [89].

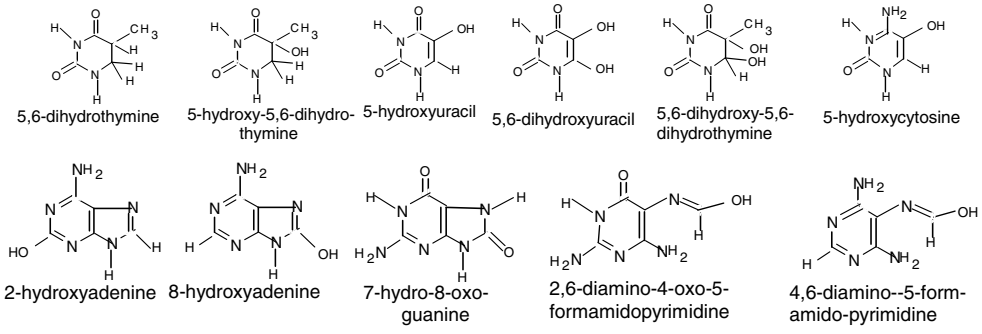
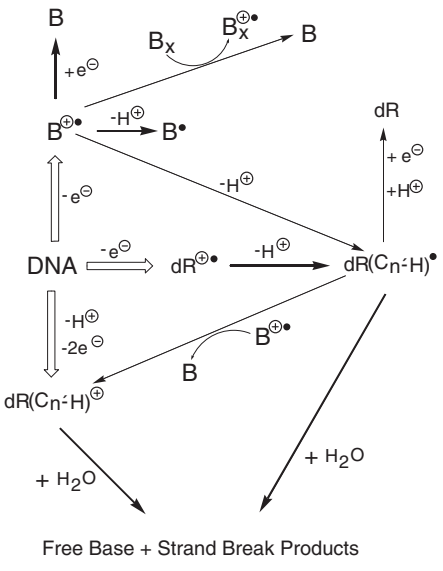


Chart 5.5 Chemical structures of selected base-damage products identified by gas chromatography/mass spectrometry-selective ion monitoring (*GC/MS-SIM*) technique [89].

Lam Research Ex. 1047 - Page 276
Lam Research Corp. v. Inpria Corp.
IPR2024-00033 - U.S. Patent No. 9,823,564



Scheme 5.18 Product formation by direct ionization of DNA at exposure to high-energy radiation. B, base; dR, deoxyribose [87].

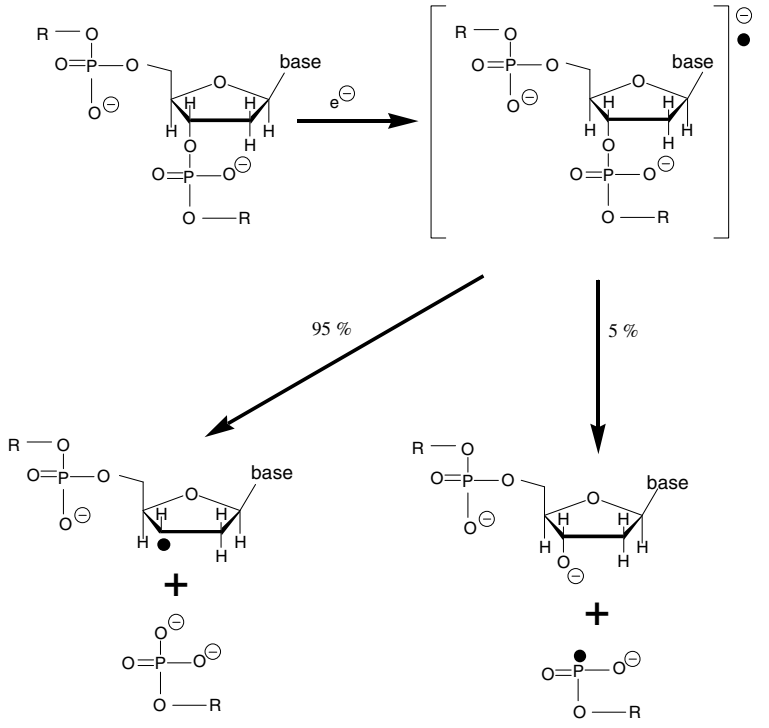
Mechanistic studies based on both ESR and product analysis have revealed the importance of hole and spin transfer in irradiated DNA. To a great extent, holes are transferred rapidly from adenine (A), cytosine (C) and thymine (T) base-cation radicals, and from sugar-phospate (*SP*)-backbone radical cations to guanine (G) sites, most preferably to codons containing three G moieties, so-called *GGG triplets*. Guanine sites have the lowest ionization potential, with about 78% of the initially formed electron-loss radicals ending up in G moieties and about 22% in backbone sites [90]. Electrons are captured at T and C moieties. Scheme 5.18 explains the primary reactions that occur in bulk DNA; these pertain to one-electron-loss processes at bases and backbone moieties, leading to base-radical cations ($B^{+\bullet}$) and deoxyribose-radical cations, $dR(C_{n'}\text{-}H)^{+\bullet}$. The latter are converted to deoxyribose radicals, $dR(C_{n'}\text{-}H)^{\bullet}$, by deprotonation. Deoxyribose carbocations, $dR(C_{n'}\text{-}H)^{+}$, are generated by spur reactions that involve the loss of two electrons and one proton. $dR(C_{n'}\text{-}H)^{\bullet}$ and $dR(C_{n'}\text{-}H)^{+}$ are converted to products when the irradiated specimen are dissolved in water.

Notably, sub-ionization low-energy electrons have been found to cause single-strand breaks in DNA, which is thought to be consistent with a dissociative electron-attachment mechanism, according to Scheme 5.19 [93,103].

5.4.3 Polysaccharides

When polysaccharides such as starch, cellulose, chitosan, amylose and dextran are subjected to high-energy radiation, a vast number of substances including

Lam Research Ex. 1047 - Page 277
Lam Research Corp. v. Inpria Corp.
IPR2024-00033 - U.S. Patent No. 9,823,564



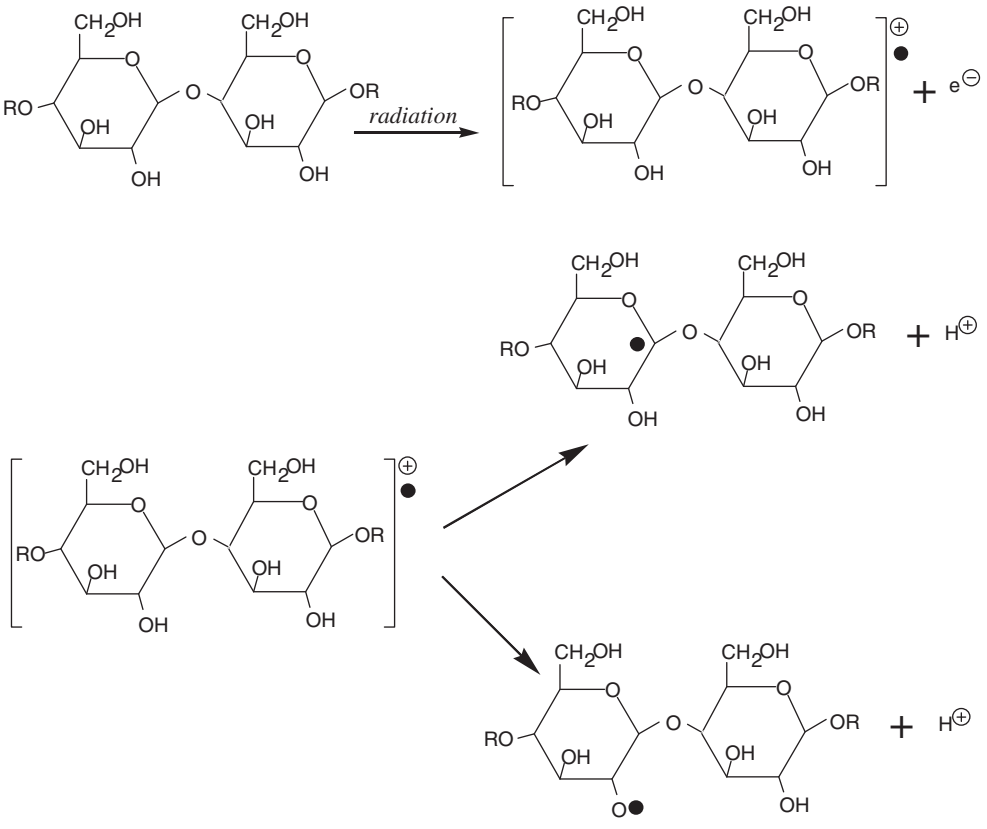
Scheme 5.19 Single-strand breakage in DNA caused by low-energy electrons [103].

gaseous materials such as H_2, CH_4, CO, CO_2, as well as other low-molar-mass substances such as water, formaldehyde, methanol, aldehydes, ketones and sugars, are produced [80,82,83,95,96]. The remaining polymer contains carbonyl, carboxyl and aldehyde functions. Moreover, the average molar mass is reduced due to the predominant main-chain cleavage which is most likely mainly caused by cleavage of the C—O—C glycoside linkages between base units [82,83,95,96].

When high-energy radiation is directly absorbed by polysaccharides, electronically excited moieties, radical cations and electrons are generated. To date, little is known of the mechanism of any subsequent processes leading to the formation of radiolysis products, but results obtained with low-molar-mass models have helped to provide an understanding to some extent of the radiation-induced chemical processes in polysaccharides [80,83]. Apparently, free-radical processes play an important role, as confirmed by ESR studies [83,95]. It is assumed that radical cations generated initially are rapidly transformed to free radicals by deprotonation, as illustrated in Scheme 5.20.

Typical free-radical reactions causing the radiation-induced cleavage of glycoside linkages are presented in Scheme 5.21 for the case of cellobiose. To some extent, fragmentation reactions might occur in the bulk of polysaccharides, whilst others

Lam Research Ex. 1047 - Page 278
Lam Research Corp. v. Inpria Corp.
IPR2024-00033 - U.S. Patent No. 9,823,564



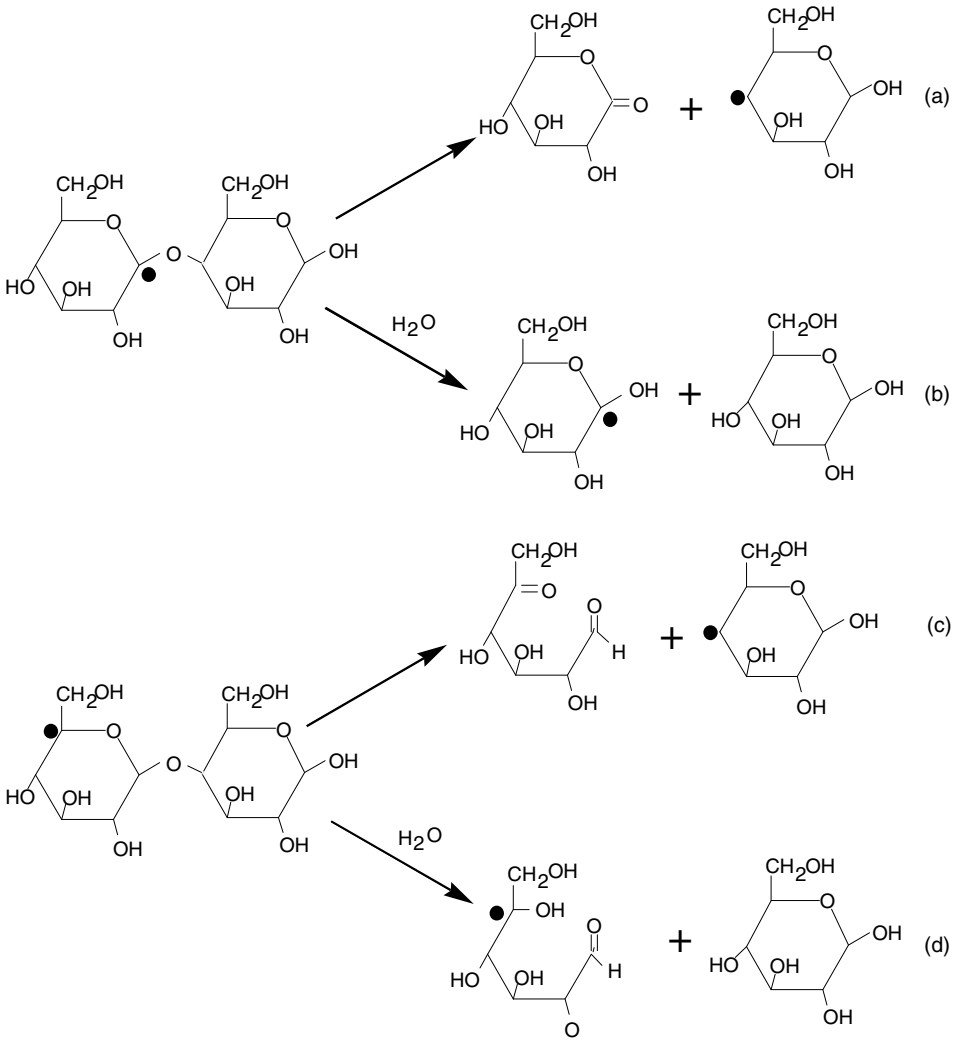
Scheme 5.20 Formation of free radicals in polysaccharide via deprotonation of radical cations.

might take place when the irradiated polymer is dissolved in water and buried radicals become accessible to the solvent. In this case, hydrolytic reactions (reactions (b) and (d) in Scheme 5.21) are feasible.

Prior to the formation of any final products, free radicals commonly undergo various transformations and reactions, both with intact moieties and other free radicals. The mechanisms of these processes have been proposed in the literature [80,83].

Radiation-induced main-chain degradation renders polysaccharides soluble, or at least increases their solubility, and therefore technical interests have focused on the radiation-induced main-chain degradation of certain biopolymers, such as cellulose, chitin and chitosan [96,104–107]. In being the main component of plants, cellulose is a widespread biopolymer. In technical processes, high-energy radiation treatment is applied to increase the solubility and to alleviate the hydrolysis of the constituent cellulose of plant-based raw materials. The G-values of the main radiolysis products, as reported by Ershov,

Lam Research Ex. 1047 - Page 279
Lam Research Corp. v. Inpria Corp.
IPR2024-00033 - U.S. Patent No. 9,823,564



Scheme 5.21 Decay of carbon-centered cellobiose radicals resulting in cleavage of glycoside linkages [83].

are listed in Table 5.6 [96]; these values correspond approximately to the material balance presented in Equation 5.10, according to which the yield of carbonyl groups is approximately equal to the scission yield, and each chain scission is accompanied by the formation of approximately one CO_2 molecule and one carbonyl group in the remaining polymer.

$$2G(H_2) = G(S) \approx G(\text{carbonyl}) \approx G(CO_2) + G(CO) \tag{5.10}$$

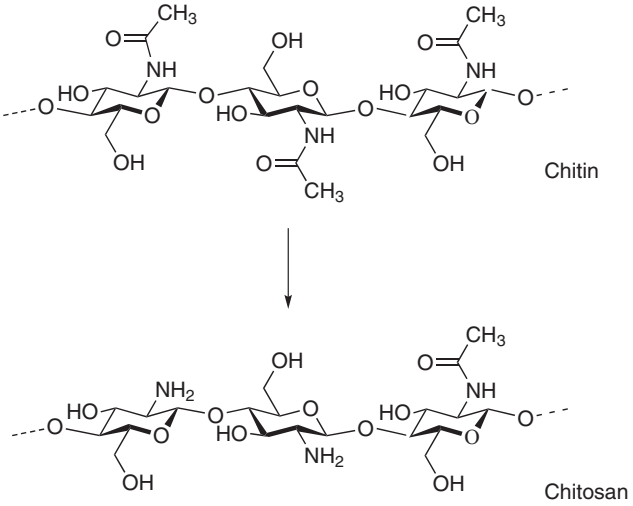
Lam Research Ex. 1047 - Page 280
Lam Research Corp. v. Inpria Corp.
IPR2024-00033 - U.S. Patent No. 9,823,564

Table 5.6 ^{60}Co-γ-ray-induced radiolysis of cellulose at room temperature in the absence of O_2. Data given are 100 eV yields (G-values) of products [96].

G(S)[a]	G(carbonyl)[b]	$G(H_2)$	$G(CO_2)$	G(CO)
6.0	6.5	3.2	6.0	0.9

a) Main-chain scission.
b) Carbonyl groups in irradiated polymer.

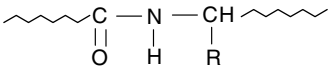
Chitosan, prepared by the alkaline N-deacetylation of chitin at 60 °C (Scheme 5.22), is converted by high-energy radiation to oligomers that dissolve readily in water. The oligomeric product is antibacterial, antifungal and blood-staunching, and has been applied to many different fields including medicine, pharmaceutics, agriculture, the textile- and paper-industries, and waste-water treatment [107]. The key advantage of the radiation degradation method, as compared to alternative methods such as chemical (oxidative) degradation, is its improved energy efficiency [15].



Scheme 5.22 Formation of chitosan by alkaline N-deacetylation.

5.4.4 Proteins

Proteins are copolymers composed of various amino-acid moieties of the general structure:



Lam Research Ex. 1047 - Page 281
Lam Research Corp. v. Inpria Corp.
IPR2024-00033 - U.S. Patent No. 9,823,564

where R denotes H (in glycine), CH_3 (in alanine), $(CH_2)_4NH_2$ (in lysine), and so on.

The most important chemical alterations that dry proteins undergo under the influence of high-energy radiation include main-chain cleavage in conjunction with the formation of amide groups, crosslinking and the formation of low-molar-mass products such as H_2, CO, and NH_3. Additional features are changes in conformation and the degree of crystallinity, as well as the inactivation of enzymes. Relatively little is known about the mechanism of the radiolytic events [84–86]. Holes – that is, radical cations – generated together with swift electrons in primary ionization acts, give rise to the formation of macroradicals and protons, probably after hole transfer. After thermalization, the ejected electrons add to sites of high electron-affinity, including cystine S—S bonds, peptide carbonyl groups, protonated amino groups (in lysine and arginine moieties) and aromatic side groups (in phenylalanine, tyrosine and tryptophan moieties). Typical reactions are shown in Scheme 5.23. The formation of free radicals in these cases has been revealed using ESR analyses [84].

Free-radical reactions bringing about the formation of CO and NH_3 are shown in Scheme 5.24.

It should be noted that the breakage of intra-chain disulfide linkages can be evidenced on the basis of electron density maps obtained with irradiated crystalline proteins by applying sophisticated X-ray diffraction methods [97]. In this way, it is possible to prove whether a radiation damage is truly nonspecific, as is usually presumed. Relevant studies with hen-egg-white lysozyme, a protein containing four intra-chain –S–S–linkages, revealed that such linkages can be discriminated with respect to damage susceptibility; that is, there is a specific order of cleavage, with Cys6–Cys127 being the most susceptible linkage.

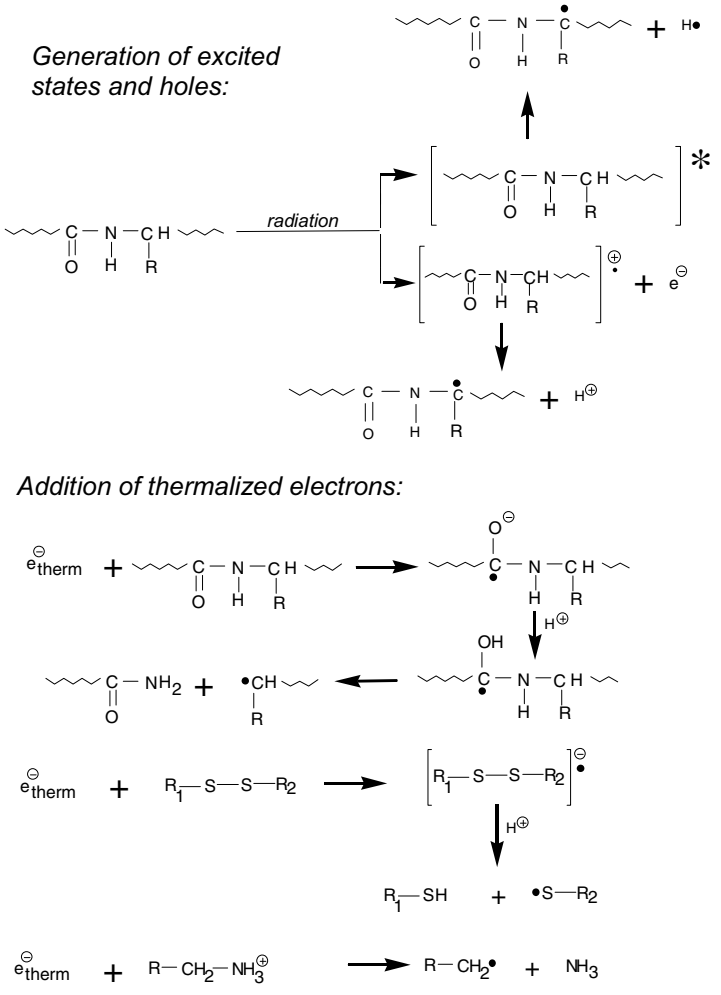
5.5
Radiolysis of Polymers in Solution

When polymers are irradiated in solution, both the polymer and the solvent will undergo radiolysis, and the portion of energy absorbed by each component will be proportional to its electron density fraction. Reactive species stemming from both polymer and solvent can interact in various manners; this is demonstrated in Scheme 5.25 which, for reasons of simplicity, is restricted to free-radical processes.

Commonly, the terms *direct* and *indirect effect* of radiation are used to discriminate between chemical transformations of the polymer that are related to the energy absorbed directly by the polymer and to the energy absorbed by the solvent, respectively.

Most synthetic polymers of the crosslinking type are crosslinked more effectively in solution than in the solid state. This is shown schematically in Figure 5.11, where D_{gel}, the dose for incipient gelation, is plotted versus the

Lam Research Ex. 1047 - Page 282
Lam Research Corp. v. Inpria Corp.
IPR2024-00033 - U.S. Patent No. 9,823,564

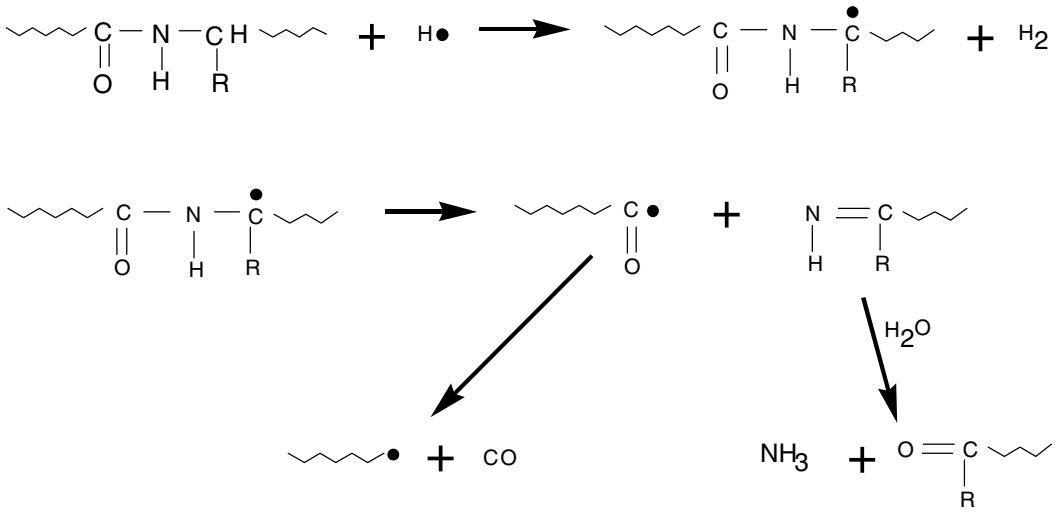


Scheme 5.23 Basic reactions occurring during the radiolysis of dry proteins.

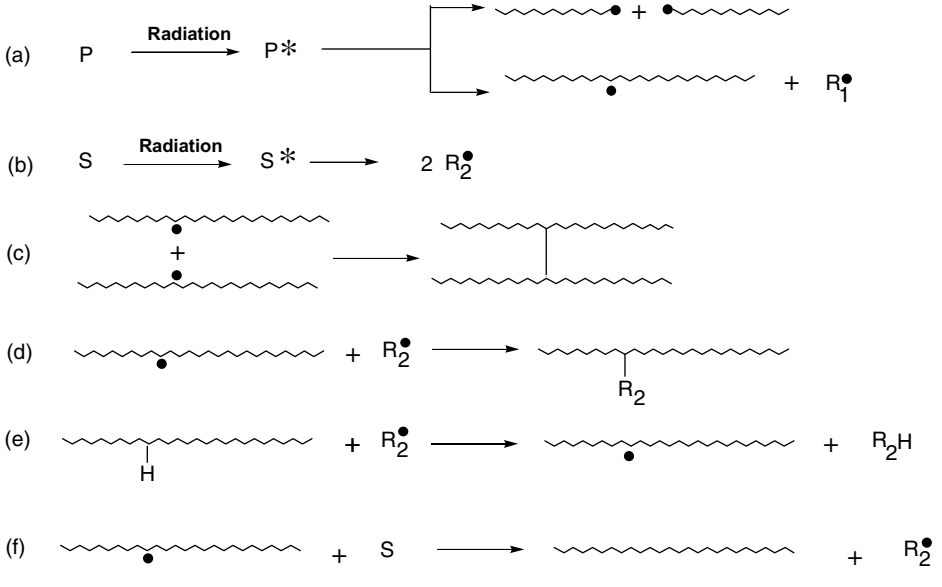
polymer concentration. D_{gel} is reciprocally proportional to G(X), the radiation chemical yield for crosslinking – that is, low values of D_{gel} correspond to high values of G(X).

In *organic solvents,* the increased crosslinking yields, when compared to the rigid state, are due mainly to an improved molecular mobility. While the coupling of free macroradicals is strongly restricted in rigid polymers, it becomes more probable in solution. Above a critical concentration c_{crit}, crosslinking in solution results in the formation of a macroscopic gel, which becomes visible after the absorbed dose exceeds the gel dose D_{gel}. However, below c_{crit} the macroradicals couple predominantly with radicals stemming from solvent

Lam Research Ex. 1047 - Page 283
Lam Research Corp. v. Inpria Corp.
IPR2024-00033 - U.S. Patent No. 9,823,564



Scheme 5.24 High-energy radiation-induced free-radical reactions in proteins resulting in the formation of CO and NH_3.



Scheme 5.25 Elementary free-radical processes occurring during the radiolysis of polymer solutions. P and S: polymer and solvent; P^* and S^*: electronically excited or ionized polymer and solvent molecules, respectively.

Lam Research Ex. 1047 - Page 284
Lam Research Corp. v. Inpria Corp.
IPR2024-00033 - U.S. Patent No. 9,823,564

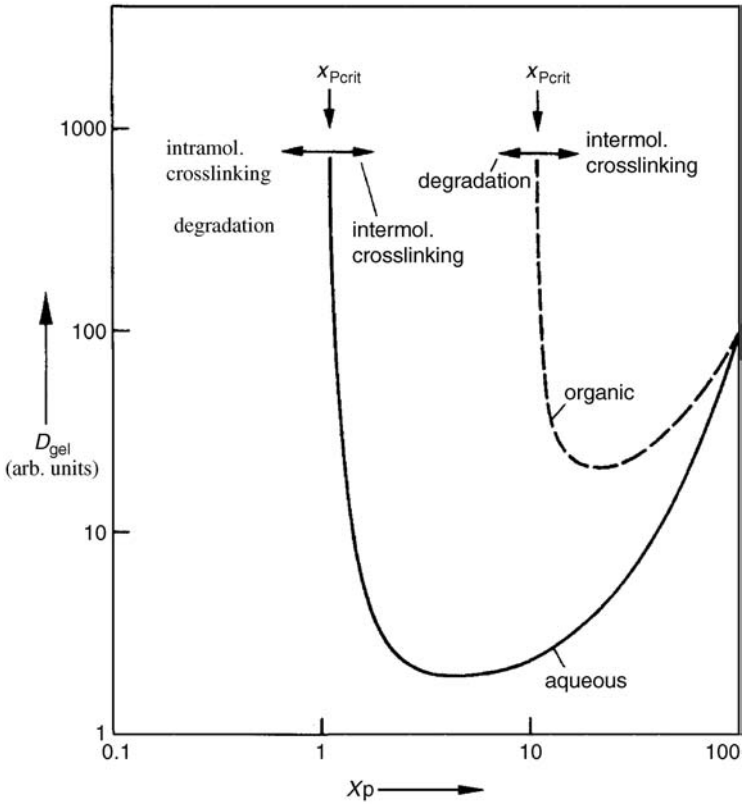


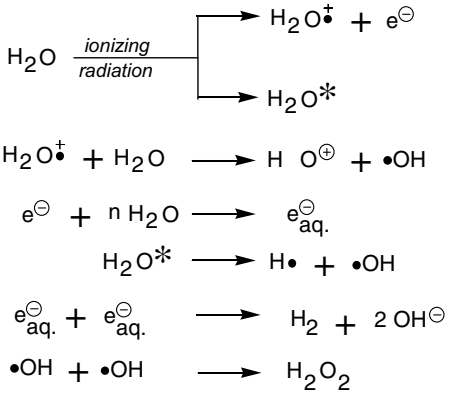
Figure 5.11 Schematic presentation of the dependence of D_{gel}, the dose for incipient gelation, on the polymer concentration x_P, expressed in terms of mole-fraction percentage. Adapted with permission from Ref. [108]; © 1966, Elsevier.

radiolysis. Moreover, main-chain scissions due either to the direct effect or to polymer attack by reactive solvent intermediates, can proceed unimpeded at polymer concentrations below c_{crit}.

In *aqueous solution*, the indirect action of radiation plays an important role, since the primary radiolysis products (Scheme 5.26) – that is, hydroxyl radicals, hydrogen atoms and hydrated electrons – are highly reactive. They are formed with $G(OH^{\bullet}) = 2.7$, $G(H^{\bullet}) = 0.55$, and $G(e^{-}_{aq.}) = 2.65$.

Rather than coupling with macroradicals, $OH^{\bullet}$, $H^{\bullet}$ and $e^{-}_{aq.}$ react with intact macromolecules. Moreover, $OH^{\bullet}$ and $H^{\bullet}$ abstract hydrogens, thus forming H_2O and H_2, respectively. Finally, they also add to unsaturations and aromatic groups. Generally, the reactivity of $OH^{\bullet}$ is much higher than that of $H^{\bullet}$, with the rate constants differing by one order of magnitude. Hydrated electrons add to functional groups of high electron affinity such as carbonyl, S—S, and aromatic groups.

Lam Research Ex. 1047 - Page 285
Lam Research Corp. v. Inpria Corp.
IPR2024-00033 - U.S. Patent No. 9,823,564



Scheme 5.26 Radiolysis of water. Formation of primary and secondary products.

In aqueous solutions saturated with N_2O, hydrated electrons are converted to hydroxyl radicals according to Equation 5.11. In this case, dissolved macromolecules may undergo chemical transformations, unperturbed by reactions of solvated electrons, that is, mainly due to the attack by OH radicals:

$$e_{aq}^- + N_2O \xrightarrow{H_2O} {}^{\bullet}OH + N_2 + OH^- \tag{5.11}$$

One frequently used technique relies on the conversion of OH to azide radicals, which takes place in aqueous solution containing sodium azide, NaN_3 (see Equation 5.12):

$$N_3^- + \bullet OH \rightarrow \bullet N_3 + OH^- \tag{5.12}$$

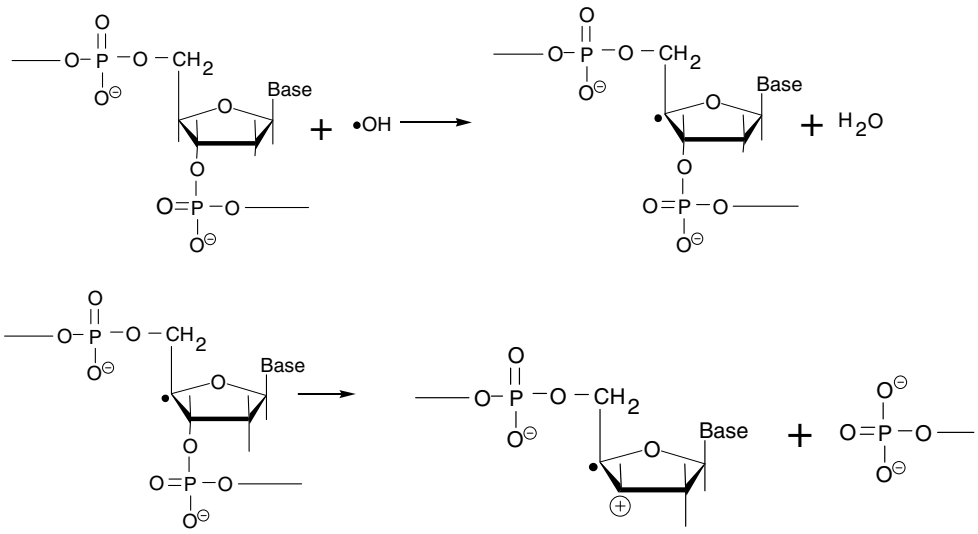
The azide radicals react selectively with certain amino acid residues of proteins including tryptophan, tyrosine and cysteine; this is especially advantageous when investigating the mechanism of reactions of free radicals formed from these residues.

All biological objects, including biological cells, contain water to different extents, and therefore the indirect radiation effect will play an important role in radiation biology. Typical cases relating to the radiolysis of biopolymers in aqueous solution include:

a) *Nucleic acids*: OH radicals interact with either the sugar phosphate by H-atom abstraction (ca. 20%) or by addition to the nucleobases (ca. 80%). H atoms and hydrated electrons react predominantly with the bases [81–94]. It is shown in Scheme 5.27 how OH radicals can attack DNA and cause main-chain cleavage of nucleic acids in aqueous solution.

   OH-radical attack on the sugar moieties with resultant backbone cleavage is a sensitive probe for the folding of nucleic acids. In fact, OH-induced backbone cleavage is predominantly dependent on the solvent accessibility of the

Lam Research Ex. 1047 - Page 286
Lam Research Corp. v. Inpria Corp.
IPR2024-00033 - U.S. Patent No. 9,823,564



Scheme 5.27 Main-chain cleavage of ribonucleic acid induced by OH-radical attack at the 4′-position.

phosphodiester backbone, and therefore the frequently present associated regions in nucleic acids are much less sensitive to OH-radical attack than are non-associated regions; that is, they are *protected* against OH attack. Taking advantage of this fact, folding pathways and rates can be studied by irradiating dilute aqueous solutions with synchrotron X-ray pulses of varying length [109,110]. Appropriate gel electrophoretic and mass spectrometric techniques are applied to analyze the fragments generated by nucleic acid cleavage. A high-resolution map of solvent accessibility obtained from the data leads to the desired information on folding pathways and rates. This method is referred to as s*ynchrotron X-ray foot printing*, and represents an approach to study time-resolved conformational changes of nucleic acids and protein–nucleic acid complexes. Typical studies in this area concern analyses of the Mg^{2+}-dependent folding of ribozyme RNA [111].

b) *Polysaccharides*: OH radicals can abstract hydrogen at every C—H bond of a regular polysaccharide (Chart 5.6), thus forming different carbon-centered free radicals as shown in Scheme 5.28.

The primary radical can undergo various reactions including rearrangement, fragmentation and elimination to yield a secondary radical [80,83]. Since the secondary radicals may undergo various different reactions, a vast number of products can principally be formed. Glycoside bond cleavage resulting in a reduction of the molar mass reportedly occurs mainly via β-scission and hydrolysis of C-1 radicals, as shown in Scheme 5.21 (reactions (a) and (b)) [80]. Scheme 5.29 presents an additional route involving C-2 radicals, that has been discussed recently [112].

Lam Research Ex. 1047 - Page 287
Lam Research Corp. v. Inpria Corp.
IPR2024-00033 - U.S. Patent No. 9,823,564

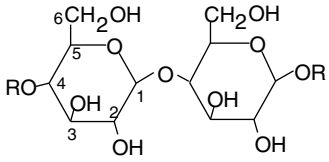
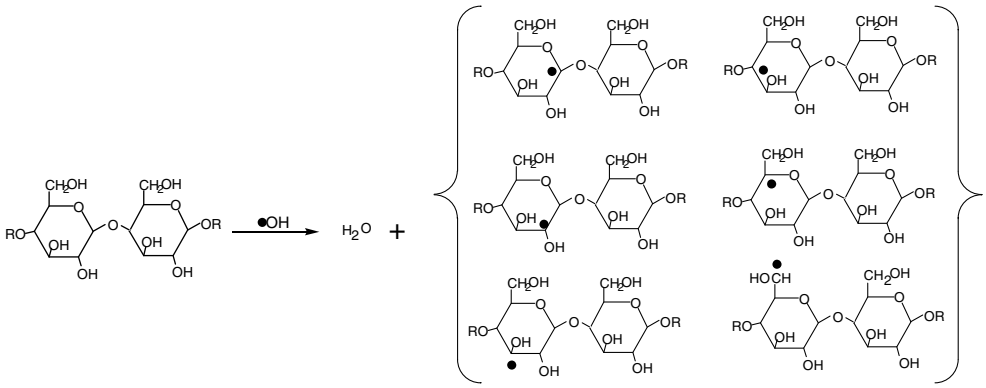
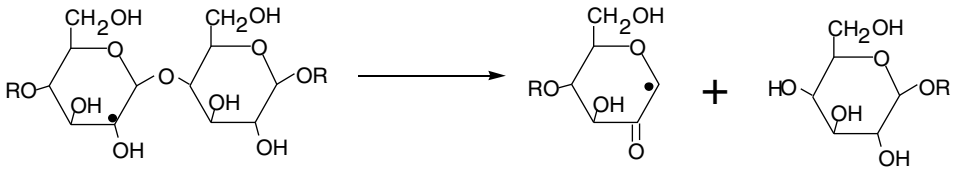


Chart 5.6 Chemical structure of a polysaccharide.



Scheme 5.28 Hydrogen abstraction from polysaccharides by OH radicals in aqueous solution.



Scheme 5.29 Radiolysis of polysaccharides in aqueous solution. Glycoside bond cleavage involving C-2 radicals.

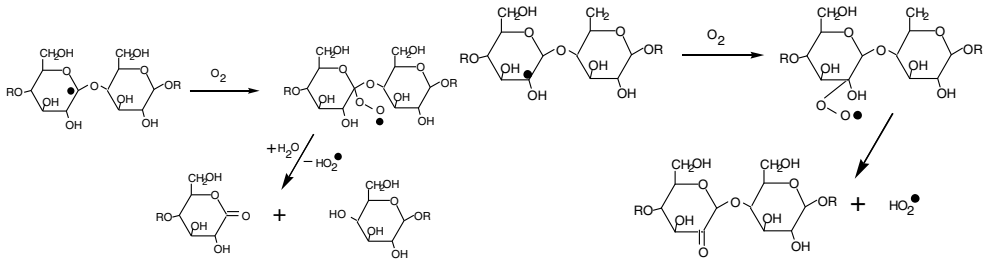
Chain scission in polysaccharides is prevented to a certain extent by molecular oxygen, as demonstrated for dextran in Table 5.7. Actually, the inhibitive action of O_2 may be related to glycoside bond-cleavage involving C-2-type radicals. When O_2 reacts with C-1-type radicals, it does not prevent glycoside bond cleavage, as can be seen from Scheme 5.30.

In the context with OH-radical attack of polysaccharides it is notable that cellulose derivatives bearing side groups, including carboxymethylcellulose, hydroxyethylcellulose and carboxymethyl starch (carboxymethyl amylopectin, carboxymethyl amylase), are predominantly intermolecularly crosslinked in aqueous solution (20–30 wt%), whereas they undergo predominantly

Lam Research Ex. 1047 - Page 288
Lam Research Corp. v. Inpria Corp.
IPR2024-00033 - U.S. Patent No. 9,823,564

Table 5.7 Radiolysis of dextran ($M = 1.15 \times 10^5$ g mol^{-1}) in aqueous solution (0.6%). G(S)-values for chain-scission [112].

Atmosphere	Ar	N_2O	O_2
G(S)	1.1	1.6	0.6



Scheme 5.30 Reaction of O_2 with carbon-centered polysaccharide radicals.

main-chain scission when they are irradiated in the solid state [113,114]. When OH radicals abstract hydrogens from the side groups of the polymer, macroradicals are generated that can couple and form crosslinks.

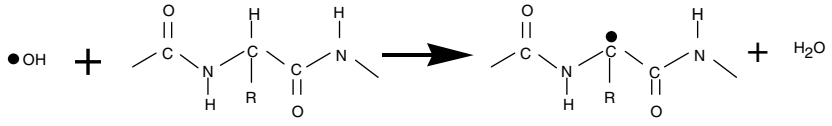
c) *Proteins*: OH radicals, H atoms and hydrated electrons react very rapidly with proteins, with rate constants on the order of 10^{10} to 10^{11} L mol^{-1} s^{-1}. Due to the given geometric structure of most proteins, the probability of a certain site to become attacked depends on its location. In other words, amino acid moieties situated in the inner part of a protein are less likely to be attacked by reactive species than are those in outer parts. OH radicals may abstract hydrogen from the backbone or side groups and add to aromatic rings or sulfur atoms, as shown in Scheme 5.31.

In proteins, hydrated electrons may react with carbonyl groups (ca. 80%), or with S—S bridges and the protonated imidazole ring of histidine (ca. 20%). In the case of redox proteins, hydrated electrons may react with the metal center. For example, the iron of the heme groups in cytochrome C is reduced from the ferric to the ferrous state. The reactions of H atoms are similar to those of either OH radicals or hydrated electrons. One interesting aspect of biological importance concerns crosslinking – that is, the dimerization and multi-merization of proteins in aqueous media. Mechanisms leading to crosslinking include the formation of intermolecular S—S bonds due to the oxidation of thiol groups, and the dimerization of tyrosine and phenylalanine residues (Scheme 5.32).

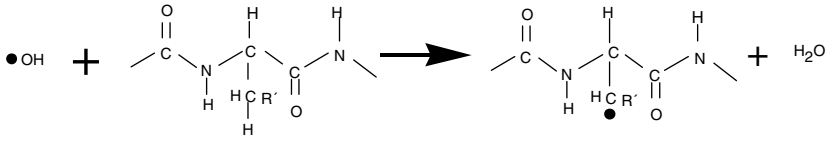
Another interesting topic concerning radiation-induced reactions in proteins in aqueous solution concerns *intramolecular long-distance electron transfer* in proteins [85,98,101]. Respective studies were performed using pulse radiolysis

Lam Research Ex. 1047 - Page 289
Lam Research Corp. v. Inpria Corp.
IPR2024-00033 - U.S. Patent No. 9,823,564

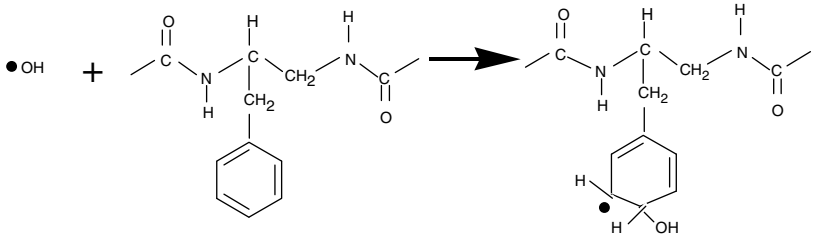
Hydrogen abstraction from backbone:



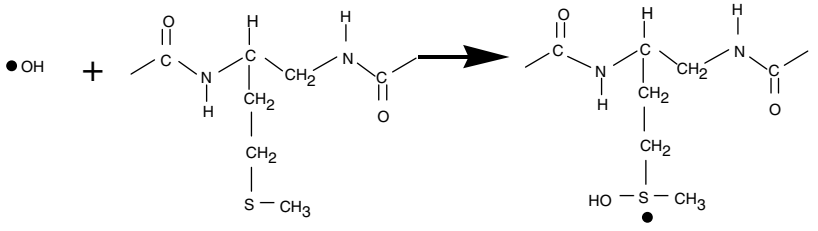
Hydrogen abstraction from side chain :



Addition to aromatic ring :



Addition to sulfur atoms :



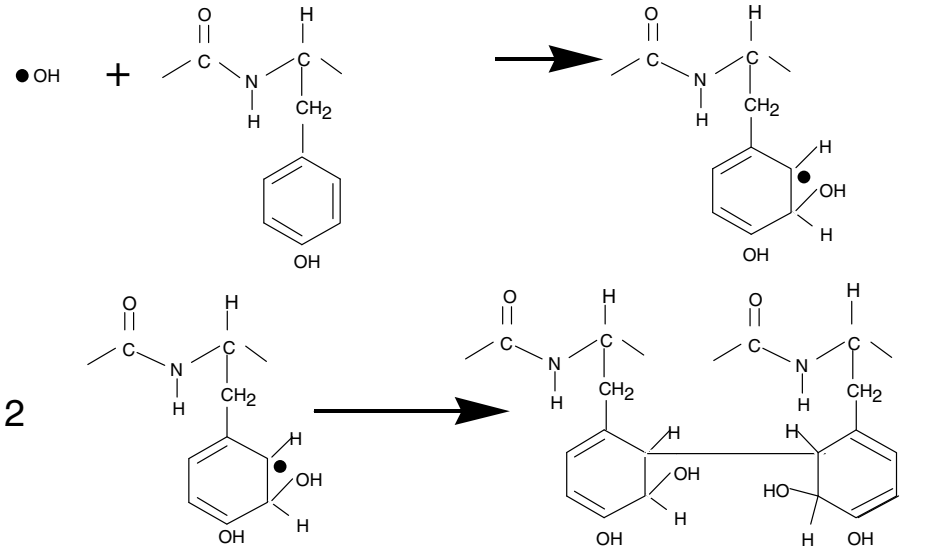
Scheme 5.31 Reactions of OH radicals with proteins.

experiments to demonstrate the efficiency of this powerful method. For example, tryptophyl radicals may be reduced by tyrosine residues, as shown in Scheme 5.33.

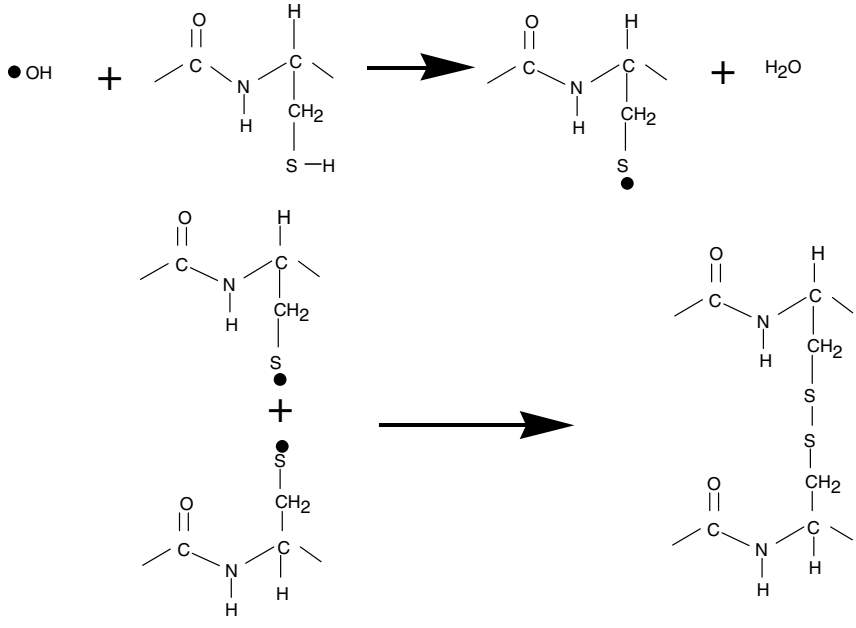
An intermediate complex is presumably formed in this process, as direct electron transfer can be ruled out [100]. Rate constants as determined by Prütz *et al.* [98] are $k_{ET} = 10^2\,s^{-1}$ for lysozyme and $k_{ET} = 2 \times 10^4\,s^{-1}$ for trypsin. Generally speaking, the initial damage to a particular amino-acid residue may migrate intramolecularly to another residue. Intramolecular electron transfer

Lam Research Ex. 1047 - Page 290
Lam Research Corp. v. Inpria Corp.
IPR2024-00033 - U.S. Patent No. 9,823,564

Coupling of tyrosyl-type radicals:



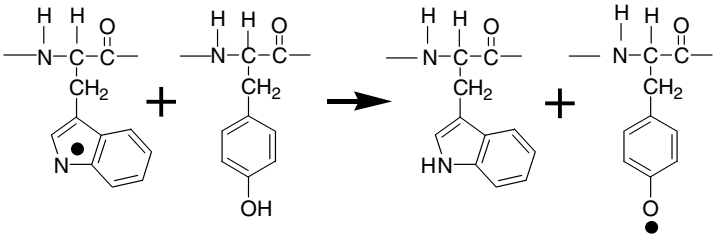
Formation of disulfide bridges :



Scheme 5.32 Radical-induced crosslinking of proteins.

Lam Research Ex. 1047 - Page 291
Lam Research Corp. v. Inpria Corp.
IPR2024-00033 - U.S. Patent No. 9,823,564

has also been proved for other couples of amino-acid residues, such as between those bearing aromatic and sulfur-containing groups [99]. Further information on this topic, which is of pronounced relevance to enzymology, is available from the literature [85,101].



Scheme 5.33 Intramolecular long-distance electron transfer between tryptophan and tyrosine residues in proteins.

The examples given above are restricted to certain basic aspects concerning the interaction of high-energy radiation with biopolymers in aqueous systems. Extensive information on this subject is available elsewhere [78,81,82,102].

5.6 Technical Developments

5.6.1 General Aspects

Technical processes using ionizing radiation have been widely applied to the field of polymers for many years [115–128]. Processes of commercial and industrial importance include the production of crosslinked wire insulation and of heat-shrink products (food wraps and tubing for electrical connections), the vulcanization of rubber tires and of rubber lattices, and the curing of coatings and inks. Some typical applications of high-energy radiation being used in technical processes are listed in Table 5.8. It should be recalled at this point, that fast electrons generated by accelerators produce similar chemical effects in polymers as do γ- and X-rays. Consequently, for most technical applications electron-beam irradiation is the preferred method because accelerators can be conveniently turned on and off, which is not possible with radioactive sources.

Radiation processing plays a major role in *nanotechnology* [118], as structures as small as 10 nm can be generated with the aid of electron beams, ion beams or X-rays. Ion-track-polymer membranes with track diameters between 10 and 100 nm (created by swift heavy ions penetrating the membrane) are used as

Lam Research Ex. 1047 - Page 292
Lam Research Corp. v. Inpria Corp.
IPR2024-00033 - U.S. Patent No. 9,823,564

Table 5.8 Applications of electron-beam and γ-radiation in technical processes.

Method	Principle	Characteristics
Crosslinking of linear polymers	Crosslinking of polymers lacking functional groups (such as polyethylene)	Established method in the wire and cable industry to improve properties such as strength and resistance to impact and stress cracking, creep resistance and often chemical resistance. Procedure to make highly shrinkable materials. Procedure to make crosslinked aqueous gels (hydrogels) by irradiating water-soluble polymers
Curing	Polymerization of reactive small molecules often in conjunction with crosslinking of oligomers	Commercially used in large scale for the production of improved coatings, lacquers and inks. Important for the production of special surface coatings and for printing in graphic arts and in packaging industries
Grafting	Attachment of side chains to a substrate polymer by radiation-induced polymerization of a monomer	Powerful method for modifying the properties of polymers and for making entirely new materials. Important for the introduction of polar groups in the bulk or at the surface of nonpolar polymeric materials to improve wettability and compatibility to specific coatings
Microdevice production, Microlithography	Generation of fine structures in polymer layers placed on an inorganic substrate by irradiation with X-rays or ion beams	Method for the production of electronic microdevices at the surface of inorganic substrates (silicon wafers). Computer-controlled ion beam lithography is used to make masks for photolithography
Main-chain degradation of polymers	Scissioning of linear polymers	Method applied to convert waste polymer material into low molecular weight compounds. Typically, waste poly(tetrafluoro ethylene) is converted to a material applicable as lubricant. Degraded chitin/chitosan is used in different fields including medicine, pharmaceuticals, textile and paper industries, waste-water treatment

Lam Research Ex. 1047 - Page 293
Lam Research Corp. v. Inpria Corp.
IPR2024-00033 - U.S. Patent No. 9,823,564

Table 5.9 Applications of high-energy radiation techniques in nanotechnology [118].

Method	Characteristics	Radiation
Generation of fine structures in polymer layers	Structures as small as 10 nm	X-ray, electron-beam, ion beam
Production of ion track membranes	Track diameters from 10 to 100 nm. Membranes can be used as templates for electroplating of nanowires	Heavy-ion beam
Production of nanoparticles	Metal nanoclusters are generated by radiation-induced reduction of metal ions within a polymer matrix (e.g., Ag clusters in poly(vinyl alcohol)	γ-ray, X-ray
Production of intercalated inorganic-organic nanocomposites	Molecular polymer layers are inserted into clay interlayers, where they are crosslinked by irradiation	γ-ray, X-ray
Surface grafting	Layers of 100 nm thickness are formed on polymer surfaces by irradiation and subsequent grafting of a monomer	X-ray, electron-beam

such or as templates for the electroplating of metal nanowires. These and other applications of high-energy radiation in nanotechnology are listed in Table 5.9.

5.6.2 Lithography

5.6.2.1 Introduction

The principle of the lithographic method to pattern surfaces of solids is described in Chapter 1 (Section 1.2.3.2), and illustrated in Figure 1.7, while optical lithography employing UV light is described at some length in Section 3.3.3. According to Equation 3.31a the minimum achievable feature size is directly proportional to the wavelength of the radiation, and therefore a reduction in wavelength proved to be the key strategy when following industry's roadmap for the miniaturization of electronic devices. Indeed, a significant enhancement in resolution was achieved with the migration to 248 nm, 193 nm, and 157 nm laser light. Moreover, because of the very short wavelength (see Tables 5.10 and 5.11), high-energy radiation possesses the potential to generate very small fine-line structures. As can be seen from a plethora of articles and books, extensive studies have focused on high-energy radiation lithography [129–147], and it is described in the following sections how extreme ultraviolet (*EUV*) light, X-rays or EB radiation can be technically applied to generate fine-line structures, and what types of resist are applicable in these cases. It might again be noted why EB radiation, in being a particle

Lam Research Ex. 1047 - Page 294
Lam Research Corp. v. Inpria Corp.
IPR2024-00033 - U.S. Patent No. 9,823,564

Table 5.10 Wavelength–energy correlation for photons.

	g-line	i-line	KrF	ArF	F_2	EUV	X-rays
Photon wavelength (nm)	436	365	248	193	157	13.5	1
Photon energy (eV)	2.84	3.40	5.00	6.42	7.90	91.8	1240

Table 5.11 Wavelength–energy correlation for electrons.

Electron wavelength (nm)	0.0708	0.0388	0.0173	0.0123	0.0078	0.0055	0.0039
Electron energy (keV)	0.3	1	5	10	25	50	100

radiation, is detailed in a book that is devoted to electromagnetic radiation. The reason is simply the fact that the polymer is affected by analogous chemical mechanisms, and differences exist only with respect to the primary absorption processes.

5.6.2.2 **Technical Performance**

Extreme Ultraviolet (EUV) Lithography Optical lithography using ArF lasers ($\lambda = 193$ nm), as discussed in Section 3.3.3.3, allows the high-volume production of devices with 45 nm structures [148]. A further size reduction became feasible with the advent of EUV light sources generating light of $\lambda = 13.5$ nm. Such sources are plasma-based, the plasmas being generated either by electrical gas discharges or by pulsed laser radiation [148]. EUV lithography is operated with imaging systems that are substantially different from those used in photolithography, as there is no material transmitting 13.5 nm light. However, projection optics – and particularly reduction optics – operating on the basis of reflection with all of the optical elements being mirrors have been developed [133,145]. Mirrors of reflectivity in the range of 60–70% are multilayer reflectors consisting of alternate 50- to 60-layer pairs of Mo and Si. The combination of high- and low-Z materials yields a small difference in refractive indices at each interface, and thus a fraction of 1.5–2% of the light penetrating to the lower layers will be reflected at each layer. EUV masks are similarly configured, that is, they are reflective masks. Materials used for absorber layers on top of the mask include Al, Cr, TaN, TaBN, and W. Schematic illustrations of a multilayer reflector and an EUV mask are presented in Figure 5.12.

Since all materials – including air – absorb EUV radiation, EUV lithography must be performed *in vacuo*. A schematic illustration of the optical layout of the EUV lithography system is shown in Figure 5.13.

Lam Research Ex. 1047 - Page 295
Lam Research Corp. v. Inpria Corp.
IPR2024-00033 - U.S. Patent No. 9,823,564

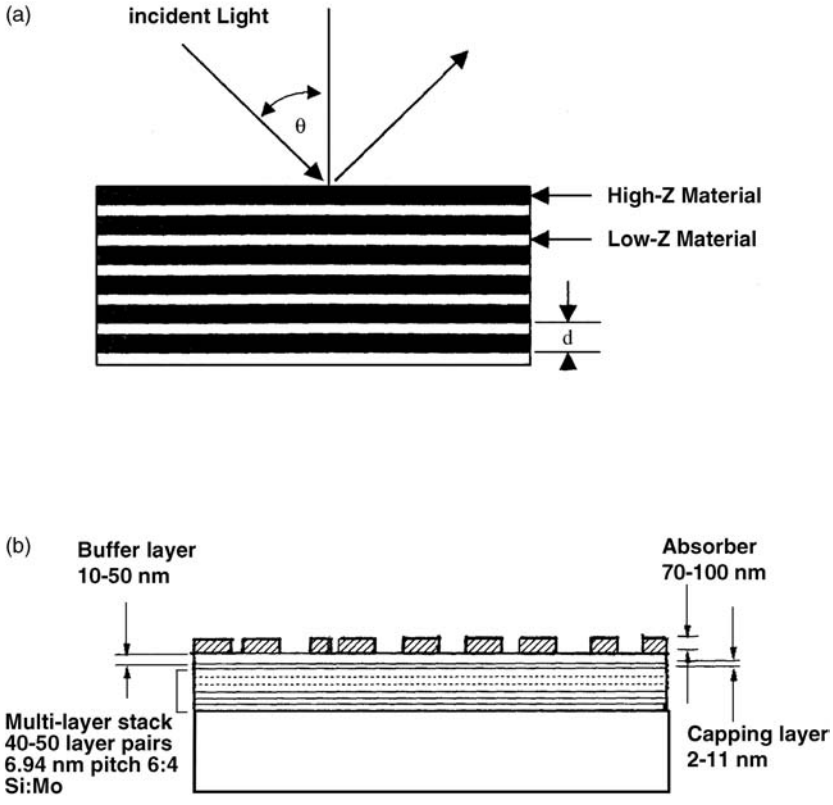


Figure 5.12 Schematic illustrations demonstrating the mode of action of (a) multilayer reflectors and (b) extreme ultraviolet (EUV) masks. (a) Adapted with permission from Ref. [133]; © 2011, SPIE Books; (b) Adapted with permission from Ref. [145]; © 2010, SPIE Books.

X-Ray Lithography Technical applications of X-ray lithography became of interest when electron synchrotrons, in being apt to generate high-intensity-X-ray beams and thus allowing rapid exposure, first entered operation. The use of a projection system is excluded in this case, because there are no image-forming lenses or mirrors applicable at X-ray wavelengths, and therefore there is no projection lithography, as in the case of photolithography. To date, all X-ray lithographic techniques that have been deployed operate in a 1 : 1 printing mode, which is also referred to as *proximity printing*. In this case, the X-rays illuminate a mask placed in close proximity (within a few micrometers) to a resist-coated wafer. The mask consists of an absorber pattern that is typically composed of gold or compounds of tantalum or tungsten, and is fixed onto a membrane, typically made of silicon carbide or diamond, that is transparent to X-rays.

Lam Research Ex. 1047 - Page 296
Lam Research Corp. v. Inpria Corp.
IPR2024-00033 - U.S. Patent No. 9,823,564

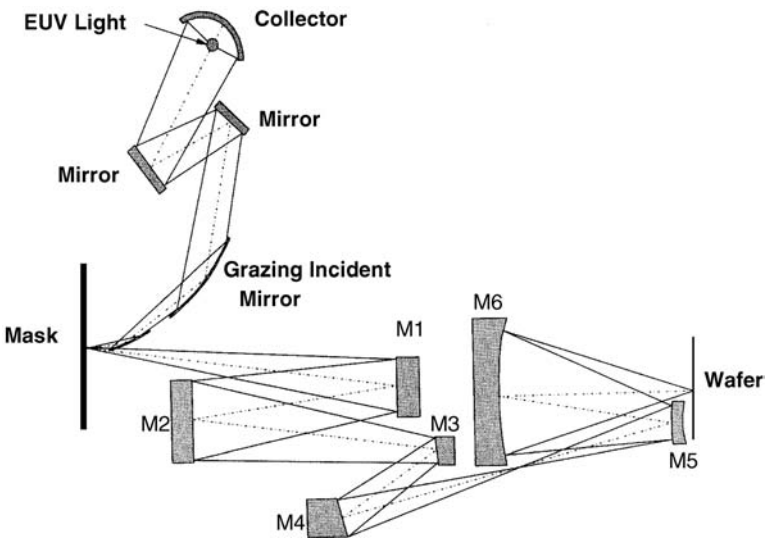


Figure 5.13 Optical layout of an extreme ultraviolet (EUV) lithography system. Adapted with permission from Ref. [145]; © 2010, SPIE Books.

In recent times, a novel lithographic method departing from the concept of fidelity in reproducing the mask pattern onto the wafer has been developed by Bourdillon and Vladimirsky [134]. This method, denoted as near-field X-ray lithography (*NFXrL*), relies on the fact that an X-ray beam passing through a small aperture or slit of the mask is diffracted (Fresnel diffraction); that is, the beam width varies and resumes a minimum diameter at a critical distance G_c from the mask located at the sweet spot. G_c depends on the width of the mask feature W and the wavelength λ, and can be also expressed in terms of the demagnification factor $M = W\,\omega^{-1}$, according to Equation 5.13:

$$G_c = \frac{W^2}{3\lambda} = \frac{\omega^2 M^2}{3\lambda} \tag{5.13}$$

where ω denotes the print feature size.

It follows, that the gap between mask and resist layer is increased in comparison with 1× exposure. For example, a demagnification factor $M = 3$ corresponds to a gap increase by a factor of nine.

If special conditions are observed – that is, a single development of the resist layer to a limited thickness and the employment of multiple exposures (Figure 5.14) – then an ultrahigh resolution beyond 25 nm can be achieved.

Electron Beam (EB) Lithography As a maskless imaging technique, EB lithography has the potential for very high resolution and to create images with an extremely large depth-of-focus. In EB lithography, the patterns are formed with the aid of a beam of high-energy electrons that is incident on a

Lam Research Ex. 1047 - Page 297
Lam Research Corp. v. Inpria Corp.
IPR2024-00033 - U.S. Patent No. 9,823,564

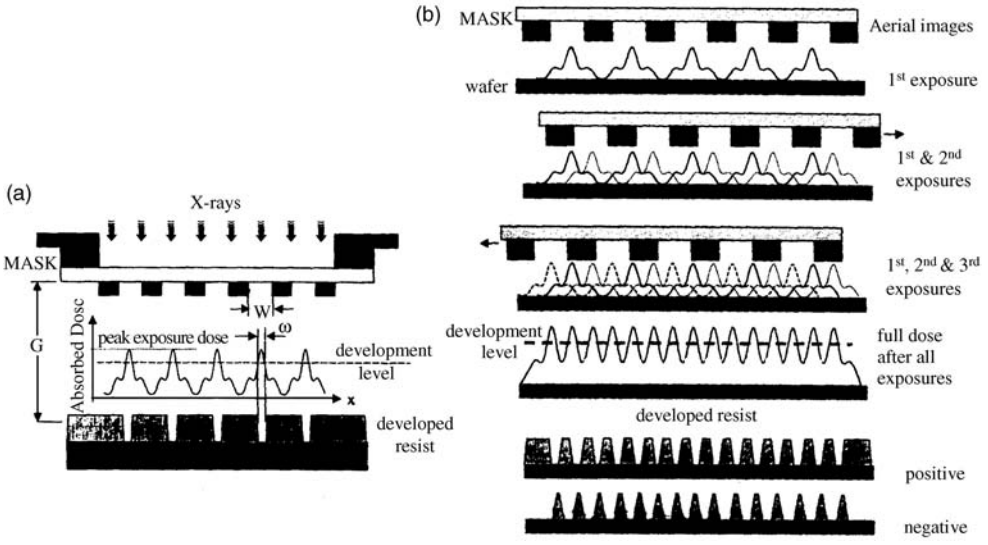


Figure 5.14 Near-field X-ray lithography. Schematic illustrations. (a) Method. The aerial image in the middle shows the absorbed dose in the resist. G, distance between mask and resist; ω: pattern width at the development level selected; W: width of the mask feature; (b) Feature formation in positive and negative resists by performing multiple sequential exposures with an X-ray stepper and subsequent single development. Adapted with permission from Ref. [134]; © 2006, Institute of Physics Publishing.

resist layer placed on top of a wafer. The beam is guided over the layer with the aid of a computer program, such that features as small as 10 nm can be produced [146]. Resolution-limiting effects for electron-direct-writing lithography include space-charge effects, imperfections in the electron optics, and scattering in the recording medium [145]. The initial expectations in replacing optical lithography with EB lithography were hampered by problems of achieving high production throughputs, yet today EB lithography is used commercially to directly write masks for photolithography. In order to circumvent the throughput problem, novel methods – referred to as *massively parallel E-beam maskless imaging* techniques – have been developed that include multiple electron optical columns or multibeam systems that allow high throughputs and yield a higher resolution and a larger depth-of-focus than can be achieved with 193 nm optical and 13.5 nm EUV lithography. For example, features of 45 nm half-pitch are generated with the aid of a writing scheme consisting of 13 000 beams distributed 150 μm apart over a 26×10 mm area [147]. Details on these interesting developments have been reported by Slot *et al.* [147] and by B. J. Lin [145].

Lam Research Ex. 1047 - Page 298
Lam Research Corp. v. Inpria Corp.
IPR2024-00033 - U.S. Patent No. 9,823,564

5.6.2.3 **Resists**

General Aspects As in photolithography, the basic principle of microstructure generation by high-energy radiation relies on the formation of a latent image during exposure, and its subsequent development. State-of-the-art techniques related to liquid development are based on the generation of differences in solubility between the exposed and unexposed regions of the resist. In polymeric resist materials, such differences can be achieved by main-chain cleavage or intermolecular crosslinking, by destruction or chemical alteration of a dissolution inhibitor, or by the generation of a catalyst that is capable of inducing chemical alterations in the resist material either during or after exposure by heating (post-exposure bake; PEB). The latter method – commonly referred to as *chemical amplification* – is most effective for practical applications which require, above all, a high radiation sensitivity. Currently, a vast number of publications is available describing the application of polymeric compounds as X-ray and EB resists [131,143,144], and some relevant studies are discussed in the following subsection. In fact, resist formulations applicable in conjunction with the chemical amplification method currently play a key role in industrial lithographic applications, and a part of this section is dedicated to this topic. Chemical amplification is of key importance for EUV lithography, and this topic is covered at the end of this section.

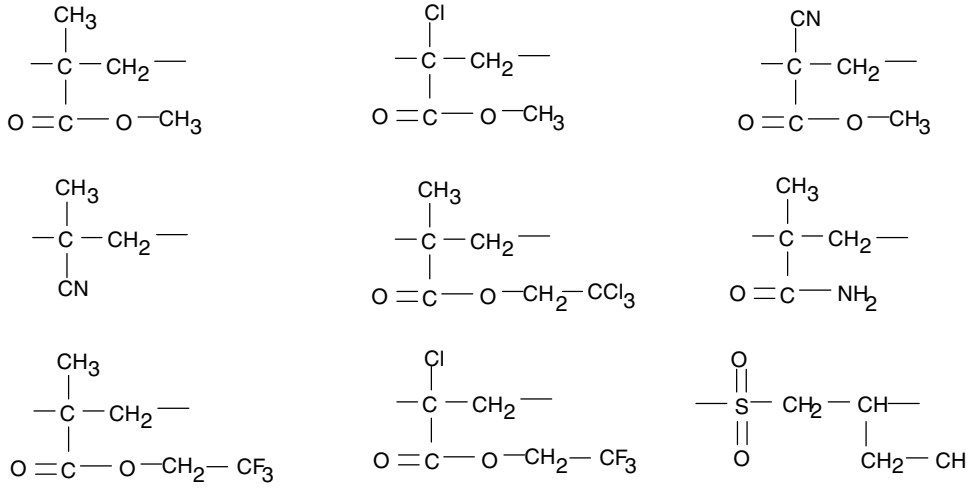
Classical X-Ray and EB Lithography Early studies performed on polymer resists for X-ray and EB lithography during the 1970s originated from the fact that there are two classes of linear polymer, depending on whether main-chain degradation or intermolecular crosslinking is the predominant chemical process upon irradiation (see Section 5.3). Main-chain scission causes a reduction, and crosslinking an increase, in molar mass, with the consequence of an increased or decreased solubility of the irradiated resist areas in a solvent. Therefore, the post-irradiation liquid development of latent structures results in positive-tone or negative-tone imaging, respectively. PMMA and polystyrene, which represent these two classes of linear polymer, achieved parent status with respect to positive-tone and negative-tone lithography, but it soon emerged that these parent substances did not fulfill the resist requirements satisfactorily, and consequently improvements were attempted by synthesizing derivatives. Details on these studies have been reported elsewhere [131,132]. The chemical structures of typical homo- and copolymers, the imaging applicability of which were tested, are shown in Charts 5.7 and 5.8.

The radiation sensitivity of negative-tone resists can be increased with the aid of crosslinking boosters, for example, by adding 20 wt% trimethylolpropane trimethacrylate (TPTM) or dipentaerythrityl pentaacrylate (DPEPA) (Chart 5.9) to polychloromethylstyrene [149].

Another chemical strategy for microstructure generation is related to the dissolution inhibitor principle, whereby a polymeric matrix is rendered insoluble in a certain solvent by admixing with a particular compound.

Lam Research Ex. 1047 - Page 299
Lam Research Corp. v. Inpria Corp.
IPR2024-00033 - U.S. Patent No. 9,823,564

Monomer units in homopolymers:



Monomer units in copolymers with methyl methacrylate:

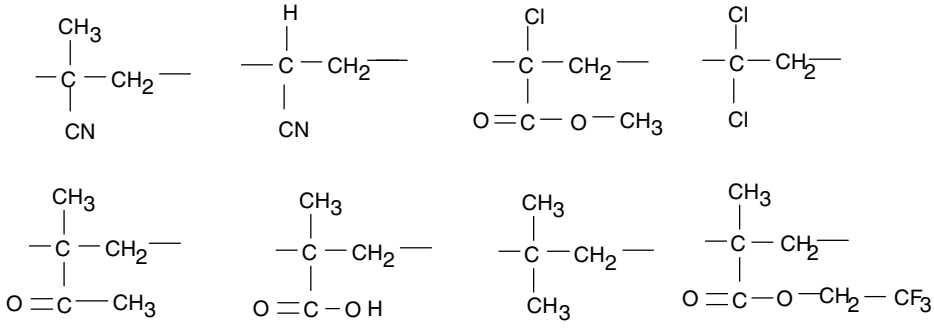


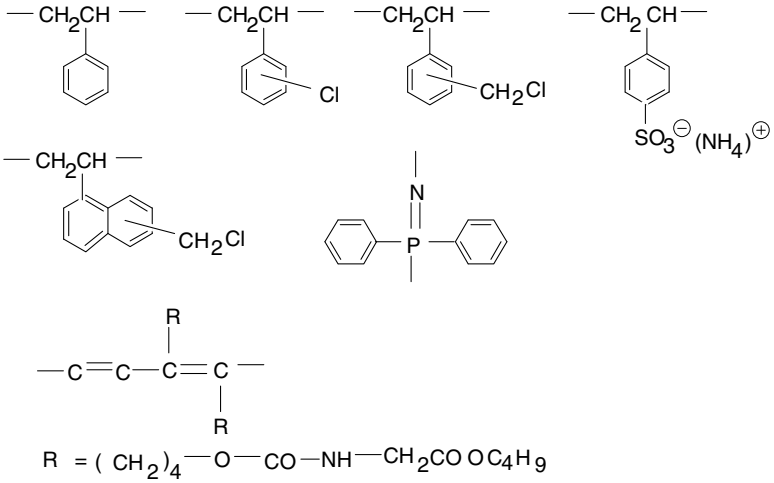
Chart 5.7 Chemical structure of polymers and copolymers applied as positive-tone resists.

Radiation-induced decomposition or chemical alteration of the dissolution inhibitor restores the solubility of the polymeric matrix. For example, certain polysulfones and polyaldehydes (for general structures, see Chart 5.10) will act as dissolution inhibitors when blended with phenol formaldehyde or cresol formaldehyde resins.

It emerged that several resist formulations which have proved to provide excellent fine line structures are applicable for mask generation (see further below in this section), although the radiation sensitivity was not sufficiently high to permit other applications.

Lam Research Ex. 1047 - Page 300
Lam Research Corp. v. Inpria Corp.
IPR2024-00033 - U.S. Patent No. 9,823,564

Homopolymers :



Copolymer :

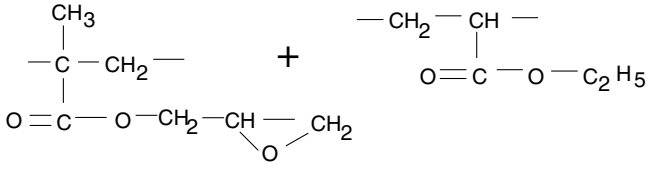


Chart 5.8 Chemical structures of polymers applied as negative-tone resists.

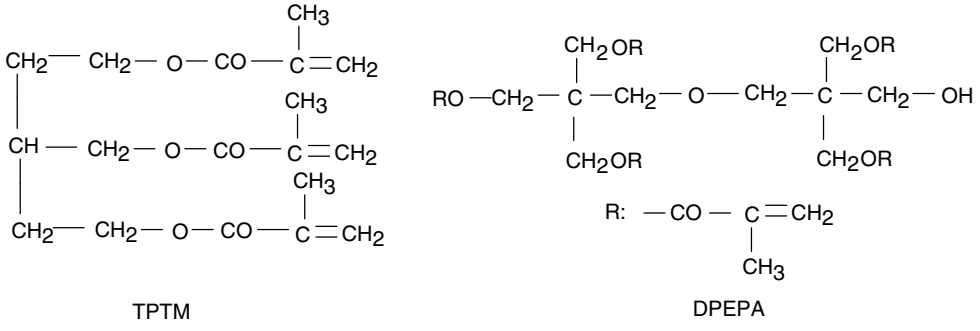


Chart 5.9 Chemical structures of crosslinking boosters.

Chemical Amplification All resists must comply with numerous additional requirements, referring among others to radiation sensitivity, resolution, contrast, aspect ratio, line edge roughness (*LER*), heat resistance, and shelf-life. With regards to the large-volume fabrication of microdevices, *chemical*

Lam Research Ex. 1047 - Page 301
Lam Research Corp. v. Inpria Corp.
IPR2024-00033 - U.S. Patent No. 9,823,564

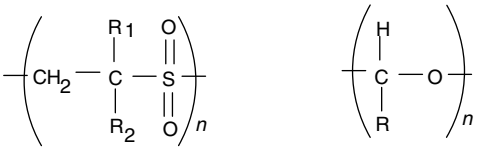
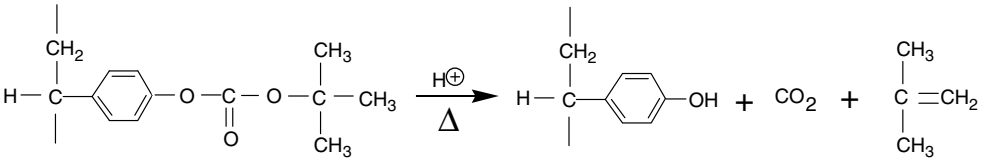


Chart 5.10 Chemical structures of polymeric dissolution inhibitors for novolak resins.

amplification functioning on the basis of radiation-induced acid generation (see Section 3.3.3) was found to meet the key requirement of high radiation sensitivity best for EUV, X-ray, and EB resists. Notably, this method does not demand high radiation-chemical yields (G-values) nor sophisticated development procedures. Currently, three classes of acid-catalyzed processes have been identified that play important roles in high-energy-radiation lithography, namely deprotection, crosslinking, and depolymerization. Moreover, the dissolution–inhibitor principle has been adopted in conjunction with chemical amplification.

Deprotection involves the decomposition of functional groups attached to the backbone of linear polymers, while the acid-catalyzed release of protecting groups renders the resist soluble in an appropriate solvent. The mechanism of acid-catalyzed deprotection of poly(*t*-butoxycarbonyloxystyrene) (PBOCST), the classical *t*BOC resist, is presented in Scheme 5.34 [146]. Decomposition of the protecting groups by post-exposure baking at about 100 °C converts the initially lipophilic polymer to a hydrophilic polymer, which in turn permits development in an aqueous basic solution (typically industrially applied 0.26 N tetramethyl ammonium hydroxide; TMAH).

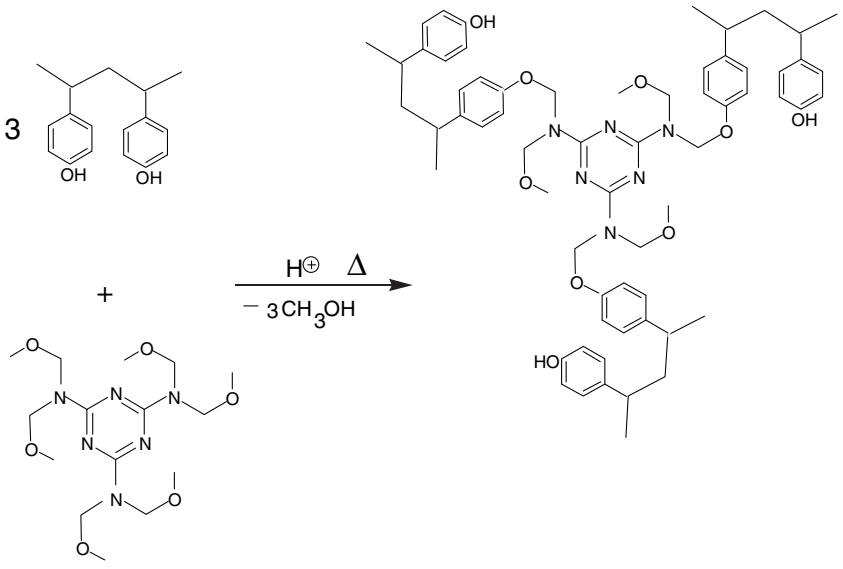


Scheme 5.34 Acid-catalyzed deprotection of poly(*t*-butoxycarbonyloxystyrene).

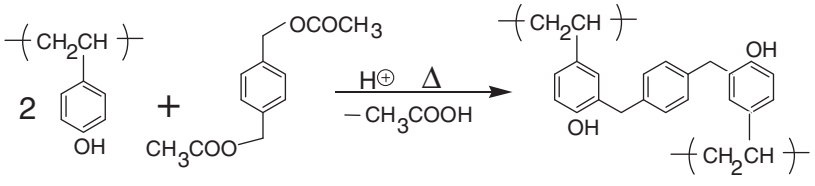
Crosslinking (for negative imaging) can be achieved through various acid-catalyzed reactions, including condensation, electrophilic substitution, and cationic polymerization. Schemes 5.35 and 5.36 present typical examples of the crosslinking of poly-4-hydroxystyrene by condensation and electrophilic substitution, respectively.

Other phenolic polymers such as novolak resins (Chart 5.11) can also be crosslinked using these methods, resulting in the formation of insoluble polymer

Lam Research Ex. 1047 - Page 302
Lam Research Corp. v. Inpria Corp.
IPR2024-00033 - U.S. Patent No. 9,823,564



Scheme 5.35 Crosslinking of poly-4-hydroxystyrene by acid-catalyzed condensation with a hexamethylolmelamine.



Scheme 5.36 Acid-catalyzed electrophilic substitution. Crosslinking of poly-4-hydroxystyrene with the aid of 1,4-di(acetoxymethyl)benzene.

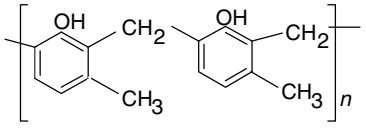


Chart 5.11 Chemical structure of a typical aqueous base-soluble novolak resin.

networks that are three-dimensionally chemically connected – that is, the respective resist formulations exhibit a negative-tone behavior.

Polymers carrying epoxide side groups (Chart 5.12) can be transformed into intermolecularly crosslinked networks by acid-catalyzed polymerization of the epoxide groups. Formulations comprised of commercially available epoxide resins and an acid generator have been employed in lithography [150].

Lam Research Ex. 1047 - Page 303
Lam Research Corp. v. Inpria Corp.
IPR2024-00033 - U.S. Patent No. 9,823,564

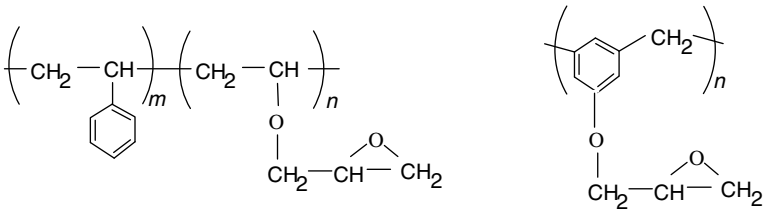
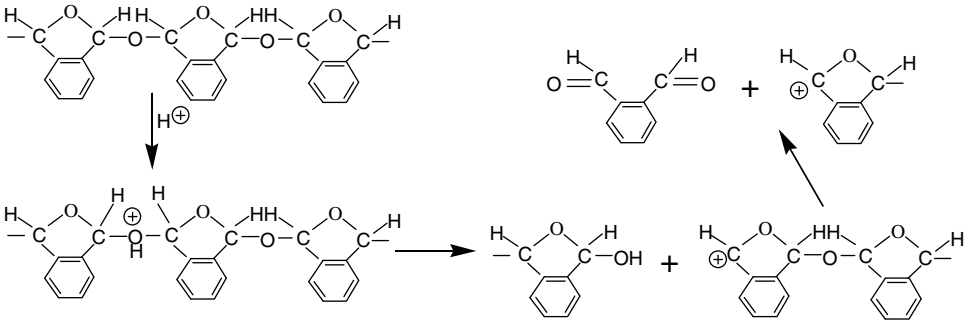


Chart 5.12 Chemical structures of epoxy resins.

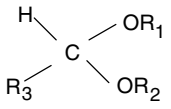
The *depolymerization* of thermodynamically labile polymers stabilized by end-capping is induced when chemical bonds are cleaved either at the end-caps or in the main chain. This behavior is exhibited by polyacetals and polyaldehydes possessing a very low ceiling temperature. Scheme 5.37 shows the acid-initiated depolymerization of poly(phthalic aldehyde) (PPA). In terms of kinetics, depolymerization is a chain reaction whereby each single proton initiates the formation of a large number of phthalaldehyde molecules. At concentrations <10 wt%, PPA is miscible with cresol-formaldehyde novolak resins, and inhibits the dissolution of blends in aqueous alkaline solution. Resist formulations of a novolak containing PAA and a sulfonium salt become soluble upon exposure to EB radiation. The sensitivity amounts to $S(EB) = 1\,\mu C\,cm^{-2}$, where S is defined in analogy to photolithography (see Section 3.3.3.1 and Figure 3.20).



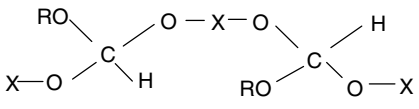
Scheme 5.37 Proton-initiated catalyzed depolymerization of poly(phthalic aldehyde).

Depolymerization occurring in exposed resist areas either causes or increases solubility. Both, X-ray and EB resists operating on the basis of the *dissolution inhibitor principle* in conjunction with acid amplification, have been commercialized, and sensitivity values $S(EB) = 9\,\mu C\,cm^{-2}$ and $S(X) = 10–30\,mJ\,cm^{-2}$ have been obtained with formulations containing a novolak resin, an acetal (AC) or orthoester (OE) as dissolution inhibitor and trichloromethyltriazine or tetrabromobisphenol as acid generators (Chart 5.13) [151a,b]. Here, S(EB) and S(X) are related to EB and X-ray radiation, respectively.

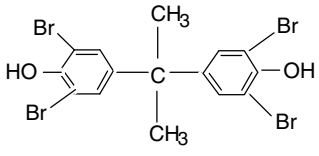
Lam Research Ex. 1047 - Page 304
Lam Research Corp. v. Inpria Corp.
IPR2024-00033 - U.S. Patent No. 9,823,564



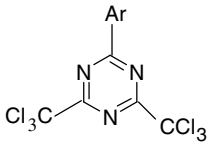
AC



OE



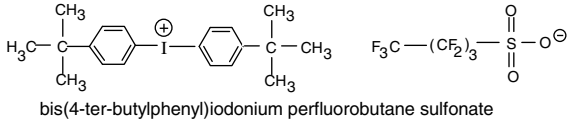
Tetrabromobisphenol A



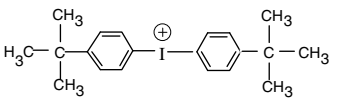
2-Aryl-4,6-bis(trichloromethyl)-1,3,5-triazine

Chart 5.13 Chemical structures of compounds used in acid-amplified resist formulations operating on the basis of the dissolution inhibitor principle.

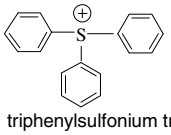
Finally, it has to be discussed why certain chemically amplified resists (*CARs*), that are applied successfully in photolithography and function on the basis of radiation-induced acid generation, are applicable also in high-energy radiation lithography. Sulfonium and iodonium salts, such as those presented in Chart 5.14, are typical acid generators in this context.

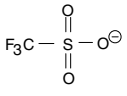


bis(4-ter-butylphenyl)iodonium perfluorobutane sulfonate



bis(4-ter-butylphenyl)iodonium perfluorooctane sulfonate





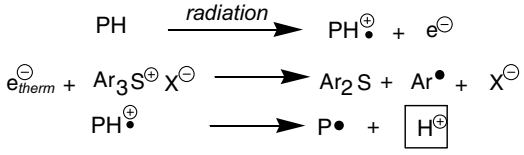
triphenylsulfonium trifluoromethane sulfonate

Chart 5.14 Chemical structures of typical sulfonium and iodonium salts used in X-ray and electron beam resist formulations.

These compounds play a different role in EB or X-ray resists compared to photoresists. Because, in being nonselective, the absorption of high-energy radiation is proportional to the electron density fraction of the components, the matrix material of the resist formulation absorbs almost all, and the small amount of acid generator only an almost negligible fraction of the total absorbed energy. On the other hand, the acid generator concentration is sufficiently high to scavenge thermalized secondary electrons generated by absorption in the matrix material, thus preventing the neutralization of radical cations and allowing them to release

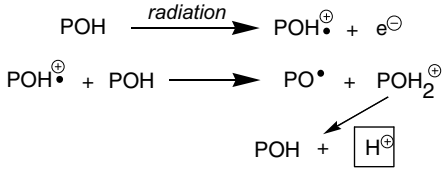
Lam Research Ex. 1047 - Page 305
Lam Research Corp. v. Inpria Corp.
IPR2024-00033 - U.S. Patent No. 9,823,564

protons by *deprotonation*. A mechanism involving a triaryl sulfonium salt as acid generator is shown in Scheme 5.38.



Scheme 5.38 Generation of protonic acid in resist matrix PH containing an triaryl sulfonium salt $Ar_3S^+X^-$ as acid generator [152,153].

Protons may be generated also by ion–molecule reactions of radical cations with surrounding intact macromolecules. This is shown schematically in Scheme 5.39 for the case of 4-hydroxystyrene moieties contained in poly-4-hydroxystyrene. In this context it is notable that protons can be generated only from nonprotected and not from protected 4-hydroxystyrene moieties [152,153].



Scheme 5.39 Generation of protonic acid via ion molecule reactions in POH, poly-4-hydroxystyrene [152,153].

Practical Applications of X-Ray and EB Resists Today, EB lithography is applied industrially as the primary tool of choice for fabricating masks for other lithographies, and occasionally it is also used for the production of special microdevices. Commercially available resists that can be used for mask making are listed in Table 5.12.

One remarkable application is a lithographic microtechnical fabrication process denoted as LIGA, which is a German acronym for Lithographie, Galvanoformung (electroplating), Abformung (molding) [122,161]. LIGA is used to fabricate microdevices including microscopic motors, sensors and actuators. In the process, an X-ray-sensitive polymer resist, typically PMMA, is cast onto an electrically conductive substrate and exposed to a parallel X-ray beam generated by an electron synchrotron through a mask consisting of X-ray-absorbing material. Subsequent removal of the exposed areas through solvent development results in a three-dimensional structure, which can be

Lam Research Ex. 1047 - Page 306
Lam Research Corp. v. Inpria Corp.
IPR2024-00033 - U.S. Patent No. 9,823,564

Table 5.12 Commercially available EB resists [160].

Resist		Tone	Resolution (nm)	Sensitivity ($\mu C\,cm^{-2}$)
PMMA	Poly(methyl methacrylate)	Positive	10	100
EBR	Poly(2,2,2-trifluoroethyl-chloroacrylate)	Positive	200	10
PBS	Poly(butene-1 sulfone)	Positive	250	1
ZEP	Alternating copolymer: α-chloromethacrylate and α-methylstyrene	Positive	10	30
AZ 5206		Positive	250	6
COP	Copolymer: glycidyl methacrylate and ethylacrylate	Negative	1000	0.3
SAL 606	Novolak matrix containing acid generator and crosslinking agent	Negative	100	8.4

used as template in a step involving the galvanic deposition of metal. In this way, rather thick microstructures with a very high aspect ratio (e.g., height >300 μm at 4 μm wall thickness) can be created. The resist is then chemically stripped away to produce a metallic mold that can be used to fabricate multiple plastic micro parts by injection molding, resin casting, or hot embolding. These plastic parts can also serve as "lost forms" for the production of ceramic micro parts.

EUV Resists Certain polymer formulations of the types used for KrF and ArF photolithography are capable also of serving as EUV resists (for chemical structures, see Sections 3.3.3.2 and 3.3.3.3) [130]. This pertains, for instance, to copolymers containing alicyclic groups and fluorine atoms (Chart 5.15).

The strong attenuation of the EUV radiation by organic materials (see Section 4.2) may be a serious problem with regards to the required total penetration of the resist layer, although this situation can be overcome by

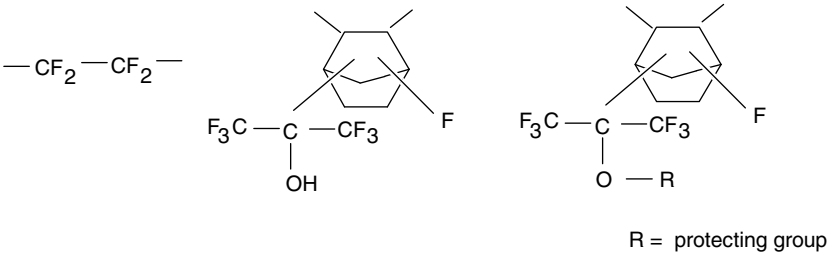


Chart 5.15 Chemical structure of copolymer units used for EUV resist formulations.

Lam Research Ex. 1047 - Page 307
Lam Research Corp. v. Inpria Corp.
IPR2024-00033 - U.S. Patent No. 9,823,564

applying thin resist layers. By using an ESCAP resist material (see Chart 3.16) at a film thickness of 1174 Å, 70 nm features were obtained at an exposure dose of 6–7 mJ cm^{-2} [154]. In this way, 26 nm dense lines have been printed using an 80 nm-thick resist layer [155]. A high sensitivity is attained with the aid of acid-amplified resists, though any image blur caused by acid diffusion into unexposed areas of the resist leads to high values of LER, and this is an important problem when generating fine line features in the sub-100 nm region. Moreover, image blur can only be limited but not eliminated. Both, LER and resolution can be significantly improved by enhancing the rate of diffusion of the acid generated in the exposed resist areas [156]. This can be achieved with a resist material consisting of star-shaped polymers with an acid-cleavable core unit and linear polymer arms with partially protected side groups. The radiation-generated acid may act in two ways: (1) the core units may decompose, causing a significant reduction in the molar mass and simultaneously promoting acid diffusion; and (2) the labile side groups of the arms may be cleaved, causing the resist material to become soluble in alkaline developers. The latter method has been used successfully to generate 30 nm patterns with the aid of formulations containing star-shaped polymers of the type shown in Chart 5.16 [157].

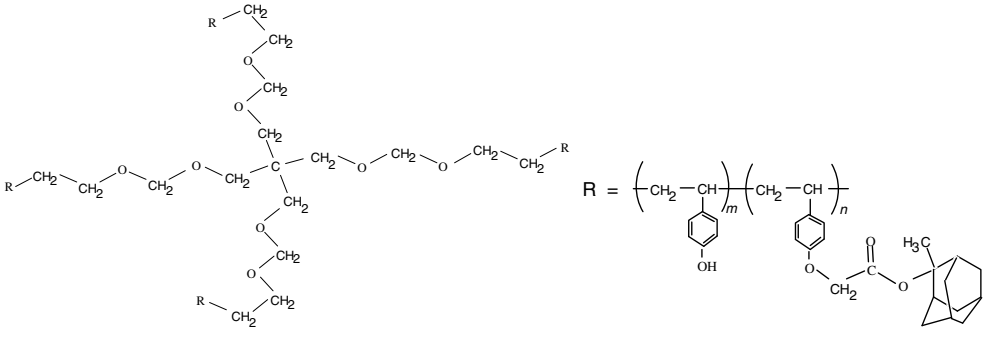


Chart 5.16 Chemical structures of a main-chain degradable star-shaped polymer applicable in EUV lithography [157].

Another approach to controlling acid diffusion involves the use of linear polymers with chemically bound acid generator groups [158,159]. The chemical structure of a copolymer consisting of various methacrylates with cycloaliphatic leaving groups and a moiety with a chemically bound acid generator is shown in Chart 5.17 (note that the anion is bound to the polymer backbone). It was reported that a commercial resist corresponding to this structure yielded 30 nm half-pitch line patterns upon EUV irradiation (exposure dose: 13.4 mJ cm^{-2}) [158].

Lam Research Ex. 1047 - Page 308
Lam Research Corp. v. Inpria Corp.
IPR2024-00033 - U.S. Patent No. 9,823,564

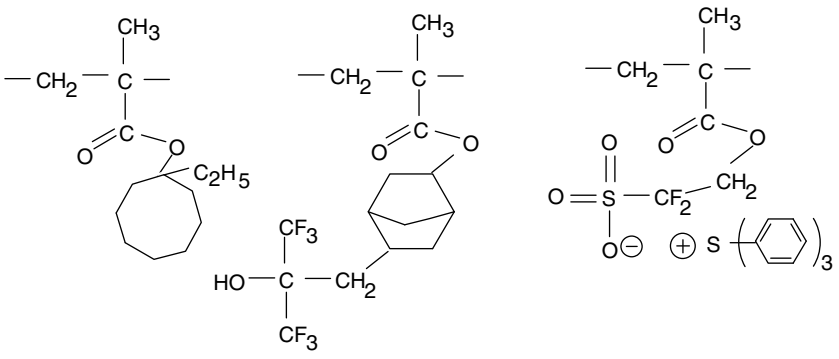


Chart 5.17 Chemical structures of repeating units of a copolymer with backbone-bound acid generator [159].

Frequently, a base (Chart 5.18) has been added to resist formulations, the aim being to neutralize any acid molecules that diffuse from the exposed into the unexposed areas. However, the base also acts in the exposed areas and thereby increases the exposure dose afforded for fine line generation. Consequently, the addition of a base leads to the establishment of a trade-off between LER and sensitivity.

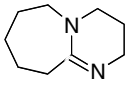


Chart 5.18 Chemical structure of 1,8-diazabiclyo[5.4.0]undec-7-ene, a typical base used to neutralize acid in exposed resists.

Future Outlook At present, the large-volume production of computer chips and other microdevices is based exclusively on photolithographic techniques. Applications of X-ray lithography in this area are not foreseeable, and euphoric plans regarding industrial applications were recently damped drastically with the advent of novel photolithographic methods that permit the generation of features in the sub-100 nm region (see Section 3.3.3). For some time, X-ray lithography appeared to be a promising method that would proceed along the pathway of the "international roadmap" for miniaturization. Interest in the technique soared when electron synchrotrons capable of generating high-intensity X-ray beams and, therefore, allowing rapid exposures were moving towards operation. It is likely that, in the near future, X-ray lithography will remain an important tool for microfabrication (e.g., the LIGA process), while EB lithography will be applied for the fabrication of masks. Regarding EUV lithography applications, the prognosis for the commercial production of microelectronic devices is poor as the method seems not to be cost-effective and the exposure costs and raw-energy consumption are both very high.

Lam Research Ex. 1047 - Page 309
Lam Research Corp. v. Inpria Corp.
IPR2024-00033 - U.S. Patent No. 9,823,564

Moreover, the actual systems are physically huge, they must be operated under vacuum, and consequently production-worthy hardware is very expensive to build and maintain [145]. Other significant problems include the lack of appropriate power sources and defect-free masks.

5.6.3 Crosslinking

Radiation crosslinking of certain polymers is technically applied with the purpose of improving important properties such as toughness, impact resistance, resistance to solvents and service temperature, and also to prevent plastic flow at elevated temperatures [115]. Radiation crosslinking has the advantage over chemical crosslinking by organic peroxides or silanes of affording a much shorter production line and a much lower energy consumption. The use of industrially applied radiation crosslinking of polymeric wire and cable insulations has been steadily expanding over the past decades such that, today, polymers used for wire and cable insulation include polyolefins (e.g., polyethylene) and certain halogen-containing polymers such as poly(vinyl chloride). Other polymers that are industrially crosslinked by irradiation are ethylene propylene rubber (*EPR*) and fluoropolymers [115]. The blending of EPR with polyolefins such as low-density polyethylene improves the material's processibility. At elevated temperatures, radiation crosslinking also improves the mechanical properties and crack resistance of widely used fluoropolymers such as copolymers of ethylene with tetrafluoroethylene, poly (vinylidene fluoride) and poly(vinyl fluoride) [115].

Some polymers (e.g., polypropylene) simultaneously undergo both main-chain cleavage and crosslinking upon irradiation; in this case, rather low absorbed doses for crosslinking are achieved with the assistance of additives that accelerate crosslinking, termed *prorads* or *crosslinking boosters*. Typical prorads include triallyl cyanurate and dipropargyl succinate (Chart 5.19). Low-molar-mass compounds containing C—C double bonds, such as ethylene propylene diene monomer (M-class) rubber compounds (known as EPDM rubber) or butadienes, are appropriate crosslinking boosters.

Electron beam processing in the manufacture of polyolefin foams is another important technical application, whereby (mostly) polyethylene is irradiated in the

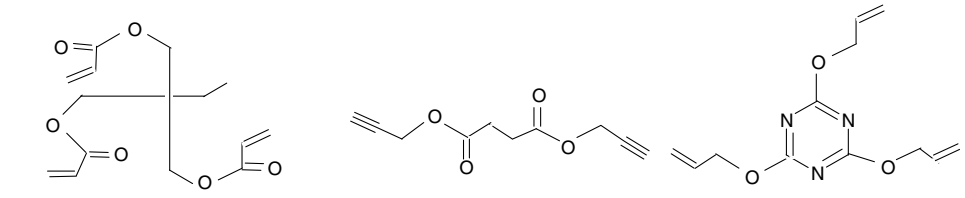


Chart 5.19 Chemical structures of compounds that boost radiation-induced crosslinking.

Lam Research Ex. 1047 - Page 310
Lam Research Corp. v. Inpria Corp.
IPR2024-00033 - U.S. Patent No. 9,823,564

melt at about 150 °C after the addition of a blowing agent such as azodicarbonamide. Subsequent heating in a foaming chamber to 200–210 °C causes decomposition of the blowing agent and an expansion of the sheet [115]. By using this process, both polyethylene and polypropylene foam sheets are produced on a commercial basis [115]. Another important technical application involves the EB-induced crosslinking of natural and synthetic rubber at room temperature, in the absence of any chemical additives [115,116]. Processes for the production of *automobile tires* operating on this basis have been commercialized about 50 years ago. Tire components such as inner liners, body plies, sidewalls, chafer strips, inner strips and tread ply skims are partially crosslinked by irradiation before the tire is assembled. The main advantages of this approach are fast production rates and reduced total manufacturing costs, as well as an ability to obtain an improved dimensional stability of the components during tire construction. Radiation-induced crosslinking not only results in a higher-quality tire with a more uniform thickness and better balance, but also allows the tire to be made thinner and to generate less frictional heating when in contact with the road.

5.6.4 Curing

Curing is a pollution-free method that is used to harden liquid coatings (that generally consist of multifunctional vinyl monomers) onto substrates, and can be performed either thermally or with the aid of UV-light or high-energy radiation. Unlike photocuring (see Section 3.3.2), high-energy radiation curing does not need an initiator and can also be applied for the rather thick layers of formulations that may be heavily pigmented. Traditionally, these formulations will contain various reactive compounds (frequently multifunctional acrylate and methacrylate monomers) that are readily polymerized when subjected to high-energy radiation. In general, high-energy curing is performed with the aid of EB radiation, and the mode of action may be either free-radical or free-cationic polymerization. However, as free-cationic polymerizations are observed only when scrupulously dry, oxygen-free and ultrapure monomers are used, they are not suitable for practical applications. Typically, EB-cured coatings adhere well to a variety of surfaces such as paper, wood, glass, metals, plastics, and textiles. The advantages of radiation curing relate to the use of solvent-free systems, a high extent of cure, and a high throughput rate. Moreover, as EBs are able to penetrate heavily pigmented formulations, adhesive layers lying between two opaque layers are also curable [23].

5.6.5 Grafting

High-energy radiation grafting is a powerful method that is used to alter or improve the surface properties of polymeric materials [162]. The principal points of the process were described in Section 5.2.3, and several applications are listed in Table 5.13.

Lam Research Ex. 1047 - Page 311
Lam Research Corp. v. Inpria Corp.
IPR2024-00033 - U.S. Patent No. 9,823,564

Table 5.13 Modification of polymers by high-energy radiation-induced grafting. Adapted in part from Ref. [126].

Polymer	Monomer	Modification of properties
Polyethylene	Acrylic acid	Hydrophilicity, wettability, antistatic behavior
Polyethylene	Acrylamide	Adhesion, permeability, permselectivity
Poly(ethylene terephthalate)	Acrylic acid	Hydrophilicity
Poly(ethylene terephthalate)	Acrylamide	Biocompatibility
Polyamide	Acrylic acid	Hydrophilicity, antistatic behavior
Polyamide	Hydroxyethyl methacrylate	Biocompatibility
Polyacrylonitrile	Acrylic acid	Moisture absorption, antistatic behavior
Polypropylene	Styrene, acrylic acid, methacrylates	Functionalization, ion exchange
Fluoropolymers	Styrene, *N*,*N*-diethylacrylamide, *N*-vinylpyrrolidone	Functionalization, hemocompatibility

Radiation grafting can be used to improve the dyeability of fabrics and fibers of nonpolar polymers, and to enhance the biocompatibility or to generate desired biochemical properties. The grafting of acrylic acid onto polymer substrates can be employed to immobilize enzymes; likewise, grafting can also be used to enhance the adhesion of biological cells onto polymer substrates [163]. A typical application is shown in Figure 5.15, where it is shown how glycidyl methacrylate is grafted

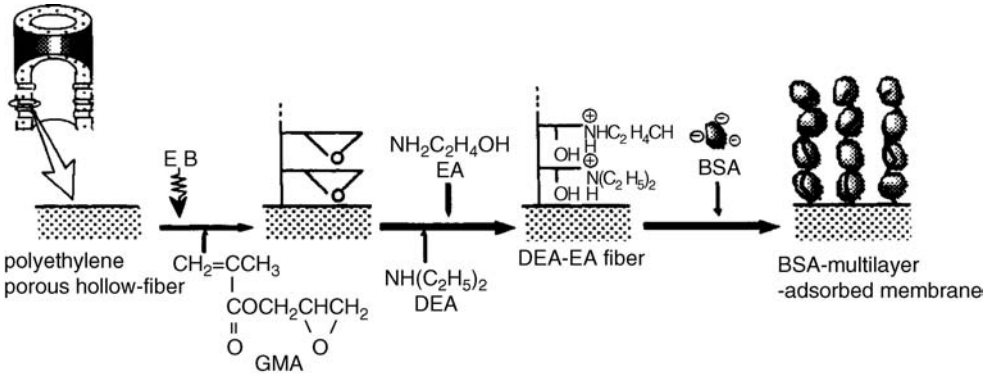


Figure 5.15 Electron beam grafting of polyethylene with glycidyl methacrylate and multilayer binding of bovine serum albumin (*BSA*) after conversion of the epoxide groups. Adapted with permission from Ref. [163]; © 2001, Elsevier.

Lam Research Ex. 1047 - Page 312
Lam Research Corp. v. Inpria Corp.
IPR2024-00033 - U.S. Patent No. 9,823,564

onto the surface of polyethylene hollow fibers, after which the epoxide groups are converted by reaction with diethylamine and ethanolamine. The resultant anion-exchange membranes are capable of adsorbing several layers of bovine serum albumin. Hollow-fiber sets treated in this way can be used for the chiral separation of racemic mixtures, for example of D,L-tryptophan [163].

Although the potential of high-energy radiation-induced grafting for practical applications has been described quite frequently elsewhere [123,126,163], at present very few commercial applications of high-energy-induced radiation grafting have been identified. One important example, however, is the production of battery separators made from polyethylene or polypropylene membranes grafted with acrylic acid and diethylene glycol dimethacrylate [165,166].

5.6.6 Hydrogels

Hydrogels consist of an interpenetrating polymer network, that is prepared by intermolecular crosslinking. Although, the base polymer is water-soluble, the crosslinked network only swells and does not dissolve in water – that is, it can take up only a limited amount of water. Polymers capable of forming hydrogels by radiation-induced crosslinking include poly(*N*-vinyl pyrrolidone), poly(acryl amide), poly(vinyl alcohol), and poly(*N*-vinyl imidazole) [15]. Hydrogels may also be formed by irradiating polysaccharide derivatives such as hydroxypropylcellulose in highly concentrated solutions [113,164].

Hydrogels can be prepared conveniently with the aid of γ-rays, starting with aqueous solutions of the respective monomer [16]. The process consists of two radiation-induced steps: (i) polymerization of the monomer; and (ii) crosslinking of the polymer formed in the first step (see Section 5.2.1). In fact, the process can commence with the OH radical-induced polymerization of monomers. With prolonged irradiation, the initially formed macromolecules such as poly(vinyl pyrrolidone) and polyacrylamide undergo crosslinking by OH radical attack [15,115].

The hydrogels produced can be loaded with a wide variety of compounds, including metal ions and biologically active compounds such as enzymes. For example, poly(*N*-vinyl imidazole) hydrogels loaded with Co and Cu ions can be used to immobilize the enzyme glucose oxidase [167]. Likewise, poly(*N*-vinyl pyrrolidone)-based hydrogels can be loaded with antibacterial acting compounds such as chitosan, which leads in turn to the creation of hydrogel wound dressings composed of poly(*N*-vinyl pyrrolidone), poly(ethylene glycol), agar and water [168]. Indeed, wound dressings prepared via radiation crosslinking were first commercialized almost 20 years ago, during the 1990s [168]. It should be noted here that γ-radiation is able to crosslink and sterilize simultaneously, a subject that is reviewed in detail by Makuuchi [15].

Lam Research Ex. 1047 - Page 313
Lam Research Corp. v. Inpria Corp.
IPR2024-00033 - U.S. Patent No. 9,823,564

References

1 Allen, N.S. and Edge, M. (1993) UV and electron-beam curable pre-polymers and diluent monomers: classification, preparation and properties, in *Radiation Curing in Polymer Science and Technology*, vol. **I** (eds J.P. Fouassier and J.F. Rabek), Elsevier Applied Science, London, Ch. 5.

2 Morrison, R.M. (June 1989) *An Economic Analysis of Electron Accelerators and Cobalt-60 Sources for Irradiating Food*, Technical Bulletin No. 1762, U.S. Department of Agriculture, Washington, DC.

3 Auslender, V.L., Bryazgin, A.A., Faktorovich, B.L., Gorbunov, V.A., Kokin, E.N., Korobeinikov, M.V., Krainov, G.S., Lukin, A.N., Maximov, S.A., Nekhaev, V.E., Panfilov, A.D., Radchenko, V.N., Tkachenko, V.O., Tuvik, A.A., and Voronin, LA. (2002) Accelerators for E-beam and X-ray processing. *Rad. Phys. Chem.*, **63**, 613–615.

4 Krenev, S. (2004) Critical analysis of industrial electron accelerators. *Rad. Phys. Chem.*, **71**, 537.

5 Ausloos, P. (ed.) (1968) *Fundamental Processes in Radiation Chemistry*, John Wiley & Sons, New York.

6 Mozumber, A. (1999) *Fundamentals of Radiation Chemistry*, Academic Press, London.

7 Wishart, J.F. and Rao, B.S.M. (2010) *Recent Trends in Radiation Chemistry*, World Scientific, Singapore.

8 Jonah, C.D. and Rao, B.S.B. (eds) (2001) *Radiation Chemistry: Present Status and Future Trends*, Elsevier Science, Amsterdam.

9 Garrison, W.M. (1987) Recent trends in radiation chemistry: present status and future trends. *Chem. Rev.*, **87**, 381.

10 Farhataziz and Rodgers, M.A.J. (1987) *Radiation Chemistry, Principles and Applications*, VCH Publishers, Weinheim.

11 Henglein, A., Schnabel, W., and Wendenburg, J. (1969) *Einführung in die Strahlenchemie*, Akademie-Verlag, Berlin.

12 Chapiro, A. (1962) *Radiation Chemistry of Polymeric Systems*, Interscience Publishers, New York.

13 Hagiwara, M., Mitsui, H., Machi, S., and Kagiya, T. (1968) Liquid carbon dioxide as a solvent for the radiation polymerization of ethylene. *J. Polym. Sci.: Part A-a*, **6**, 603.

14 Caputo, G., Galia, A., Scrò, F., Spandaro, G., and Filardo, G. (2002) Gamma radiation induced polymerization of vinyl monomers in dense CO_2. *Rad. Phys. Chem.*, **63**, 45.

15 Makuuchi, K. (2010) Critical review of radiation processing of hydrogel and polysaccharide. *Rad. Phys. Chem.*, **79**, 267.

16 Rosiak, J.M. (1991) Hydrogel Dressings, in *Radiation Effects on Polymers* (eds R.L. Clough and S.W. Shalaby), American Chemical Society, Washington DC, Ch. 17.

17 Friedrich, T. and Tieke, B. (2010) Intelligent hydrogels via gamma-ray induced polymerization of micellar monomer solutions and microemulsions. *Macromol. Symp.*, **287**, 16.

18 Friedrich, T., Tieke, B., Meyer, M., Pyckhout-Hintzen, W., and Pipich, V. (2010) Thermoresponsive copolymer hydrogels based on n-isopropylacrylamide and cationic surfactant monomers from micellar solutions and microemulsions in a one-step reaction. *J. Phys. Chem.*, **114**, 5666.

19 Ueno, K., Williams, F., and Hayashi, K. (1967) Radiation-induced polymerization by free ions. Part 1. - polymerization of styrene under anhydrous conditions. *Trans. Faraday Soc.*, **63**, 1478.

20 Naylor, D.M., Stannett, V.T., Deffieux, A., and Sigwalt, D. (1990) Radiation-induced polymerization of dimethylcyclosiloxane in the liquid state, 1. Influence of drying and mechanism. *Polymer*, **31**, 954.

21 Yamamoto, Y. (1993) Pulse radiolysis of onium salts and radiation-induced cationic polymerization, in *Radiation Curing in Polymer Science and Technology*, vol. **II** (eds J.P. Fouassier and J.F Rabek), Elsevier Applied Science, London.

22 Crivello, J.V. (1999) UV and electron beam-induced cationic polymerization. *Nucl. Instr. Meth. Phys. Res. B*, **151**, 8.

23 Davidson, R.S. (1993) Mechanism of electron beam curing, chapter 9, in *Radiation Curing in Polymer Science and*

Lam Research Ex. 1047 - Page 314
Lam Research Corp. v. Inpria Corp.
IPR2024-00033 - U.S. Patent No. 9,823,564

Technology, vol. **III** (eds J.P. Fouassier and J.F. Rabek), Elsevier Applied Science, London.

24 Yamaoka, H., Williams, F., and Hayashi, K. (1967) Radiation-induced polymerization of nitroethylene. *Trans. Faraday Soc.*, **63**, 376.

25 Dinh-Ngoc, B. and Schnabel, W. (1977) Anionic polymerization of β-Nitrostyrene under the influence of high energy radiation. *J. Macromol. Sci. Chem.*, **A1**, 1637.

26 Dinh-Ngoc, B. and Schnabel, W. (1978) Primary reactions during the free anionic polymerization of β-nitrostyrene. *Naturforschung*, **33a**, 253.

27 Schmitz, J.K. and Lawton, E.J. (1951) Initiation of vinylpolymerization by means of high energy electrons. *Science*, **113**, 718.

28 Henglein, A. and Schulz, R.C. (1954) Die Einwirkung von γ-Strahlen auf festes Acrylamid. *Z. Naturforsch.*, **9b**, 617.

29 Mesrobian, R.B., Ander, P., Ballantine, D.S., and Dienes, G.J. (1954) Gamma-ray polymerization of acrylamide in the solid state. *J. Chem. Phys.*, **22**, 565.

30 Chapiro, A. (1966) Polymérisations en phase solide amorcée par les radiations, in *Actions Chimiques et Biologiques des Radiations, dixième série* (ed. M. Haissinsky), Masson et Cie, Paris.

31 Nishii, M. and Hayashi, K. (1975) Solid-state polymerization. *Annu. Rev. Mater. Sci.*, **5**, 135.

32 Okamura, S., Hayashi, K., and Nishii, N. (1962) Polymer crystals obtained by radiation polymerization of trioxane in solid state. *J. Polymer Sci.*, **60**, −26.

33 Hayashi, K., Ochi, H., and Okamura, S. (1964) Radiation-induced post-polymerization of trioxane in the solid state. *J. Polymer Sci. A*, **2**, 2929.

34 Chance, R.R. and Patel, G.N. (1978) Solid-state polymerization of a diacetylene crystal: thermal, ultraviolet, and γ-ray polymerization of 2,4-hexadiyne-1,6-diol bis-(*p*-toluene sulfonate). *J. Polym. Sci., Polym. Phys. Ed.*, **16**, 859.

35 Patel, G.N. (1977) Diacetylenes as radiation dosage indicators. *Rad. Phys. Chem.*, **18**, 913.

36 Mod Ali, N., Tucker, C.E., and Smith, F.A. (1996) Consideration of radiation-induced polymerization of diacetylene LB films for dosimetry. *Thin Solid Films*, **289**, 267.

37 Butson, M.J., Cheung, T., and Yu, P.K.N. (2006) Visible absorption spectra of radiation exposed SIRAD dosimeters. *Phys. Med. Biol.*, **51**, N417.

38 Bovey, F.A. (1958) *The Effects of Ionizing Radiation on Natural and Synthetic High Polymers*, Interscience Publishers, New York.

39 (a) Charlesby, A. (1960) Chapter 10, in *Atomic Radiation and Polymers*, Pergamon Press, Oxford; (b) Saito, O. (1972) Statistical Theory of Crosslinking, in *The Radiation Chemistry of Macromolecules*, (ed. M. Dole), vol. **I**, Academic Press, New York, Ch. 11.

40 (a) Dole, M. (ed.) (1972) *The Radiation Chemistry of Macromolecules*, vol. **I**, Academic Press, New York; (b) Dole, M. (ed.) (1973) *The Radiation Chemistry of Macromolecules*, vol. **II**, Academic Press, New York.

41 Clough, R.L. and Shalaby, S.W. (eds) (1991) *Radiation Effects on Polymers*, American Chemical Society, Washington, DC.

42 Clough, R.L. and Shalaby, S.W. (eds) (1996) *Irradiation of Polymers*, American Chemical Society, Washington, DC.

43 Knolle, W. and Trautman, C. (eds) (1999) *Ionizing radiation and polymers*. Elsevier Science.

44 Ivanov, V.S. (1992) *Radiation Chemistry of Polymers*, VSP International Science Publ., Leiden, NL.

45 Woods, R.J., and Pikaev, A.K. (1994) *Applied Radiation Chemistry: Radiation Processing of Polymers*, John Wiley & Sons, New York.

46 Clegg, D.W., and Collyer, A.A. (1991) *Irradiation Effects on Polymers*, Elsevier Applied Science, London.

47 Adams, M.R. and Garton, A. (1996) Far ultraviolet degradation of selected polymers, in *Polymer Durability* (eds R.L. Clough, N.C. Billingham, and K.T. Gillen), American Chemical Society, Washington, DC, Ch. 9.

48 Dawes, K., Glover, L.C., and Vroom, D.A. (1996) Effects of electron beam and γ-irradiation on polymeric materials, in *Physical Properties of Polymers Handbook* (ed. J.E. Mark), American Institute of Physics Press, Woodbury, NY, Ch. 41.

Lam Research Ex. 1047 - Page 315
Lam Research Corp. v. Inpria Corp.
IPR2024-00033 - U.S. Patent No. 9,823,564

49 O'Donnell, J.H. (1991) Chemistry of radiation degradation of polymers, in *Radiation Effects on Polymers* (eds R.L. Clough and S.W. Shalaby), American Chemical Society, Washington, DC, Ch. 24.

50 Forsythe, J.S. and Hill, D.J.T. (2000) The radiation chemistry of fluoropolymers. *Prog. Polym. Sci.*, **25**, 101.

51 Moad, C.L. and Winzor, D.J. (1998) Quantitative characterization of radiation degradation in polymers by evaluation of scission and cross-linking yields. *Prog. Polym. Sci.*, **23**, 759.

52 Chapiro, A. (2002) Polymer irradiation: past, present and future. *Rad. Phys. Chem.*, **63**, 207.

53 Makhlis, F.A. (1975) *Radiation Physics and Chemistry of Polymers*, John Wiley & Sons, New York.

54 Schnabel, W. (1978) Degradation by high energy radiation, in *Aspects of Degradation and Stabilization of Polymers* (ed. H.H.G. Jellinek), Elsevier Scientific, Amsterdam, Ch. 4.

55 Matheson, M.S. and Dorfman, L.M. (1961) *Pulse Radiolysis*, MIT Press, Cambridge, MA.

56 Baxendale, J.H. and Busi, F. (eds) (1982) *The Study of Fast Processes and Transient Species by Electron Pulse Radiolysis*, Reidel, Dordrecht.

57 Tabata, Y. (ed.) (1991) *Pulse Radiolysis*, CRC Press, Boca Raton.

58 Warman, J.M. and de Haas, M.P. (1991) Time Resolved Conductivity Techniques, DC to Microwaves, in *Pulse Radiolysis* (ed. Y. Tabata), CRC Press, Boca Raton, Ch. 6.

59 Schnabel, W. (1991) Time-Resolved Light Scattering Study, in *Pulse Radiolysis* (ed. Y. Tabata), CRC Press, Boca Raton, Ch. 7.

60 Schnabel, W. (1979) Application of the light scattering detection method to problems of polymer degradation, in *Developments in Polymer Degradation – 2* (ed. N. Grassie), Applied Science Publishers, London, Ch. 2.

61 Busfield, W.K. and Watson, G.S. (1996) Radiation Chemistry of Polybutene-1, in *Irradiation of Polymers* (eds R.L. Clough and S.W. Shalaby), American Chemical Society, Washington, DC, Ch. 5.

62 Ichikawa, T. and Yoshida, H. (1990) Mechanism of radiation-induced degradation of poly(methyl methacrylate) as studied by ESR and electron spin echo methods. *J. Polym. Sci.: Part A: Polym. Chem.*, **28**, 1185.

63 Nakano, A., Okamoto, K., Kozawa, T., and Tagawa, S. (2004) Pulse radiolysis study on proton and charge transfer reactions in solid poly(methyl methacrylate). *Jpn. J. Appl. Phys.*, **43**, 4363.

64 Wündrich, K. (1974) The dependence of radiation-induced polyisobutylene degradation on molecular mobilities. *Eur. Polym. J.*, **10**, 341.

65 Schnabel, W. (1970) The temperature dependence of degradation and cross-linking at the ^{60}Co-γ-irradiation of poly (ethylene oxide) (in German). *Makromol. Chem.*, **131**, 287.

66 Sun, J., Zhang, Y., Zhong, X., and Zhu, X. (1994) Modification of polytetrafluoroethylene by radiation – 1. Improvement in high temperature properties and radiation stability. *Radiat. Phys. Chem.*, **44**, 655.

67 Lappan, U., Geißler, U., and Scheler, U. (2007) The influence of the irradiation temperature on the ratio of chain scission to branching reactions in electron beam irradiated polytetrafluoroethylene (PTFE). *Macromol. Mater. Eng.*, **292**, 641.

68 Lappan, U., Geißler, U., Häußler, L., Jehnichen, D., Pompe, G., and Lunkwitz, K. (2001) Radiation-induced branching and crosslinking of polytetrafluoroethylene (PTFE). *Nucl. Instrum. Meth. Phys. Res. B*, **185**, 178.

69 Tabata, Y., Ikeda, S., and Oshima, A. (2001) Radiation-induced cross-linking and grafting of polytetrafluoroethylene. *Nucl. Instr. Meth. Phys. Res. B*, **185**, 169.

70 Brown, J.R. and O'Donnell, J.H. (1972) γ-Radiolysis of poly(butene-1 sulfone) and poly(hexene-1 sulfone). *Macromolecules*, **5**, 109.

71 Bhatta, U.M., Ghatak, J., Mukhopadhyay, M., Wang, J., Narayanan, S., and Satyam, P.V. (2009) Synchrotron X-ray induced damage in polymer thin films. *Nucl. Instr. Meth. Phys. Res. B*, **267**, 1807.

Lam Research Ex. 1047 - Page 316
Lam Research Corp. v. Inpria Corp.
IPR2024-00033 - U.S. Patent No. 9,823,564

72 Briskman, B.A. (2007) Be careful when using X-ray exposure analysis for polymers. *Nucl. Instr. Meth. Phys. Res. B*, **265**, 276.

73 Holton, J.M. (2009) A beginner's guide to radiation damage. *Synchrotron Rad.*, **16**, 133.

74 Wilski, H. (1973) The behavior of low pressure polyethylene under the influence of ionizing radiation (in German). *Kolloid Z. Z. Polym.*, **251**, 703.

75 Scroog, C.E., Endrey, A.L., Abramo, S.V., Berr, C.E., Edwards, W.M., and Olivier, K. L. (1965) Aromatic polypyromellitimides from aromatic polyamic acids. *J. Polym. Sci. A*, **3**, 1373.

76 Bowmer, T.N., Cowen, L.K., O'Donnell, J. H., and Winsor, D.J. (1979) Degradation of polystyrene by gamma irradiation: effect of air on the radiation-induced changes in mechanical and molecular properties. *J. Appl. Polym. Sci.*, **24**, 425.

77 Sonntag, C.v. and Schulte-Frohlinde, D. (1978) Radiation-induced degradation of the sugar in model compounds and in DNA, in *Effects of Ionizing Radiation on DNA* (ed. A.J. Bertinchamps), Springer, Berlin, p. 204.

78 Sonntag, C.v. (2006) *Free-Radical-Induced DNA Damage and its Repair. A Chemical Perspective*, Springer, Berlin.

79 Sonntag, C.v. (2010) Radiation-induced DNA damage: indirect effects, in *Recent Trends in Radiation Chemistry* (eds J.F. Wishart and B.S.M. Rao), World Scientific, New Jersey, Ch. 19.

80 Sonntag, C.v. and Schuchmann, H.-P. (2001) Carbohydrates, in *Radiation Chemistry: Present Status and Future Trends* (eds C.D. Jonah and B.S.B. Rao), Elsevier Science, Amsterdam, p. 481.

81 Sonntag, C.v. (1987) *The Chemical Basis of Radiation Biology*, Taylor and Francis, London.

82 Sharpatyi, V.A. and Zaikov, G.E. (2006) *Radiation Chemistry of Biopolymers*, Brill Academic Publ., Leiden.

83 Sharpatyi, V.A. (2007) Free radical mechanisms of irradiation of polysaccharides. radiation destruction products, in *Polymers and Composites: Synthesis, Properties and Application* (eds R.A. Pethrick, G.E. Zaikov, and D. Horak), Nova Science Publ., New York, Ch. 6.

84 Sharpatyi, A. (2007) The problems of radiation chemistry of protein molecules, in *Polymers and Composites: Synthesis, Properties and Application* (eds R.A. Pethrick, G.E. Zaikov, and D. Horak), Nova Science Publ., New York, Ch. 7.

85 Houée-Levin, C. and Sicard-Roselli, C. (2001) Radiation Chemistry of Proteins, in *Radiation Chemistry: Present Status and Future Trends* (eds C.D. Jonah and B.S.B. Rao), Elsevier Science, Amsterdam, p. 553.

86 Kempner, E.S. (1993) Damage to proteins due to direct action of ionizing radiation. *Q. Rev. Biophys.*, **26**, 27.

87 Sharma, K.K.K., Tyagi, R., Purkayastha, S., and Bernhard, W.A. (2010) One-electron oxidation of DNA by ionizing radiation: competition between base-to-base hole transfer and hole-trapping. *J. Phys. Chem. B*, **114**, 7672.

88 Sharma, K.K.K., Swarts, S.G., and Bernhard, W.A. (2011) Mechanisms of direct damage to DNA: the effect of base sequence on the base end products. *J. Phys. Chem. B*, **115**, 4843.

89 Swarts, S.G., Becker, D., Sevilla, M., and Wheeler, K.T. (1996) Radiation-induced DNA damage from electron-loss centers. *Radiat. Res.*, **145**, 304.

90 Becker, D., Adhikary, A., and Sevilla, M. D. (2010) Mechanisms of Radiation-Induced DNA Damage to DNA: Direct Effects, in *Recent Trends in Radiation Chemistry* (eds J.F. Wishart and B.S.M. Rao), World Scientific, Singapore., Ch. 18.

91 Yokoya, A., Cunniffe, S.M.T., and O'Neill, P. (2002) Effect of hydration on the induction of strand breaks and base lesions in plasmid DNA films by radiation. *J. Am. Chem. Soc.*, **124**, 8856.

92 Shukla, M.K. and Leszczynski, J. (eds) (2008) *Radiation-Induced Molecular Phenomena in Nucleic Acids, A Comprehensive Theoretical and Experimental Analysis*, Springer, Berlin.

93 Sanche, L. (2008) Low-Energy Radiation Damage to DNA, in *Radiation-Induced Molecular Phenomena in Nucleic Acids, A Comprehensive Theoretical and Experimental Analysis* (eds M.K. Shukla

Lam Research Ex. 1047 - Page 317
Lam Research Corp. v. Inpria Corp.
IPR2024-00033 - U.S. Patent No. 9,823,564

and J. Leszczynski), Springer, Berlin, Ch. 19.

94 O'Neill, P. (2001) Radiation-Induced Damage in DNA, in *Radiation Chemistry: Present Status and Future Trends* (eds C.D. Jonah and B.S.B. Rao), Elsevier Science, Amsterdam, p. 5.

95 Ershov, B.G. and Klimentov, A.S. (1984) The radiation chemistry of cellulose. *Russ. Chem. Rev.*, **53**, 1195.

96 Ershov, B.G. (1998) Radiation chemical degradation of cellulose and other polysaccharides. *Russ. Chem. Rev.*, **67**, 315.

97 Weik, M., Ravelli, R.G.B., Kryger, G., McSweeney, S., Raves, M.L., Harel, M., Gros, P., Silman, I., Kroon, J., and Sussman, J.L. (2000) Specific chemical structure damage to proteins produced by synchrotron radiation. *Proc. Natl Acad. Sci. USA*, **97**, 623.

98 Prütz, W.A., Butler, J., Land, E.J., and Swallow, A.J. (1980) Direct demonstration of electron transfer between tryptophan and tyrosine in proteins. *Biochem. Biophys. Res. Commun.*, **96**, 408.

99 Prütz, W.A., Butler, J., Land, E.J., and Swallow, A.J. (1986) Unpaired electron migration between aromatic and sulfur peptide units. *Free Rad. Res. Commun.*, **2**, 69.

100 Jovanovic, S.V., Harriman, A., and Simic, M.G. (1986) Electron transfer reactions of tryptophan and tyrosine derivatives. *J. Phys. Chem.*, **90**, 1935–1939.

101 Lin, N.Y. (1990) Radiation-induced long range electron transfer in biological systems. *Res. Chem. Intermed.*, **14**, 209.

102 Lehnert, S. (2008) *Biomolecular Action of Ionizing Radiation*, CRC Press, Boca Raton, FL, USA.

103 Boudaiffa, B., Cloutier, P., Hunting, D., Huels, M.A., and Sanche, L. (2000) Resonant formation of DNA strand breaks by low-energy (3–20eV) electrons. *Science*, **287**, 1658.

104 Chmielewski, A. (2010) Chitosan and radiation chemistry. *Radiat. Phys. Chem.*, **79**, 272.

105 Philipchatina, O.A. and Sharpatyi, V.A. (2007) Free-radical mechanism of chitosan radiation degradation and problems of the chemical antiradiation protection. *Radiats. Biol. Radioecol.*, **47**, 717 (in Russian).

106 Ulanski, P. and Rosiak, J.M. (1992) Preliminary studies on radiation-induced changes in chitosan. *Radiat. Phys. Chem.*, **39**, 53.

107 Tahtat, D., Uzun, C., Mahlous, M., and Güven, O. (2007) Beneficial effects of γ-irradiation on the N-deacetylation of chitin to form chitosan. *Nucl. Instrum. Meth. Phys. Res. B*, **265**, 425.

108 Henglein, A. and Schnabel, W. (1966) Radiation chemistry of synthetic macromolecules in solution, LET effects. *Curr. Topics Radiat. Res.*, **I**, 1.

109 Chance, M.R., Brenowitz, M., Sullivan, M., Scalvi, B., Maleknia, S.D., and Ralston, C. (1998) A new method for examining the dynamics of macromolecules: time-resolved synchrotron X-Ray "Footprinting". *Synchrotron Rad. News*, **11**, 7.

110 Maleknia, S.D., Ralston, C.Y., Brenowitz, M., Downard, K.M., and Chance, M.R. (2001) Determination of macromolecular folding and structure by synchrotron X-ray radiolysis techniques. *Anal. Biochem.*, **289**, 103.

111 Scalvi, B., Woodson, S., Sullivan, M., Chance, M.R., and Brenowitz, M. (1997) Time-resolved synchrotron X-ray "Footprinting", a new approach to the study of nucleic acid structure and function: application to Protein-DNA interactions and RNA folding. *J. Mol. Biol.*, **266**, 144.

112 Edimecheva, I.P., Kisel, R.M., Shadyro, O.I., Kazem, K., Murase, H., and Kagiya, T. (2005) Homolytic cleavage of the O-glycoside bond in carbohydrates: a steady-state radiolysis study. *J. Radiat. Res.*, **46**, 319.

113 Yoshii, F., Zhao, L., Wach, R.A., Nagasawa, N., Mitomo, H., and Kume, T. (2003) Hydrogels of polysaccharide derivatives crosslinked with irradiation at paste-like condition. *Nucl. Instrum. Meth. Phys. Res. B*, **208**, 320.

114 Nagasawa, N., Yagi, T., Kume, T., and Yoshii, F. (2004) Radiation crosslinking of carboxymethyl starch. *Carbohydr. Polym.*, **58**, 109.

Lam Research Ex. 1047 - Page 318
Lam Research Corp. v. Inpria Corp.
IPR2024-00033 - U.S. Patent No. 9,823,564

115 Drobny, J.G. (2010) *Radiation Technology for Polymers*, 2nd edn, CRC Press, Boca Raton, FL, USA.

116 Machi, S. (2011) Trends for electron beam accelerator applications in industry. *Rev. Accelerator Sci. Technol.*, **4**, 1.

117 Czvikovszki, T. (2003) Expected and unexpected achievements and trends in radiation processing of polymers. *Radiat. Phys. Chem.*, **67**, 437.

118 Chmielewski, A.G., Chmielewska, D.K., Michalik, J., and Sampa, M.H. (2007) Prospects and challenges in application of gamma, electron and ion beams in processing of nanomaterials. *Nucl. Instr. Meth. Phys. Res. B*, **265**, 339.

119 Chmielewski, A.G. (2007) Practical applications of radiation chemistry. *Russian J. Phys. Chem. A*, **81**, 1488.

120 Chmielewski, A.G., Haji-Saied, M., and Ahmed, S. (2005) Progress in radiation processing of polymers. *Nucl. Instr. Meth. Phys. Res. B*, **236**, 44.

121 Chmielewski, A.G. and Haji-Saied, M. (2004) Progress in radiation technologies: past, present and future. *Radiat. Phys. Chem.*, **71**, 16.

122 Saile, V. (2009) *LIGA and its Applications*, Wiley-VCH, Weinheim.

123 Clough, R.L. (2001) High-energy radiation and polymers: a review of commercial processes and emerging applications. *Nucl. Instr. Meth. Phys. Res. B*, **185**, 8.

124 Clough, R.L. and Shalaby, S.W. (eds) (1996) *Irradiation of Polymers: Fundamentals and Technological Applications*, American Chemical Society, Washington, DC.

125 Bhattacharya, A. (2000) Radiation and industrial polymers. *Prog. Polym. Sci.*, **25**, 371.

126 Mehnert, R., Bögl, K.W., Helle, N., and Schreiber, G.A. (1993) *Radiation Chemistry, Ulmann's Encyclopedia of Industrial Chemistry*, vol. **A22**, VCH, Weinheim, p. 471.

127 Singh, A. and Silverman, J. (eds) (1992) *Radiation Processing of Polymers*, Hanser, München.

128 Heger, A., Dorschner, H., Dunsch, L., Ihme, B., and Lunkwitz, K. (1990) *Technologie der Strahlenchemie der Polymeren*, Akademie Verlag, Berlin.

129 Rai-Choudhury, P. (ed.) (1997) *Microlithography*, vol. **1**, *Handbook of Microlithography, Micromachining and Microfabrication*, SPIE Press, Bellingham, Washington.

130 Okoroanyanwu, U. (2010) *Chemistry and Lithography*, SPIE Press, Bellingham, Washington.

131 Schlegel, L. and Schnabel, W. (1993) Polymers in X-ray, electron beam and ion beam lithography, in *Radiation Curing in Polymer Science and Technology*, vol. **I** (eds J.P. Fouassier and J.F. Rabek), Elsevier Applied Science, London, Ch. 2.

132 Schnabel, W. and Sotobayashi, H. (1983) Polymers in electron beam and X-ray lithography. *Prog. Polym. Sci.*, **9**, 297.

133 Levinson, H.J. (2011) *Principles of Lithography*, 3rd edn, SPIE Press.

134 Bourdillon, A. and Vladimirsky, Y. (2006) *X-Ray Lithography on the Sweet Spot*, UHRL, San Jose, USA.

135 Rousseaux, F., Haghiri-Gosnet, A.M., Chen, Y., Ravel, M.F., and Launois, H. (1994) X-ray lithography: an overview and recent activities at super-ACO. *J. de Physique*, **I**, C-237.

136 Wu, B. and Kumar, A. (2009) *Extreme Ultraviolet Lithography*, McGraw-Hill.

137 Atwood, D. (2000) *Soft X-Rays and Extreme Ultraviolet Radiation. Principles and Applications*, Oxford University Press, Oxford.

138 (a) Bakshi, V. (ed.) (2009) *EUV Lithography*, John Wiley & Sons, Hoboken, NJ, USA; (b) Bakshi, V. (ed.) (2006) *EUV Sources for Lithography*, SPIE Press, Bellingham, Washington.

139 Cerrina, F. (1997) X-Ray Lithography, in *Microlithography* (ed. P. Rai-Choudhury), vol. **1**, *Handbook of Microlithography, Micromachining and Microfabrication*, SPIE Press, Bellingham, Washington, Ch. 3.

140 Cobb, J.L., Brainard, R.L., O'Connell, D.J., and Dentinger, P.M. (2002) EUV lithography: patterning to the end of the road. *Proc. Mater. Res. Soc. Symp.*, **705**, 91.

141 Brainard, R.L., Trefonas, P., Lammers, J.H., Cutler, C.A., Mackevich, J.F., Trefonas, A., and Robertson, S.A. (2004) Shot noise, LER, and quantum efficiency of EUV photoresists. *Proc. SPIE*, **5374**, 74.

Lam Research Ex. 1047 - Page 319
Lam Research Corp. v. Inpria Corp.
IPR2024-00033 - U.S. Patent No. 9,823,564

142 Brainard, R.L., Cobb, J.L., and Cutler, C.A. (2003) Current status of EUV photoresists. *J. Photopol. Sci. Technol.*, **16**, 401.

143 Brainard, R.L. (2009) Photoresists for extreme ultraviolet lithography, in *EUV Lithography* (ed. V. Bakshi), John Wiley & Sons, Hoboken, NJ, USA, Ch. 8.

144 Ito, H. (2005) Chemical amplification resists for microlithography. *Adv. Polym. Sci.*, **172**, 37.

145 Lin, B.J. (2010) *Optical Lithography. Here is Why*, SPIE Press, Bellingham, Washington, USA.

146 Craighead, H.G. (1984) 10-nm Resolution electron beam lithography. *J. Appl. Phys.*, **55**, 4430.

147 Slot, E., Wieland., M.J., de Boer, G., Kruit, P., ten Berge, G.F., Houkes, A.M.C., Jager, R., van de Peut, T., Pleijster, J.J., Steenbrink, S.W.H., Teepen, T.F., van Veen, A.H.V., and Kampherbeek, B.J. (2008) Mapper: High-throughput maskless lithography. Proceedings of SPIE, vol. **6921**, 69211P1–69211P9.

148 Schriever, G. and Zink, P. (2008) EUV sources for lithographic applications. *Optik Photonik*, **3**, 40.

149 Namaste, Y.M.N., Obendorf, S.K., and Rodriguez, D. (1988) Reactive plasticizers in negative E-beam resists. *J. Vac. Sci. Technol. B*, **6**, 2245.

150 Reichmanis, E., Houlihan, F.M., Nalamasu, O., and Neenan, T.X. (1991) Chemical amplification mechanisms for microlithography. *Chem. Mater.*, **3**, 394.

151 (a) Dössel, K.-F., Huber, H.L., and Oertel, H. (1986) Highly-sensitive novolak-based positive X-ray resist. *Microelectron. Eng.*, **5**, 97; (b) Pongratz, S., Demmeler, R., Ehrlich, C., Kohlmann, K., Reimer, K., Dammel, R., Hessemer, W., Lingnau, J., Scheunemann, U., and Theis, J. (1989) E-beam application of highly sensitive positive and negative-tone resists for X-ray mask making. *Proc. SPIE*, **1089**, 303.

152 Kozawa, T., Yoshida, Y., Uesaka, M., and Tagawa, S. (1992) Radiation-induced acid generation reactions in chemically amplified resists for electron and X-ray lithography. *Jpn. J. Appl. Phys.*, **31**, 4301.

153 Kozawa, T. and Tagawa, S. (2010) Radiation chemistry in chemically amplified resists. *Jpn. J. Appl. Phys.*, **49**, 030001.

154 Rao, V., Cobb, J., Henderson, C., Okoroanyanwu, U., Bozman, D., Mangat, P., Brainard, R., and Mackevich, J. (1999) Ultrathin photoresists for EUV lithography. *Proc. SPIE*, **3676**, 615.

155 Golovkina, V.N., Nealey, P.F., Cerrina, F., Taylor, J.W., Solak, H.H., David, C., and Gobrecht, J. (2004) Exploring the ultimate resolution of positive-tone chemically amplified resists: 26nm dense lines using extreme ultraviolet interference lithography. *J. Vac. Sci. Technol. B*, **22**, 99.

156 Kozawa, T., Tagawa, S., Santillan, J.J., and Itani, T. (2008) Impact of nonconstant diffusion coefficient on latent image quality in 22nm fabrication using extreme ultraviolet lithography. *J. Photochem. Sci. Technol.*, **21**, 421.

157 Iwashita., J., Mimura, T., Hirayama, T., and Iwai, T. (2009) Main chain decomposable star shaped polymer for EUV resist. *Proc. SPIE*, **7273**, 727330.

158 Thackeray, J.W., Aqad, E., Kang, S.J., and Spear-Alfonso, K. (2009) Design considerations for EUV resist materials. *J. Photopolym. Sci. Technol.*, **22**, 65.

159 Bozano, L.D., Brock, P.J., Truong, H.D., Sanchez, M.I., Wallraff, G.M., Hinsberg, W.D., Allen, R.D., Fujiwara, M., and Maeda, K. (2011) Bound PAG resists: an EUV and electron beam lithography performance comparison of fluoropolymers. *Proc. SPIE*, **7972**, 797218–1.

160 McCord, M.A. and Rooks, M. (1997) Electron Beam Lithography, in *Microlithography* (ed. P. Rai-Choudhury), vol. **1**, *Handbook of Microlithography, Micromachining and Microfabrication*, SPIE Press, Bellingham, Washington., Ch. 2.

161 Ehrfeld, W. and Lehr, H. (1995) Deep X-ray lithography for the production of three-dimensional microstructures from metals, polymers and ceramics. *Rad. Phys. Chem.*, **45**, 349.

162 Berejka, A.J. (2004) Advances in Radiation Chemistry of Polymers. Proceedings of a technical meeting, 13–17 September 2003, Notre Dame, Indiana, USA. International Atomic Energy Agency.

Lam Research Ex. 1047 - Page 320
Lam Research Corp. v. Inpria Corp.
IPR2024-00033 - U.S. Patent No. 9,823,564

163 Saito, K. and Sugo, T. (2001) High-performance polymeric materials for separation and reaction, prepared by radiation-induced graft polymerization, in *Radiation Chemistry: Present Status and Future Trends* (eds C.D. Jonah and B.S.B. Rao), Elsevier Science, Amsterdam, Ch. 24.

164 Wach, R.A., Nagasawa, N., Mitomo, H., Yoshii, F., and Kume, T. (2002) Hydrogel of radiation-induced crosslinked hydroxypropylcellulose. *Macromol. Mater. Eng.*, **287**, 285.

165 Arora, P. and Zhang, Z.M. (2004) Battery separators. *Chem. Rev.*, **104**, 4419.

166 Gineste, J.L. (1995) Polypropylene separator grafted with hydrophilic monomers for lithium batteries. *J. Membr. Sci.*, **107**, 155.

167 Pekel, N., Salih, B., and Güven, O. (2003) Activity studies of glucose immobilized onto poly(*N*-vinyl imidazole) and metal ion chelated poly (*N*-vinyl imidazole) hydrogels. *J. Mol. Catalysis B: Enzym.*, **21**, 273.

168 Rosiak, J.M. and Olejniczak, J. (1993) Medical applications of radiation formed hydrogels. *Rad. Phys. Chem.*, **42**, 903.

Lam Research Ex. 1047 - Page 321
Lam Research Corp. v. Inpria Corp.
IPR2024-00033 - U.S. Patent No. 9,823,564

6
Applications of High-Energy Radiation in Polymer Physics

6.1
General Aspects

This chapter is devoted to various X-rays methods which have been applied successfully to the characterization and analysis of polymers. These methods have contributed substantially to the characterization of polymer surfaces and the determination of the structure of proteins and other biological polymers. X-rays passing through matter are attenuated both by absorption and scattering. The absorption of X-ray photons results in the formation of unstable reactive species, namely radical ions, excited molecules and free radicals, which interact with intact surrounding molecules thus leading to chemical alterations of the absorbing matter. However, X-ray absorption can be used as an analytical tool when the absorbed radiation dose is kept low and deleterious radiation effects are negligible. In fact, the methods described in Section 6.2, namely near-edge X-ray absorption fine structure (*NEXAFS*) spectroscopy, extended X-ray absorption fine structure spectroscopy (*EXAFS*), UV-photoelectron spectroscopy (*UPS*) and X-ray photoelectron spectroscopy (*XPS*) are widely used in the polymer field. In addition, X-ray imaging and X-ray microscopy (see Section 6.3) are techniques that allow the derivation of quantitative composition maps of polymer surfaces.

As noted above, X-rays passing through matter are attenuated to some extent also by scattering processes. The scattering phenomenon forms the basis of techniques that serve to characterize semicrystalline synthetic polymers, to elucidate the chemical structure of biopolymers capable of crystallizing such as certain proteins, and to determine the size, shape and state of aggregation of macromolecules in solution (see Section 6.4). In fact, solution scattering is an important tool for characterizing biopolymers such as proteins and nucleic acids in the native state.

The advances in X-ray applications are closely related to the development of X-ray sources, and within this context recently constructed electron-synchrotron facilities are to be noted in particular. Synchrotrons produce high-intensity beams of photons that cover a broad range of energies. The fact that

Polymers and Electromagnetic Radiation: Fundamentals and Practical Applications, First Edition. Wolfram Schnabel
© 2014 Wiley-VCH Verlag GmbH & Co. KGaA. Published 2014 by Wiley-VCH Verlag GmbH & Co. KGaA.

Lam Research Ex. 1047 - Page 322
Lam Research Corp. v. Inpria Corp.
IPR2024-00033 - U.S. Patent No. 9,823,564

synchrotron radiation is polarized can also be of use. There are today also new, more powerful X-ray (bremsstrahlung) sources that are based on electron beam/X-ray conversion and continue to open up routes to as-yet unexplored application modes [1].

6.2
X-Ray Spectroscopy

6.2.1
General Aspects

X-ray absorption spectroscopy is used as an analytical tool for quantitative analyses of the chemical composition of polymer blends and copolymers. It serves to study the interaction of molecules with surfaces and the orientation of molecules on surfaces [2–11]; exploration of the structure of metal-containing proteins is another interesting application [12–14]. As noted in Section 4.1, X-ray absorption causes the excitation of tightly bound core electrons and, therefore, X-ray absorption spectra are characterized by edges which correspond to the binding energy of electrons in specific shells of specific atoms, denoted by uppercase letters K, L, M, N, and so on. With increasing core–shell distance the binding energy decreases. The drastic increase in the absorption coefficient at the edge signals the presence of a certain element, and since electron binding energies are well known, the elemental composition of a sample is readily accomplished. The observed X-ray spectrum – that is, the absorption recorded as a function of photon energy – is the sum of the contributions related to excitations occurring in the elements in the sample. Figure 6.1 depicts schematically the shape of an X-ray absorption spectrum of a polymer containing carbon, nitrogen, and oxygen.

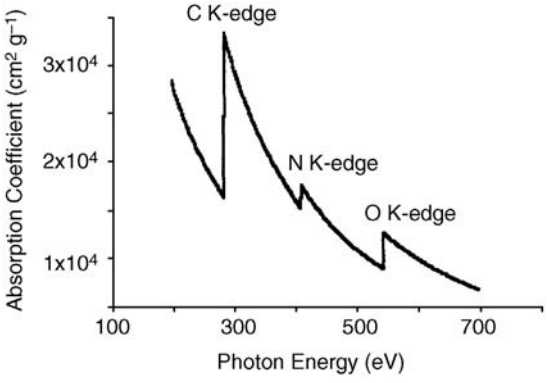


Figure 6.1 X-ray absorption spectrum of a typical polymer containing carbon, nitrogen, and oxygen. Adapted from Ref. [15].

Lam Research Ex. 1047 - Page 323
Lam Research Corp. v. Inpria Corp.
IPR2024-00033 - U.S. Patent No. 9,823,564

6.2.2
Near-Edge X-Ray Absorption Fine Structure (NEXAFS) Spectroscopy

NEXAFS, which is also referred to as X-ray absorption near-edge spectroscopy (*XANES*), concerns spectral features appearing around the absorption edge up to about 30 eV above the edge. These features are related to electronic transitions of core electrons from the ground state into unoccupied molecular orbitals of π and σ symmetry below and above the ionization energy (see Figure 4.6). The energies of molecular orbitals depend on the nature of chemical bonding of the constituting atoms, which in turn implies a dependence of the transition energies on the chemical nature of functional groups bound to the atom from which a core electron is released. Differences in the magnitude of the transition energies are reflected by differences in the peak positions in the absorption spectrum. Notably, NEXAFS spectra of different polymers can differ significantly even for rather similar structures [15]. A typical NEXAFS spectrum recorded with a copolymer of styrene and acrylonitrile is shown in Figure 6.2.

NEXAFS spectroscopy can be applied for quantitative analyses of the chemical composition of polymer blends and copolymers [9]. An interesting application concerns *NEXAFS microscopy* (see Section 6.3). Moreover, the application of NEXAFS spectroscopy to surface studies – and in particular to studies related to the adsorption of organic molecules onto the surfaces of metals and polymers – is of particular interest. For example, the NEXAFS spectra of a monolayer of poly-3-methylthiophene, electrochemically grafted onto Pt, revealed that the aromatic rings in the polymeric layer are π-bonded to the Pt(111) surface [16]. In addition, NEXAFS spectroscopy provides answers to questions such as "How do molecules interact with surfaces?" or "How do molecules orient on surfaces?"

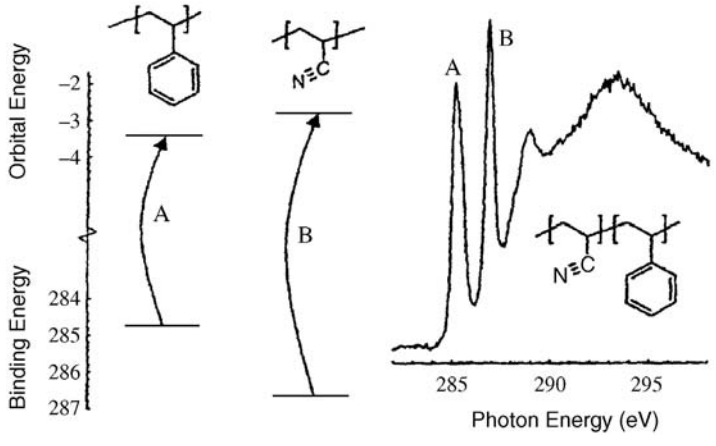


Figure 6.2 NEXAFS spectrum of poly(styrene-*co*-acrylonitrile). Left: Energy schemes related to the electronic transitions C 1s → $\pi_{C=C}$ (A) and C 1s → $\pi_{C\equiv N}$ (B). Adapted with permission from Ref. [9]; © 2002, World Scientific Publishing.

Lam Research Ex. 1047 - Page 324
Lam Research Corp. v. Inpria Corp.
IPR2024-00033 - U.S. Patent No. 9,823,564

6.2.3
Extended X-Ray Absorption Fine Structure (EXAFS) Spectroscopy

At photon energies which exceed the NEXAFS range – that is, from about 30 to 1000 eV – X-ray absorption spectra are characterized by wavy fine structures. The oscillatory nature of these fine structures is thought to be due to interference caused by interaction of the outgoing photoelectron wave with the wave(s) backscattered from surrounding atoms (see Section 4.3). The interference depends on the distance $R_{a\text{-}b}$ between the absorbing atom and the backscattering atoms. $R_{a\text{-}b}$ can be determined from EXAFS spectra with the aid of an appropriate theory (see Ref. [10]). EXAFS spectroscopy allows the determination of local structures element-specifically in almost any mixture, independent of the sample's physical state. With regards to complexes, EXAFS spectroscopy can provide structural information on the first shell of coordination around an atom including accurate interatomic distances, together with estimates of the type (atomic number) and number of the surrounding atoms. EXAFS spectroscopy has also been widely applied to biochemical systems, in particular to proteins containing metal centers; examples include Mn in photosystem II, Cu in blue copper proteins, Cu and Zn in superoxide dismutase, and Fe and Cu in cytochrome c oxidase [12,13]. The metal centers are coordinated by amino acid residues; for example, in the case of cytochrome c oxidase, the Cu center is coordinated by two histidine and two cystine moieties, with $R_{Cu\text{-}N} = 1.97$ Å and $R_{Cu\text{-}S} = 2.28$ Å [14].

Polarized EXAFS spectra of oriented thin films can reveal information about the ordering of the molecules, as in the case of poly(di-*n*-hexyl silane) films. In relevant experiments, spectra were recorded on carbon and silicon edges [17].

6.2.4
X-Ray Photoelectron Spectroscopy (XPS)

X-ray photoelectron spectroscopy, which was developed as an extension of UV photoelectron spectroscopy (see Section 3.2.3.1) by K. Siegbahn (who was awarded the Nobel Prize 1981) is an important analytical tool for the analysis of surfaces [18–23]. The method, which is also referred to as electron spectroscopy for chemical analysis (*ESCA*), is based on the photoelectric effect according to which the absorption of an X-ray photon results in the emission of an electron possessing a certain kinetic energy (see Section 4.3). In most cases, samples are irradiated with monoenergetic soft X-rays (typically Mg K_α, 1253.6 eV, or Al K_α, 1486.6 eV) and the energy distribution of electrons emitted after the absorption of photons is measured. The mean free path of the emitted electrons in solid polymer sheets is very short, and therefore detectable electrons originate from only the top atomic layers of the irradiated surface (ca. 1 nm). Commonly, XPS spectra are presented as plots of the number of emitted electrons versus the binding energy; the latter is obtained on the basis of measured kinetic-energy values with the aid of Equation 4.4. The peaks of the spectra correspond to the

Lam Research Ex. 1047 - Page 325
Lam Research Corp. v. Inpria Corp.
IPR2024-00033 - U.S. Patent No. 9,823,564

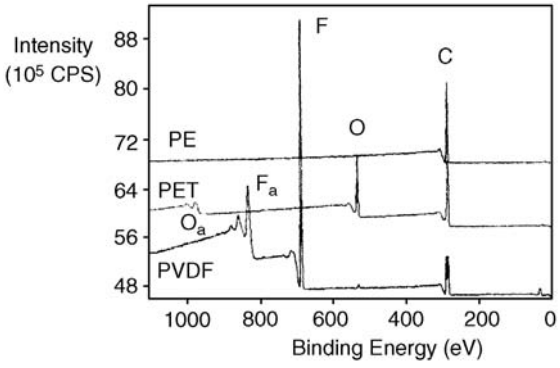


Figure 6.3 XPS spectra of polyethylene (PE), poly(ethylene terephthalate) (PET) and poly (vinylidene fluoride) (PVDF). The peaks denoted as F_a and O_a are related to the emission of Auger electrons. Adapted with permission from Ref. [22]; © European Polymer Federation.

electron configuration within the atom – that is, 1s, 2s, 2p, 3s, and so on. The overwhelming portion of X-ray photons interacts with core electrons (1s transitions), and each element contained in the sample produces a characteristic peak at an element-characteristic binding energy. The elements contained in the surface of the sample are identified from the position of the peaks. The element spectra of three polymers shown in Figure 6.3 exhibit strong peaks that correspond to the elements carbon, oxygen, and fluorine, respectively.

With high-resolution techniques the rather weak influence of valence electrons on the binding strength of core electrons is detectable. This essential feature of XPS is demonstrated in Figure 6.4, where C_{1s} spectra of polyethylene (*PE*), poly (ethylene terephthalate) (*PET*) and poly(vinylidene fluoride) (*PVDF*) are shown. While the spectrum of PE contains only a single peak at 285.0 eV, assigned to aliphatic carbon (C—C, C—H), the spectrum of PET exhibits three peaks assigned to aromatic carbon (C_{arom}) at 285 eV, C—O-bonded carbon at 286.6 eV, and carboxylic carbon (O—C=O) at 289.9 eV. The C_{1s} spectrum of PVDF shows two carbon lines at 285.0 eV (aliphatic carbon) and 290.0 eV (CF_2 carbon) in the stoichiometric ratio.

A small fraction of soft X-ray photons being absorbed by matter (1% or less) interact with valence electrons (C_{2s}, O_{2s} transition, etc.). The corresponding tiny lines of the spectrum can be detected and satisfactorily resolved with modern techniques. As the binding energy of valence electrons depends significantly on the nature of the chemical bond, valence-photoelectron spectroscopy has been developed as a powerful tool for chemists, especially for those involved in studies with polymers. Typical valence energy level spectra, recorded with acetates and polyacrylates, are depicted in Figure 6.5, where the overall band profiles are fingerprints for each particular compound with band assignments related to

Lam Research Ex. 1047 - Page 326
Lam Research Corp. v. Inpria Corp.
IPR2024-00033 - U.S. Patent No. 9,823,564

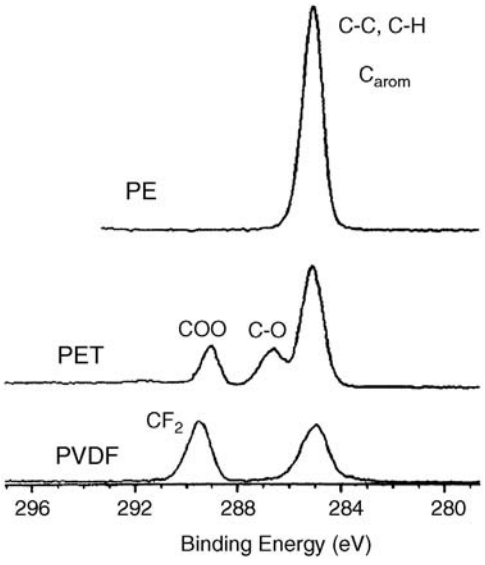


Figure 6.4 XPS spectra (C_{1s} spectra) of polyethylene (PE), poly(ethylene terephthalate) (PET) and poly(vinylidene fluoride) (PVDF). Adapted with permission from Ref. [22]; © European Polymer Federation.

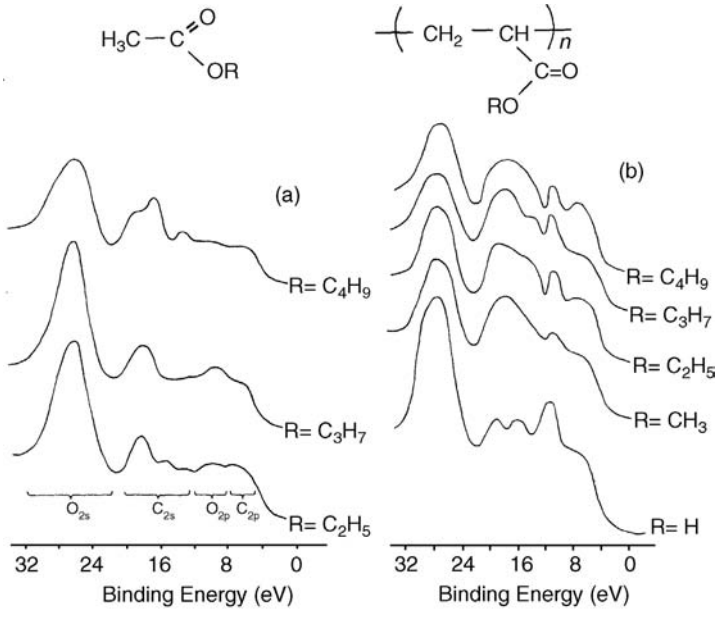


Figure 6.5 Valence energy level spectra of (a) alkyl acetates and (b) poly(alkyl acrylates). Adapted with permission from Ref. [23]; © 1976, John Wiley.

Lam Research Ex. 1047 - Page 327
Lam Research Corp. v. Inpria Corp.
IPR2024-00033 - U.S. Patent No. 9,823,564

electron transitions involving the orbitals O_{2s} (21 to 32 eV), C_{2s} (12 to 21 eV), O_{2p}, and C_{2p} (the latter two in the region below 12 eV) [23].

Important applications of XPS pertain to the characterization of polymer surfaces. These applications include the detection of oxidation products and impurities, and observations of molecular rearrangements and chemical modifications of polymer chains. Moreover, XPS is an appropriate tool to follow up flame and plasma treatments of polymers. In polymer processing, XPS can help to optimize surface properties while retaining desirable bulk properties.

6.3 X-Ray Imaging and Microscopy

Interesting X-ray applications involve the imaging of tiny areas of polymer specimens. This will be demonstrated in the following by reference to NEXAFS microscopy (see Section 6.2.2) and XPS (see Section 6.2.4) [9]. NEXAFS microscopy techniques operating in the 200 to 900 eV range are utilized to characterize thin films and surfaces. These techniques allow the probing of micrometer-sized areas with a spatial resolution better than 50 nm, both in transmission mode to measure bulk properties, and in reflection mode to study surfaces. Among others, NEXAFS microscopy has proved successful for studying thin bilayer and multilayer polymer films, multicomponent and multiphase polymer blends. As a typical example, Figure 6.6 shows the NEXAFS

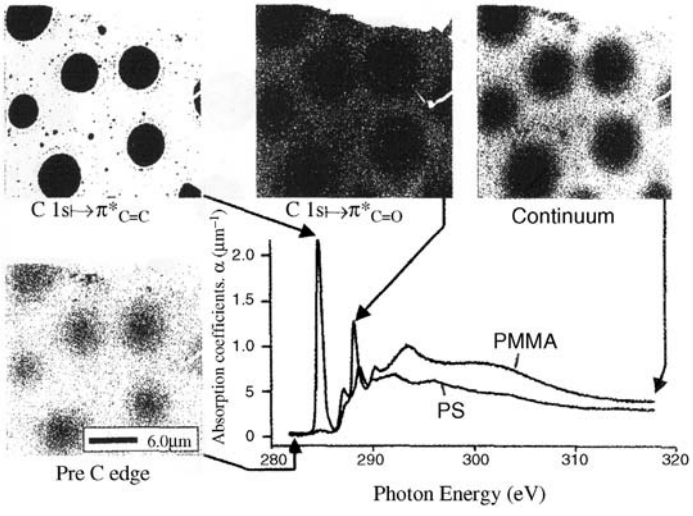


Figure 6.6 NEXAFS reference spectra of polystyrene (*PS*) and poly(methyl methacrylate) (*PMMA*) and transmission images of a PS/PMMA blend recorded at four different photon energies as indicated. Adapted with permission from Ref. [9]; © 2002, World Scientific Publishing.

Lam Research Ex. 1047 - Page 328
Lam Research Corp. v. Inpria Corp.
IPR2024-00033 - U.S. Patent No. 9,823,564

transmission images of a polystyrene/poly(methyl methacrylate) blend. The figure shows that NEXAFS microscopy is based on recording images at various photon energies that are sensitive to specific functional groups.

6.4 X-Ray Scattering

6.4.1 General Aspects

X-rays passing through matter are attenuated to some extent both by absorption and scattering processes. Scattering is commonly interpreted by the following model, which has been briefly introduced already in Section 3.2.3.2 and is related to the scattering of visible light: The oscillating electrical field of an X-ray wave causes vigorous vibrations of the shell electrons of atoms, thus forming oscillating dipoles. Such dipoles are themselves the source of electromagnetic waves being of the same wavelength as that of the incident wave and being emitted over the whole space. The scattering, which is said to be *coherent* and is referred to as *Rayleigh* scattering, can also be seen as an elastic collision process of photons with electrons – that is, as a process in which the photons do not lose energy. There exists a definite relationship between the phase of the incident and outgoing wave which implies the possibility of interference of X-rays scattered by different scattering centers.

Scattering phenomenons form the basis of techniques used for the characterization of semicrystalline synthetic polymers and the elucidation of the chemical structure of crystalline biopolymers, such as proteins. Moreover, the size, shape and state of aggregation of macromolecules in solution can be determined using X-ray scattering techniques. This subject has been covered extensively elsewhere [24–54].

6.4.2 Crystalline Polymers

X-ray interference plays a key role in the characterization of rigid polymers, as it allows the detection of crystallinity [24,55–60]. Interference occurring in crystals can be understood in terms of X-ray waves being reflected from the internal atomic planes of the crystal, in the same way that visible light waves are reflected by a mirror (specular reflection); this point is illustrated in Figure 6.7.

Each plane reflects a very small fraction of the X-ray beam of wavelength λ which is incident at a glancing angle Θ. The reflected waves can interfere either constructively or destructively. Constructive interference occurs when the glancing angle satisfies Bragg's law (see Equation 6.1), that is, when the path length difference of waves reflected from adjacent planes, is an integral

Lam Research Ex. 1047 - Page 329
Lam Research Corp. v. Inpria Corp.
IPR2024-00033 - U.S. Patent No. 9,823,564

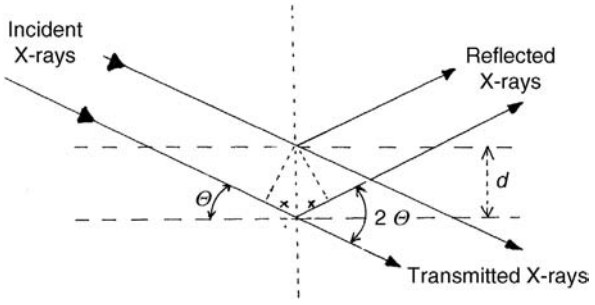


Figure 6.7 Illustration of the reflection of X-rays from the internal atomic planes of a crystal.

multiple of the wavelength. The waves reflected from different planes will be in phase when

$$n\lambda = 2d \sin \Theta \tag{6.1}$$

where $n = 1, 2, 3$, and so on, and d is the distance between parallel lattice planes.

It follows, that a characteristic diffraction pattern is obtained, when the scattered radiation intensity is measured as a function of Θ. Actually, a well-defined angular pattern is indicative of a medium of high orderliness, and in this case the term *diffraction* is commonly used instead of *scattering*.

On flat detection films, wide angle X-ray diffraction (*WAXD*) from crystalline polymers yields circle-shaped patterns, the circles being related to reflections from different lattice planes, as can be seen in Figure 6.8. By contrast, amorphous polymers yield diffuse halos.

The scattering data collected from crystalline material are in reciprocal space and must be analyzed using various mathematical operations to construct the information in real space. The transformation from reciprocal space to real space affords a modeling approach to obtain structural information, and sources of further reading on this topic are available elsewhere [61]. From the angles and intensities of the diffracted beams, a three-dimensional (*3-D*) picture of the electron-density distribution within the crystal is produced; subsequently, the mean positions of the atoms in the molecule can be determined from the electron-density distribution, as shown schematically in Figure 6.9.

In this way, many thousands of crystal structures of proteins, nucleic acids and other biological molecules have been determined using X-ray scattering. The crystal structures of proteins were first resolved during the late 1950s, starting with the structure of sperm whale myoglobin by M. Perutz and J. C. Kendrew (who were awarded the Nobel Prize in 1962). Today, X-ray crystallography is used routinely to resolve the structures of arbitrarily large molecules.

Moreover, WAXD has been used to determine how the addition of a low-molecular-weight material to a polymer causes the latter to start crystallizing at a concentration in excess of a critical value.

Lam Research Ex. 1047 - Page 330
Lam Research Corp. v. Inpria Corp.
IPR2024-00033 - U.S. Patent No. 9,823,564

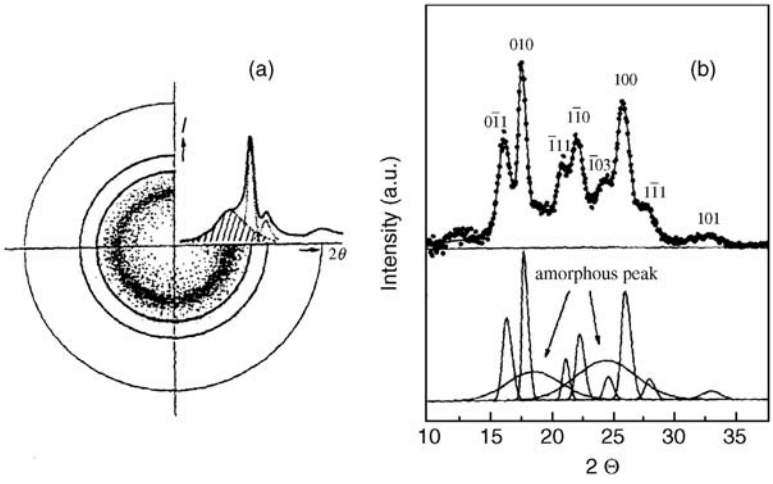


Figure 6.8 (a) Schematic presentation of a wide-angle-diffraction diagram of an unoriented crystalline polymer. The radial intensity distribution is given in the first quadrant; (b) WAXD profile of a poly(ethylene terephthalate) sample having a degree of crystallinity equal to 57% recorded at 38 °C, $\lambda = 1.307$ Å, sample–detector distance = 100 mm. Panel (a) adapted with permission from Ref. [36]; © 2005, Springer; panel (b) adapted with permission from Ref. [59]; © 2000, Elsevier.

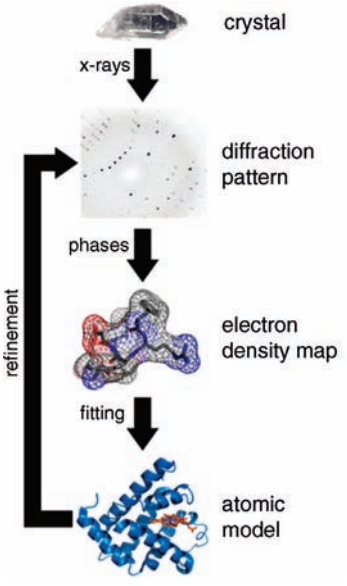


Figure 6.9 Evaluation of the structure of a protein from wide-angle X-ray scattering data. Adapted from Ref. [24].

Lam Research Ex. 1047 - Page 331
Lam Research Corp. v. Inpria Corp.
IPR2024-00033 - U.S. Patent No. 9,823,564

An alternative important application of WAXD relates to the determination of the degree of crystallinity in synthetic rigid polymers. Moreover, the morphology – that is, the arrangement of the crystalline and amorphous regions – can also be studied and crystallites characterized with regards to their size and lattice distortion [36,61,63]. From the plot of the scattering intensity versus the scattering angle depicted in Figure 6.8b the degree of crystallinity x_{crst} of unoriented partially crystalline PET can be determined. The plot shows sharp crystalline diffractions overlapped by peaks of amorphous halos. Subsequent to deconvolution and corrections for incoherent scattering (not shown in Figure 6.8b), the degree of crystallinity is obtained by dividing the area corresponding to the crystalline reflection intensities by the area of the overall intensity: $x_{cryst} = a_{crystalline}/a_{total}$. Subsequently, by means of time-resolved measurements, information on the mechanism of crystallization is obtained. A typical example related to the formation of crystallites by rapid cooling of liquid PE from 150 °C to 122 °C is shown in Figure 6.10.

A further interesting application of WAXD concerns the orientation of macromolecules in natural fibers, and in fibers of synthetic polymers drawn under the influence of an outer mechanical force. Fibers produce patterns that resemble those of single crystals of inorganic salts. Figure 6.11a and b illustrate, schematically, WAXD by a specimen with axial orientation, where the fiber axis is normal to the incident X-ray beam. Spot locations at the detector screen can be denoted by a radial distance from the primary beam, and by an azimuth β with respect to the meridian. The diffraction patterns of undrawn and drawn specimens of silicone rubber are shown in Figure 6.12, as a typical example.

Frequently employed WAXD techniques use X-rays or synchrotron radiation of wavelengths in the range of 0.1 to 0.2 nm, while the sample–detector distance ranges from 0.05 to 0.2 m. According to Bragg's law (Equation 6.1),

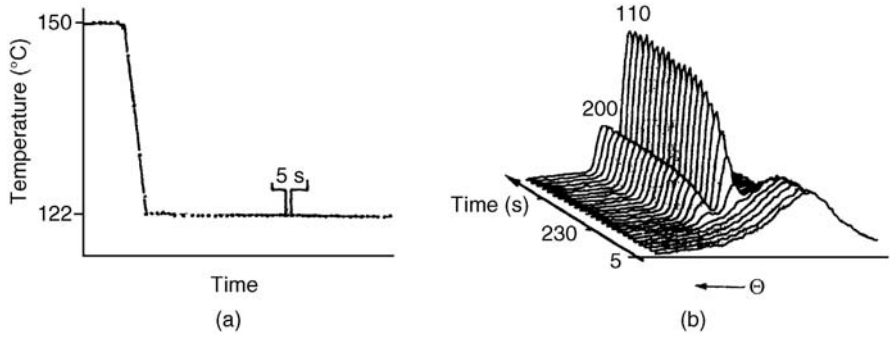


Figure 6.10 Formation of crystallites by rapid cooling of liquid polyethylene from 150 °C to 122 °C. (a) Temperature/time profile; (b) Wide-angle scattering diagrams illustrating the formation of crystallites. Adapted with permission from Ref. [43]; © 1985, Springer Verlag.

Lam Research Ex. 1047 - Page 332
Lam Research Corp. v. Inpria Corp.
IPR2024-00033 - U.S. Patent No. 9,823,564

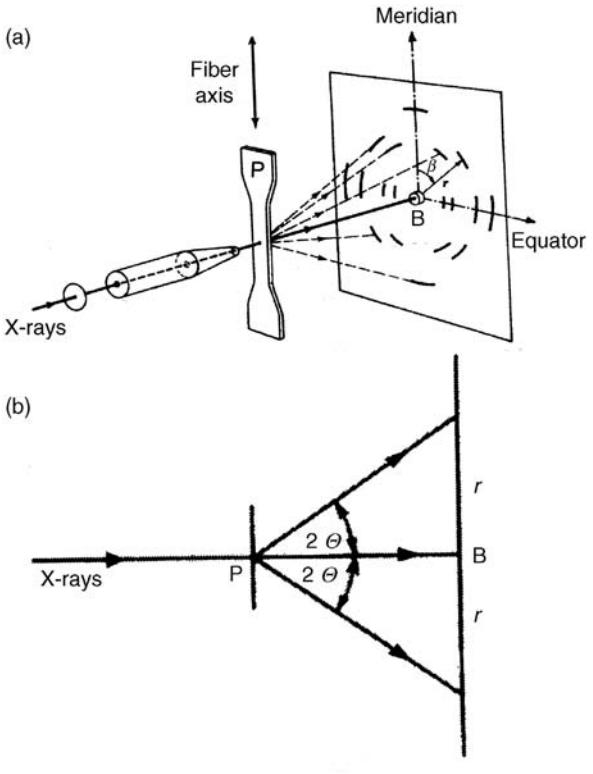


Figure 6.11 (a) Schematic illustration of WAXD by a specimen with axial orientation; (b) Dimensional relationships related to panel (a). Adapted with permission from Ref. [37]; © 1979, John Wiley.



Figure 6.12 Influence of orientation induced by elongation on the diffraction pattern of silicone rubber. Drawing by a factor of 6.5 was performed at −60 °C. Adapted with permission from Ref. [62]; © 1958, John Wiley.

Lam Research Ex. 1047 - Page 333
Lam Research Corp. v. Inpria Corp.
IPR2024-00033 - U.S. Patent No. 9,823,564

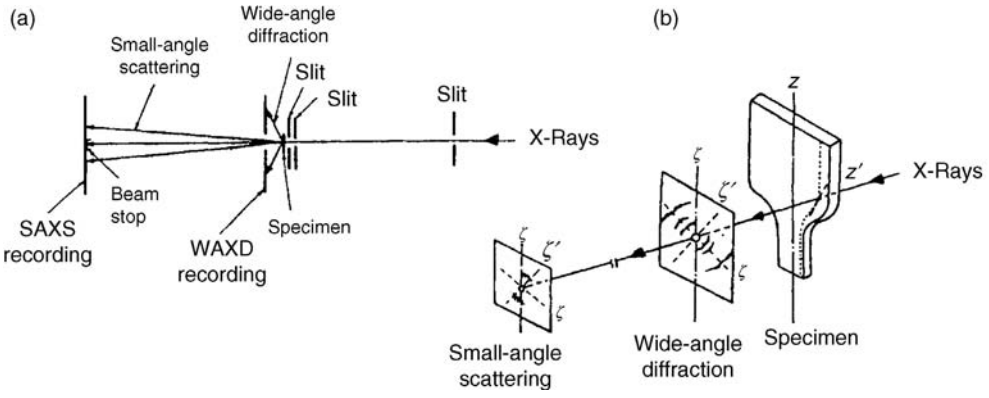


Figure 6.13 Simultaneous recording of WAXS and SAXS patterns. (a) The set-up used; (b) Pattern generation. Adapted with permission from Ref. [36]; © 2005, Springer.

the dimensions of objects reflecting this radiation measure about 0.1 nm (1 Å), that is, d and λ are of the same order of magnitude. Because of the reciprocal relationship between d and sin Θ, objects of larger dimensions are expected to reflect X-rays of the same wavelengths (0.1 to 0.2 nm) at very low angles. Therefore, small-angle X-ray scattering (*SAXS*) at angles between 0.1° and 10°, $\lambda = 0.1$ nm and sample–detector distances ranging from 1 to 3 m can reveal the existence of inhomogeneities extending up to several hundred nanometers in polymeric materials. Such inhomogeneities include crystallites in semicrystalline materials or gaseous or liquid domains in solid polymers. For example, SAXS resulting from voids can indicate the presence of pores generated in amorphous material by aging. In this case, the scattering intensity at very small angles is systematically increasing as a function of aging [61]. SAXS is applied to measure the size and size distributions of crystallites in partially crystalline polymers. In order to characterize such polymers in detail, set-ups allowing simultaneous WAXS and SAXS measurements are used; such an arrangement is shown schematically in Figure 6.13a and b.

From the SAXS profiles of two PET samples, as shown in Figure 6.14, the long period – that is, the average distance between crystalline lamellae in the amorphous matrix – is calculated as 77 Å ($x_{crys} = 57\%$) and 118 Å ($x_{crys} = 40\%$). The long period represents the average distance between regions of equivalent electron density. The shape of the SAXS patterns reflects characteristic morphological textures of the scattering specimen. Typical SAXS patterns of partially crystalline polymers are presented in Figure 6.15.

Generally, diffraction lines and spots are broadened due to instrumental effects. Apart from this, there is *true broadening* which can be due to two factors: broadening due to crystallite size and broadening due to strain-induced lattice distortion inside the crystallites (crystalline regions), as illustrated in Figure 6.16.

Lam Research Ex. 1047 - Page 334
Lam Research Corp. v. Inpria Corp.
IPR2024-00033 - U.S. Patent No. 9,823,564

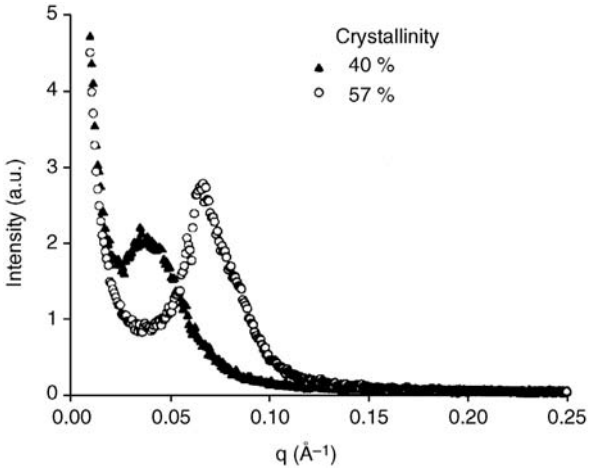


Figure 6.14 SAXS profiles of two PET samples recorded at 38 °C, $\lambda = 1.307$ Á, sample–detector distance 1950 mm. $q = (4\pi/\lambda)\sin\Theta$. Scattering angle 2Θ. Adapted with permission from Ref. [59]; © 2000, Elsevier.

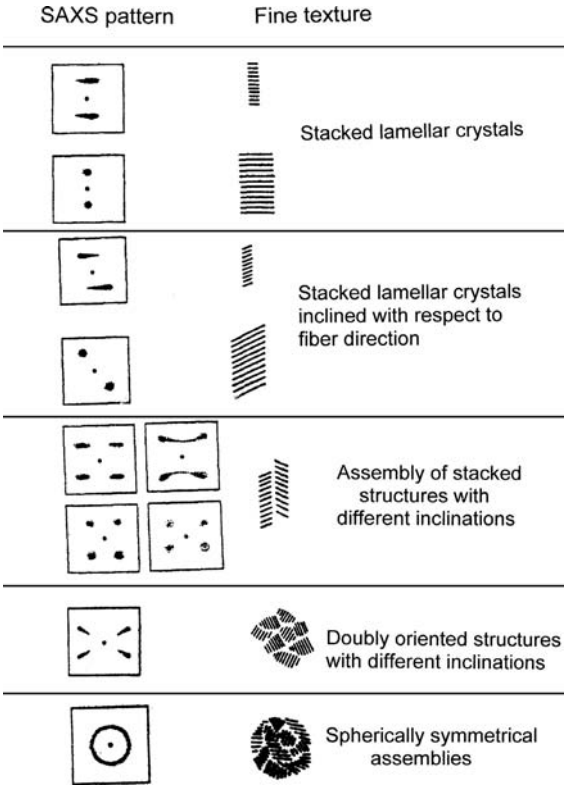


Figure 6.15 SAXS patterns related to typical morphological textures in partially crystalline polymers. Adapted with permission from Ref. [36]; © 2005, Springer.

Lam Research Ex. 1047 - Page 335
Lam Research Corp. v. Inpria Corp.
IPR2024-00033 - U.S. Patent No. 9,823,564

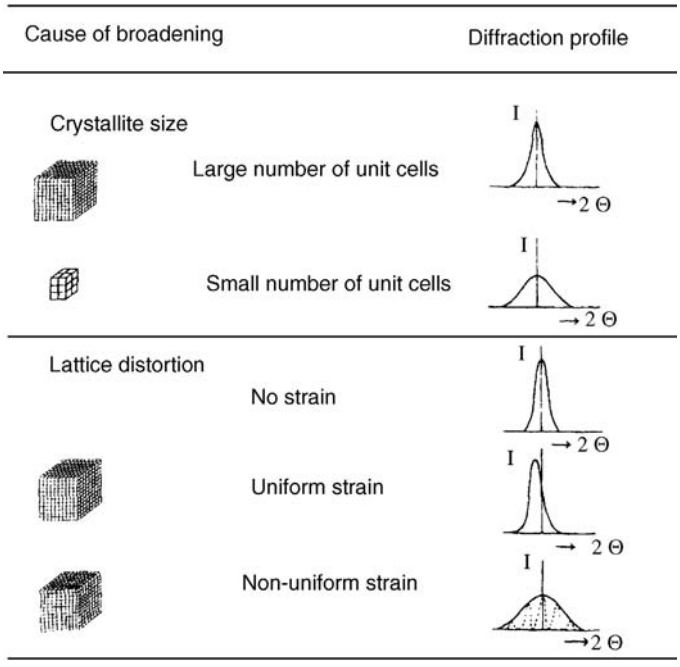


Figure 6.16 Illustration of broadening of lines observed at X-ray scattering by crystallites. Adapted with permission from Ref. [36]; © 2005, Springer.

As has been demonstrated by Bodor [65], the number distribution of the crystalline particle size in partially crystalline polymers can be determined by a method related to line broadening of X-ray scattering peaks. Figure 6.17 shows the particle size distribution of a linear PE sample that was cooled down from the melt at 160 °C to 125 °C.

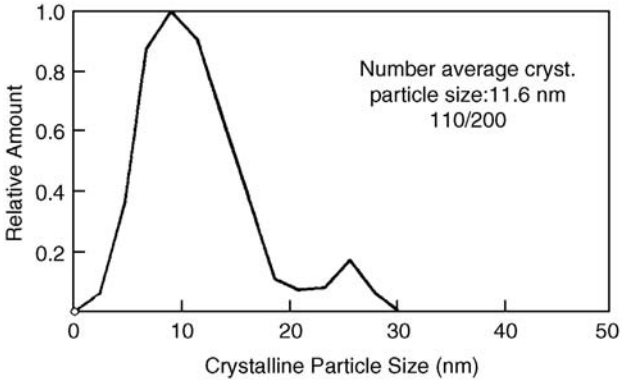


Figure 6.17 Number distribution of crystalline particle size of a linear polyethylene sample melted for 2 h at 160 °C and annealed for two days at 125 °C. Adapted with permission from Ref. [63]; © 1985, Springer.

Lam Research Ex. 1047 - Page 336
Lam Research Corp. v. Inpria Corp.
IPR2024-00033 - U.S. Patent No. 9,823,564

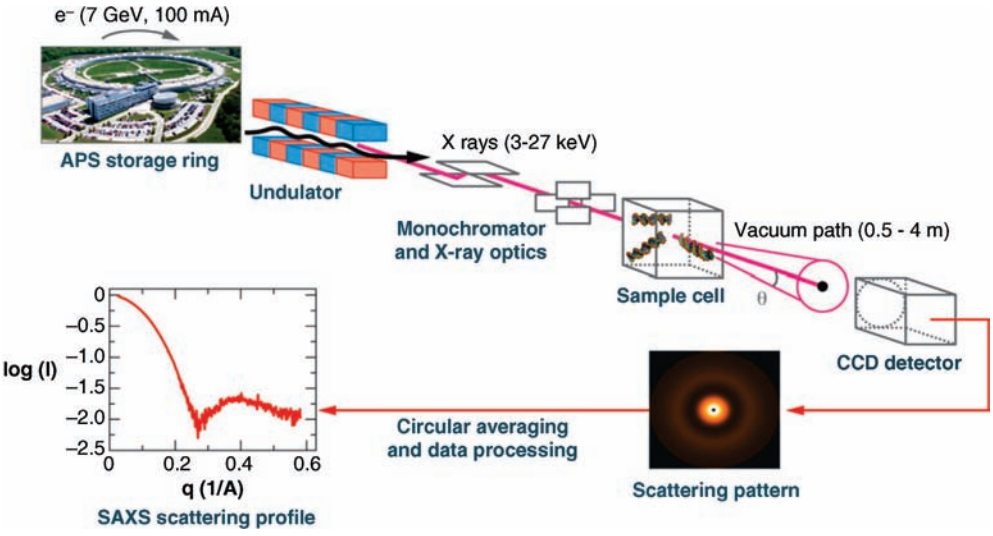


Figure 6.18 X-ray scattering set-up employing an electron synchrotron. Adapted with permission from Ref. [27]; © 2007, from Annual Reviews.

Modern scattering techniques employ electron synchrotrons, generating electromagnetic radiation of high intensity and high brightness, in conjunction with sophisticated detection systems based, for example, on CCD (charge coupled device) area detectors. A typical set-up is shown schematically in Figure 6.18.

6.4.3 Polymer Solutions

Solution scattering is an important tool to characterize biopolymers in the native state [53,64–68]. Relevant methods applicable to dilute solutions of macromolecules are related to the diffuse scattering at angles in close proximity to the primary X-ray beam, which is produced in systems containing regions of nonuniform electron density. The scattering signal is determined by the difference in average electron density $\Delta\rho(r)$ of the solute $\rho(r)$ and solvent ρ_s molecule. $\Delta\rho(r) = \rho(r) - \rho_s$ is also referred to as excess scattering length density or contrast. Typical $\rho(r)$ values (in electrons nm^{-3}) are 550 (DNA), 420 (proteins), and 334 (pure water) [66]. Since the scattering depends on the geometric structure of the inhomogeneous regions, it is possible to establish the size, shape and state of aggregation of the macromolecules by an analysis of the scattering pattern. First reports on the diffuse scattering phenomenon observed with dilute polymer solutions date back to the 1930s [69]. Since then SAXS methods related to the characterization of macromolecules in dilute solution have been developed and theoretical studies have been devoted to the quantitative treatment of the experimental results obtained [29,31,33,37,70,71]. The subject has been treated systematically by Kasai and Kakudo [38], and

Lam Research Ex. 1047 - Page 337
Lam Research Corp. v. Inpria Corp.
IPR2024-00033 - U.S. Patent No. 9,823,564

relevant investigations have been critically reviewed with respect to recent achievements by Stribeck [63].

In practice, SAXS studies on macromolecules in solution are performed by recording separately the scattering curves (intensity I_q versus momentum transfer q) for the polymer solution and the solvent and subtracting the latter from the former. q is equal to $(4\pi/\lambda)$ sin Θ, where 2Θ is the scattering angle. Any dependence of I_q on the concentration c is considered by extrapolating I_q to $c \rightarrow 0$. In the case of monodisperse systems consisting of dilute solutions of noninteracting arbitrarily oriented identical particles, the scattering intensity can be expressed by Equation 6.2:

$$I_q = I_0 P_q \tag{6.2}$$

where I_0 is the forward scattering intensity, and P_q the scattering function of the particle, also referred to as the *form factor.*

P_q is originating from intramolecular interferences of the polymer and is, therefore, characteristic of the size and the shape of the macromolecule. It is defined according to Equation 6.3 [54]:

$$P_q = \frac{1}{z^2} \sum_{i=1}^{z} \sum_{j=1}^{z} \left\langle \frac{\sin q r_{ij}}{q r_{ij}} \right\rangle \tag{6.3}$$

where r_{ij} is the vector joining two scattering points, z is the number of scattering points, and $\langle\ \rangle$ indicates average value over all orientations and conformations. For globular particles, P_q is given by Equation 6.4:

$$P_q = \exp\left[-\frac{4\pi^2 R_g^2 q^2}{3} \right] \tag{6.4}$$

where R_g is the radius of gyration. On inserting P_q, given by Equation 6.4, into Equation 6.2, the dependence of the scattering intensity on q is obtained (see Equation 6.5).

$$I_q = I_0 \exp\left[-\frac{4\pi^2 R_g^2 q^2}{3} \right] \tag{6.5}$$

A plot of ln I_q versus q^2 should result in a straight line, the intercept of which with the ordinate yields I_0. I_0 is proportional to the molar mass M and the volume V of the macromolecules. Details for determination can be found elsewhere in the literature [64]. The radius of gyration is obtained from the slope α of the straight line (see Equation 6.6).

$$R_g = \left(\frac{3\lambda^2 \alpha}{16\pi^2} \right)^{\frac{1}{2}} \tag{6.6}$$

Equations 6.4 to 6.6 represent the widely used *Guinier approximation* for globular particles. Approximations pertaining to rod-like and disc-shaped particles using appropriate particle scattering functions can be found in the

Lam Research Ex. 1047 - Page 338
Lam Research Corp. v. Inpria Corp.
IPR2024-00033 - U.S. Patent No. 9,823,564

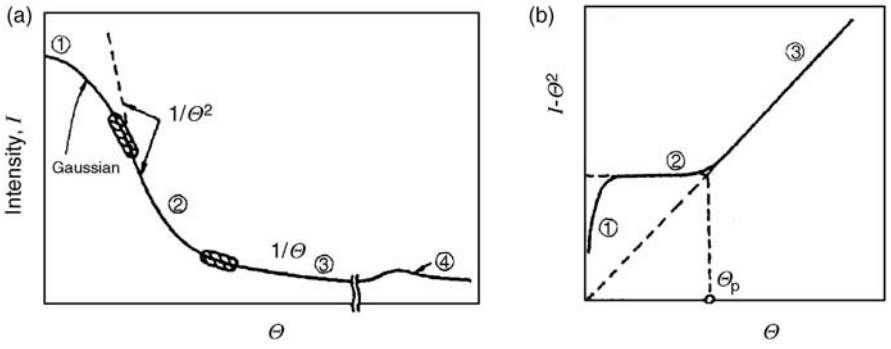


Figure 6.19 (a) Schematic presentation of the X-ray scattering curve (I versus Θ) of a dilute solution of a coiled linear chain polymer; (b) Kratky plot of $I{\cdot}\Theta^2$ versus Θ. For details, see text. Adapted with permission from Ref. [29]; © 1952, Springer.

literature [36]. Notably, the Guinier equation (Equation 6.5) applies only to very small scattering angles, that is, only to a short section of the scattering curve (I versus q) obtained with a dilute polymer solution. Generally, different zones of the total scattering curve can be discriminated, as shown schematically in Figure 6.19a, where zone ① exhibits a Gaussian curve and is related to the overall size of the macromolecules. As noted above, a plot of ln I versus Θ^2 or q^2 would result in a straight line, for small scattering angles. Zone ③ is due to the interference of atoms in linear portions of the polymer chain; here, I is proportional to Θ^{-1}. The intermediate region, denoted as zone ②, is characterized by I being proportional to Θ^{-2}. In this region, a so-called *Kratky plot* of $I{\cdot}\Theta^2$ versus Θ yields an almost horizontal straight line up to a critical value Θ_p (see Figure 6.19b). In this plot, the portion related to zone ③ yields another straight line which extrapolates to the origin. Θ_p corresponds to the point of intersection of the straight lines pertaining to zone ② and zone ③. In the case of worm-like linear chain polymers, Θ_p is correlated with the *persistence length* p, according to Equation 6.7, with $s_p = 4\pi\ \Theta_p/\lambda$.

$$p = \frac{6}{\pi s_p} = \frac{1.5\lambda}{\pi^2 \Theta_p} \tag{6.7}$$

It was noted in Section 3.2.3.2 that the stiffness of worm-like chain polymers can be characterized by the persistence length, p. According to X-ray scattering studies, p is about 50 nm (150 base pairs) in the case of double-stranded DNA [72], and about 5 nm in the case of cellulose nitrate [31].

At large angles corresponding to zone ④ in Figure 6.19a, the scattering is due to short-range interatomic interferences involving solvent molecules and monomer base units. As noted in Ref. [33], the tail end of the scattering curve originates solely from the interface between particle phase and solvent phase. Here, the scattering intensity drops with a high power of q according to Equation 6.8, where $\Delta\rho$ denotes the difference in electron density between

Lam Research Ex. 1047 - Page 339
Lam Research Corp. v. Inpria Corp.
IPR2024-00033 - U.S. Patent No. 9,823,564

particle and solvent phase:

$$\lim_{q\to\infty} I_\Theta = \frac{\Delta\rho}{8\pi^2 q^d} A_P \tag{6.8}$$

Equation 6.8, with $d = 4$, is referred to as *Porod's law*, and allows the particle surface area A_p to be determined. More recently, based on the fractal theory and assuming a fractally rough particle surface, the dimensionality d in Porod's law (Equation 6.8) resumes values between 3 and 4 [25].

It should be noted that a straightaway interpretation of scattering curves is possible only in the case of large discrete molecules – that is, in the case of monodisperse systems such as certain proteins (see below), when all scattering particles are identical in size and shape. In the case of polydisperse systems, only average parameters concerning the size and shape of macromolecules in solution can be deduced from X-ray scattering curves [37].

The scattering curve may be described in terms of the *pair distribution function* $p(r)$ (also called the *distance distribution function*), according to Equation 6.9, where r is the intramolecular atomic distance and D_{max} the maximum intramolecular distance [31]:

$$I(q) = \int_0^{D_{max}} p(r)\frac{\sin(qr)}{qr}\,dr \tag{6.9}$$

Here, $p(r)$, as obtained by an indirect Fourier transform of the scattering curve, is presented by Equation 6.10:

$$p(r) = \frac{1}{2\pi^2}\int_0^\infty I(q)(qr)\sin(qr)\,dq \tag{6.10}$$

Since $p(r)$ is zero at $r = 0$ and $r = D_{max}$, the latter can be obtained from plots of $p(r)$ versus r. Typical experimental SAXS curves and related plots (Guinier and pair-distribution plots) of four different proteins are presented in Figure 6.20. A Kratky plot of unfolded apomyoglobin is shown in Figure 6.21a. Kratky plots of extended macromolecules yield a plateau or a slightly increasing course, in contrast to folded or partially folded macromolecules, as shown in Figure 6.21b.

In recent times, broad interest has been focused on biological macromolecules in solution, aiming at elucidating their structures as well as any structural changes [27,53,64–68]. In this context, SAXS emerged as a key technique for determining the structural conformation of proteins and nucleic acids, as well as of related complexes in solution – that is, in an almost native state. The basic problem in structural analysis involves the question: How can the 3-D structure of particles be derived from a one-dimensional scattering curve (I_q versus q)? Many proteins, for example, yield similar scattering curves, and to overcome this problem algorithms for the reconstruction of 3-D-electron density maps from 1-D scattering profiles, based on different models,

Lam Research Ex. 1047 - Page 340
Lam Research Corp. v. Inpria Corp.
IPR2024-00033 - U.S. Patent No. 9,823,564

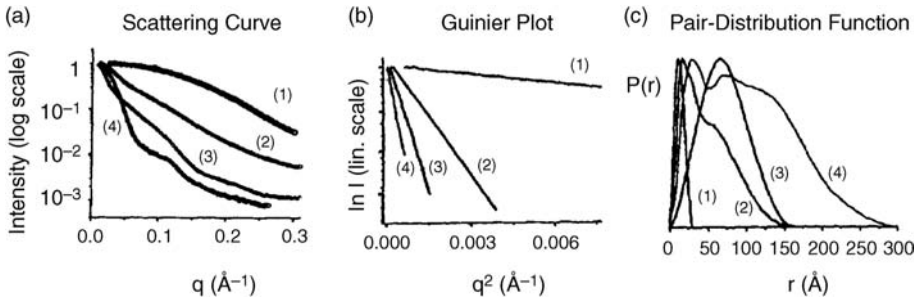


Figure 6.20 Small-angle X-ray scattering of four proteins in solution. (a) Experimental scattering curves; (b) Guinier plots; (c) Plots of pair-distribution functions. The denotations refer to values of R_g (nm) and M ($g\,mol^{-1}$), respectively: (1) 1.1 and 9×10^3; (2) 4 and 3.8×10^4; (3) 5.6 and 4.7×10^5; (4) 8.2 and 2.8×10^5. Adapted with permission from Ref. [64]; © 2007, Cambridge University Press.

have been developed [26,27,64–66,74]. One approach uses an ensemble of dummy residues to build a locally chain-compatible structure model inside a sphere of diameter D_{max} (the maximum intraparticle distance) which is determined from the scattering data. Another program operates with a sphere of diameter D_{max} and fills it with beads, where each bead belongs either to the particle or to the solvent. Interestingly, multidomain proteins and macromolecular complexes have also been studied, and in these cases solution scattering curves were fitted using models built from structures of individual domains or subunits that are known from high-resolution nuclear magnetic resonance or X-ray crystallography measurements. An example of the application of a certain algorithm (DAMMIN) to RNA of known crystal structure is shown in

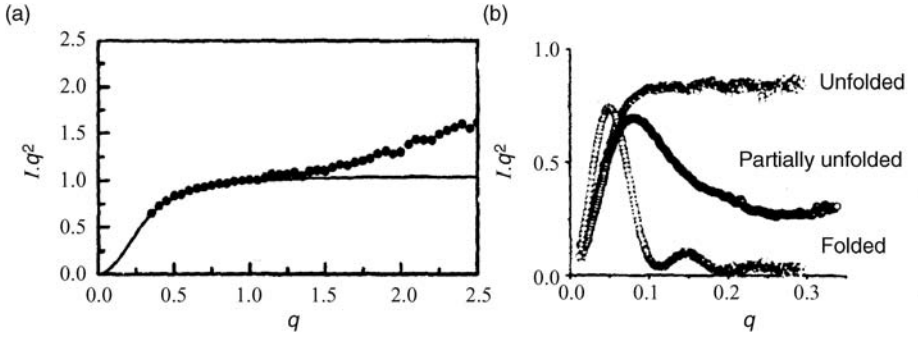


Figure 6.21 (a) Kratky plot recorded with urea-denatured (unfolded) apomyoglobin in buffer solution at pH 6.0. Adapted with permission from Ref. [73]; © 2007, American Chemical Society; (b) Schematic representation of Kratky plots resulting from different folding states of a macromolecule. Adapted with permission from Ref. [64]; © 2007, Cambridge University Press.

Lam Research Ex. 1047 - Page 341
Lam Research Corp. v. Inpria Corp.
IPR2024-00033 - U.S. Patent No. 9,823,564



Figure 6.22 Three-dimensional shape of RNA sample reconstructed from the SAXS curve. Adapted with permission from Ref. [27]; © 2007, Annual Reviews.

Figure 6.22; from this it can be seen that the shape determined from the SAXS curve coincides well with that obtained from the crystal structure [27].

References

1 Stichelbaut, S.F., Bol, J.-L., Cleland, M.R., Gregoire, O., Herer, A.S., Jongen, Y., and Mullier, B. (2004) The Palletron™: A high dose uniformity pallet irradiator with X-rays. *Radiat. Phys. Chem.*, **71**, 291.

Lam Research Ex. 1047 - Page 342
Lam Research Corp. v. Inpria Corp.
IPR2024-00033 - U.S. Patent No. 9,823,564

2 Koningsberger, D.C. and Prins, R. (eds) (1988) *X-Ray Absorption, Principles, Applications, Techniques of EXAFS, SEXAFS and XANES*, John Wiley, New York.

3 Bianconi, A. (1988) XANES spectroscopy, in *X-Ray Absorption, Principles, Applications, Techniques of EXAFS, SEXAFS and XANES* (eds D.C. Koningsberger and R. Prins), John Wiley, New York, Ch. 11.

4 Tsakanov, V. and Wiedemann, H. (eds) (2007) *Brilliant Light in Life and Material Sciences*, Springer, Berlin.

5 Sham, T.K. (ed.) (2002) *Chemical Applications of Synchrotron Radiation*, World Scientific Publishing, Singapore.

6 Als-Nielsen, J. and McMorrow, D. (2001) *Elements of Modern X-ray Physics*, John Wiley, New York.

7 Stöhr, J. (1992) *NEXAFS Spectroscopy*, 1st edn, Springer-Verlag, Berlin, (corrected printing 1996).

8 Seki, K., Ishii, H., and Ouchi, Y. (2002) Functional organic materials studied using UPS and NEXAFS, in *Chemical Applications of Synchrotron Radiation* (ed. T.K. Sham), World Scientific Publishing, Singapore, p. 386.

9 Ade, H. and Urquhart, S. (2002) NEXAFS spectroscopy and microscopy of natural and synthetic polymers, in *Chemical Applications of Synchrotron Radiation* (ed. T.K. Sham), World Scientific Publishing, Singapore, p. 285.

10 Sayers, D.E. and Bunker, B.A. (1988) Data analysis, in *X-Ray Absorption, Principles, Applications, Techniques of EXAFS, SEXAFS and XANES* (eds D.C. Koningsberger and R. Prins), John Wiley, New York, Ch. 6.

11 Fuller, M.L.S., Kasrai, M., and Bancroft, G.M. (2002) Application of X-ray absorption spectroscopy in tribology, in *Chemical Applications of Synchrotron Radiation* (ed. T.K. Sham), World Scientific Publishing, Singapore, p. 1091.

12 Cramer, S.P. (1988) Biochemical application of X-ray absorption spectroscopy, in *X-Ray Absorption, Principles, Applications, Techniques of EXAFS, SEXAFS and XANES* (eds D.C. Koningsberger and R. Prins), John Wiley, New York, Ch. 7.

13 Garner, C.D. (1995) XAS studies of metal centres in proteins. *Physica B: Condensed Matter*, **208-209**, 714.

14 Li, P.M., Gelles, J., Chan, S.I., Sullivan, R.J., and Scott, R.A. (1987) Extended X-ray absorption fine structure of copper in CuA-depleted, *p*-(hydroxymercuri)benzoate-modified, and native cytochrome c oxidase. *Biochemistry*, **26**, 2091.

15 Koprinarov, I. and Hitchcock, A.P. (2000) X-Ray Spectromicroscopy of Polymers: An Introduction for the Non-specialist. Available at: http://unicorn.chemistry.mcmaster.ca/research/stxm-intro/polystxmintro-all.pdf.

16 Stöhr, J., Gland, J.L., Kollin, E.B., Koestner, R.L., Johnson, A.L., Muetterties, E.L., and Sette, F. (1984) Desulfurization and structural transformation of thiophene on the Pt(111) surface. *Phys. Rev. Lett.*, **53**, 2161.

17 McCrary, V.R., Sette, F., Chen, C.T., Lovinger,, A.J., Robin, M.B., Stöhr, J., and Zeigler, J.M. (1988) Polarization effects in the valence and inner-shell spectra of poly(*n*-hexyl silane). *J. Chem. Phys.*, **88**, 5925.

18 Siegbahn, K. (1970) Electron spectroscopy for chemical analysis (e.s.c.a.). *Phil. Trans. Roy. Soc. London A*, **268**, 33.

19 Crist, B.V. (2000) *The Handbook of Monochromatic XPS Spectra, Part 2, Polymers and Polymers Damaged by X-rays*, John Wiley, Chichester.

20 Endo, K., Kaneda, Y., Okada, H., Chong, D.P., and Duffy, P. (1996) Analysis of X-ray photoelectron spectra of eight polymers by demon density-functional calculations using the model oligomers. *J. Phys. Chem.*, **100**, 19455.

21 Wagner, C.D., Riggs, W.M., Davis, L.E., Moulder, J.F., and Muilenberg, G.E. (eds) (1979) *Handbook of X-Ray Photoelectron Spectroscopy*, Perkin-Elmer Corp., Eden Prairie, Minnesota, USA.

22 Kaufmann, R., Höcker, H., and Möller, M. XPS – an analytical tool for the characterization of surfaces and their modifications. *The Scientific e-only Polym. J.*

23 Clark, D.T. and Thomas, H.R. (1976) Applications of ESCA to polymer chemistry. X. Core and valence energy levels of a series of polyacrylates. *J. Polym. Sci., Polym. Chem. Ed.*, **14**, 1671.

24 Splettstoesser, T. (2006) http://en.wikipedia.org/wiki/X-ray_crystallography.

Lam Research Ex. 1047 - Page 343
Lam Research Corp. v. Inpria Corp.
IPR2024-00033 - U.S. Patent No. 9,823,564

25 http://en.wikipedia.org/wiki/Small-angle_X-ray_scattering.
26 http://en.wikipedia.org/wiki/Biological_small-angle_scattering.
27 Lipfert, J. and Doniach, S. (2007) Small-angle X-ray scattering from RNA, proteins, and protein complexes. *Annu. Rev. Biophys. Biomol. Struct.*, **36**, 307.
28 Hengstenberg, J. and Mark, H. (1932) *Physik und Chemie der Cellulose* (ed. H. Mark), Springer, Berlin, p. 139.
29 Kratky, O. and Porod, G. (1952) Röntgenkleinwinkelstreuung von makromolekularen Lösungen, in *Physik der Hochpolymeren*, vol. **II** (ed. H.A. Stuart), Springer, Berlin, p. 515.
30 Kratky, O. (1952) Natural high polymers in the dissolved and solid state, in *Physik der Hochpolymeren*, vol. **II** (ed. H.A. Stuart), Springer, Berlin, p. 361.
31 Glatter, O. and Kratky, O. (eds) (1982) *Small Angle X-ray Scattering*, Academic Press, London.
32 Guinier, A. and Fournet, G. (1955) *Small Angle-Scattering of X-rays*, Chapman and Hall, London.
33 (a) Porod, G. (1951) Die Röntgenkleinwinkelstreuung von dichtgepackten kolloiden Systemen 1. *Kolloid-Z.*, **124**, 83; (b) Porod, G. (1952) Die Röntgenkleinwinkelstreuung von dichtgepackten kolloiden Systemen 2. *Kolloid-Z.*, **125**, 51.
34 Baltá-Calleja, F.J. and Vonk, C.G. (1989) *X-ray Scattering of Synthetic Polymers*, Elsevier, Amsterdam.
35 Reimers, W., Pyzalla, A.R., Schreyer, A.K., and Clemens, H. (eds) (2008) *Neutrons and Synchrotron Radiation in Engineering Materials Science. From Fundamentals to Material and Component Characterization*, Wiley-VCH, Weinheim.
36 Kasai, N. and Kakudo, M. (2005) *X-ray Diffraction by Macromolecules*, 2nd edn, Springer, Berlin.
37 Alexander, L.E. (1979) *X-ray Diffraction Methods in Polymer Science*, Wiley, New York.
38 Roe, R.J. (2000) *Methods of X-ray and Neutron Scattering in Polymer Science*, Oxford University Press, Oxford.
39 Chu, B. and Hsiao, B.S. (2001) Small angle scattering of polymers. *Chem. Rev.*, **101**, 1727.
40 Langridge, R., Wilson, H.R., Hooper, C.W., Wilkins, M.H.F., and Hamilton, L.D. (1960) The molecular configuration of deoxyribonucleic acid I. X-ray diffraction study of a crystalline form of lithium salt. *J. Mol. Biol.*, **2**, 19–37.
41 Zabel, H. (ed.) (1992) Surface X-ray and neutron scattering, in *Springer Proceedings in Physics*, vol. 61, Springer, Berlin.
42 Lindner, P. (ed.) (1991) Neutron, X-ray and light scattering, in *Proceedings of the European Workshop on Neutron, X-ray and Light Scattering as an Investigative Tool for Colloidal and Polymeric Systems, Bombannes, France*, North-Holland, Amsterdam.
43 Elsner, G., Riekel, C., and Zachmann, H.G. (1985) Synchrotron radiation in polymer science. *Adv. Polym. Sci.*, **67**, 1.
44 Stuhrmann, H.B. (1985) Resonance scattering in macromolecular structure research. *Adv. Polym. Sci.*, **67**, 123.
45 Hosemann, R. and Bagchi, S.N. (1962) *Direct Analysis of Diffraction by Matter*, North-Holland, Amsterdam.
46 Hsiao, B.S. and Chu, B. (2002) Chemical applications of small angle scattering, in *Chemical Applications of Synchrotron Radiation* (ed. T.K. Sham), World Scientific Publishing, Singapore, p. 799.
47 Hayashi, H., Udagawa, Y., Gillet., J.-M., Caliebe, W.A., and Kao, C.-C. (2002) Chemical applications of inelastic X-ray scattering, in *Chemical Applications of Synchrotron Radiation* (ed. T.K. Sham), World Scientific Publishing, Singapore, p. 850.
48 Brumberger, H. (1995) *Modern Aspects of Small Angle Scattering*, Kluwer Academic Publ., Amsterdam.
49 Agarwal, B.K. (1979) *X-ray Spectroscopy. An Introduction*, Springer, Berlin.
50 Russel, T.P. (1991) Small angle scattering at synchrotron radiation sources, in *Handbook of Synchrotron Radiation*, vol. 3 (eds G.S. Brown and D.E. Moncton), North-Holland, Amsterdam, p. 379.
51 Pietsch, U., Holy, V., and Baumbach, T. (2004) *High Resolution X-ray Scattering. From Thin Films to Lateral Nanostructures*, 2nd edn, Springer, Berlin.
52 Brown, W. and Mortensen, K. (2000) *Scattering in Polymeric and Colloidal Systems*,

Lam Research Ex. 1047 - Page 344
Lam Research Corp. v. Inpria Corp.
IPR2024-00033 - U.S. Patent No. 9,823,564

Gordon & Breach Science Publ., Amsterdam.
53 Oliveira, C.L.P., Vorup-Jensen, T., Andersen, C.B.F., Andersen, G.R., and Pedersen, J.S. (2009) Discovering new features of protein complexes structures by small-angle X-ray scattering, in *Applications of Synchrotron Light to Scattering and Diffraction in Materials and Life Sciences* (eds T.A. Ezquerra, M.C. Garcia-Gutiérrez,A. Nogales, and M.A. Gomez), Springer, Berlin, Ch. 11.
54 Higgins, J.S. and Benoit, H.C. (1994) *Polymers and Neutron Scattering*, Clarendon Press, Oxford.
55 Drenth, J. (1999) *Principles of Protein Crystallography*, Springer, Berlin.
56 McPherson, A. (2003) *Introduction to Macromolecular Crystallography*, Wiley, New York.
57 Helliwell, J.R. (1992) *Macromolecular Crystallography with Synchrotron Radiation*, Cambridge University Press, Cambridge.
58 Rupp, B. (2009) *Biomolecular Crystallography. Principles, Practice and Application to Structural Biology*, Garland Science, New York.
59 Wang, Z.-G., Hsiao, B.S., Sirota, E.B., and Srinivas, S. (2000) A simultaneous small- and wide-angle X-ray scattering study of the early stages of melt crystallization in polyethylene. *Polymer*, **41**, 8825.
60 Zachmann, H.G. (1997) Wide angle and small angle X-ray scattering for studies of the crystallization of polymers, in *Röntgen Centennial. X-rays in Natural and Life Sciences* (eds A. Haase, G. Landwehr, and E. Umbach), World Scientific, Singapore, p. 659.
61 Stribeck, N. (2007) *X-ray Scattering of Soft Matter*, Springer, Berlin.
62 Ohlberg, S.M., Alexander, L.E., and Warrick, E.L. (1958) Crystallinity and orientation in silicone rubber. I. X-ray studies. *J. Polym. Sci. A-1*, **27**, 19.
63 Bodor, G. (1985) X-ray line shape analysis. A means for the characterization of crystalline polymers. *Adv. Polym. Sci.*, **67**, 165.
64 Putnam, C.D., Hammel, M., Hura, G.L., and Tainer, J.A. (2007) X-ray solution scattering (SAXS) combined with crystallography and computation: defining accurate macromolecular structure, conformation and assemblies in solution. *Q. Rev. Biophys.*, **40**, 191.
65 Koch, M.H.J., Vachette, P., and Svergun, D.I. (2003) Small-angle scattering. A view on the properties, structure and structural changes of biological macromolecules in solution. *Q. Rev. Biophys.*, **36**, 147.
66 Svergun, D.I. and Koch, M.H.J. (2003) Small-angle scattering studies of biological macromolecules in solution. *Rep. Prog. Phys.*, **66**, 1735.
67 Ezquerra, T.A., Garcia-Gutiérrez, M.C., Nogales, A., and Gomez, M.A. (eds) (2009) *Applications of Synchrotron Light to Scattering and Diffraction in Materials and Life Sciences*, Springer, Berlin.
68 Buey, R.M., Chacon, P., Andreu, J.M., and Fernando Diaz, J. (2009) Protein shape and assembly studied with X-ray solution scattering: Fundamentals and practice, in *Applications of Synchrotron Light to Scattering and Diffraction in Materials and Life Sciences* (eds T.A. Ezquerra, M.C. Garcia-Gutiérrez, A. Nogales, and M.A. Gomez), Springer, Berlin, Ch. 12.
69 Krishnamurti, P. (1930) Studies in X-Ray diffraction, Part II and III. *Indian J. Phys.*, **5**, 489 and 543.
70 Kratky, O. (1938) Die Berechnung der Mizelldimensionen von Faserstoffen aus den unter kleinsten Winkeln abgebeugten Interferenzen. *Naturwissenschaften*, **26**, 94.
71 Guinier, A. (1939) La diffraction des Rayons X aux Très petits angles: application à l' etude de phénomènes ultramicroscopiques. *Ann. Phys. (Paris)*, **12**, 161.
72 Mastroianni, A.J., Sivak, D.A., Geissler, P.L., and Alivisatos, P.A. (2009) Probing the conformational distributions of subpersistence length DNA. *Biophys. J.*, **97**, 1408.
73 Seki, Y., Tomizawa, T., Hiragi, Y., and Soda, K. (2007) Global structure analysis of acid-unfolded myoglobin with consideration to effects of intermolecular coulomb repulsion on solution X-ray scattering. *Biochemistry*, **46**, 234.
74 Chacon, P., Moran, F., Diaz, J.F., Pantos, E., and Andreu, J.M. (1998) Low resolution structures of proteins in solution retrieved from X-ray scattering with a genetic algorithm. *Biophys. J.*, **74**, 2760.

Lam Research Ex. 1047 - Page 345
Lam Research Corp. v. Inpria Corp.
IPR2024-00033 - U.S. Patent No. 9,823,564

Index

a
absorption
– anisotropic 61
– bands of polyacrylonitrile 62
– in biopolymers 118
– broadband 64
– coefficient 63, 64, 75–78, 82, 101, 152, 192, 201, 231, 316
– mid-IR radiation by organic matter 65
– of sub-THz radiation by organic materials 16
– of swift electrons 235–237
–– branched tracks 236
–– δ-electrons 236
–– energy deposited in spurs 236
–– fraction of energy loss in solid dry DNA 236
– in synthetic conjugated polymers 115–117
– in synthetic nonconjugated polymers 114, 115
– of X-ray photons 315
absorption spectra
– DNA and bovine serum albumin 119
– polymer films 83
– synthetic conjugated polymers 117
– synthetic nonconjugated polymers 115
– synthetic polar polymers 63
– synthetic unpolar polymers 64
– typical unconjugated linear polymers 114
– X-ray absorption spectra, corresponding electron transitions 232
acetophenones 125
acid-catalyzed deprotection 295
acidolysis 192
– poly(*t*-butoxycarbonyloxystyrene) 187, 188
– proton generation by 188
acriflavin 128
acrylamide 135, 254
acrylic acid 28, 36, 37, 135
acrylonitrile 254
acrylonitrile/butadiene/styrene (ABS) copolymer 151
acryloxypropyltrimethoxysilane (APTMS) 95
11-acryloyloxyundecyltrimethylammonium bromide (AUTMAB) 246
activation energy 16, 22, 26, 40, 243
acylphosphine oxides 125
adhesion, improvement of 136
adhesion-promoting polymer layer 37
alkyl acetates 320
alkyl acrylate 127
allyl alcohol 28, 36, 37
angular frequency 9
anharmonicity 92
– constant 57
anionic photopolymerization 132
anisotropy 44, 61, 79, 82, 85, 86
– microwave anisotropy images 45
anthraquinone 128
antibonding orbital 111–113
antioxidants 151
APTMS. *see* acryloxypropyltrimethoxysilane
aromatic amino acids 119
aromatic ketones 126
2-aryl-4,6-bis(trichloromethyl)-1,3,5-triazine 298
5-arylthianthrenium salts 130
atomic vibrations 57
attenuated total reflectance (ATR) method 65, 96
attenuation coefficients 224, 228–230
Auger effect 231
AUTMAB. *see* 11-acryloyloxyundecyltrimethylammonium bromide
autoxidation 145, 148–151
Avogadro's number 111, 143
azo dye 206

Polymers and Electromagnetic Radiation: Fundamentals and Practical Applications,First Edition. Wolfram Schnabel
© 2014 Wiley-VCH Verlag GmbH & Co. KGaA. Published 2014 by Wiley-VCH Verlag GmbH & Co. KGaA.

Lam Research Ex. 1047 - Page 346
Lam Research Corp. v. Inpria Corp.
IPR2024-00033 - U.S. Patent No. 9,823,564

b

β- and γ-relaxation 15
benzil 128
benzil ketals 125
benzoin 125
benzoin ethers 125
benzophenone 135
benzophenone derivatives 126
benzothiadiazolepyrrole copolymer 194
5-benzyl-1,5-diazabicyclo[4.3.0]nonane 132, 133
beryllium-doped germanium (Ge:Be) lasers 67
bicyclo[2.2.1]hept-2-ene group 38
binding energies 7, 16, 59, 232, 316
biopolymers 58, 64
– absorption in 118
– dimerization 158, 159, 161
– formation of quinoid structures in lignins 164
– high-energy radiation with 285
– modification 158–164
– photoionization 159
– photolysis of proteins 161
– photoreactions of lignins 163
– radiolysis (*see* radiolysis)
– rupture of cystine bridges 161
– UV/Vis light, effects 158
bisphenol-A polycarbonate 207
bis(4-tert-butylphenyl)iodonium perfluorobutane sulfonate 298
bis(4-tert-butylphenyl)iodonium perfluorooctane sulfonate 298
blepharismins 121
blobs 236
block copolymers 133, 134
Boltzmann's constant 14
bovine serum albumin (BSA) 64
– absorption spectra 118, 119
– biopolymers examined with THz spectroscopy 77
– electron beam grafting of polyethylene 305
β-propiolactone 255
Bragg's law 322, 325
brilliance 233
BSA. *see* bovine serum albumin
bulk biopolymers, radiolysis 268
– nucleic acids 268–270
– polysaccharides 270–274
– proteins 274, 275
bulk synthetic polymers, radiolysis 257, 258
butadiene-styrene rubber 10

c

camphor quinone 128
ε-caprolactam 19
ε-caprolactone 19
carbocations 132
carbon black 46, 152
carotenoids 120
CARs. *see* chemically amplified resists
CAs. *see* 2-cyanoacrylates
cationic photoinitiators 130
cationic photopolymerization 127
cationic polymerization 127, 130, 133
– of epoxide 94
CD spectroscopy. *see* circular dichroism spectroscopy
cellulose 10, 22, 64, 77, 270, 272
– photochemistry 162
– THz absorption spectrum 64
CF_4 plasma 32
CGL. *see* charge generation layer
chain-growth polymerizations 17
chain terminators 154
chalcogenide, inorganic glasses 204
charge generation layer 205–207
charge transport layer (CTL) 205–207
chemical amplification 292, 294–299
chemical etching 33
chemically amplified resists (CARs) 189, 298
chiral molecules 164
chitosan 306
chlorophyll *a* 121
chromophores 144, 147, 224
chromophoric groups 109, 110, 119, 133–135, 139, 151
– for visible and ultraviolet 110
circular dichroism (CD) spectroscopy 164
– spectra of poly(L-lysine) 165
11-*cis* retinal 120
CN-PPV 193, 195
coherent microwave transient spectroscopy 43
coherent synchrotron radiation 67
coinitiator 126
Cole–Cole equation 12
color mixing 204
Compton scattering 224, 234, 235
continuous wave (CW) plasmas 27
copolymerization of monomers 37
core electron transitions, in diatomic molecule 233
corrosion phenomena 45
crosslinking boosters 294
crystal band splitting 61

Lam Research Ex. 1047 - Page 347
Lam Research Corp. v. Inpria Corp.
IPR2024-00033 - U.S. Patent No. 9,823,564

crystalline polyethylene 61
crystalline polymers 322–330
CTL. *see* charge transport layer
cyanine dye 128
cyanoacrylates 152, 153
– intramolecular charge separation in 152
2-cyanoacrylates (CAs) 132
cyano polymers 198
cyclic imide 38
cycloaddition, of cyclopentadiene 37
cyclobutane 159
cyclohexene oxide 255

d

data extraction algorithms 75
DBANS. *see* 4,4′-(*N*,*N*-dibutylamino)-*(E)*-nitrostilbene
DBN. *see* 1,5-diazabicyclo[4.3.0]non-5-ene
DC (direct current) accelerator 243
Debye function equation 11
Debye model 13
dehydrochlorination 144, 258
deoxyribonucleic acid (DNA)
– absorption bands 70
– absorption spectra 118, 119
– dimerization of adjacent thymine moieties 159, 160
– direct and indirect radiation effects 268
– 2D-IRS characterization 93
– effects of UV/Vis light on biopolymers 158
– high-energy-induced lesions generated in 269
– product formation by direct ionization 270
– single-strand breakage in 271
– THz spectroscopy 77
– twisting and vibrational modes 62
– typical damage sites in 269
depolymerization 23, 265, 295
– poly(phthalic aldehyde) 297
deprotection 187, 189, 295
– acid-catalyzed, poly(t-butoxycarbonyloxystyrene) 295
deprotonation 270–272, 299
diacetylenes 136–138, 255, 256
diacylgermane 129
dialkene 136, 137, 140
dialkyl dithiocarbamates 155
dialkylphenacyl sulfonium salts 130
diaryl iodonium salts 130
diaryl ketone 127
diatomic oscillator 56
1,5-diazabicyclo[4.3.0]non-5-ene (DBN) 132, 133
diazonium salts 130
diblock copolymer 135
dichroic difference 61
dichroic ratio 61
– cyano group band 88
dielectric anisotropy 44
dielectric dispersion 11
dielectric function 11
dielectric loss 11
– heating 7
dielectric performance, of materials 9
dielectric properties
– nonpolar and polar polymers 9, 10
– of polyamide 6,6 14
dielectric relaxations 8
– multiplicity 12
dielectric response
– polar amorphous polymer 14
dielectric spectroscopy 8, 12, 16
– of polymers 38–40
Diels–Alder cycloaddition 37
diglycol diallylcarbonate resin 207
diketene 255
1,2-diketones (benzils and camphorquinone) 126
dimethylacetamide 20
diolefinic crystals 137
dipentaerythrityl pentaacrylate (DPEPA) 292, 294
diphenyl iodonium ions 131
dipolar reorientation 8
dipole moment 8, 55, 109
dipole vectors 8
dipropargyl succinate 303
discoloration 144
dissolution inhibitors 187, 293, 297
– radiation-induced decomposition/chemical alteration 293
2,5-distyrylpyrazine 139
dithioalkyl propionates 155
dithiophosphates 155
DLS. *see* dynamic light scattering
DNA. *see* deoxyribonucleic acid
DPEPA. *see* dipentaerythrityl pentaacrylate
DRAM devices. *see* dynamic random access memory devices
dyes 128
– applicable as dopants 206
dynamic absorption spectroscopy 89
dynamic dichroic absorption difference 89
dynamic light scattering (DLS) 171–174
– autocorrelation function 171, 172
– CONTIN algorithm, use of 173

Lam Research Ex. 1047 - Page 348
Lam Research Corp. v. Inpria Corp.
IPR2024-00033 - U.S. Patent No. 9,823,564

– distribution of relaxation times 173, 174
– processes investigated by 166
dynamic random access memory (DRAM) devices 46, 184

e

EB lithography. *see* electron beam lithography
effective loss factor 9
EL. *see* electroluminescence
electrical conductivity 42, 99
– benzene solutions 42
– in stretch-oriented polymers 43
electric dipole moment 55
electroluminescence (EL) 115, 196, 197
electromagnetic spectrum 7
electromagnetic waves 8
electron accelerators 242, 243
electron-beam, applications 286
electron beam grafting 305
electron beam (EB) lithography 290, 291
electron-density distribution 323
electron distortion polarization 11
electronic transition 110
– allowedness 111
– and optical absorption 113
electron-positron pair production 235
– triplet production 235
elementary processes occurring by
– interaction of high-energy photons with matter 228
energy 8
– absorption 8, 9
– dissipation 9
– translational 7
energy quenchers 153
– action of 154
– nickel chelates used as 154
enthalpy 14
entropy 14
environmentally stable chemical amplification positive photoresist (ESCAP) 188, 301
EPDM. *see* ethylene-propylene-diene-terpolymer
epoxide
– difunctional epoxide with trifunctional polyol 182
– initiation, of anionic polymerization 132
– monomers employed in holography 204
epoxide side groups 296
3,4-epoxy-cyclohexylcarboxylate 19
3,4-epoxycyclohexylmethylcarboxylate 19
epoxy resins 297
EPR. *see* ethylene propylene rubber
erbium and germania-doped silica fibers 207
ESCAP. *see* environmentally stable chemical amplification positive photoresist
ESIPT. *see* excited state intramolecular proton transfer
ethyl 4-(dimethylamino)benzoate 127
ethylene oxide 83
ethylene-propylene-diene-terpolymer (EPDM) 46, 303
ethylene propylene rubber (EPR) 303
EXAFS. *see* extended X-ray absorption fine structure spectroscopy
excited state intramolecular proton transfer (ESIPT) 152
– 2-hydroxybenzophenone 152
exposure characteristic curves, for resists 186
extended X-ray absorption fine structure spectroscopy (EXAFS) 232, 233, 315, 318
extreme ultraviolet (EUV) lithography 288, 289
– copolymer units used for EUV resist formulations 300
– star-shaped polymer applicable in 301

f

far-IR analysis of polymers. *see* terahertz spectroscopy
far-IR radiation 62–64
ferrocenium hexafluorophosphate 128
fiber optic sensors 207
fiber-to-the-home systems 207
flash photolysis 97, 121, 122
flavins 120
fluorescence 231
– deactivation route 231
fluoropolymers 303
folding, of proteins 100
– rate of subsequent refolding 100
– THz detection method 100
– ubiquitin 100, 101
form factor 331
four-center-type polymerization 137
Fourier transform infrared (FTIR) spectra 66
Fourier transforms, of pulse profiles 75
Franck–Condon factor 110
free radicals 17, 134, 242
– cationic polymerization 123, 132, 243–247
– generation by photoreactions of impurity chromophores 148
– from metal salts 148
Fresnel transmission equation 75
FTIR microspectroscopy
– mapping set-ups 90

Lam Research Ex. 1047 - Page 349
Lam Research Corp. v. Inpria Corp.
IPR2024-00033 - U.S. Patent No. 9,823,564

– secondary structure motifs of poly-L-lysine 93
FTIR spectra. *see* Fourier transform infrared spectra
fundamental (normal) transition 57

g

Ge:Be lasers. *see* beryllium-doped germanium lasers
gel dose 144
glass transition temperature 202
glycidyl acrylate 135
glycidyl methacrylate 305
glycoside 273
graft copolymerization 133, 251–253
graft copolymers 133, 134
grafting 251
– high-energy radiation 304–306
– surface 135
Guinier and pair-distribution plots 333
Guinier approximation for globular particles 331
Guinier equation 332
G-value 242

h

HALSs. *see* hindered amine light stabilizers
harmonic oscillations 56
HASs. *see* hindered amine stabilizers
Havriliak–Negami equation 12
HDPE. *see* high-density polyethylene
heterogeneities, in plastic articles 16
heterogeneous dielectric systems 9
Hevea rubber 10
hexamethyl cyclotrisiloxane 255
hexamethyl disilazane 28
high-density polyethylene (HDPE) 23, 64, 101
high-energy photon radiations, denotations 228
high-energy radiation-induced grafting
– modification of polymers 305
high-energy radiation techniques, in nanotechnology 287
high resolution capability 186
hindered amine light stabilizers (HALSs) 154
hindered amine stabilizers (HASs) 154, 156, 157
holography 201–204
– component segregation 203
– epoxide monomers employed in 204
– photopolymerizable systems 202
– reconstruction of image of object recorded in hologram 202
– recording of hologram of object 202
– volume 201
homopolymers 134
– monomer moieties 191
hot band transition 58
hydrogels 306
– creation of hydrogel wound dressings 306
– poly(*N*-vinyl imidazole) hydrogels 306
– poly(*N*-vinyl pyrrolidone)-based hydrogels 306
hydroperoxide decomposers 157
hydrophilicity 35, 36, 136, 305
hydrophobic polymers 136
hydroxyalkylphenones 125
2-hydroxybenzophenone 152
4-hydroxycinnamate 120
2-(2-hydroxyphenyl)benzotriazoles 153
2-(2-hydroxyphenyl)-1,3,5-triazines 153
2-hydroxypropyl cellulose (HPC-C16) 86

i

I_2-doped polyacetylene 43
immersion grafting 136
indium tin oxide (ITO) 196, 199, 201
industrial plasma modification of textile surfaces 47
infrared reflection absorption spectroscopy (IRRAS) 66, 79, 82–84
– change in reflectance 82
– polarization modulation technique 84
– reflectance absorbance 82
– techniques 82–85
iniferter (initiator-transfer-agent-terminator) 135
injection molding of plastic articles 45
inorganic crystals 204
interfacial polarization 9
interpenetrating polymer networks (IPNs) 95
intrachain hole mobility 41
intramolecular/intermolecular vibrational modes 55
ionic polymerization 18, 19, 127, 247–251
IPNs. *see* interpenetrating polymer networks
IR absorption spectra
– of polyethylene 58
IR dichroism 86
– technique 85
IR ellipsometry (IRE) 66, 79
– optical system used for 80
– pseudo-optical constant 81
– techniques 79–82
– wavelength dependence 81

Lam Research Ex. 1047 - Page 350
Lam Research Corp. v. Inpria Corp.
IPR2024-00033 - U.S. Patent No. 9,823,564

IR imaging 90, 91
IR linear dichroism 61
IR mapping technique 90
IR microspectroscopy 90, 91
IR photon energies 55
IRRAS. *see* infrared reflection absorption spectroscopy
IR spectroscopy 65
– attenuated total reflection 65
– critical angle, defined 66
– for polymer characterization 65
– recorded during uniaxial deformation of isotactic polypropylene 87
– stretched poly(vinylidene fluoride) 89
– two-dimensional 65, 91–93
IR synchrotron radiation 90
isobornyl acrylate 203
isoquinolinium salt 130
ITO. *see* indium tin oxide

j

Jablonski diagram 113, 114

k

Kratky plot 332–334

l

ladder-type poly(*p*-phenylene)s (LPPPs) 41–43
Lambert– Beer law 64, 111
LANs. *see* local area networks
laser ablation 155
– polymers appropriate for 157
laser desorption mass spectrometry (LDMS) 157
LCDs. *see* liquid-crystal displays
LDMS. *see* laser desorption mass spectrometry
light-emitting diodes 196, 198
– multilayer polymer 199
– polymers employed in 198
– poly(p-phenylene vinylene)s used in 197
– single-layer polymer 199
light-induced chemical alterations 144
– mechanism 145
– photo-Fries rearrangement 146
–– main chain of polycarbonate 146
–– *o*-nitrobenzyl ester rearrangement in pendant groups 146
– rearrangement of constituent groups 146
light scattering 166–171
– characterizing chain stiffness of linear polymers 170
– data obtained with dilute polymer solutions 169
– intramolecular interference 168
– light scattering intensity (LSI) 167
– Rayleigh ratio 168
– static and dynamic 166
– Zimm plot 169, 170
light stabilizers 150, 151
lignins
– formation of quinoid structures in 164
– photoreactions of 163
linear polymers 16
– characterization 143, 144
– crosslinking 241
line edge roughness (LER) 186, 294
liquid-crystal displays (LCDs) 196
liquid immersion lithography 184
lithographic microtechnical fabrication process denoted (LIGA) 299
lithography 183–187, 287–289
– chemical amplification 187
– electron beam (EB) 290, 291
– exposure characteristic curves 186
– extreme ultraviolet 288, 289
– line edge roughness 186
– liquid immersion 184
– miniaturization 184
– near-field X-ray 290, 291
– 157 nm 190–192
– 193 nm 189, 190
– 248 nm 187–189
– optical projection system employed in 185
– radiation sensitivity 186
– resolution capability 186
local area networks (LANs) 207
loss factor 9
LPPPs. *see* ladder-type poly(*p*-phenylene)s

m

MA1. *see* 4-*N*-ethyl-*N*-(2-methacryloxyethyl) amine-4′-nitroazobenzene
MALDI. *see* matrix-assisted laser desorption/ionization
maleic anhydride 38
MAPTMS. *see* methacryloxypropyl trimethoxysilane
matrix-assisted laser desorption/ionization (MALDI) 157
Maxwell's equations 13
Maxwell–Wagner polarization 9
MDMO-PPV 193
media-oriented system transport (MOST) devices 207

Lam Research Ex. 1047 - Page 351
Lam Research Corp. v. Inpria Corp.
IPR2024-00033 - U.S. Patent No. 9,823,564

MEH-CN-PPV 193
MEH-PPV. *see* poly(2-methoxy-5-(2′ethylhexyloxy)-*p*-phenylene-vinylene
membrane filtration 25
methacryloxypropyl trimethoxysilane (MAPTMS) 95
methane 28
5,10-methenyltetrahydrofolate (MTHF) 120
methyl diethanolamine 127
methylene bending mode 61
methyl methacrylate (MMA) 79, 293
4-methyl pentene-1 102
1-methyl-2-pyrrolidone 25
N-methylpyrrolidone 20
Michelson interferometer 66
microspectroscopy mapping technique 90
microwave
– absorption 8
– anisotropy images 45
– effects 16
– heating 16, 17, 25
– irradiation 16
– linacs 243
– near field imaging 44
– nondestructive testing
–– dielectric polymeric coatings 44
– probing of electrical conductivity in polymers 40–43
– radiation 7
– testing 45
mid-IR analysis 67
– identification of synthetic polymers 67
– nucleic acids 69, 70
– proteins 67–69
mid-IR spectra, of nucleic acids 59
miniaturization 46, 184, 287, 302
MMA. *see* methyl methacrylate
molar extinction coefficients
– biopolymers 64
molar mass distribution 143
molecular orbital (MO) model 111–113
– assumptions 112
– electronic transitions, induced by absorption of photon 112
– energy of molecular orbitals 112
– molecular orbitals, type 112
–– with respect to electron occupancy 113
molecular oxygen (O_2) product formation
– in absence of 258–265
– in presence of 265
monomer conversion *vs*, absorbed dose 256
monomers, photopolymerized by cationic mechanism 129
4-morpholino-α-dialkylamino acetophenones 125
MOST devices. *see* media-oriented system transport devices

n

N-alkoxy pyridinium salt 130
nanotechnology 285
naphthodianthrones 121
Nd^{3+}:YAG systems 122
near-edge X-ray absorption fine structure spectroscopy 315, 317, 321, 322
near-field geometry 44
4-*N*-ethyl-*N*-(2-methacryloxyethyl)amine-4′-nitroazobenzene (MA1) 79
Newton–Raphson algorithm 75
NEXAFS spectroscopy. *see* near-edge X-ray absorption fine structure spectroscopy
nickel chelates, as quenchers in polyalkenes 154
NIR spectroscopy 58
– analysis of synthetic organic polymers 70–73
N-*i*sopropyl acrylamide (NIPAAM) 246
o-nitrobenzyl 146
nitroxyl(aminoxyl) radicals 154
NMP. *see* 1-methyl-2-pyrrolidone
4,4′-(*N*,*N*-dibutylamino)-*(E)*-nitrostilbene (DBANS) 39
non-destructive testing
– microwave testing of polymer materials 43–45
– of plastic articles 76, 77
non-equilibrium plasmas 32
non-thermal effects 16, 25, 26
Norrish type reaction 145, 148
novolak resins 295
N-vinyl carbazole 203, 254

o

o-acyl-α-oximo ketones 125
o-cresol 20
o-hydroxybenzophenones 153
OLEDs. *see* organic light-emitting diodes
onium ion 131
optical fibers 207
optical waveguides 207–209
organic light-emitting diodes (OLEDs) 196, 201
organic photoacid generators 189
organic polymers
– mid-IR absorption bands of typical chemical groups 60

Lam Research Ex. 1047 - Page 352
Lam Research Corp. v. Inpria Corp.
IPR2024-00033 - U.S. Patent No. 9,823,564

– near-IR absorption bands of hydrogenic functional groups 60
organic solar cell devices 193
– semiconducting polymers used in 193
organometallic initiators 124
overtone transitions 57
oxadiazole-containing polymers 198
oxanilides 153
2-oxazolines 18
oxidation, of hindered amine stabilizers 157
oxonium ions 182
oxygen anions, mobility 43
oxygen plasma treatment 36
oxyl radicals 150
– reactions 151

p

parallel-plate plasma reactor 46
PBOCST. *see* poly-(*t*-butoxycarbonyloxystyrene)
PEDOT. *see* poly(3,4-ethylenedioxy thiophene)
Penning ionization 30
perfluorinated polymer poly(perfluorobutenyl vinyl ether) 207
perfluorohexylethyl methacrylate (PFMA) 83
perylene dye 206
phenanthrene quinone 128
phenylalanine(Phe) 119, 282
phenylene-vinylene polymers 41
phenylglyoxylates 125
phenyl salicylates 153
S-phenyl thiobenzoates 125
phosphonium salts 130
photoactive chromophores 120, 121
photoconductivity, of conjugated polymers 98–100
photo-crosslinking, of linear polymers 142
photocuring 178, 179, 182, 183
– di- and trifunctional compounds used for 179
– letterpress technique 182
– photocuring of inks 183
– printing plate fabrication techniques 183
photocurrent 194
photodecomposition, of azides 142
photodegradation 151
photodimers 159
photoelectric effect 230–234
photofragmentation 126
photo-Fries rearrangement 146
photogeneration 100
– of charge carriers in MEH-PPV 100
photografting 135
– advantages 135
photoinitiation 124
– free-radical polymerization of alkyl acrylate 127
photoinitiators 123
– type I 123
– type II 123, 126, 127
– for visible light 128
photolabile groups 133, 134
photolithographic structuring 46
photolithography. *see* lithography
photolysis 131
– diphenyl iodonium ions 131
– free radicals generated by 132
– onium ion 131
– polystyrene 141
photolytic cleavage
– of diacylgermane 129
photonuclear absorption 235
– giant resonance, characterized by 235
photo-oxidation 144
photoreactions 144
– of carbonyl groups 149
photorearrangements, in polymers 146
photoreceptors 206
– dual-layer 205, 206
– xerographic process 205
photovoltaics 192, 194–196
phytochromes 120
phytochromobilin 120
picarin 101
– transmission spectra 102
pigments 152
Planck's constant 14
plasma-assisted chemistry 16, 26–29
– mechanistic aspects 29–32
– surface modifications of polymeric substrates 35
– technical applications 33–35
plasma-assisted surface modification, of polymers 37
plasma-deposited polymer films 37
plasma etching 27, 33, 46
– industrial, of wafers 48
plasma-induced formation 36
plasma-induced modifications of polymer surfaces 36
plasma-initiated homopolymerization 37
plasma polymerization 27–29, 36, 37, 82
plasma-polymerized maleic anhydride 37
– attachment of bicyclo[2.2.1]hept-2-ene groups 38
plasma reactor configurations 47, 48

Lam Research Ex. 1047 - Page 353
Lam Research Corp. v. Inpria Corp.
IPR2024-00033 - U.S. Patent No. 9,823,564

plasma techniques, for production of microelectronic devices 46
plasma-treated fiber, in a composite matrix 37
plasma treatment, of yarn of polymer fibers 36
plasticizers 145
PMMA. *see* poly(methyl methacrylate)
polar amorphous polymer 12
– dielectric response 12
polarization 11
– of incident radiation 61
polarized IR spectroscopy 62
polar polymers 63
poled polymers 78, 79
poly (vinylidene fluoride) 89
– infrared spectra 89
polyacetylene 43
poly(acryl amide) 306
polyacrylonitrile 62
polyalkenes 135, 147, 153
poly(alkyl acrylates) 320
polyamic acid 21
polyamide-6 10, 23
polyaniline 116
polyaramide 63
polycarbonate 63, 205, 207
polychloromethylstyrene 292
polychloroprene (1,4-poly(2-chloro-1,3-butadiene)) 10
poly(dialkyl fluorene) 116
poly(dichlorophosphazene) 22
polyenes 144
poly(ethyl acrylate) 91
polyethylene 8, 58, 63, 146, 241, 305, 320
– transmission spectra 102
poly(3,4-ethylenedioxy thiophene) (PEDOT) 194
poly(ethylene oxide) 24
poly(ethylene terephthalate) (PET) 10, 13, 23, 63, 320, 324, 328
poly(2-ethyl-2-oxazoline) 18
polyfluorenes 198
polyglucose 64
poly(3-hydroxybutyrate) 91
poly-4-hydroxystyrene 296, 299
polyimide 33, 267
poly(isooctyl acrylate) 17
poly(lactic acid) 91
poly(L-lysine) 93, 165
polymer-based electroluminescence (EL) 196
polymer degradation 22, 23
polymeric dissolution inhibitors, for novolak resins 295
polymeric light sources 196, 197, 199, 201
polymeric photovoltaic cells 194
polymer-supported reagents (PSRs) 24
poly(2-methoxy-5-(2′ethylhexyloxy)-*p*-phenylene-vinylene (MEH-PPV) 99, 100, 193, 197
poly(methyl methacrylate) (PMMA) 10, 17, 63, 79, 91, 114, 207, 259, 261, 262, 265, 299
poly(4-methyl pentene-1) 102
poly(methyl vinyl ketone) 114
poly[*N*-(1-adamantyl)vinylsulfonamide-*co*-(2-methyl)adamantyl methacrylate 190
poly(*N*-vinyl imidazole) 306
poly(*N*-vinyl pyrrolidone) 306
poly[3-(4′-octylphenyl) thiophene] 193
polyolefins 144
polyols 132
poly(perfluorobutenyl vinyl ether) 209
poly(*p*-phenylene vinylene) 116
poly(phenyl vinyl ketone) 114
poly(phthalic aldehyde) (PPA) 297
poly-*p*-phenylenes 41–43, 116, 197, 198
poly(*p*-phenylene vinylene) 196
– derivative 116
– used in light-emitting diodes 197
polypropylene 8, 10, 46, 61, 63, 87, 101, 146, 303
polysaccharides 270–274
polysiloxane 23
polysiloxane/polyurethane copolymer 88
polysilylene 116
polystyrene 17, 91, 114, 139, 141, 207
polystyrene-*b*-poly(ethylene-propylene) 173
poly(styrene-*co*-acrylonitrile) 317
polysulfone 267
poly-(*t*-butoxycarbonyloxystyrene) (PBOCST) 187, 188, 295
poly(*t*-butyl-*p*-vinyl benzoate) 187
poly(tetrafluoroethylene) (PTFE) 8, 63, 64, 101, 264, 265
poly(tetrafluoroethylene-*co*-hexafluoropropene) 10
polythiophenes 116, 198
polyurethane 136
poly(vinyl acetate) 114
poly(vinyl alcohol) 306
poly(vinyl butyral) 205
poly(9-vinylcarbazole) 17
poly(vinyl chloride) (PVC) 81, 144–148, 180, 229, 257
– dehydrochlorination 257
poly(vinylidene fluoride) 89, 320
POPT. *see* poly[3-(4′-octylphenyl) thiophene]
Porod's law 333

Lam Research Ex. 1047 - Page 354
Lam Research Corp. v. Inpria Corp.
IPR2024-00033 - U.S. Patent No. 9,823,564

PPV. *see* poly(*p*-phenylene vinylene)
proteins 274, 275
– radiolysis 275–285
– structure, evaluation 324
pterins 120
PTFE. *see* polytetrafluoroethylene
pulse radiolysis method 258
pyridine-containing polymers 198

q
quantum yields, of photoproducts 142, 143
quinoid structures 164
quinone dye 206

r
γ-radiation 306
– in technical processes 286
radiation-chemical yield 242
– G-value 242
radiation crosslinking 303, 304
radiation-cured coatings
– commercial applications 180
radiation grafting, importance of 305
radiation-induced orientation polarization 8
radiation processing, role in nanotechnology 285
radiation protection 265–267
radiation sensitivity 186
radiation sources 242, 243
radiation stability 265–267
radical-induced crosslinking, of proteins 284
radical migration, via hydrogen atom transfer 241
radical polymerization, of acrylate monomer 94
radiolysis
– bulk biopolymers 268–275
– bulk synthetic polymers 257, 258
– proteins, polymers in solution 275–285
RAIRS. *see* reflection absorption infrared spectroscopy
Raman images, of polystyrene beads 177
Raman scattering 174–176
Raman-spectroscopic imaging 91
Rayleigh light scattering 207
Rayleigh radiation 176
Rayleigh ratio 168
reflection absorption infrared spectroscopy (RAIRS) 79
relaxation 8
resists 292
– chemical amplification 294–299
– classical X-ray and EB lithography 292, 293
–– practical applications 299, 300
– commercially available EB resists 300
– crosslinking boosters 294
– EUV resists 300–302
– formulations 300, 302
– polymers/copolymers applied
–– as negative-tone resists 294
–– as positive-tone resists 293
– radiation sensitivity, of negative-tone 292
resonant vibration frequencies 59
RF (radio frequency) linacs 243
RF (radio frequency) linear accelerators 243
ring-opening polymerization 204
Rose Bengal 128
rubber tires 285
Rutherford scattering 237

s
SAXS. *see* small-angle X-ray scattering
self-indicating-instant- radiation-alert dosimeter (SIRAD) 256
– diacetylene applicable for dosimetry 256
semiconducting polymers, for organic solar cell devices 193
sensitizers 46
– electronically excited, oxidation 131
Si-and SiO_2-selective plasmas 34
signal-to-noise ratio 45
SIRAD. *see* self-indicating-instant- radiation-alert dosimeter
size-exclusion chromatography 25
small-angle X-ray scattering (SAXS) 327
– broadening of lines 329
– profiles of PET samples 328
– proteins in solution 334
solar cells 196
solid-phase organic synthesis (SPOS) 23–25
solid-state polymerization 253, 256
– monomers, experimental evidence 256
solution scattering, tool to characterize biopolymers 330
spurs 235
squaraine dye 206
stentorin 121
step-growth polymerization 19–21
Stokes–Einstein equation 172
stress-induced changes in orientation of domains 88
sub-THz radiation 7, 13
– induced chemical reactions 16
– materials absorbing 15
– plasma generated by 16

Lam Research Ex. 1047 - Page 355
Lam Research Corp. v. Inpria Corp.
IPR2024-00033 - U.S. Patent No. 9,823,564

surface grafting 135
surface wettability, of selected polymers 36
swift electrons 235–237
synchrotron FTIR microspectroscopy 91
synchrotrons 315
– radiation 316

t
terahertz (THz) spectroscopy 66, 73, 76–78, 98, 100, 101
– absorption spectra
–– biopolymers 77
–– synthetic polar polymers 63
–– synthetic unpolar polymers 64
– angular frequency 75
– biopolymers in liquid water, studies 77, 78
– complex transmittance 75
– external reflection methods, for thin films 79
– generation of THz radiation in poled polymers 78, 79
– nondestructive testing of plastic articles 76, 77
– refractive index, calculation 76
– time-domain spectrometer, illustration 73
– time-resolved 98, 100, 101
– waveforms of THz pulses propagation 74
terahertz-time-domain spectroscopy 73
terephthalophenones 126
tetrabromobisphenol A 298
tetrabutyl ammonium bromide (TBAB) 22
tetrafluoromethane 31
tetrahydrofuran (THF) 22
2,2′,6,6′−tetramethylpiperidine (TMP) 154
tetramethylsilane 28
thickness, measurements 44
– nondestructive 45
thiobenzoates 125
thiohydantoins 25
– microwave-assisted synthesis 25
thioxanthone derivatives 126
thymine moieties 159, 160
THz optics, made from polymers 101, 102
– polymeric materials 101
– transmission spectra, of polyethylene/picarin 102
THz radiation 67
THz spectroscopy. *see* terahertz spectroscopy
time-resolved measurements, in mid-IR range 93
– *in-situ* monitoring of chemical reactions 93–96
time-resolved microwave absorption measurements 41
time-resolved THz spectroscopy 98, 121, 122
– flash photolysis 97, 121, 122
– folding of proteins 100, 101
– photoconductivity of conjugated polymers 98–100
Ti:sapphire laser, used in THz spectroscopy 66
Ti:sapphire oscillators 122
titanocene 124
TMP. *see* 2,2′,6,6′-tetramethylpiperidine
TNF. *see* trinitrofluorenone
topochemical polymerization 136, 137
– diacetylene derivatives 136
– dialkenes, capable of undergoing 137
– four-center-type polymerization 137
–– crystalline 2,5-distyrylpyrazine 139
– [2+2] photocyclopolymerization of a dialkene 140
– photopolymerization of diolefinic crystals 137
– polymerization of assembled functional diacetylenes 138
TPTM. *see* trimethylolpropane trimethacrylate
transient two-dimensional IR spectroscopy 96
– flash photolysis 97, 98
– folded and unfolded ubiquitin, structures 97
– temperature jump (T-jump) studies 96, 97
– transient 2D-IR difference spectra of ubiquitin 97
transition metal complexes 128
transition moments 55, 61, 109–111
– integrals 109, 110
trans-polyacetylene 116
triallyl cyanurate 303
triaryl sulfonium salts 130, 299
triethanolamine 127
2,4,6-trimethylbenzoyl diphenylphosphine oxide 126
1,1,1-trimethylolpropane triacrylate 303
trimethylolpropane trimethacrylate (TPTM) 292, 294
trinitrofluorenone (TNF) 205
trioxane 254
triphenyl amine triazo pigment AZO-3 207, 208
triphenylsulfonium trifluoromethane sulfonate 298
tryptophan (Trp) 119, 306
two-dimensional IR spectroscopy 91, 92
– polymer characterization 91–96
– secondary structure motifs of poly-L-lysine 93

Lam Research Ex. 1047 - Page 356
Lam Research Corp. v. Inpria Corp.
IPR2024-00033 - U.S. Patent No. 9,823,564

type I free-radical photoinitiators 125
tyrosine (Tyr) 119, 282

u

ubiquitin
– folding 101
– structures 96, 97
– transient 2D-IR difference spectra 97
– unfolding 100
ultraviolet photoelectron spectroscopy (UPS) 165, 166, 315
ultraviolet (UV) radiation 228, 240
unpolar polymers 63
– THz absorption spectra 64
UPS. *see* ultraviolet photoelectron spectroscopy
UV absorbers 152, 153
UV-curing of coatings 178
UV-light-initiated polymerization
– urethane-acrylate system 94

v

valence electrons 109
vapor-phase grafting 136
vibrations 55
– energy levels 58
– frequency 56
vibronic molecular energy levels 56, 57
vinyl monomers 136
4-vinyl pyridine plasma 37
vinylstearate 254
vulcanization
– carbon black-filled rubber 46
– rubber tires and lattices, and curing 285
vulcanized rubber 23

w

water contact angle 36
water-soluble aromatic ketones 126
wavelength-energy correlation
– for electrons 288
– for photons 288
WAXD. *see* wide angle X-ray diffraction
wettability 136
wide angle X-ray diffraction (WAXD) 323, 325, 326
– applications 324, 325
– evaluation of structure of protein 324
– profile of poly(ethylene terephthalate) 324
– recording of pattern, simultaneous with SAXS 327
– specimen with axial orientation, illustration 326

x

xanthopsins 120
xerography 204–207
X-ray absorption near-edge structure 232, 233
X-ray absorption spectra, with corresponding electron transitions 232
X-ray imaging 315, 321, 322
X-ray interference, role in characterization of rigid polymers 322
X-ray lithography 289, 290
– applications 302, 303
– near-field 291
X-ray microscopy 315, 321, 322
X-ray photoelectron spectroscopy (XPS) 315, 318–321
X-ray scattering 322. *See also* small-angle X-ray scattering
– crystalline polymers 322–330
– overview 322
X-ray spectroscopy 233, 316

z

Zimm plot 169, 170
zone-plate array lithography 185

Lam Research Ex. 1047 - Page 357
Lam Research Corp. v. Inpria Corp.
IPR2024-00033 - U.S. Patent No. 9,823,564